UNIVERSITY OF SOUTHAMPTON

FACULTY OF NATURAL AND ENVIRONMENTAL SCIENCES

School of Chemistry

THE DEVELOPMENT OF SMALL MOLECULE TRANSMEMBRANE ANION TRANSPORTERS FOR THE TREATMENT OF DISEASE

by

Stephen John Moore

Thesis for the degree of Doctor of Philosophy

June 2012

UNIVERSITY OF SOUTHAMPTON

UNIVERSITY OF SOUTHAMPTON

ABSTRACT

FACULTY OF NATURAL AND ENVIRONMENTAL SCIENCES

Chemistry

Doctor of Philosophy

THE DEVELOPMENT OF SMALL MOLECULE TRANSMEMBRANE ANION TRANSPORTERS FOR THE TREATMENT OF DISEASE

by Stephen John Moore

Within this thesis novel receptors capable of binding and facilitating the transmembrane transport of biologically relevant anions are reported. Molecules based on the diindolylurea and tris(2-aminoethyl)amine scaffolds are described and their anion binding properties in both solution and in the solid state are reported. Inspired by the high affinities for oxo-anions measured for these molecules in polar solvent mixtures, the anion transport properties of structurally simple ureas and thioureas were studied. The high Cl^-/NO_3^- and Cl^-/HCO_3^- antiport activity observed with some of the thiourea compounds led to the development of more 'drug-like' transporters containing trifluoromethyl substituents. Fluorination of the transporter scaffold in this manner enhanced the lipophilicity and increased the acidity of the NH hydrogen-bond donor groups, leading to improvements in both anion affinity and transport activity. This work ultimately produced compounds capable of facilitating ion transport *in vitro*.

A series of bisurea compounds based on the *ortho*-phenylenediamine scaffold are reported as potent ion transporters, capable of facilitating a range of ion transport processes. The introduction of electron withdrawing substituents was found to increase transporter activity. Of particular note is a *para*-nitrophenyl functionalised bisurea that facilitates chloride transport at a loading of 0.1 mmol % (with respect to lipid), the lowest loading of a synthetic mobile carrier to facilitate anion transport reported to date.

Dual host systems for both M^+/Cl^- symport (M = Na, K or Rb) and Cl^-/HCO_3^- antiport are also described. By using different transporters to facilitate each uniport pathway in these coupled transport processes, it was possible to achieve enhanced ion transport rates. Remarkably, this is the first reported example of a dual host approach towards anion antiport.

Contents

DECLARATION OF AUTHORSHIP

I, Stephen John Moore, declare that the thesis entitled

The development of small molecule transmembrane anion transporters for the treatment of disease

and the work presented in the thesis are both my own, and have been generated by me as the result of my own original research. I confirm that:

- This work was done wholly or mainly while in candidature for a research degree at this University;
- Where any part of this thesis has previously been submitted for a degree or any other qualification at this University or any other institution, this has been clearly stated;
- Where I have consulted the published work of others, this is always clearly attributed;
- Where I have quoted from the work of others, the source is always given. With the exception of such quotations, this thesis is entirely my own work;
- I have acknowledged all main sources of help;
- Where the thesis is based of work done by myself jointly with others, I have made clear exactly what was done by others and what I have contributed myself;
- Parts of this work have been published as:

"Anion-anion proton transfer in hydrogen bonded complexes" P. A. Gale, J. R. Hiscock, S. J. Moore, C. Caltagirone, M. B. Hursthouse and M. E. Light, *Chem. -Asian J.*, 2010, **5**, 555-561

"Tripodal transmembrane transporters for bicarbonate" N. Busschaert, P. A. Gale, C. J. E. Haynes, M. E. Light, S. J. Moore, C. C. Tong, J. T. Davis and W. A. Harrell, Jr., *Chem. Commun.*, 2010, **46**, 6252-6254

"Structurally simple lipid bilayer transport agents for chloride and bicarbonate" N. J. Andrews, C. J. E. Haynes, M. E. Light, S. J. Moore, C. C. Tong, J. T. Davis, W. A. Harrell, Jr. and P. A. Gale, *Chem. Sci.*, 2011, **2**, 256-260

"A dual host approach to transmembrane transport of salts" S. J. Moore, M. G. Fisher, M. Yano, C. C. Tong and P. A. Gale, *Chem. Commun.*, 2011, **47**, 689-691

"A synergistic approach to anion antiport" S. J. Moore, M. G. Fisher, M. Yano, C. C. Tong and P. A. Gale, *Dalton Trans.*, 2011, **40**, 12017-12020

"Tunable transmembrane chloride transport by bis-indolylureas" C. J. E. Haynes, S. J. Moore, J. R. Hiscock, I. Marques, P. J. Costa, V. Félix and P. A. Gale, *Chem. Sci.*, 2012, **3**, 1436-1444

"Towards "drug-like" indole-based transmembrane anion transporters" S. J. Moore, M. Wenzel, M. E. Light, R. Morely, S. J. Bradberry, P. Gómez-Iglesias, V. Soto-Cerrato, R. Péréz-Tomás and P. A. Gale, *Chem. Sci.*, 2012, **3**, 2501-2509

"Chloride, carboxylate and carbonate transport by *ortho*-phenylenediamine-based bisureas" S. J. Moore, C. J. E. Haynes, J. González, J. L. Sutton, S. J. Brooks, M. E. Light, J. Herniman, G. J. Langley, V. Soto-Cerrato, R. Péréz-Tomás, I. Marques, V. Félix and P. A. Gale [Manuscript in preparation]

Signed:.....

Date:.....

Acknowledgements

Firstly I would like to thank my supervisor Prof. Philip Gale for his support and guidance, and for giving me the opportunity to work in his research group. I would like to thank the members of the Gale group past and present; Masafumi 'Yopparai' Yano, Pete 'Mr. Magic' Edwards, Matt Fisher, Christine Tong, 'Uncle' Marco Wenzel, Sarah Young, Noémie Lalaoui, Raj 'Caribbean Cruise Gold Membership' Gosain, Yoshinori Takashima, Issy 'Parrots and Goats' Kirby, Agnieszka Krajewska, Louise Karagiannidis, Pip 'Ninja' Simpson, Dale Kelpie, Nathalie 'Body in the Freezer' Busschaert, Michele Bruschini and Cally 'Leprosy' Haynes.[1] I would also like to thank everyone on Level 4 for making it such a nice place to work. I must thank all the people that directly contributed towards my work, in particular Mark Light who ran and solved all the crystal structures, John Langley and Julie Herniman for their help with the mass spectroscopy, Ricardo Péréz-Tomás and Vanessa Soto-Cerrato at the University of Barcelona for devising and running the *in vitro* assays and also Rebeka Morley, Patricia Gómez-Iglesias and Jorge González for their contributions to the work discussed in **Chapters 3** and **4**.

I would like to thank all my friends in Southampton, Poole, Reading and elsewhere. Honourable mentions go to Michael 'Wild Bill' Bodnarchuk, Jon 'Lindley' Blaine, Sam 'Never Made a MOF' Keltie, John Blake, Jon Burns, Dave Xuereb, Andrew 'Militant' Guy, Dan 'Nit' Mason, Letty Dormandy, Licia Biserna, Rob Hudson, Charles 'IR' Taylor, Nathan 'King of the Jungle' Bartlett, Jason Petrou, Montse Shelbourne, Scott Twiddy, Rob 'Safehands' Johnson, 'Uncle' Pete Horton, Dave 'N' Robson, Matt Hart, Chris Hyde, Gary 'Woodpigeon' Edwards, Sam Hanson, Jason Moors, Adrian Rowland, Matthew Butler, Simon Aitchison and Andrew 'Shandy-Andy' Smart. I must also thank Penny Martin, David Leah, Rhiannon Smith, John Fosbraey, Colin Flowers, the Stores Staff (Keith, Clive, Karl, Tony and Graham), Len Lindoy, Bricio Boni, Calden Carrol, Will Harrell and Fumiaki Ito.

Special thanks goes to my parents; Sharon and Jim, my grandparents; Eric, Betty, Eric and Rosemary, my brother Tom and also John, Helen, Nathalie, Olivia, Debs, Olly and Sam for their support and encouragement over the course of the last 26 years. Finally, I would like to thank Rachael for putting up with me throughout.

“I am the farmer. Bang! You are the crops.”

(Sam Keltie, 2011)

Abbreviations

Å	Angstrom
ADMET	Absorption, distribution, metabolism, excretion and toxicity
AmB	Amphotericin B
AO	Acridine orange
ATP	Adenosine triphosphate
AVD	Apoptotic volume decrease
bipy	2,2'-bipyridine
Bn	Benzyl
Bu	Butyl
BzO^-	Benzoate
C	Celcius
c	Calculated
CD	Cyclodextrin
CDI	1,1'-carbonyldiimidazole
CF	Cystic fibrosis
CFTR	Cystic fibrosis transmembrane conductance regulator
CLC	Chloride channel protein
CNS	Central nervous system
CyPLOS	Cyclic phosphate linked oligosaccharide
Da	Daltons
DIQ	Diindolylquinoxaline
DMEM	Dulbecco's Modified Eagle Medium
DMF	*N,N*-dimethylformamide
DMPC	1,2-dimyristoyl-*sn*-glycero-3-phosphocholine
DMSO	Dimethyl sulfoxide
DNA	Deoxyribonucleic acid
DOPA	1,2-dioleoyl-*sn*-glycero-3-phosphate
DOPC	1,2-dioleoyl-*sn*-glycero-3-phospocholine

Dpa	2,2'-dipicolylamine
DCM	Dichloromethane
DPPC	1,2-dipalmitoyl-*sn*-glycero-3-phosphocholine
EDTA	Ethylenediaminetetraacetic acid
ESI-MS	Electrospray ionisation mass spectrometry
EYPC	Egg yolk phosphatidyl choline
FBS	Foetal bovine serum
FTIR	Fourier Transform Infrared Spectroscopy
HEPES	4-(2-hydroxylethyl)-1-piperazineethanesulfonic acid
HPTS	Hydroxylpyrene-1,3,6-trisulfonic acid
HRMS	High resolution mass spectrometry
Hz	Hertz
IR	Infrared
ISE	Ion selective electrode
ITC	Isothermal titration calorimetry
J	Joule
K	Kelvin
K_a	Association constant
K_{sv}	Stern-Volmer constant
L	Litres
LRMS	Low resolution mass spectrometry
M	Molar concentration
MDCK	Madin Darby canine kidney
mins	Minutes
mol	Moles
MTT	3-(4,5-Dimethylthiazol-2-yl)-2,5-Diphenyltetrazolium bromide
NADPH	Nicotinamide adenine dinucleotide phosphate
NBD	7-nitrobenz-2-oxa-1,3-diazol-4-yl
NMR	Nuclear magnetic resonance
NOE	Nuclear Overhauser Effect
O-NDI	oligo-(*p*-phenylene)-*N*,*N*-naphthalenediimide

O-PDI	oligo-(p-phenylene)-*N*,*N*-perylenediimide
P	Patition coefficient
PBS	Phosphate buffered saline
Ph	Phenyl
PLB	Planar lipid bilayer
POPC	1-palmitoyl-2-oleoyl-*sn*-glycero-3-phosphocholine
POPG	1-palmitoyl-2-oleoyl-*sn*-glycero-3-phospho-(1'-*rac*-glycerol)
POPS	1-palmitoyl-2-oleoyl-*sn*-glycero-3-phospho-*L*-serine
ppm	parts per million
s	Seconds
SCLC	Small-cell lung carcinoma
SCMTR	Synthetic chloride membrane-insertable transporter
SPQ	6-methoxy-*N*-(3-sulfopropyl)quinolinium
t	time
TBA	Tetrabutylammonium
TEA	Tetraethylammonium
TEG	Tetraethylene glycol
THP	1,4,5,6-tetrahydropyrimidine
TMA	Tetramethylammonium
TPSA	Topological polar surface areas
TTF	Tetrathiafulvalene
UV-vis	Ultraviolet-visible spectroscopy
VSOR	Volume sensitive outwardly rectifying
wc	Wildman-Crippen

Quick Reference

This page is designed to serve as a quick reference for some of the most frequently discussed compounds within **Chapter 2**.

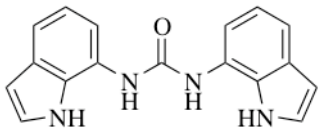

118

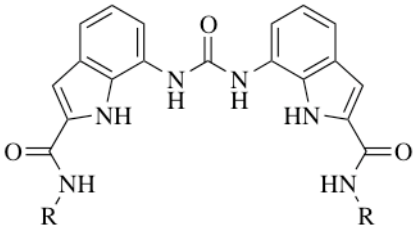

152 R = Bn

153 R = 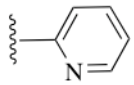

154 R = Ph

129 R = $(CH_2)_3CH_3$

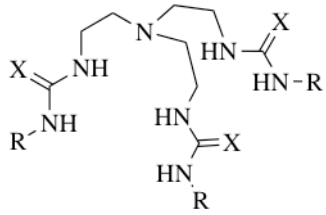

155 R = ^{n}Bu, X = O

156 R = ^{n}Bu, X = S

143 R = Ph, X = O

144 R = Ph, X = S

Quick Reference

This page is designed to serve as a quick reference for some of the most frequently discussed compounds within **Chapter 3**.

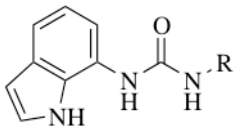

202 R = $(CH_2)_3CH_3$
203 R = $(CH_2)_4CH_3$
204 R = $(CH_2)_5CH_3$
205 R = $(CH_2)_6CH_3$
206 R = $(CH_2)_7CH_3$
207 R = $(CH_2)_8CH_3$
208 R = $(CH_2)_9CH_3$
209 R = $(CH_2)_{10}CH_3$
210 R = $(CH_2)_{11}CH_3$

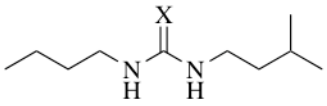

211 X = O
212 X = S

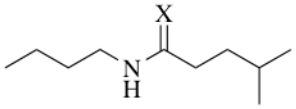

217 X = O
218 X = S

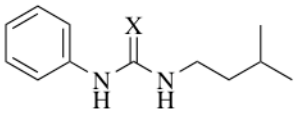

213 X = O
214 X = S

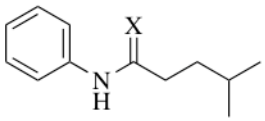

219 X = O
220 X = S

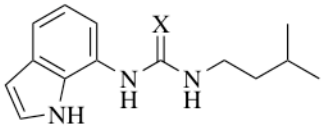

215 X = O
216 X = S

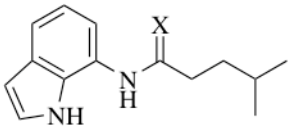

221 X = O
222 X = S

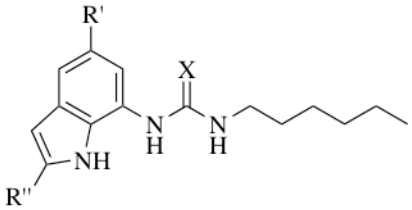

204 X = O, R' = H, R'' = H
223 X = S, R' = H, R'' = H
224 X = O, R' = CF_3, R'' = ^nBu
225 X = S, R' = CF_3, R'' = ^nBu

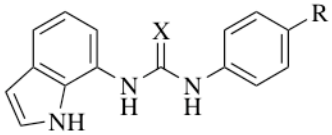

226 X = O, R = H
227 X = S, R = H
228 X = O, R = CF_3
229 X = S, R = CF_3

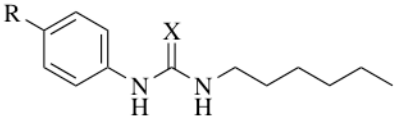

230 X = O, R = H
231 X = S, R = H
232 X = O, R = CF_3
233 X = S, R = CF_3

Quick Reference

This page is designed to serve as a quick reference for some of the most frequently discussed compounds within **Chapter 4**.

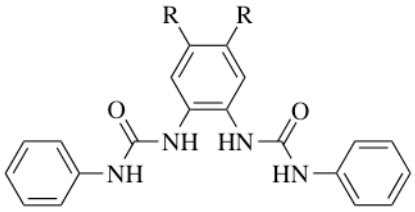

244 R = H
262 R = F
245 R = Cl

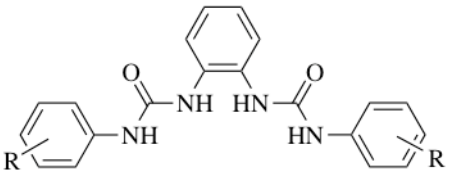

263 R = *p*-CN
264 R = *p*- CF_3
247 R = *p*-NO_2
265 R = *m*-NO_2
248 R = *o*-NO_2

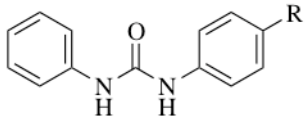

266 R = CN
267 R = CF_3
268 R = NO_2

Quick Reference

This page is designed to serve as a quick reference for some of the most frequently discussed compounds within **Chapter 5**.

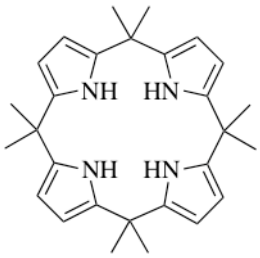

178

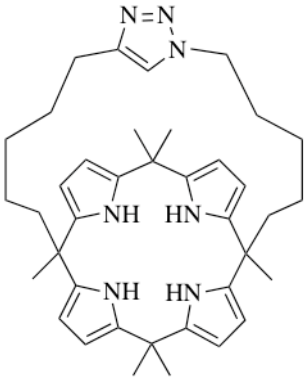

286

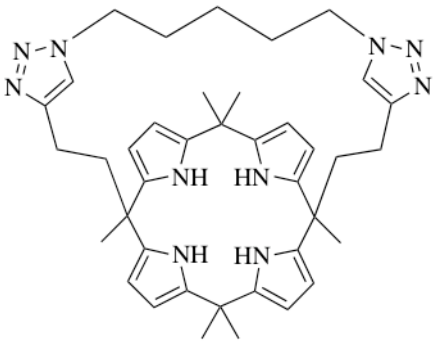

287

Chapter 1
Introduction

Supramolecular chemistry is the study of the intermolecular bond, encompassing all systems wherein two or more chemical species associate.[2] This broad definition has grown to encompass a diverse range of fields, the transmembrane transport of anions being a relatively new supramolecular discipline that has attracted considerable attention from research groups around the world.[3-10] By developing simple organic molecules that are capable of binding anions and facilitating their transport across phospholipid bilayers, it may be possible to develop new approaches for the treatment of disease. This chapter examines the biological importance of membrane transport, the most recent advances in the development of synthetic anion transporters and gives an overview of the methods used to monitor the movement of ionic species across a membrane.

1.1 The Structure of Biological Membranes

Cellular organisation in biological systems is achieved using biomembranes. These membranes are involved in a diverse range of processes including protein biosynthesis, small molecule transport, regulation of ion gradients, pinocytosis, phagocytosis, intermediary metabolism and controlled cell growth and division.[11]

The biomembranes that fulfil these functions are composed of a mixture of lipids, proteins and oligosaccharides.[12] The organisation of these components to form a membrane is described by the fluid mosaic model.[13] The amphiphilic nature of lipid molecules leads to the formation of a bilayer structure, with the hydrophilic fatty acid 'tails' directed inwards and the polar phospholipid 'head groups' in direct contact with the aqueous phase (**Figure 1.1**). The bilayer is a dynamic structure wherein lipid molecules are laterally mobile, but the transport of lipids between leaflets is energetically unfavourable and must be facilitated by a protein. Proteins responsible for a range of membrane functions are found either within the bilayer (integral) or associated to the membrane surface by non-covalent interactions (peripheral).[14] Carbohydrate chains are

commonly anchored onto the extracellular bilayer surface and are involved in cellular recognition.[15]

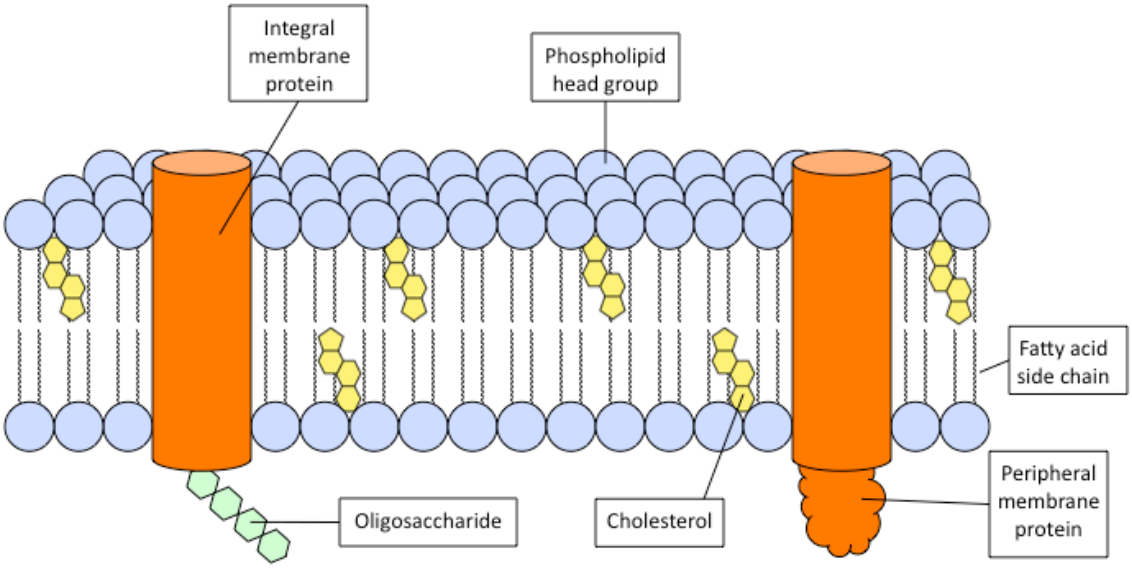

Figure 1.1: Fluid mosaic model of a biological membrane.

Biomembranes serve as a barrier between the cystolic and exoplasmic environments. Consequently, the free diffusion of chemical species across phospholipid bilayers is limited to gases and some hydrophobic steroid hormones.[16] Small uncharged polar molecules display a range of membrane permeabilities whilst large uncharged polar molecules such as glucose and charged polar molecules such as adenosine triphosphate (ATP) are membrane impermeable.[17] Anions exhibit very low permeability towards pure phospholipid bilayers.[18, 19] The ease of ion permeation through biomembranes is predicted by the Hofmeister series, which reflects the lipophilicity and extent of hydration of the ionic species.[20, 21] The hydration energies of some of the ions relevant to the transport assays discussed in **Section 1.9** are displayed in **Table 1.1**. To overcome the inherently low permeability of ionic species biomembranes are endowed with proteins that selectively transport ions across the hydrophobic membrane interior (see **Section 1.4**).

Ion	Na^+	K^+	Rb^+	Cs^+	Cl^-	NO_3^-	HCO_3^-	SO_4^{2-}
$\Delta_{hyd}G_{calc}$ (kJ mol^{-1})	-385	-305	-285	-245	-270	-275	-310	-1145

Table 1.1: Calculated molar Gibbs energies of the hydration of ions relevant to transport.[22]

1.2 Transport Pathways

Transmembrane ion transport can occur by one of three pathways (**Figure 1.2**);

- **Uniport** – A chemical species is transported in a single direction.
- **Symport** – A co-transport process wherein two different chemical species are transported in the same direction.
- **Antiport** – A co-transport process wherein two different chemical species are transported in opposite directions.

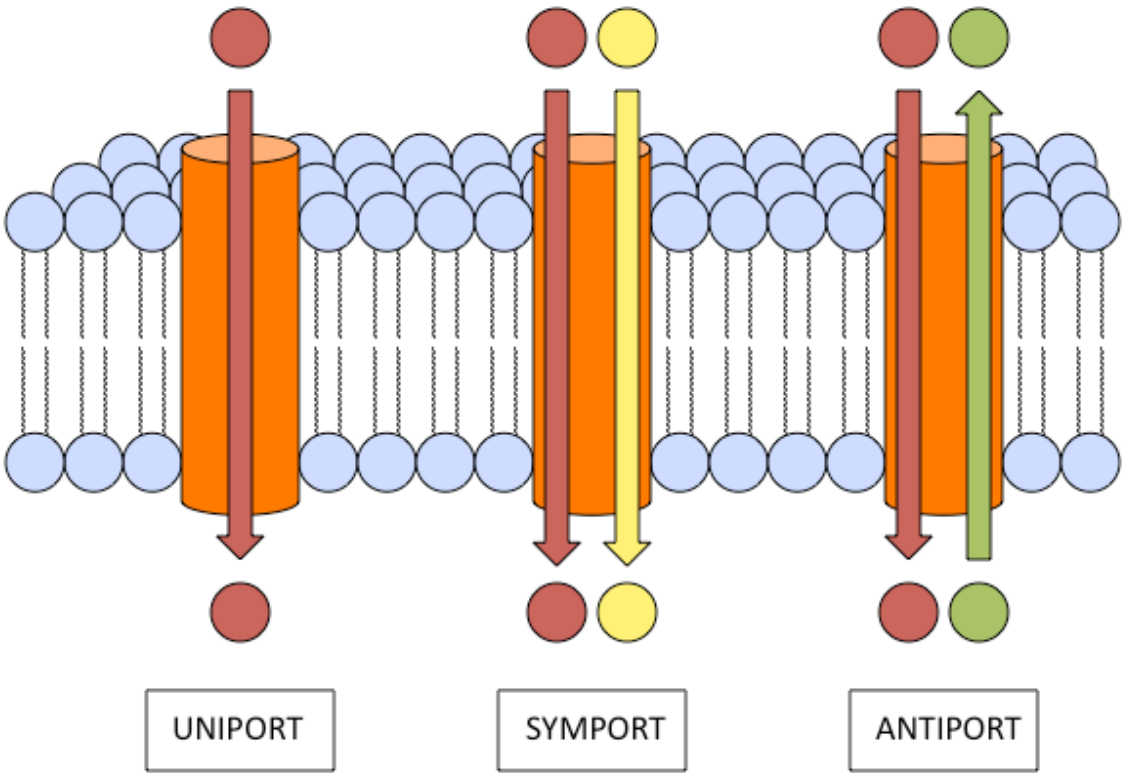

Figure 1.2: Uniport, symport and antiport transport pathways.

These processes can be passive; responding to established electrochemical gradients, or active; using the energy derived from the hydrolysis of ATP to transport against the gradient. In nature the situation is usually more complex, with multiple transport processes coupled to one-another (see **Section 1.5**). When considered as isolated processes, the symport of ions of opposite charge or the antiport of ions of the same charge are required to maintain charge neutrality.

1.3 Transport Mechanisms

Molecules that facilitate the transmembrane transport of ionic species chiefly operate by either a channel mechanism or by a mobile carrier mechanism (some exotic transport mechanisms are discussed in **Section 1.8.8**). Channels are semi-permanent, membrane spanning structures that facilitate the transmembrane transport of ionic species by providing a hydrophilic pathway through the membrane, through which the transported ions avoid interaction with the hydrophobic membrane interior. Mobile carriers are typically small, organic molecules that partition into phospholipid bilayers. These molecules bind ions at the polar membrane interface, carry them across the hydrophobic membrane interior by diffusion and then release them on the opposite side of the membrane in response to electrochemical ion gradients (**Figure 1.3**). The transport rates achieved by channels are typically faster than the rates achieved by carriers (with channel ion conductance rates of up to 10^8 ions s^{-1}).[23] However synthetic carriers can exhibit strong ion selectivity, which upon synthetic modification can be tuned for different ionic guests.[12] Examples of both ion channels and mobile carriers are found in nature (see **Sections 1.4** and **1.6**).

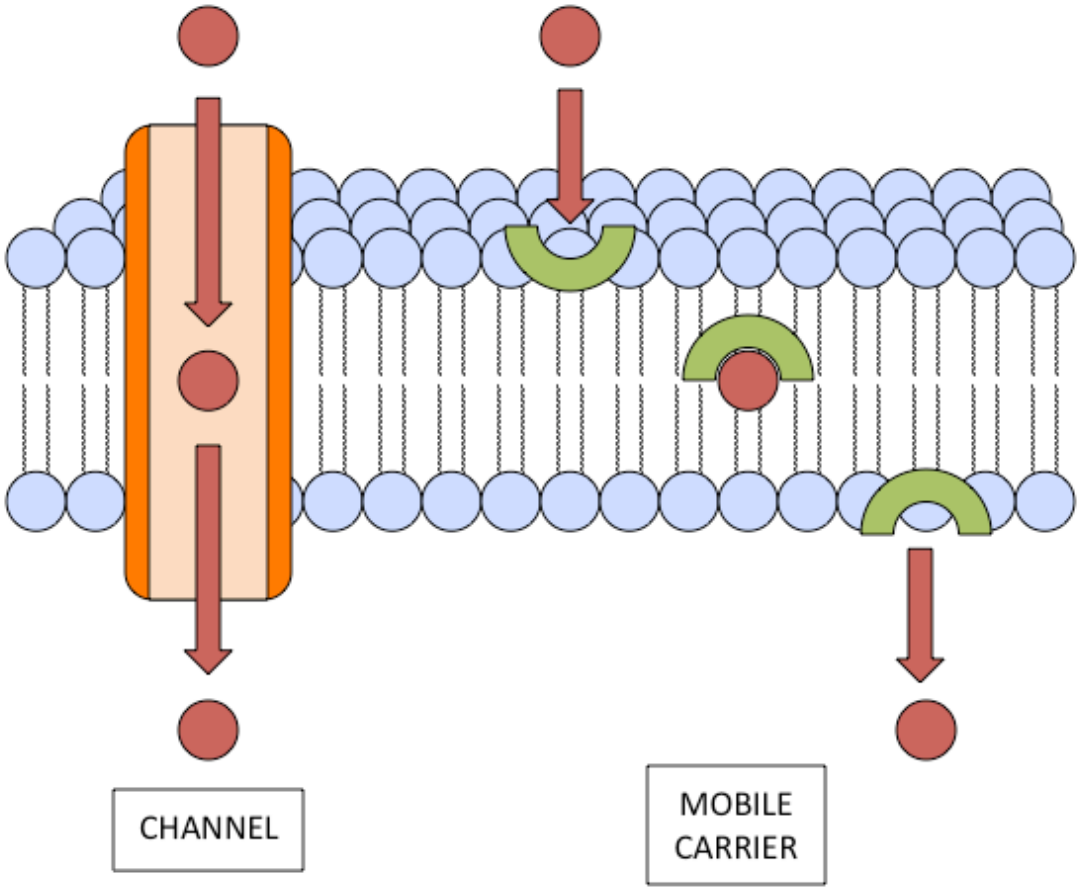

Figure 1.3: The mobile carrier and channel mechanisms for transmembrane ion transport.

1.4 Biological Channels

Biological ion transport is typically achieved by membrane spanning proteins. These proteins provide an ion conductance pathway across the membrane, preventing hydrophilic ions from coming into contact with the hydrophobic membrane interior.[7] Gated channels can switch between open and closed states in response to external stimuli (ligand binding, changes in membrane potential or a mechanical stimulus).[4, 24, 25] In all instances the stimulus causes a conformational change in the channel protein that will either block or open the pore.[26] The relative sizes of the ion and the conductance pore influence ion channel permeability, as large ions are physically unable to permeate small pores. Aside from this steric requirement, ion selectivity may also be achieved using a selectivity filter located at the narrowest region of the channel. The selectivity filter is a collection of amino acid residues that 'screens' ions according to their charge, size and

hydrophobicity. At least partial desolvation of the ion is required to pass through such filters and thus the interactions between the selectivity filter(s) and the ion must compensate this desolvation penalty.[26]

Chloride channels are a typical example of a biological ion channel and are critical for a diverse range of biological processes (see **Section 1.5.1**). Channel mediated chloride transport occurs by either a uniport mechanism or is coupled to sodium, potassium or bicarbonate transport.[27] Chloride channels are characterised by their gating mechanisms, of which there are several. Gating can occur in response to changes in membrane potential, cell volume, intracellular calcium concentration, ligand binding or phosphorylation. The CLC family of voltage-gated chloride channels are ubiquitous in cellular organisms. All CLC channels selectively conduct chloride, bromide and nitrate.[28] The low abundance of nitrate and bromide in biological systems means that the fundamental selectivity is that between chloride and phosphate, sulphate, bicarbonate, and anionic proteins. The elucidation of the *Escherichia coli* and *Cyanidioschyzon merolae* CLC structures by X-ray diffraction techniques have provided mechanistic insights into how this selectivity is achieved.[29, 30] The extracellular surface of the channel leading to the selectivity filter is lined with positive dipoles, attracting anions whilst repelling cations.[31] The filter itself is wide enough for chloride but not larger competing anions.[30] Chloride ions are bound by hydrogen-bonding interactions within the selectivity filter, and stabilised by positive dipoles.[32] A glutamate residue (E148) occludes the filter when the channel is in the closed state.[33] A conformational change occurs upon protonation of this residue, opening the channel (**Figure 1.4**).[34, 35]

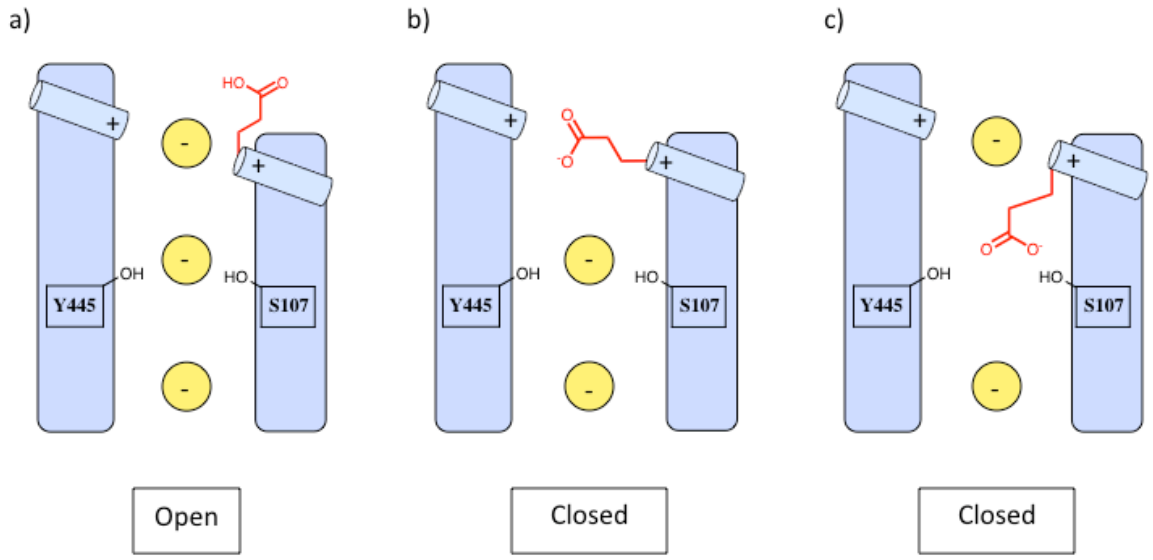

Figure 1.4: Model for gating in CLC transporters. Residues corresponding to S107, E148 (red) and Y445 are shown as schematic drawings. Yellow spheres represent chloride ions. Blue cylinders represent the 'positive' N termini of alpha helicies. Open state and two closed states are shown; a) open state with three chloride ions occupying the three binding sites within the pore, b) closed state with carboxylate of E148 binding to the 'positive' dipole of the selectivity filter, c) alternative closed state with carboxylate of E148 binding to central binding site.

1.5 Ion Channels and Disease

1.5.1 Diseases Associated with Defective Chloride Transport

Chloride channels are found in a diverse range of tissues and consequently are vital for a range of biological processes including blood pressure regulation, chloride reabsorption, salt and fluid secretion, electrical response generation and programmed cell death (apoptosis).[29] Mutation of chloride channels vital to these processes can lead to a myriad of disease states. Defects in the CLC-1 chloride channel, which is widely expressed in skeletal muscle, can result in electrical hyperexcitability.[27] Reduced chloride uptake leads to destabilisation of the resting potential, resulting in continued firing of action potentials.[36] This impaired muscle relaxation causes myotonia (muscle stiffness).[26]

Mutations in renal chloride transport proteins are responsible for a number of disorders. Bartter's syndrome type III is a disease of the voltage gated chloride channel, CLC-Kb. In the ascending loop of Henle, NaCl reabsorption is facilitated by the NaK2Cl co-transporter. Energy for this process comes from the Na^+ gradient generated by the action of a Na/K-ATPase. The return of imported chloride to the blood is facilitated by

the CLC-Kb chloride channel (**Figure 1.5**). Failure of the CLC-Kb channel leads to chloride accumulation, lowering the activity of the NaK2Cl co-transporter. Thus, patients with Bartter's syndrome type III suffer from salt-wasting (excessive NaCl excretion), hypokalaemia (low blood potassium) and hypercalciuria (excessive urinary calcium excretion).[36]

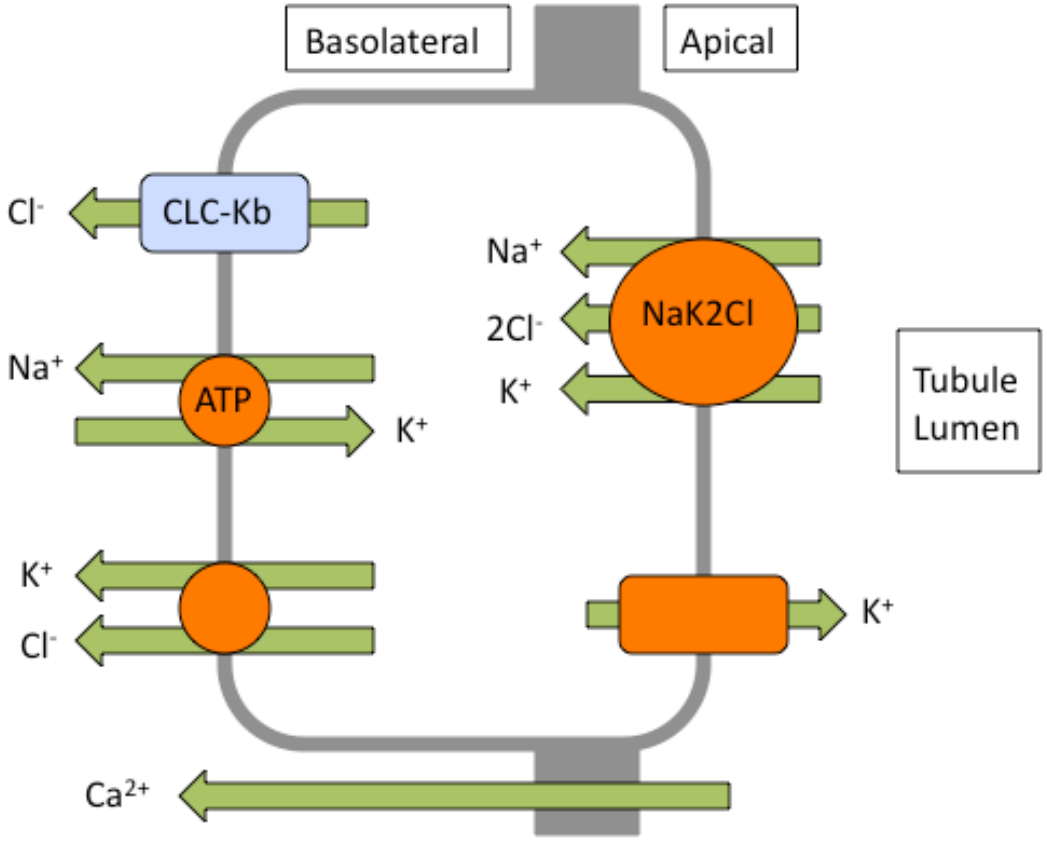

Figure 1.5: Ion transport pathways in the thick ascending loop of Henle.[26]

Similarly, kidney stones (nephrolithiasis) often result from hypercalciuria caused by defects in the renal chloride channel, CLC-5. Elevated levels of salts (usually calcium) precipitate out from the urine, causing pain and infection.[26] Other disorders with suspected links to defective channel mediated chloride transport include epilepsy, Best's disease, malaria and ostropetrosis.[36, 37]

1.5.2 Diseases Associated with Defective Bicarbonate Transport

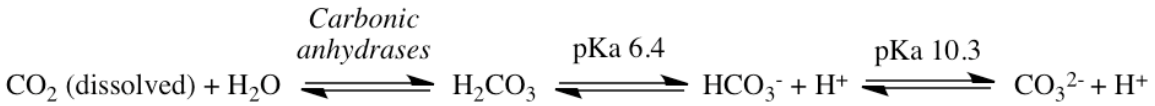

Figure 1.6: Bicarbonate equilibrium

Bicarbonate transporters (predominantly Cl^-/HCO_3^- exchangers and Na^+/HCO_3^- co-transporters) are expressed in a diverse range of tissues.[38] These transporters serve many different roles facilitating the transport of the CO_2 respiratory load, regulating cellular pH, controlling cell volume and facilitating the excretion of HCO_3^-. Bicarbonate plays a key role as a biological buffer owing to the equilibrium shown in **Figure 1.6**. This equilibrium is exploited in the conversion of carbon dioxide (a major metabolic waste product) into bicarbonate, to facilitate transport within the blood.[39, 40]

Bicarbonate is secreted by the pancreas in order to neutralise stomach acid entering the intestine. Within the intestine Cl^-/HCO_3^- exchangers are coupled to NHE3 Na^+/H^+ exchangers to facilitate NaCl reabsorption. The osmotic gradient created by these coupled transport processes drives the reabsorption of water, however defective bicarbonate transport can lead to congenital chloride diarrhea. The misregulation of bicarbonate transport has also been linked to epilepsy, renal tubular acidosis, and ocular disorders.[41] Interestingly, bicarbonate transport plays a vital role in recovery from ischemic acidosis of the cardiac muscle, as the contractile activity of the heart is highly sensitive to pH. The transport of bicarbonate has also been linked to cardiac hypertrophy, a contributing factor to heart failure.[38] Bicarbonate transport is also linked to infertility; capacitation of sperm cells requires a rise in intracellular pH, corresponding to an influx of bicarbonate, whilst uterine bicarbonate secretion is similarly dependent on chloride coupled bicarbonate transport.[42, 43]

1.5.3 Cystic Fibrosis

Cystic fibrosis (CF) is a genetic disorder of the cystic fibrosis transmembrane conductance regulator (CFTR), a voltage independent chloride channel found in the epithelial cells of the intestine, lungs, secretory glands and reproductive tract.[27] Mutation

of the CFTR causes a reduction in epithelial chloride conductance, leading to the secretion of thick, sticky mucus that blocks ducts and tubes (mucoviscidosis).

Patients suffering from CF typically have elevated NaCl concentrations in their sweat. This is due to failure of the CFTR to reabsorb chloride in the sweat duct. Chloride transport is coupled to sodium uptake in this instance. The uptake of sodium is unhindered but causes membrane depolarisation (due to the lack of accompanying chloride transport), reducing the driving force for further sodium reabsorption. More complex transport networks involving CFTR facilitated chloride transport are evidenced in the pancreas and in the lungs.[22] In the pancreas bicarbonate transport is coupled to the transmembrane transport of chloride (**Figure 1.7**). Bicarbonate is generated within the pancreatic epithelial cells by carbonic anhydrase. Transporter mediated Cl^-/HCO_3^- exchange moves bicarbonate out of the cell down its concentration gradient. The CFTR channel facilitates the movement of chloride out of the cell. The protons produced by the action of carbonic anhydrase are exchanged for sodium ions. Sodium ion concentration gradients are maintained by the action of both Na/K-ATPase and the NaK2Cl co-transporter and the removal of imported potassium is facilitated by the action of potassium channels. The net movement of chloride and bicarbonate into the lumen drives sodium uptake, accompanied by the osmotic movement of water. In CF patients chloride accumulates within the pancreatic epithelial cells, removing the driving force for bicarbonate secretion and consequently removing the driving force for water and sodium uptake. Dealkalisation of the pancreas leads to premature activation of digestive enzymes, damaging the pancreatic tissue and leading to malabsorption in the gut.[44]

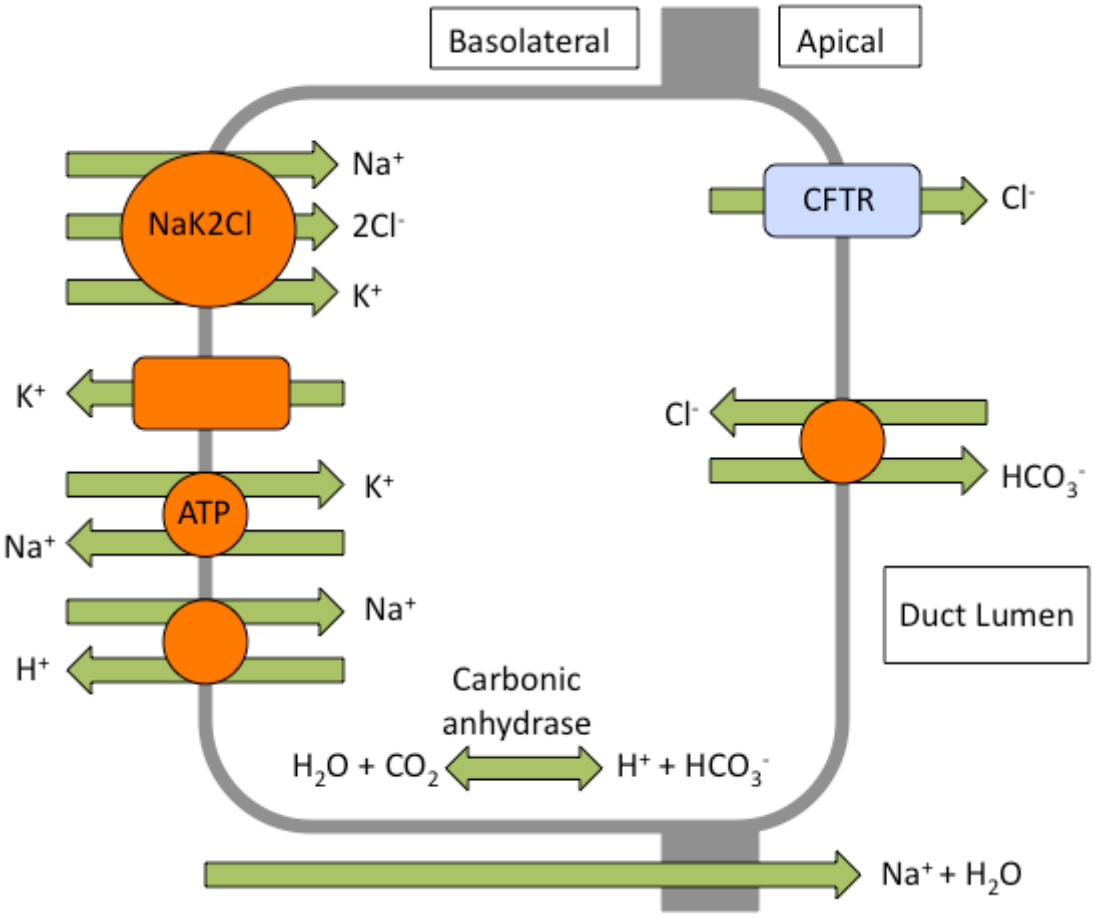

Figure 1.7: Secretion in the pancreatic duct.[26]

In the lungs the mechanism of fluid secretion is not fully understood but is believed to resemble that in the pancreas. Fluid secretion is driven by osmosis linked directly to chloride efflux. CFTR mutation inhibits chloride secretion and removes its inhibitory influence on ENaC sodium channels, promoting sodium (and therefore fluid) uptake. In CF patients, mucus secreted in the lungs is thick and becomes easily trapped. Bacteria can proliferate within the mucus leading to infection and the subsequent damage of lung tissue.[26]

In general, CF epithelia show reduced chloride and bicarbonate transport.[45] Owing to the complex transport networks involved, the correction of defective chloride transport alone is unlikely to alleviate the symptoms of CF.[46-48] The situation is further complicated by recent findings that show CFTR to be permeable to bicarbonate ions.[49] Thus, strategies

that redress bicarbonate transport as well as chloride transport may have medical efficacy.[50]

1.5.4 Regulation of pH

In human biology the regulation of pH is achieved by the action of ATP driven proton pumps, Na^+/H^+ exchange, Cl^-/HCO_3^- exchange and Na^+/HCO_3^- co-transport processes.[51, 52] Misregulation of these transport processes directly affects cellular pH and has been shown to contribute to visual and auditory dysfunction, and metabolic bone disorders.[52-54]

Cancer cells maintain abnormal organelle and cystolic pH; typically by acidification of intracellular organelles.[55] By reducing intracellular organelle pH tumour cells avoid apoptotic cell death, since mitochondrial alkalinization and cystol acidification are early events in apoptosis that modulate caspase activation.[56] Acidification of intracellular organelles can be facilitated by the action of chloride coupled H^+ transport and thus organelle deacidifaction may be an effective strategy to selectively target cancerous cells.[57] Indeed, the anticancer properties of the prodigiosins are though to be due to their ability to deacidify intracellular organelles, *via* H^+/Cl^- co-transport (see **Section 1.6.1**).[58, 59]

Additionally, the disruption of intracellular pH gradients may help to overcome multidrug resistance in tumour cells, wherein the toxic effects of anti-cancer drugs are evaded.[60] Chemotherapeutics are often weakly basic and concentrate inside acidified organelles, because upon protonation the drug molecules become less membrane permeable. This leads to only low concentrations of therapeutic agent accumulating within the nucleus.[61] By disrupting the acidification of organelles normal drug distribution can be achieved, rendering tumour cells again susceptible to chemotherapy.[62] The weakly basic breast cancer drug Tamoxifen influences transmembrane pH gradients, partitioning into acidified organelles and therein mediating H^+/Cl^- co-transport. Tamoxifen administration has consequently been observed to re-sensitise cells to chemotherapies (**Figure 1.8**).[63] It is postulated that the transmembrane transport of bicarbonate could achieve similar organelle deacidification.[64]

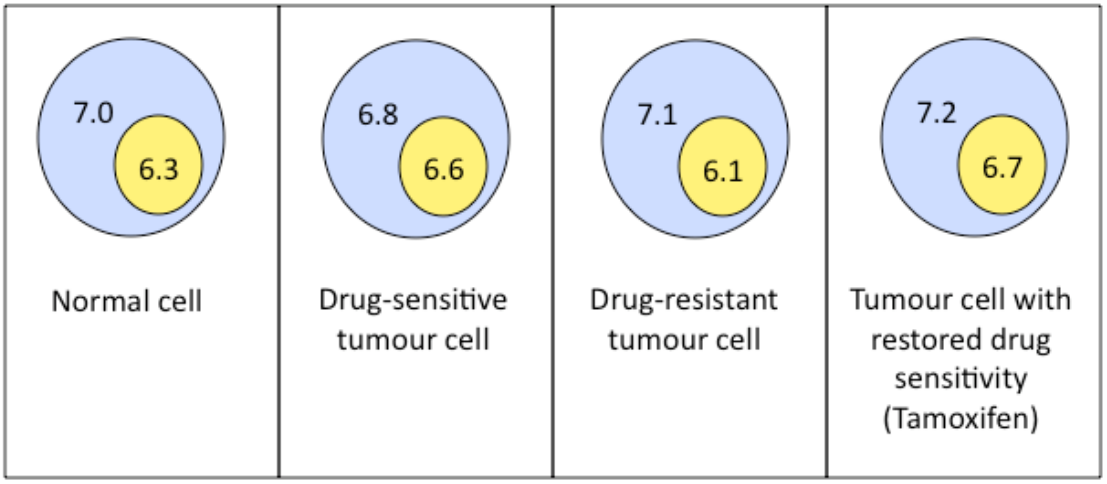

Figure 1.8: The effect of the chemotherapeutic agent Tamoxifen on cytoplasmic (blue) and intracellular organelle (yellow) pH.

The transmembrane transport of chloride is also linked to apoptosis.[65] Chloride and potassium efflux in response to cellular signalling or stress leads to apoptotic volume decrease (AVD) through the loss of water by osmosis.[28, 66] Blocking volume sensitive outwardly rectifying (VSOR) chloride channels prevents cell death by inhibition of AVD, and the loss of VSOR chloride channel activity has been shown to confer resistance to cisplatin in human epidermoid cancer cell lines.[67, 68]

1.6 Naturally Occurring Anion Carriers

Naturally occurring molecules that function as anionophores are rare, but examples include the prodiginine and tambjamine alkaloids and the sphingolipid ceramide.[4, 69, 70]

1.6.1 Prodiginines

The red pyrrole containing alkaloids of the prodigiosin family are secondary metabolites produced by microorganisms including members of the *Serratia* and *Streptomyces* genera. Prodigiosin **1** (**Figure 1.9**) is characteristic of this group of molecules, and contains a pyrrolylpyrromethene core appended with alkyl substituents.[71]

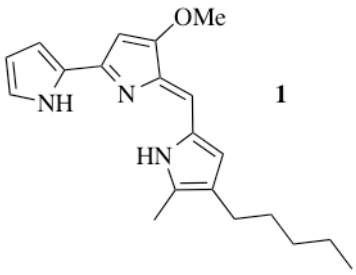

1

Figure 1.9: Prodigiosin **1**, a naturally occurring ionophore.

The prodigiosins display a broad range of activity against pathogenic bacteria, protozoa and fungi.[72] Bioactivity has been observed in the malaria parasite and in human cancer cell lines, whilst some prodiginines exhibit potent immunosuppressive activity suggesting potential applications in the treatment of disease.[73-83] The anticancer activity of these compounds is believed to stem from either copper-mediated DNA cleavage or the alteration of intracellular pH by H^+/Cl^- co-transport.[84-87]

Chloride binding is facilitated by protonation of the azafulvene site, resulting in ion pair formation.[83] The crystal structure of a synthetic prodigiosin·HCl complex (**Figure 1.10**) shows a chloride ion bound by a combination of electrostatic and hydrogen bonding interactions.[88] The resulting complex is stabilised through extensive π-electron conjugation.

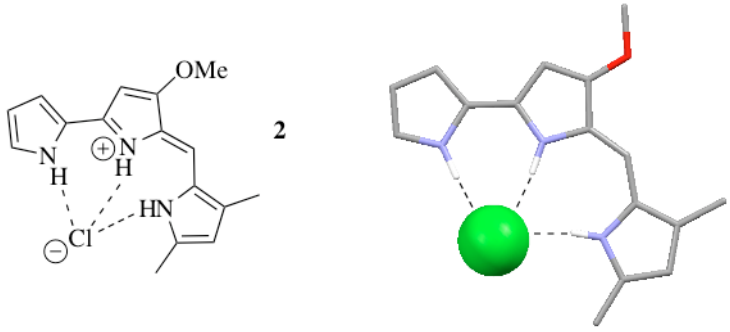

2

Figure 1.10: H^+/Cl^- binding mode of synthetic prodigiosin **2** and the X-ray crystal structure of the H^+/Cl^- salt complex. The ligand is represented as a wireframe and the guest anion is represented as a spacefilling model (0.6 times the van der Waals radius); hydrogen (white), carbon (grey), nitrogen (blue), oxygen (red), chlorine (green). Non-interacting hydrogen atoms have been omitted for clarity.[88]

The prodiginine·HCl complexes are suitably lipophilic to function as ion carriers in phospholipid bilayers. Prodigiosin **1** (**Figure 1.9**) was shown to facilitate H^+/Cl^- symport, Cl^-/NO_3^- antiport and Cl^-/HCO_3^- antiport in phospholipid vesicles.[89, 90] The transmembrane transport of bicarbonate was verified using ^{13}C labelled bicarbonate, the movement of which could be monitored by NMR techniques (see **Section 1.9.5**). To test if the anticancer activity of the prodigiosins is the result of transmembrane ion transport, Sessler and co-workers examined the transport properties and *in vitro* anticancer activity of prodigiosin analogues **3**-**7** (**Figure 1.11**).[91] The *in vitro* antiproliferative activity against human lung cancer cells was found to match trends in the Cl^-/NO_3^- antiport activity observed in phospholipid vesicles, rather than the chloride affinity as measured by isothermal titration calorimetry (ITC) in acetonitrile. In particular, prodiginine **3** exhibited a strong antiproliferative effect in both A549 human lung cancer and PC3 human prostate cell lines.

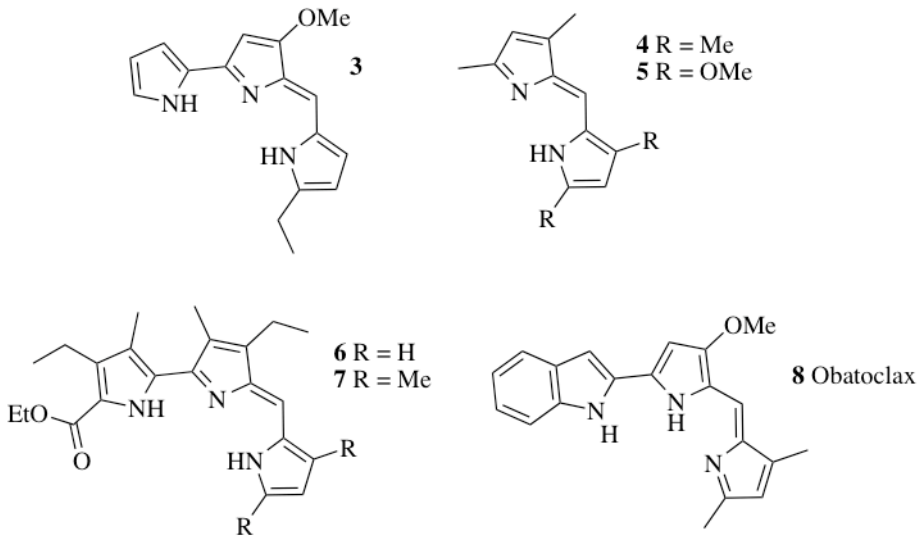

Figure 1.11: Synthetic prodigiosins **3**-**8** that have been studied as ion transport agents.

Obatoclax **8** is structurally similar to the aforementioned prodiginines and has reached phase II clinical trials.[92] Despite anticancer activity primarily stemming from the initiation of autophagocytosis, Obatoclax has been demonstrated to bind and transport chloride and bicarbonate through bilayers composed of 1-palmitoyl-2-oleoyl-*sn*-glycero-

3-phosphocholine (POPC).[93] Anion transport activity has also been demonstrated *in vitro*; in GLC4 lung cancer cells organelle deacidification was observed upon exposure to Obatoclax, resulting in apoptotic cell death.[94]

1.6.2 Tambjamines

The tambjamine alkaloids are derived from marine sources and are structurally related to the prodiginines, with an enamine functionality in the place of a pyrrole ring.[95-97] They similarly show interesting biological activity, with several studies examining their potential uses as anticancer agents.[98-100] As with the prodiginines, the route cause of the bioactivity remains controversial, but a recent study has shown that tambjamines **9-14** (**Figure 1.12**) function as anion transporters.[85, 101]

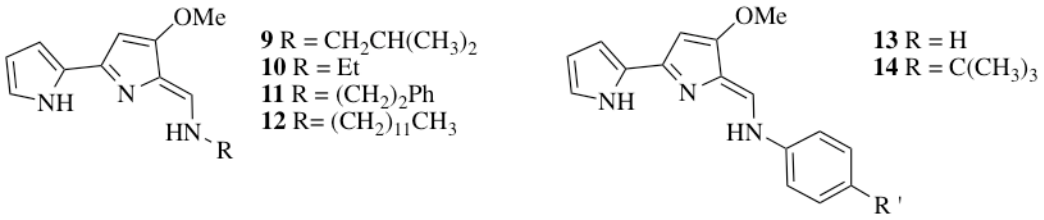

Figure 1.12: Tambjamine anion transporters.

Solution phase binding studies with tambjamines **9-14** in DMSO-d_6 reveal a 1:1 binding stoichiometry with tetrabutylammonium (TBA) chloride. Ion transport assays in phospholipid vesicles indicate that the tambjamines function as Cl^-/NO_3^- and Cl^-/HCO_3^- antiport agents. The transport activity was not enhanced in the presence of a pH gradient, suggesting that these compounds do not facilitate H^+/Cl^- symport. Compounds **12** and **14**, the most active in the study, were shown to deacidify organelles in a series of fluorescence assays. Presumably, the mechanism underlying this deacidification is bicarbonate transport. Compound **10** was found to be the least active transporter in the series as a consequence of its lower lipophilicity.

1.6.3 Ceramides

Ceramides are spingolipid proapoptotic agents that form pores in biological membranes at high concentrations (> 10 mol % with respect to lipid).[102-106] C_2-ceramide **15** (**Figure 1.13**) has been shown to transport ions *via* an alternative mobile carrier mechanism at lower concentrations.[107] The activity of compound **15** was compared to the analagous isopropylidine **16** to assess the contributions towards ion transport from the 1,3-diol motif. Chloride complexation was observed by electospray ionisation mass spectrometry (ESI-MS) for compound **15** but not **16**, and binding constants of 1730 M^{-1} and 27 M^{-1} respectively were obtained by NMR titration with TBA chloride in wet CD_2Cl_2.

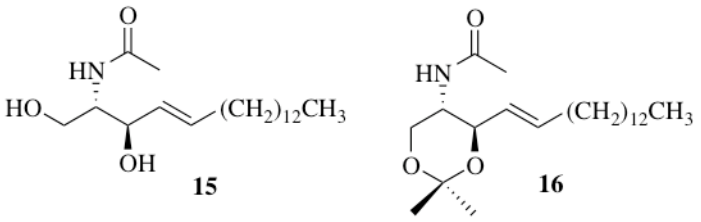

Figure 1.13: Ceramide **15** and the analogous isopropylidine **16**.

At 1 mol % (with respect to lipid) loadings, carboxyfluorescein release assays (see **Section 1.9.3**) indicated that neither compound **15** or **16** formed large channels. Lucigenin fluorescence assays (see **Section 1.9.3**) in phospholipid vesicles indicated that compound **15** can facilitate both Cl^-/NO_3^- and Cl^-/HCO_3^- antiport, whilst compound **16** is inactive. These findings emphasise the importance of the 1,3-diol in the ceramide scaffold for both the binding and transmembrane transport of anions.

1.7 The Design of Synthetic Molecules to Facilitate Transport

Ion transport processes in cells seldom occur in isolation, often forming complex transport networks.[108] Multiple disease states have been shown to arise from the failure of one transport pathway within a networked transport system, as exemplified by defective chloride transport by the CFTR protein in cystic fibrosis (see **Section 1.5.3**). It has been proposed that correction of such defective transport processes with synthetic transporter

molecules will serve to treat channelopathies.[109] Indeed, both synthetic channel forming peptides and synthetic chloride carriers have been shown to improve the secretory properties of CF epithelial cells.[110-112]

Several important factors must be considered in the design of synthetic carriers. They are required to be sufficiently hydrophobic to allow partitioning into the phospholipid bilayer, whilst retaining sufficient aqueous solubility to permit successful delivery to the target membrane. Strong ion binding is needed to facilitate the extraction of the transported ion from aqueous solution, whilst the binding must be reversible to permit ion release at the opposite side of the membrane. In addition to these factors, binding selectivity is highly desirable so as to facilitate a specific transport processes. The binding of anionic species requires at least partial desolvation of the anionic guest. The resulting desolvation penalty must be compensated for by favourable interactions between the host and guest species (see **Section 1.1**).[113] A wide range of different interactions have been utilized to achieve anion capture including covalent, aromatic and electrostatic interactions, or combinations thereof.[114-121] The most widely utilized interaction, particularly in the development of hosts created to function as anion transporters, is the use of convergent arrays of hydrogen-bond donors.[122-124] Hydrogen-bonds are highly directional, hence the spatial arrangement of hydrogen-bond donor functionalities can impart anion selectivity, whilst the comparatively weak nature of hydrogen-bonding interactions (4-120 kJ mol^{-1}) permits reversible solution phase binding.[3] Of the known hydrogen-bond donor functionalities, NH groups are the most widely reported for anion complexation.[122-124] Indeed, the diverse range of NH groups, including indole, pyrrole, carbazole, (thio)amide, (thio)urea, guanidine and amine make such scaffolds highly tunable towards the size and shape of the anionic guest. Other donor groups have also been reported including OH, CH, and halogen bond donors.[125-127] Many of these donor groups have been successfully used in transporter scaffolds (see **Section 1.8**) and offer supramolecular chemists a diverse 'toolbox' for the construction of new mobile carriers.

1.8 Synthetic Anion Transporters

1.8.1 Cholapods

Davis and co-workers have pioneered the use of the steroidal cholic acid podand (cholapod) scaffold as a motif for anion binding and transmembrane anion transport.[128, 129] As a building block, cholic acid **17** (**Figure 1.14**) has several advantages; it is cheap, naturally occurring, amphiphilic, and provides a rigid framework for the attachment of additional hydrogen-bond donor groups. Additionally, extension of the scaffold at the 7- and 12- hydroxyl groups results in conformational preorganisation of pendant hydrogen-bond donor groups as a result of 1,3-diaxial interactions.

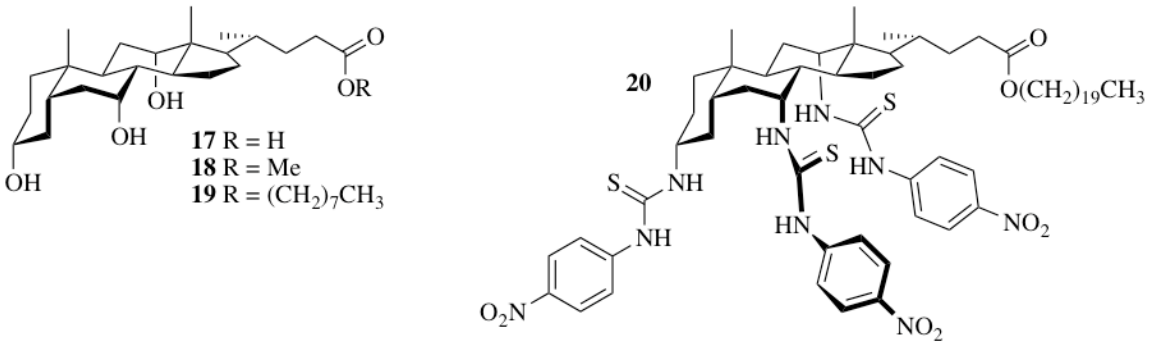

Figure 1.14: Cholic acid **17** and structurally related cholapods **18**-**20**.

In initial studies Davis and co-workers found that the cholate alkyl esters **18** and **19** (**Figure 1.14**) bound both sulfonates and phosphonates in apolar media, the three hydroxyl groups functioning as hydrogen-bond donors.[130] These early results led to the development of cholapods with alternative hydrogen-bond donor groups, tuned to operate in polar environments.[131] Anion affinity and selectivity were enhanced by increasing both the number and the acidity of hydrogen-bond donor groups on the cholapod scaffold, culminating in the formation of cholapod **20** (**Figure 1.14**).[132] Cholapod **20** possesses six hydrogen-bond donor groups, the acidity of which has been tuned through the use of thiourea and *para*-nitrophenyl functionalities. The ester alkyl chain enhances lipophilicity, resulting in a remarkably high binding constant of 1.8×10^{11} M^{-1} with tetraethylammonium (TEA) chloride in wet chloroform.[133, 134] Owing to the promising

anion extraction properties exhibited by these compounds, it was hypothesised that cholapod compounds could function as transmembrane anion transporters.[134, 135]

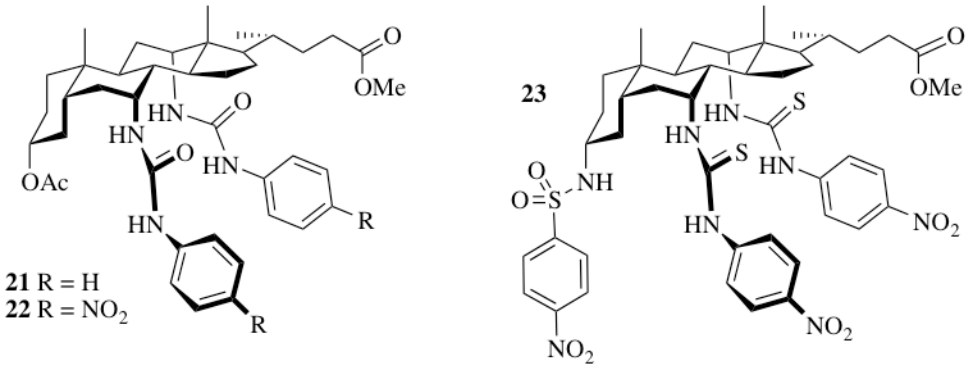

Figure 1.15: Second generation cholapods **21**-**23**.

Compounds **21** and **22** (**Figure 1.15**) were found to facilitate chloride efflux from phospholipid vesicles containing NaCl suspended in a solution of $NaNO_3$ at carrier loadings of 0.4 mol % (with respect to lipid).[136] Transport rates were unaltered upon changing the encapsulated cation to potassium or caesium, suggesting that the metal cation was not involved in the transport process. In addition, changing the external anion to sulphate drastically reduced the rate of chloride efflux, confirming a Cl^-/NO_3^- antiport mechanism. Having shown antiport activity in ion selective electrode (ISE) assays, chloride transport was demonstrated *in vitro* using Madin Darby canine kidney (MDCK) epithelial cells, suggesting that these molecules are compatible with biological systems. The most active cholapod transporter to date, compound **23** (**Figure 1.15**), was found to facilitate Cl^-/NO_3^- antiport at loadings as low as 0.4 mmol % (with respect to lipid) in vesicle based lucigenin fluorescence assays (see **Section 1.9.3**).[137] Despite this high activity, it should be noted that compound **23** could not be tested by conventional ISE methods due its limited solubility, and thus had to be pre-incorporated into the phospholipid vesicles.

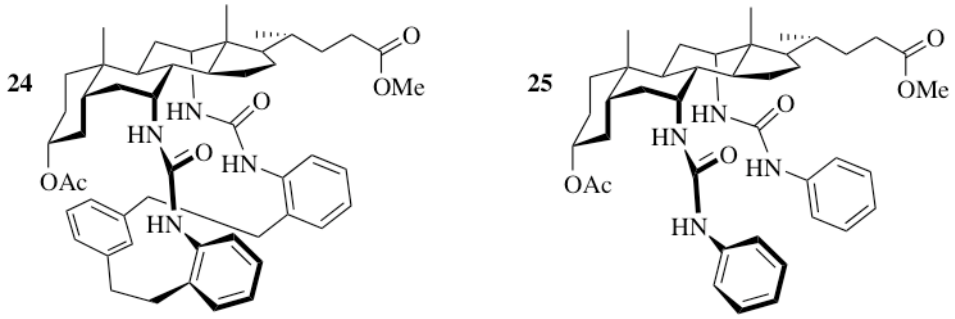

Figure 1.16: Cholaphane **24** and the analogous cholapod **25**.

In general, the most potent cholapod transporters are those compounds that exhibit the strongest interaction with TEA chloride in extraction studies. Davis and co-workers have found that increasing the acidity of the hydrogen-bond donor groups appended to the 7- and 12- positions increases transport activity. However, the transport activity observed upon modification at the 3- position does not correlate to such a simple trend.[138] It is believed that modification at the 3- position dramatically influences the ability of cholapod transporters to facilitate phospholipid translocation (see **Section 1.8.3**) through interaction with the polar phosphate head group, and it is this interaction that obscures trends in carrier activity across the series.[139, 140] In an attempt to inhibit the scramblase activity, cholaphanes such as **24** (**Figure 1.16**) were synthesised. This type of molecule possesses an enclosed binding site that sterically hinders binding to bulky phospholipid head groups. Lucigenin fluorescence assays (see **Section 1.9.3**) reveal that cholaphane **24** displays an eighteen-fold enhancement in Cl^-/NO_3^- antiport activity in phospholipid vesicles, compared to the acyclic analogue **25**. Computer modelling suggests that bound anions (and their solvating waters) are more effectively shielded from the lipophilic membrane interior by the cholaphane, reducing competitive interactions with bulk water.[141]

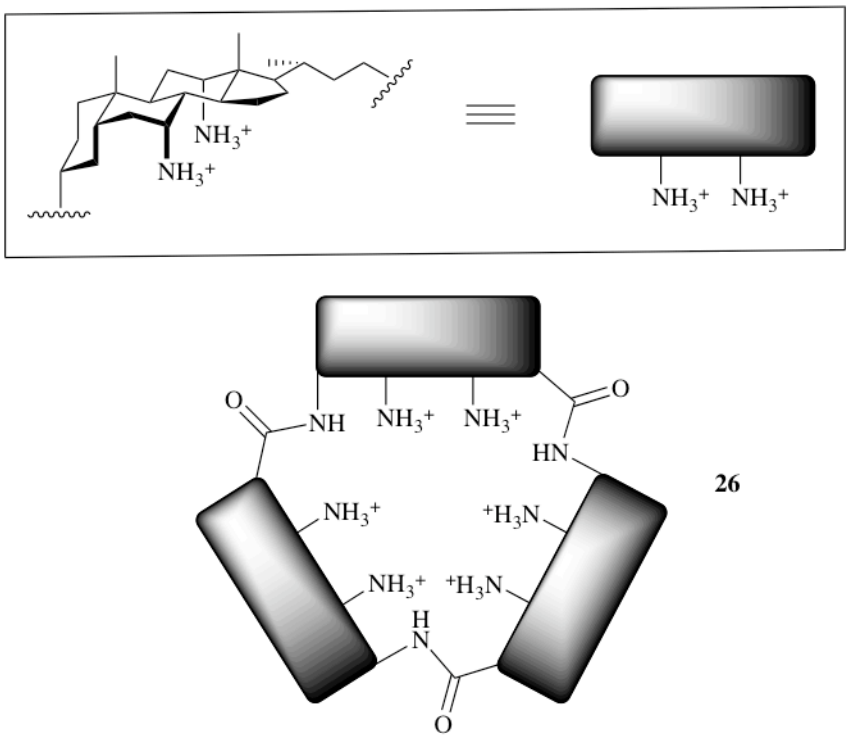

Figure 1.17: Cationic cholapod macrocycle **26**.

Cationic molecules based on the cholapod scaffold have been reported to discharge pH gradients in vesicle assays.[142, 143] Based on this finding, Davis and co-workers synthesised macrocyclic cholamide **26** (**Figure 1.17**) and its cyclodimeric and cyclotetrameric analogues. Molecular modelling suggested that molecule **26** favours a conformation with the NH_3^+ functionalities directed inwards, creating a toroidal facial amphiphile with a lipophilic exterior surface and a hydrophilic interior. Cholamide **26** facilitated Cl^-/NO_3^- antiport in phospholipid vesicles, with no obvious cation dependence. Experiments using vesicles containing cholesterol showed a reduction in transport rates implying a mobile carrier mechanism for transport (see **Section 1.9.7**).[144]

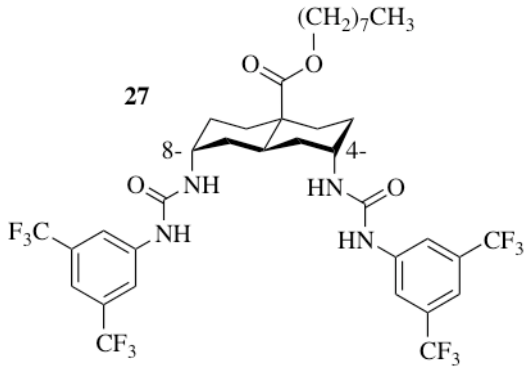

Figure 1.18: Decalin **27** with urea functionalities at the decalin 4- and 8- positions.

In an effort to make the cholapod transporters more 'drug-like' Davis and co-workers developed decalin as a transporter scaffold.[145] As with the cholapods, 1,3-diaxial interactions prevent substituent rotation at the 4- and 8- positions, preorganising the pendant hydrogen-bond donor motifs at these positions for anion binding. Like the cholapods, receptor lipophilicity could be tuned through modification of the alkyl ester functionality, with Cl^-/NO_3^- transport activity increasing with alkyl chain length. Compound **27** (**Figure 1.18**) was found to be the most active decalin anion transporter, facilitating Cl^-/NO_3^- antiport at loadings of 0.4 mmol % (with respect to lipid); activity comparable to the most active cholapod transporter, compound **23**. Additionally, decalin **27** facilitated Cl^-/HCO_3^- antiport. The cholapods and structurally related compounds demonstrate that convergent arrays of hydrogen-bond donor groups attached to a lipophilic scaffold can yield potent anion transporters.

1.8.2 Isophthalamides

The isophthalamides are structurally simple receptors that can be readily functionalized through variation of the amide substituents. To examine the role of preorganisation on the transport activity of this type of scaffold, Gale and co-workers synthesised isophthalamides **28**-**30** (**Figure 1.19**).[146] Intramolecular hydrogen-bonding in compounds **29** and **30** results in *syn-syn* and *anti-anti* favoured conformations respectively, whilst the unfunctionalised cleft receptor **28** preferentially adopts the *syn-anti* conformation. The *syn-syn* conformation of compound **29** creates a hydrogen-bond

donating cleft suitable for anion coordination. Indeed, both compounds compounds **28** and **29** bind chloride selectively over the other halides whilst compound **30** cannot interact with these anions as the amide NH groups are involved in intramolecular hydrogen-bonding interactions. Only preorganised isophthalamide **29** was found to facilitate chloride influx into phospholipid vesicles. Interestingly, the transport activity of **29** was found to be pH dependent, with decreasing activity observed upon increasing the pH and a total loss of activity observed at pH 9.1. This is consistent with the deprotonation of the phenolic hydroxyl groups and the subsequent loss of cleft preorganisation.

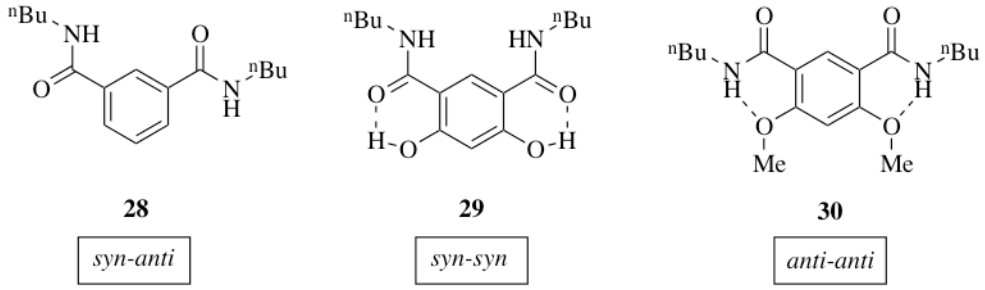

Figure 1.19: Favoured conformations of isophthalamides **28**-**30**.

Preorganisation can also be achieved in isophthalamides by introducing a heteroatom to the aromatic core, as demonstrated with isophthalamides **31** and **32** (**Figure 1.20**).[147] Both compounds exhibited weak affinity for chloride under neutral conditions (K_a < 10 M^{-1}) in DMSO-d_6 but compound **32** showed enhanced chloride affinity under acidic conditions (K_a = 56 M^{-1}). Only compound **32** facilitated chloride efflux from phospholipid vesicles under neutral conditions, but the chloride transport activity of both **31** and **32** was enhanced in the presence of a pH gradient suggesting that this type of compound can facilitate H^+/Cl^- co-transport. The higher activity of compound **32** was attributed to a more preorganised and hence convergent binding pocket. Building on this study Gokel and co-workers examined the transport properties of isophthalamides **33**-**36** (**Figure 1.20**).[148] The *para*-nitrophenyl functionalized compounds **34** and **36** were shown to have higher chloride affinities than their unfunctionalised analogues **33** and **35** in both the solution phase (DMSO-d_6) and the gas phase, and were also found to be more

active as chloride transporters. Characteristic open-close behaviour was demonstrated using planar bilayer conductance techniques (see **Section 1.9.10**), indicating channel formation at receptor concentrations 0.45 M. This evidence for channel formation was supported by fluorescence studies that inferred receptor stacking in solution (1 % DMSO/H_2O). Hill plot analysis suggested that at lower concentrations (< 20 μM) a carrier mechanism may also operate.

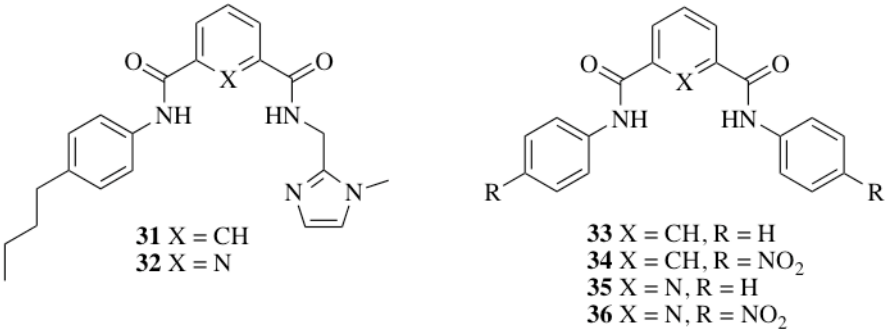

Figure 1.20 Isophthalamides **31**-**36**.

Yang and co-workers have developed α-aminoxy acid functionalised isophthalamide **37** (**Figure 1.21**) to investigate the compatibility of the scaffold with biological systems.[149] Chloride transport was observed in both phospholipid vesicles and Madin-Darby canine kidney (MDCK) cells using the chloride sensitive fluorescent dye 6-methoxy-*N*-(3-sulfopropyl)quinolinium (SPQ). Patch clamp experiments (see **Section 1.9.10**) showed single-channel currents indicating that like isophthalamides **33**-**36**, compound **37** forms functional ion channels. The action of compound **37** was also examined in A7r5 smooth muscle cells. The activation of voltage gated Ca^{2+} channels that resulted was the consequence of membrane polarization caused by transmembrane chloride transport.[150]

The isophthalamide receptors discussed thus far facilitate chloride transport by either an anion antiport or H^+/Cl^- symport pathway. By tethering an isophthalamide unit to a crown ether, receptor flexibility is dramatically reduced. The combination of an anion and a cation binding site in this manner yields the ditopic salt-binding macrocycle **38**, (**Figure 1.21**) that facilitates Na^+/Cl^- symport at loadings as low as 0.04 mol % (with respect to lipid).[151] The Na^+/Cl^- symport process was directly observed using ^{23}Na and

^{35}Cl NMR transport assays. Chloride efflux from phospholipid vesicles was found to be dependent on the metal cation with chloride transport rates significantly reduced with encapsulated CsCl. Significantly, the uncoupled crown ether and isophthalamide subunits were inactive when added together, demonstrating the importance of contact ion-pairing to create a membrane permeable neutral species.

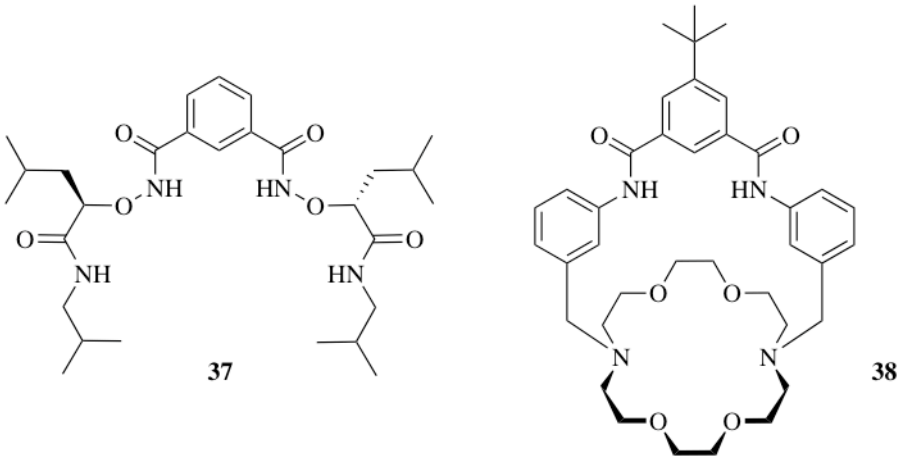

Figure 1.21: Biologically active chloride transporter **37** and ditopic salt-binding macrocycle **38**.

Inspired by the structural simplicity of these isophthalamide transporters and the H^+/Cl^- co-transport properties of the prodigiosins (see **Section 1.6.1**), methylimidazole appended amidopyrrole **39** was studied by Gale and co-workers.[152] Enhanced chloride binding was observed in acetonitrile-d_3 under acidic conditions (K_a = 60 M^{-1} and 397 M^{-1} in the absence and presence of one equivalent of HPF_6 respectively). The solid state structure of **39**·HCl revealed the formation of a '2+2' dimer, with each chloride ion bound by three hydrogen-bonds. The lipophilic functionalities were found to reside on the exterior of the dimer with the bound anions residing within this lipophilic coat (**Figure 1.22**).

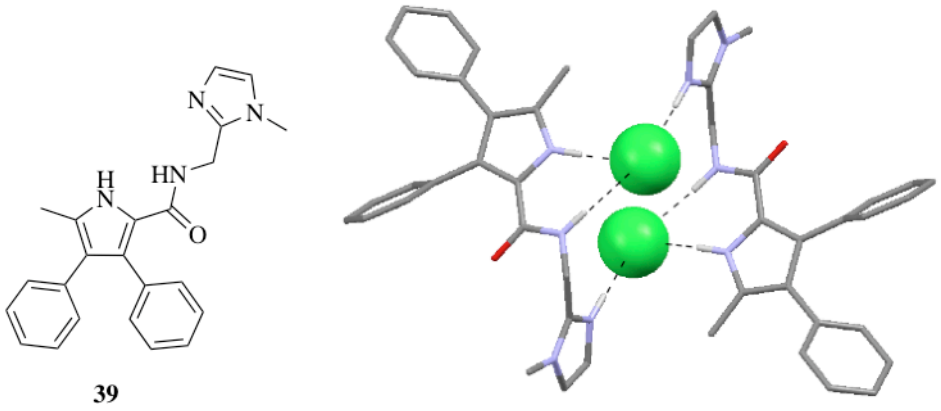

39

Figure 1.22: Crystal structure of the **39**·HCl '2+2' hydrogen-bonded dimer. The ligands are represented as wireframes and the guest anions are represented as a spacefilling models (0.6 times the van der Waals radius); hydrogen (white), carbon (grey), nitrogen (blue), oxygen (red), chlorine (green). Solvent molecules and non-interacting hydrogen atoms have been omitted for clarity.[152]

Chloride transport facilitated by compound **39** was measured in phospholipid vesicles containing NaCl and suspended in $NaNO_3$ under a range of pH conditions. Chloride transport was detected at pH 7.2, but not at pH 4.0. Under pH gradient conditions (intravesicular pH 4.0, extravesicular pH 7.2) the highest transport rates were observed. The H^+/Cl^- co-transport mechanism suggested by these findings was confirmed using a fluorescence assay to monitor H^+ transport (see **Section 1.9.3**).[153]

1.8.3 Tripodal Transporters and Flippases

The tris(2-aminoethyl)amine scaffold can be readily functionalised to afford tripodal anion hosts. The catechol motif **40** (**Figure 1.23**) has been shown to selectively complex chloride anions over bromide and iodide anions in CD_3CN (K_a [Cl^-] = 1570 M^{-1}, K_a [Br^-] = 55 M^{-1}, K_a [I^-] < 5 M^{-1}), utilising the hydroxyl groups as hydrogen-bond donors.[154] The introduction of further hydrogen-bond donor groups into the scaffold enhances anion affinity, and hence catechol bearing tripodal compounds **41**-**43** (**Figure 1.23**) were investigated for H^+/X^- symport activity with a range of anions.[155, 156] Methylation of the catechol hydroxyl functionalities or altering the position of these moieties to produce a less convergent hydrogen-bond donor array resulted in transport inactivity (compound **42** and **43** respectively), whilst variation of the alkyl chain length

similarly resulted in reduced transport activity, suggesting that the pentyl chain is the optimal length to facilitate effective membrane partitioning.

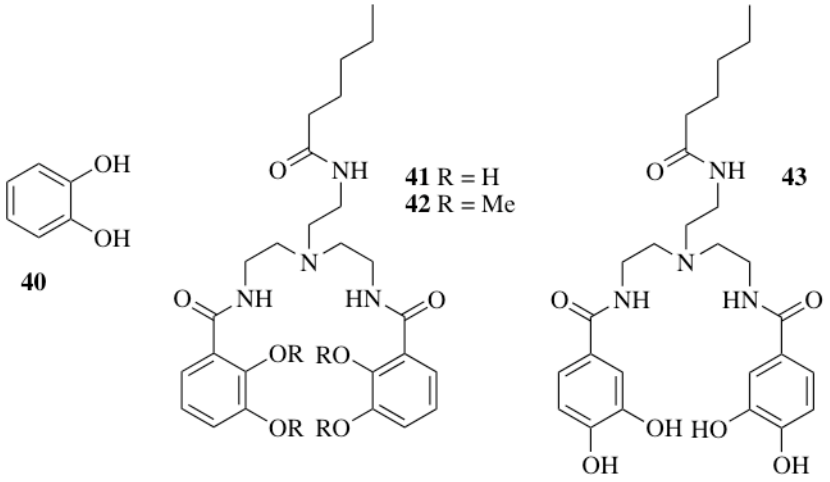

Figure 1.23: Catechol **40** and tripodal receptors **41**-**43** containing the catechol motif.

Tripodal compounds have been studied by Smith and co-workers as flippases (molecules capable of promoting phospholipid translocation between the inner and outer membrane leaflets).[157] In biological systems this process is utilised in the regulation of enzyme activity and membrane-protein interactions, and also in cell recognition.[158-160] Phospholipid translocation was observed upon the addition of compounds **44**-**46** (**Figure 1.24**) to POPC vesicles containing 7-nitrobenz-2-oxa-1,3-diazol-4-yl (NBD) fluorescently labeled phospholipids in the outer membrane leaflet. The movement of phospholipids was monitored by examining changes in NBD fluorescence on addition of dithionite to the extravesicular solution (dithionite is an NBD fluorescence quenching agent).[161] The retention of NBD fluorescence with compounds **44** and **45** indicated that some of the fluorescently tagged phospholipids had translocated to the inner membrane leaflet, a region inaccessible to the extravesicular dithionite anions. The lack of phospholipid translocation with compound **46** indicated that NH hydrogen-bonding interactions with the phospholipid head groups were critical for flippase activity. Significantly, flippase activity was observed for compounds **44** and **45** in human erythrocytes, indicating that these compounds can function within biological systems.[162]

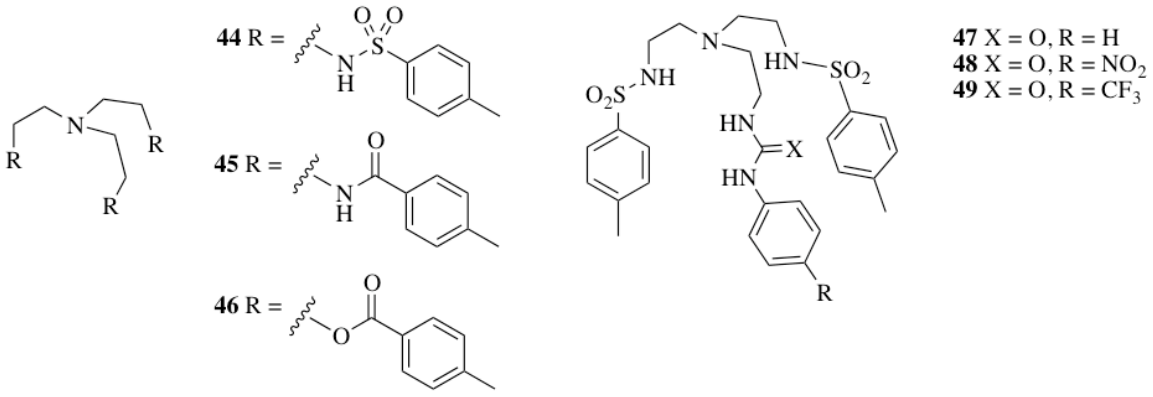

Figure 1.24: Tripodal compounds studied by Smith and co-workers.

Having thoroughly examined the flippase activity of tripodal amides, the same group examined the influence of incorporating urea moieties into the tris(2-aminoethyl)amine scaffold, producing compounds **47-49** (**Figure 1.24**).[163-166] Tripodal urea **47** was capable of transporting phosphatidylcholine and also anionic phosphatidylserine lipids between membrane leaflets (see **Section 1.9.9**). Compounds bearing electron withdrawing substituents, such as **48** and **49,** facilitated enhanced rates of phospholipid translocation. The authors hypothesized that the increased translocation activity was the consequence of increased affinity towards the phospholipid head groups.

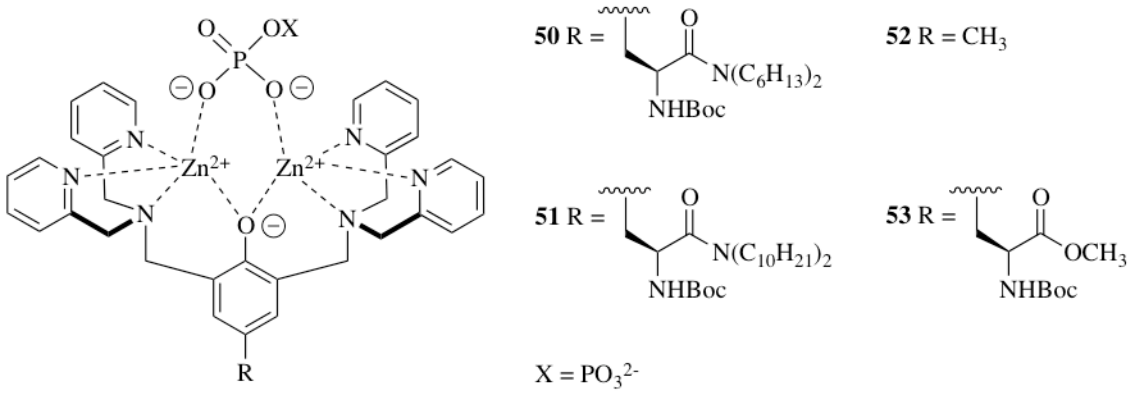

Figure 1.25: Proposed binding mode of binuclear Zn(II) 'flippases' **50-54** to phosphates.

Binuclear Zn(II) complexes of 2,2'-dipicolylamine (Dpa) are reported to function as effective binding motifs for phosphate, with binding constants in water of the order of

10^4-10^6 M^{-1}.[167-169] This phosphate binding can be utilized to produce molecules that interact with phospholipid head groups in biological membranes, functioning as optical probes for the imaging of sites of bacterial infection and necrotic tissue in tumors.[170-172] Introducing a phenoxide as the linker unit in the bis(Dpa) scaffold preorganises the binding pocket formed by the two Zn^{2+}-Dpa units.[173] Lipophilic binuclear Zn(II) complexes **50** and **51** (**Figure 1.25**) partition into both uncharged and anionic vesicles, promoting the translocation of fluorescently labeled phospholipids from the outer membrane leaflet to the inner membrane leaflet.[174] Analogous hydrophilic compounds **52** and **53** (**Figure 1.25**) are selectively toxic towards *Staphylococcus aureus* bacteria. Interestingly, an analogous scaffold containing four Zn^{2+}-Dpa subunits facilitates the delivery of short anionic phosphorylated peptide sequences into HeLa cells.[175] Transport can be turned off by the addition of pyrophosphate ($H_2P_2O_7^{2-}$), which competes for the zinc binding sites.

1.8.4 Anion-π Slides

Amphotericin B (AmB) **54** (**Figure 1.26**) is a naturally occuring macrocyclic polyene that exhibits antifungal activity as a consequence of its ability to form transmembrane ion channels.[176] Computer simulations reveal that the formation of channels permeable to water, ions and non-electrolytes is the result of AmB aggregation, facilitated by interaction with sterol molecules within the membrane. These interactions orientate the AmB perpendicular to the membrane surface in a functional 'barrel' aggregate.[177] Charged residues line the mouth of the resulting channel, and it is the ionization state of these groups that dictates the pH tunable anion *vs* cation selectivity of the channels formed.[178]

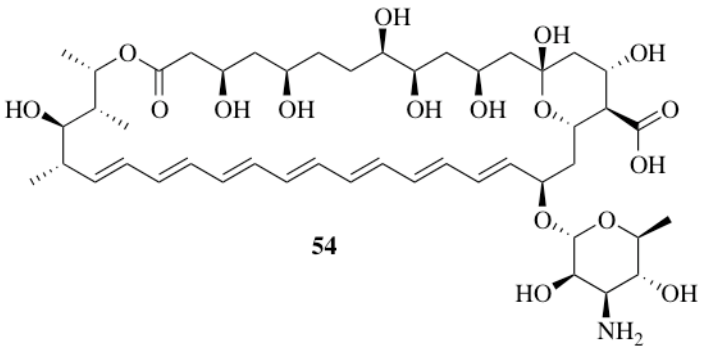

54

Figure 1.26: Amphotericin B (**54**), a naturally occurring ion channel.

The rigid AmB polyene backbone inspired Matile and co-workers to examine channel formation by rigid molecules containing conjugated backbones. Oligo(*p*-phenylene) compound **55** (**Figure 1.27**) shares several structural features with AmB; the rigid phenylene backbone permits cooperative van der Waals interactions with components of biological membranes, whilst the hydroxyl groups function as an ionophoric relay.[179] Evidence of both H^+/Na^+ antiport and H^+/Cl^- symport were obtained in egg yolk phosphatidyl choline (EYPC) vesicles. The authors reasoned that as the calculated length of octamer **55** (34 Å) is close to the thickness of the EYPC bilayer (36 Å), and that since shorter analogous oligo(*p*-phenylene) compounds showed significantly reduced transport activity, compound **55** functions as a membrane spanning channel.[180] The finding that rigid molecules such as **55** can promote ion translocation led the same group to investigate rigid electron deficient systems as anion transporters that utilise anion-π interactions, synthesising rigid oligo-(*p*-phenylene)-*N*,*N*-naphthalenediimide (O-NDI) rods such as **56** (**Figure 1.27**).[181] Computational modelling revealed that the NDI motif **56** is an excellent electron acceptor and is consequently well suited for use as an anion-π slide.[182] Proton transport was found to be anion dependent, with multiple anions bound simultaneously. This behaviour confirmed the 'slide' function attributed to these compounds.[183] The O-NDI scaffold could be tuned in various ways; introduction of a single charged terminal residue increased transport activity whilst the introduction of charges at both termini deactivated the slide, presumably due to the inability of such a molecule to translocate across the membrane.[184] Covalent linkage of O-NDI units, as in **57** (**Figure 1.27**), yielded 'hairpins' with enhanced chloride selectivity whilst attachment

of a hydrophilic polyhistidine anchor dramatically enhanced transport activity, an approach also demonstrated in the simpler oligo(*p*-phenylene) scaffold.[185, 186] Molecules based on oligo-(*p*-phenylene)-*N,N*-perylenediimide (O-PDI) scaffold **58** (**Figure 1.27**) containing a hydrophilic anchor in the form of an anionic triglutamic acid tail, function as anion-π slides in an analogous fashion to O-NDI rods.[187] Chloride transport facilitated by these structures can be coupled to the transmembrane transport of electrons in the opposite direction. This electron coupled transport was demonstrated in phospholipid vesicles loaded with $[Co(bpy)_3]^{3+}$ and suspended in a solution containing ethylenediaminetetraacetic acid (EDTA), a photoinducible electron donor. Electron transport coupled to the movement of chloride was 'observed' by the reduction of the encapsulated $[Co(bpy)_3]^{3+}$. This finding reveals that such compounds are able to combine both ion channel function and photosynthetic activity.

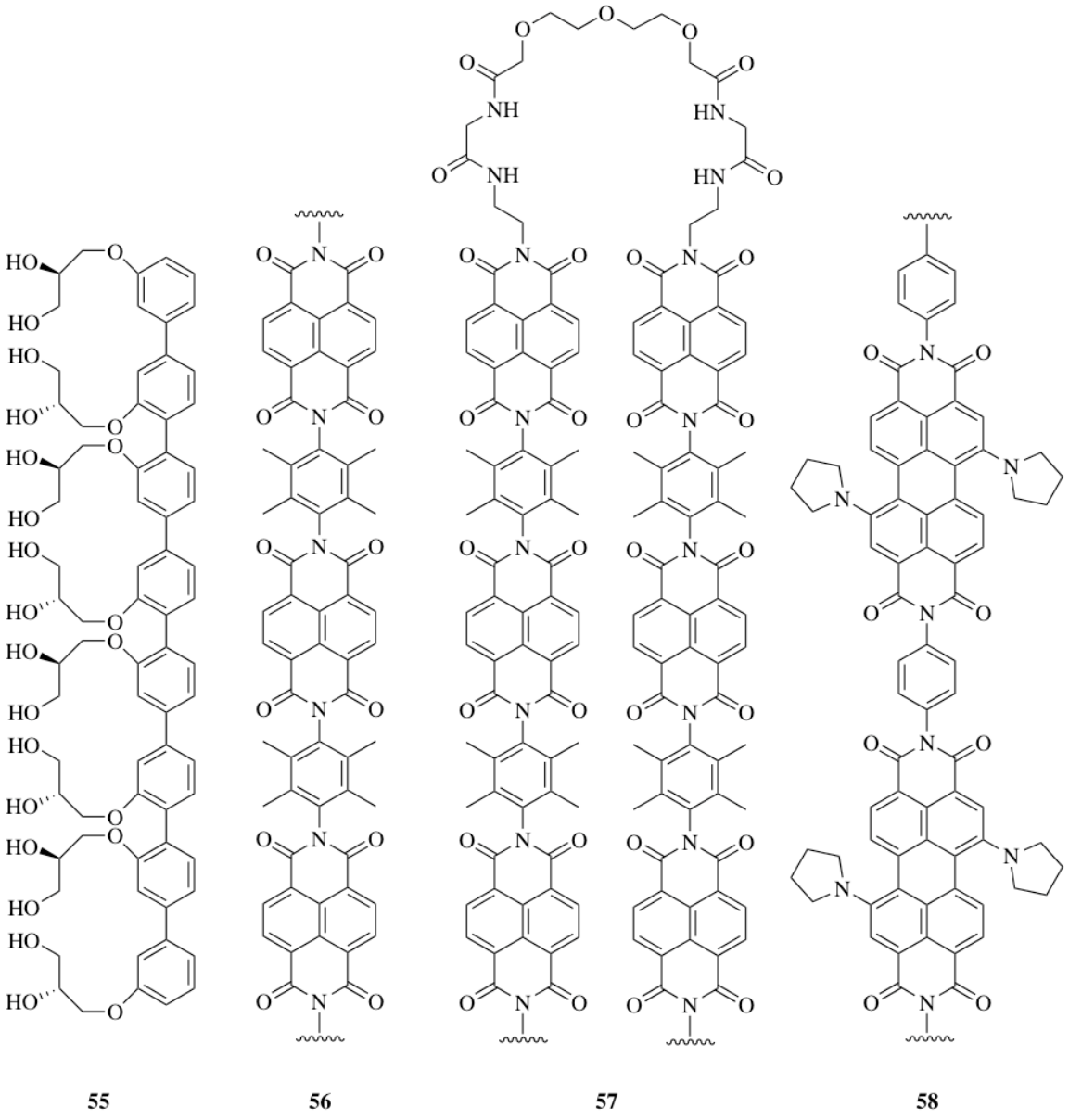

Figure 1.27: Rigid, membrane spanning transporters **55**-**58**.

Anion-π interactions have also been used by ion transporter **59** (**Figure 1.28**).[188] Compound **59** was shown to facilitate Cl^-/NO_3^- antiport, with chloride efflux from phospholipid vesicles monitored *via* changes in the fluorescence intensity of encapsulated lucigenin (see **Section 1.9.3**). Computer modelling revealed that the monomer was inactive and that the formation of an active aggregate was required for transport. This hypothesis was tested by adding α-cyclodextrin (α-CD) to the vesicle suspension. The

aromatic arms of compound **59** are accommodated into the hydrophobic cavity of α-CD, preventing aggregate formation and thus inhibiting channel formation.

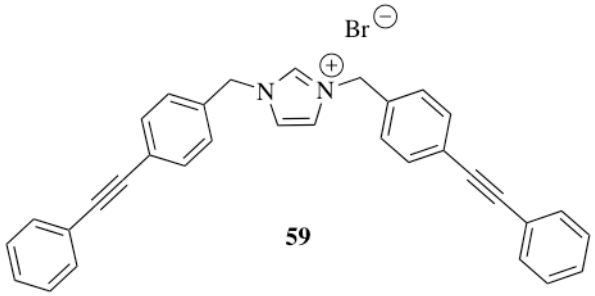

Figure 1.28: Transporter **59** utilizes anion-π interactions.

1.8.5 Calixarenes

Davis and co-workers have studied the ion transport propertes of acyclic calixarene derivatives **60**-**62** (**Figure 1.29**).[189, 190] A study of polyphenoxyacetamides of varying length indicated that the trimer **60** was the most active chloride transporter. A combination of ^{35}Cl NMR experiments and hydroxylpyrene-1,3,6-trisulfonic acid (HPTS) fluorescence assays confirmed the transmembrane transport of chloride *via* an H^+/Cl^- symport mechanism. Compound **60** was found to generate a stable potential gradient owing to a difference in H^+ and Cl^- transport rates. The formation of a stable negative charge within vesicles containing Na_2SO_4 and suspended in NaCl was observed by fluorescence techniques (see **Section 1.9.3**). Structurally related compounds **61** and **62** were inactive as ion transport agents since compound **61** lacks the NH hydrogen-bond donor groups needed for chloride complexation, whilst compound **62** bears bulky *tert*-butyl substituents that inhibit transporter aggregation. The self-association of compound **60** into channel structures was confirmed by a 1,2-dipalmitoyl-*sn*-glycero-3-phosphocholine (DPPC) assay (see **Section 1.9.7**).

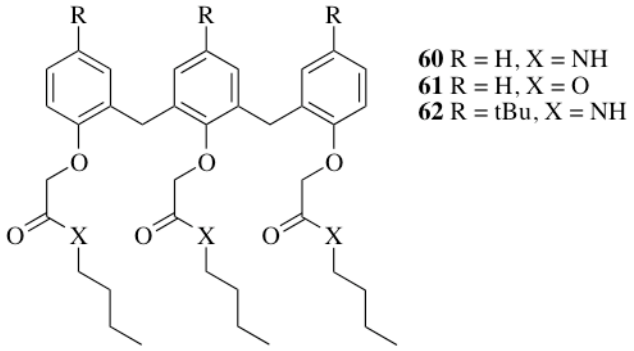

Figure 1.29: Acyclic polypheoxyacetamides **60-62**.

In addition to the acyclic calixarene structures, amide substituted calix[4]arene **63** (**Figure 1.30**) was studied by Davis and co-workers for anion transport function.[191] In a series of HPTS vesicle assays (see **Section 1.9.3**) compound **63**, a substituted calix[4]arene in the *1,3-alt* conformation, was shown to selectively transport chloride in a cation dependent manner. Proton NMR experiments revealed that **63** bound HCl as an ion pair in $CDCl_3$. As with the acyclic compounds **60-62**, the amide NH groups were required for chloride binding and thus transport, whilst the alkyl amide substituent permitted tuning of receptor lipophilicity. Channel formation was verified using a voltage clamp assay (see **Section 1.9.10**). The abrupt changes in current intensity indicated that **63** is capable of aggregating into channel-like structures. The ion transport properties of the *cone* and *paco* isomers (**64** and **65** respectively) were also studied.[192] The calixarene conformation was demonstrated to influence chloride transport rates, with the *cone* conformation being the more active. Replacement of one of the amide arms with a hydroxyl group yielded receptor **66** (**Figure 1.30**), which displayed remarkable pH sensitive chloride transport (a property not observed with analogous compound **64**). Transport activity was diminished by increasing the pH of the system from 6.4 to 9.0. From these results it appears that deprotonation of the hydroxyl group introduces unfavourable electrostatic interactions between the calixarene and the chloride ions, inhibiting chloride binding and consequently impeding transport.[193] In addition, patch clamp experiments in HEK-293 cells revealed the formation of voltage-dependent channels *in vitro*, demonstrating the suitability of such molecules for applications in biological systems. Indeed, further functionalisation of the calix[4]arene scaffold with

chiral substituents may yield receptors capable of facilitating the enantioselective transport of biomolecules.[194] Inspired by the finding that *paco* calixarene **65** can facilitate Cl^-/NO_3^- antiport, Davis and co-workers constructed tripodal receptor **67** (**Figure 1.30**) which, like calixarene **65**, contains three convergent NH groups.[195] Compound **67** displayed high affinity for nitrate in CD_2Cl_2 (K_a = 326 M^{-1}). In a series of HPTS base pulse assays, compound **67** facilitated H^+ efflux from EYPC vesicles loaded with $NaNO_3$ but not from vesicles loaded with NaCl. Direct evidence for nitrate transport was obtained using a nitrate reductase assay. In this assay the nitrate released from EYPC vesicles was reduced by nitrate reductase in the presence of nicotinamide adenine dinucleaotide phosphate (NADPH), producing nitrite and $NADP^+$. The enzymatically generated nitrite was then used in the formation of diazo dye **68** (**Figure 1.30**).[196, 197] Consequently, nitrate efflux could then be monitored by following the decrease in the ultraviolet-visible (UV-vis) absorbance of NADPH at 340 nm and the increase in the UV-vis absorbance of diazo-dye **68** at 543 nm.

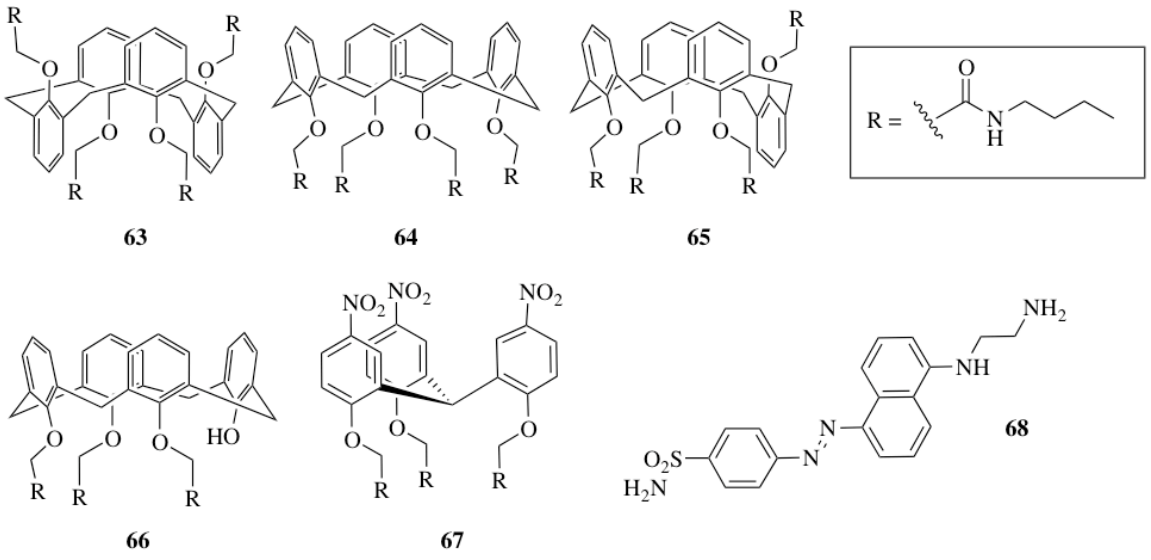

Figure 1.30: Calixarenes **63**-**66**, tripodal nitrate transporter **67** and diazo dye **68**.

Inspired by the transport activity of the aforementioned calixarenes, Matile and co-workers developed ditopic ion transporters **69** and **70** (**Figure 1.31**) that utilise anion-π and halogen-bonding interactions respectively to facilitate anion transport.[198] In a series

of HPTS fluorescence assays (see **Section 1.9.3**), compounds **69** and **70** were shown to facilitate the dissipation of an applied pH gradient only in the presence of tetramethylammonium (TMA) cations, by a combination of TMA^+/Cl^- and TMA^+/OH^- antiport processes. The TMA selectivity of the observed transport processes serves as conformation that TMA complexation with the calixarene upper rim is essential for transport function. Channel formation was disproved by the inability of these compounds to facilitate carboxyfluorescein release from phospholipid vesicles (see **Section 1.9.3**).

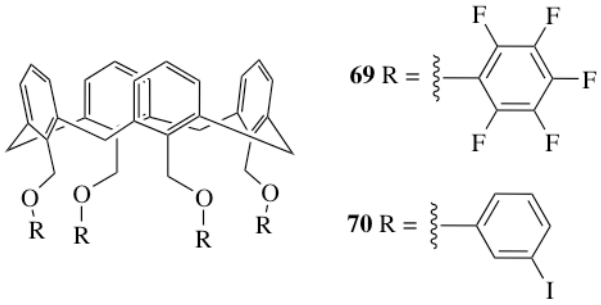

Figure 1.31: Calixarenes **69** and **70** utilise non-hydrogen-bonding interactions to facilitate anion transport.

1.8.6 Cyclodextrins

Aminocyclodextrin **71** (**Figure 1.32**) was synthesised by Gin and co-workers and was found to form a highly active, monomeric ion channel with selectivity for anions over cations.[199] Compound **71** appears well suited towards channel function, with a polar β-cyclodextrin (β-CD) head group and pendant oligoether chains. These chains are suitably hydrophobic to promote membrane insertion and of sufficient length to span the entire membrane. In a series of lucigenin fluorescence assays (see **Section 1.9.3**), halide transport into phospholipid vesicles was shown to be dependent on the protonation state of the amines lining the channel pore.[200] Under acidic conditions (pH 5.6) chloride and bromide import rates were diminished, indicating that electrostatic interactions between the positively charged amines and the anionic substrate retards anion conduction through the channel.

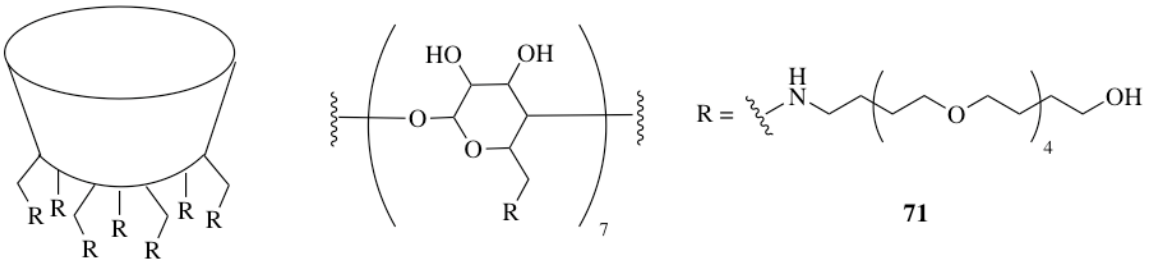

Figure 1.32: Cyclodextrin ion channel **71**.

The same group has appended an azobenzene group onto β-CD transporter motifs to create a light-switchable gated channel, compound **72** (**Figure 1.33**).[201] Irradiation converts the covalently linked azobenzene from the *trans* to the *cis* conformation. In the *trans* form the azobenzene moiety can bind within the hydrophobic β-CD cavity, occluding the pore and thus inhibiting the passage of halide ions. Photoisomerization to the *cis* form reduces the binding affinity of the azobenzene with the β-CD cavity, resulting in an 'open' conformation (**Figure 1.33**). The rate of chloride transport was consequently enhanced by a factor of 2.5 for the *cis* form of **72**, compared to the *trans* isomer.

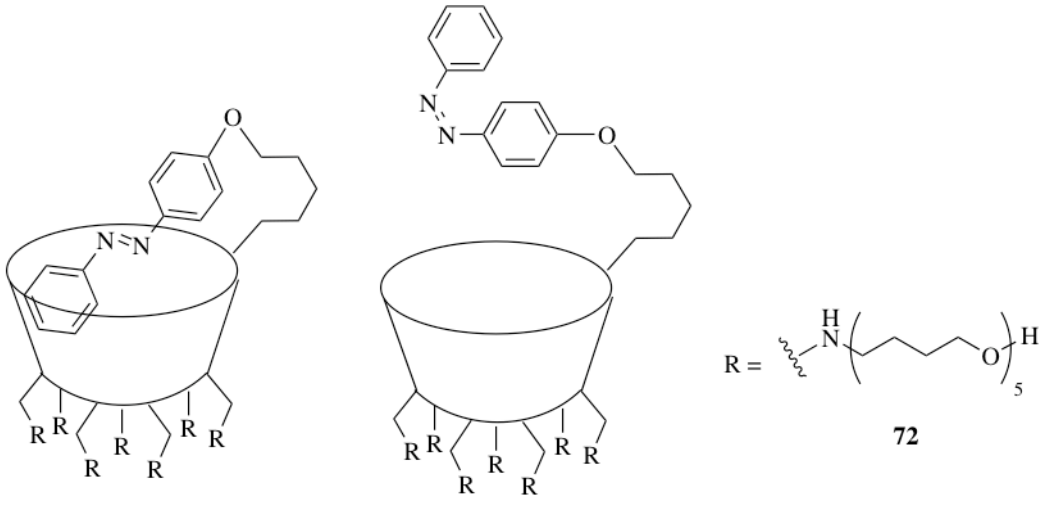

Figure 1.33: Light gated cyclodextrin channel **72**.

Inspired by Gin's cyclodextrins, Montesarchio and Tecilla developed ionophores based on cyclic phosphate linked oligosaccharide (CyPLOS) macrocycles.[202] Compounds **73**-**75** (**Figure 1.34**) comprise of an anionic macrocycle with varying numbers of pendant tetraethylene glycol (TEG) chains. In a series of HPTS fluorescence assays (see **Section 1.9.3**) compound **73** was shown to facilitate the re-equilibration of an applied pH gradient in phospholipid vesicles. Transport rates were dependent on the nature of the anion but not the cation, implying an H^+/Cl^- symport (or analgous OH^-/Cl^- antiport) mechanism. The loss of TEG chains drastically reduced the transport activity in **74** and **75** whilst neutral compound **76** and the non-macrocyclic compound **77** (**Figure 1.34**) still retained some transport activity. Based on these findings the authors rationalized that the macrocycle partitions into the polar region of the phospholipid membrane, with the amphiphilic TEG chains permeating the hydrophilic region, destabilizing the bilayer and facilitating pore formation.

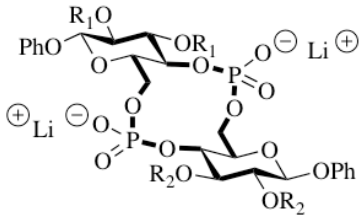

73 $R_1 = R_2 = (CH_2CH_2O)_4Bn$
74 $R_1 = CH_2(CH_2)_9CH_3$
$R_2 = (CH_2CH_2O)_4Bn$
75 $R_1 = R_2 = CH_2(CH_2)_9CH_3$

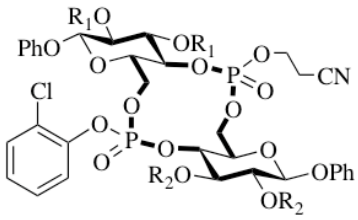

76 $R_1 = R_2 = (CH_2CH_2O)_4Bn$

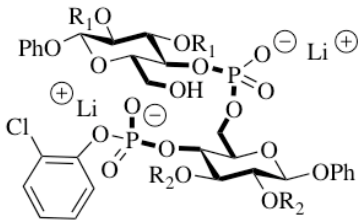

77 $R_1 = R_2 = (CH_2CH_2O)_4Bn$

Figure 1.34: CyPLOS macrocycles **73**-**75**, neutral analogue **76** and acyclic analogue **77**.

1.8.7 Synthetic Peptides

Examples of channel forming peptides that selectively transport anions are comparatively rare. Kissiper **78** (**Figure 1.35**) is a thirty-nine residue peptide isolated from kiwi fruit that functions as a pore forming agent in synthetic phospholipid bilayers, acting as a voltage-gated ion channel with selectivity for chloride over potassium.[203] Similarly duramycins, a series of nineteen residue polycyclic peptide derived from *Streptomyces,* form channels in both artificial and biological membranes.[204] Owing to

their propensity to selectively transport chloride they have undergone clinical trials for the treatment of CF.[205]

H_2N-ISSCNGPCRDLNDCDGQLICIKGKCNDDPQVGTHICRGT-COOH **78**

H_2N-PARVGLGITTVLTMTTQSSGSRA-COOH **79**

H_2N-KKKKPARVGLGITTVLTMTTQSSGSRA-COOH **80**

H_2N-KKKKPARVGLGITTVLTMTTQS-COOH **81**

H_2N-KKKKPARVGLGITTVLTMTTQW-COOH **82**

Figure 1.35: Kissiper peptide sequence **78** and short peptide sequences **79-82** studied for ion transport (see **Appendix 1** for a list of amino acid codes).

Tomich and co-workers discovered that a twenty-three residue peptide M2GlyR **79** (**Figure 1.35**) from a transmembrane segment of the spinal cord glycine receptor functions as a chloride selective channel in POPC membranes.[206] As part of a study of over 200 structurally related peptide sequences, Tomich and co-workers modified the transport active M2GlyR sequence, incorporating four lysines at the N-teminus to produce NK_4-M2GlyR **80** (**Figure 1.35**). The aqueous solubility of the peptide sequence was greatly enhanced by the lysine residues and the peptide displayed channel activity in MDCK cells.[207, 208] The sequence was further optimised for improved solubility by the removal of the five C-terminal amino acids to yield peptide **81** (**Figure 1.35**). Importantly, this new sequence retained the N-terminal arginine required for anion selectivity.[209] The most active sequence was found to be peptide **82** (**Figure 1.35**), with a C-terminal serine replaced by an indole containing tryptophan. This tryptophan residue has a dual function; preventing the aggregation of peptide monomers and also anchoring the protein into the membrane.[210]

Building on these findings Gokel and co-workers have developed a synthetic chloride membrane-insertable transporter (SCMTR) **83** (**Figure 1.36**).[211] Structurally, SCMTR **83** has several important features; an N-terminal lipophilic anchor, a 'mid-polar' connector, a short peptide sequence found in CLC chloride channels, and a C-terminal lipophilic anchor. NMR studies revealed that the glycine NH groups in **83** hydrogen-bond with chloride in solution; an association constant of 1700 M^{-1} was measured for this

interaction in $CDCl_3$.[212, 213] Voltage clamp experiments with planar phospholipid bilayers revealed that **83** functions as a dimeric channel with a 10:1 selectivity for Cl^- over K^+.[211] By systematically modifying parts of the SCMTR **83**, Gokel and co-workers gained insights into the mechanism of channel operation. Shortening the C- and N- terminal anchor groups, making the midpolar linker region less polar, and extending the peptide sequence with glycines were all found to improve chloride transport efficacy.[214-218] Increasing the steric bulk of the anchor groups was found to prevent dimer formation and thus resulted in a loss of channel activity.[219] Replacement of the peptidic proline residue with pipecolic acid in compound **84** (**Figure 1.36**) resulted in a dramatic loss of transport activity.[220, 221] This finding shows that the proline residue induces a 'kink' in the peptide sequence, fundamentally contributing to the structure of the pore.[222] To investigate the effect of charged residues on channel activity, glutamic acid functionalised receptor **85** and lysine functionalised receptor **86** (**Figure 1.36**) were studied. The glutamic acid residue was included so as to mimic the gating glutamate (E148) found in natural CLC chloride channels (see **Section 1.4**), however receptor **85** showed reduced transport activity compared to **83**, indicating that the presence of a negative charge in the ion conduction pathway hinders chloride transport.[223] Similarly, the positively charged lysine did little to enhance the transport activity of **86**. The authors postulated that this could be the consequence of favourable electrostatic interaction between the lysine residue and the anion.[224]

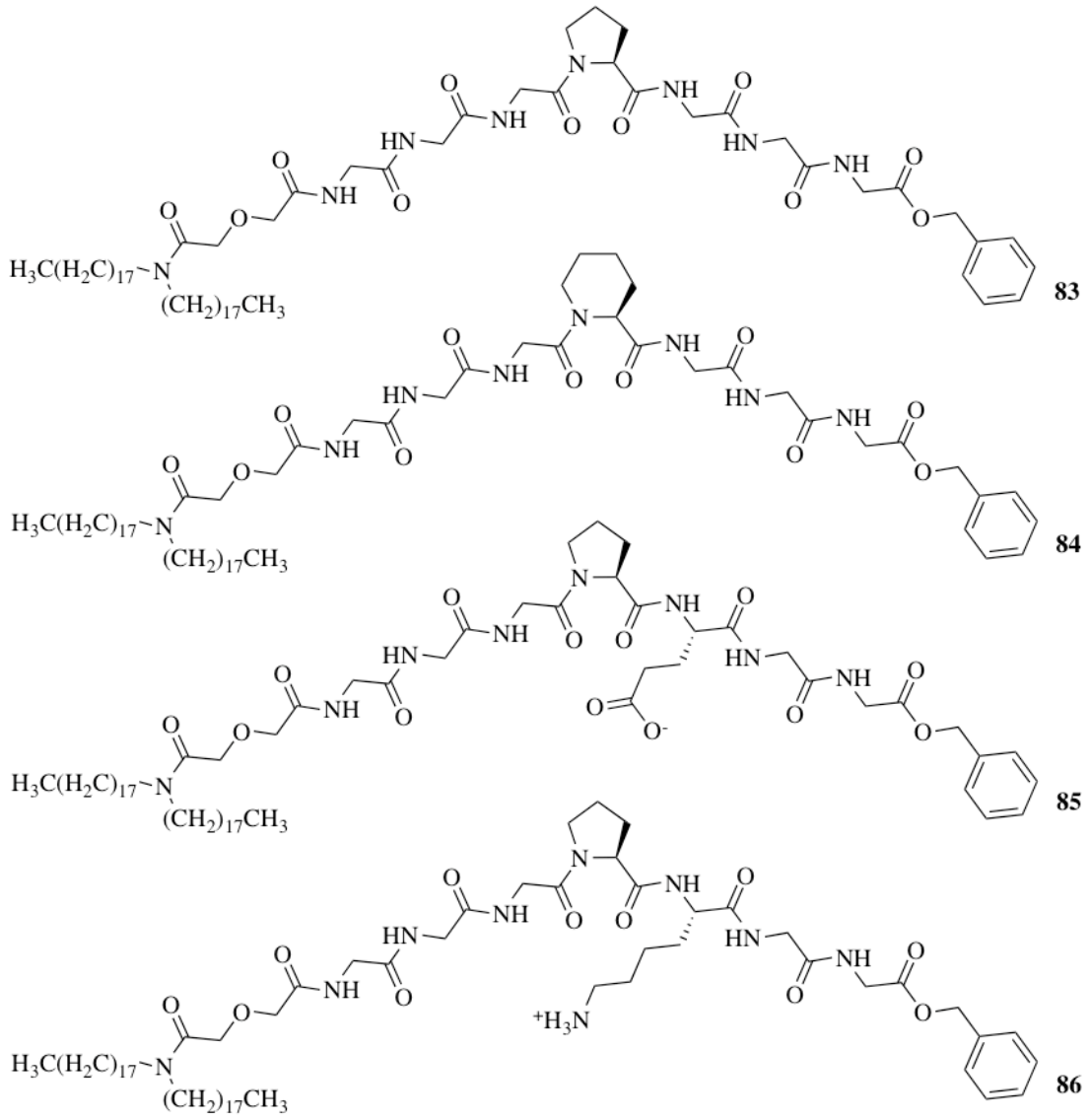

Figure 1.36: SCMTR **83** and structural analogues **84-86**.

Evidence for channel formation was obtained by a range of means.[225] NMR chemical shift changes observed upon dilution were consistent with self association for structural analogues of compound **83**. In addition, covalent linkage of two SCMTR **83** units at either the N- or C- termini resulted in pseudo-dimer compounds that retained chloride transport activity.[226] The attachment of fluorescent groups onto the SCMTR scaffold allowed direct measurement of aggregation and partitioning phenomena (**Figure 1.37**). The tryptophan residue in compound **87** absorbs at λ = 283 nm and fluoresces at λ = 345 nm, whilst pyrenyl compound **88** absorbs at λ = 345 nm. A mixture of compounds

87 and **88** was added to a suspension of phospholipid vesicles. Following excitation at λ = 283 nm, Gokel and co-workers observed that indole fluorescence was lost, suggesting that compounds **87** and **88** aggregate forming a pore. In addition, the fluorescence shift of indolyl compound **87** was found to be solvent dependant. By comparing the fluorescence maxima in a range of solvents it could be determined that in liposomes composed of a mixture of 1,2-dioleoyl-*sn*-glycero-3-phosphocholine (DOPC) and dioleoyl-sn-glycero-3-phosphate (DOPA) the tryptophan residue was located at the polar membrane interface.[227]

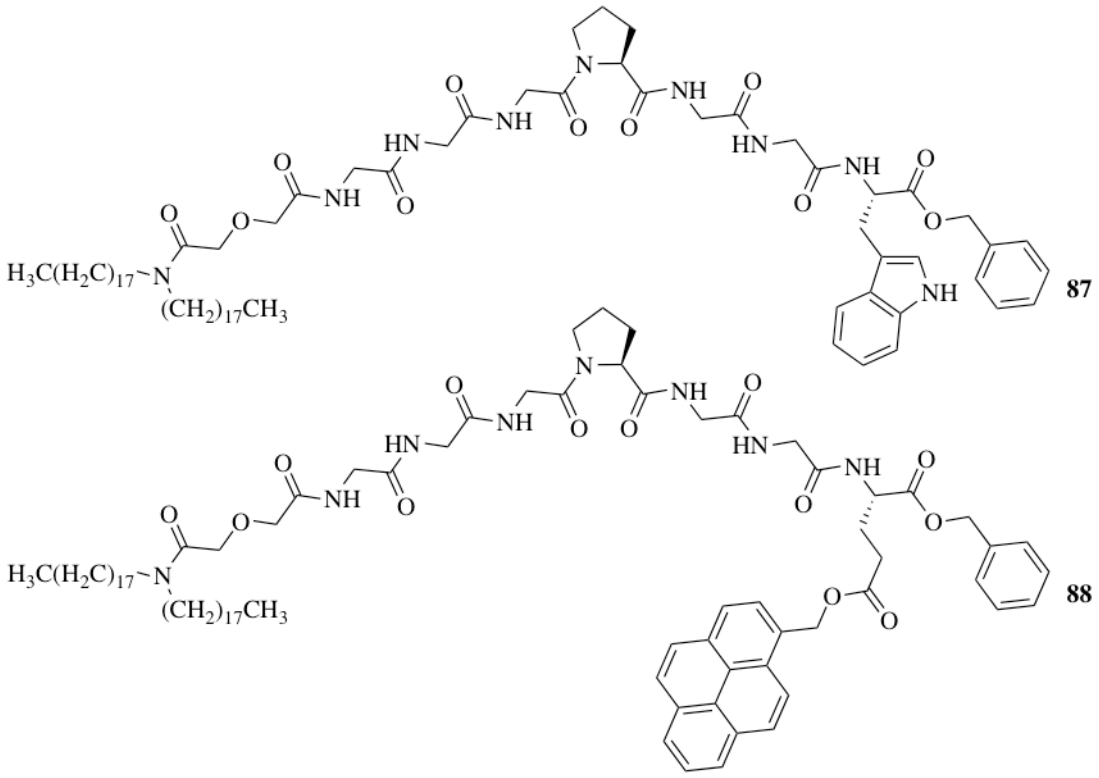

Figure 1.37: Fluorescently tagged SCMTRs **87** and **88**.

1.8.8 Exotic Transport Mechanisms

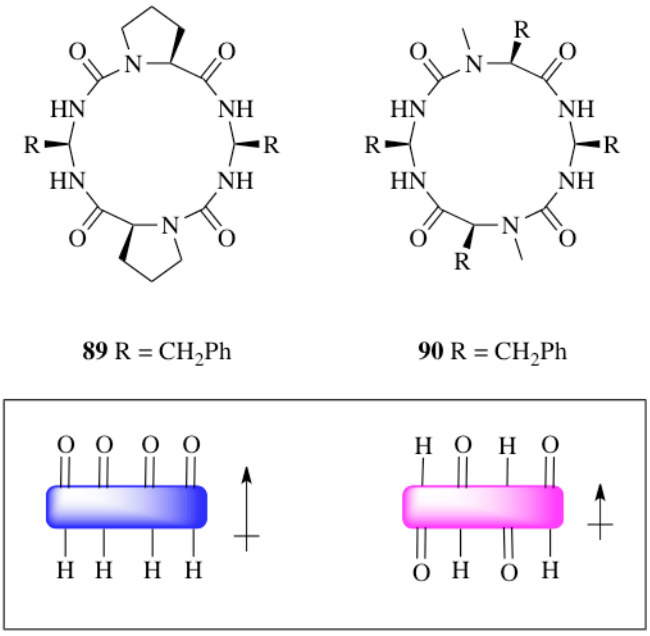

Figure 1.38: Macrocyclic peptides **89** and **90**.

Transporters usually operate by a mobile carrier or channel mechanism. Interest has grown in alternative modes of ion translocation, exemplified by Matile and co-workers' utilization of the self-assembly properties of cyclic peptides to construct amide containing macrocycles **89** and **90** (**Figure 1.38**).[228, 229] HPTS assays in phospholipid vesicles revealed that these compounds facilitate H^+/Cl^- co-transport. Chloride is too large to pass through the macrocycle (d ≈ 3.5 Å and 1.8 Å respectively) ruling out a conventional channel mechanism, whilst a carrier mechanism was considered unlikely owing to Hill coefficients of $n > 1$.[230] The authors proposed a novel transport mechanism coined a 'Jacob's ladder' (**Figure 1.39**) wherein anions bind to the NH hydrogen-bond donor groups at the positive end of the macrocyclic dipole. Rotation of the macrocycle and subsequent binding to the next macrocycle in the nanotube leads to anion conduction. Protonation of a bridging water provides a H^+ conduction pathway, completing a charge neutral H^+/Cl^- co-transport process. A similar mechanism can be applied to compound **90**, which has a smaller macrocyclic dipole, although in this case macrocycle dimers are believed to bind anions weakly and then rotate to conduct anions across the membrane.

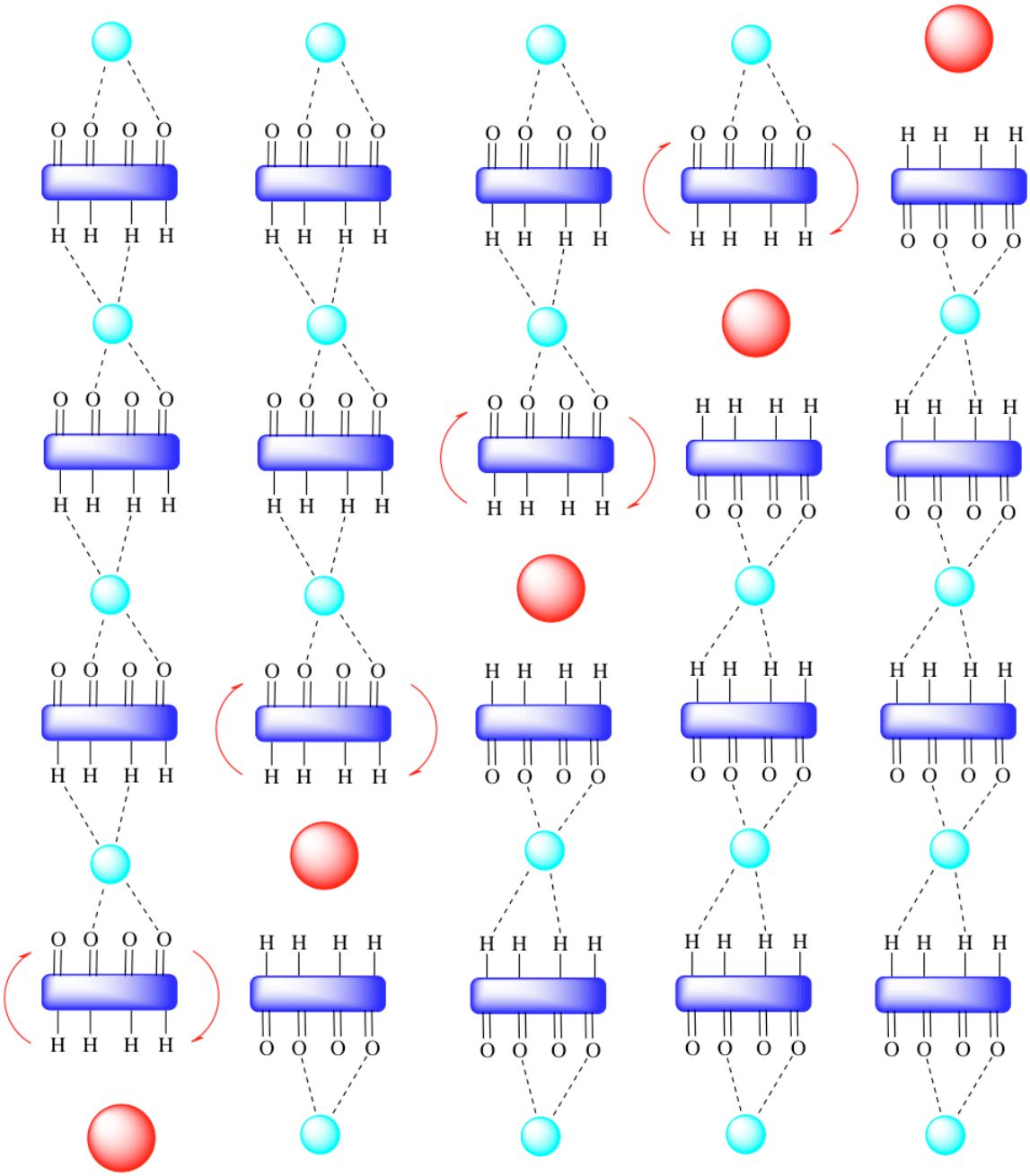

Figure 1.39: The 'Jacob's ladder' mechanism for anion transport (red circles) facilitated by macrocycle **89**. Water or H_3O^+ (blue circles) link the macrocycle units through hydrogen bonding interactions.

Regen and co-workers have utilized the facial amphiphilicity of the cholic acid scaffold (see **Section 1.8.1**) to produce transporters that operate *via* a 'molecular umbrella' mechanism.[231] The guanidine group facilitates anion co-ordination by compound **91** (**Figure 1.40**) and ATP release from phospholipid vesicles has been

observed using UV-vis spectroscopy techniques.[232] Fluorescence experiments with fluorescently tagged analogues of umbrella **91** reveal that this type of structure favours a shallow membrane-bound state, with the hydrophobic cholate faces directed towards the membrane interior and the hydrophilic faces orientated towards the polar external medium. Transport is facilitated by the rotation of the cholate groups, shielding the polar cholate faces from the hydrophobic membrane interior.[233] Extension of the umbrella scaffold through the addition of extra cholic acid functionalities increases transport rates owing to improved shielding of the bound anions from the hydrophobic membrane interior.[234] Further investigations revealed that these extended structures aggregate, forming channels suitable for the passage of chloride, sucrose and ribonucleic acid.[235-237]

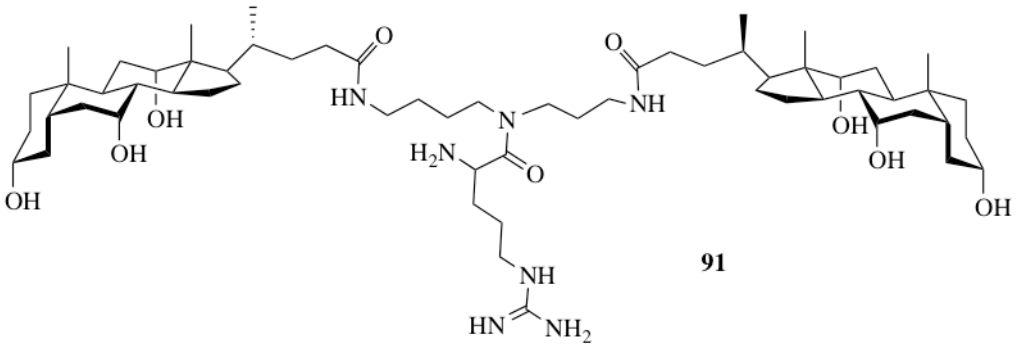

91

Figure 1.40: 'Molecular umbrella' **91**.

Smith and co-workers investigated phospholipid derivatives bearing covalently linked anion binding units.[238] Preincorporation of compounds **92** and **93** (**Figure 1.41**) into phospholipid vesicles containing lucigenin, facilitated chloride influx upon addition of NaCl to the external solution. The addition of an electron withdrawing nitro group into the phenylurea scaffold was found to enhance the rate of chloride transport into the vesicles. UV absorption experiments revealed that to facilitate chloride transport compound **93** was required to populate both the inner and outer leaflets of the vesicle membrane. Kinetic analysis revealed that in vesicles composed of 1,2-dimyristoyl-*sn*-glycero-3-phosphocholine (DMPC) and cholesterol (7:3 molar ratio) aggregates of two transporter molecules were required to facilitate ion transport, whilst in vesicles composed of POPC and cholesterol (7:3 molar ratio), a thicker membrane, transport

function was reduced with kinetic studies suggesting that aggregates of four transporters were responsible for transport function. In both cases a relay mechanism was proposed (**Figure 1.42**). The transporter molecules assemble into the phospholipid bilayer, with the flexible urea arms 'fishing' for the anion in the aqueous phase. The anion is bound at the polar membrane interface and is then carried into the hydrophobic membrane interior, wherein a transporter molecule incorporated into the opposite membrane leaflet can bind the anion and facilitate its release on the opposite side of the membrane.

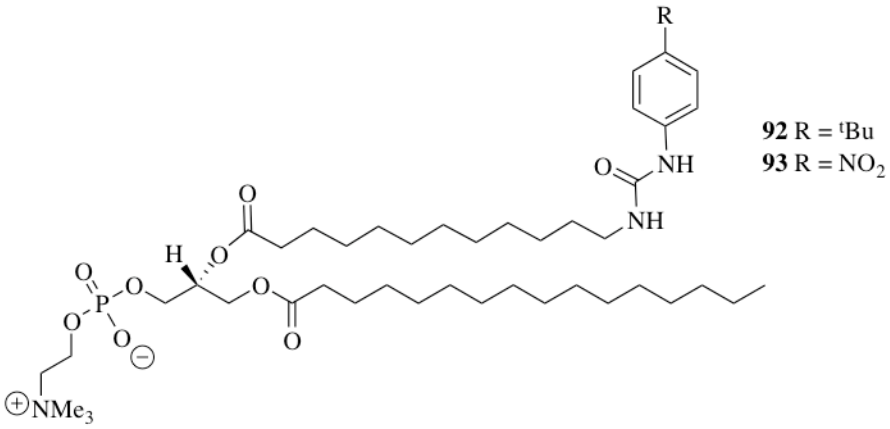

Figure 1.41: Urea functionalized phospholipids **92** and **93**.

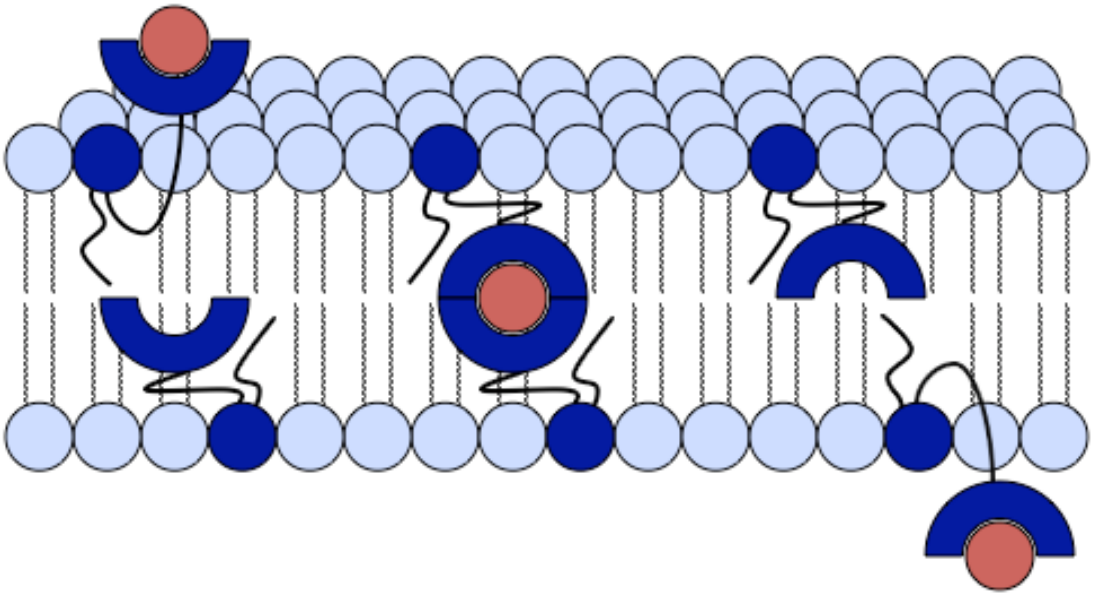

Figure 1.42: A schematic drawing of the 'relay' mechanism of ion transport facilitated by compounds **92** and **93**.

1.9 Ion Transport Assays

Direct comparison of transport data between different sets of compounds is seldom straightforward as different research groups utilize alternative methods to assay for transport activity. Even assays that utilize the same method for the detection of ion transport can differ in the concentrations of salt and buffer species, the loading of transporter, the method of transporter administration and the composition of the phospholipid bilayer. In this thesis the assay methods are such that they conform to those previously published by the Gale group.[5]

1.9.1 Unilamellar Vesicles

200 nm diameter unilamellar vesicles are prepared by the hydration of a thin film of phospholipid, followed by multiple freeze/thaw cycles and then extrusion through a polycarbonate membrane.[239] This technique for vesicle preparation was developed by Smith and co-workers.[240] Vesicles formed in this manner serve as a simplified model of a cell membrane, enabling easily reproducible experiments to be performed rapidly. Additionally, this system permits control of the composition of the intravesicular and

extravesicular solutions, allowing a variety of experimental conditions to be tested (see **Section 1.9.4**). Uniform ionic strength of the intravesicular and extravesicular solutions is maintained throughout the assays, preventing osmotic disruption of the bilayer.[241] Uniform pH is also maintained across the bilayer through the use of buffered solutions, ensuring that transport is not driven by a pH gradient (unless so desired). Transporters can either be preincorporated into the bilayer or added as a solution in a water miscible solvent such as DMSO. This latter approach also tests the delivery of the transporter through aqueous media.

1.9.2 Ion Selective Electrodes (ISE)

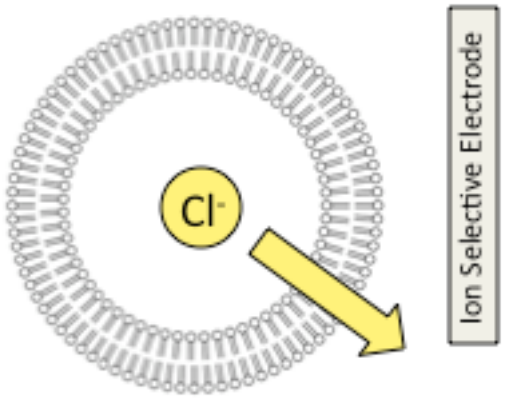

Figure 1.43: Chloride efflux from phospholipid vesicles can be measured using a chloride ISE.

Chloride selective electrodes make it possible to monitor the chloride concentration in the extravesicular solution. Typically vesicles are made containing chloride. The encapsulated chloride is 'invisible' to the chloride ISE and consequently chloride efflux facilitated by a transporter can be followed by changes in the measured electrode potential (**Figure 1.43**). Lysis of the vesicles with a non-chloride containing detergent enables determination of 100 % chloride efflux, allowing the system to be calibrated against solutions of known chloride concentration. Ions other than chloride, for example sodium and carbonate, can be measured in a similar fashion using an appropriate ISE.[242-244]

1.9.3 Fluorescent Dyes

A range of membrane impermeable fluorescent probes can be encapsulated within phopholipid vesicles, allowing the influx or efflux of ionic species to be monitored. Lucigenin and 6-methoxy-*N*-(3-sulfopropyl)quinolinium (SPQ) fluorescence is quenched by halides, thus these probes can be used to monitor halide transport.[149, 245] 8-Hydroxypyrene-1,3,6-trisulfonic acid (HPTS) permits the measurement of pH changes and is typically used to monitor H^+/X^- symport (or analogous X^-/OH^- antiport) processes.[246] Safranin-O is a potential sensitive dye that allows changes in membrane potential arising from ion transport to be monitored.[247] The fluorescence intensity of some dyes is dependent on concentration, examples include carboxyfluorescein and calcein.[174, 191] These self-quenching dyes can be used to monitor membrane integrity as the release of carboxyfluorescein and calcein from phospholipid vesicles implies either pore formation or the development of membrane defects.[248]

1.9.4 Composition of Intravesicular and Extravesicular Solutions

The variation of the composition of the intravesicular and extravesicular solutions can help to determine the underlying transport mechanism. An initial test for anion transport activity uses vesicles containing NaCl suspended in a solution of $NaNO_3$. Chloride efflux can be the consequence of H^+/Cl^- symport, Na^+/Cl^- symport or Cl^-/NO_3^- antiport. Changing the external anion to sulphate enables testing for an anion antiport mechanism. The sulphate anion is very hydrophilic (see **Table 1.1**) and consequently its transport is facilitated by only a select group of transporters to date.[249] If chloride efflux is inhibited under these conditions then H^+/Cl^- symport and Na^+/Cl^- symport can be ruled out, owing to the anion selectivity of the transport process. Davis and co-workers have pioneered the use of bicarbonate 'pulse' assays under these conditions to examine Cl^-/HCO_3^- antiport.[90] The transport of other species such as carboxylic acids (see **Section 4.2.5**) can be examined by analogous 'pulse' assays. If chloride efflux is observed with SO_4^{2-} as the external anion then assays using different encapsulated MCl salts will reveal if an M^+/Cl^- symport pathway is in operation, enabling cation selectivity to be studied. H^+/Cl^- transport can be further examined using a pH gradient assay.[152] By making the intravesicular solution more acidic than the extravesicular solution a proton gradient in

the same direction as the chloride gradient is created, resulting in an enhanced rate of chloride efflux if an H^+/Cl^- cotransport process is facilitated.

1.9.5 NMR Assays

Ion transport can be directly monitored by NMR techniques. The detection of $^{23}Na^+$, $H^{13}CO_3^-$, or $^{35}Cl^-$ is possible by NMR methods, and the vesicular import or export of these species can be examined, owing to the difference in chemical shift of the encapsulated and unencapsulated ions.[90, 199, 250-252] The addition of a membrane impermeable, paramagnetic $MnCl_2$ contrast reagent broadens the signal of unencapsulated ions, permitting differentiation between intravesicular and extravesicular anions.

1.9.6 U-tube Assays

U-tubes are simple models for transport through biological membranes, consisting of two aqueous phases separated by a water immiscible organic phase such as chloroform, dichloromethane (DCM) or nitrobenzene in a U-shaped piece of apparatus. The movement of ions across the bulk organic phase can be monitored by following changes in the ion concentration in each of the aqueous phases. This assay is highly tunable as the content of the source and receiving phases can be easily altered, and has been used previously to demonstrate a range of proton-coupled transport processes.[253-255] Additionally, U-tube experiments serve as proof that a transporter can function as a mobile carrier, since the large distance that separates the two aqueous phases ensures that a channel transport mechanism is not possible.

1.9.7 Mobility Assays

A carrier mechanism for transport can be tested by the addition of cholesterol to phospholipid vesicles. Cholesterol has been shown to exhibit a range of effects on phospholipid membranes, the most relevant being the reduction of membrane fluidity.[256-262] Molecules operating by a mobile carrier mechanism are under diffusion control and thus the increase in membrane viscocity results in an observable reduction in transport activity. Conversely, molecules that function by a channel mechanism are membrane

spanning, and thus the decreased membrane fluidity should have little effect on the observed transport rates for these structures.

Vesicles composed of DPPC can also be used to assay for mobile carrier activity. DPPC undergoes a gel to fluid phase transition at 314 K. At temperatures above 314 K, the membrane is in the fluid phase and thus molecules that function as mobile carriers and molecules that function as channels will both exhibit ion transport function. At temperatures below 314 K mobile carriers will show reduced activity as the gel phase hinders diffusion through the DPPC bilayer. The activity of channel forming compounds remain unaffected under the same conditions.[263] It should be noted that the reliability of this technique is contested, as there is some evidence of phase-induced ionophore expulsion from DPPC bilayers.[264]

1.9.8 Hill Plots

The Hill equation was initially used to describe the cooperative binding of oxygen to haemoglobin and has subsequently found diverse applications in biological systems.[265, 266] In an anion transport context the Hill equation can be expressed in its simplest form as **Equation 1.1**, where E is the observed ion flux, C is the receptor concentration, EC_{50} is the concentration of the transporter required to achieve 50 % of the maximum ion flux and n is the Hill coefficient. In this context n refers to the number of transporter molecules that facilitate a single ion transport event.

$$E = EC_{max}C^n/(EC_{50}{}^n + C^n)$$

Equation 1.1: The Hill equation as used for ion transport calculations

In this way EC_{50} values can be used to enable direct comparison of ion transporter activity, provided the values are calculated under identical assay conditions. The calculated values for the Hill coefficients are similarly informative, as they indicate the likely transport stoichiometry.[198]

1.9.9 Phospholipids

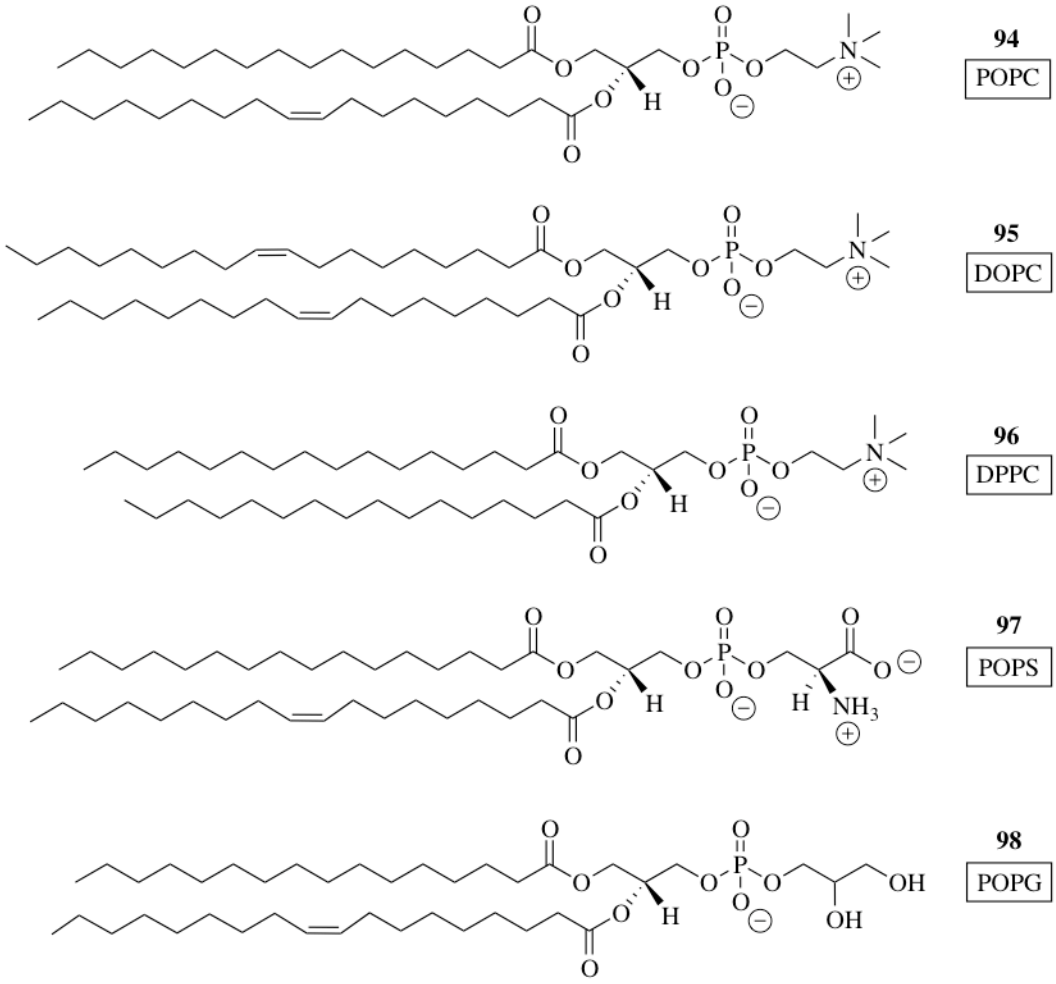

Figure 1.44: Commonly used phospholipids for vesicle based transport assay.

A range of phospholipids can be used to construct vesicles suitable for ion transport assays (**Figure 1.44**), with POPC the predominant lipid used in the experiments described within this thesis. Phosphatidylcholines are the major component of cell membranes and hence this class of lipid is widely used in vesicle assays aiming to produce a 'model cellular environment'.[17] The choice of phospholipid imparts different properties on the vesicle membrane, influencing the dipole moment, fluidity and stability.[267] For this reason a range of other phospholipids are utilized in membrane transport assays including EYPC (a complex mixture of phosphatidylcholines), DOPC,

DPPC, 1-palmitoyl-2-oleoyl-*sn*-glycero-3-phospho-*L*-serine (POPS) and 1-palmitoyl-2-oleoyl-*sn*-glycero-3-phospho-(1'-*rac*-glycerol) (POPG).[268] Variation of membrane thickness is readily achieved by alteration of phospholipid hydrocarbon chain length, and can be used to probe the mode of action of a transporter molecule. Transport rates achieved by channel structures are expected to be unaffected by membrane thickness, with a dramatic reduction in activity only when membrane thickness exceeds the length of the channel, whilst carriers (which operate under diffusion control) are expected to show simple correlation between transport rate and membrane thickness.[269] In two recent studies a carrier mechanism has thus been demonstrated using phospholipids of differing hydrocarbon chain length, with reduced activity observed upon increasing the phospholipid chain lengths.[138, 270]

1.9.10 Conductance Measurements

Conductance measurements across membranes can be measured using planar lipid bilayer (PLB) or patch clamp techniques. These experiments allow the membrane to be held at a constant potential and thus the current flowing through the membrane at the fixed potential can be measured.[26] The transmembrane current is directly related to the transport of ions across the bilayer and consequently it is possible to record single channel activity and observe the characteristic 'open-close' behaviour of individual channels.[9] These methods can be used to unequivocally confirm channel function.[271] In the PLB experiment a lipid bilayer is 'painted' across a hole linking two vessels containing electrolyte solution. Electrodes placed in each solution measure the membrane conductance. In the patch clamp experiment a thin glass tube is used to capture a 'patch' of cell or vesicle membrane.[272, 273] This separates the inside of the tube and the external solution with a membrane, permitting conductance studies to be performed in an analogous manner to the aforementioned PLB methods. The transporter molecule for examination can be delivered to the aqueous solution or preincorporated if using synthetic vesicles.

1.9.11 Cell Based Assays

Patch clamp methods can be used to measure the transport current in whole cells.[274] In a similar fashion the use of an Ussing chamber can be employed to study transmembrane ion transport across a tissue sample, and has been successfully used to study CFTR mediated chloride transport across airway and intestinal epithelia.[275] Additionally, the use of cell permeable fluorescent dyes such as SPQ (see **Section 1.9.3**) and the pH sensitive dye acridine orange (AO) can be used to monitor transmembrane transport *in vitro*.[276] Despite widespread use of these techniques to assess channel function, few examples of the *in vitro* testing of synthetic carriers are known.[26] Cholapod mediated chloride selective discharge of an electrochemical gradient has been used to demonstrate chloride transport in Madin Darby canine kidney (MDCK) cells using the Ussing chamber technique (see **Section 1.8.1**).[136] Isophthalamide mediated chloride transport has similarly been demonstrated in MDCK cells loaded with the chloride sensitive dye SPQ (see **Section 1.8.2**).[149] R. Pérez-Tomás and co-workers have pioneered the study of synthetic carriers in small cell lung cancer (GLC4) cells; monitoring the deacidification of acidic cellular organelles by synthetic prodiginine and tambjamine alkaloids, and fluorinated tripodal molecules through changes in AO fluorescence (see **Sections 1.6** and **3.1.3**).[94, 101, 249] These studies provide direct evidence for the transmembrane transport of H^+, likely coupled to the transmembrane transport of chloride.

1.10 Aims of this Thesis

This chapter has examined the most recent advances in the development of synthetic anion transporters. The potential for such compounds to be used in biological systems for the treatment of disease has been discussed. The work within this thesis aims to examine new, simple structural motifs for the complexation and membrane transport of biologically relevant anions such as chloride and bicarbonate. The anion binding properties of new transporters has been examined in solution and in the solid state where possible. Ion transport has been studied using a range of vesicle-based assays utilising both ISE and fluorescence methods, whilst *in vitro* testing has revealed the suitability of some of the compounds for biological applications.

The work in **Chapter 2** examines the anion binding properties of a range of diindiolylurea and tripodal urea scaffolds, bearing NH hydrogen-bond donor arrays. In **Chapters 3** and **4** the anion transport properties of structurally simple urea containing scaffolds are examined. In both chapters receptor structure is modified to optimize both transport activity and 'drug-like' properties. In **Chapter 5** a dual host approach to ion transport is explored. This approach utilises a combination of carriers to facilitate coupled transport processes, and appears to be of relevance in biological systems.

Chapter 2
From Anion Binding to Anion Transport

2.1 Introduction

In this chapter the development of neutral organic molecules suitable for the binding of anionic species are discussed. Two scaffolds are examined; the diindolylurea motif and tripodal ureas based on the tris(2-aminoethyl)amine scaffold. Both of these types of structure contain urea groups as a key anion binding motif. The hydrogen-bond donor ability of urea groups can be readily tuned through N,N'-substitution, with the directional nature of hydrogen-bonding enabling ureas to form complexes with a variety of different anion geometries (**Figure 2.1**).

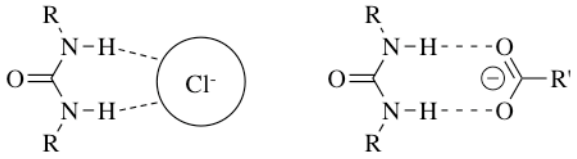

Figure 2.1: Urea binding modes for the spherical chloride anion and Y-shaped carboxylate anions.

Common strategies for the optimisation of ureas as anion hosts include increasing NH acidity through the introduction of electron withdrawing substituents, the introduction of additional hydrogen-bond donor groups onto the urea scaffold or preorganisation of the binding cavity.[277] In this chapter the effect of incorporating additional hydrogen-bond donor groups into the receptor scaffold is explored with amide substituted diindolylureas (see **Section 2.2**) whilst the assembly of multiple urea groups into a convergent array is achieved using a tripodal scaffold (see **Section 2.3**). The influence of these structural changes on both anion binding and transmembrane ion transport activity are examined, with the aim of examining how anion binding properties can be used to inform anion transporter design.

2.1.1 Indole in Nature

Neutral molecules containing arrays of hydrogen-bond donor groups have been extensively reported as anion hosts.[122-124] Following the successful development of pyrrole containing anion receptors, significant progress has been made in the construction of anion receptors containing indole functionalities.[278] This is partly owing to the similarity in the pK_a values for indole (21.0 in DMSO) and pyrrole (23.0 in DMSO).[279] Nature uses indole in the form of the amino acid tryptophan. Tryptophan is found in the binding site of several proteins, the indolyl NH functioning as a hydrogen-bond donor to anionic guests.[280] The structure of the cyanobacterial bicarbonate CmpA transport protein bears striking similarity to that of the NrtA nitrate transporter. In both cases a tryptophan residue contributes a single hydrogen-bonding interaction to stabilise the binding of the anionic guest at the protein binding site (**Figure 2.2**).[281, 282] In addition, X-ray crystal structure analysis of haloalkane dehalogenase isolated from *Xanthobacter autotrophicus* reveals that tryptophan is used to bind chloride in the enzyme active site (**Figure 2.2**).[283] These natural examples of indole playing a functionally important role in anion binding have led to the development of synthetic molecules that can similarly bind halides and oxo-anions (see **Section 2.1.2**).

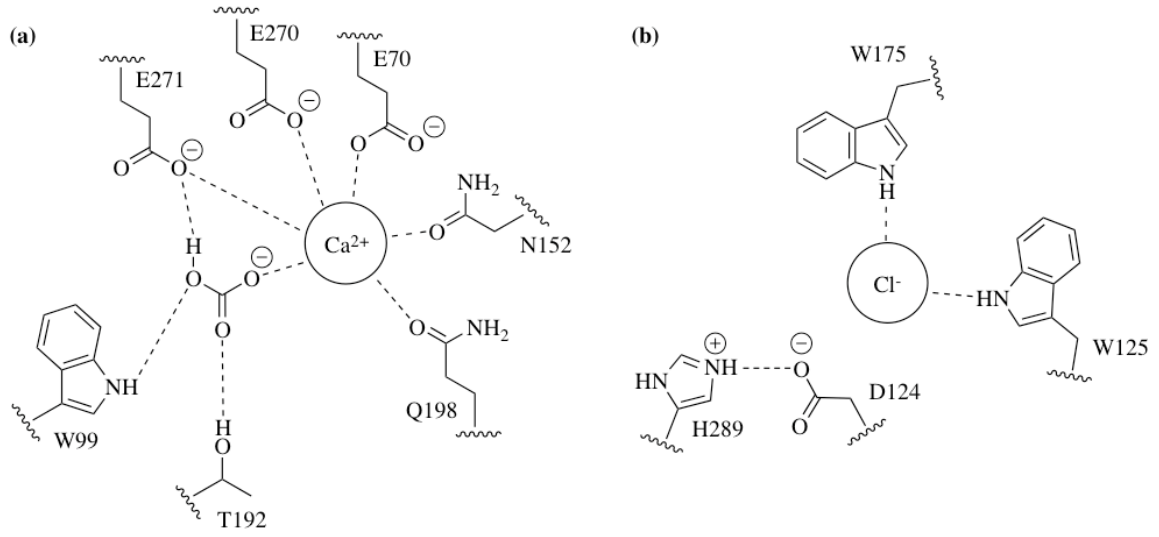

Figure 2.2: Schematic diagrams of; **(a)** The binding site of the bacterial CmpA bicarbonate transporter; the simultaneous binding of a calcium cation facilitates bicarbonate binding. **(b)** The active site of haloalkane dehalogenase, wherein two tryprophan residues can simultaneously bind to a chloride ion.

2.1.2 Bisindole Anion Hosts

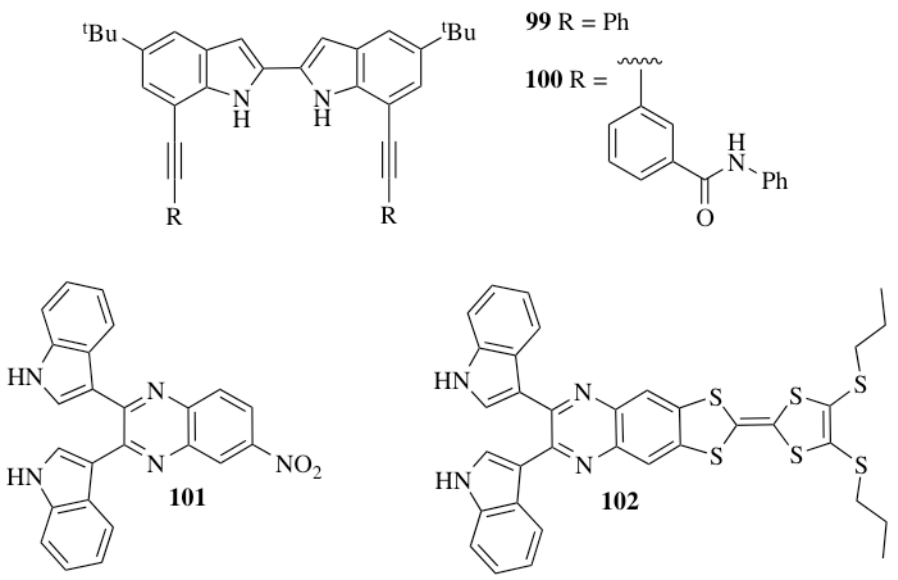

Figure 2.3: Bisindoles **99** and **100**, and flexible diindolylquinoxaline (DIQ) compounds **101** and **102**.

Jeong and co-workers have produced cleft receptors **99** and **100** (**Figure 2.3**) with indole functionalities directly bonded to one another at the 2- position.[284] The additional amide NH hydrogen-bond donors in receptor **100** enhanced the chloride affinity of the scaffold 40-fold in acetonitrile. The introduction of an azobenzene functionality onto this type of scaffold can yield colorimetric anion sensors whereby hydrogen-bonding interactions are transmitted through resonance to the azobenzene chromophore.[285] Rigidifying the scaffold to form an indolocarbazole has been found to dramatically improve anion affinity through removal of the conformational flexibility provided by the 2,2'-biindolyl linkage. Molecules based on the indolocarbazole functionality have found application in the fields of anion sensing and anion directed assembly.[286-289]

The DIQ motif is structurally similar to the indolocarbazole group. Sessler and co-workers have demonstrated that adding a nitro group to the quinoxaline core yields a colorimetric receptor for phosphate, compound **101**, whilst incorporation of tetrathiafulvalene (TTF) into the DIQ scaffold yields compound **102**, a dual optical-electrochemical sensor for dihydrogen phosphate.[290, 291] Phosphate binding was monitored by both the quenching of DIQ fluorescence and also electrochemically;

electron density from the bound dihydrogen phosphate anion was judged to extend into the TTF core making the molecule easier to oxidise. UV-vis experiments in DCM revealed that both **101** and **102** displayed good affinity and selectivity for dihydrogen phosphate over benzoate, hydrogen sulphate and chloride ($K_a[H_2PO_4^-]$ = 6500 M^{-1} and 20000 M^{-1} respectively). The authors ascribed the high affinity for the bulky dihydrogen phosphate anion in both these compounds as resulting from the large, flexible anion binding cavity created by the beta-connectivity linking the two indole motifs.

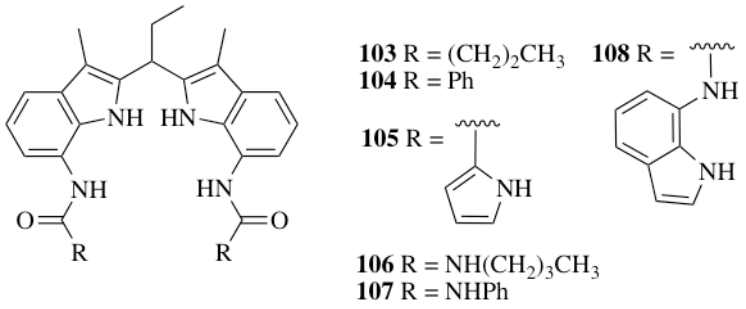

Figure 2.4: Diindolylmethane based oxo-anion hosts.

Jurczak and co-workers have developed the 7,7'-diamido-2,2'-diindolylmethane scaffold, with compounds **103-108** (**Figure 2.4**) displaying strong affinity towards oxo-anions.[292, 293] Amide compounds **103-105** displayed remarkable affinity for oxoanions even in highly polar 25 % H_2O/DMSO solvent mixtures, with K_a = 210 M^{-1} measured for compound **103** with TBA dihydrogen phosphate. The lower affinity observed with compounds **104** (K_a < 2 M^{-1}) and **105** (130 M^{-1} in 5 % H_2O/DMSO) was attributed to steric factors. Additionally, solid state analysis revealed that the pyrrolic substituents in **105** formed intramolecular hydrogen-bonds to the amide carbonyl oxygen, resulting in unfavourable preorganisation of the receptor.[292] Additional hydrogen-bond donors were incorporated into the receptor scaffold, and the resulting urea compounds **106-108** were found to bind oxo-anions in MeOH-d_3, a highly competitive solvent. The introduction of additional pendant indole groups in **108** did not enhance anion affinity, but did increase selectivity towards dihydrogen phosphate.[293]

The role of preorganisation in this type of bisindole receptor appears to be very important. This was demonstrated by Gale and co-workers by changing the indole linker unit to a 2,2'-bipyridine (bipy) motif.[294] Compound **109**, which shows moderate affinity for dihydrogen phosphate in 0.5 % H_2O/DMSO-d_6 (K_a = 90 M^{-1}) can be preorganised by reaction with $PtCl_2(DMSO)_2$ to form complex **110** (**Figure 2.5**) Formation of the platinum complex prevents rotation about the pyridine-pyridine bond and consequently receptor **110** displays enhanced affinity for dihydrogen phosphate (K_a = 3640 M^{-1}) in the same solvent mixture.

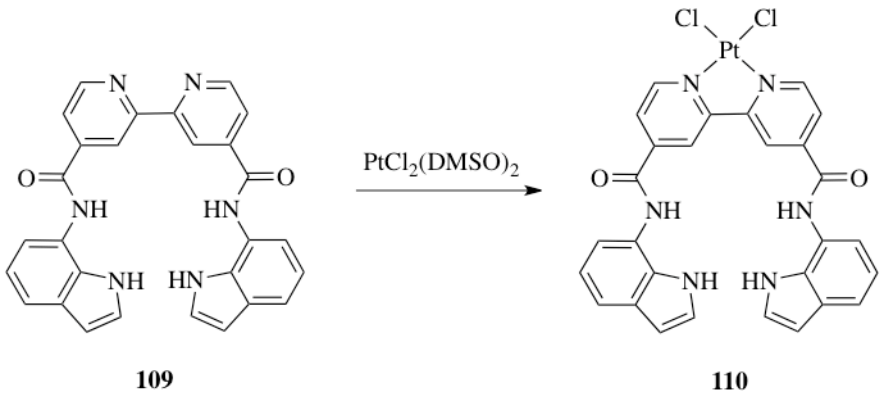

Figure 2.5: Preorganisation of receptor **109** is induced by the formation of a platinum complex.

In a similar set of studies inspired by the work of both Crabtree and Hunter, independent work by Gale and co-workers and Jurczak and co-workers explored different aromatic linker groups; pyrrole **111**, benzene **112**, and pyridine **113** (**Figure 2.6**).[295-298]

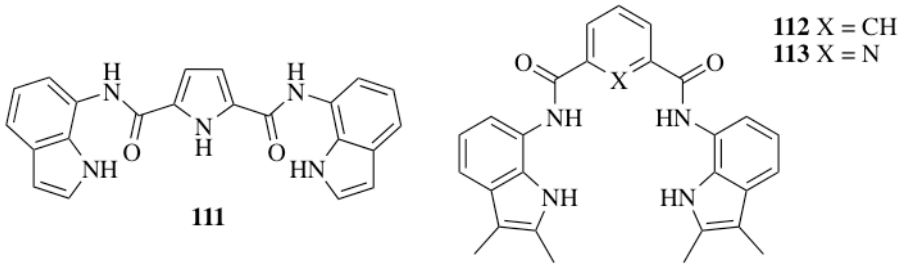

Figure 2.6: Bis(indole)s with indolyl groups connected by different linker functionalities. Compound **111** is shown in the *anti-anti* conformation.

Molecular modelling revealed that the lowest energy conformation of pyrrole compound **111** was the *anti-anti* conformer (**Figure 2.6**). The authors judged that strong intramolecular hydrogen-bonding and the consequent unfavourable host preorganisation diminished the supposedly advantageous addition of an extra hydrogen-bond donor group. Strong binding selectivity for fluoride over chloride was observed for compounds **112** and **113**, with the strong interaction between **113** and fluoride in 5 % H_2O/DMSO (K_a = 1360 M^{-1}) attributed to preorganisation of the binding cleft by intramolecular hydrogen-bonding. Solid state analysis of the fluoride and chloride complexes revealed that the fluoride ion was encapsulated by twisted conformations of receptors **112** and **113**; one indole positioned above the central aromatic ring and the other below, thus coordinating the fluoride ion with four hydrogen-bonds (an additional isophthalamide CH interaction was observed with **112**). The larger chloride ion was instead bound on one face of the receptors, coordinated by four hydrogen-bonding interactions (**Figure 2.7**).

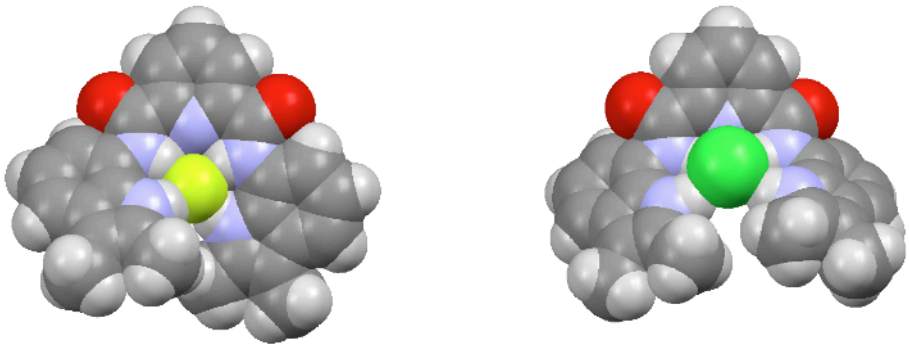

Figure 2.7: Spacefilling structures of the fluoride (left) and chloride (right) complexes of **113**; hydrogen (white), carbon (grey), nitrogen (blue), oxygen (red), fluorine (pale green), chlorine (green). TBA counterions have been omitted for clarity.[297]

Alternatively, pendant indole groups can be connected to the receptor scaffold using flexible *n*-pentyl or 1,3-dimethylphenyl linkers to give receptors **114-117** (**Figure 2.8**). These compounds exhibited moderate affinity for anions in 0.5 % H_2O/DMSO, with selectivity for oxo-anions and in particular dihydrogen phosphate, over halide anions.[299] The addition of electron withdrawing nitro functionalities was expected to increase stability constants but enhanced binding was only observed for acetate, presumable due to unfavourable steric interactions. Interestingly a combination of enhanced flexibility and

steric constraints imposed by the nitro substituents enabled compound **117** to bind dihydrogen phosphate as a cooperative 1:2 (host:guest) complex (K_{a1} = 108 M^{-1} and K_{a2} = 216 M^{-1}).

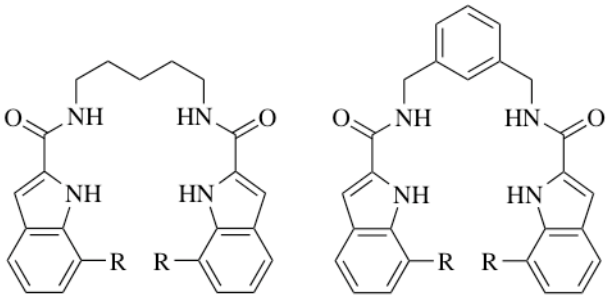

114 R = H
115 R = NO_2

116 R = H
117 R = NO_2

Figure 2.8: Bisindoles with flexible linker groups.

2.1.3 Diindolylureas as Anion Hosts

The development of bisindole scaffolds for anion binding has culminated in the investigation of the diindolylurea receptor scaffold. Using a urea as a linker unit has the advantage of providing two additional hydrogen-bond donor groups for anion coordination. Gale and co-workers synthesised diindolylureas **118** and **119** (**Figure 2.9**) and investigated their anion coordination properties.[300] These compounds were found to be selective for oxo-anions, with urea receptors **118** and **119** binding benzoate, acetate and dihydrogen phosphate with $K_a > 10^4$ M^{-1} in 0.5 % H_2O/DMSO-d_6. Further investigation revealed that all four compounds had the highest affinity for dihydrogen phosphate out of all the anions tested (chloride, acetate, benzoate, dihydrogen phosphate). Increasing the polarity of the solvent mixture to 25 % H_2O/DMSO-d_6 gave a binding constant for compound **118** with dihydrogen phosphate of 160 M^{-1}, whilst the additional methyl functionalities rendered compound **119** insoluble in this solvent mixture. Computer modelling of the dihydrogen phosphate complex of compound **118** revealed that in addition to the expected four hydrogen-bonding interactions between the receptor and the dihydrogen phosphate anion, favourable interactions between the indolyl hydrogen atoms in the 6- position and the urea oxygen stabilise the complex (**Figure 2.9**).

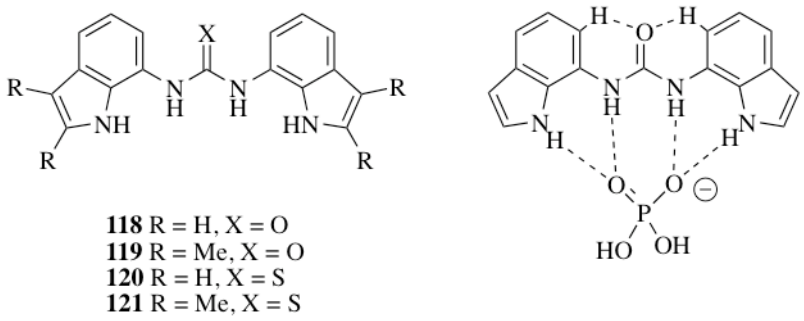

118 R = H, X = O
119 R = Me, X = O
120 R = H, X = S
121 R = Me, X = S

Figure 2.9: Indolylureas and indolylthioureas **118-121** and the calculated binding mode of receptor **118** to dihydrogen phosphate.

The X-ray crystal structure of the TBA benzoate complex of compound **119** reveals a 1:1 complex with the indole groups twisted with respect to one another. The benzoate anion is bound by four hydrogen-bonding interactions with N···O distances of 2.868-2.907 Å and N-H···O bond angles between 159-176 ° (**Figure 2.10**).

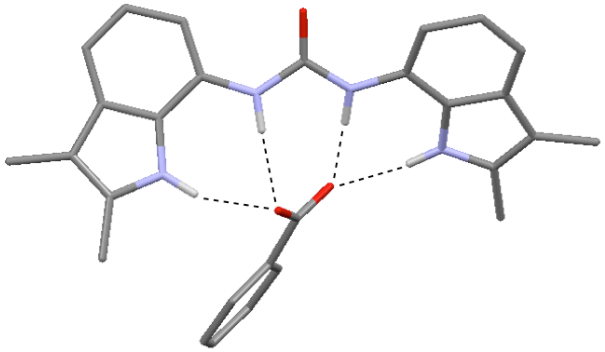

Figure 2.10: X-ray crystal structure of the complex formed by TBA benzoate and compound **119**, showing the benzoate anion bound by four hydrogen-bonding interactions. The ligand and guest anion are represented as wireframes; hydrogen (white), carbon (grey), nitrogen (blue), oxygen (red). TBA counterions and non-interacting hydrogen atoms have been omitted for clarity.[300]

Investigation of the analogous thiourea compounds **120** and **121** revealed that the thiourea compounds exhibited lower binding constants than their urea counterparts.[301] Despite apparently binding anions 1:1 in solution, solid state analysis revealed a range of binding stoichiometries. In the solid state compound **121** binds chloride 1:1, but forms a 2:2 complex with bicarbonate and as in the benzoate complex of **119**, the indole groups

adopted a twisted conformation. Crystal structures were also obtained with deprotonated anions. With TEA bicarbonate compound **119** formed a 2:1 (host:guest) carbonate complex, which was stabilised by eight hydrogen-bonds. With TBA dihydrogen phosphate compound **118** formed a 3:1 (host:guest) phosphate complex with the bound phosphate anion coordinated by twelve hydrogen bonds. Clearly, the large number of hydrogen-bonding interactions stabilises the formation of deprotonated anion complexes in the solid state.

Interesting tautomerisation was observed upon addition of acetate to a 0.5 % H_2O/DMSO-d_6 solution of the dibenzimidazole analogue of **118**, compound **122**.[302] At low concentrations acetate was bound primarily by the benzimidazole NH groups, but addition of more than two equivalents of acetate triggered a conformational change, resulting in acetate binding *via* both the urea and benzimidazole NH groups (**Figure 2.11**). Such conformational switching was also reported with sulphate and dihydrogen phosphate anions, but not with chloride and benzoate. The protonatable benzimidazole nitrogen facilitates stronger chloride binding under acidic conditions than with **118**, with solution phase nitrate binding also observed with the diprotonated complex. This type of switching behaviour increases selectivity for basic ions and demonstrates how such a scaffold can be 'tuned' to achieve anion selectivity.

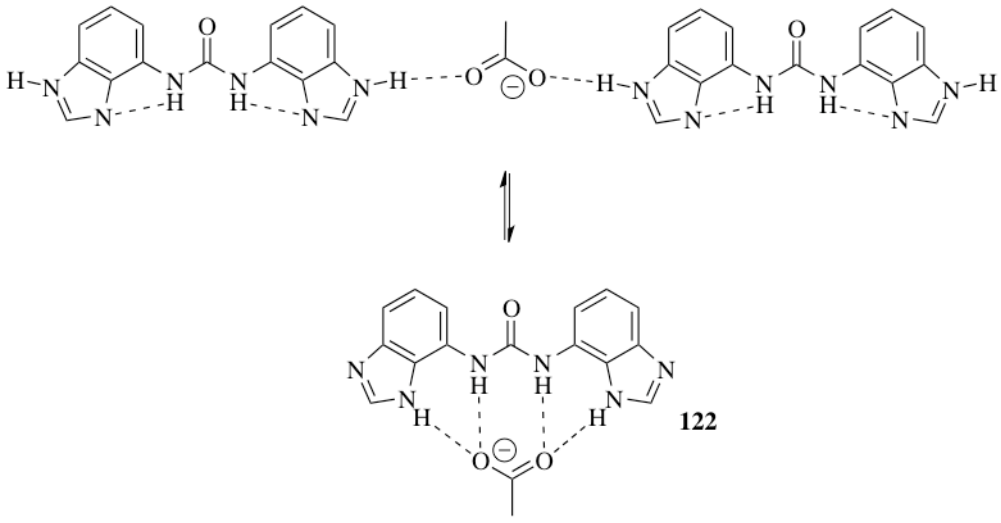

Figure 2.11: Acetate binding equilibrium for compound **122**.

Gale and co-workers have also investigated the anion complexation properties of carbazole containing receptors **123-128** (**Figure 1.12**).[303, 304] Like the aforementioned diindolylureas, urea compounds **123**, **125** and **127** displayed high affinity towards oxo-anions, with binding constants of > 10^4 M^{-1} measured with acetate and bicarbonate in 0.5 % H_2O/DMSO-d_6. Solid state analysis revealed similar anion binding modes to the aforementioned diindolyureas. The thiourea compounds **124**, **126** and **128** exhibited lower anion affinities than their analogous ureas. The authors rationalised that despite the increased acidity of the thiourea NHs relative to the urea, the size of the sulphur atom may force the thioureas to adopt a twisted conformation. The introduction of a fluorescent carbazole functionality permitted anion binding to be studied by fluorescence techniques. In 0.5 % H_2O/DMSO compound **123** functioned as a selective ON-OFF receptor for benzoate. The authors attributed the fluorescence quenching behaviour triggered by benzoate binding to π-π interactions in the excited state between the carbazole and benzoate aromatic electrons.

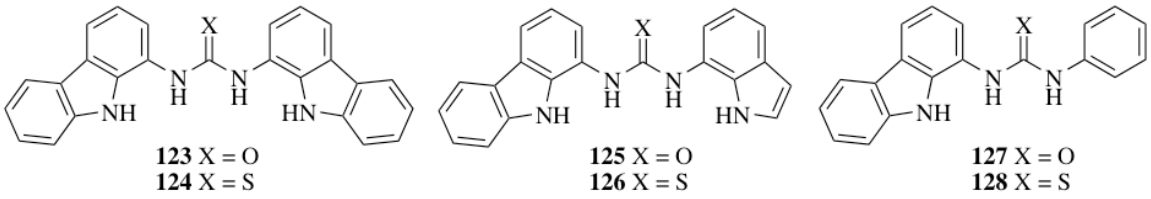

Figure 2.12: Carbazole functionalised ureas and thioureas **122-128**.

Gale and co-workers investigated potential applications for this type of anion receptor in the field of carbon dioxide fixation.[305, 306] Compounds **118**, **123** and **125** were found to stabilise alkylcarbamate anions formed by the reaction of carbon dioxide with amines (**Figure 2.13**).

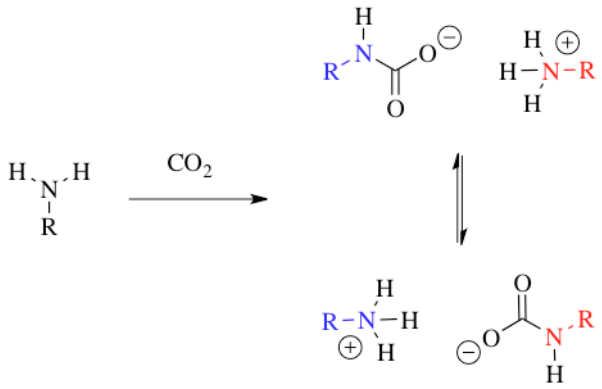

Figure 2.13: Rapid exchange of carbon dioxide between two amines.

The receptors were dissolved in DMSO and amines (*n*-butylamine, 1,3-diaminopropane or 1,4,5,6-tetrahydropyrimidine (THP)) were added. Carbon dioxide was then bubbled through the solution and receptor mediated stabilisation of the carbamate anion was assessed by monitoring changes in the urea NH chemical shift using ^{1}H NMR. Downfield shifts were observed in all instances, indicating binding and thus stabilisation of the carbamate anions through hydrogen-bonding to the receptors (**Figure 2.14**). The addition of 18-crown-6 was found to stabilise the cationic component of the system, leading to increased downfield shifts of the receptor NH groups upon addition of the carbamate to a solution of the receptor in DMSO-d_6. This stabilisation was clearly demonstrated in the solid state; a crystal structure of the complex formed between the amide appended diindolylurea **129,** 18-crown-6 and the 1,3-diaminopropane zwitterion shows the crown ether binding to the ammonium group and receptor **129** hydrogen-bonding to the carbamate anion, with one amide side chain orientated to accept a hydrogen-bond from the carbamate NH group. This finding demonstrates that pendant amide functionalities can be used to achieve additional interactions with anions bound by the diindolylurea cleft, and has led to the development of the amide functionalised diindolylureas described in **Section 2.2**.

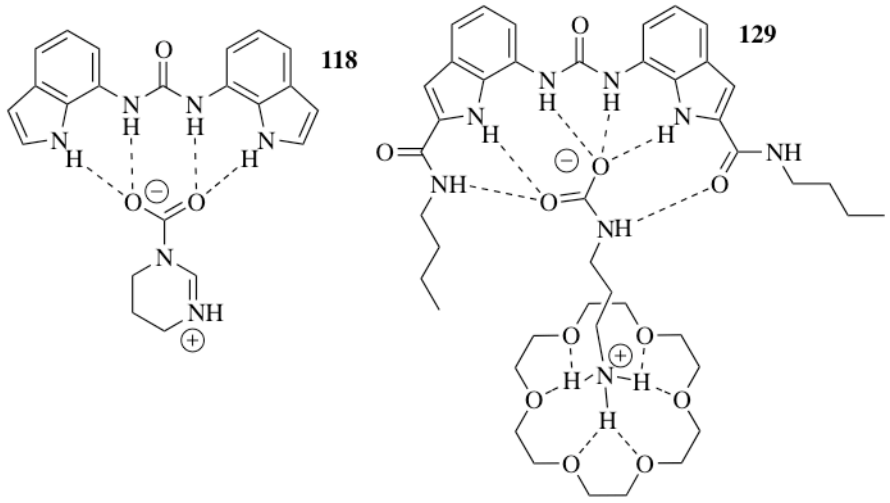

Figure 2.14: Proposed mode of carbamate stabilisation; zwitterionic THP carbamate bound by diindolylurea **118** (left) and the alkylammonium-alkylcarbamate zwitterion formed by reaction of 1,3-diaminopropane with carbon dioxide stabilised by hydrogen-bonding interactions with both diindolylurea **129** and 18-crown-6 (right).

2.1.4 Tripodal Scaffolds in Anion Recognition

Tripodal scaffolds have been widely used in use in the construction of anion hosts. The use of the 1,3,5-trialkylbenzene cores to create tripodal anion receptors is well examined. Ghosh and co-workers have produced nitro-functionalised receptors **130** and **131** (**Figure 2.15**) that show interesting anion complexation behaviour in the solid state.[307, 308] Crystallographic analysis of the complexes formed by compound **130** with acetate, fluoride and chloride reveal the formation of dimeric capsules each containing two anions and hydrating water molecules. The *ortho*-nitro functionalities in compound **131** inhibit capsule formation, and it instead forms non-capsular aggregates with chloride, nitrate and acetate, and only forms a dimeric capsule with fluoride. The covalent linkage of such dimeric capsules can lead to the development of more rigid structures, that similarly function as an anion hosts.[309] An interesting application of tripodal receptors bearing a trialkylbenzene core was demonstrated by Anzelbacher and co-workers.[310] The attachment of fluorophores to the trialkylbenzene scaffold *via* a urea or thiourea linkage produced tripodal receptors capable of binding multiple phosphate anions. Fluorescence amplification was observed upon phosphate complexation, which the authors attributed to restriction of conformational freedom within the receptor. Embedding this type of receptor within polyurethane films produced an array for the detection of biologically

relevant phosphates in blood serum. Gunnlaugsson and co-workers have also demonstrated that a simple aromatic scaffold can yield tripodal receptors that display good anion affinity in DMSO-d_6.[311] The attachment of urea-amide pendant arms onto the phenyl core resulted in the construction of compounds such as **132**. This compound displays good affinity for dihydrogen phosphate and acetate in DMSO-d_6 (16000 M^{-1} and 620 M^{-1}). The role of the amide NHs in anion binding appears less significant than the urea groups, with only small changes observed in the chemical shifts of the amide NH groups. Molecular modelling also suggested that only the urea NH groups are directly involved in anion binding.

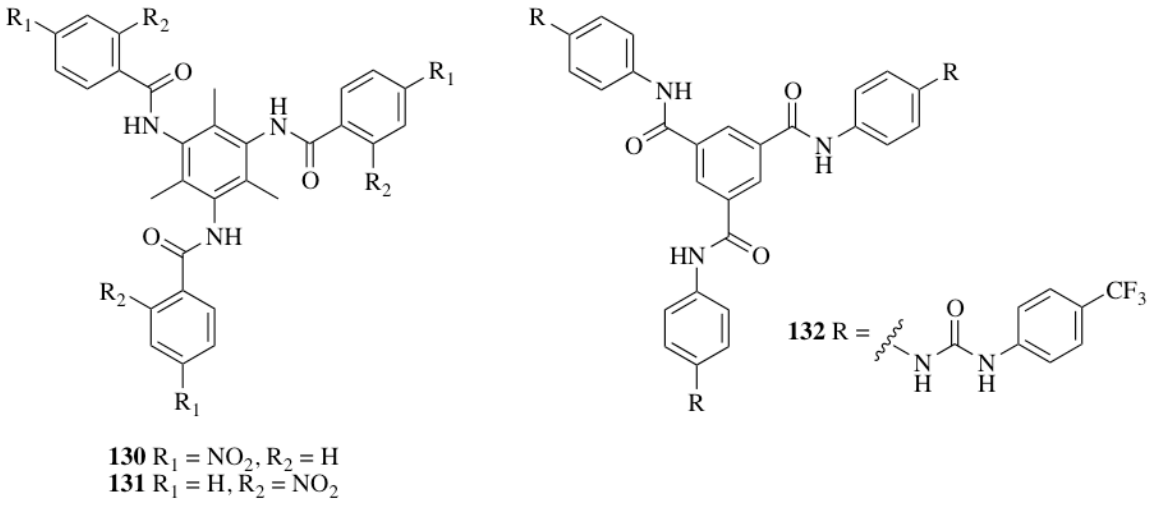

130 $R_1 = NO_2, R_2 = H$
131 $R_1 = H, R_2 = NO_2$

Figure 2.15: Tripodal receptors **130-132** containing an aromatic core.

The construction of receptors that adopt bowl conformations can also be achieved with a cyanuric acid core. Ghosh and co-workers have demonstrated that the attachment of pentafluorphenylurea arms to this scaffold yields compound **133**, a receptor that selectively binds sulphate over dihydrogen phosphate, acetate and chloride in DMSO-d_6 (**Figure 2.16**).[312] Sulphate (added as the TBA salt) is bound by six hydrogen-bonding interactions to the urea NH groups ($K_a > 10^4$ M^{-1}). At 298 K two TBA counter ions cap the complex, forming a contact ion-pair. These cations coordinate to the sulphate anion through a total of five C-H···O interactions.

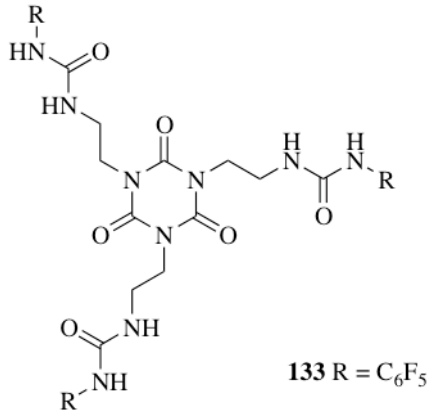

Figure 2.16: Tripodal cyanuric sulphate receptor **133**.

Jolliffe and co-workers have developed the use of cyclic peptides as a scaffold for the attachment of pendant urea and thiourea functionalities.[313] ^{1}H NMR titrations reveal that tripodal urea **134** (**Figure 2.17**) is a high affinity, selective receptor for sulphate ($K_a > 10^4$ M^{-1} in 10 % DMSO-d_6/$CDCl_3$), with the observed changes in chemical shift indicating that the tetrahedral sulphate anion is bound by a total of nine hydrogen-bonding interactions with both urea and amide NH groups. The peptide NH groups were found to only interact with tetrahedral anions such as sulphate, dihydrogen phosphate and hydrogen sulphate. Dilution studies revealed that **134** can self-associate, with intermolecular hydrogen-bonding between urea functionalities facilitating dimerisation.

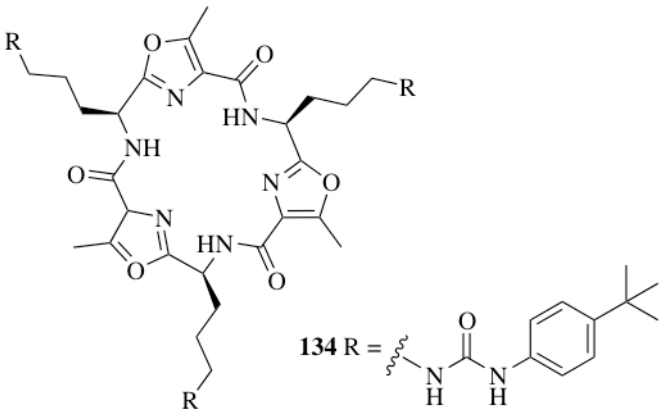

Figure 2.17: Tripodal anion host with a cyclic peptide core.

2.1.5 Tripodal Tris(2-aminoethyl)amine Based Anion Hosts

The tris(2-aminoethyl)amine core provides a tripodal scaffold for the construction of anion hosts and contains a protonatable tertiary nitrogen, facilitating the construction of receptors that can coordinate anionic species through a combination of electrostatic and hydrogen-bonding interactions. Amide substituted compounds such as **135**-**142** (**Figure 2.18**) are one of the simplest types of anion host that can be built using the tris(2-aminoethyl)amine scaffold.[314] In the solid state protonation of the tertiary nitrogen in compound **135** results in intramolecular hydrogen-bonding between the alkyl ammonium NH group and an amide oxygen atom, occluding the binding cavity.[315] Smith and co-workers investigated the ability of structurally related tripodal amides **136**-**141** to facilitate H^+/Cl^- symport in a series of U-tube experiments (see **Section 1.9.6**). By monitoring the pH of the aqueous receiving phase, the transport of protons across the DCM organic phase could be detected.[316] The authors judged that H^+/Cl^- transport rates within the series were determined by the degree of encapsulation afforded by the HCl binding site, with longer alkyl substituents more effectively screening the anion from the apolar membrane interior. The addition of phenyl substituents onto the tripodal amide scaffold was achieved by Ghosh and co-workers through the synthesis of *ortho*-nitrophenyl substituted amide **142**.[317] Solution phase studies in DMSO-d_6 revealed that **142** is a selective host for fluoride (over chloride, bromide, iodide, dihydrogen phosphate, nitrate and perchlorate), binding the fluoride anion using a combination of NH and aromatic CH hydrogen-bond donor groups. X-ray crystal structures of the complexes of protonated **142** with perchlorate and hexafluorosilicate anions revealed that these large anions were not encapsulated by the receptor, but were instead were bound peripherally.

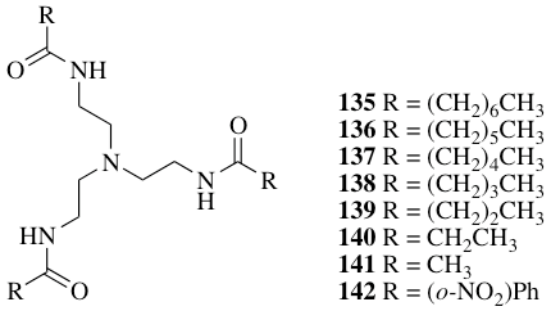

Figure 2.18: Tripodal amides **135**-**142**.

Replacing the amide functionality with a urea endows the receptor with additional NH hydrogen-bond donor groups that are suitably orientated to achieve tetrahedral anion complexation.[318] Expanding the size of the anion binding cavity by increasing the length of the alkyl core linkages has been shown to be detrimental to anion binding as the increased receptor flexibility results in a favoured open receptor conformation.[319] Alternative strategies to tune receptor selectivity must therefore be adopted.[320]

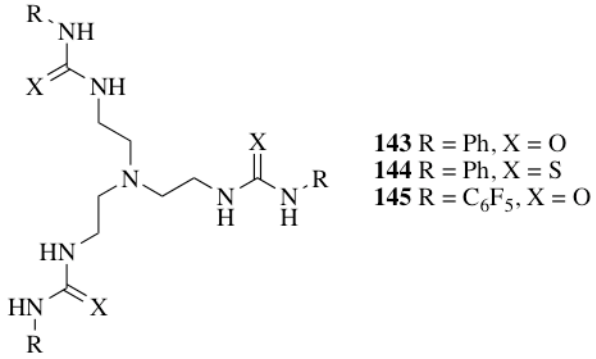

Figure 2.19: Tripodal ureas/thioureas **143**-**145**.

NH group acidity can be modified through the use of a thiourea functionality in place of the urea (compound **144**) or by the introduction of electron withdrawing substituents onto the urea scaffold, as demonstrated with tripodal pentafluorophenyl substituted urea **145** (**Figure 2.19**).[321, 322] The increased urea NH acidity of pentafluorophenyl substituted urea **145** combined with stabilising anion-π interactions yielded unique anion complexation behaviour.[323] Solution phase binding studies in

DMSO-d_6 revealed 1:1 binding interactions with halides, dihydrogen phosphate and acetate, whilst 2:1 (host:guest) binding stoichiometry was observed with sulphate and bicarbonate, with anion affinity following the Hofmeister series.[324, 325] Tripodal urea **145** has been found to complex fluoride, sulphate, dihydrogen phosphate and carbonate in the solid state through a variety of binding modes.[324, 325] Fluoride is bound as a 1:1 complex in the solid state with the encapsulated fluoride ion bound by six hydrogen-bonding interactions with urea NH groups (**Figure 2.20**).

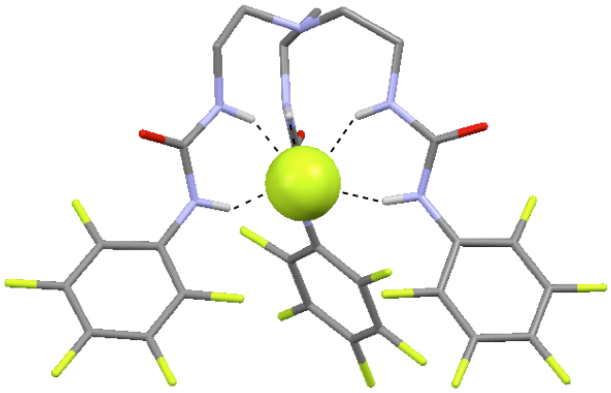

Figure 2.20: Crystal structure of the 1:1 fluoride complex of **145**. The ligand is represented as a wireframe and the guest anion is represented as a spacefilling model (0.6 times van der Waals radius); hydrogen (white), carbon (grey), nitrogen (blue), oxygen (red), fluorine (pale green). TBA counterions and non-interacting hydrogen atoms have been omitted for clarity.[324]

Sulphate is bound as the 2:1 (host:guest) complex, with all twelve urea NH groups involved in sulphate binding. Carbonate is also bound by all twelve urea NH groups as a 2:1 (host:guest) complex, and in both cases the two host molecules forming the 'capsule' are held together by π-π interactions between pentafluorophenyl substituents. In contrast, dihydrogen phosphate is bound in the solid state as a '2+2' complex (**Figure 2.21**), the tripodal urea **145** forms a dimeric cage hosting a dihydrogen phosphate dimer. Each dihydrogen phosphate is bound to its dimeric partner by two hydrogen-bonding interactions, and is bound to the tripodal hosts by a combination of hydrogen-bonding interactions with the urea NH groups, and anion-π interactions with the electron deficient pentafluorophenyl rings.

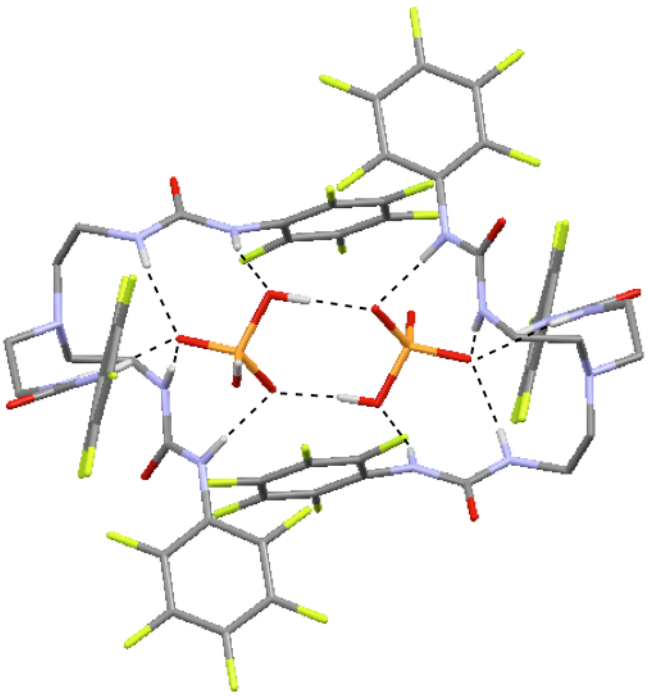

Figure 2.21: X-ray crystal structure of '2+2' dihydrogen phosphate complex of **145**. The ligands and guest anions are represented as wireframes; hydrogen (white), carbon (grey), nitrogen (blue), oxygen (red), fluorine (pale green), phosphorous (orange). TBA counterions and non-interacting hydrogen atoms have been omitted for clarity.[323]

The encapsulation of sulphate by tripodal compounds has been used in the assembly of metal organic frameworks. Tripodal compounds with pyridyl or cyanophenyl urea substituents (compounds **146** and **147** respectively, **Figure 2.22**) can coordinate to hydrated metal clusters, resulting in the formation of three dimensional extended networks in the solid state.[326-330] Both 1:1 and 2:1 (host:guest) sulphate complexes have been observed, with the nature of the secondary coordination sphere dictating binding stoichiometry.[328] Typically, the six urea NH groups on each tripodal scaffold are directed inwardly towards a tetrahedral sulphate ion, forming a 2:1 (host:guest) sulphate complex stabilised by twelve hydrogen-bonding interactions. The high stability of this complex is exemplified by competitive crystallisation experiments wherein the 2:1 sulphate complex is formed even in the presence of carbonate and selenate anions.[326] 2:1 (host:guest) sulphate complexation has also been noted in a range of other tripodal scaffolds, including *para*-nitrophenyl substituted tripodal urea **148** (**Figure 2.22**), which forms a

unique sulphate-$(H_2O)_3$-sulphate adduct.[331, 332] Slow evaporation of an acetonitrile solution of the analogous thiourea **149** (**Figure 2.22**) and TBA dihydrogen phosphate yielded a 2:1 (host:guest) complex with the deprotonated phosphate anion (PO_4^{3-}) as the bound guest.[333] The bound phosphate is stabilised by twelve hydrogen-bonding interactions to the twelve thiourea NH groups, with the capsule stabilised by two separate π-stacking interactions. ^{1}H NMR solution phase analysis in DMSO-d_6 revealed slow exchange behaviour upon addition of TBA dihydrogen phosphate to a solution of **149**. The authors rationalised that the receptor initially complexes dihydrogen phosphate ($H_2PO_4^-$), but beyond addition of more than one equivalent of the anion a 2:1 (host:guest) complex with the deprotonated phosphate anion (PO_4^{3-}) is formed. Deprotonation of the bound dihydrogen phosphate is facilitated by hydrogen-bonding activated proton transfer between the free and bound dihydrogen phosphate.

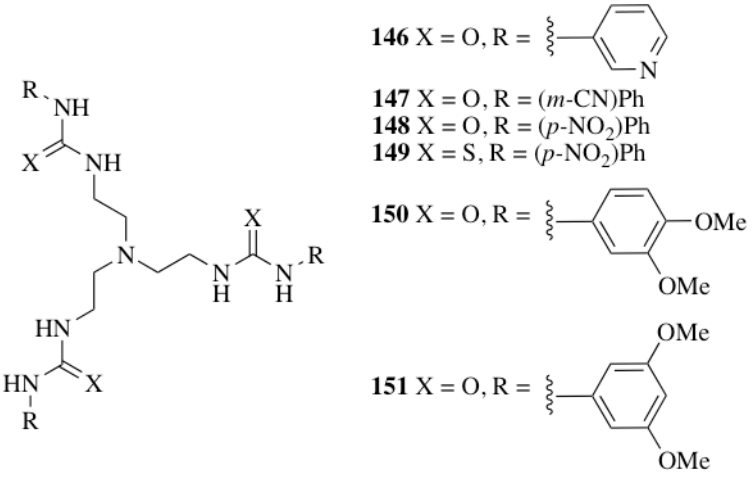

Figure 2.22: Tripodal ureas **146-151**.

Owing to the interesting ion complexation behaviour observed with tripodal ureas, the use of these compounds as anion extractants has been explored. Compounds **150** and **151** (**Figure 2.22**) were found to facilitate the extraction of the hexachloroplatinate anion ($PtCl_6^{2-}$) from aqueous solution into chloroform under acidic conditions.[334, 335] Protonation of the tris(2-aminoethyl)amine bridgehead nitrogen atoms in the 2:1 (host:guest) complex created a neutral species that was soluble in organic solvents,

facilitating high recovery of the platinum species (> 90 %).[334] In light of the above, amide functionalised diindolylureas and tripodal tris(2-amino)ethyl (thio)ureas were investigated as anion hosts and anion transport agents.

2.2 Amide Substituted Diindolylureas as Anion Hosts

Two 1,3-diindolylurea compounds, **152** and **153**, have been synthesised and their solution phase anion binding behaviour was examined by ^{1}H NMR titration techniques. The pyridyl diindolylurea **153** was synthesised in an attempt to achieve additional hydrogen-bonding interactions with anions containing hydrogen-bond donor groups.[336] These compounds possess amide substituents at the 2- position of the indole ring, introducing an additional pair of NH hydrogen-bond donor motifs onto the scaffold.[287, 337] In addition the X-ray crystal structure of compound **152** with TBA benzoate is discussed along with the anion transport properties of compounds **152** and **153**, and structurally related compounds **154** and **129 (Figure 2.23)**.

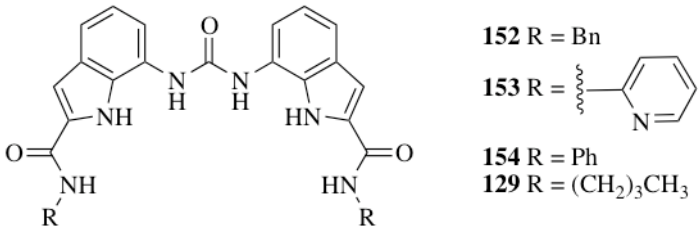

Figure 2.23: Diindolylureas with pendant amide functionalities.

2.2.1 Synthesis

Compounds **152** and **153** were synthesised by a 1,1'-carbonyldiimidazole (CDI) coupling reaction between commercially available 7-nitroindole-2-carboxylic acid and either benzylamine or 2-aminopyridine. The 2-carboxamido-7-nitroindole derivatives were obtained in yields of 90 % and 80 % respectively. The nitro compounds were reduced using hydrogen and a Pd/C catalyst in ethanol to afford the amines, which were coupled using triphosgene in a two phase DCM/$NaHCO_3$ (aq) mixture (**Figure 2.24**).[338] Compounds **152** and **153** were afforded in 56 % and 55 % yields respectively. Compounds **154** and **129** were synthesised by J. R. Hiscock.

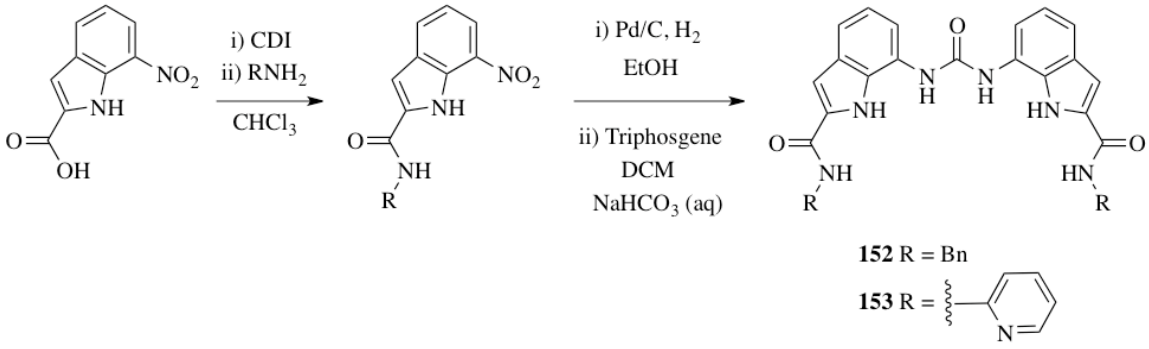

Figure 2.24: Synthetic scheme for diindolylureas **152** and **153**.

2.2.2 Anion Binding Studies

Stability constants for compounds **152** and **153** with a range of anionic guests were determined using ^{1}H NMR titration techniques in both 0.5 % H_2O/DMSO-d_6 and 10 % H_2O/DMSO-d_6.[339] Stability constants were obtained by curve fitting using WinEQNMR2 computer software (see **Appendix A2.1** for fitted curves).[340] The results of these studies are shown in **Tables 2.1** and **2.2**.

Anion [a]	Indole CH (0.5 % H_2O)	Urea NH (0.5 % H_2O)	Indole CH (10 % H_2O)	Urea NH (10 % H_2O)
Cl^-	[b]	[c]	[d]	[d]
BzO^-	1490	1580	368	284
AcO^-	$> 10^4$	$> 10^4$	278	293
$H_2PO_4^-$	[e]	[c]	2960	812
HCO_3^-	1420	[c]	319	[c]

Table 2.1: Apparent stability constants K_a (M^{-1}) determined by ^{1}H NMR titration techniques with compound **152** in H_2O/DMSO-d_6 mixtures at 298 K following urea NH and indole CH (6-position) groups. Data fitted to a 1:1 binding model. Errors < 15 %. [a] Added as TBA salts, except bicarbonate which was added as the TEA salt. [b] No significant interaction. [c] Peak broadening. [d] Not determined. [e] Isotherm could not be fitted to a 1:1 or a 1:2 binding model.

Anion [a]	Indole CH (0.5 % H_2O)	Urea NH (0.5 % H_2O)	Indole CH (10 % H_2O)	Urea NH (10 % H_2O)
Cl^-	[b]	<10	[c]	[c]
BzO^-	2430 (± 19%)	4760	298	304
AcO^-	> 10^4	> 10^4	485	544
$H_2PO_4^-$	[d]	[e]	2560	128
HCO_3^-	7660	[e]	149	[e]

Table 2.2: Apparent stability constants K_a (M^{-1}) determined by ^1H NMR titration techniques with compound **153** in H_2O/DMSO-d_6 mixtures at 298 K following urea NH and indole CH (6-position) groups. Data fitted to a 1:1 binding model. Errors < 15 % unless stated otherwise. [a] Added as TBA salts, except bicarbonate which was added as the TEA salt. [b] No significant interaction. [c] Not determined. [d] Isotherm could not be fitted to a 1:1 or a 1:2 binding model. [e] peak broadening

The stability constants obtained for the carboxylate anions generally show a good agreement between the values obtained from the shift of the urea NH protons and the values determined from the shift of the indole CH protons in the indole 6- position. The receptors were found to have a low affinity for chloride in the solvent mixtures tested, but did display high affinity towards the oxo-anions studied. Binding isotherms for the carboxylate anions fitted a 1:1 binding model, however the binding of dihydrogen phosphate appeared more complex and could not be adequately fitted to a suitable binding model in some instances.

Examination of the change in chemical shift of the indole, urea and amide NH protons upon addition of the various anions reveals details of the anion binding modes (see **Appendix A4.1**). With chloride, no significant interaction was observed with compound **152**, but with compound **153** a downfield shift of the urea NHs was observed. Strong binding interactions with the carboxylate anions (benzoate and acetate) were observed for both compounds; the indole and urea NH groups are shifted downfield, but the amide NH groups do not exhibit a significant downfield shift. This suggests a binding mode such as that displayed in **Figure 2.25**. Significant NH broadening prevents clear determination of the bicarbonate binding mode, however it appears that the indole and urea NH groups are predominantly responsible for bicarbonate complexation. Similar broadening is observed with dihydrogen phosphate, however in the case of compound **152** significant amide NH downfield shifts are observed in both 0.5 % H_2O/DMSO-d_6

and 10 % H_2O/DMSO-d_6 solvent mixtures, suggesting a possible binding mode utilising all six NH hydrogen bond donors (**Figure 2.25**).

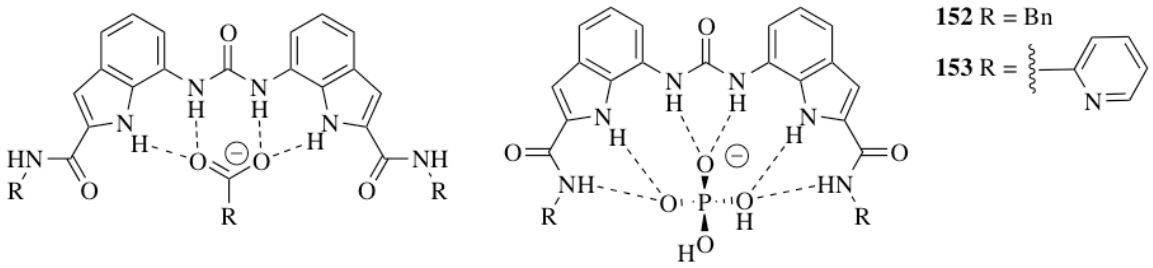

Figure 2.25: Possible anion binding modes of diindolylureas **152** and **153**.

A recent NMR study by Plavec and co-workers examined the conformations adopted by diindolylurea **118** and compound **154** upon addition of anion salts in DMSO-d_6.[341] The *anti-anti* conformer of **118** predominates in solution in the absence of anions, whilst examination of Nuclear Overhauser Effect (NOE) enhancements led the authors to conclude that the *syn-anti* conformation is adopted in the presence of chloride. Oxo-anions such as acetate, benzoate and dihydrogen phosphate induced anion binding by the *syn-syn* conformer. Significant peak broadening hindered the conformational study of compound **154**, although the behaviour of the diindolylurea core in compounds **152**-**154** is likely to be analogous to that of compound **118** (**Figure 2.26**). Significantly, NOE experiments indicated that the amide protons in compound **154** do not interact with carboxylate ions. The authors postulated that this lack of interaction (mirrored in the chemical shift changes of compounds **152** and **153**) is the consequence of strong carboxylate binding to the urea NH protons, preventing interaction with the amide NH groups.

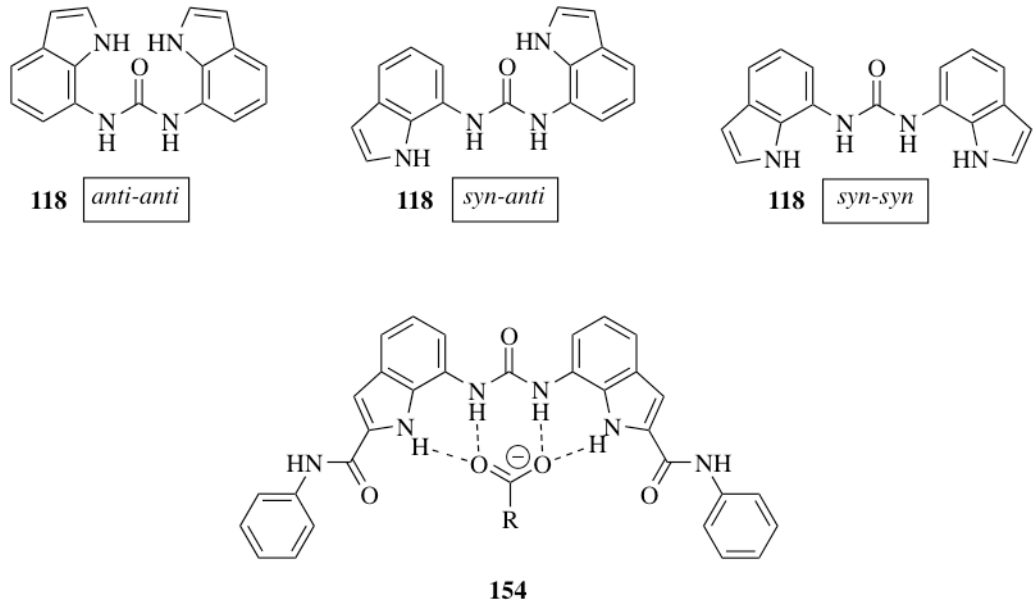

Figure 2.26: Possible conformations of diindolylurea **118** and the carboxylate binding conformation of **154** observed by NOE experiments in DMSO-d_6.

J. R. Hiscock studied the solution phase and solid state anion binding properties of compounds **154** and **129** and found that compound **129** exhibits slow exchange behaviour upon titration with TBA dihydrogen phosphate. This behaviour was attributed to the receptor binding of dihydrogen phosphate lowering the pKa of the bound species, resulting in deprotonation of the bound anion upon addition of further equivalents of TBA dihydrogen phosphate.[342] The broadening of the NH resonances upon addition of dihydrogen phosphate or a binding isotherm that could not be fitted to a suitable binding model with compounds **152** and **153** suggests that proton transfer processes may also be occurring, but that the equilibrium between the monohydrogen phosphate and dihydrogen phosphate complexes is not slow on the NMR timescale.

2.2.3 Solid State Studies

Crystals of compound **152** with TBA benzoate were obtained by slow evaporation from DMSO. X-ray crystal structure analysis on these crystals was performed by M. E. Light (see **Appendix A3.1**). In the solid state two independent hydrogen-bonded chains were observed. A single benzoate ion was bound within the diindolylurea 'cleft' by hydrogen-bonding interactions with urea and indolyl NH groups (**Figure 2.26**). Urea N-

H···O distances varied between 2.800(9)-2.846(9) Å with NHO bond angles between 168.0-171.4 °, whilst indolyl NH···O distances varied between 2.799(9)-2.809(8) Å with NHO bond angles between 144.1-160.1 °. The amide NH groups were found to point outside of the binding "cleft", coordinating to an additional peripheral benzoate ion. Amide N-H···O distances varied between 2.774(10)-2.869(11) Å with NHO bond angles between 149.0-165.0 °. This structure supports the proposed carboxylate binding model illustrated in **Figure 2.25**, with the indolyl and urea NH groups primarily responsible for carboxylate anion complexation.

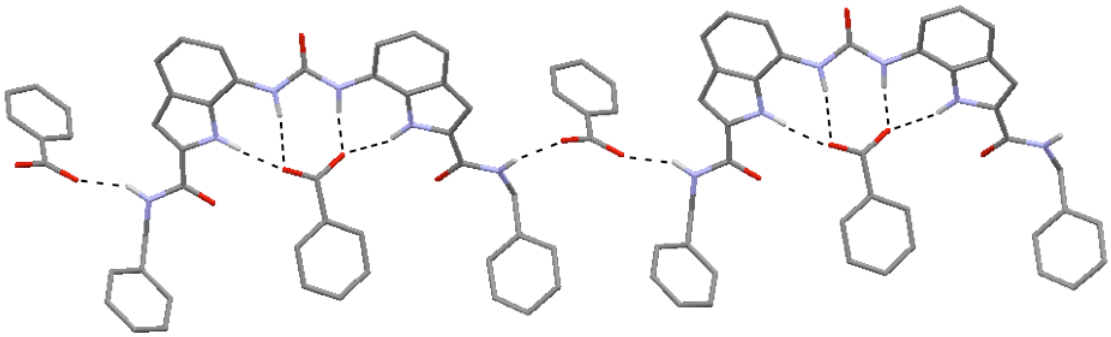

Figure 2.27: X-ray crystal structure of part of one of the two independent hydrogen bonded chains of the complex formed between compound **152** and TBA benzoate. Ligands and guest anions are represented as wireframes; hydrogen (white), carbon (grey), nitrogen (blue), oxygen (red). TBA counterions and non-interacting hydrogen atoms have been omitted for clarity.

2.2.4 Ion Transport Studies

Owing to the promising solution phase anion binding properties of compounds **152**, **153**, **154** and **129**, these compounds were tested for the ability to transport anions across phospholipid bilayers. Diindolylurea **118** (**Figure 2.28**) was synthesised by J. R. Hiscock and was tested to evaluate the impact of the additional amide substituents on transport activity.[300] POPC vesicles were prepared containing 488 mM NaCl buffered to pH 7.2 with 5 mM sodium phosphate salts, suspended in 488 mM $NaNO_3$. To initiate the experiment compounds **152**, **153**, **154**, **129** or **118** were added as solutions in DMSO at loadings of 2 mol % (with respect to lipid). Chloride efflux from the vesicles was measured using a chloride ISE and at the end of the experiment the vesicles were lysed with detergent to calibrate the ISE to 100 % chloride efflux. Of the amide substituted

compounds tested, only butyl functionalised compound **129** facilitated significant chloride release (**Figure 2.29**). Even in this instance, the transport activity was comparable with unfunctionalised diindolylurea **118**.

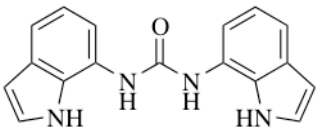

118

Figure 2.28: Diindolylurea **118** served as a control compound for the ion transport assays.

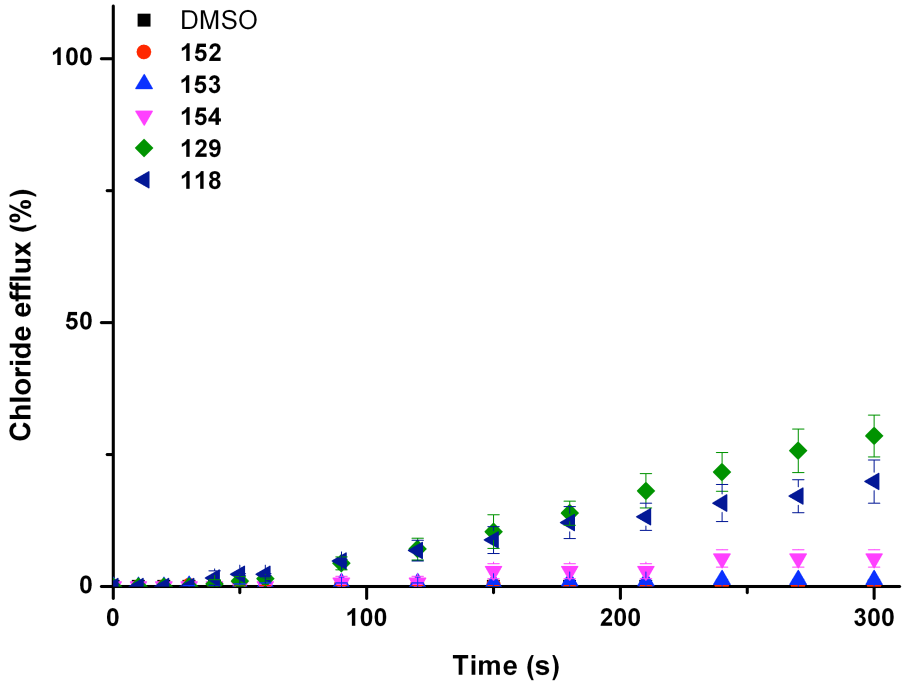

Figure 2.29: Chloride efflux promoted by addition of receptors **152**, **153**, **154**, **129** and **118** (2 mol % with respect to lipid) from unilamellar POPC vesicles loaded with 488 mM NaCl buffered to pH 7.2 with 5 mM sodium phosphate salts and suspended in 488 mM $NaNO_3$ buffered to pH 7.2 with 5 mM sodium phosphate salts. At the end of the experiment, detergent was added to lyse the vesicles and calibrate the ISE to 100 % chloride efflux. Each point represents an average of three trials.

To assess the ability of compounds **152**, **153**, **154** and **129** to facilitate Cl^-/HCO_3^- antiport, these compounds were added to POPC vesicles containing 451 mM NaCl buffered to pH 7.2 with 20 mM sodium phosphate salts, suspended in 150 mM Na_2SO_4

buffered to pH 7.2 with 20 mM sodium phosphate salts. At t = 120 s a 'pulse' of $NaHCO_3$ was added such that the external concentration of bicarbonate was 40 mM. Chloride efflux from the vesicles was measured using a chloride ISE and at the end of the experiment the vesicles were lysed with detergent to calibrate the ISE to 100 % chloride efflux. Diindolylurea **118** was again used as a control to assess the contribution of the amide substituents to transport activity. None of the compounds facilitated significant chloride efflux in this assay (**Figure 2.30**), suggesting that the enhanced lipophilicity of bicarbonate relative to nitrate (see **Section 1.1**) may hinder transport *via* an antiport mechanism with these compounds.

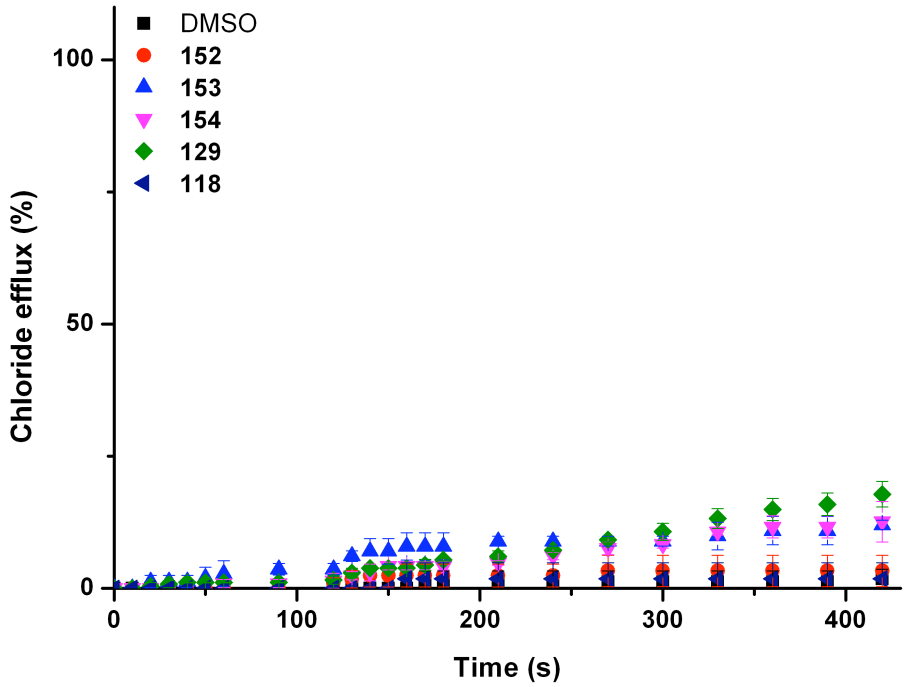

Figure 2.30: Chloride efflux promoted by addition of receptors **152**, **153**, **154**, **129** and **118** (2 mol % with respect to lipid) from unilamellar POPC vesicles loaded with 451 mM NaCl buffered to pH 7.2 with 20 mM sodium phosphate salts upon addition of a $NaHCO_3$ 'pulse' such that the extravesicular concentration of bicarbonate was 40 mM. The vesicles were suspended in 150 mM Na_2SO_4 buffered to pH 7.2 with 20 mM sodium phosphate salts. At the end of the experiment, detergent was added to lyse the vesicles and calibrate the ISE to 100 % chloride efflux. Each point represents an average of three trials.

In summary, solution phase binding studies show that compounds **152** and **153** exhibit good affinity for oxoanions in H_2O/DMSO-d_6 mixtures. Examination of the

changes in chemical shift indicates that binding modes such as those in **Figure 2.24** may be adopted in solution. This suggests that upon binding carboxylate anions the amide NH groups are not orientated towards the binding 'cleft'. The anion transport properties of diindolylurea compounds **152**, **153**, **154**, **129** and **118** have been examined and indicate that these compounds display poor activity in Cl^-/NO_3^- and Cl^-/HCO_3^- antiport assays, with the additional amide hydrogen-bond donor functionalities having little effect on the transport activity of the diindolylurea scaffold. This is perhaps unsurprising, as the amide NH groups were not observed to interact with either chloride or bicarbonate anions in the solution phase binding studies. The low levels of chloride efflux facilitated by compounds **129** and **118** suggest that upon further modification the indolylurea motif may hold potential as a transporter functionality (see **Chapter 3**).

2.3 Tripodal Molecules for Anion Complexation

Tripodal tris(2-amino)ethyl receptors **155**,[314, 319, 335] **156**,[343, 344] **143**,[314, 318, 324, 334, 335, 345] and **144** [318, 346] (**Figure 2.31**) were synthesised by N. Busschaert and thiourea compounds **156** and **144** were found to be potent anion transport agents, facilitating Cl^-/HCO_3^- antiport in phospholipid vesicles (see **Section 2.3.3**).[347] In this instance the tripodal thioureas are more lipophilic than their analogous ureas (see **Appendix A4.1**). To provide insights into the observed transport activity the solution phase anion binding properties were examined by ^{1}H NMR titration techniques, and anion complexation in the solid state was examined by X-ray crystallography.

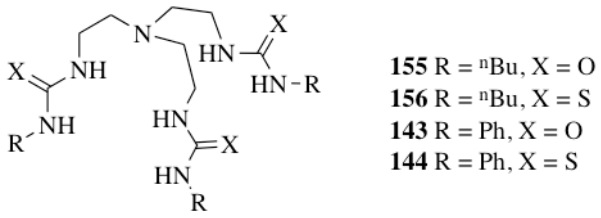

155 R = ^{n}Bu, X = O
156 R = ^{n}Bu, X = S
143 R = Ph, X = O
144 R = Ph, X = S

Figure 2.31: Tripodal ureas and thioureas.

2.3.1 Anion Binding Studies

The solution phase anion binding properties of compounds **155**, **156**, **143** and **144** were examined by ^{1}H NMR titration in 0.5 % H_2O/DMSO-d_6 with a range of anions. Stability constants were obtained by curve fitting using WinEQNMR2 computer software (see **Appendix A2.1** for fitted curves).[340] The results of this study are displayed in **Table 2.3**.

Anion [a]	**155**	**156**	**143**	**144**
Cl^-	655 [b]	440	777 [b]	191 [b]
NO_3^-	[c]	[c]	[c]	[c]
HCO_3^-	[d]	451	[d]	[e]
$H_2PO_4^-$	3450	540	$> 10^4$	[e]
SO_4^{2-}	$> 10^4$	$> 10^4$	$> 10^4$	$> 10^4$

Table 2.3: Apparent stability constants K_a (M^{-1}) determined by ^{1}H NMR titration techniques with compounds **155**, **156**, **143** and **144** in 0.5 % H_2O/DMSO-d_6 at 298 K following the most downfield urea/thiourea NH group. Data fitted to a 1:1 binding model. Errors < 15 %. [a] Added as TBA salts, except bicarbonate which was added as the TEA salt. [b] Fitted using raw data collected by N. Busschaert. [c] No significant interaction. [d] Binding isotherm did not fit available binding models. [e] Significant broadening of NH signals.

The results show that in all cases receptors **155**, **156**, **143** and **144** bind sulphate strongly with $K_a > 10^4$ M^{-1}. High stability constants were measured for compounds **155**, **156**, **143** and **144** with chloride, the tripodal architecture showing enhanced chloride affinity compared to the diindolylurea motif in compounds **152** and **153** which also contains six NH hydrogen-bond donors (see **Section 2.2**). Job plot analysis with chloride, sulphate and dihydrogen phosphate (in the absence of peak broadening) confirmed 1:1 binding stoichiometry. Titrations with bicarbonate showed significant downfield NH shifts, but only with compound **156** could the data be adequately fitted to a 1:1 binding model. Job plot analysis suggested that compounds **155**, **156** and **144** all bind bicarbonate as a 1:1 complex, whilst the Job plot with compound **143** implies more complicated solution phase behaviour.

2.3.2 Solid State Studies

Crystals of urea **155** with TBA sulphate, thiourea **156** with TBA dihydrogen phosphate and TBA chloride, and thiourea **144** with TEA bicarbonate were obtained by slow evaporation from H_2O/DMSO mixtures. The X-ray crystal structures of these complexes were obtained and solved by M. E. Light (see **Appendix A3.1**). The X-ray crystal structure of urea **155** with TBA sulphate revealed the formation of a 2:1 (host:guest) complex, wherein each sulphate oxygen atom is bound by hydrogen-bonding interactions with three urea NH groups (**Figure 2.32**). The NH···O bond distances were found to be between 2.872(3)-3.291(4) Å with NHO bond angles of 117.8-171.4 º. Interestingly, the dimeric capsules are linked to neighbouring capsules by two bridging water molecules that hydrogen-bond to the urea oxygen atoms.

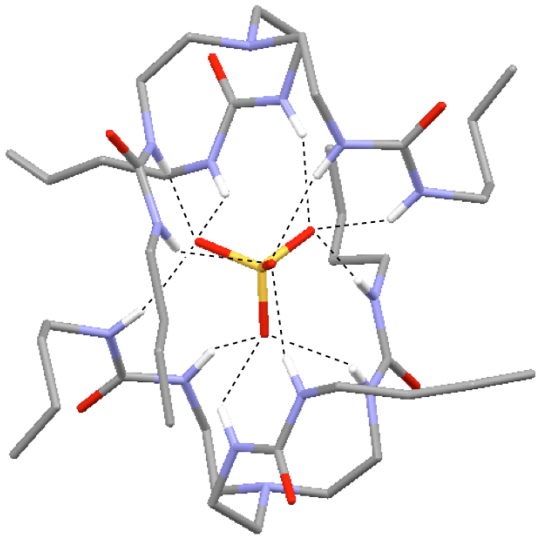

Figure 2.32: X-ray crystal structure of the 2:1 (host:guest) complex formed by compound **155** with TBA sulphate. Ligands and the guest anion are represented as wireframes; hydrogen (white), carbon (grey), nitrogen (blue), oxygen (red), sulphur (yellow). TBA counterions, bridging water molecules, disorder in the trenurea butyl chains and non-interacting hydrogen atoms have been omitted for clarity.

The structure of thiourea **156** with TBA dihydrogen phosphate shows that the dihydrogen phosphate anion is complexed by hydrogen-bonding interactions with all six thiourea NH groups, with NH···O distances ranging between 2.950(2)-3.100(2) Å and NHO bond angles between 142.4-172.0 º. Two identical capsules are linked by hydrogen-

bonding interactions between complexed dihydrogen phosphate anions, O-H···O distance 2.530(2) Å, creating a '2+2' (host:guest) motif as was observed previously for pentafluorophenyl substituted tripodal urea **145** (**Figure 2.21**).

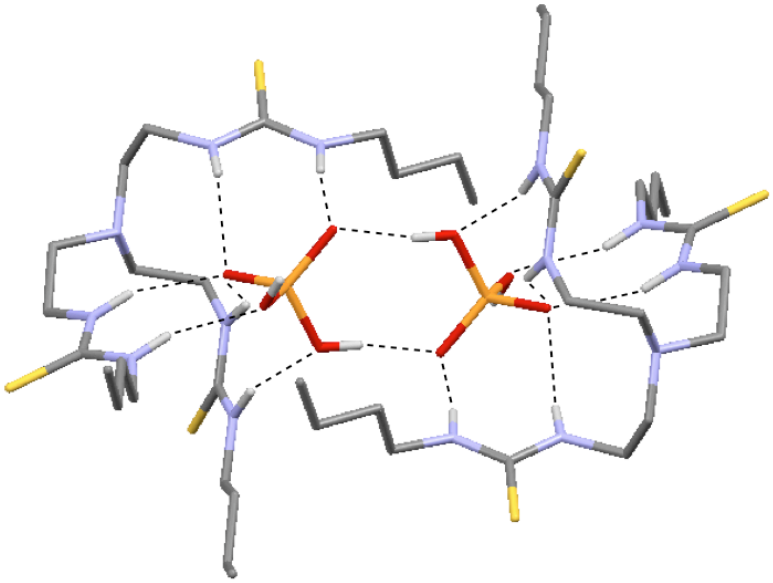

Figure 2.33: X-ray crystal tructure of the '2+2' complex formed by compound **156** with TBA dihydrogen phosphate. Ligands and guest anions are represented as wireframes; hydrogen (white), carbon (grey), nitrogen (blue), oxygen (red), phosphorous (orange), sulphur (yellow). TBA counterions, solvent molecules and non-interacting hydrogen atoms have been omitted for clarity.

In the solid state thiourea **156** was also observed to complex chloride. X-ray crystallography of the TBA chloride complex reveals two discrete 1:1 (host:guest) complexes, with the chloride anion bound by six hydrogen-bonding interactions with the thiourea NH groups (**Figure 2.34**). The NH···Cl distances are generally shorter (3.119(8)-3.404(9) Å) for the thiourea NH groups adjacent to the butyl functionality, compared to the NH groups closer to the tris(2-aminoethyl)amine centre (3.213(9)-3.516(8) Å).

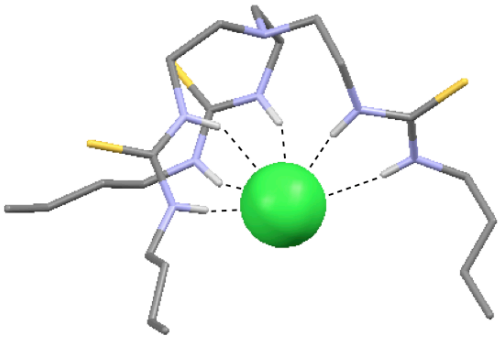

Figure 2.34: X-ray crystal structure of the 1:1 complex formed by compound **156** with TBA chloride. The ligand is represented as a wireframe and the guest anion is represented as a spacefilling model (0.6 times van der Waals radius); hydrogen (white), carbon (grey), nitrogen (blue), sulphur (yellow), chlorine (green). TBA counterions and non-interacting hydrogen atoms have been omitted for clarity.

Solid state X-ray crystallographic studies of the crystals grown from a H_2O/DMSO solution of tripodal thiourea **144** with TEA bicarbonate reveal a 2:1 (host:guest) complex with carbonate (**Figure 2.35**). The centrally bound carbonate ion is bound by twelve hydrogen-bonds with thiourea NH groups (NH···O distances between 2.824(6)-3.070(7)Å) and some longer range interactions. Multiple hydrogen-bonding to oxo-anions has been reported to alter the pK_a of the bound guest and may therefore result in guest deprotonation by unbound anions.[342] Such behaviour in solution may account for the difficulty in fitting the ^{1}H NMR titrations with TEA bicarbonate to the available binding models.

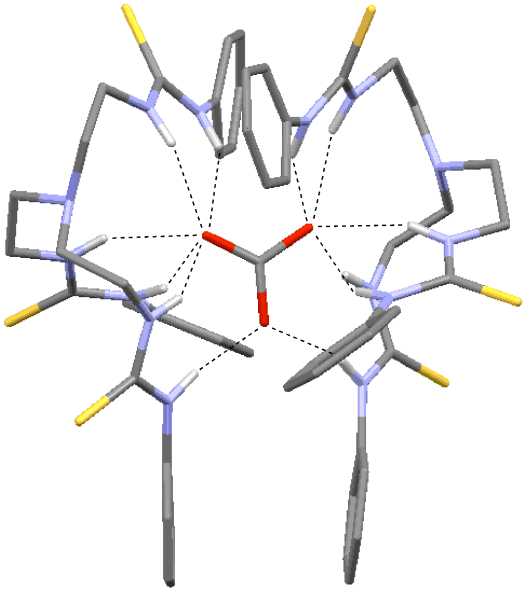

Figure 2.35: X-ray crystal structure of the 2:1 (host:guest) complex formed by compound **144** with TEA bicarbonate. Ligands and the guest anion are represented as wireframes; hydrogen (white), carbon (grey), nitrogen (blue), oxygen (red), sulphur (yellow). TEA counterions and non-interacting hydrogen atoms have been omitted for clarity.

The spacefilling models of the aforementioned chloride and carbonate complexes reveal that the tripodal thiourea compounds encapsulate the bound anion, with the thiourea sulphur atoms decorating the exterior surface of the capsule (**Figures 2.36** and **2.37**). This type of encapsulation screens the bound anion from the external environment, and by surrounding the anion with lipophilic groups may aid anion transport through phospholipid bilayers (see **Section 2.3.3**).

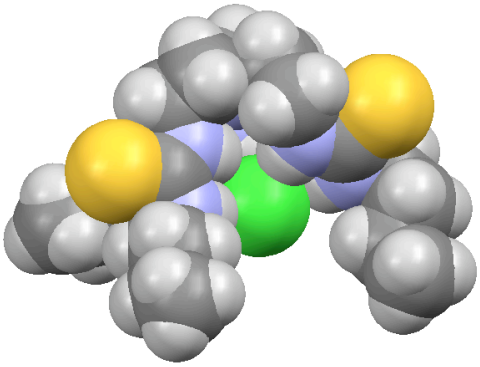

Figure 2.36: Spacefilling model of the chloride complex of **156**; hydrogen (white), carbon (grey), nitrogen (blue), sulphur (yellow), chlorine (green). TBA counterions have been omitted for clarity.

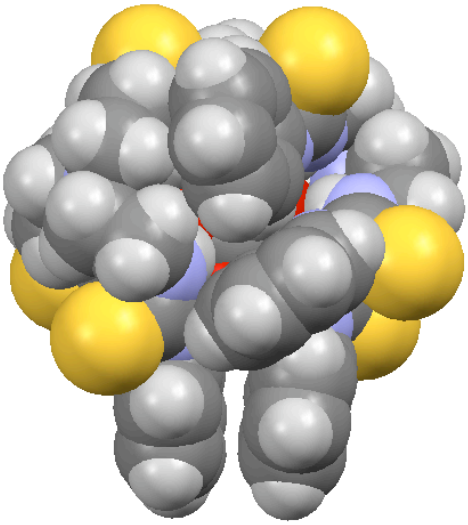

Figure 2.37: Spacefilling model of the carbonate complex of **144**; hydrogen (white), carbon (grey), nitrogen (blue), oxygen (red), sulphur (yellow). TEA counterions have been omitted for clarity.

2.3.3 Ion Transport Studies

The ion transport studies described in this section were performed by N. Busschaert, C. J. E. Haynes and C. C. Tong. Compounds **155**, **156**, **143** and **144** were tested in a Cl^-/NO_3^- antiport ISE assay (see **Section 2.2.4**). Urea compound **155** was inactive whilst urea **143** displayed moderate activity. Thioureas **156** and **144** were considerably more active than their analogous ureas, facilitating almost 100 % chloride efflux during the course of the experiment at loadings of 2 mol %. Transport rates were

unchanged when KCl was encapsulated within the vesicles, instead of NaCl. Repeating the assay under pH gradient conditions did not enhance transport rates. These results suggest that chloride efflux under these assay conditions is primarily due to Cl^-/NO_3^- antiport and not Na^+/Cl^- or H^+/Cl^- symport. The transport mechanism was tested by repeating the Cl^-/NO_3^- antiport assay with vesicles composed of a mixture of POPC and cholesterol (7:3 molar ratio). Reduced ion transport rates were measured in the cholesterol containing vesicles suggesting that transporters **156**, **143** and **144** function as mobile carriers (see **Section 1.9.7**). The transmembrane transport of bicarbonate was tested using a bicarbonate 'pulse' assay to examine Cl^-/HCO_3^- antiport. Again urea compounds **155** and **143** displayed lower transport activity than thioureas **156** and **144**. Direct evidence for the transmembrane transport of bicarbonate facilitated by thioureas **156** and **144** was obtained using ^{13}C labelled bicarbonate, in a series of vesicle based NMR assays (see **Section 1.9.5**).

In summary, tripodal urea and thiourea compounds **155**, **156**, **143** and **144** have been shown to complex chloride and bicarbonate in both solution and in the solid state. X-ray crystallographic studies have revealed that the bound anions are encapsulated by the lipophilic tris(2-aminoethyl)amine scaffold. Ion transport studies have confirmed that thiourea compounds **156** and **144** are potent Cl^-/NO_3^- and Cl^-/HCO_3^- antiport agents. A combination of strong anion binding and effective anion encapsulation are likely to aid the transmembrane transport of anions facilitated by these compounds.

2.4 Conclusions

Both the diindolylurea and tripodal scaffolds examined in this chapter contain urea (or thiourea functionalities). Urea groups have been widely employed in the field of anion complexation owing to the diverse anion binding modes available, and the readily tuneable nature of the urea scaffold.[348] By varying the urea substituents NH acidity can be increased, additional hydrogen-bonding interactions can be provided and the spatial orientation of urea functionalities can be modified to enhance anion affinity and selectivity.[349]

Owing to the high affinity of urea containing diindolylureas **152-153** and tripodal compounds **155**, **156**, **143** and **144** towards anions, and the encouraging transmembrane

anion transport properties that these scaffolds posses, urea functionalities feature prominently in the design of the anion transporters discussed in **Chapter 3** and **Chapter 4**.

Chapter 3
Indolylurea and Indolylthiourea Anion Transporters

3.1 Introduction

In **Chapter 2** diindolylureas were shown to selectively bind oxo-anions in polar H_2O/DMSO-d_6 solvent mixtures. Despite the strong anion affinity exhibited by these receptors, they displayed poor anion transport activity in phospholipid vesicles. In this chapter the anion transport activity of a series of simple monoindolylureas and thioureas is examined. The development of these receptors to optimise their 'drug-like' properties is discussed and applied to the development of a second generation of transporter molecules bearing trifluoromethyl substituents. The *in vitro* anion transport properties of this second generation of compounds are also examined.

3.1.1 Indolylureas in Supramolecular Systems

Work by Pfeffer and co-workers demonstrated that receptor scaffolds containing a mixture of indole, amide and urea/thiourea hydrogen-bond donors can complex anions.[350] Compounds **157-159** (**Figure 3.1**) link an indole to a urea/thiourea *via* a flexible alkyl chain. The interaction of these molecules with a variety of anions was examined using ^{1}H NMR techniques. Addition of TBA fluoride resulted in the deprotonation of all the receptors, whilst chloride was bound predominantly by the urea/thiourea NH groups. Acetate was also found to bind predominantly to the urea/thiourea NH groups, but the tetrahedral dihydrogen phosphate anion was bound by all the available NH hydrogen-bond donor groups.

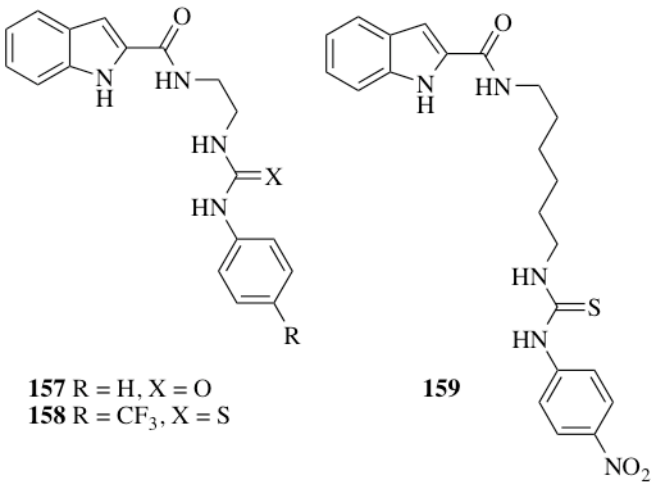

Figure 3.1: Pfeffer's mixed NH hydrogen-bond donor anion receptors.

Building on these promising results Gale, Albrecht and co-workers studied the anion binding properties of indoles functionalised with amides or ureas/thioureas in the 2- and 7- positions, compounds **160**-**165** (**Figure 3.2**).[351] NMR titration experiments in 0.5 % H_2O/DMSO-d_6 revealed that compounds **160**-**165** bind anions in the order $AcO^- > H_2PO_4^- > BzO^- > Cl^-$.

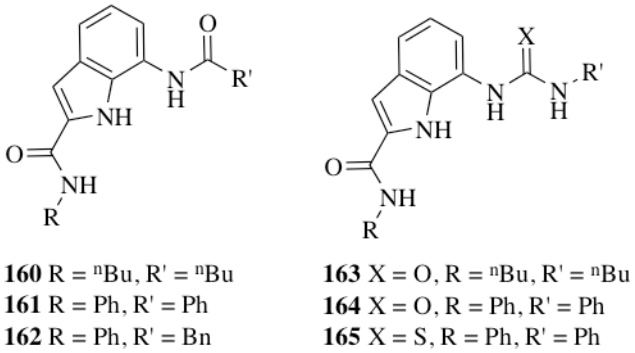

Figure 3.2: Amide and urea functionalised indoles **160**-**165**.

Urea-containing receptors **163** and **164** were found to display significantly higher anion affinity than their amide functionalised analogues. Replacement of the urea functionality in **164** with a thiourea (compound **165**) resulted in lower binding constants,

despite the increase in NH acidity. The authors attributed this decrease in anion affinity to the steric interactions between the thiourea sulphur atom and the aromatic CH groups destabilising a receptor conformation with a convergent hydrogen-bond donor array. NMR studies on these, and structurally related compounds indicated that the *anti-anti* conformation is favoured in solution (**Figure 3.3**).[352, 353] In the presence of anions, NOE experiments in acetone-d_6 indicated that the conformation of these receptors changes. Addition of TBA acetate results in the host adopting the *syn-syn* conformation, permitting all NH functionalities to hydrogen-bond with the carboxylate ion. NOE experiments confirmed that the amide NH in the 2- position does not interact significantly with chloride or bromide ions, a finding mirrored in the solid state.

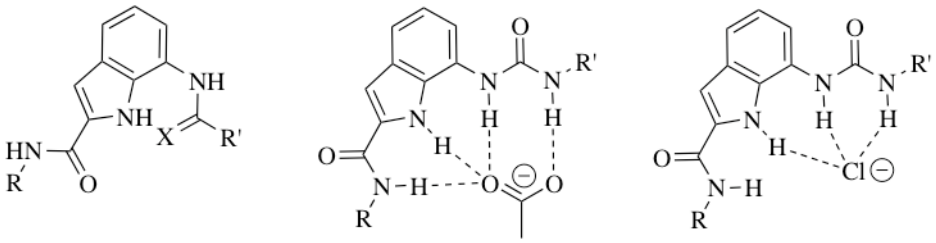

Figure 3.3: Favoured *anti-anti* conformation, and acetate and chloride binding modes observed in solution for indoles functionalised at the 2- and 7- positions.

Gale and co-workers covalently linked two indolylurea units together with flexible alkyl chains of varying length, producing compounds **166-174** (**Figure 3.4**).[270] Increasing the length of the alkyl linker resulted in an increase in Cl^-/NO_3^- antiport activity in phospholipid vesicles for compounds **166-172**. This effect was attributed to the enhanced membrane partitioning properties afforded by an increase in lipophilicity (see **Section 3.1.2**). Increasing the alkyl linker length to more than ten carbon atoms (compounds **173** and **174**) reduced transporter activity, an effect attributed to impeded delivery through the aqueous phase caused by the higher hydrophobicity of these compounds.

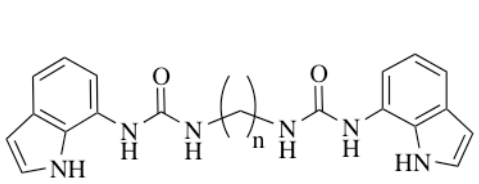

166 n = 4
167 n = 5
168 n = 6
169 n = 7
170 n = 8
171 n = 9
172 n = 10
173 n = 11
174 n = 12

Figure 3.4: Bis(indolylurea)s with alkyl linkers of different lengths.

Complicated solution phase behaviour was observed during binding studies, the authors rationalising that the high flexibility of the receptors and the large distances between the two discrete anion binding sites presented a multitude of binding stoichiometries. In the solid state, a rod of dihydrogen phosphate anions was bound by a helical arrangement of bis(indolylurea) host **168** with a pseudo 1:2 (host:guest) binding stoichiometry (**Figure 3.5**). The indole NH groups were found to hydrogen-bond to the adjacent urea oxygen, whilst the dihydrogen phosphate anions were bound by the urea NH groups.

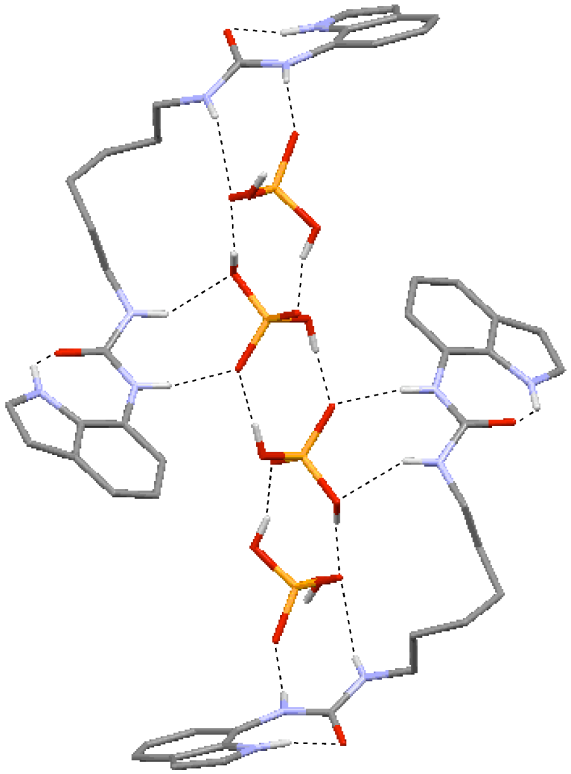

Figure 3.5: TBA dihydrogen phosphate complex of bis(indolylurea) **168**, showing a dihydrogen phosphate oligomeric rod bound in a 1:2 (host:guest) conformation. Ligands and the guest anions are represented as wireframes; hydrogen (white), carbon (grey), nitrogen (blue), oxygen (red), phosphorous (orange). TBA counterions and non-interacting hydrogen atoms have been omitted for clarity.[270]

3.1.2 Medicinal Chemistry Considerations for Transporter Design

Synthetic molecules capable of functioning as transmembrane ion transporters *via* a mobile carrier mechanism are atypical of the type of compound conventionally developed as drugs. The overwhelming majority of drug compounds are designed to interact with protein-based targets; usually enzymes or cell receptors.[354] An understanding of absorption, distribution, metabolism, excretion and toxicity (ADMET) parameters is critical for the successful development of 'drug-like' molecules. Despite the obvious differences between drugs designed as ion carriers and those designed as protein ligands, guidelines for developing the latter are likely to be informative towards transporter design.

Several sets of guidelines have been produced that are intended to aid drug design.[355] Lipinski and co-workers developed a set of rules from the statistical analysis of

compounds that had reached phase II clinical trials.[356] Lipinski's rules state that a molecule will exhibit poor absorption and poor membrane permeation properties if it has:

- More than 5 hydrogen-bond donors
- More than 10 hydrogen-bond acceptors
- Molecular weight greater than 500 Da
- LogP greater than 5

Veber and co-workers produced a similar set of rules having examined the oral bioavailability of drug compounds in rat models.[357] Good oral bioavailability was observed when a molecule had:

- Less than 10 rotatable bonds
- A polar surface area of less than 140 $Å^2$

Optimisation of lipophilicity (as measured by the partition coefficient, P) is important in the design of anion transporters that function as mobile carriers, since these compounds are required to partition into the hydrophobic membrane interior. Unlike conventional drugs these compounds are not required to cross the bilayer, thus high logP values are desired to facilitate partitioning.[358] Simultaneously, high logP can be detrimental to aqueous solubility, an important consideration in delivery of the transporter to the membrane.[359] The role of logP on transporter activity was studied by Quesada and co-workers using a series of alkyl substituted tambjamines (see **Section 1.6.2**).[360] Similar trends were observed to those reported by Gale and co-workers in their bis(indolylurea) study (see **Section 3.1.1**), with the rate of transport activity (in this case Cl^-/HCO_3^- antiport) found to be dependent on the length of an alkyl substituent. Increasing the alkyl chain length was found to enhance initial transport rates owing to increased receptor lipophilicity, but beyond an optimal length chloride transport rates were diminished. The authors rationalised that these compounds (the most lipophilic in the series) suffered from poor delivery from the aqueous phase into the phospholipid membrane and possibly lower mobility within the membrane interior.

Toxicological considerations are also of paramount importance in the design of anion transporters. A compound that has undesirable toxic side effects will require modification to make it suitable for use as a drug. A common strategy in drug design is to replace toxicophores with alternative, less toxic functionalities. Gale and co-workers have demonstrated this approach through their examination of thiourea isosteres for the structurally simple transporter **175** (**Figure 3.6**).[361] Toxicity has been previously shown with thiourea motifs, although the mechanism of toxicity is poorly understood.[362-364] The Cl^-/NO_3^- antiport activity of isosteres of **175** were tested in POPC vesicles loaded with KCl and suspended in KNO_3 using ISE assays. In the presence of valinomycin (a potassium ionophore) chloride transport rates under the same conditions were enhanced (see **Section 5.2**). Compound **176**, based upon the 3-amino-1,2,4-benzothiadiazie-1,1-dioxane scaffold displayed poor transport activity at 2 mol % loading. Replacement of the thiourea group with a cyanoguanidine and fluorination of the phenyl ring yielded compound **177**. This molecule was found to be as potent as the original thiourea compound **175** in the aforementioned transport assay. These results confirm that the cyanoguanidine is a suitable substitute for the potentially toxic thiourea functionality, and demonstrate isosteric replacement in a transport context.

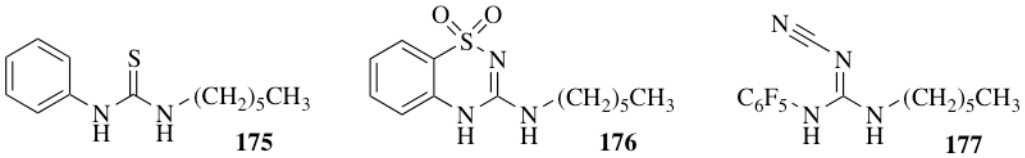

Figure 3.6: Thiourea **175** and thiourea isosteres **176** and **177**.

3.1.3 Fluorination as a Strategy to Enhance Transporter Activity

A range of transporters exist wherein ion transport activity has been optimised by fluorination. Fluorination of *meso*-octamethylcalix[4]pyrrole **178** (discussed in detail in **Section 5.2.2**) yields compound **179** (**Figure 3.7**).[365] Due to the addition of electron withdrawing fluorine atoms, fluorinated calix[4]pyrrole **179** has a higher affinity for anionic guests than compound **178** ($K_a[Cl^-] > 10^4$ M^{-1} and $K_a[Cl^-] = 5{,}000$ M^{-1} respectively in 0.5 % D_2O/Acetonitrile-d_3).[366] In addition, the primary transport

mechanism adopted by **179** differs from that of compound **178**, which has only been reported to facilitate Cs^+/Cl^- symport (see **Section 5.2.2**).[367] The incorporation of fluorine atoms into the calix[4]pyrrole scaffold produces a receptor that no longer facilitates Cs^+/Cl^- symport, but can instead facilitate both Cl^-/NO_3^- and Cl^-/HCO_3^- antiport. DPPC mobility assays (see **Section 1.9.7**) indicate that like **178**, compound **179** functions *via* a mobile carrier mechanism.

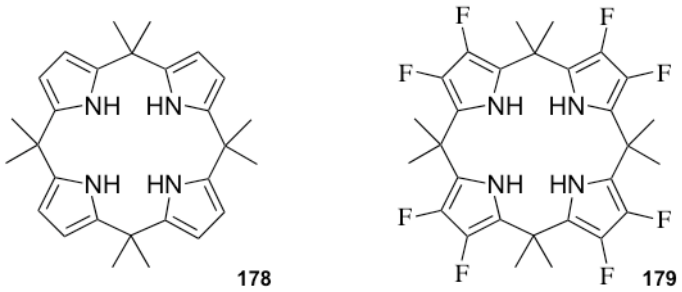

Figure 3.7: Fluorination of calix[4]pyrrole **178** alters the available chloride transport pathways.

In an extensive study of structure activity relationships in cholapod ion transporters Davis and co-workers found that the addition of a trifluoromethyl functionality at the cholapod 3- position yielded potent chloride transporters **180** and **181** (**Figure 3.8**). The trifluoromethyl substituent was judged to enhance both the strength of anion binding and the observed transport rates.[138]

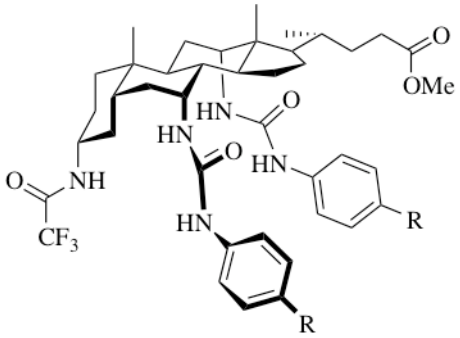

180 R = H
181 R = NO_2

Figure 3.8: Trifluoromethyl substituted cholapods **180** and **181**.

Developing the tripodal urea/thiourea motif discussed in **Chapter 2**, Gale and co-workers synthesised fluorinated compounds **145** and **182-188** (**Figure 3.9**).[249] Proton NMR titrations revealed that compounds **145** and **182-188** are selective receptors for TBA sulphate, with strong 1:1 binding ($K_a > 10^4\ M^{-1}$) measured in 0.5 % H_2O/DMSO-d_6. In POPC vesicles all of the compounds functioned as mobile carriers facilitating both Cl^-/NO_3^- and Cl^-/HCO_3^- antiport. In an HPTS assay (see **Section 1.9.3**) an increase in intravesicular pH was observed upon addition of compounds **145** and **182-188** to vesicles containing NaCl suspended in Na_2SO_4, supporting a H^+/Cl^- symport mechanism. The authors proposed that the neutral receptor transports chloride across the membrane, but receptor deprotonation occurs upon chloride release (facilitated by the increased urea NH acidity as a consequence of receptor fluorination). The deprotonated receptor then diffuses back across the membrane in its anionic form completing the transport cycle. The possibility of transmembrane sulphate transport was examined using vesicles loaded with NaCl and lucigenin in a solution of NaCl. Addition of a Na_2SO_4 'pulse' to the external medium resulted in an increase in lucigenin fluorescence intensity, indicating chloride efflux (as a consequence of Cl^-/SO_4^{2-} exchange) in the presence of compound **186**, but not with any of the other compounds. A clear correlation was observed between the lipophilicity of urea compounds **145** and **182-184**, and the measured ion transport activity. Thioureas **185-188** are more lipophilic than the analogous ureas and again similar trends were observed, with increasing lipophilicity resulting in improved transport activity. However the two most lipophilic compounds, **187** and **188** (clogP = 8.26 and 11.03 respectively) showed lower activity than anticipated. The authors rationalised that the most lipophilic transporters were less able to effectively partition into the polar membrane region to facilitate anion binding and release, resulting in reduced transport rates. Transporters **183**, **184**, **186**, **187** and **188** were tested *in vitro* and were found to facilitate the deacidification of organelles in GLC4 cells, thus showing promise as anticancer agents that promote apoptosis in cancerous cell lines (see **Section 3.4.5**).

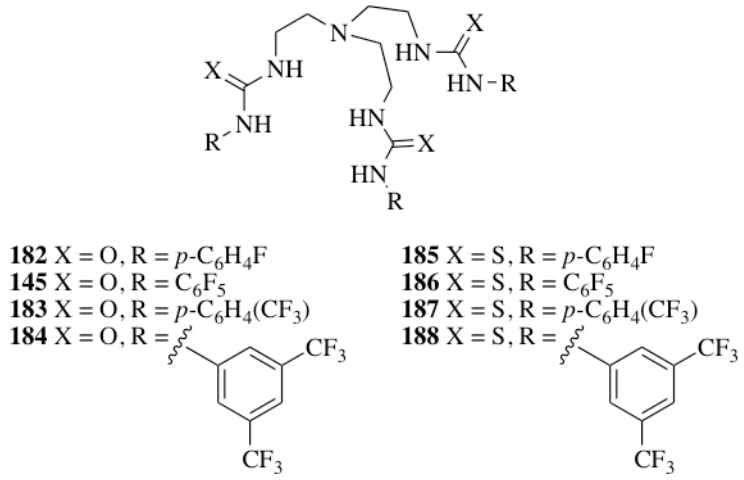

Figure 3.9: Fluorinated tripodal ureas and thioureas.

Research by Matile and co-workers has shown that small perfluorinated molecules with halogen-bond donor moieties can facilitate chloride transport in EYPC vesicles (**Figure 3.10**).[368] The introduction of fluorine atoms onto iodine-bearing alkyl compound **189** and phenyl compound **190** resulted in a dramatic enhancement in transporter activity, owing to the electron withdrawing fluorine atoms increasing the acidity of the iodine halogen-bond donor atom in compounds **191** and **192**. Computer modelling revealed that aggregates of **191** and **192** are responsible for chloride encapsulation and subsequent membrane transport, functioning *via* a mobile carrier mechanism. Structurally related fluorinated compounds **193**, **194** and **195** were also active transporters. Intriguingly, compounds **194** and **195** were found to facilitate chloride transport in the gas phase.

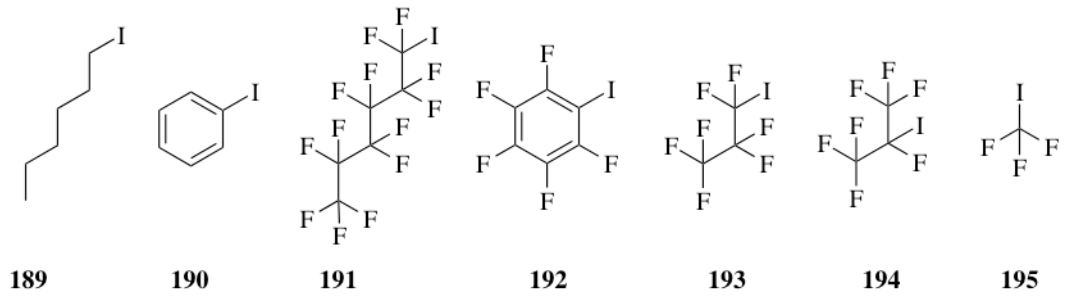

Figure 3.10: Matile's structurally simple fluorinated anion transporters.

In an attempt to uncover new isosteres for the thiourea group, Gale and co-workers have investigated the use of squaramides and their fluorinated analogues as ion transport agents, synthesising compounds **196-201** (**Figure 3.11**).[369] Trifluoromethyl bearing compounds **197**, **199** and **201** all exhibit significantly enhanced Cl^-/NO_3^- and Cl^-/HCO_3^- antiport activity in POPC vesicles, in comparison to their unfluorinated analogues **196**, **198** and **200**. The introduction of the trifluoromethyl group was found to increase the lipophilicity of the receptors but despite the squaramides showing the fastest transport rates, calculations reveal that they are significantly less lipophilic than analogous thioureas. Proton NMR titrations in 0.5 % H_2O/DMSO-d_6 revealed that the observed differences in transport activity are likely due to the increased chloride affinity exhibited by the squaramides ($K_a[Cl^-]$ = 43 M^{-1} and 260 M^{-1} for compound **199** and compound **201** respectively).

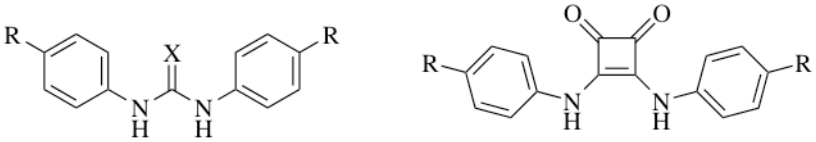

196 X = O, R = H
197 X = O, R = CF_3
198 X = S, R = H
199 X = S, R = CF_3

200 R = H
201 R = CF_3

Figure 3.11: Simple trifluoromethyl bearing ureas, thioureas and squaramides.

Owing to the abundance of the indole moiety in both nature and in synthetic anion hosts, a range of simple indolyl(thio)urea scaffolds were studied as transporters. Fluorination has been shown to be a successful strategy for the construction of potent ion transporters and hence the transport properties of a series of fluorinated indolyl(thio)ureas were also examined (see **Section 3.4**).

3.2 Indolylureas as Anion Transport Agents

To investigate if improving receptor lipophilicity enhances transporter activity, the transport properties of indolylureas **202-210** were studied (**Figure 3.12**). Alkyl chain

length was increased from *n*-butyl (C_4) to *n*-dodecyl (C_{12}) across the series. Compounds **202** and **206** were studied previously by Albrecht and Plavec, with a binding constant for TBA chloride of 442 M^{-1} in $CDCl_3$ at 296 K reported for compound **202**.[370]

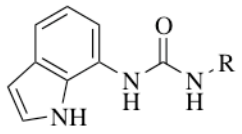

202 R = $(CH_2)_3CH_3$
203 R = $(CH_2)_4CH_3$
204 R = $(CH_2)_5CH_3$
205 R = $(CH_2)_6CH_3$
206 R = $(CH_2)_7CH_3$
207 R = $(CH_2)_8CH_3$
208 R = $(CH_2)_9CH_3$
209 R = $(CH_2)_{10}CH_3$
210 R = $(CH_2)_{11}CH_3$

Figure 3.12: Alkyl substituted monoindolylureas.

3.2.1 Synthesis

Compounds **202-210** were synthesised by reaction of *N*-(1*H*-indol-7-yl)-1*H*-imidazole-carboxamide with the appropriate amine in DCM.[371] Compounds **209** and **210** were synthesised by C. J. E. Haynes using a similar method.

3.2.2 Ion Transport Studies

To assess the anion transport properties of compounds **202-210**, a Cl^-/NO_3^- ISE antiport assay was performed (see **Section 2.2.4**). Compounds **202-210** were found to facilitate low levels of chloride efflux at loadings of 2 mol % (with respect to lipid), although activity was too low to discern trends across the series (**Figure 3.13**).

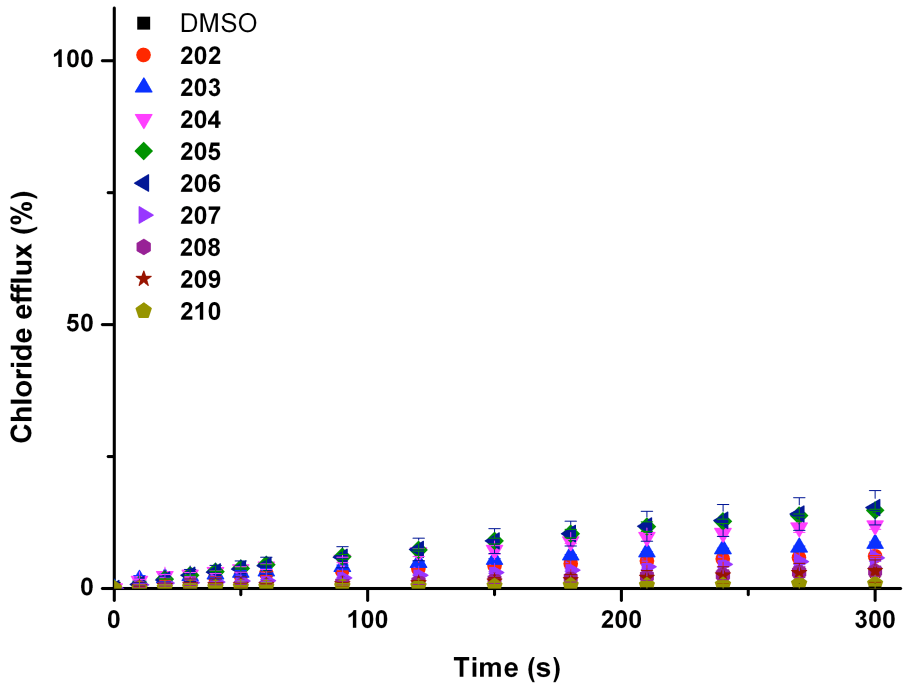

Figure 3.13: Chloride efflux promoted by addition of receptors **202**-**210** (2 mol % with respect to lipid) from unilamellar POPC vesicles loaded with 488 mM NaCl buffered to pH 7.2 with 5 mM sodium and suspended in 488 mM $NaNO_3$ buffered to pH 7.2 with 5 mM sodium phosphate salts. At the end of the experiment, detergent was added to lyse the vesicles and calibrate the ISE to 100 % chloride efflux. Each point represents an average of three trials.

To explore the possibility of transmembrane bicarbonate transport, a Cl^-/HCO_3^- antiport ISE transport assay was performed (see **Section 2.2.4**). No significant chloride efflux was observed for compounds **202**-**210** at loadings of 2 mol % (with respect to lipid) (**Figure 3.14**).

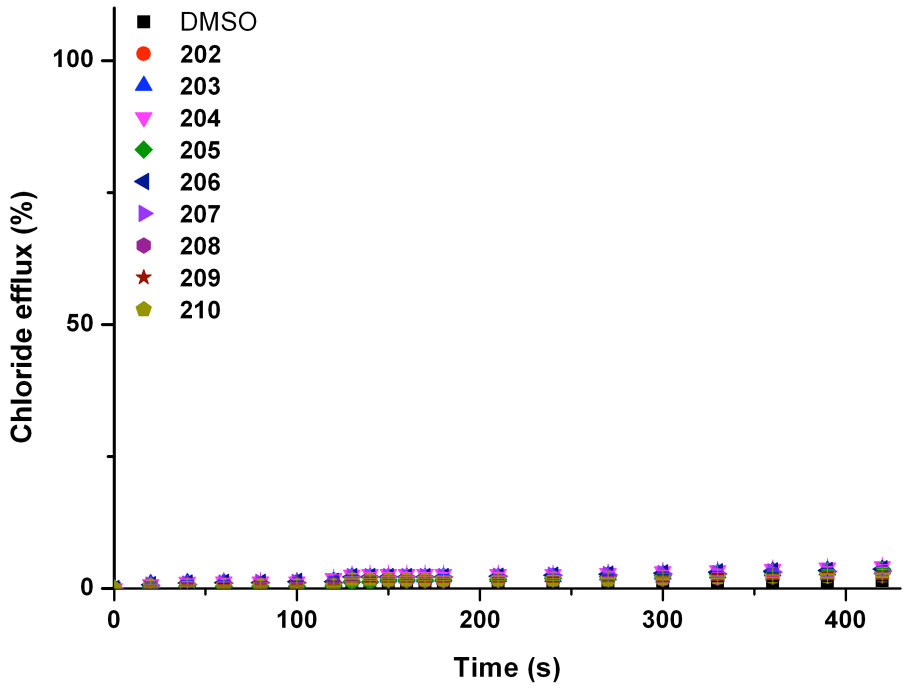

Figure 3.14: Chloride efflux promoted by addition of receptors **202**-**210** (2 mol % with respect to lipid) from unilamellar POPC vesicles loaded with 451 mM NaCl buffered to pH 7.2 with 20 mM sodium phosphate salts upon addition of a $NaHCO_3$ 'pulse' to make the extravesicular bicarbonate concentration 40 mM. The vesicles were suspended in 150 mM Na_2SO_4 buffered to pH 7.2 with 20 mM sodium phosphate salts. At the end of the experiment, detergent was added to lyse the vesicles and calibrate the ISE to 100 % chloride efflux. Each point represents an average of three trials.

The low transport activity of these simple urea compounds may be the consequence of poor partitioning into the lipid bilayer. Another factor likely to limit the transport activity of these compounds is the propensity of simple urea compounds to aggregate in solution.[372, 373] In an attempt to enhance the transport activity of such indolylurea motifs simple thiourea containing compounds were investigated for anion transport activity.

3.3 Structurally Simple Ureas and Thioureas

Owing to the abundance of urea and thiourea groups in motifs capable of anion recognition and transport (see **Chapters 1** and **2**) a series of structurally simple urea and thiourea molecules **211**-**212** and their analogous amides and thioamides **218**-**222** were

studied (**Figure 3.15**). Each molecule bears an *iso*-pentyl side chain as a common substituent across the series. This functionality was selected because it has been used previously in successful transporter designs.[90] The other side chain was varied across the series to *n*-butyl, phenyl or indolyl to examine the electronic impact of different substituents and to examine the effect of incorporating an additional indole NH hydrogen-bond donor into the scaffold.

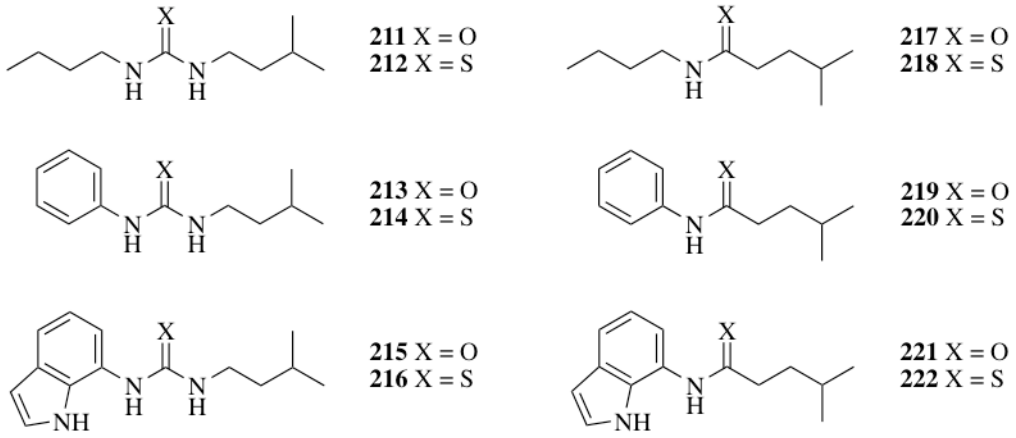

Figure 3.15: Structurally simple ureas and thioureas and their analogous amides and thioamides.

3.3.1 Synthesis

Compounds **211-214** and **216-222** were synthesised by N. J. Andrews, C. J. E. Haynes and C. C. Tong. Compound **215** was prepared by the reduction of 7-nitro-1*H*-indole to the amine, followed by reaction with CDI. The isolated white solid was reacted with *iso*-pentylamine in DCM to afford compound **215** in 53 % overall yield.

3.3.2 Anion Binding Studies

Stability constants for compounds **211-216** with chloride, nitrate (added as the TBA salts) and bicarbonate (added as the TEA salt) were determined by ^{1}H NMR titration. For consistency with previous anion binding studies (see **Section 2.2.2** and **2.3.1**), titrations were performed in a solution of 0.5 % H_2O/DMSO-d_6 at 298 K and stability constants were obtained by curve fitting using WinEQNMR2 computer software

(see **Appendix A2.2** for fitted curves).[340] The results of these studies are shown in **Table 3.1**.

Compound	Cl^{-} [a]	HCO_3^{-} [a]	NO_3^{-} [a]
211	< 10	18	[b]
212	10	58	[b]
213	21	135	[b]
214	22	343 [c]	[b]
215	96	1170	[b]
216	28	516	[b]

Table 3.1: Apparent stability constants K_a (M^{-1}) determined by ^1H NMR titrations with compounds **211-216** in 0.5 % H_2O/DMSO-d_6 at 298 K following the shift of the *iso*-pentyl NH group. Data was fitted to a 1:1 binding model. Errors < 10 %. [a] Added as TBA salts, except bicarbonate which was added as the TEA salt. [b] No significant interaction. [c] Significant broadening of NH signals.

Compounds **211**-**216** did not interact with nitrate in this solvent mixture, however interactions were observed with both chloride and bicarbonate. The indolyl compounds **215** and **216** displayed the highest affinity for both of these anions, with the indolylurea compound **215** showing higher anion affinity than its thiourea analogue.

3.3.3 Solid State Studies

Crystals of compound **213** were grown by slow evaporation from a DMSO solution. The X-ray crystal structure was obtained and solved by M. E. Light (see **Appendix A3.2**). In the solid state characteristic hydrogen-bonded urea tapes were observed, with N···O distances between 2.788-2.933 Å and N-H···O bond angles in the range of 136.4-158.1° (**Figure 3.16**).[374]

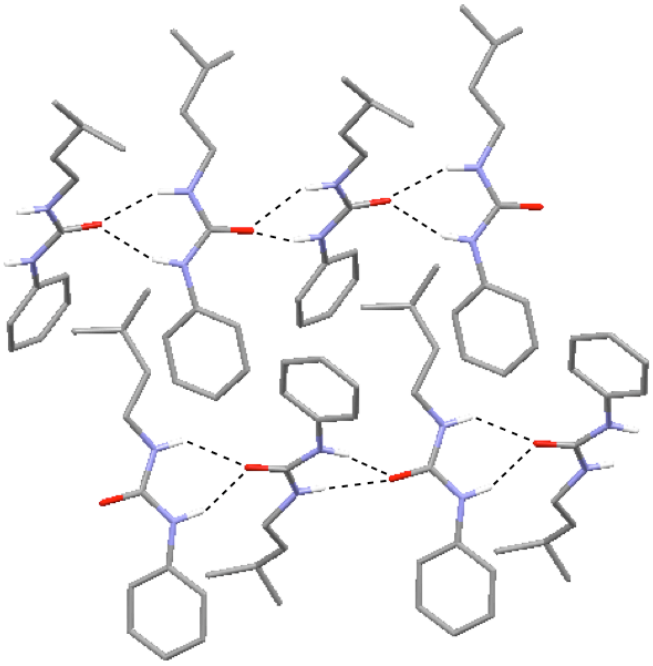

Figure 3.16: X-ray crystal structure of compound **213**. Ligands are represented as wireframes; hydrogen (white), carbon (grey), nitrogen (blue), oxygen (red). Non-interacting hydrogen atoms have been omitted for clarity.

3.3.4 Ion Transport Studies

Experiments by C. J. E. Haynes confirmed that compounds **211-216** can facilitate Cl^-/NO_3^- antiport. Owing to this finding, the bicarbonate transport activity of compounds **211-216** was assessed using a Cl^-/HCO_3^- antiport ISE transport assay (see **Section 2.2.4**). Significant chloride efflux was not observed in this assay with the urea compounds, but was observed with the thiourea compounds **212**, **214** and **216** (**Figure 3.17**). NMR techniques were used to directly monitor the transmembrane transport of ^{13}C labelled bicarbonate in phospholipid vesicles, facilitated by thiourea compounds **212**, **214** and **216** (see **Section 1.9.5**). These experiments were performed by W. A. Harrell Jr. at the University of Maryland.

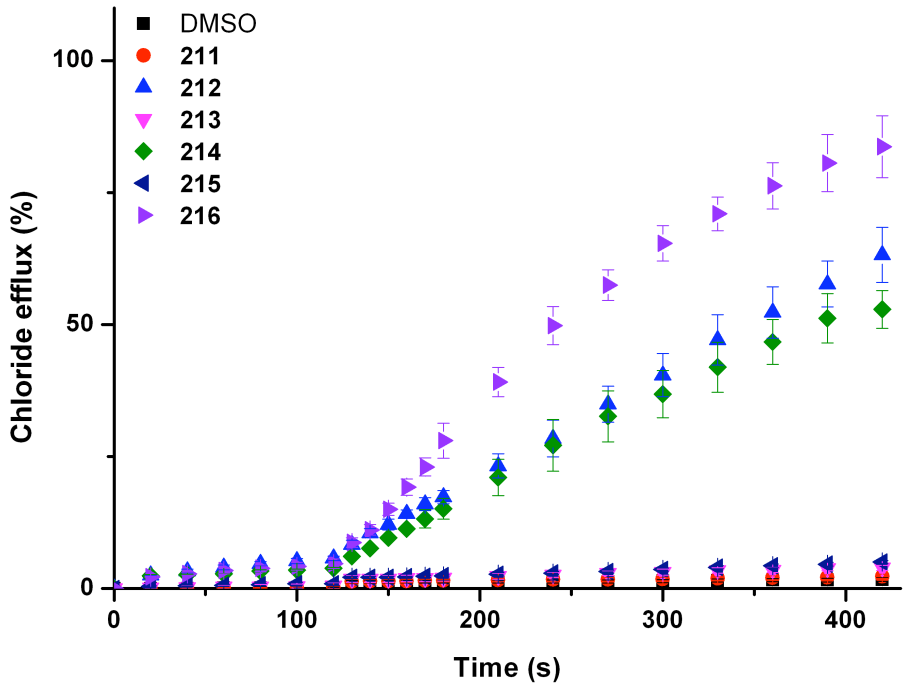

Figure 3.17: Chloride efflux promoted by addition of receptors **211**-**216** (2 mol % with respect to lipid) to unilamellar POPC vesicles loaded with 451 mM NaCl buffered to pH 7.2 with 20 mM sodium phosphate salts upon addition of a $NaHCO_3$ 'pulse' to make the extravesicular bicarbonate concentration 40 mM. The vesicles were suspended in 150 mM Na_2SO_4 buffered to pH 7.2 with 20 mM sodium phosphate salts. At the end of the experiment, detergent was added to lyse the vesicles and calibrate the ISE to 100 % chloride efflux. Each point represents an average of three trials.

To confirm that these transporters operate *via* a mobile carrier mechanism POPC/cholesterol (7:3 molar ratio) vesicles were prepared containing NaCl (see **Section 1.9.7**). These vesicles were suspended in a solution of $NaNO_3$ and the chloride efflux observed upon addition of compounds **212**, **214** and **216** was compared to that observed in vesicles made entirely from POPC. A slight reduction in the rate of chloride efflux was observed in all three cases with the cholesterol containing vesicles (see **Appendix A5.1**), and these results coupled with the low n values obtained by Hill analysis (**Table 3.2**) imply a mobile carrier mechanism.

Hill analysis of the thiourea receptors was performed by conducting the aforementioned bicarbonate 'pulse' assay at a range of carrier concentrations. A summary of the $EC_{50,\ 270\ s}$ values obtained by this method and calculated wclogP values are shown

in **Table 3.2**. The Wildman-Crippen logP (wclogP) values and topological polar surface areas (TPSA) are useful indicators for suitability as a mobile carrier (see **Section 3.1.2**).[375, 376] The wclogP and TPSA values were calculated using Fieldview Version 2.0.2 computer software.[377]

Compound	$EC_{50,\ 270\ s}$ [a] (Cl^-/HCO_3^-)	n [b] (Cl^-/HCO_3^-)	wclog P [c]	TPSA[c] ($Å^2$)
211	[d]	[d]	2.13	41.1
212	0.640	0.69	2.30	24.1
213	[d]	[d]	2.85	41.1
214	2.83	0.60	3.02	24.1
215	[d]	[d]	3.34	56.9
216	0.041	1.59	3.50	39.8

Table 3.2: $EC_{50,\ 270\ s}$ values and Hill coefficients for compounds **211-216** for the release of chloride in a Cl^-/HCO_3^- antiport assay. Values for wclogP and TPSA are also displayed. [a] $EC_{50,\ 270\ s}$ defined as concentration (mol % carrier with respect to lipid) needed to achieve 50 % chloride efflux after 270 s. [b] Hill coefficient.[c] Calculated using Fieldview Version 2.0.2 for Macintosh. [d] Hill analysis not performed due to low activity.

Analysis of this data reveals that bicarbonate transport activity is of the order **216** > **212** > **214**. Interestingly the thiourea compounds have higher wclogP and lower TPSA values than their urea analogues. This likely reflects the ability of these compounds to effectively partition into the lipid bilayer. Indolylthiourea **216** was found to be extremely active, facilitating Cl^-/HCO_3^- antiport at loadings as low as 5 mmol % (with respect to lipid). This highlights the impact of introducing an additional indolyl NH hydrogen-bond donor group onto the receptor scaffold.

Amide and thioamide compounds **217-222** were also tested as transporters owing to their structural similarity to compounds **211-216**. Compounds **217-222** showed low chloride transport activity in a Cl^-/NO_3^- antiport assay (**Figure 3.18**) suggesting that the thiourea motif is vital for transport activity in this type of receptor.

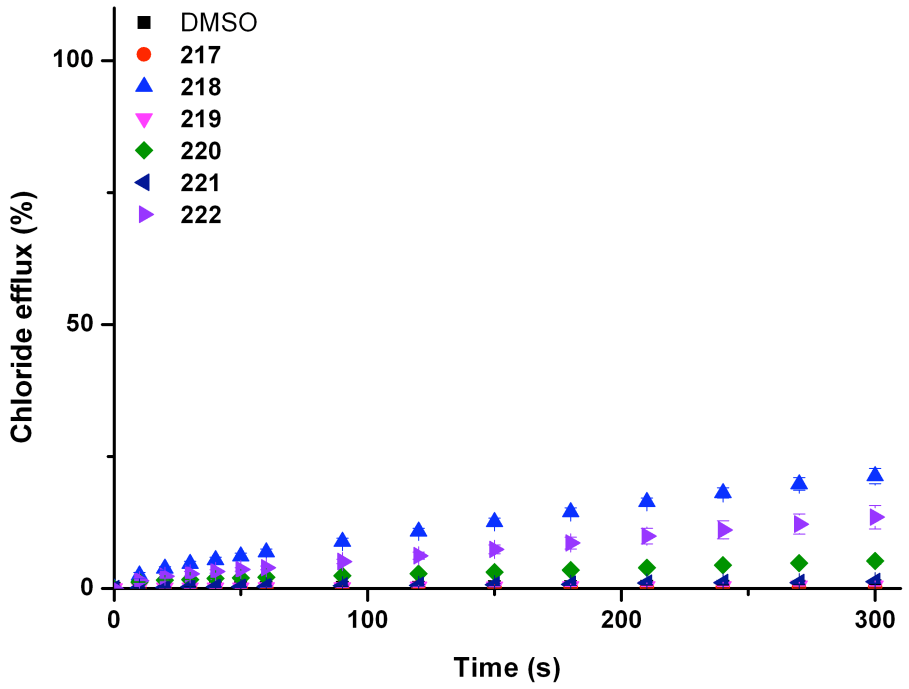

Figure 3.18: Chloride efflux promoted by addition of receptors **217**-**222** (2 mol % with respect to lipid) from unilamellar POPC vesicles loaded with 488 mM NaCl buffered to pH 7.2 with 5 mM sodium phosphate salts and suspended in 488 mM $NaNO_3$ buffered to pH 7.2 with 5mM sodium phosphate salts. At the end of the experiment, detergent was added to lyse the vesicles and calibrate the ISE to 100 % chloride efflux. Each point represents an average of three trials.

In summary, these results show that thiourea compounds **212**, **214** and **216** show promising activity as Cl^-/HCO_3^- antiport agents. The most active compound **216**, has a higher wclogP and a lower TPSA than its significantly less active urea analogue **215**. NMR binding studies show that the indolylurea and indolylthiourea motifs have a high affinity for bicarbonate and thus it seems likely that the high transport activity of indolylthiourea **216** is the result of a favourable balance between anion affinity and lipophilicity. Additionally, indolylthiourea **216** facilitates higher Cl^-/HCO_3^- antiport activity than the tripodal thiourea compounds **156** and **144** discussed in **Chapter 2** (see **Appendix A5.1**), thus representing an improvement on this transporter design.

3.4 Development of 'Drug-like' Indole-based Anion Transporters

In **Section 3.3** *iso*-pentyl functionalised indolylthiourea **216** was found to facilitate the transmembrane transport of chloride, bicarbonate and nitrate.[371] Transporters for use in biological systems should ideally facilitate high ion fluxes at low carrier concentrations and have suitable ADMET characteristics. Strategies for the optimisation of 'drug-like' properties in anion transporters were discussed in **Section 3.1**, including the replacement of a potentially toxic moiety with a suitable isostere.[361] An alternative strategy is to fluorinate the mobile carrier (see **Section 3.1.3**). Fluorinated drug molecules often display lower toxicity and higher metabolic stability than their unfluorinated analogues.[378-382] Aromatic fluorination can increase both lipophilicity and hydrogen-bond acidity, leading to enhanced membrane partitioning and stronger anion-receptor interactions.[383] In **Section 3.1.3** fluorination was demonstrated to enhance the transport activity of cholapods, calix[4]pyrroles and tripodal urea and thioureas.[138, 249, 365] In this latter case, fluorination of the tripodal transporters led to compounds that displayed *in vitro* activity, inducing apoptosis in human cancer cells. Examination of the Lipinski guidelines described in **Section 3.1.2** suggest that these tripodal transporters have molecular masses outside the acceptable range and that the most active compounds have lipophilicities that also exceed the appropriate range.[356, 384] Thus the indolylurea/thiourea scaffold is a promising candidate for the development of low molecular weight fluorinated anion transporters.

To examine the effect of fluorination on low molecular weight transporters indolylurea/thiourea compounds **204** and **223**-**229**, and structurally related urea/thiourea compounds **230**-**233** were synthesised (**Figure 3.19**). The anion transport properties of compound **204** were examined in **Section 3.2**, whilst the transport activity of compound **231** was described in **Section 3.1.2**.[270, 361] The carbamate complexation properties of compound **226** were described in **Section 2.1**.[305, 306]

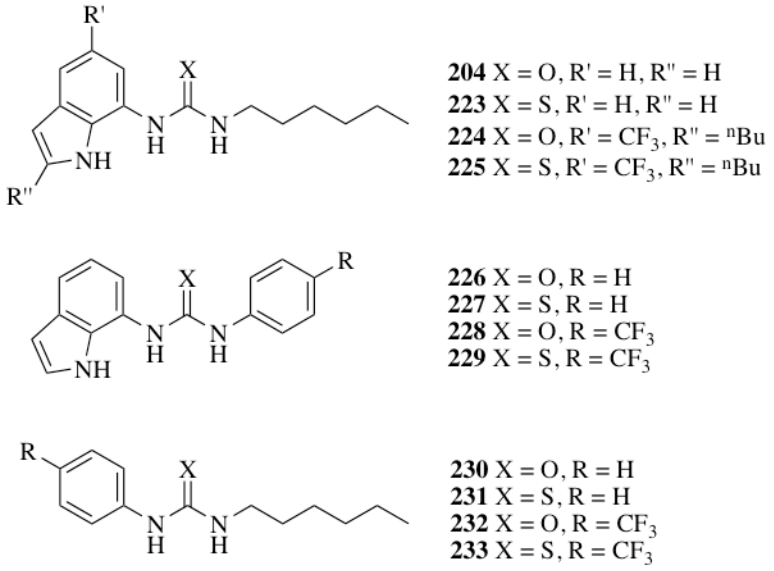

Figure 3.19: Trifluoromethyl substituted urea and thiourea compounds.

3.4.1 Synthesis

The synthesis of compound **204** is described in **Section 3.2.1**.[270] Compound **223** was synthesised in 64 % yield using a published method for the synthesis of indolylthioureas.[371] Compounds **224** and **225** were derived from 2-butyl-7-nitro-5-(trifluoromethyl)-1*H*-indole,[385, 386] and synthesised in 60 % and 47 % yields respectively.

Compounds **226**,[305, 306] **227**, **228** and **229** were prepared from 7-nitro-1*H*-indole. In all cases 7-nitroindole was hydrogenated in methanol with Pd/C catalyst. Reaction with CDI followed by reaction with aniline gave compound **226** in 21 % yield. Reaction with 4-(trifluoromethyl)phenylisocyanate in DCM afforded compound **228** in 51 % yield, whilst reaction with the corresponding isothiocyanates gave compounds **227** and **229**, each in 20 % yield.

Compounds **230** [387-389] and **231** [361] were synthesised by M. Wenzel. Compounds **232** and **233** were obtained by reaction of hexylamine with the corresponding isocyanate or isothiocyanate in DCM in 69 % and 47 % yields respectively.

3.4.2 Anion Binding Studies

The ability of compounds **223**-**233** to bind anions in solution was investigated using ^{1}H NMR titration techniques in 0.5 % H_2O/DMSO-d_6. The binding studies were

performed with anions (added as either the TBA or TEA salts) relevant to both biological systems and the transmembrane transport assays described in **Section 3.4.4**. Where possible the change in chemical shift of the most upfield urea/thiourea NH signal was fitted to a 1:1 binding model using WinEQNMR2 software (see **Appendix A2.2** for fitted curves).[340] A summary of the results is presented in **Table 3.3**. Previously reported stability constants are included for comparison.[270, 361]

Compound	Cl^- [a]	HCO_3^- [a]	NO_3^- [a]
204	64 [b]	2330	[c]
223	17	414	[c]
224	154	$>10^4$	[c]
225	40	2150 [d]	[c]
226	95	3860	[c]
227	25	[e]	[c]
228	101	4050 (19 % error)	[c]
229	26	[e]	[c]
230	16	121	[c]
231	14	262	[c]
232	23	329	[c]
233	26	931 [f]	[c]

Table 3.3: Apparent stability constants K_a (M^{-1}) determined by ^1H NMR titration techniques with compounds **204** and **223**-**233** in 0.5 % H_2O/DMSO-d_6 at 298 K following the most upfield urea NH signal unless stated otherwise. Data fitted to a 1:1 binding model. Errors < 15 % unless stated otherwise. [a] Added as TBA salts, except bicarbonate which was added as the TEA salt. [b] Binding constant obtained by following the downfield urea NH signal due to peak overlap. [c] No significant interaction. [d] Binding constant obtained by following indole NH due to broadening of urea NH signals. [e] Sigmoidal curve could not be fitted to a suitable binding model. [f] Binding constant obtained by following an aromatic CH signal due to significant broadening of thiourea NHs, fitted using raw data collected by M. Wenzel.

Compounds **204** and **223**-**233** were found to exhibit strong 1:1 binding with bicarbonate, moderate 1:1 interactions with chloride and no significant interaction with nitrate ions. Peak broadening of the urea NH signals was observed with the basic bicarbonate anion for compounds **225** and **233**. Compounds **227** and **229** exhibited

thiourea NH peak broadening upon addition of TEA bicarbonate and the resulting sigmoidal binding curves did not fit available models. Although Job plot analysis suggests 1:1 binding in both instances, the observed binding curve is perhaps indicative of more complex solution phase behaviour, or even deprotonation.[390] The self association of urea and thiourea functionalities is widely reported in both solid state and solution.[391-394] Generally the thiourea sulphur is a poor hydrogen-bond acceptor compared to the analogous urea oxygen owing to the difference in electronegativities (2.58 and 3.44 respectively on the Pauling scale).[395] Additionally, thioureas are more acidic than their analogous ureas and consequently would be expected to display higher stability constants with anionic guests.[396, 397] This trend was observed with structurally simple urea/thiourea compounds **230**-**233**, but the trend was reversed with indolyl compounds **204** and **223**-**229**, as has been observed previously (see **Section 3.3.2**).[371] Across the series the introduction of trifluoromethyl substituents onto the receptor scaffold was found to increase receptor affinity for both chloride and bicarbonate, presumably due to the increased acidity of the NH hydrogen bond donor groups.[378-382]

Conformational properties may also dictate anion affinities in solution. The *cis*-*cis* conformation of urea and thiourea compounds is more preorganised for anion binding than the *cis*-*trans* conformation. Computational modelling suggests that the urea *cis*-*cis* conformation is more stable than the analagous thiourea *cis*-*cis* conformation.[398, 399] This effect has been shown experimentally with a range of anion hosts, wherein the steric bulk of the thiourea sulphur atom results in the receptor adopting a twisted conformation. This twisting effect hinders the creation of a convergent hydrogen-bonding array, thus lowering the anion affinity of some thiourea receptors in comparison to the analogous urea compounds.[301, 304]

3.4.3 Solid State Studies

The solid state behaviour of compounds **224**, **227**, **231** and **232** was examined by single-crystal X-ray diffraction techniques. The X-ray crystal structures were obtained and solved by M. E. Light (see **Appendix A3.2**). Structures were obtained for the free receptors **231** and **232**. Crystals of compound **232** were grown by slow evaporation of a DCM/hexane mixture. The crystal structure shows characteristic intermolecular

hydrogen-bonding between urea NHs and adjacent urea oxygen atoms (N-O distances 2.923(3) and 2.936(3) Å, N-H···O angles 146.9 and 150.3° (**Figure 3.20**).[374] Crystals of compound **231** were grown by slow evaporation of a DMSO solution. In the solid state compound **231** also forms a hydrogen-bonded tape (N-H···S distances 3.363 and 3.437 Å, N-H···S angles 158 and 174°). In stark contrast to the solid state structure observed for compound **232**, adjacent thiourea molecules are bound perpendicular to one another (H···S-C angles 93.5 and 103.9°) (**Figure 3.21**). The differences in crystal packing observed with these compounds may correspond to the abilities of ureas and thioureas to self-associate, which could be reflected in the ion transport activity observed in the vesicle based assays (see **Section 3.4.4**).

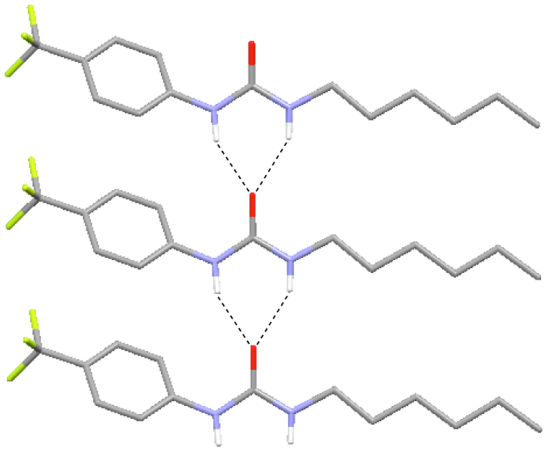

Figure 3.20: X-ray crystal structures of **232** (free receptor). Ligands are represented as wireframes; hydrogen (white), carbon (grey), nitrogen (blue), oxygen (red), fluorine (pale green). Non-interacting hydrogen atoms have been omitted for clarity.

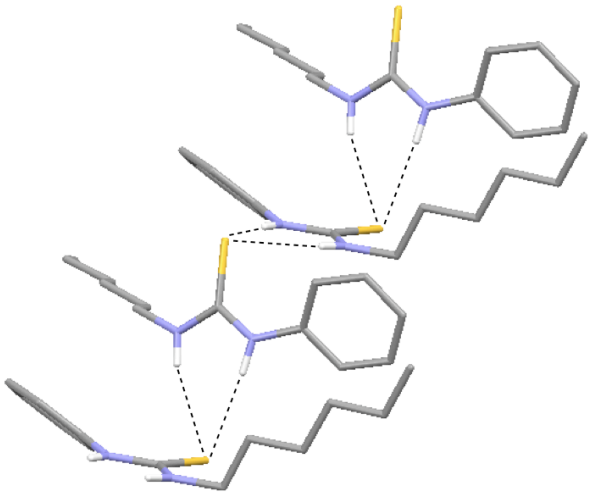

Figure 3.21: X-ray crystal structures of **231** (free receptor). Ligands are represented as wireframes; hydrogen (white), carbon (grey), nitrogen (blue), sulphur (yellow). Non-interacting hydrogen atoms have been omitted for clarity.

Crystal structures were obtained for complexes of **224** and **227** with TBA chloride. Crystals of the chloride complex of compound **224** were grown by slow evaporation of a DMSO solution. In the solid state compound **224** forms three N-H hydrogen bonds with the chloride ion (N-Cl distances 3.140(5)-3.406(5) Å, N-H···Cl angles 151.2-170.1°) (**Figure 3.22**). Crystals of the chloride complex of thiourea **227** were grown by slow evaporation of a diethylether/DCM/*iso*-propanol mixture. Compound **227** similarly forms three N-H hydrogen-bonds with the chloride ion (N-Cl distances 3.181(2)-3.235(2)Å, N-H···Cl angles 141.6-160.1°) with the thiourea group twisted with respect to the indole functionality (**Figure 3.23**).

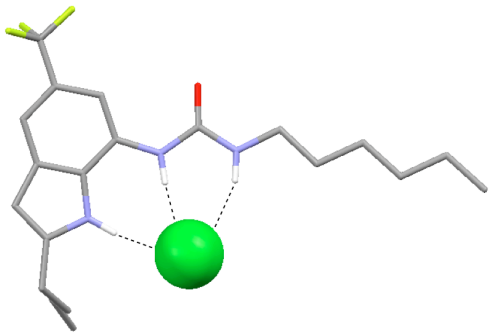

Figure 3.22: X-ray crystal structures of the 1:1 complex formed by compound **224** with TBA chloride. The ligand is represented as a wireframe and the guest anion is represented as a spacefilling model (0.6 times van der Waals radius); hydrogen (white), carbon (grey), nitrogen (blue), oxygen (red), fluorine (pale green), chlorine (green). TBA counterions and non-interacting hydrogen atoms have been omitted for clarity.

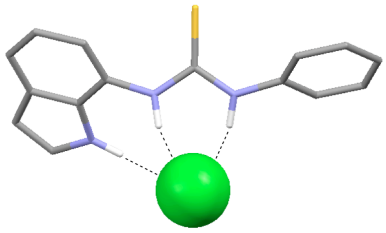

Figure 3.23: X-ray crystal structures of the 1:1 complex formed by compound **227** with TBA chloride. The ligand is represented as a wireframe and the guest anion is represented as a spacefilling model (0.6 times van der Waals radius); hydrogen (white), carbon (grey), nitrogen (blue), sulphur (yellow), chlorine (green). TBA counterions and non-interacting hydrogen atoms have been omitted for clarity.

3.4.4 Ion Transport Studies

The ion transport properties of compounds **204** and **223-233** were examined using a combination of ion selective electrode and fluorescence techniques. Initially, a Cl^-/NO_3^- antiport assay was performed (see **Section 2.2.4**). Under these conditions, the transmembrane transport of ions across a lipid bilayer is a passive process, wherein charge balance across the membrane is maintained by either a symport or an antiport mechanism. The chloride efflux in **Figures 3.24-3.26** could be the consequence of Na^+/Cl^- or H^+/Cl^- symport processes, or a Cl^-/NO_3^- antiport process. Previous studies have shown that similar carriers operate predominately *via* an antiport mechanism, and it is likely that the observed chloride efflux is predominantly due to Cl^-/NO_3^- exchange. [361, 371]

To confirm an antiport transport mechanism in this experiment, encapsulated NaCl was replaced with CsCl. No significant changes in chloride transport rates were observed upon changing the encapsulated metal cation, ruling out the possibility of M^+/Cl^- co-transport (see **Appendix A5.1**).

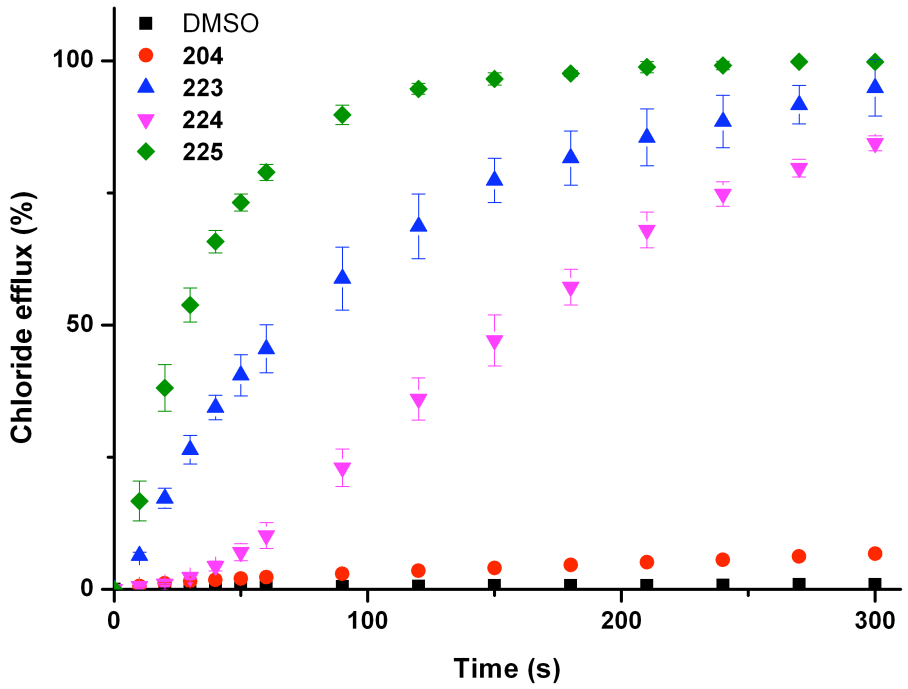

Figure 3.24: Chloride efflux promoted by a DMSO solution of compounds **204** and **223**-**225** (2 mol % with respect to lipid) from unilamellar POPC vesicles loaded with 488 mM NaCl buffered to pH 7.2 with 5 mM sodium phosphate salts. The vesicles were dispersed in 488 mM $NaNO_3$ buffered to pH 7.2 with 5 mM sodium phosphate salts. At the end of the experiment, detergent was added to lyse the vesicles and calibrate the ISE to 100 % chloride efflux. Each point represents an average of three trials.

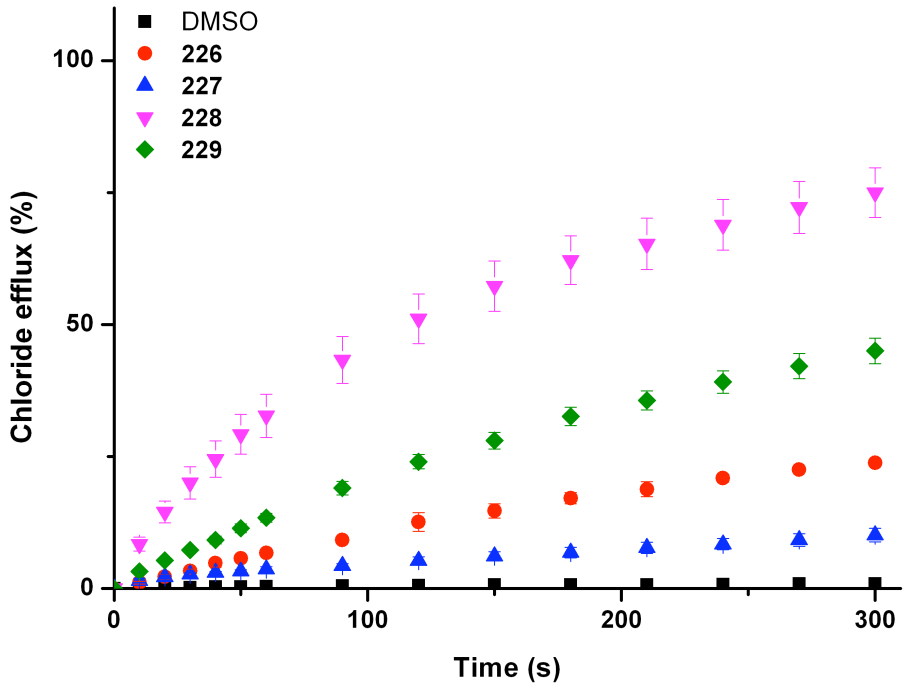

Figure 3.25: Chloride efflux promoted by a DMSO solution of compounds **226**-**229** (2 mol % with respect to lipid) from unilamellar POPC vesicles loaded with 488 mM NaCl buffered to pH 7.2 with 5 mM sodium phosphate salts. The vesicles were dispersed in 488 mM $NaNO_3$ buffered to pH 7.2 with 5 mM sodium phosphate salts. At the end of the experiment, detergent was added to lyse the vesicles and calibrate the ISE to 100 % chloride efflux. Each point represents an average of three trials.

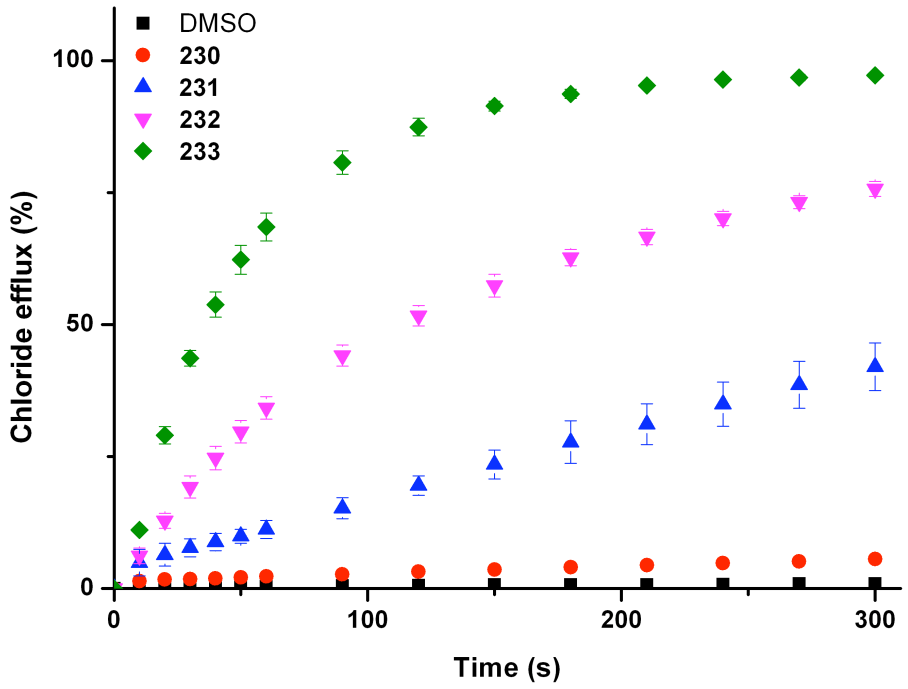

Figure 3.26: Chloride efflux promoted by a DMSO solution of compounds **230-233** (2 mol % with respect to lipid) from unilamellar POPC vesicles loaded with 488 mM NaCl buffered to pH 7.2 with 5 mM sodium phosphate salts. The vesicles were dispersed in 488 mM $NaNO_3$ buffered to pH 7.2 with 5 mM sodium phosphate salts. At the end of the experiment, detergent was added to lyse the vesicles and calibrate the ISE to 100 % chloride efflux. Each point represents an average of three trials.

Compounds **204** and **223-233** were also tested in POPC vesicles for their ability to mediate the more biologically relevant Cl^-/HCO_3^- antiport process using a bicarbonate 'pulse' ISE assay (see **Section 2.2.4**).[50, 53, 54, 400, 401] The results of this assay are shown in **Figures 3.27-3.29**.

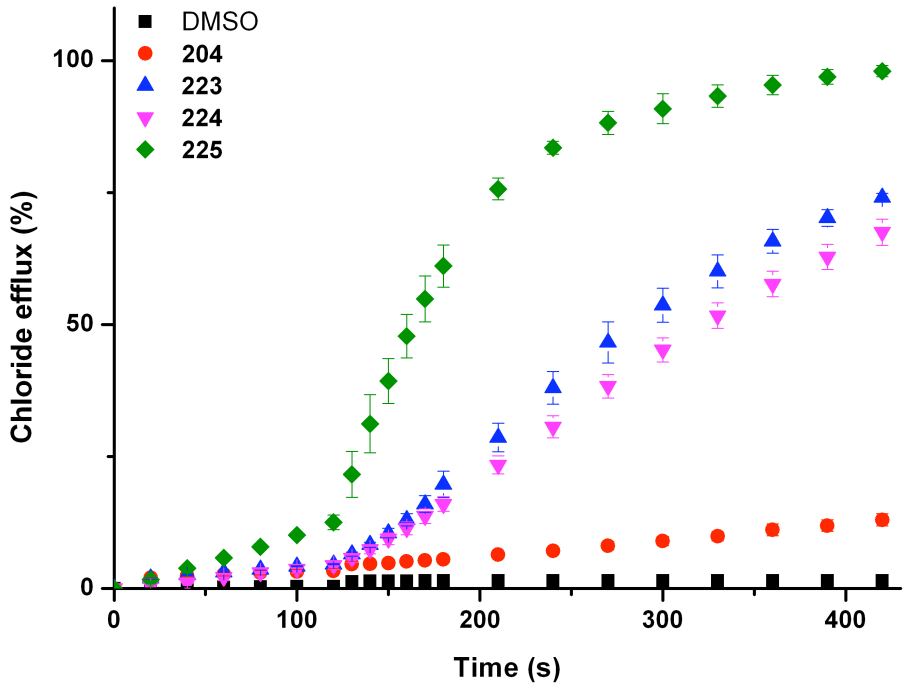

Figure 3.27: Chloride efflux promoted by a DMSO solution of compounds **204** and **223**-**225** (2 mol % with respect to lipid) from unilamellar POPC vesicles loaded with 451 mM NaCl buffered to pH 7.2 with 20 mM sodium phosphate salts. The vesicles were dispersed in 150 mM Na_2SO_4 buffered to pH 7.2 with 20 mM sodium phosphate salts. At t = 120 s a sodium bicarbonate 'pulse' was added such that the external concentration of bicarbonate was 40 mM. At the end of the experiment, detergent was added to lyse the vesicles and calibrate the ISE to 100 % chloride efflux. Each point represents an average of three trials.

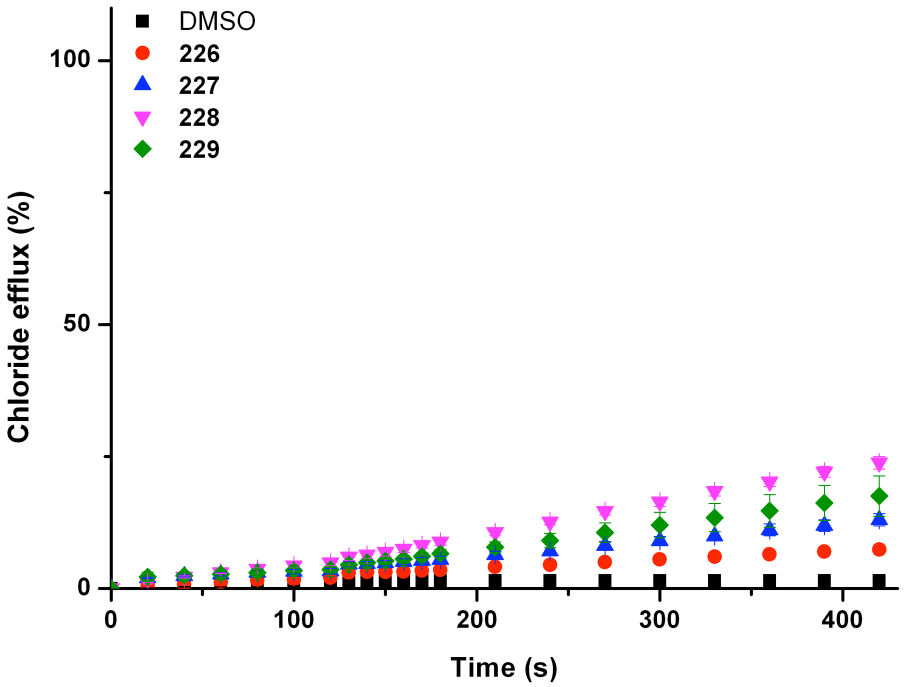

Figure 3.28: Chloride efflux promoted by a DMSO solution of compounds **226-229** (2 mol % with respect to lipid) from unilamellar POPC vesicles loaded with 451 mM NaCl buffered to pH 7.2 with 20 mM sodium phosphate salts. The vesicles were dispersed in 150 mM Na_2SO_4 buffered to pH 7.2 with 20 mM sodium phosphate salts. At t = 120 s a sodium bicarbonate 'pulse' was added such that the external concentration of bicarbonate was 40 mM. At the end of the experiment, detergent was added to lyse the vesicles and calibrate the ISE to 100 % chloride efflux. Each point represents an average of three trials.

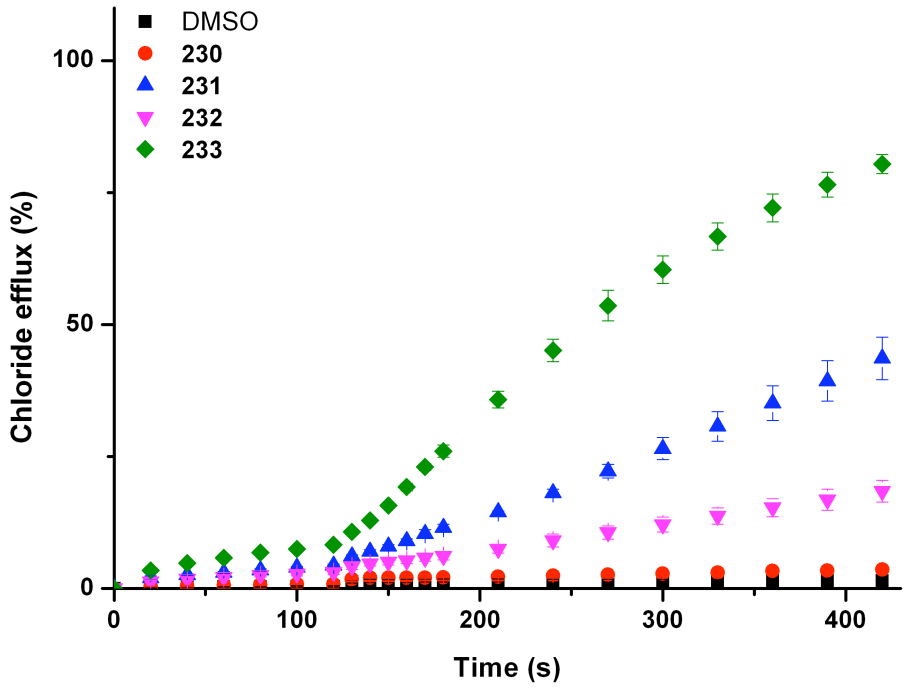

Figure 3.29: Chloride efflux promoted by a DMSO solution of compounds **230**-**233** (2 mol % with respect to lipid) from unilamellar POPC vesicles loaded with 451 mM NaCl buffered to pH 7.2 with 20 mM sodium phosphate salts. The vesicles were dispersed in 150 mM Na_2SO_4 buffered to pH 7.2 with 20 mM sodium phosphate salts. At t = 120 s a bicarbonate 'pulse' was added such that the external concentration of bicarbonate was 40 mM. At the end of the experiment, detergent was added to lyse the vesicles and calibrate the ISE to 100 % chloride efflux. Each point represents an average of three trials.

Due to the difference in hydrophilicity, the doubly negatively charged sulfate anion is more difficult to transport across lipid bilayers than the nitrate anion.[22] Thus, for the first two minutes of the bicarbonate 'pulse' assay (before the 'pulse') chloride transport cannot occur as the result of an antiport mechanism. Upon addition of the bicarbonate 'pulse', Cl^-/HCO_3^- exchange becomes possible, and a marked increase in chloride efflux for the majority of the compounds was observed (**Figures 3.27-3.29**).

For some of the compounds, low levels of chloride efflux were recorded in the two minutes before the chloride pulse in the aforementioned assay. To investigate this effect further, the experiment was repeated without the bicarbonate 'pulse'. Significant chloride efflux (> 15 % after 420 s) was observed only for thiourea compound **225** (**Figure 3.30**). Under the experimental conditions, chloride efflux could only be due to

H^+/Cl^- symport or Cl^-/SO_4^{2-} antiport.

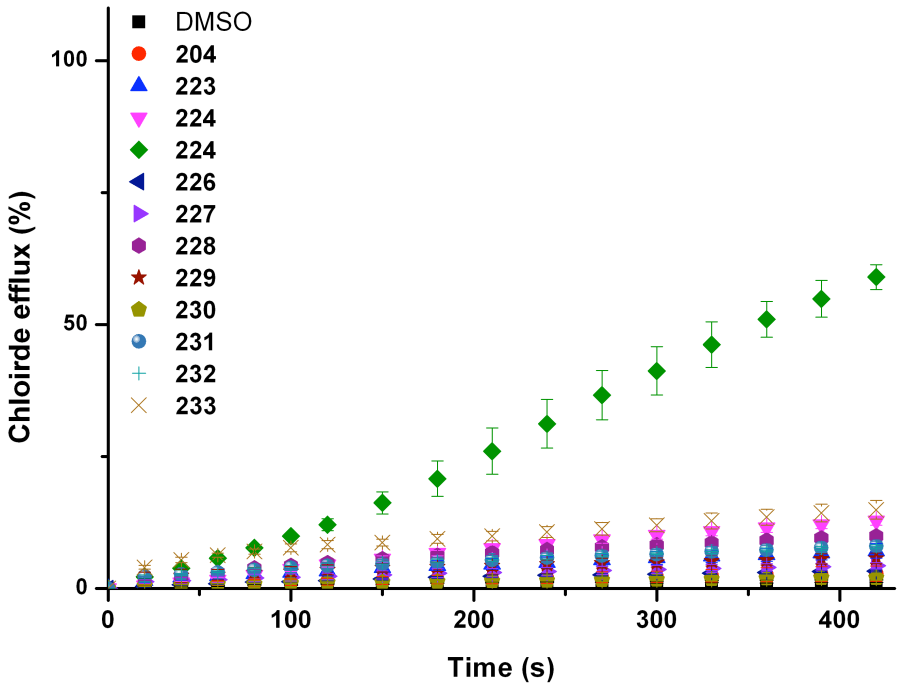

Figure 3.30: Chloride efflux promoted by a DMSO solution of compounds **204** and **223-233** (2 mol % with respect to lipid) from unilamellar POPC vesicles loaded with 451 mM NaCl buffered to pH 7.2 with 20 mM sodium phosphate salts. The vesicles were dispersed in 150 mM Na_2SO_4 buffered to pH 7.2 with 20 mM sodium phosphate salts. At the end of the experiment, detergent was added to lyse the vesicles and calibrate the ISE to 100 % chloride efflux. Each point represents an average of three trials.

To examine the possibility transmembrane sulfate transport unilamellar POPC vesicles were prepared containing 100 mM NaCl and 2 mM lucigenin buffered to pH 7.2 with 20 mM phosphate buffer.[249] These vesicles were suspended in 100 mM NaCl solution buffered to pH 7.2 with 20 mM phosphate salts. A 'pulse' of sodium sulfate was added such that the external concentration of sulfate was 40 mM. For compounds **204** and **223-233** no evidence of sulphate transport was observed using this assay (see **Appendix A5.1**). To confirm that the chloride efflux observed with compound **225** was therefore the result of H^+/Cl^- co-transport, a pH gradient study was performed.[147] Vesicles containing 451 mM sodium chloride buffered to pH 4.0 with 20 mM citric acid buffer were suspended in a solution of 150 mM sodium sulfate buffered to pH 7.2 with 20 mM sodium phosphate salts. **Figure 3.31** shows that the rate of chloride transport facilitated

by compound **225** under gradient conditions is greater than in the absence of a pH gradient, supporting an H^+/Cl^- symport mechanism.

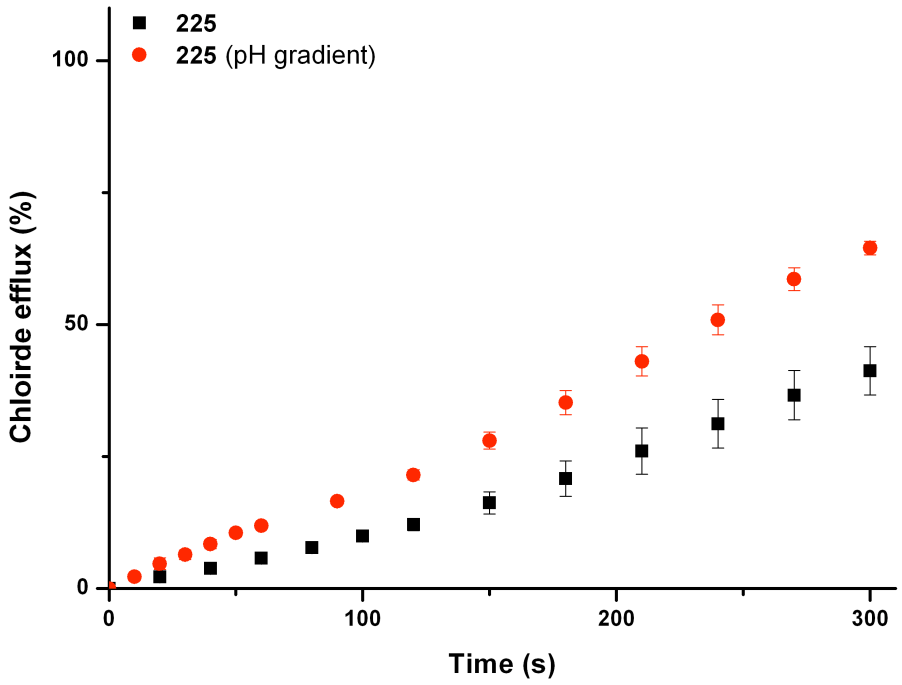

Figure 3.31: Chloride efflux promoted by a DMSO solution of compound **225** (2 mol % with respect to lipid) from unilamellar POPC vesicles loaded with either 451 mM NaCl buffered to pH 7.2 with 20 mM sodium phosphate salts or 451 mM NaCl buffered to pH 4.0 with 20 mM sodium citrate salts. The vesicles were dispersed in 150 mM Na_2SO_4 buffered to pH 7.2 with 20 mM sodium phosphate salts. At the end of the experiment, detergent was added to lyse the vesicles and calibrate the ISE to 100 % chloride efflux. Each point represents an average of three trials.

Proton transport was confirmed directly with POPC vesicles loaded with NaCl (451 mM) and HPTS (see **Section 1.9.3**).[246] These vesicles were suspended in a solution of Na_2SO_4 (150 mM) and the HPTS fluorescence was measured upon addition of a DMSO solution of compound **225**. An increase in intravesicular pH was observed, corresponding to deacidification of the vesicles *via* either H^+/Cl^- co-transport or an equivalent Cl^-/OH^- antiport pathway (see **Appendix A5.1**).

Cholesterol mobility assays (see **Section 3.3.4**) proved inconclusive, hence U-tube assays (see **Section 1.9.6**) were used to examine the transport mechanism. In these assays the membrane is modelled by a bulk organic phase separating two aqueous phases.

For solubility reasons nitrobenzene was used as the organic phase. The source phase was loaded with sodium chloride (488 mM buffered to pH 7.2 with 5 mM sodium phosphate salts) and the receiving phase was loaded with sodium nitrate (488 mM buffered to pH 7.2 with sodium phosphate salts). The carrier (1 mM) and TBA hexafluorophosphate (1 mM) was dissolved in the nitrobenzene organic phase and chloride transport into the receiving phase was monitored using an ion selective electrode. Owing to the separation of the two aqueous phases, transport by a channel mechanism is not possible.[402] Compounds **223**-**225**, **228**, **229**, **232** and **233** were tested by this method. In all cases a higher concentration of chloride was measured in the receiving phase, than was observed in the control experiment (see **Appendix A5.1**). These results, coupled with low n values by Hill analysis (**Table 3.4**) suggest that this series of compounds facilitate ion transport *via* a mobile carrier mechanism rather than by channel formation.

Compound	$EC_{50,\,270\,s}$ [a] (Cl^-/NO_3^-)	n [b] (Cl^-/NO_3^-)	$EC_{50,\,270\,s}$ [a] (Cl^-/HCO_3^-)	n [b] (Cl^-/HCO_3^-)	wclogP [c]
204	[d]	[d]	[d]	[d]	3.87
223	0.029	0.8	0.18	0.7	4.03
224	0.47	1.3	1.2	2.0	6.23
225	0.016 [e]	1.7 [e]	0.081 [e]	1.5 [e]	6.40
226	[d]	[d]	[d]	[d]	3.81
227	[d]	[d]	[d]	[d]	3.98
228	1.1	1.6	[d]	[d]	4.83
229	2.6	1.2	[d]	[d]	5.00
230	[d]	[d]	[d]	[d]	3.39
231	2.9	1.4	3.1	0.6	3.55
232	1.4	2.4	[d]	[d]	4.41
233	0.44	1.6	0.59	1.1	4.57

Table 3.4: Overview of transport assays for compounds **204** and **223**-**233**. Values for wclogP are also displayed. [a] $EC_{50,\,270\,s}$ defined as concentration (mol % carrier with respect to lipid) needed to achieve 50 % chloride efflux after 270 s. [b] Hill coefficient. [c] Calculated using Fieldview Version 2.0.2 for Macintosh. [d] Hill analysis not performed due to low activity. [e] Some of the observed activity is from H^+/Cl^- co-transport.

To quantify the transport activity of compounds **204** and **223-233** Hill analyses (see **Section 9.8**) for the Cl^-/NO_3^- and Cl^-/HCO_3^- antiport assays were performed (see **Appendix A5.1**). Hill analysis allowed determination of an $EC_{50,\ 270\ s}$ value; the concentration of carrier (mol % with respect to lipid) required to afford 50 % chloride efflux 270 s after addition of the carrier (or after the bicarbonate 'pulse'), enabling comparison of the transport activity of the compounds. These values are summarised in **Table 3.4**, together with the Hill coefficients and the calculated values for wclogP. This data reveals that the trifluoromethyl functionalised receptors are more active than their unfluorinated analogues in the Cl^-/NO_3^- and Cl^-/HCO_3^- assays in all instances. Correspondingly, the wclogP of the trifluoromethyl functionalised compounds is higher than that of their unfluorinated analogues. It is known that the introduction of a trifluoromethyl group onto an aromatic system increases lipophilicity.[378-382] The enhanced membrane partitioning afforded by the addition of the trifluoromethyl moiety, combined with stronger anion binding properties through electron withdrawing effects (see **Section 3.4.2**) afford the trifluoromethyl functionalised compounds enhanced ion transport activity. Thiourea transporters are often more active than their analogous ureas owing to differences in lipophilicity.[347, 371] In this series the thioureas are more active than the analogous ureas for compounds **204** and **223-225**, and **230-233**. The reverse is true for compounds **226-229**, although it should be noted that this series of compounds is significantly less active as anion transporters. For these latter compounds there may be a steric factors to consider, since we observed twisting of the indole moiety in the solid state for compound **227** (see **Section 3.4.3**).

3.4.5 Cell Based Assays

The cell based assays described in this section were performed by V. Soto-Cerrato at the University of Barcelona. Modulation of intracellular pH (pH_i) is a promising new strategy for cancer treatment (see **Section 1.5.4**).[403] The promising ion transport activity of the series led to the investigation of the *in vitro* cytotoxicity of receptors **204** and **223-233** in a diverse range of cancerous cell lines (human melanoma A375, human small-cell lung carcinoma (SCLC) GLC4, human colon adenocarcinoma SW480, and human oral adenosquamos carcinoma CAL27). A single point screening at receptor concentrations of

10 μM was performed using a 3-(4,5-dimethylthiazol-2-yl)-2,5-diphenyltetrazolium bromide (MTT) cell viability assay. **Figure 3.32** shows that 48 hours after receptor exposure significant cytotoxicity was observed with compounds **224**, **225**, **228**, **232** and **233**, especially in GLC4 and A375 cells. The other compounds did not display a significant cytotoxicity at this dose and time interval.

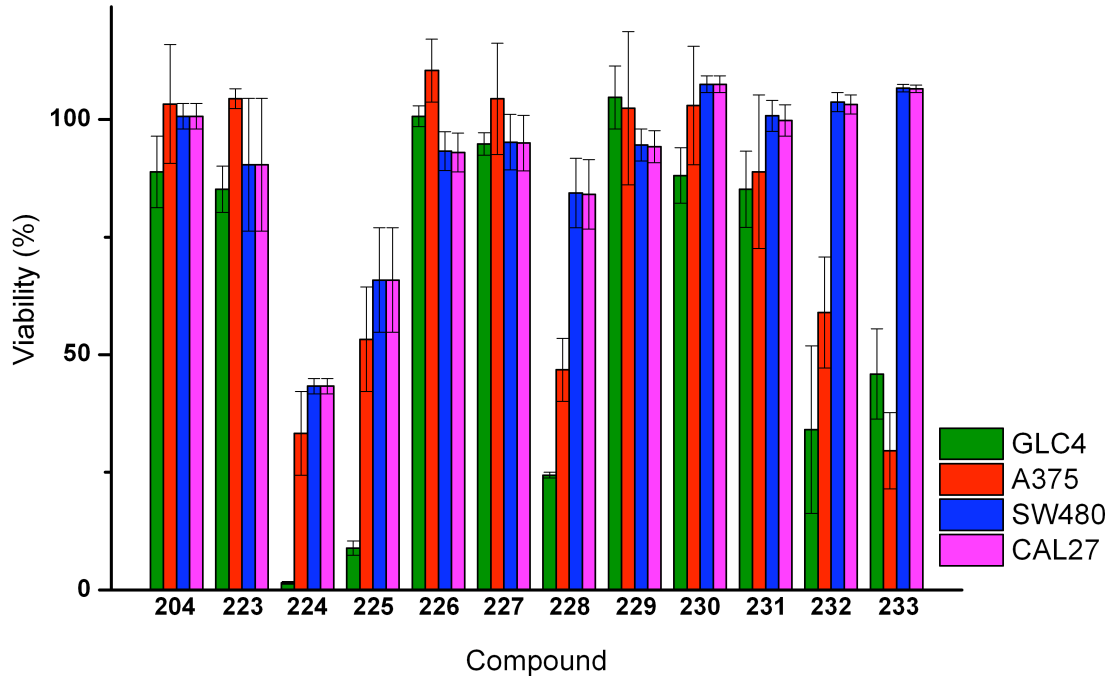

Figure 3.32: Cell viability 48 hours after exposure to compounds **204** and **223**-**233** (10 μM) on a range of cancer cell lines, measured by MTT assay.

Dose-response curve experiments were performed to determine IC_{50} values (inhibitory concentration of 50 % of the cell population) for the cytotoxic compounds in the most sensitive cancerous cell lines. IC_{50} values were also determined in non-cancerous human MCF10A mammary epithelial cells. The results of these studies are displayed in **Table 3.5**. High potency is observed in the GLC4 cell line, with IC_{50} values of around 10 μM. The reduction in cytotoxicity towards non-cancerous MCF10A cells suggests that these receptors have some specificity towards cancerous cells.

Compound	GLC4	A375	MCF10A
224	6.0 ± 1.1	17.4 ± 5.5	> 70
225	6.3 ± 0.5	14.3 ± 0.1	> 40
228	9.7 ± 1.7	22.9 ± 2.6	> 200
232	16.8 ± 0.4	13.7 ± 2.0	> 200
233	14.9 ± 0.1	21.1 ± 0.8	> 30

Table 3.5: IC_{50} values (μM) of cytotoxic compounds **224**, **225**, **228**, **232** and **233** on GLC4 (cancerous), A375 (cancerous) and MCF10A (non-cancerous) cell lines.

All of the significantly active compounds in the MTT assay contain a trifluoromethyl group. In the vesicle based ion transport assays the fluorinated compounds exhibit higher anion affinity in solution and improved ion transport properties, compared to their unfluorinated analogues (see **Sections 3.4.2** and **3.4.4**). The one fluorinated compound that did not show significant cytotoxic properties, **229**, was found to have the lowest transport activity of all the fluorinated compounds in the series in ISE experiments.

The control of pH_i is essential for regulation of the cell cycle, proliferation and cell death (see **Section 1.5.4**). This is achieved biologically by several transport mechanisms including Na^+/H^+ and Na^+/HCO_3^- co-transport, Cl^-/HCO_3^- antiport and H^+ uniport.[404] Owing to the ability of the receptors to facilitate transmembrane ion transport in vesicle based assays, transport activity within a biological context was examined in A375 melanoma cells using vital staining with acridine orange (AO), a cell-permeable fluorescent dye.[405] Within acidic cellular compartments AO becomes protonated and exhibits orange fluorescence, whilst in the more basic cytosol it exhibits green fluorescence.[406]

Cells in basal conditions were stained with AO (**Figure 3.33a** and **3.33b**). Acidic cellular compartments (such as lysosomes) were found to display granular orange fluorescence. Following exposure to cytotoxic compounds **224**, **225**, **228**, **232** and **233** (**Figure 3.33c**, **3.33d**, **3.33e**, **3.33f** and **3.33g** respectively) the orange fluorescence disappeared, indicating an increase in the pH of the acidified organelles. Following exposure to non-cytotoxic compound **226** (**Figure 3.33h**), pH_i was not sufficiently altered

to cause the disappearance of the orange fluorescence.

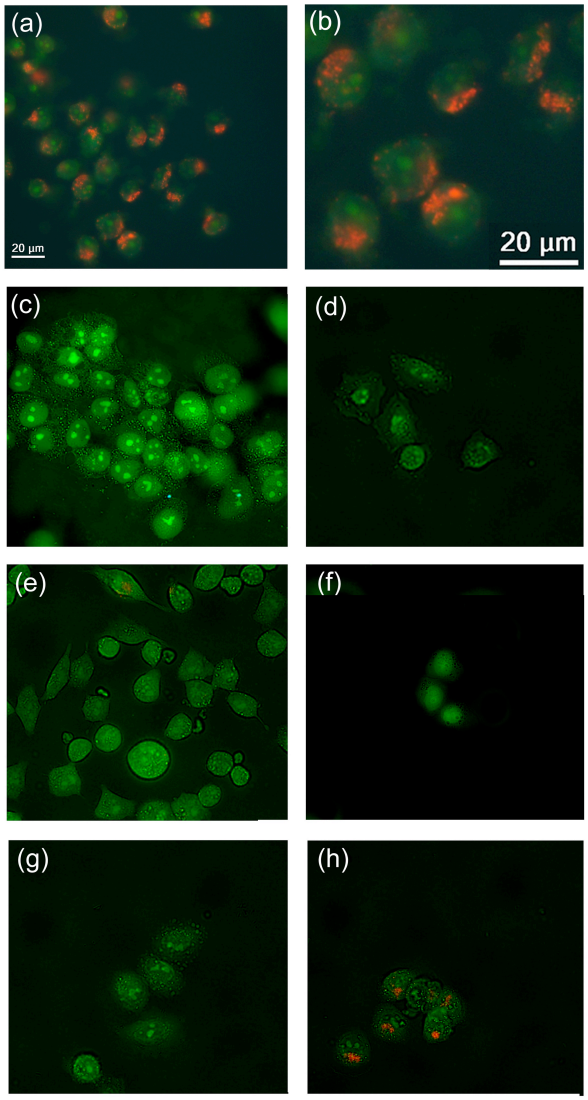

Figure 3.33: Acridine orange (AO) staining of melanoma A375 cells 1 hour after exposure (10µM) to: (a, b) Untreated cells, (c) **224**, (d) **225**, (e) **228**, (f)**232**, (g) **233** and (h) **226**.

Reduction of pH_i disrupts normal cellular function, inducing cell damage. Sufficiently large reductions in pH_i have been shown to promote apoptosis in cancer cells.[406] Apoptosis is programmed cell death, leading to the removal of damaged cells without causing inflammation (a feature of non-apoptotic cell death). Several types of cytotoxic compound, such as prodiginines, tambjamines, and fluorinated tripodal moleucles have been shown to promote apoptosis through the lowering of pH_i.[81, 101, 249] The modification of pH_i has been attributed to either H^+/Cl^- co-transport or Cl^-/HCO_3^-

antiport in all of these cases. All of the compounds that facilitated a decrease in pH_i in the AO assay are potent Cl^-/NO_3^- antiport agents. In addition compounds **224**, **225** and **233** are potent Cl^-/HCO_3^- antiport agents and compound **225** can facilitate H^+/Cl^- co-transport (see **Section 3.4.4**). The biological activity of these molecules may originate from the transmembrane transport of HCl or bicarbonate, but equally could be the consequence of an ion transport process coupled to the uniport of chloride.[407]

Apoptosis can be induced by changes in pH_i, suggesting that compounds **224**, **225**, **228**, **232** and **233** may induce this type of cell death.[408, 409] Apoptosis is characterised by changes is nuclear morphology including nuclear condensation, fragmentation and the formation of apoptotic bodies. These changes in nuclear structure can be observed by Hoechst 33342 staining, a fluorescent nuclear dye. Cancerous A375 cells were exposed to cytotoxic compounds **224**, **225**, **228**, **232** and **233** and were stained with Hoechst 33342 to evaluate whether these compounds trigger apoptosis. The results of this assay are shown in **Figure 3.34**. Untreated cells have typical rounded nuclear morphology (**Figure 3.34a**), whilst cells treated with cytotoxic compounds **224**, **225**, **228**, **232** and **233** show nuclear condensation and the formation of apoptotic bodies (**Figures 3.34b**, **3.34c**, **3.34d**, **3.34e** and **3.34f** respectively). These results confirm that the type of cell death induced by these compounds is apoptosis.

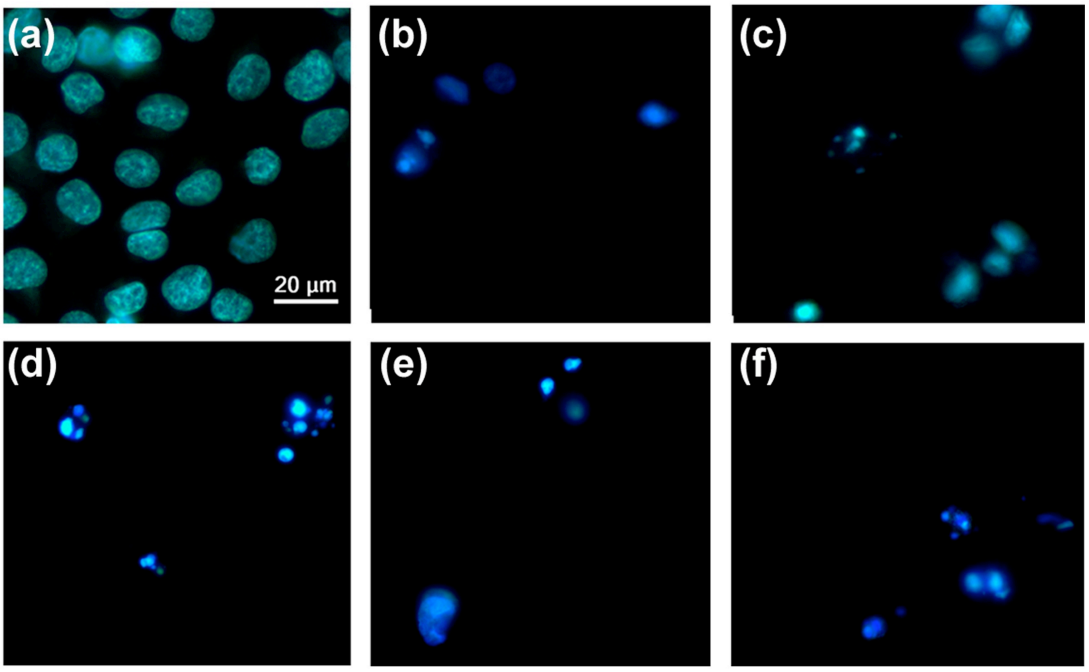

Figure 3.34: Hoechst 33342 staining of cancerous A375 cells 48 hours after exposure (10 µM) to: (a) untreated cells, (b) **224**, (c) **225**, (d) **228**, (e) **232**, (f) **233**.

3.5 Conclusions

It has been shown that fluorination of structurally simple ureas and thioureas yields a significant increase in transmembrane transport activity, and can even promote new transport pathways (H^+/Cl^- symport was observed with compound **225**). Introduction of a trifluoromethyl group increased the anion affinity and lipophilicity of the receptors and yielded compounds that facilitated ion transport *in vitro*. Trifluoromethyl bearing compounds **224**, **225**, **228**, **232** and **233** were found to be cytotoxic towards cancerous cells, inducing apoptosis as a consequence of sustained changes in internal pH regulation. Critically, the ability of the transporters to partition within bilayers (either in POPC vesicles or in live cells) is likely to have been enhanced by fluorination.[410-412] Significantly, these molecules represent an improvement in the 'drug-like' characteristics of anion transporters.[249] All of these molecules adhere to the Lipinski parameters with the exception of compounds **224** and **225** which have wclogP values greater than 5 (6.23 and 6.40 respectively).[356] Even this may be within the acceptable range for molecules desired to function as mobile carriers, since the Lipinski parameters are guidelines to achieve membrane permeation rather than partitioning into the bilayer.

Chapter 4
Bisurea Anion Transporters

4.1 Introduction

The development of new motifs that facilitate the transmembrane transport of ionic species can uncover molecules with often surprising and novel transport activity. In **Chapter 2** ureas were shown to be useful motifs for anion binding and in **Chapter 3** the indolylurea/thiourea motif was used to create molecules capable of facilitating ion transport within living cells. In this chapter the *ortho*-phenylenediamine based bisurea system is studied as a motif for the transmembrane transport of chloride, nitrate, bicarbonate and carboxylate anions.

4.1.1 Bisureas as Anion Hosts

The urea group has been successfully utilised in a diverse range of anion receptors, and consequently bisureas have been widely used in the construction of anion hosts.[348, 349] Steed and co-workers have pioneered the use of chiral bisurea compounds as anion sensitive gelators.[413, 414] Gelation of bisurea **234** (**Figure 4.1**) was observed in a range of solvents including acetonitrile, chloroform and DMSO, owing to the formation of antiparallel hydrogen-bonded urea chains. Gel stability was disrupted by the addition of bromide, chloride and acetate, since anion binding by the urea NH groups inhibited the intermolecular hydrogen-bonding interactions required for bisurea gelation.

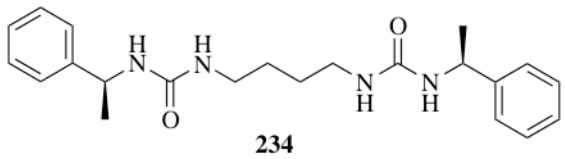

234

Figure 4.1: Bisurea gelator **234**.

There are numerous published examples of convergent bisureas as motifs for anion recognition. A rigid naphthalene group can be functionalised at the 1- and 8-

positions to produce receptors with two adjacent urea groups. Owing to the small anion binding pocket produced by such an arrangement of hydrogen-bond donor groups, receptor **235** (**Figure 4.2**) displays a forty-fold selectivity for fluoride over chloride, and exhibits fluoride selective fluorescent effects.[415] Compounds **236-238** (**Figure 4.2**) were based on a similar design and formed gels in a range of solvents including ethyl acetate, *N,N'*-dimethylformamide (DMF) and butan-1-ol. Addition of fluoride (but not the larger halides such as chloride, bromide or iodide) induced a gel-sol transition, owing to the disruption of intermolecular hydrogen-bonding.[416, 417]

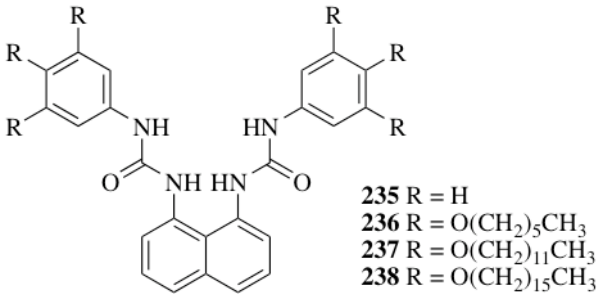

Figure 4.2: Bisureas **235-238** contain a rigid naphthalene core.

A range of other scaffolds have been utilised that can accommodate the attachment of two urea functionalities. The attachment of *para*-nitrophenyl groups onto a twelve-membered tetra-aza macrocycle, yields receptor **239** (**Figure 4.3**) that is selective for acetate. UV-vis studies in 0.5 % H_2O/DMSO, reveal that compound **239** forms a 1:2 (host:guest) complex with TBA acetate.[418] Johnson and co-workers showed that attachment of urea functionalities to a rigid 2,6-bis(2-anilinoethynyl)pyridine scaffold yields receptor **240** (**Figure 4.3**), which forms 1:1 complexes with halides.[419] Upon protonation the pyridyl NH supplies an additional hydrogen-bonding interaction in the binding pocket, increasing the observed binding constants for chloride in $CDCl_3$ by an order of magnitude; K_a = 2100 M^{-1} (no acid) and > 10^4 M^{-1} (with one equivalent of trifluoroacetic acid). Compound **241 (Figure 4.3)** shows how urea groups can be attached to a carbazole scaffold at the 1- and 8- positions, yielding a colorimetric sensor for the detection of basic hydroxide and fluoride ions.[420, 421]

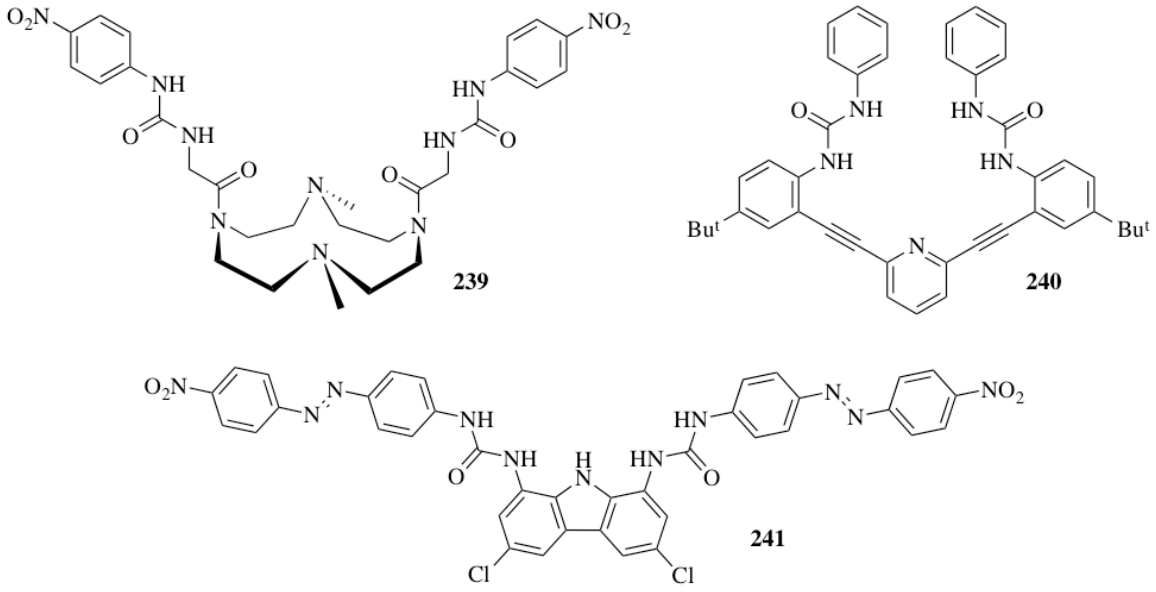

Figure 4.3: A selection of the versatile range of scaffolds from which pendant urea functionalities can be attached.

One of the simplest scaffolds that can be utilised for the attachment of urea groups is a phenyl core. Hamilton and coworkers found that reaction of 1,4-bis(aminomethyl)benzene with butylisocyanate afforded bisurea compound **242**.[422-423] The steric arrangement of urea functionalities in this molecule was found to be suitable for dicarboxylate binding; a binding constant of 640 M^{-1} was calculated by ^{1}H NMR titration with TBA glutarate in DMSO-d_6. The binding model proposed by the authors is shown in **Figure 4.4**. The analogous 1,3-phenylbisurea **243** (**Figure 4.4**) is a selective receptor for dihydrogen phosphate, although only modest anion affinities were observed in DMSO-d_6, with K_a = 110 M^{-1} for TBA dihydrogen phosphate and K_a = 43 M^{-1} for TBA acetate.[424]

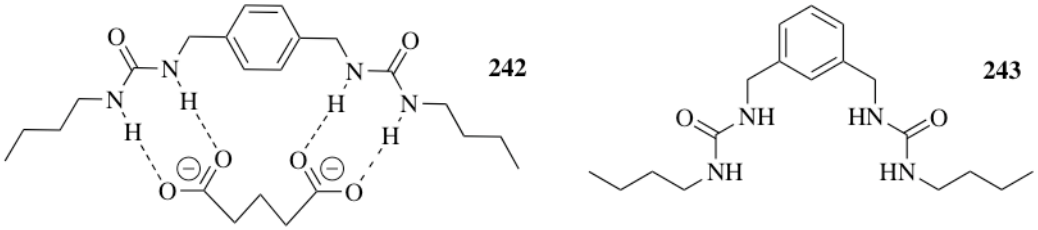

Figure 4.4: The proposed binding mode of glutarate with 1,4-phenylbisurea **242** and the analogous 1,3-phenylbisurea **243**.

A wide range of bisurea scaffolds have been studied as anion receptors, but the use of bisureas as anion transporters is less thoroughly explored.[425-427] In **Section 1.8.1** cholapods were shown to be useful scaffolds for the attachment of pendant urea functionalities producing potent lipophilic anion transporters, whilst bisindolylureas employed as transmembrane chloride transporters were discussed in **Section 3.1.1**.[270]

4.1.2 Supramolecular Chemistry of *ortho*-phenylenediamine Based Bisureas

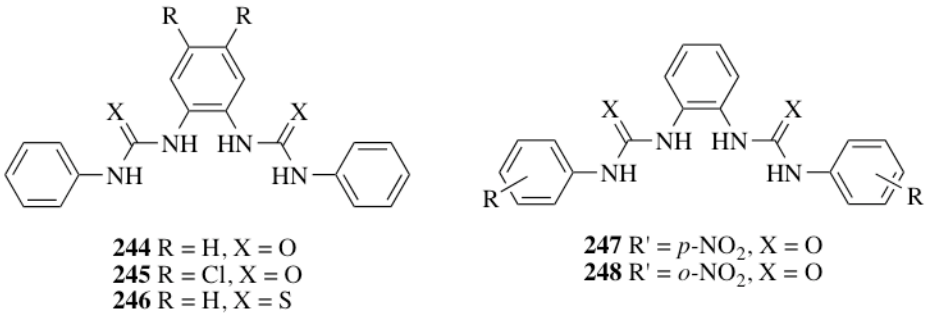

244 R = H, X = O
245 R = Cl, X = O
246 R = H, X = S

247 R' = *p*-NO_2, X = O
248 R' = *o*-NO_2, X = O

Figure 4.5: Bisureas based on the *ortho*-phenylenediamine scaffold.

Ortho-phenylenediamine based bisureas have found extensive use in the field of supramolecular chemistry. The anion complexation behaviour of compounds **244**-**248** (**Figure 4.5**) was studied by Gale and coworkers.[428, 429] The X-ray crystal structure of **244** with TBA benzoate reveals that the benzoate anion is bound by four hydrogen-bonding interactions with the receptor urea NH groups (**Figure 4.6**). The carboxylate anion was found to bridge the two urea functionalities, with hydrogen-bonds in the range 2.740(4)-2.939(4) Å (N-O distances).

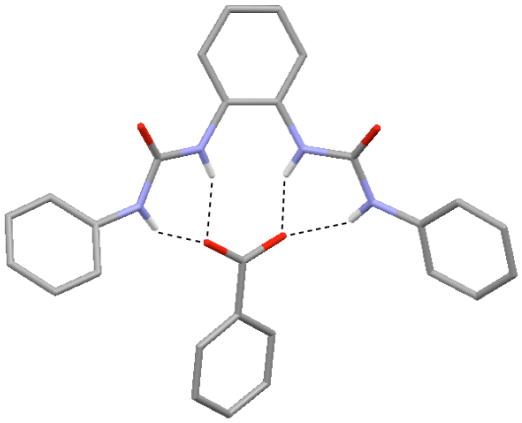

Figure 4.6: The benzoate complex of receptor **244**, showing the benzoate anion bound by four hydrogen-bonding interactions. The ligand and guest anion are represented as wireframes; hydrogen (white), carbon (grey), nitrogen (blue), oxygen (red). The TBA counterions and non-interacting hydrogen atoms have been omitted for clarity.[428]

Anion binding studies were performed using ^{1}H NMR titration techniques in a 0.5 % H_2O/DMSO-d_6 solvent mixture. Bisureas **244-248** were found to be good receptors for oxo-anions including acetate, benzoate and dihydrogen phosphate (see **Table 4.1**). The addition of chlorine substituents onto the central phenyl ring (compound **245**) was found to dramatically improve anion affinity (see **Table 4.1**). The authors attributed this enhancement to an increase in the acidity of both the urea NHs and the aromatic CHs on the central phenyl ring. This latter effect strengthens intramolecular hydrogen-bonding interactions, improving receptor preorganisation (see **Figure 4.7**).

Anion [a]	**244**	**245**	**246**	**247**	**248**
Cl^-	43	67	18	78	[b]
AcO^-	3210	8079	[c]	4018	1739
BzO^-	1330	2248	1249	1399	541
$H_2PO_4^-$	732	4724	1637	666	349

Table 4.1: Apparent stability constants K_a (M^{-1}) determined by ^{1}H NMR titrations with compounds **244-248** in 0.5% H_2O/DMSO-d_6 at 298 K.[246, 247] Data fitted to a 1:1 binding model. [a] Added as TBA salts. [b] No significant interaction. [c] Deprotonation.

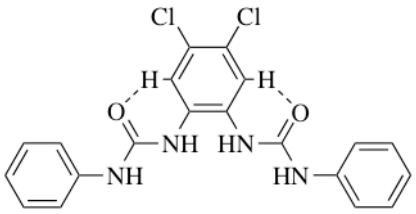

Figure 4.7: Introduction of chlorine atoms onto the central phenyl core in compound **245** improves receptor preorganisation by strengthening intramolecular hydrogen-bonding interactions.

Addition of *para*-nitro substituents to the peripheral phenyl rings in **247** led to an increase in anion affinity towards chloride and acetate (see **Table 4.1**), predominantly due to the electron withdrawing effects of the *para*-nitro substituents. However, *ortho*-nitro substituted compound **248** displayed lower binding constants with respect to 'unfunctionalised' compound **244** (see **Table 4.1**). This was due to the *ortho*-nitro substituents on the peripheral phenyl rings sterically blocking the anion binding site. Thiourea **246** displayed lowered affinity for chloride (see **Table 4.1**). X-ray crystal analysis of **246** revealed that this compound adopts a twisted conformation in the solid state (**Figure 4.8**). The authors postulated that the greater steric bulk of the sulphur in the thiourea motif may cause the binding site to twist in solution, disfavouring carboxylate binding but promoting the coordination of dihydrogen phosphate.

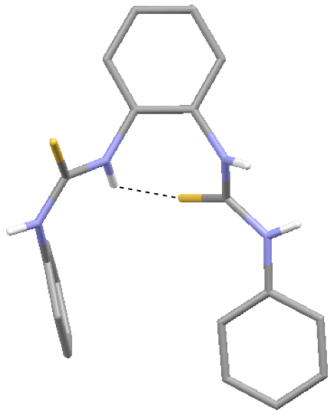

Figure 4.8: X-ray crystal structure of **246**. In solution the bulky sulphur atoms of the thiourea groups may cause the molecule to twist. The ligand is represented as a wireframe; hydrogen (white), carbon (grey), nitrogen (blue), sulphur (yellow). Non-interacting hydrogen atoms have been omitted for clarity.[429]

Bisureas based on the *ortho*-phenylenediamine scaffold have found a range of other applications. Owing to the reliable mode of carboxylate binding exhibited by this family of molecules, compound **249** (**Figure 4.9**) was synthesised for use in crystal engineering.[430] Compound **249** contains two bisurea clefts, which in the presence of suitable dicarboxylate anions can form extended hydrogen-bonded networks. Similar bisurea motifs have found applications in catalysis and as gelators.[432-434]

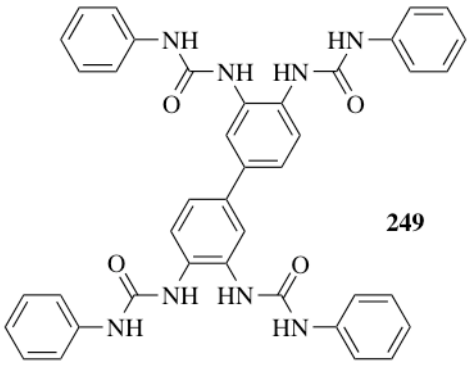

Figure 4.9: Supramolecular synthon **249** containing two bisurea functionalities can assemble into extended supramolecular networks in the presence of suitable anions.

The introduction of a chromophore into the *ortho*-phenylenediamine bisurea scaffold produces colorimetric ion sensors. Adding a *para*-nitrophenyl urea substituent onto the 4,5-dimethyl-1,2-phenylendiamine scaffold was used to construct fluoride sensor **250** (**Figure 4.10**); the colour changes caused by the addition of fluoride to a DMSO solution of the receptor were detectable with the naked eye.[434] Tweezer-like compounds containing an anthraquinone core can similarly be used for naked eye anion detection. Compounds **251** and **252** (**Figure 4.10**) both display high affinity and selectivity towards dihydrogen phosphate in 10 % DMSO/acetonitrile (K_a = 1.3 x 10^4 M^{-1} and 1.0 x 10^6 M^{-1} respectively). However, colour changes with oxoanions for urea **251** were only observed at temperatures above 333 K.[435] The authors attributed the lack of colour changes below this temperature to strong intramolecular hydrogen-bonding preventing suitable alignment of urea moieties for anion complexation. Similarly, the disruption of intramolecular hydrogen-bonding between the anthraquinone oxygen and a urea NH in compound **253** upon addition of Hg^{2+}, produces a colorimetric response.[436] Replacement

of the central phenyl core with a cyclohexyl group facilitates the production of chiral anion receptors **254** and **255** (**Figure 4.10**). Compound **255** functions as a colorimetric sensor for cyanide, whilst **254** displays enantiomeric selectivity for biologically relevant chiral phosphate anions in DMSO.[437, 438]

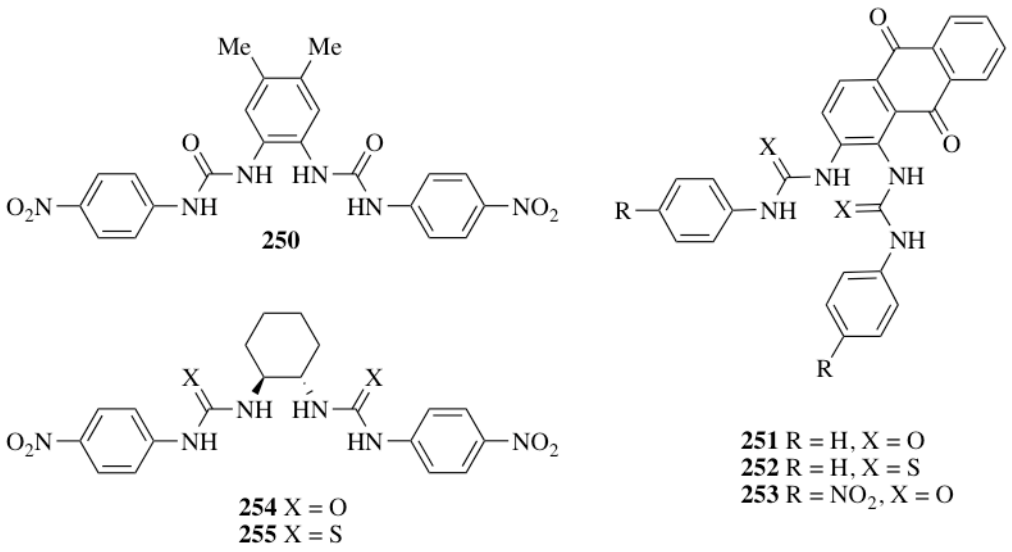

Figure 4.10: Colorimetric ion sensors **250**-**253** and chiral anion sensors **254**-**255**.

4.1.3 Extending the Bisurea Scaffold

Additional hydrogen-bonding motifs can be appended onto the *ortho*-phenylenediamine based bisurea scaffold. Appending an amide onto the pendant phenyl 2- position of compound **244** yielded compound **256** (**Figure 4.11**).[439] The amide appended compound **256** showed greater affinity for oxo-anions in 0.5 % H_2O/DMSO-d_6 than its parent compound **244**, albeit with a propensity to form 1:2 (host:guest) complexes. Amide substitution at the pendant phenyl 3- position was found to have a far less dramatic influence on the solution phase anion binding behaviour.

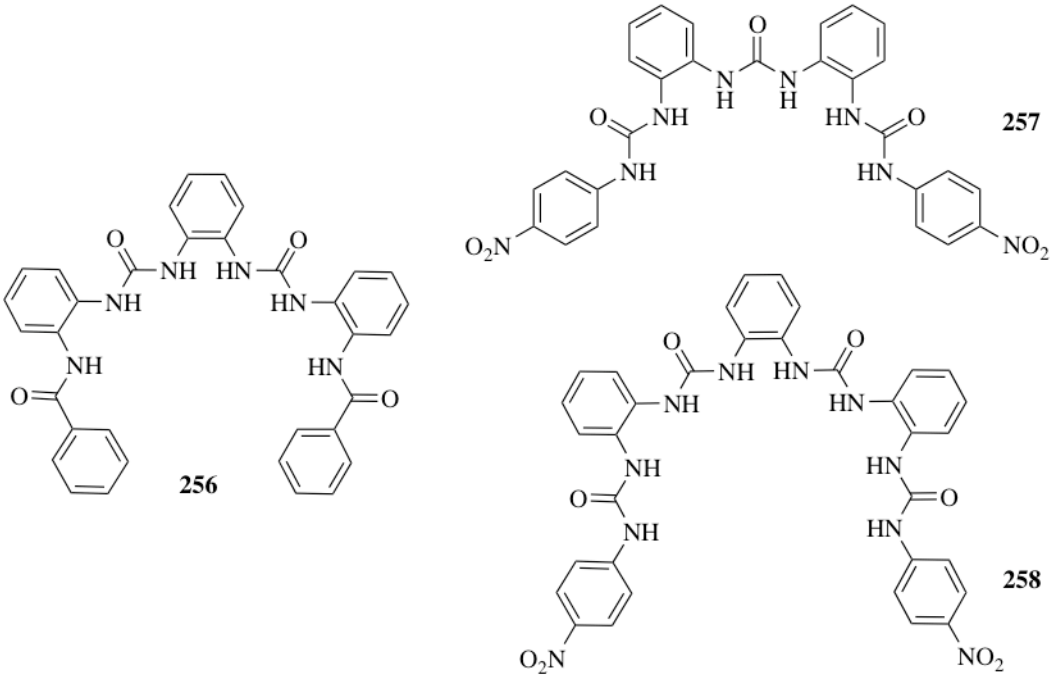

Figure 4.11: Extended bisurea scaffolds.

Wu and co-workers have examined the possibility of extending the *ortho*-phenylenediamine based bisurea scaffold further, producing analogous receptors containing multiple urea functionalities.[440, 441] Trisurea **257** and tetraurea **258** (**Figure 4.11**) were shown to be selective receptors for tetrahedral anions, particularly sulphate. Compound **257** showed strong solution phase sulphate binding due to good conformational complementarity with tetrahedral sulphate ($K_a > 10^6$ M^{-1} in DMSO), whilst the tetraurea scaffold was found to complex sulphate in polar 10 % H_2O/DMSO-d_6 solvent mixtures ($K_a > 10^4$ M^{-1}). Solid state analysis revealed that all available urea NH groups were used to complex tetrahedral anions in both scaffolds. Further expansion of the scaffold, with molecules containing up to six urea functionalities has been achieved.[442] These larger structures form molecular barrels, templated by interactions with tetraalkylammonium halides and illustrate the diversity of the *ortho*-phenylenediamaine based urea core in the development of anion hosts.

Building on the successful sulphate complexation by the polyurea containing scaffolds, Wu and co-workers developed tripodal compound **259** (**Figure 4.12**), containing '*ortho*-phenylenediamine-like' units.[443] This compound contains six urea

groups, providing twelve NH hydrogen-bonds to a tetrahedral sulphate anion. A high binding constant with TBA sulphate ($K_a > 10^4$ M^{-1}) was measured in a highly polar solvent mixture of 25 % H_2O/DMSO-d_6. This finding prompted the investigation of the extraction of Na_2SO_4 from aqueous solution into a chloroform solution of TBA chloride. A high sulphate extraction yield (> 95 %) was achieved under these conditions, and was preserved in the presence of aqueous sodium nitrate.

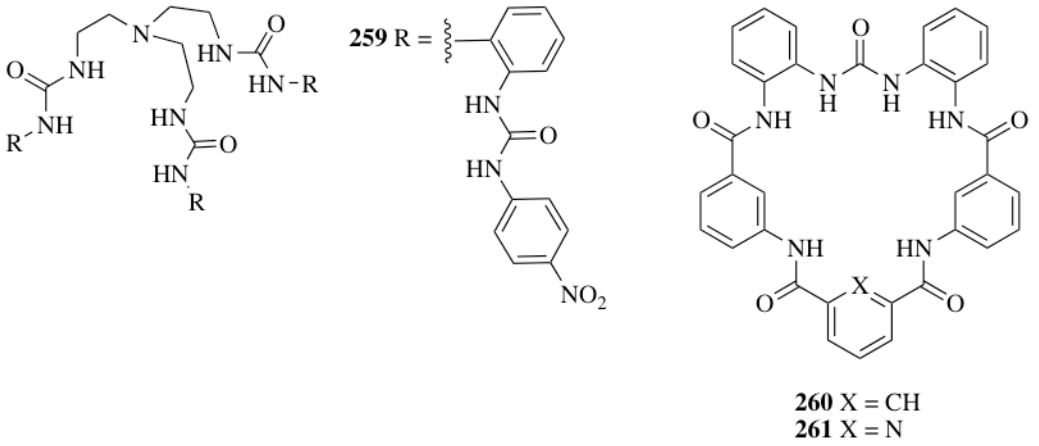

Figure 4.12: Extended structures based on the *ortho*-phenylenediamine scaffold.

Macrocyclisation has proven an effective strategy to convert *ortho*-phenylenediamine based ureas into carboxylate selective hosts. Macrocycles **260** and **261** (**Figure 4.12**) contain two '*ortho*-phenylenediamine-like' 1,2-appended phenyl rings, and were shown to posses high selectivity for carboxylates, particularly acetate, over other anions.[444] Selectivity and anion affinity were highest for macrocycle **261** ($K_a[CH_3CO_2^-]/K_a[H_2PO_4^-]$ = 116 in 0.5 % H_2O/DMSO) owing to the preorganising influence of the pyridine group, preventing the macrocycle from adopting a twisted conformation. Crystals grown from a DMSO solution of TBA fluoride and **261** contained carbonate ions (CO_3^{2-}) bound by six urea/amide NH hydrogen-bonding interactions (**Figure 4.13**). The bound carbonate ions were judged not to originate from solution and thus implied that macrocycle **261** can extract atmospheric carbon dioxide.[445]

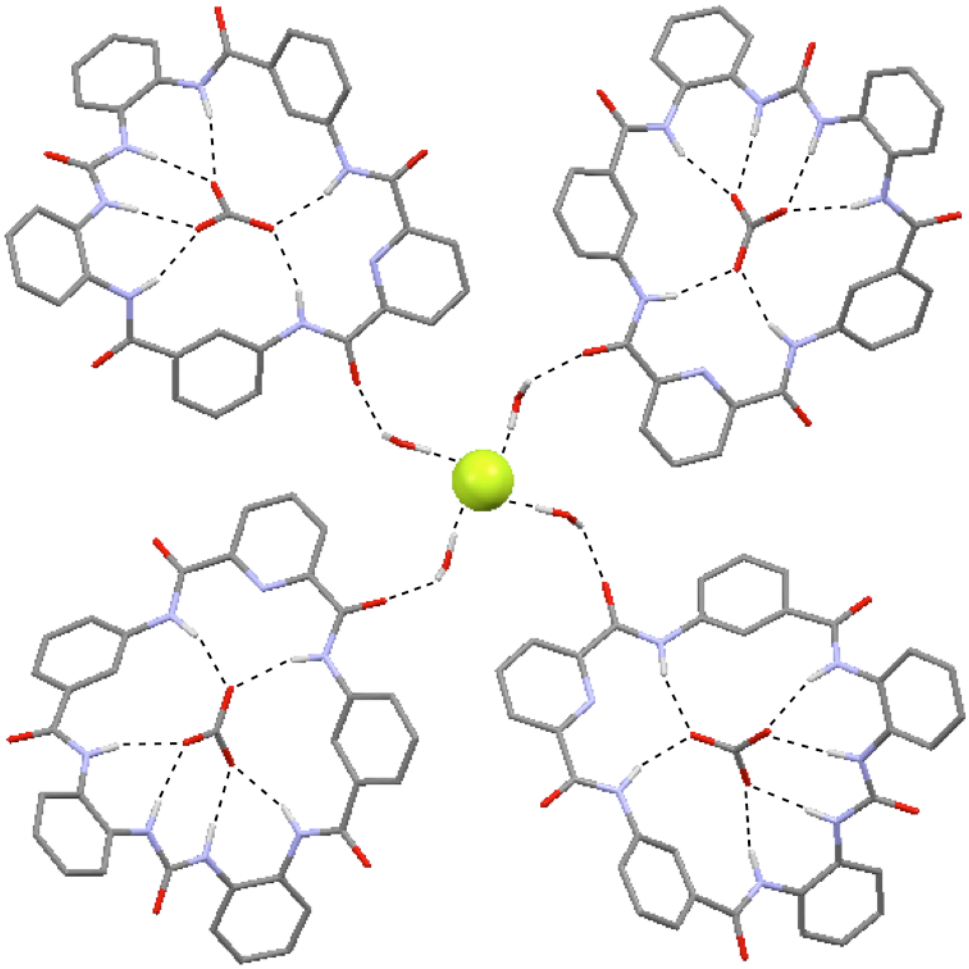

Figure 4.13: X-ray crystal structure of macrocycle **261** with carbonate bound in the macrocyclic cleft and a fluoride ion coordinated by hydrogen-bonding interactions with water at the periphery. The ligand, carbonate ions and coordinating water molecules are represented as wireframes and the fluoride anion is represented as a spacefilling model (0.6 times van der Waals radius); hydrogen (white), carbon (grey), nitrogen (blue), oxygen (red), fluorine (pale green). TBA counterions and non-interacting hydrogen atoms have been omitted for clarity.[445]

In light of the above, a series of bisurea compounds were examined as ion transport agents. The introduction of electron withdrawing substituents was performed to examine the importance of anion binding in the transport process.

4.2 Transmembrane Ion Transport Facilitated by Bisureas

In **Chapter 3** medicinal chemistry guidelines were used in the optimisation of indolylurea molecules to yield biologically active transporter motifs. Consequently, discovering new motifs capable of functioning as anion transporters may help to identify

future drug molecules. It has been shown previously that bisurea receptors can promote chloride transport across phospholipid bilayers (see **Section 4.1.1**) and hence a series of *ortho*-phenylenediamine-based bisureas were synthesised and tested for their ability to facilitate Cl^-/NO_3^-, Cl^-/HCO_3^- and Cl^-/carboxylate antiport, and H^+/Cl^- symport using a combination of ISE and fluorescence assays.[270]

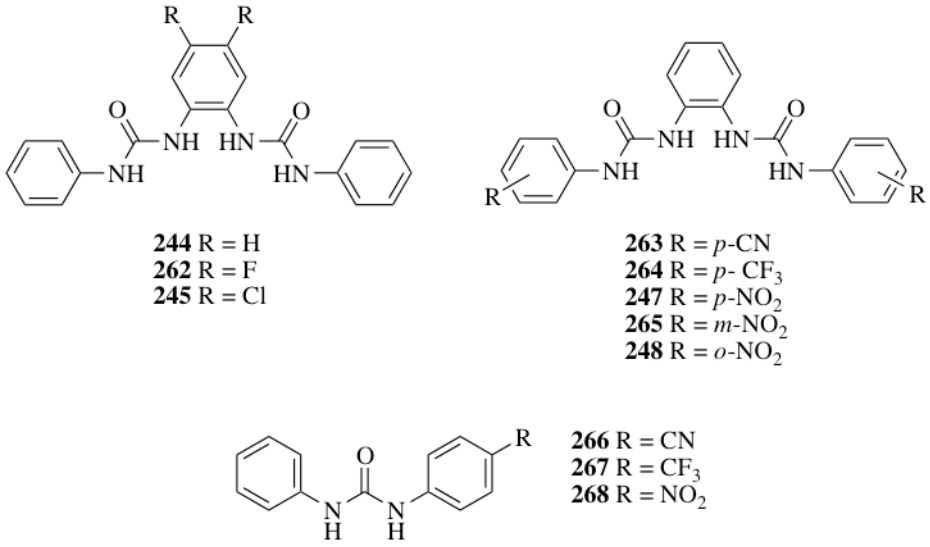

Figure 4.14: The *ortho*-phenylenediamine based bisureas studied as ion transport agents.

Compounds **244**, **245**, **247**, **248** and **262-265** were selected for the study. Compound **244**[428, 446] is an unfunctionalised *ortho*-phenylenediamine based bisurea and compounds **262** and **245**[429] place electron withdrawing halogen atoms on both the 3- and 4- positions of the central phenyl ring. Compounds **263**, **264** and **247**[429, 436] place electron withdrawing functionalities on the *para* position of the peripheral phenyl groups, whilst compounds **265** and **248**[429, 439, 441] were made to examine how varying the position of an electron withdrawing substituent nitro on the peripheral phenyl groups affects transport activity. Monourea compounds **266**,[447-451] **267**,[450-453] and **268** [448-451, 454] are analogues of the most active transporters. These compounds were made to examine if the spatial orientation of the two urea groups in the *ortho*-phenylenediamine based bisurea system influences the transport activity observed with these compounds.

4.2.1 Synthesis

Compounds **244**, **245**, **247** and **248** were synthesised by S. J. Brooks. Compounds **266**, **267** and **268** were synthesised by J. González. Reaction of the appropriate isocyanate with *ortho*-phenylenediamine in DCM/pyridine afforded compounds **263**, **264** and **265** in 39 %, 84 % and 82 % yields respectively. Compound **262** was prepared by a similar method, using 4,5-difluoro-2-nitroaniline as the starting material. Hydrogenation using Pd/C in methanol, followed by reaction with phenylisocyanate in DCM/pyridine yielded compound **262** in 37 % yield.

4.2.2 Anion Binding Studies

The ability of compounds **244**, **245**, **247**, **248** and **262**-**268** to bind anions in solution was investigated using ^{1}H NMR techniques in 0.5 % H_2O/DMSO-d_6. The binding studies were performed for anions relevant to both the transmembrane transport assays and biological systems. Where possible the change in chemical shift of the most downfield urea NH signal was fitted to a 1:1 binding model using WinEQNMR2 software (see **Appendix A2.3** for fitted curves).[340] The results of this study are shown in **Table 4.2**. Previously reported stability constants are included for comparison.[428, 429]

Compound	Cl^{-} [a]	HCO_3^{-} [a]	NO_3^{-} [a]
244	43[b]	1370	[c]
262	73	[d,e]	[c]
245	67[b]	2570[e]	[c]
263	74	[f]	[c]
264	78	2090[e]	[c]
247	78[b]	3770[e,g]	[c]
265	81	3140[e,g]	[c]
248	< 10[b]	826[g]	[c]
266	41	2580	[c]
267	61	1380	[c]
268	57	1630[e,g]	[c]

Table 4.2: Apparent stability constants K_a (M^{-1}) determined by ^1H NMR titrations with compounds **244**, **245**, **247**, **248** and **262-268** in 0.5 % H_2O/DMSO-d_6 at 298 K, following the most downfield urea NH unless stated otherwise. Data fitted to a 1:1 binding model. Errors < 15 %. [a] Added as TBA salts, except bicarbonate which was added as the TEA salt. [b] Binding constant determined by S. J. Brooks.[428, 429] [c] No significant interaction. [d] Sigmoidal curve could not be fitted to a suitable binding model. [e] Significant broadening of urea NH signals. [f] Reliable binding constant could not be obtained due to broadening of urea NHs and significant overlap of aromatic CH signals. [g] Dramatic colour change.

In general compounds **244**, **245**, **247**, **248** and **262-268** exhibit strong 1:1 binding with TEA bicarbonate, moderate 1:1 binding with TBA chloride and no significant interaction with TBA nitrate. A sigmoidal binding curve was obtained for compound **262** with TEA bicarbonate, which could not be fitted to a suitable binding model. Job plot analysis suggested 1:1 binding, however the plot was an unusual shape, implicit of more complex solution phase behaviour.[390] Significant urea NH peak broadening was observed upon addition of TEA bicarbonate to compounds **262**, **245**, **263**, **264**, **247**, **265**, **248** and **268**. A stability constant could not be determined for compound **263** with TEA bicarbonate due to this broadening effect, however Job plot analysis confirmed 1:1

binding. Comparing functionalised receptors **245**, **247** and **262**-**265** with receptor **244**, it can be observed that addition of electron withdrawing substituents to either the phenylene core or the peripheral phenyl groups increases anion affinity. In addition, it has been suggested that halogenation of the phenylene core (**262** and **245**) can aid receptor preorganisation by increasing the acidity of the phenylene CH groups, strengthening intramolecular hydrogen-bonding interactions (**Figure 4.7**).[429] For compounds **245**, **247** and **262**-**265** the binding constants obtained with TBA chloride are of a similar magnitude whilst no significant interaction was previously reported between compound **248** and TBA chloride.[429] This lack of interaction was attributed to intramolecular hydrogen-bonding between the urea NH groups and the *ortho*-nitro functionalities. The *ortho*-nitro substituents may also provide a steric constraint on the binding site. Similarly, compound **248** has a significantly lower binding constant with TEA bicarbonate than compounds **247** and **265**.

Colour changes were observed upon addition of TEA bicarbonate to nitro functionalised compounds **247**, **265**, **248** and **268**. Such behaviour has been reported previously in the presence of basic anions and has been attributed to deprotonation in analogous systems.[429, 434, 437, 455-459]

Interestingly, the two least active ion transporters (**244** and **248**) display the lowest affinity for both chloride and bicarbonate. The most active transporter **247** has the highest binding constant of the series for bicarbonate. In addition, the monourea compounds **266**, **267** and **268** show reduced anion affinity compared to their bisurea analogues (**263**, **264** and **247** respectively), demonstrating the impact of incorporating additional convergent hydrogen-bond donor groups into the receptor scaffold.

To complement the transport studies (see **Section 4.2.5**), titrations of compounds **263**, **264** and **247** with TBA maleate and fumarate salts in 0.5 % H_2O/DMSO-d_6 were attempted.[460] Addition of the TBA dicarboxylate to the receptor solution resulted in the formation of a precipitate in both instances, preventing determination of a binding constant by ^{1}H NMR methods. Instead ESI mass spectrometry was used to examine the interaction between the bisureas and carboxylate anions. Compound **264** was studied owing to both its good solubility and high transport activity (see **Section 4.2.4**). Negative ESI experiments with both maleic and fumaric acid revealed the formation of 1:1

bisurea/carboxylate complexes in the gas phase. Further, by analysing samples containing different ratios of compound **264** and carboxylate ions it was possible to deduce that **264** binds maleate more strongly than fumarate (see **Appendix 6**).[461, 462] These mass spectrometry experiments were performed by G. J. Langley and J. Herniman.

4.2.3 Solid State Studies

An X-ray crystal structure of compound **265** with TEA bicarbonate was obtained by slow evaporation of a H_2O/methanol solution. X-ray crystal structure analysis on these crystals was performed by M. E. Light (See **Appendix A3.3**). Analysis revealed that the *meta*-nitro functionalised bisurea forms a 2:1 (host:guest) complex with carbonate, the encapsulated carbonate anion bound by eleven hydrogen-bonding interactions. All the available urea NH groups hydrogen bond to the carbonate ion (N-O distances 2.726(2)-3.368(2) Å, N-H···O angles 139.0-166.9°). It appears that in the solid state the *meta*-nitro group does not hinder guest inclusion.

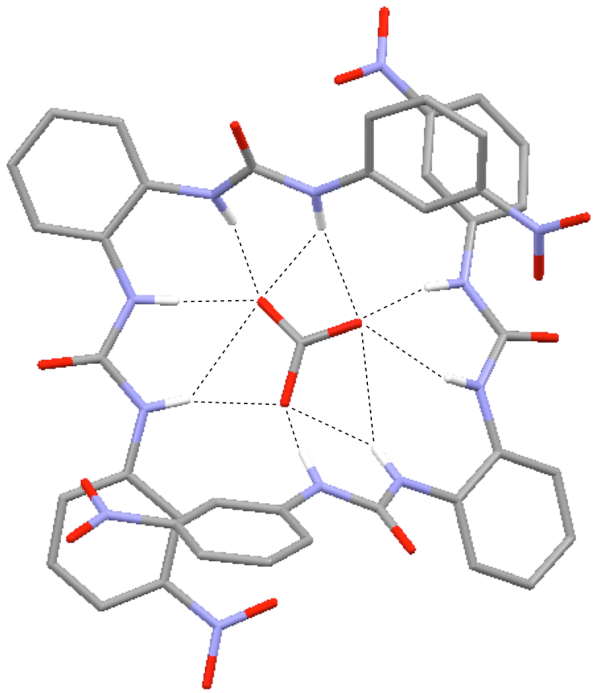

Figure 4.15: X-ray crystal structure of the 2:1 (host:guest) complex formed by compound **265** with TEA bicarbonate. Ligands and the guest anion are represented as wireframes; hydrogen (white), carbon (grey), nitrogen (blue), oxygen (red). TBA counterions and non-interacting hydrogen atoms have been omitted for clarity.

4.2.4 Ion Transport Studies

Compounds **244**, **245**, **247**, **248** and **262-268** were tested in a Cl^-/NO_3^- antiport ISE assay (see **Section 2.2.4**). The results of these assays are shown in **Figures 4.16** and **4.17**. To maintain charge balance, ion transport must occur by either a symport or an antiport mechanism.[136, 240] Hence, the chloride efflux in **Figures 4.16** and **4.17** could therefore be the consequence of Cl^-/NO_3^- antiport, Na^+/Cl^+ symport or H^+/Cl^- symport processes.

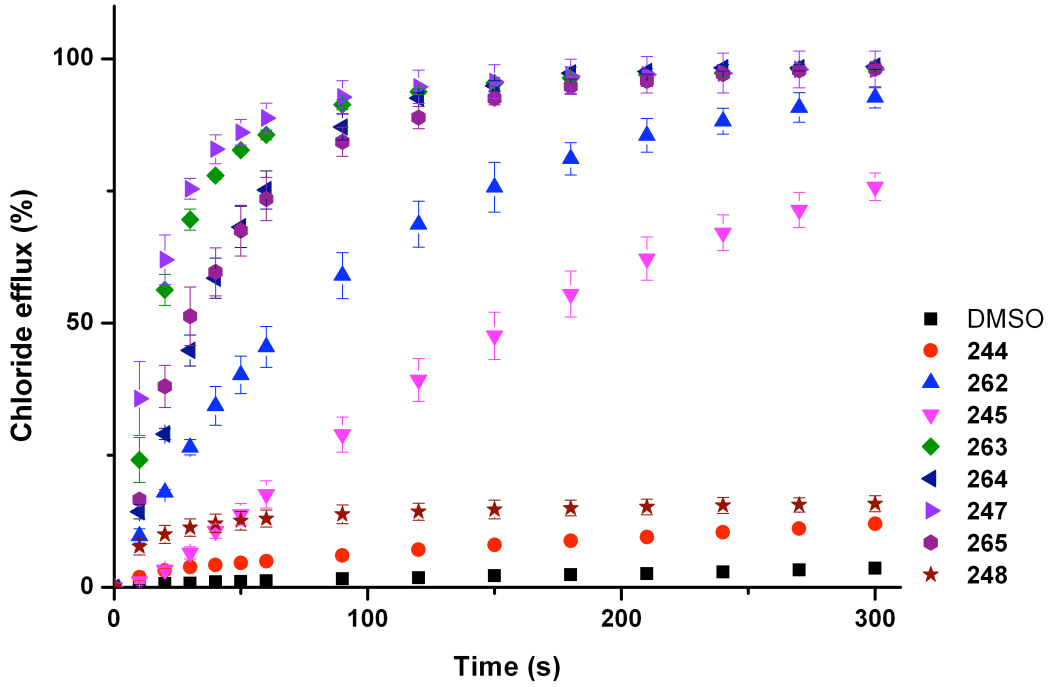

Figure 4.16: Chloride efflux promoted by a DMSO solution of compounds **244**, **245**, **247**, **248** and **262-265** (2 mol % with respect to lipid) from unilamellar POPC vesicles loaded with 488 mM NaCl buffered to pH 7.2 with 5 mM sodium phosphate salts. The vesicles were dispersed in 488 mM $NaNO_3$ buffered to pH 7.2 with 5 mM sodium phosphate salts. At the end of the experiment detergent was added to lyse the vesicles and calibrate the ISE to 100 % chloride efflux. Each point represents an average of three trials.

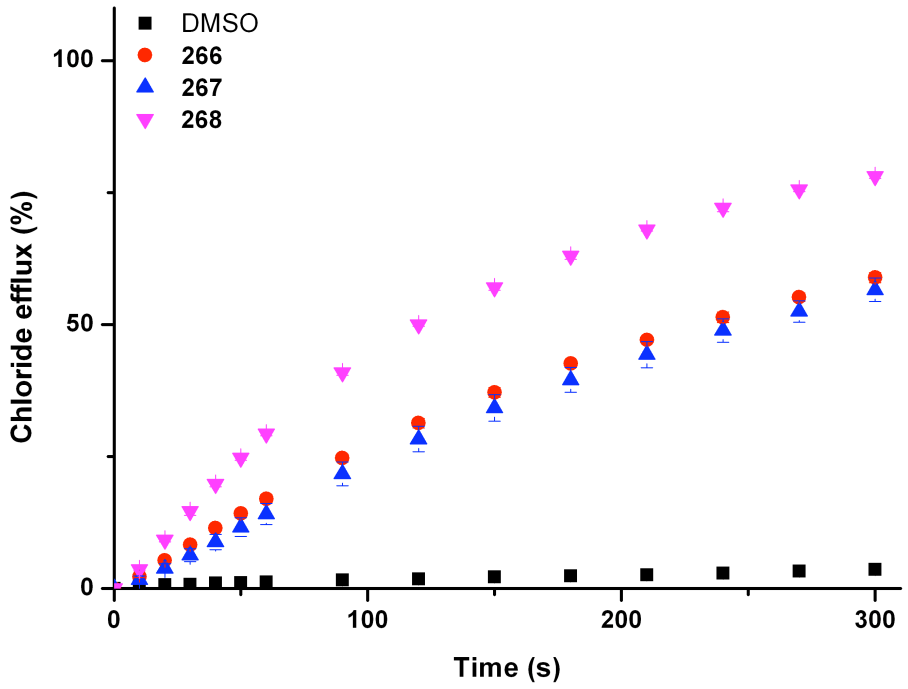

Figure 4.17: Chloride efflux promoted by a DMSO solution of compounds **266-268** (2 mol % with respect to lipid) from unilamellar POPC vesicles loaded with 488 mM NaCl buffered to pH 7.2 with 5 mM sodium phosphate salts. The vesicles were dispersed in 488 mM $NaNO_3$ buffered to pH 7.2 with 5 mM sodium phosphate salts. At the end of the experiment detergent was added to lyse the vesicles and calibrate the ISE to 100 % chloride efflux. Each point represents an average of three trials.

To examine the possibility of Na^+/Cl^- co-transport, an ISE assay was performed using vesicles containing CsCl instead of NaCl (see **Section 3.4.4**). In the event of M^+/Cl^- co-transport, the rate of chloride release is usually dependent on the nature of the metal cation.[365, 367, 463, 464] The rates of chloride release for vesicles containing NaCl were within error of those observed for vesicles containing CsCl, implying that M^+/Cl^- symport is not facilitated by these compounds (see **Appendix A5.2**).

Cl^-/HCO_3^- antiport is a biologically relevant process (see **Section 1.5**). Compounds **244**, **245**, **247**, **248** and **262-268** were tested for ability to facilitate Cl^-/HCO_3^- exchange using a bicarbonate 'pulse' ISE assay (see **Section 2.2.4**). The external sulphate is more difficult to transport through a lipid bilayer than nitrate, due to differences in hydrophilicity.[22] Consequently, chloride efflux observed in the first two minutes of the assay before the bicarbonate 'pulse' is not expected to be the result of anion antiport.

Upon addition of the bicarbonate 'pulse' a Cl^-/HCO_3^- antiport mechanism becomes possible. A marked increase in transport activity was observed for compounds **245**, **247**, **248** and **262-264** at this point (**Figures 4.18** and **4.19**).

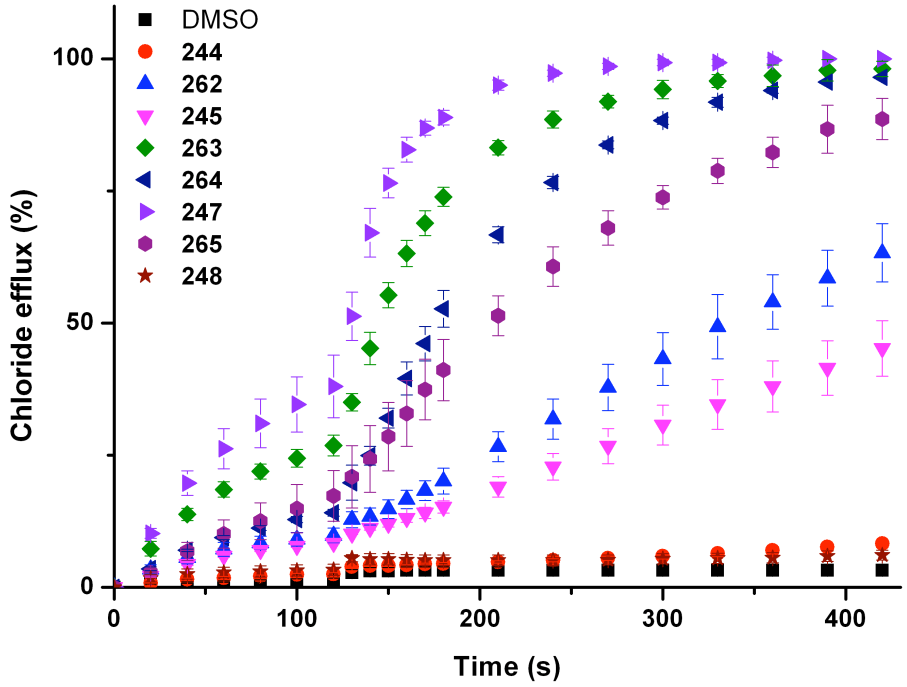

Figure 4.18: Chloride efflux promoted by a DMSO solution of compounds **244**, **245**, **247**, **248** and **262-265** (2 mol % with respect to lipid) from unilamellar POPC vesicles loaded with 451 mM NaCl buffered to pH 7.2 with 20 mM sodium phosphate salts. The vesicles were dispersed in 150 mM Na_2SO_4 buffered to pH 7.2 with 20 mM sodium phosphate salts. At t =120 s a 'pulse' of $NaHCO_3$ was added such that the external concentration of bicarbonate was 40 mM. At the end of the experiment detergent was added to lyse the vesicles and calibrate the ISE to 100 % chloride efflux. Each point represents an average of three trials.

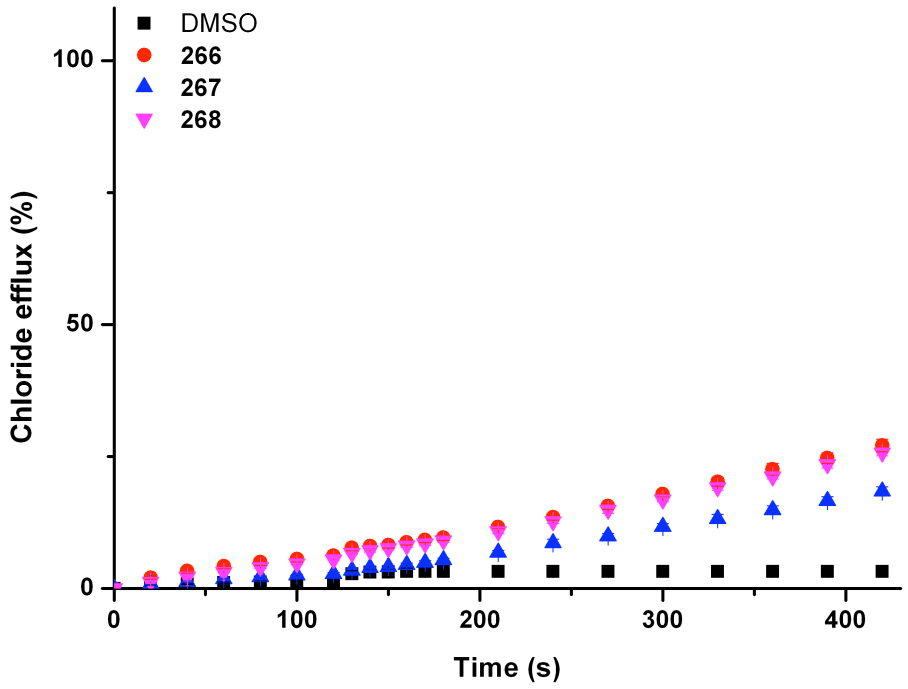

Figure 4.19: Chloride efflux promoted by a DMSO solution of **266-268** (2 mol % with respect to lipid) from unilamellar POPC vesicles loaded with 451 mM NaCl buffered to pH 7.2 with 20 mM sodium phosphate salts. The vesicles were dispersed in 150 mM Na_2SO_4 buffered to pH 7.2 with 20 mM sodium phosphate salts. At t = 120 s a 'pulse' of $NaHCO_3$ was added such that the external concentration of bicarbonate was 40 mM. At the end of the experiment detergent was added to lyse the vesicles and calibrate the ISE to 100 % chloride efflux. Each point represents an average of three trials.

Low levels of chloride efflux were observed for some of the compounds in the two minutes before the bicarbonate 'pulse' in the aforementioned assay. To investigate this effect further, the experiment was repeated without the bicarbonate 'pulse' (see **Section 3.4.4**). Significant chloride efflux was observed for some of the compounds (see **Appendix A5.2**).

Transmembrane sulphate transport has been observed previously for fluorinated tripodal ureas and thioureas.[249] To test if the chloride efflux observed in the aforementioned assay was linked to the transmembrane transport of sulphate, a sulphate 'pulse' lucigenin fluorescence assay was performed (see **Section 3.4.4**). POPC vesicles containing NaCl and lucigenin were suspended in a solution of NaCl. A 'pulse' of Na_2SO_4 was added followed by addition of a methanol solution of the test compound (2

mol % with respect to lipid). No evidence of sulphate transport was observed using this assay (see **Appendix A5.2**).

To examine the possibility of phosphate transport the assay was repeated with 20 mM 4-(2-hydroxyethyl)-1-piperazineethanesulfonic acid (HEPES) buffer (a sulfonic acid buffer) instead of 20mM phosphate buffer. No significant changes in chloride efflux were observed on comparison of the two buffer systems (see **Appendix A5.3**), suggesting that phosphate transport was not facilitated.

Compound **263** facilitated the highest chloride efflux in the sulfate 'blank' assay and was used to explore the possibility of H^+/Cl^- co-transport using a pH gradient assay (see **Section 3.4.4**).[147] Vesicles containing NaCl buffered to pH 4.0 were suspended in a solution of Na_2SO_4 buffered to pH 7.2. **Figure 4.20** shows that the rate of chloride transport facilitated by compound **263** under gradient conditions is greater than in the absence of a pH gradient (intravesicular and extravesicular pH 7.2), implying that this molecule can facilitate H^+/Cl^- symport.

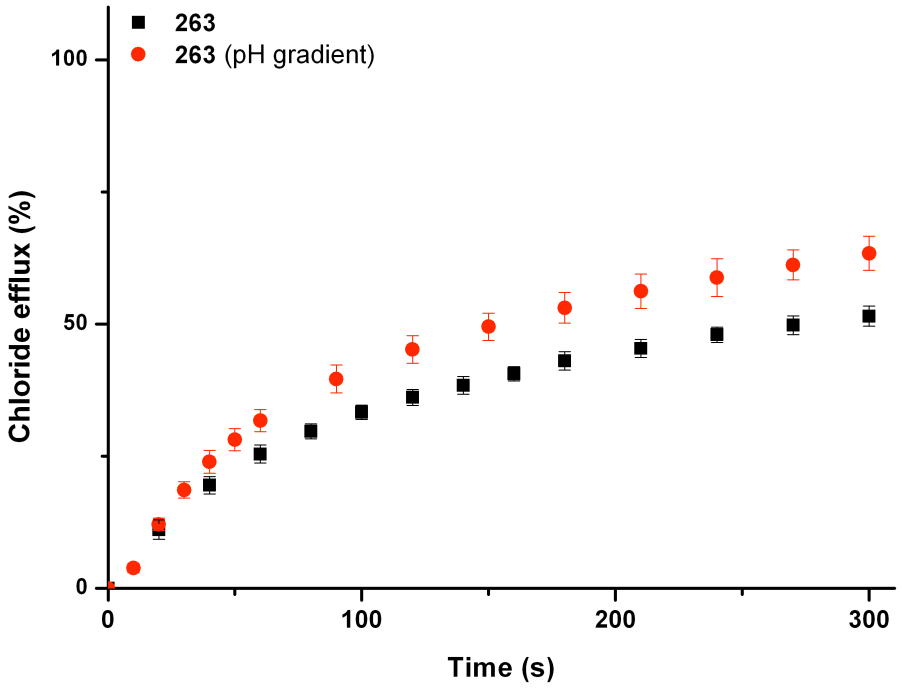

Figure 4.20: Chloride efflux promoted by a DMSO solution of compound **263** (2 mol % with respect to lipid) from unilamellar POPC vesicles loaded with either 451 mM NaCl buffered to pH 7.2 with 20 mM sodium phosphate salts or 451 mM NaCl buffered to pH 4.0 with 20 mM sodium citrate salts. The vesicles were suspended in 150 mM Na_2SO_4 buffered to pH 7.2 with 20 mM sodium phosphate salts. At the end of the experiment detergent was added to lyse the vesicles and calibrate the ISE to 100 % chloride efflux. Each point represents an average of three trials.

Proton transport was confirmed in a HPTS fluorescence assay (see **Section 3.4.4**), with POPC vesicles loaded with NaCl and HPTS.[246] These vesicles were suspended in a solution of Na_2SO_4 and the HPTS fluorescence measured upon addition of a DMSO solution of compound **263**. An increase in intravesicular pH was observed, corresponding to deacidification of the vesicles *via* either H^+/Cl^- co-transport or an equivalent Cl^-/OH^- antiport pathway (see **Appendix A5.2**).

To examine the transport mechanism of these compounds a Cl^-/NO_3^- antiport ISE assay was performed with vesicles composed of POPC/cholesterol (7:3 molar ratio). Compounds **245**, **247**, **248** and **262-264** all showed reduced chloride efflux in the POPC/cholesterol vesicles compared to POPC vesicles (see **Appendix A5.2**), indicating that transport likely occurs *via* a mobile carrier mechanism.[465] Further evidence for a carrier mechanism was obtained in U-tube experiments (see **Sections 1.9.7** and **3.4.4**).

For solubility reasons only compounds **245**, **263**, **264** and **265** could be tested in this way. All the compounds tested facilitated a higher concentration of chloride in the receiving phase than was observed in the control experiment (see **Appendix A5.2**).

Compound	$EC_{50,\,270\,s}$ [a] (Cl^-/NO_3^-)	n [b] (Cl^-/NO_3^-)	$EC_{50,\,270\,s}$ [a] (Cl^-/HCO_3^-)	n [b] (Cl^-/HCO_3^-)	wclogP [c]
244	[d]	[d]	[d]	[d]	4.97
262	0.14	0.9	1.40	0.7	5.80
245	0.39	0.7	> 5	0.9	6.33
263 [e]	0.011	0.7	0.073	1.0	4.72
264 [e]	0.018	1.2	0.15	0.9	7.01
247 [e]	0.0048	0.9	0.038	1.1	4.58
265 [e]	0.084	1.0	0.21	0.8	4.58
248	[d]	[d]	[d]	[d]	4.58
266[f]	1.76	1.8	[d]	[d]	3.20
267	1.80	2.1	[d]	[d]	4.35
268[f]	1.05	1.5	[d]	[d]	3.13

Table 4.3: Overview of transport assays for compounds **244**, **245**, **247**, **248** and **262-268**. Values for wclogP are also displayed. [a] $EC_{50,270\,s}$ defined as the concentration (mol % carrier with respect to lipid) needed to achieve 50 % chloride efflux after 270 s. [b] Hill coefficient. [c] Calculated using Fieldview Version 2.0.2 for Macintosh. [d] Hill analysis not performed due to low activity [e] Some of the observed transport activity is from H^+/Cl^- co-transport. [f] Hill analysis performed by J. González.

To quantify the transport activity of compounds **244**, **245**, **247**, **248** and **262-268** Hill analyses (see **Section 1.9.8**) for the Cl^-/NO_3^- and Cl^-/HCO_3^- antiport assays were performed (see **Appendix A5.2**), enabling comparison of the transport activity of this series of compounds. The results of this study are summarised in **Table 4.3**, together with the calculated values wclogP.[375-377]

Substituent	σ_{meta}	σ_{para}
H	0.00	0.00
F	0.34	0.06
Cl	0.37	0.23
CN	-	0.66
CF_3	-	0.54
NO_2	0.71	0.78

Table 4.4: Hammett substituent constants, σ, for moieties found in compounds **244**, **245**, **247**, **248** and **262**-**268**.[466]

In general, incorporation of electron withdrawing functionalities into the bisurea scaffold affords compounds capable of facilitating the transmembrane transport of anions. Parent compound **244**, shows poor transport activity. Halogenation of the phenyl core at both the 4- and 5- positions improved transporter activity, but to a less dramatic extent than by the addition of electron withdrawing functionalities to the 4- position of the peripheral phenyl groups. In these instances transporter activity was observed to increase with increasing electron withdrawing strength of the substituents (represented by the Hammett constants shown in **Table 4.4**); $NO_2 > CN > CF_3 > Cl \approx F > H$. This trend is also reflected in the anion binding constants, with the inactive transporter **244** exhibiting relatively low binding constants in 0.5 % H_2O/DMSO-d_6 for chloride and bicarbonate (43 M^{-1} and 1270 M^{-1} respectively), in comparison to the most active transporter **247**, (78 M^{-1} and 3770 M^{-1} respectively), reflecting the strong electron withdrawing effect of the nitro functionality. Indeed, *para*-nitro functionalised compound **247** displays very high transport activity, facilitating chloride efflux at loadings as low as 0.1 mmol % (with respect to lipid), the lowest loading of transporter that can facilitate transport reported to date (see **Figure 4.21**).

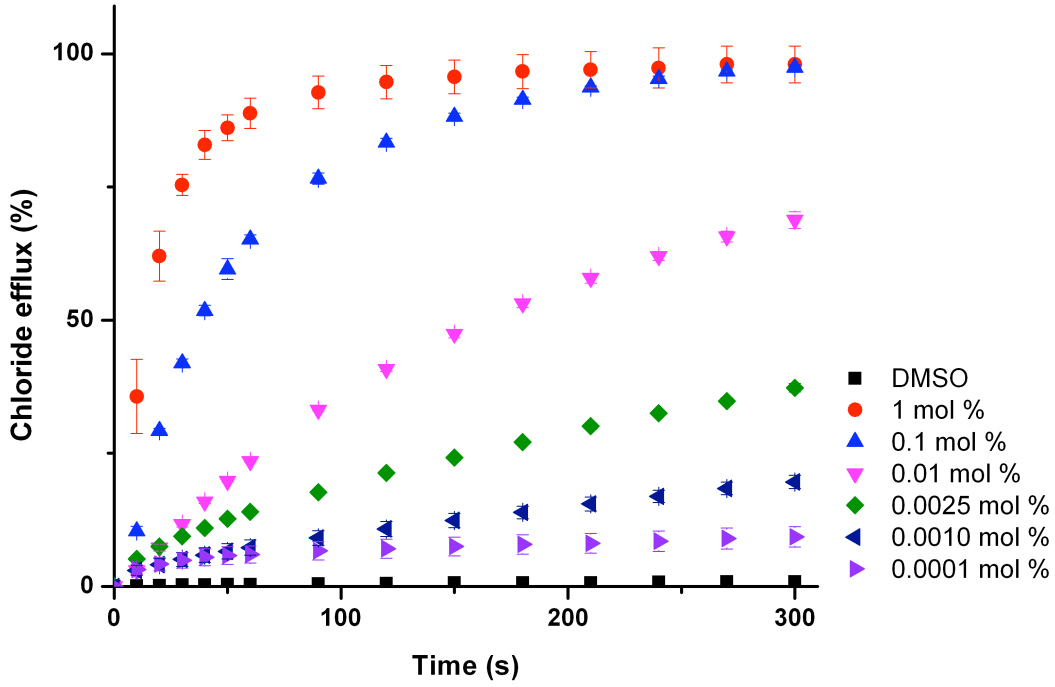

Figure 4.21: Chloride efflux promoted by a DMSO solution of compound **247** at various loadings from unilamellar POPC vesicles loaded with 488 mM NaCl buffered to pH 7.2 with 5 mM sodium phosphate salts. The vesicles were dispersed in 488 mM $NaNO_3$ buffered to pH 7.2 with 5 mM sodium phosphate salts. At the end of the experiment detergent was added to lyse the vesicles and calibrate the ISE to 100 % chloride efflux. Each point represents an average of three trials.

The effect of varying the position of electron withdrawing substituents on the peripheral phenyl rings has also been examined with compounds **247**, **265**, and **248**. The nitro functionality is the most electron withdrawing in the *ortho*- and *para*- positions.[466] The *para*-nitro functionalised compound **247** shows greater ion transport activity than *meta*-nitro functionalised compound **265**. The *ortho*-nitro functionalised compound **248** displays poor transport activity, likely due to the *ortho*-nitro groups involvement in intramolecular hydrogen bond formation and also steric hinderance of the binding site arising from its situation in the *ortho*-position.[429] This is reflected in the stability constants for compound **248** with chloride and bicarbonate (K_a < 10 M^{-1} and K_a = 826 M^{-1} respectively) which are significantly lower than those observed for compounds **247** and **265** (see **Section 4.2.2**).

The transport activity of the monourea analogues of the three most active bisurea

compounds (**263**, **264** and **247**) were tested using a Cl^-/NO_3^- antiport ISE assay (see **Section 2.2.4**). Compounds **266**, **267** and **268** were tested at loadings of 2 mol % (with respect to lipid), and the results compared to the efflux measured upon addition of compounds **263**, **264** and **247** at loadings of 1 mol % (with respect to lipid). This ensured that the concentration of 'urea groups' was the same. The results (**Figures 4.22**, **4.23** and **4.24**) show that the bisurea compounds are more active than their monourea analogues at the same 'urea group' concentration, implying that the spatial arrangement of urea groups in the bisurea receptors enhances transport activity.

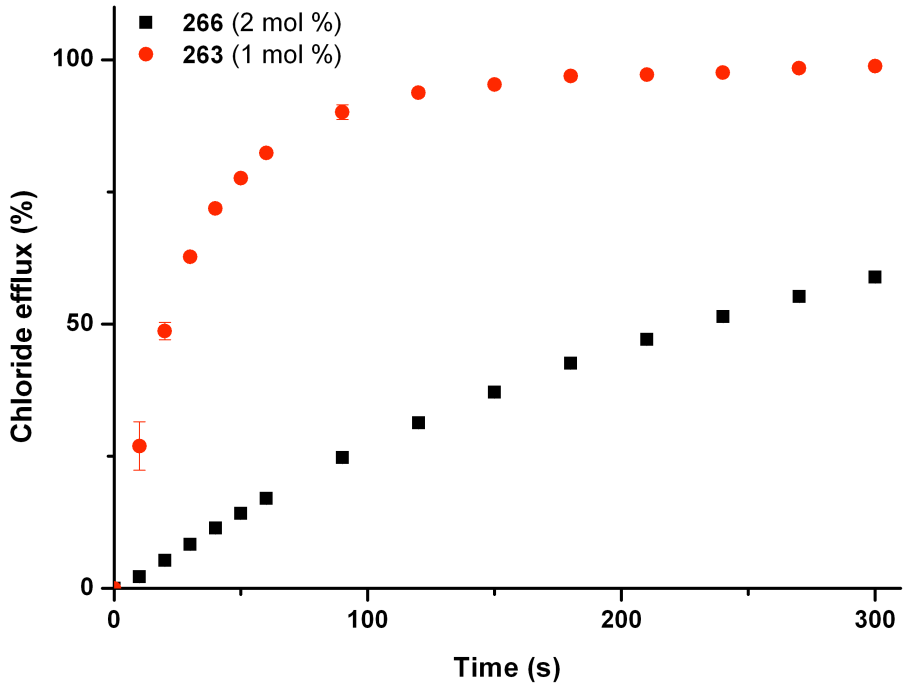

Figure 4.22: Chloride efflux promoted by a DMSO solution of monourea compound **266** (2 mol % with respect to lipid) and the analogous bisurea **263** (1 mol % with respect to lipid) from unilamellar POPC vesicles loaded with 488 mM NaCl buffered to pH 7.2 with 5 mM sodium phosphate salts. The vesicles were dispersed in 488 mM $NaNO_3$ buffered to pH 7.2 with 5 mM sodium phosphate salts. At the end of the experiment detergent was added to lyse the vesicles and calibrate the ISE to 100 % chloride efflux. Each point represents an average of three trials.

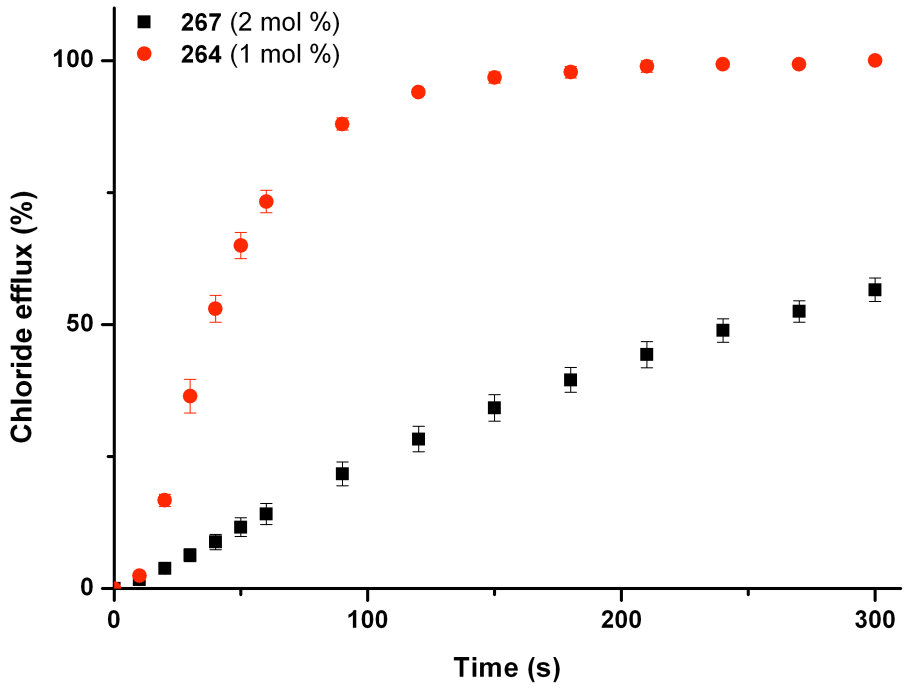

Figure 4.23: Chloride efflux promoted by a DMSO solution of monourea compound **267** (2 mol % with respect to lipid) and the analogous bisurea **264** (1 mol % with respect to lipid) from unilamellar POPC vesicles loaded with 488 mM NaCl buffered to pH 7.2 with 5 mM sodium phosphate salts. The vesicles were dispersed in 488 mM $NaNO_3$ buffered to pH 7.2 with 5 mM sodium phosphate salts. At the end of the experiment detergent was added to lyse the vesicles and calibrate the ISE to 100 % chloride efflux. Each point represents an average of three trials.

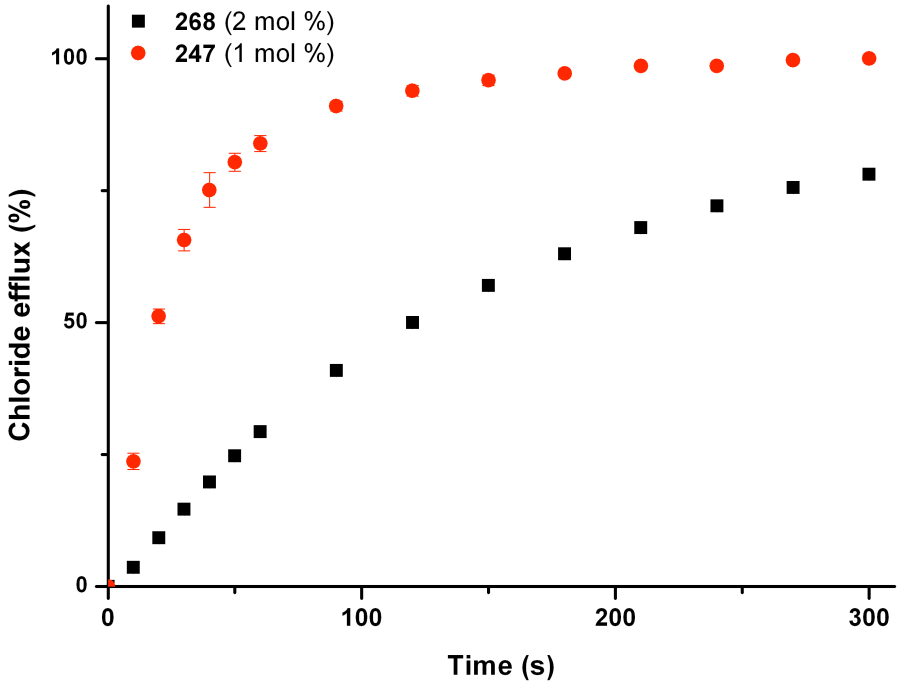

Figure 4.24: Chloride efflux promoted by a DMSO solution of monourea compound **268** (2 mol % with respect to lipid) and the analogous bisurea **247** (1 mol % with respect to lipid) from unilamellar POPC vesicles loaded with 488 mM NaCl buffered to pH 7.2 with 5 mM sodium phosphate salts. The vesicles were dispersed in 488 mM $NaNO_3$ buffered to pH 7.2 with 5 mM sodium phosphate salts. At the end of the experiment detergent was added to lyse the vesicles and calibrate the ISE to 100 % chloride efflux. Each point represents an average of three trials.

4.2.5 Dicarboxylate Transport

Considerable effort has gone into the construction of molecules capable of binding dicarboxylic acids, with many successful receptor designs utilising multiple convergent urea or thiourea moieties.[467-470] The discrimination between isomeric dicarboxylates by organic hosts has attracted particular interest, owing to the abundance of some of these anions in biological systems.[471-473] The transmembrane transport of dicarboxylates, such as glutamate and oxalate, is of biologically importance. Glutamate is the major excitatory neurotransmitter in the central nervous system (CNS). Synaptic glutamate clearance in the CNS is facilitated by glial glutamate transporters. Reduced glutamate clearance leads to the toxic accumulation of glutamate, causing nerve cell death through overstimulation (excitotoxicity). Glutamate excitotoxicity is linked to secondary injuries following traumatic brain injury, schizophrenia, bipolar disorder, and

neurodegenerative disorders including Alzheimer's and Huntingdon's disease.[474-481] Of particular note, olivopontocerebellar degeneration is a disorder caused by deficiency of the enzyme glutamate dehydrogenase, involved in glutamate metabolism. Patients exhibit high blood glutamate levels, resulting in the accumulation of glutamate within the brain and consequent excitotoxic neuronal cell death.[26, 482] In addition, glutamate analogues are produced by some plants and function as natural excitotoxins. Consumption of these compounds leads to severe neurological disorders.[483] Transmembrane oxalate transport is required for the reabsorption of water and electrolytes in the kidneys.[484] Disruption of oxalate transport can result in renal disorders such as nephrolithiasis (kidney stones), since calcium oxalate is the major component of kidney stones in humans.[485, 486]

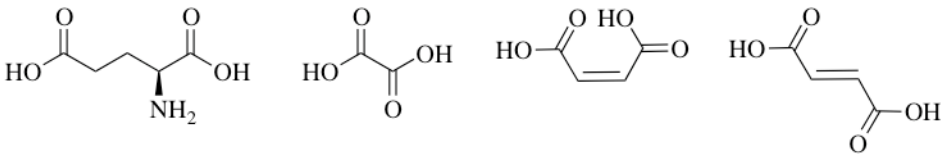

269 *L*-Glutamic acid **270** Oxalic acid **271** Maleic acid **272** Fumaric acid

Figure 4.25: Biologically relevant dicarboxylic acids.

Several examples of bisurea compounds with structural similarity to compounds **244**, **245**, **247**, **248** and **262**-**268** have been shown to selectively bind dicarboxylates.[423, 487-489] Bisurea **244** has been found to bind terephthalate in the solid state, forming a 2:1 (host:guest) complex wherein each carboxylate group of the terephthalate anion is bound by four hydrogen-bonding interactions with a single molecule of **244** (**Figure 4.26**).[430]

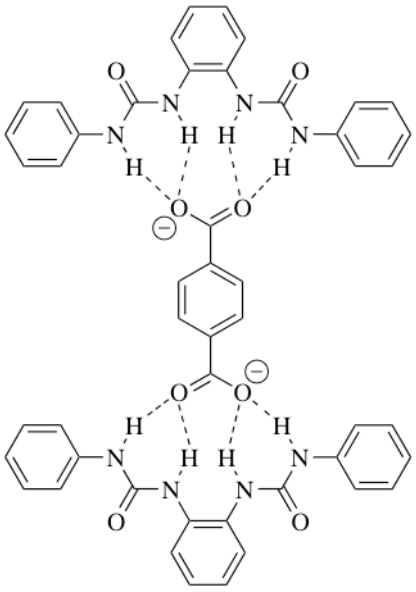

Figure 4.26: Binding mode observed in the solid state between bisurea **244** and the terephthalate anion.

Owing to this similarity, the most active transporters (**263**, **264** and **247**) were examined for their ability to facilitate the transmembrane transport of carboxylate anions, in particular fumarate and its stereoisomer, maleate.[490-492] Fumarate is a key intermediate in the citric acid cycle, whilst maleate absorption has been linked to renal disorders including Fanconi syndrome and bicarbonaturia and has also been shown to inhibit mitochondrial transaminase.[493-496]

Carboxylate transport was examined indirectly *via* antiport with chloride, using vesicles containing 451 mM NaCl buffered to pH 7.2, suspended in a solution of 151 mM Na_2SO_4 buffered to pH 7.2. Compounds **263**, **264** and **247** were added as solutions in DMSO (2 mol % with respect to lipid). After two minutes a sodium maleate or sodium fumarate 'pulse' was added such that the external concentration of the carboxylate was 40 mM. At pH 7.2 significant additional chloride efflux was observed on addition of a sodium maleate 'pulse' with all three compounds, whilst no significant enhancement in chloride efflux was seen with the sodium fumarate 'pulse'. The experiment was repeated at pH 4.0, whereupon an enhancement in chloride efflux was observed upon addition of both maleate and fumarate pulses (**Figures 4.27** and **4.28**, see also **Appendix A5.2**). These maleate and fumarate pulse assays were performed by J. González.

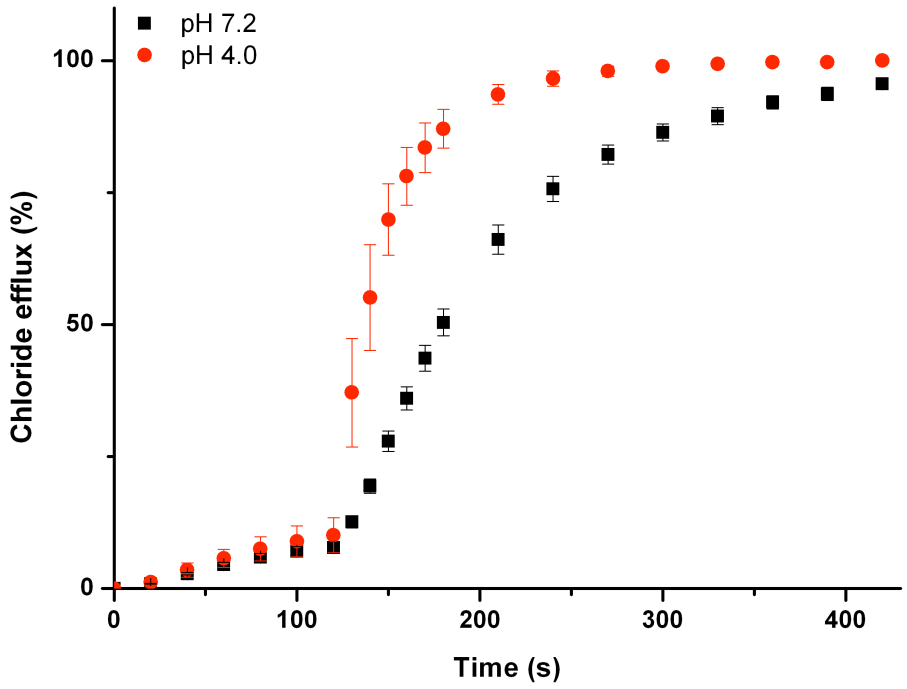

Figure 4.27: Chloride efflux promoted by a DMSO solution of compound **264** (2 mol % with respect to lipid) from unilamellar POPC vesicles loaded with either; i) 451 mM NaCl buffered to pH 7.2 with 20 mM sodium phosphate salts and dispersed in 150 mM Na_2SO_4 buffered to pH 7.2 with 20 mM sodium phosphate salts, or ii) 451 mM NaCl buffered to pH 4.0 with 20 mM sodium citrate salts and dispersed in 150 mM Na_2SO_4 buffered to pH 4.0 with 20 mM sodium citrate salts. At t = 120 s a solution of sodium maleate was added such that the external concentration of carboxylate was 40 mM. At the end of the experiment, detergent was added to lyse the vesicles and calibrate the ISE to 100 % chloride efflux. Each point represents an average of three trials.

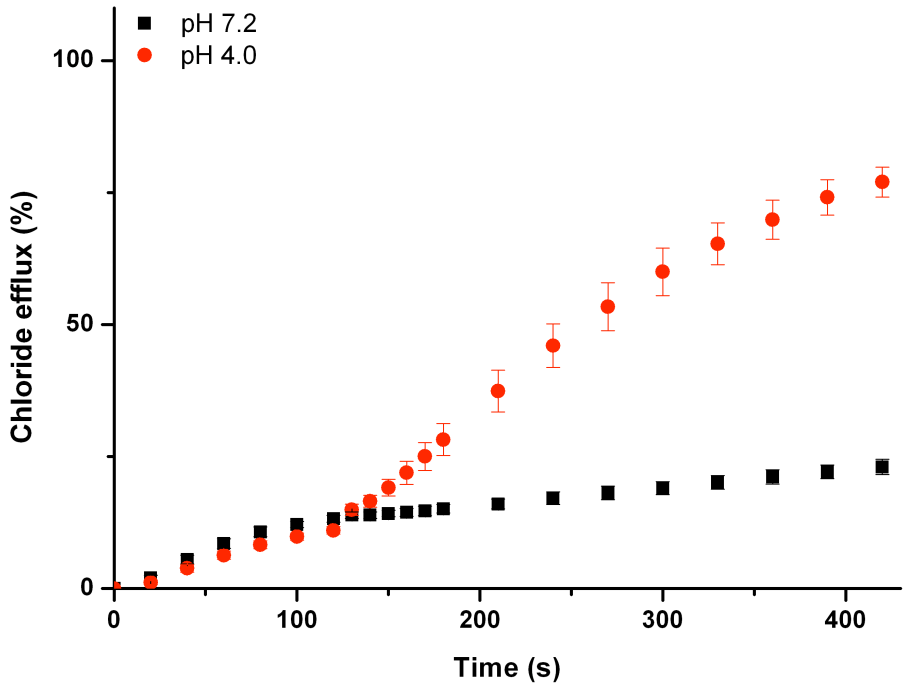

Figure 4.28: Chloride efflux promoted by a DMSO solution of compound **264** (2 mol % with respect to lipid) from unilamellar POPC vesicles loaded with either; i) 451 mM NaCl buffered to pH 7.2 with 20 mM sodium phosphate salts and dispersed in 150 mM Na_2SO_4 buffered to pH 7.2 with 20 mM sodium phosphate salts, or ii) 451 mM NaCl buffered to pH 4.0 with 20 mM sodium citrate salts and dispersed in 150 mM Na_2SO_4 buffered to pH 4.0 with 20 mM sodium citrate salts. At t = 120 s a solution of sodium fumarate was added such that the external concentration of carboxylate was 40 mM. At the end of the experiment, detergent was added to lyse the vesicles and calibrate the ISE to 100 % chloride efflux. Each point represents an average of three trials.

The pre-pulse chloride efflux is likely the consequence of H^+/Cl^- symport and not sulfate transport or Na^+/Cl^- symport (see **Section 4.2.4**). The pH dependant nature of the transport can be rationalised by considering the pK_a values for maleic acid (pK_a1 = 1.92, pK_a2 = 6.23) and fumaric acid (pK_a1 = 3.02, pK_a2 = 4.38).[497] Thus, at pH 7.2 a higher proportion of maleate exists as the monoanion than fumarate, which will exist predominantly as the dianion. Dianions are more hydrophilic than their monoanionic counterparts and will consequently be more difficult to transport.[22] Hence, at pH 7.2 an increase in chloride transport is observed upon addition of maleate, but little enhancement is observed upon addition of fumarate. At pH 4.0 the monoionic forms of both maleate and fumarate predominate, and thus increased rates of chloride transport were observed

upon addition of both the maleate and fumarate 'pulses', corresponding to Cl^-/carboxylate exchange.

4.3 Conclusions

In summary, the *ortho*-phenylenebisurea motif is a useful scaffold for the construction of transmembrane ion transporters. Bisureas based on the *ortho*-phenylenediamine scaffold that are functionalised with electron withdrawing substituents at either the central phenylene core or at the peripheral phenyl groups generally function as potent ion transporters. These compounds are capable of facilitating Cl^-/NO_3^- and Cl^-/HCO_3^- antiport. In some instances Cl^-/carboxylate antiport and H^+/Cl^- symport were observed. These compounds operate *via* a mobile carrier mechanism and sulphate transport and M^+/Cl^- symport processes are not facilitated. These findings highlight that electron withdrawing groups are a particularly useful addition to transporter scaffolds in order to improve activity. Additionally, *para*-nitrophenyl functionalised bisurea **247** has been found to facilitate transmembrane chloride transport at loadings as low as 0.1 mmol %. Compounds with electron withdrawing groups on both the peripheral phenyl groups and the central phenyl core may yield even greater transport activity.

Chapter 5
A Dual Host Approach to Ion Transport

5.1 Introduction

In **Chapters 2-4** molecules have been developed that are capable of facilitating coupled transport processes; Cl^-/NO_3^- antiport, Cl^-/HCO_3^- antiport and in some instances H^+/Cl^- symport. Fundamentally, each of these electroneutral processes can be considered to be two linked uniport transport pathways. By using a different transporter to facilitate each uniport step, synergistic transport can be achieved.

5.1.1 Dual Host Systems

Ion transport processes in biological systems seldom occur in isolation, they are often coupled together creating complex transport networks (see **Section 1.5**).[498] By examining how individual transport processes can be uncoupled, it may be possible to develop new strategies for the treatment of ion channelopathies such as cystic fibrosis (see **Section 1.5.3**), using combinations of synthetic ion transporters. With regards to ion transport, a dual host system would be appropriate for coupled transport processes (either symport or antiport). Conventionally, a single carrier molecule is used to transport both ionic components. In a dual host system a discrete carrier is used to transport each of the ionic species. A schematic diagram for a model M^+/X^- symport dual host system is shown in **Figure 5.1**. In this system one mobile carrier is responsible for the transmembrane transport of M^+, whilst another carrier is responsible for the transmembrane transport of X^-. Owing to the inherent selectivity of the transporters employed, addition of the carriers individually does not facilitate coupled transport and thus a synergistic effect is observed when carriers are added to the system in combination, through the coupling of discreet uniport transport pathways.

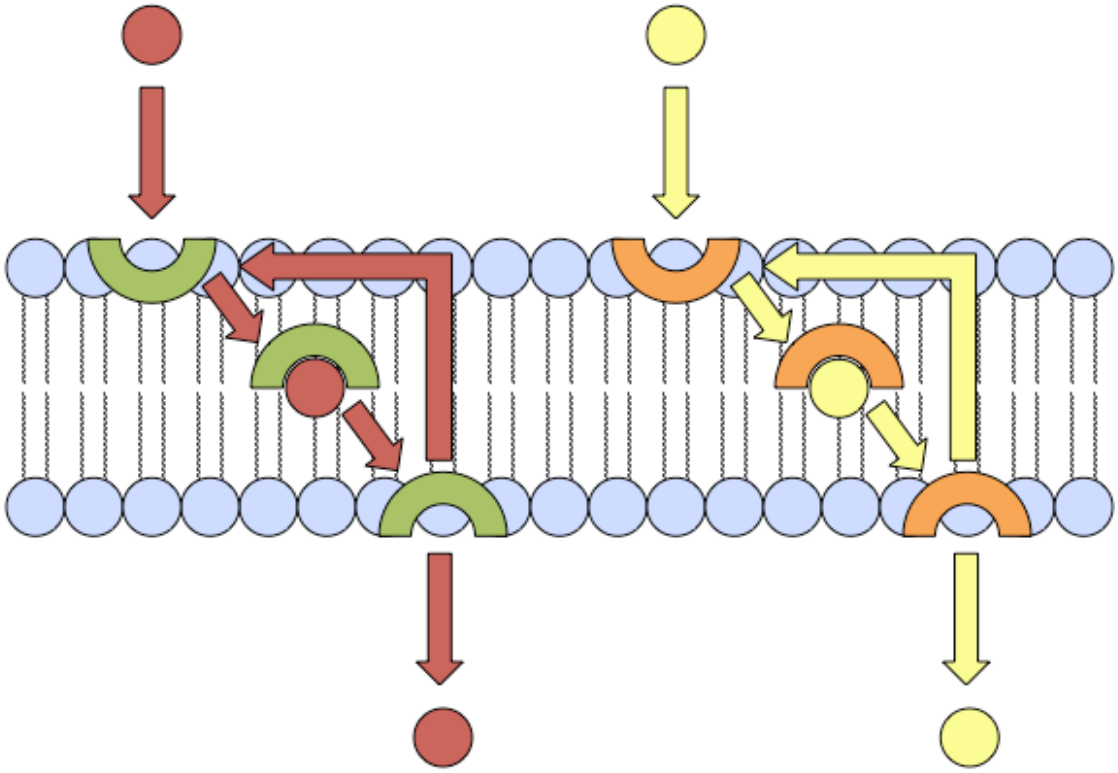

Figure 5.1: Schematic Diagram for a dual host system for M^+/X^- symport; M^+ (terracotta), X^- (yellow), M^+ carrier (green) and X^- carrier (orange).

Receptors that simultaneously bind both a cation and an anion can have advantages in terms of selectivity and affinity, arising from effects such as favourable electrostatic interaction between the bound ions.[499-503] For such transporter molecules, the simultaneous binding of both charged species advantageously results in an overall neutral complex which may have favourable connotations for transmembrane ion transport.[120, 504, 505] The field of ion extraction is closely related to that of transmembrane ion transport. There has been some progress in using a dual host approach to facilitate the extraction of ion pairs from aqueous solution into organic solvents.[343, 506] Owing to the high toxicity of the herbicide paraquat dichloride **273** (**Figure 5.2**), its extraction from aqueous solution is highly desirable.[507] Using an acetylated cyclodextrin **274** (**Figure 5.2**) to bind the dicationic paraquat, and two equivalents of an expanded calixpyrrole **275** (**Figure 5.2**) to bind the chloride counterions, 40 % extraction of **273** from D_2O into CD_2Cl_2 was

achieved. No paraquat dichloride was detected in the CD_2Cl_2 layer if only one of the complexing agents (either **274** or **275**) was used.[508]

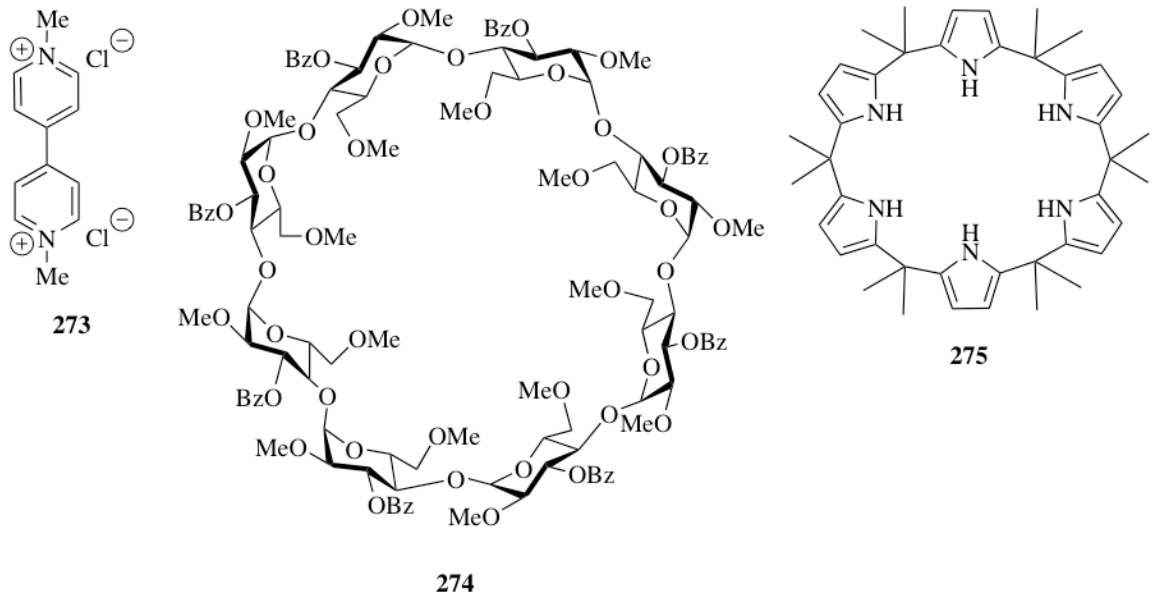

Figure 5.2: Paraquat dichloride **273** can be successfully extracted from D_2O into CD_2Cl_2 using a combination of cyclodextrin **274** and expanded calixpyrrole **275**.

Moyer and co-workers have developed dual host strategies for the extraction of $CsNO_3$ into 1,2-dichloroethane. Using tetrabenzo-24-crown-8 **276** to complex Cs^+ and tripodal receptors (either benzene-1,3,5-tricarboxamide or tripodal amide scaffolds) to selectively bind the NO_3^- counterion (**Figure 5.3**).[509, 510] In the presence of two equivalents of benzene-1,3,5-tricarboxamide **277**, the Cs^+ extraction efficiency of crown **276** was nearly doubled. In the presence of ten equivalents of tripodal amide **278** the Cs^+ extraction efficiency was increased four-fold. Using a similar strategy, Ghosh and co-workers facilitated KF and KCl extraction using 18-crown-6 **279** to selectively complex K^+ and the lipophilic tripodal molecule **280** to coordinate to the halide ion.[511] This simple modification of the dual host receptors, using a smaller crown ether, shows how dual host systems can be tuned to achieve selective ion extraction.

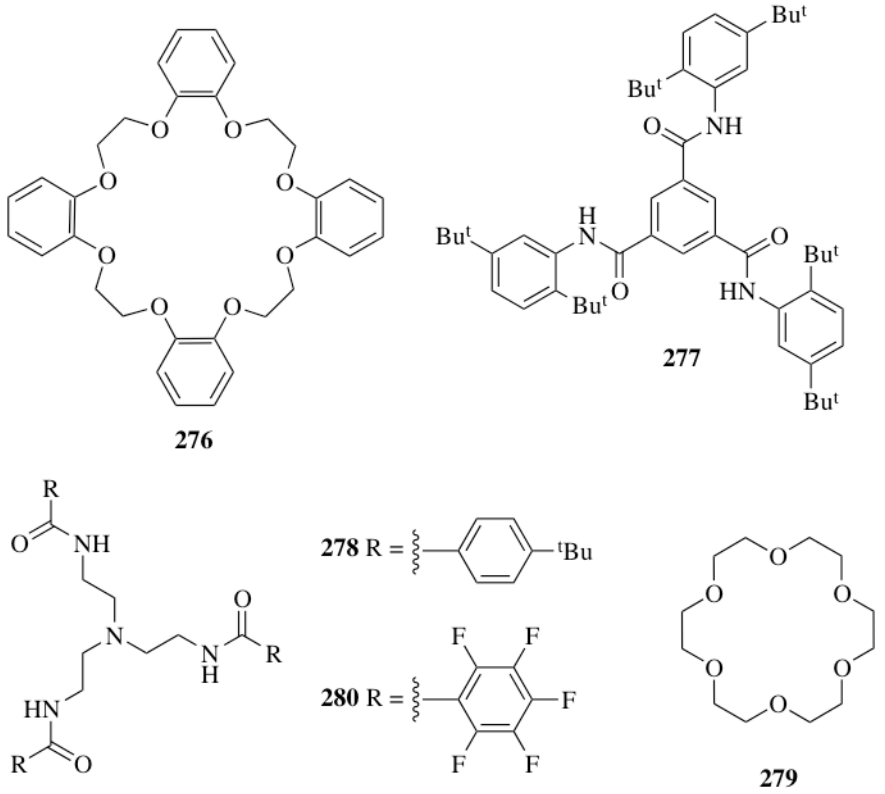

Figure 5.3: Combinations of tripodal anion hosts and crown ethers can be used to facilitate the dual host extraction of metal salts.

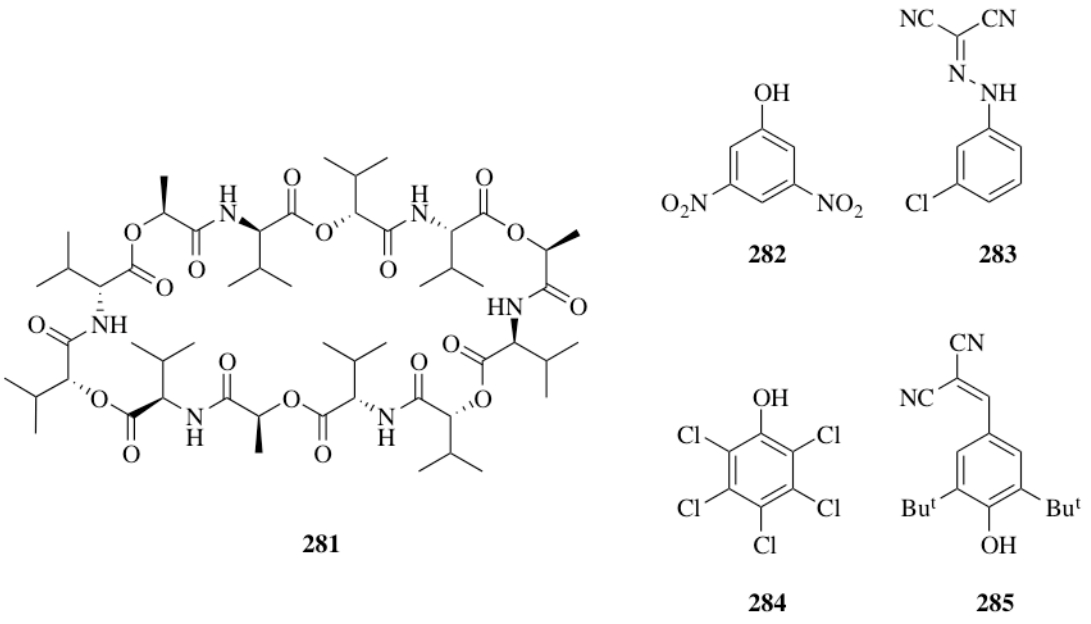

Figure 5.4: Valinomycin **281** and protonophores **282-285** can facilitate K^+/H^+ antiport processes.

There are some examples of dual host systems used in a transport context. Chloride transport through CLC-1 chloride channels can be coupled to valinomycin **281** mediated K^+ transport in planar bilayer experiments (see **Section 1.9.10**).[512] Dual-host systems comprising of valinomycin **281** and protonophores such as **282**-**285** can facilitate electroneutral K^+/H^+ antiport across phospholipid membranes (**Figure 5.4**).[513-516] **Figure 5.5** shows how valinomycin mediated K^+ transport can be linked to protonophore mediated H^+ transport. Neutral protonophore-valinomycin-potassium ion complexes are known to be stable in liposomal membranes.[517, 518] The formation of this ternary complex facilitates the transport of the deprotonated protonophore across the membrane.[514, 516]

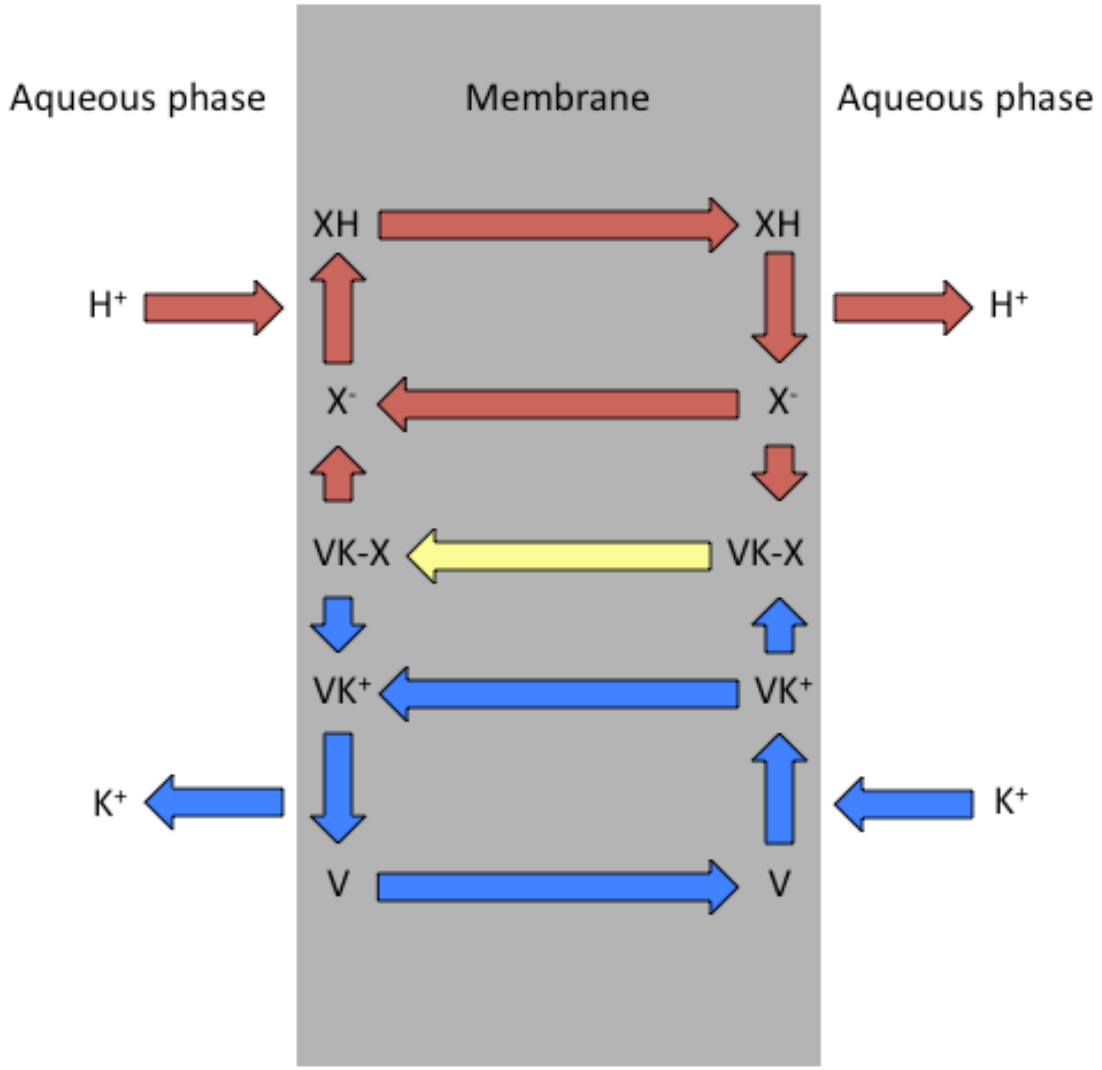

Figure 5.5: Schematic diagram indicating how protonophore (X) mediated transmembrane transport of H^+ can be linked to the valinomycin (V) mediated transport of K^+.

In summary, dual host systems have been developed for the extraction of $CsNO_3$, KF, KCl and paraquat dichloride, processes analogous to that of dual host facilitated transmembrane ion transport. Combinations of protonophores and the potassium ionophore valinomycin **281** have been shown to facilitate dual host K^+/H^+ exchange. Additionally transmembrane potassium ion transport by valinomycin **281** can be coupled to the action of biological chloride channels. By carefully selecting the appropriate ion transporters it should be possible to create dual host systems for a range of transport processes including M^+/Cl^- (M = Na, K or Rb) symport and Cl^-/HCO_3^- antiport.

5.2 A Dual Host System for M^+/Cl^- Co-transport

5.2.1 Selection of the Cationophore

Valinomycin **281** is a naturally occurring cyclic depsipeptide that has been shown to complex and transport potassium cations across cell membranes *via* a mobile carrier mechanism.[246, 519-524] Owing to its use in dual host K^+/H^+ exchange systems (see **Section 5.1.1**), and its ability to complex alkali metal cations (**Table 5.1**), valinomycin was selected as the M^+ ionophore for a dual host system for M^+/Cl^- symport.

Cation	log K_a
Li^+	< 0.7
Na^+	0.67
K^+	4.90
Rb^+	5.26
Cs^+	4.41

Table 5.1: Binding constants measured for the interaction between valinomycin and the alkali metal halides by spectrophotometry in MeOH.[525]

5.2.2 Selection of Chloride Carriers

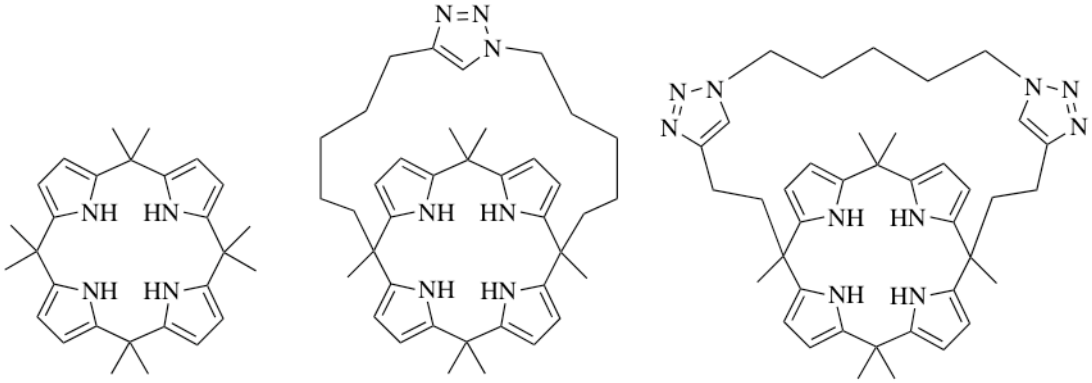

178 **286** **287**

Figure 5.6: Compounds tested as chloride carriers.

The chloride carriers tested for the M^+/Cl^- dual host system were *meso*-octamethylcalix[4]pyrrole **178** and its traizole containing strapped analogues **286** and **287** (**Figure 5.6**), owing to the interesting ion transport properties that these calix[4]pyrrole derived receptors exhibit. Sessler and co-workers discovered that calix[4]pyrrole **178** can bind halide anions *via* hydrogen bonding interactions with the four pyrrolic NH groups, achieving a binding constant of 5000 M^{-1} in 0.5 % D_2O/acetonitrile-d_3 at 295 K.[366, 526, 527] Calix[4]pyrrole **178** was found to function as a CsCl ion pair receptor in the solid state.[528] Complexation of the chloride ion preorganises the calix[4]pyrrole **178** into a cone conformation, permitting caesium ion inclusion into the aromatic 'cup' of the macrocycle. The neutral complex formed upon CsCl binding has been shown to be membrane permeable and thus calix[4]pyrrole **178** can facilitate the transmembrane transport of the Cs^+/Cl^- ion pair. Gale and co-workers demonstrated the transmembrane transport of CsCl in POPC vesicles containing CsCl suspended in a solution of Na_2SO_4. Chloride efflux (detected using an ISE) was not observed when the encapsulated salt was replaced with RbCl, KCl or NaCl supporting the hypothesis that chloride was transported out of the vesicles as an ion pair. Replacing the external sulphate with less hydrophilic nitrate resulted in only a modest enhancement in transport activity, suggesting that Cs^+/Cl^- symport is the predominant transport process.[22, 367]

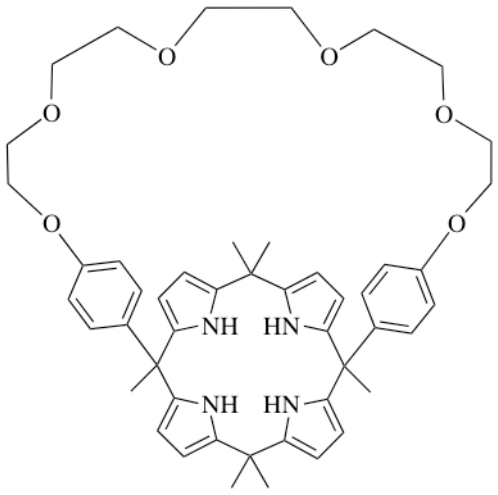

288

Figure 5.7: Oligoether strapped calix[4]pyrrole **288**.

Strapped calix[4]pyrroles have proven to be useful scaffolds for the complexation of ion pairs and can even be used to produce ditopic anion transporters. Oligoether strapped calix[4]pyrrole **288** (**Figure 5.7**) is such a ditopic ion-pair receptor, that contains multiple ion co-ordination sites.[120, 529, 530] Chloride binding is achieved by a combination of hydrogen-bonding interactions with pyrrolic NH groups and anion-π interactions with the phenyl linker groups. Cation coordination can be achieved by either the calixarene aromatic cup or by the crown ether strap. In CD_3CN solution the Li^+ ion is bound *via* the crown ether moiety, and stabilised by favourable electrostatic interactions with the neighbouring bound chloride ion. In contrast the large, charge diffuse Cs^+ ion is bound in the aromatic cup of the calixpyrrole. Neither Na^+ or K^+ ions were found to bind effectively to either cation binding site of the **288** chloride complex, and addition of these cations thus resulted in partial chloride decomplexation. In ion transport experiments cation dependent M^+/Cl^- symport was observed, with significant chloride efflux from phospholipid vesicles observed only when CsCl was the encapsulated metal salt. Chloride efflux was also observed upon addition of **288** to vesicles containing sodium chloride, suspended in a solution containing sodium nitrate. Owing to the lack of chloride efflux when the external anion was sulphate under the same conditions the mechanism was judged to be Cl^-/NO_3^- antiport, with U-tubes indicating a mobile carrier mechanism (see **Section 1.9.6**).

Triazole-strapped calix[4]pyrroles **286** and **287** have also been shown to facilitate transmembrane chloride transport.[463, 464] Isothermal titration calorimetry (ITC) with TEA chloride indicated that the association constant for **286** is considerably greater than that of parent calix[4]pyrrole **178** in acetonitrile (K_a = 4.9 x 10^4 M^{-1} and 2.7 x 10^6 M^{-1} respectively) at 303 K. Transport experiments with phospholipid vesicles loaded with metal chloride salts (M = Na^+, K^+, Rb^+ and Cs^+) showed chloride efflux when the external anion was either nitrate or sulphate. Reduced transport activity was observed for the smaller cations when nitrate was the external anion. The general trend was that as the size of the encapsulated cation decreases, the chloride efflux with external sulphate was reduced. The authors concluded that the transport mechanism changes from predominantly M^+/Cl^- symport (with caesium) to predominantly Cl^-/NO_3^- antiport (with sodium and potassium).[463] Strapped calix[4]pyrrole **287** bears a strap containing two

triazole functionalities.[464] Solid state analysis of analogous structures indicate that chloride is bound by a combination of hydrogen-bonding interactions with the four pyrrolic NH groups and triazole CH groups (**Figure 5.8**), ITC indicated strong binding with TEA chloride (K_a = 3.5 x 10^6 M^{-1}) in acetonitrile at 303 K. Transport experiments in phospholipid vesicles loaded with metal chloride salts (M = Na^+, K^+, Rb^+ and Cs^+) suspended in a solution containing Na_2SO_4 revealed that chloride efflux was cation dependant, with highest efflux rates observed with encapsulated CsCl. Exchanging the external sulphate for nitrate resulted in modest enhancements in transport activity for all anions, indicating that compound **287** can function as both a Cs^+/Cl^- symport agent and a Cl^-/NO_3^- antiport agent. As both compounds **286** and **287** have been shown to facilitate chloride transport through an antiport pathway (effectively two coupled uniport steps), they were selected as the chloride carriers for the dual host system described in subsequent sections.

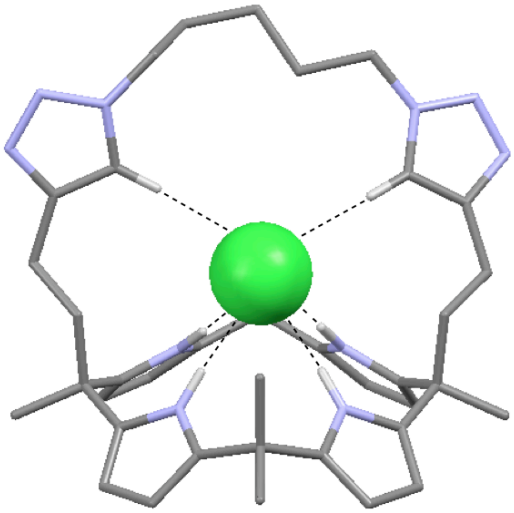

Figure 5.8: X-ray crystal structure of the chloride complex of a structural analogue of traizole strapped calix[4]pyrrole **287**, with the chloride ion bound by a combination of NH and CH hydrogen bonding interactions. The ligand is represented as a wireframe and the guest anion is represented as a spacefilling model (0.6 times van der Waals radius); hydrogen (white), carbon (grey), nitrogen (blue), chlorine (green). TBA counterions and non-interacting hydrogen atoms have been omitted for clarity.[464]

Molecules that complex ion pairs have attracted much recent interest.[120, 502] The transmembrane transport of ion pairs by a single molecule requires a receptor capable of the simultaneous binding of both the anionic and the cationic species.[367] Using separate receptors for anion and cation extraction has proven an effective strategy in the extraction of metal salts from aqueous solution.[509, 510] Building on this work experiments were undertaken to examine a two-component dual host system for the transmembrane transport of M^+/Cl^- ion pairs (M = Na, K or Rb).

5.2.3 Ion Transport Studies

Transmembrane transport assays were conducted using a dual host system comprising of one calixpyrrole compound (**178**, **286** or **287**) and valinomycin **281** (**Figures 5.6** and **5.4**). Compounds **178**, **286** and **287** were synthesised by C. C. Tong, M. G. Fisher and M. Yano. It was hypothesised that the calix[4]pyrroles would facilitate the Cl^- uniport step and valinomycin would facilitate the coupled M^+ uniport step. The metal salts tested were NaCl, KCl and RbCl. CsCl was not tested owing to the propensity of compounds **178**, **286** and **287** to facilitate Cs^+/Cl^- symport.[367, 463, 464] Chloride transport was monitored using a lucigenin fluorescence assay (see **Section 1.9.3**).

POPC vesicles were prepared containing sodium sulphate (71 mM) buffered to pH 7.2 with sodium phosphate salts (5 mM) and lucigenin (1 mM).[245, 531] To remove unencapsulated lucigenin the vesicles were passed through a Sephadex G-50 column and then diluted with a solution containing sodium sulphate (71 mM) buffered to pH 7.2 with sodium phosphate salts (5 mM). A pulse of MCl (M = Na, K or Rb) was added to the extravesicular solution such that the external concentration of the added metal salt was 100 mM. The solution was then allowed to equilibrate for 30 s. To initiate the experiment the carriers were added as solutions in acetone (2 mol % with respect to lipid). Chloride influx was calibrated by the addition of an acetone solution of melittin (0.2 mol % with respect to lipid) to vesicles containing sodium sulphate (71 mM) buffered to pH 7.2 with sodium phosphate salts (5 mM) and lucigenin (1 mM). Melittin is a peptide that forms pores large enough for the transmembrane conduction of chloride, but too small to permit lucigenin release.[532-534] The lucigenin fluorescence intensity was measured upon addition of sodium chloride 'pulses' such that each addition increased the total chloride

concentration by 2 mM. A Stern-Volmer constant (K_{sv}) of 42.55 ± 0.44 M^{-1} was calculated, in agreement with published values (see **Appendix A5.3**).[137]

The results for the addition of KCl 'pulses' are shown in **Figures 5.9**, **5.10** and **5.11** for compounds **178**, **286** and **287** respectively. In each case the results show the chloride influx observed upon adding valinomycin **281** (2 mol % with respect to lipid) and calixpyrroles **178**, **286** or **287** (2 mol % with respect to lipid) individually and the effect of adding the valinomycin and the calixpyrrole together (2 mol % each with respect to lipid). The sum of the change in chloride concentration facilitated by valinomycin and the calixpyrrole individually is shown for comparison.

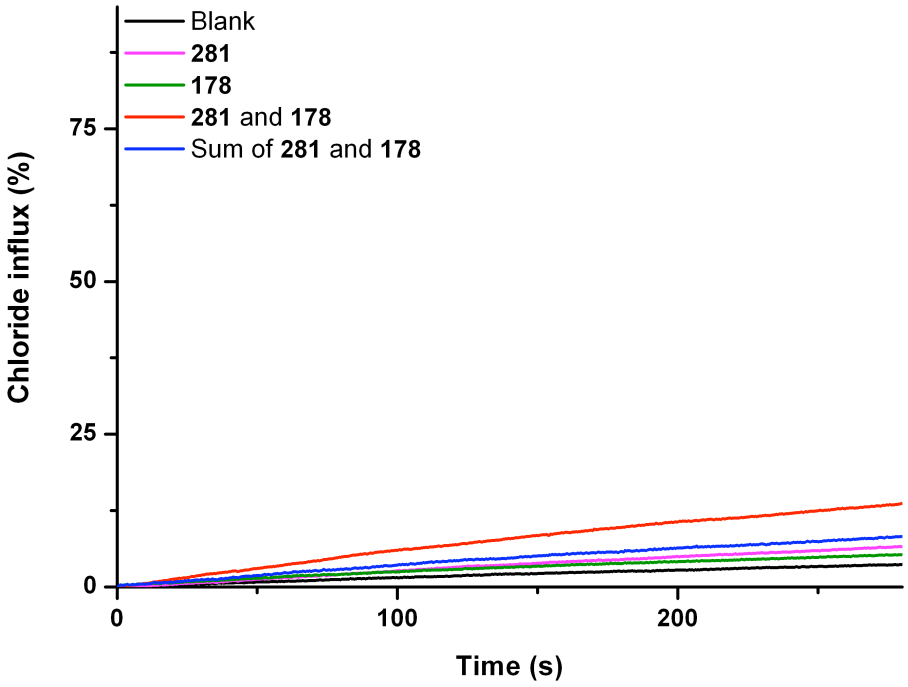

Figure 5.9: Change in internal chloride concentration of unilamellar POPC vesicles containing 1 mM lucigenin and 71 mM sodium sulphate, buffered to pH 7.2 with 5 mM sodium phosphate salts and suspended in 71 mM sodium sulphate buffered to pH 7.2 with 5 mM sodium phosphate salts, upon addition of an acetone solution of **281** (2 mol % with respect to lipid), **178** (2 mol % with respect to lipid) and both **281** and **178** (2 mol % each with respect to lipid) following a KCl 'pulse' bringing the extravesicular KCl concentration to 100 mM.

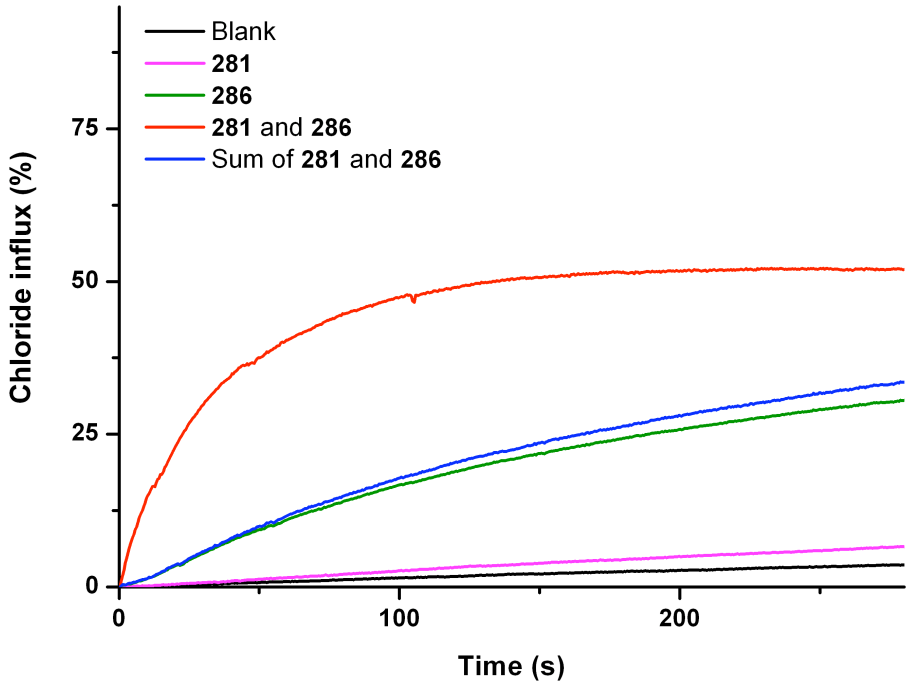

Figure 5.10: Change in internal chloride concentration of unilamellar POPC vesicles containing 1 mM lucigenin and 71 mM sodium sulphate, buffered to pH 7.2 with 5 mM sodium phosphate salts and suspended in 71 mM sodium sulphate buffered to pH 7.2 with 5 mM sodium phosphate salts, upon addition of an acetone solution of **281** (2 mol % with respect to lipid), **286** (2 mol % with respect to lipid) and both **281** and **286** (2 mol % each with respect to lipid) following a KCl 'pulse' bringing the extravesicular KCl concentration to 100 mM.

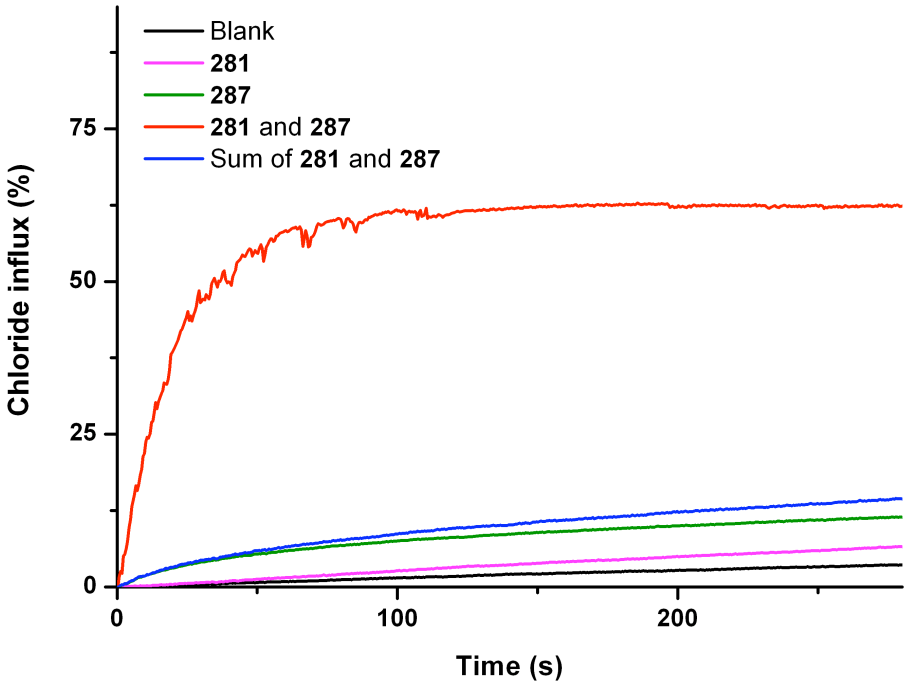

Figure 5.11: Change in internal chloride concentration of unilamellar POPC vesicles containing 1 mM lucigenin and 71 mM sodium sulphate, buffered to pH 7.2 with 5 mM sodium phosphate salts and suspended in 71 mM sodium sulphate buffered to pH 7.2 with 5 mM sodium phosphate salts, upon addition of an acetone solution of **281** (2 mol % with respect to lipid), **287** (2 mol % with respect to lipid) and both **281** and **287** (2 mol % each with respect to lipid) following a KCl 'pulse' bringing the extravesicular KCl concentration to 100 mM.

For strapped calixpyrroles **286** and **287** a significant synergistic effect on chloride influx was observed by adding the anionophore and the cationophore together (there is a significant difference between the sum of chloride influx when the ionophores are added individually and that observed when they are added simultaneously – for plots with error bars see **Appendix A5.3**). Only a small increase was observed upon addition of *meso*-octamethylcalix[4]pyrrole **178** with valinomycin, compared to the sum of chloride influx achieved by the compounds individually (**Figure 5.9**). Upon addition of compound **286** alone there is a significant increase in the internal chloride concentration (**Figure 5.10**), however chloride transport under similar conditions has been observed previously.[463]

These results can be rationalised by examining the known transport properties of these compounds. Compounds **286** and **287** are known Cl^-/NO_3^- antiport agents and can, in addition, facilitate some M^+/Cl^- co-transport.[463, 464] An antiport process is essentially a

combination of two coupled uniport steps, thus a molecule capable of facilitating ion transport by an antiport mechanism should be able to facilitate a coupled uniport step in a symport dual host system (**Figure 5.12**). Transmembrane chloride transport with compound **178** has only been observed *via* a Cs^+/Cl^- symport process, wherein CsCl is transported as an ion pair.[367] Consequently, compound **178** is unable to facilitate chloride uniport.

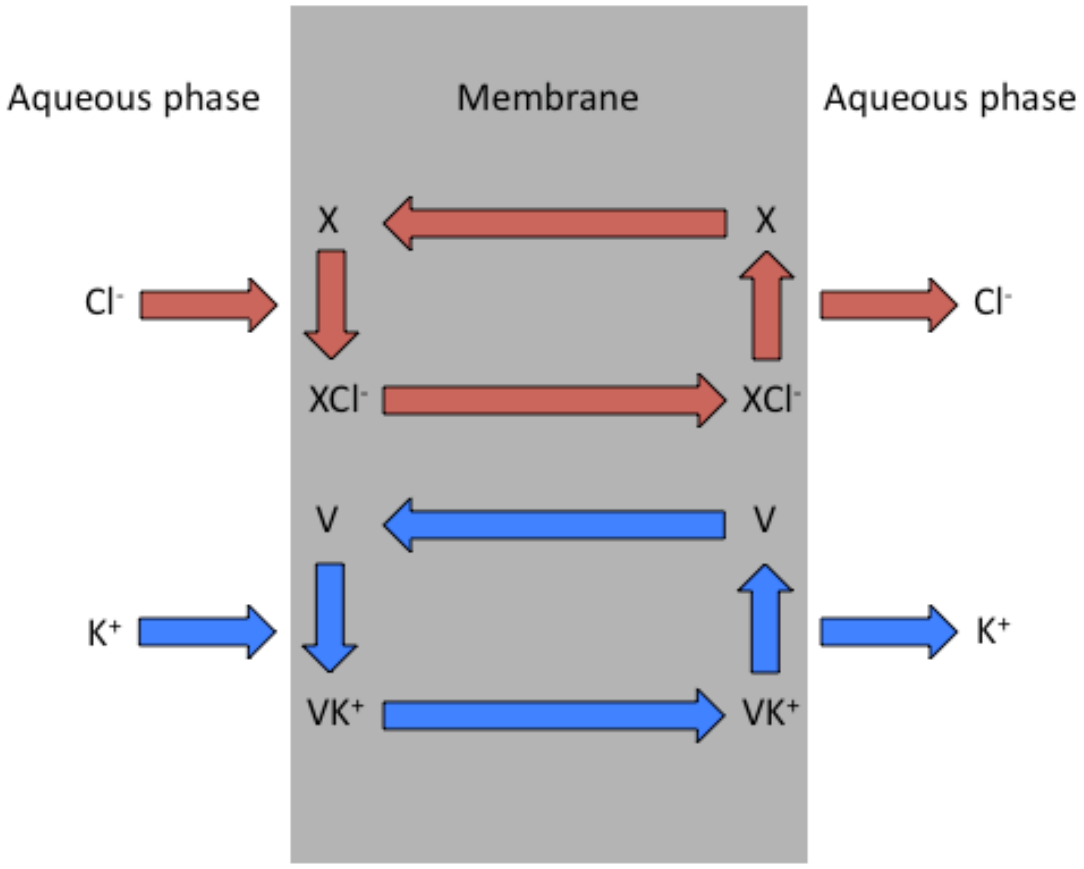

Figure 5.12: K^+/Cl^- symport by a dual host mechanism; using a discrete chloride transporter (X) and valinomycin (V) as a discrete potassium transporter.

In addition to the KCl 'pulse' experiments, assays with NaCl and RbCl 'pulses' were also conducted. Similar results to those obtained with the KCl 'pulse' experiments were obtained (see **Appendix A5.3**). These results show that the addition of both an anionophore and a cationophore together can significantly enhance the rate of ion

transport through a lipid bilayer. By separating the cotransport process into two coupled uniport processes it may be possible to optimise receptors for the transport of each ion species, individually optimising the transport rates and selectivity of each uniport pathway.[535]

5.3 A Dual Host System for Anion Antiport

Rather than occurring in isolation, transport processes in cells are coupled together. Having demonstrated that M^+/Cl^- co-transport can be facilitated in a dual host system by a combination of strapped calixpyrroles and valinomycin, focus was drawn to more biologically relevant transport systems.[535] Cl^-/HCO_3^- antiport was shown in **Section 1.5** to be biologically significant and thus facilitating such a process *via* a dual host system may aid the development of synthetic transport systems for the treatment of cystic fibrosis, infertility and heart disease.[41, 46]

5.3.1 Selection of Ionophores

In the previous study of M^+/Cl^- co-transport by a dual host mechanism, *meso*-octamethylcalix[4]pyrrole **178** and its strapped analogues **286** and **287** were tested as chloride ionophores (see **Section 5.2**).[371] Compounds **286** and **287** are known to facilitate M^+/Cl^- co-transport and Cl^-/NO_3^- antiport processes and were found to facilitate coupled chloride uniport, whilst *meso*-octamethylcalix[4]pyrrole **178** can only facilitate chloride transport *via* Cs^+/Cl^- co-transport, and is thus unsuitable for a dual host transport system.[367, 535]

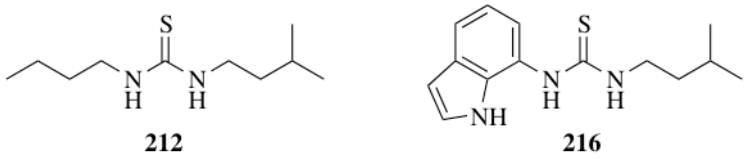

212 **216**

Figure 5.13: Thiourea containing bicarbonate transporters.

Thiourea compounds **212** and **216** (**Figure 5.13**) have been shown to facilitate both Cl^-/NO_3^- and Cl^-/HCO_3^- antiport (see **Section 3.3**). In fact, compound **216** facilitates

ion transport in POPC lipid vesicles at concentrations as low as 4 mmol % (with respect to lipid).[371] Proton NMR titrations in 0.5 % H_2O/DMSO-d_6 reveal that these compounds are selective for bicarbonate over chloride ($[K_a[HCO_3^-]/K_a[Cl^-]$ = 5.8 for **212**, 18.4 for **216**). Owing to this selectivity it was hypothesised that chloride transport may be the rate limiting step in Cl^-/HCO_3^- antiport processes with these compounds, thus using an additional chloride carrier in a dual host type system may enhance transport rates.

5.3.2 Ion Transport Studies

The effect of calixpyrroles **178**, **286** and **287** on Cl^-/HCO_3^- antiport processes mediated by thioureas **212** and **216** was examined using a chloride ISE bicarbonate 'pulse' assay (see **Section 2.2.4**). The carriers were added individually and in combination as solutions in DMSO at 2 mol % (with respect to lipid) loadings, with the exception of compound **216** which was added at 0.03 mol % (with respect to lipid) owing to its inherently higher transport activity (see **Section 3.3.4**). Control experiments were performed without the bicarbonate 'pulse' to examine the possibility of H^+/Cl^- co-transport.

The results of the bicarbonate 'pulse' experiments with thiourea **212** and calixpyrroles **178**, **286** and **287** are shown in **Figures 5.14-5.16**. In each case the results show the effect of adding the thiourea compound individually, the calixpyrroles individually and the effect of adding the two compounds simultaneously. The corrected sum of the change in chloride concentration facilitated by addition of the calixpyrrole and thiourea individually is shown for comparison.

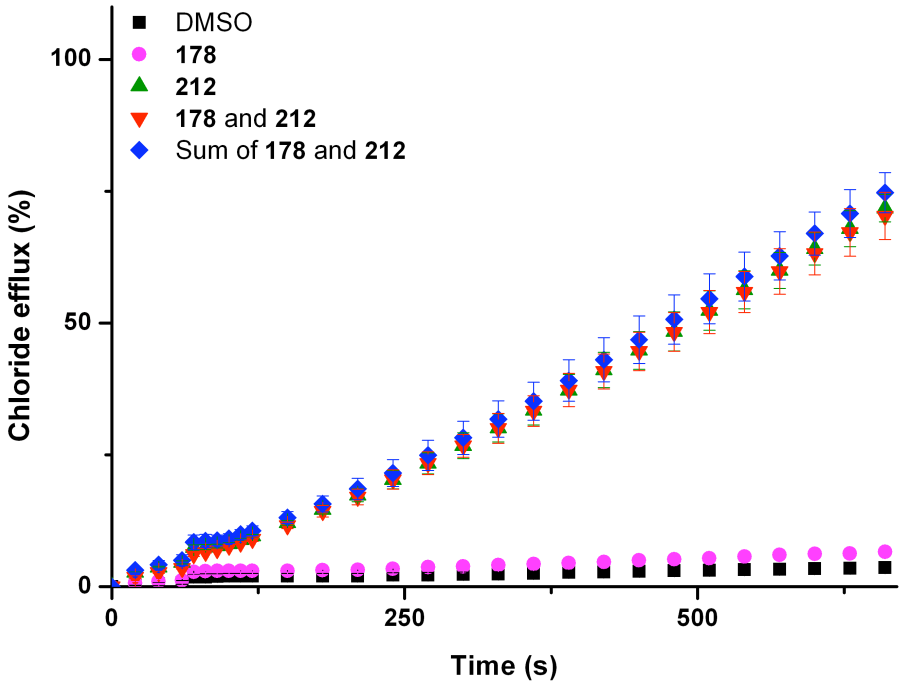

Figure 5.14: Chloride efflux from unilamellar POPC vesicles containing 451 mM sodium chloride, buffered to pH 7.2 with 20 mM sodium phosphate salts and suspended in 150 mM sodium sulphate, buffered to pH 7.2 with 20 mM sodium phosphate salts, upon addition of DMSO solutions of **178** (2 mol % with respect to lipid), **212** (2 mol % with respect to lipid) and both **178** and **212** (2 mol % each with respect to lipid). The sum of **178** and **212** (2 mol % each with respect to lipid) is shown for comparison. A sodium bicarbonate pulse was added at t = 60 s such that the external bicarbonate concentration was 40 mM. Each point represents an average of three trials.

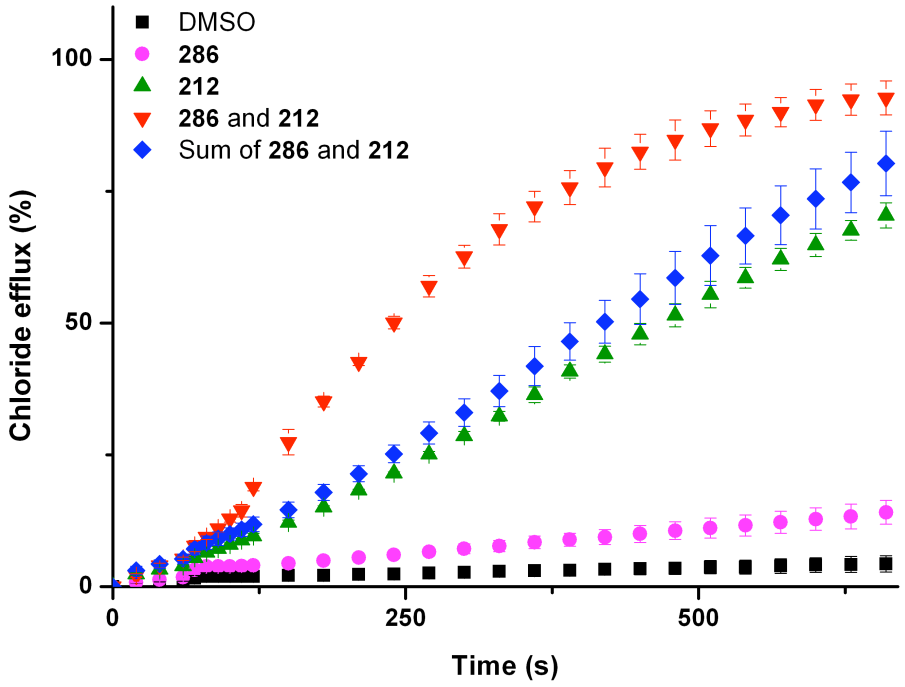

Figure 5.15: Chloride efflux from unilamellar POPC vesicles containing 451 mM sodium chloride, buffered to pH 7.2 with 20 mM sodium phosphate salts and suspended in 150 mM sodium sulphate, buffered to pH 7.2 with 20 mM sodium phosphate salts, upon addition of DMSO solutions of **286** (2 mol % with respect to lipid), **212** (2 mol % with respect to lipid) and both **286** and **212** (2 mol % each with respect to lipid). The sum of **286** and **212** (2 mol % each with respect to lipid) is shown for comparison. A sodium bicarbonate pulse was added at t = 60 s such that the external bicarbonate concentration was 40 mM. Each point represents an average of three trials.

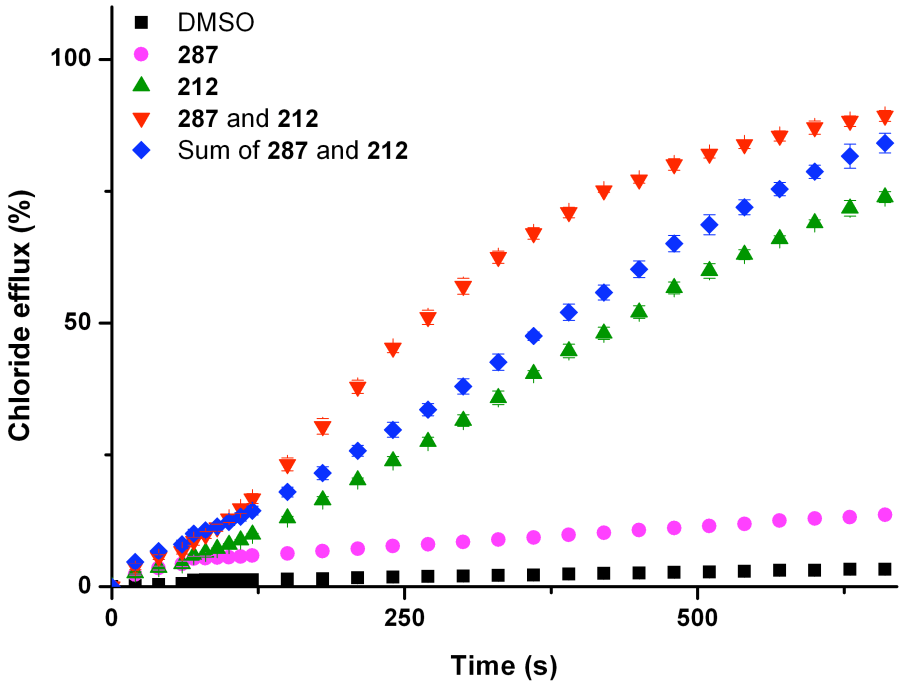

Figure 5.16: Chloride efflux from unilamellar POPC vesicles containing 451 mM sodium chloride, buffered to pH 7.2 with 20 mM sodium phosphate salts and suspended in 150 mM sodium sulphate, buffered to pH 7.2 with 20 mM sodium phosphate salts, upon addition of DMSO solutions of **287** (2 mol % with respect to lipid), **212** (2 mol % with respect to lipid) and both **287** and **212** (2 mol % each with respect to lipid). The sum of **287** and **212** (2 mol % each with respect to lipid) is shown for comparison. A sodium bicarbonate pulse was added at t = 60 s such that the external bicarbonate concentration was 40 mM. Each point represents an average of three trials.

Figures 5.14-5.16 show that an enhancement in Cl^-/HCO_3^- transport was observed when compounds **286** and **287** were added with thiourea compound **212** (compared to the sum of the chloride efflux obtained from adding the compounds separately), demonstrating a synergistic effect. Similar results were obtained with thiourea **216** and calixpyrroles **286** and **287** (see **Appendix A5.3**). These results show that these compounds can participate in a dual host system for the transmembrane transport of chloride and bicarbonate *via* two coupled uniport processes. The transport pathways in operation are shown in **Figure 5.17**. The addition of compounds **286** or **287** provide an additional chloride uniport pathway. In order to maintain charge neutrality one bicarbonate ion must be transported into the vesicle for every chloride ion transported out. Thus, the enhanced transport activity observed when compounds **286** or **287** are

added with compound **212** is the result of increased membrane permeability towards chloride in the presence of the calixpyrroles **286** and **287** (**Figure 5.17**). This enables compound **212** to transport bicarbonate at a faster rate. In agreement with the results presented in **Section 5.2**, *meso*-octamethylcalix[4]pyrrole **178** did not facilitate a significant enhancement in chloride efflux when added with thioureas **212** or **216**, owing to its inability to facilitate chloride uniport. Control experiments with no bicarbonate 'pulse' demonstrated that the observed synergy was not a consequence of dual host H^+/Cl^- co-transport (see **Appendix A5.3**).

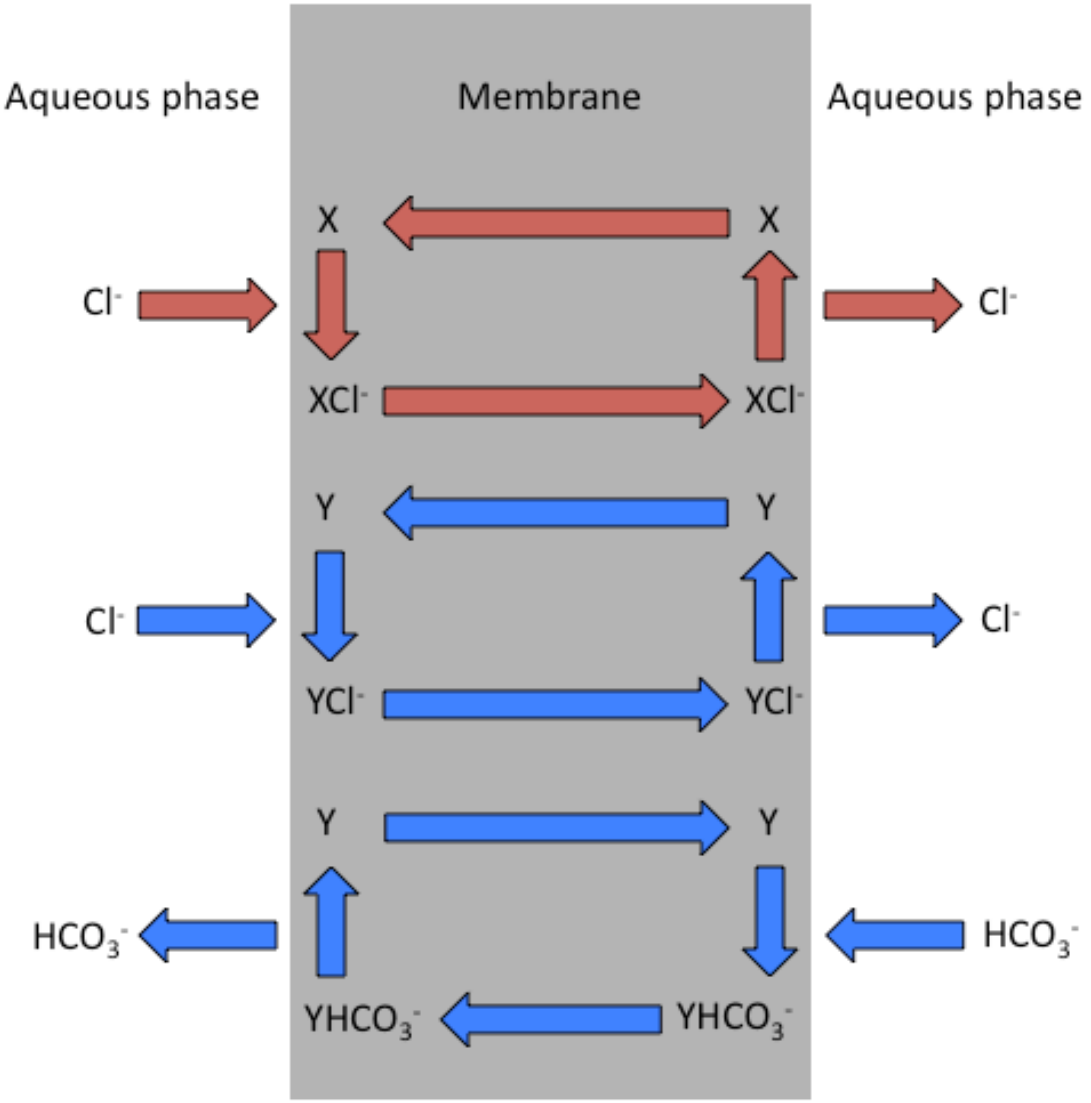

Figure 5.17: Cl^-/HCO_3^- antiport by a dual host mechanism; using a discrete chloride transporter (X) and a discrete bicarbonate carrier (Y). The bicarbonate carrier in this case can also facilitate chloride transport.

Receptors optimised for the transmembrane transport of chloride can be coupled with those optimised for the transmembrane transport of bicarbonate, to yield enhanced rates of Cl^-/HCO_3^- antiport over each receptor functioning alone.[407] These results suggest that the use of small molecule carriers in biological systems may result in enhanced rates of transport through the coupling of transport processes mediated by the synthetic carrier to other transport processes present in the cell.

5.4 Investigation of a Bioactive Molecule

Compound **289** was synthesised by the group of J. L. Sessler at the University of Texas. Compound **289** had been found to exhibit biological activity *in vitro*.[536] To better understand the origin of this activity, a range of vesicle based ion transport assays were performed.

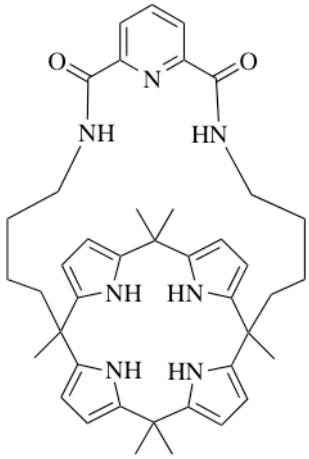

289

Figure 5.18: Isophthalamide strapped calix[4]pyrrole **289**.

5.4.1 Ion Transport Studies

M^+/Cl^- co-transport activity was assessed using unilamellar POPC vesicles containing 451 mM MCl (M = Li, Na, K, Rb or Cs) buffered to pH 7.2 with 20 mM sodium phosphate salts. The vesicles were suspended in either 150 mM sodium sulphate (M = Li, K, Rb or Cs) or 150 mM potassium sulphate (M = Na) buffered to pH 7.2 with 5 mM sodium phosphate salts. To initiate the experiment compound **289** (4 mol % with respect to lipid) was added as a solution in DMSO to the vesicle suspension and chloride efflux was monitored using a chloride ISE. The vesicles were lysed at t = 300 s to determine 100 % chloride efflux. (**Figure 5.19**)

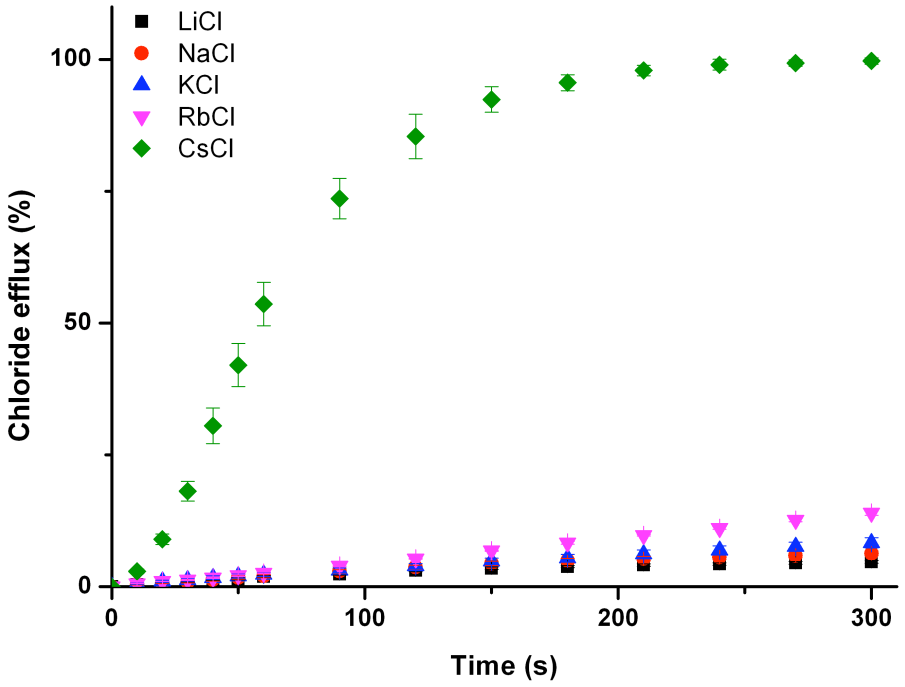

Figure 5.19: Chloride efflux mediated by receptor **289** (4 mol % with respect to lipid) from POPC vesicles containing 451 mM MCl buffered to pH 7.2 with 20 mM sodium phosphate salts (M = Li, Na, K, Rb, Cs). The vesicles were suspended in 150 mM Na_2SO_4 (except where M = Na, where K_2SO_4 was used) buffered to pH 7.2 with 20 mM sodium phosphate salts. At the end of the experiment, the vesicles were lysed to calibrate 100 % chloride efflux. Each point represents the average of three trials.

Compound **289** was found to facilitate Cs^+/Cl^- co-transport to a significantly greater extent than with the other alkali metal chloride salts. A Hill plot was performed for caesium chloride co-transport. An EC_{50} value of 0.211 mol % was obtained for Cs^+/Cl^- symport, with a Hill coefficient (n) of 1.64 (see **Appendix A5.3**).

Compound **289** was tested in a Cl^-/NO_3^- antiport ISE assay (see **Section 2.2.4**). Compound **289** was found to facilitate a limited amount of Cl^-/NO_3^- antiport (**Figure 5.20**) at loadings of 4 mol % (with respect to lipid).

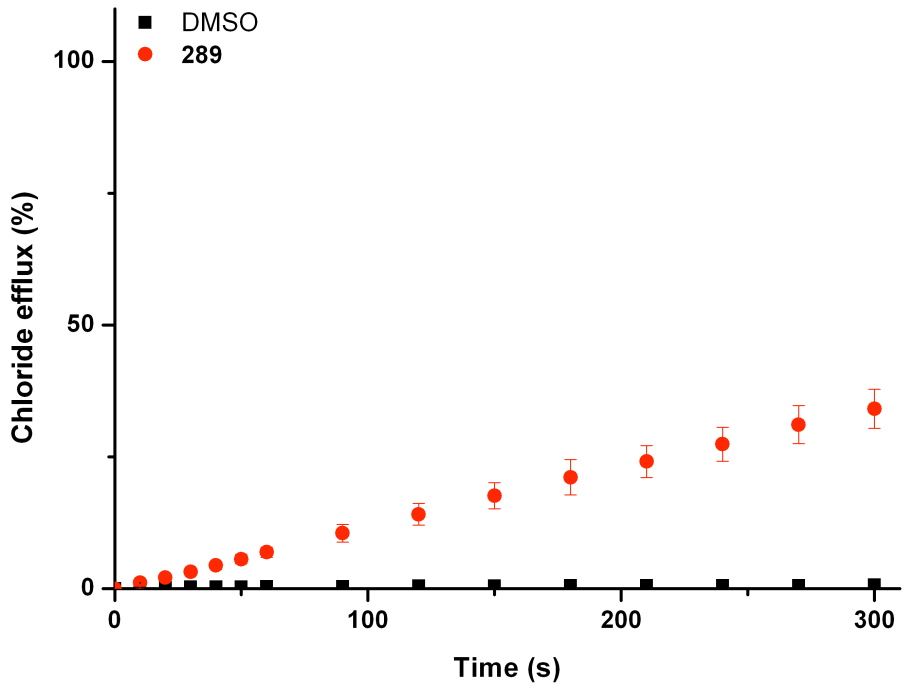

Figure 5.20: Chloride efflux mediated by receptor **289** (4 mol % with respect to lipid) from vesicles containing 488 mM NaCl buffered to pH 7.2 with 5 mM sodium phosphate salts. The vesicles were suspended in 488 mM $NaNO_3$ buffered to pH 7.2 with 5 mM sodium phosphate salts. At the end of the experiment, the vesicles were lysed to calibrate 100 % chloride efflux. Each point represents the average of three trials.

Compound **289** was also tested in a bicarbonate 'pulse' assay (see **Section 2.2.4**). The results show that upon addition of the bicarbonate 'pulse' only a small increase in chloride efflux is observed (**Figure 5.21**), suggesting that compound **289** is a poor bicarbonate transporter at loadings of 4 mol % (with respect to lipid). In addition the lack of transport before the bicarbonate 'pulse' indicates that compound **289** is unlikely to facilitate H^+/Cl^- co-transport.

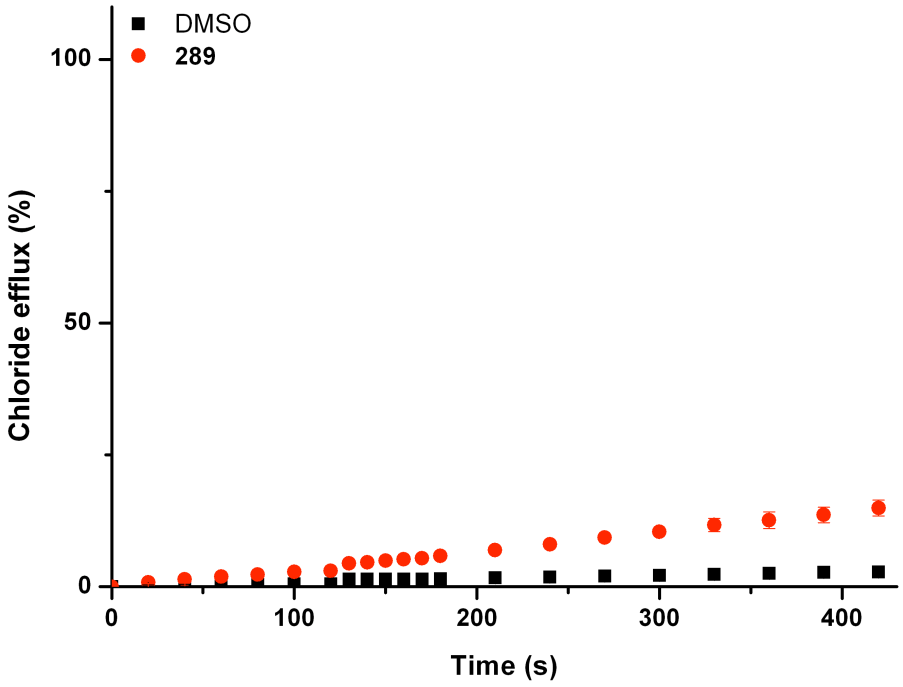

Figure 5.21: Chloride efflux mediated by receptor **289** (4 mol % with respect to lipid) from unilamellar POPC vesicles containing 451 mM NaCl buffered to pH 7.2 with 20 mM sodium phosphate salts. The vesicles were suspended in 150 mM Na_2SO_4 buffered to pH 7.2 with 20 mM sodium phosphate salts, at t = 120 s, a 'pulse' of $NaHCO_3$ was added such that the external bicarbonate concentration was 40 mM. At the end of each experiment, the vesicles were lysed to calibrate 100 % chloride efflux. Each point represents the average of three trials.

To determine if compound **289** operates *via* a mobile carrier mechanism a cholesterol mobility assay (see **Section 3.3.4**) was performed using unilamellar POPC/cholesterol (7:3 molar ratio) vesicles containing 451 mM CsCl buffered to pH 7.2 with 20 mM sodium phosphate salts. The vesicles were suspended in 150 mM Na_2SO_4 buffered to pH 7.2 with 20 mM sodium phosphate salts. To initiate the experiment compound **289** (0.25 mol % with respect to lipid) was added as a solution in DMSO to the vesicle suspension. The vesicles were lysed at t = 300 s to determine 100 % chloride efflux. The dramatic reduction in transport activity observed in the cholesterol containing vesicles compared to that observed in vesicles composed entirely of POPC at the same loading (**Figure 5.22**) indicate that the transporter operates by a diffusion mechanism. In addition, the low Hill coefficient calculated from the Hill plot for Cs^+/Cl^- co-transport suggests a mobile carrier mechanism.

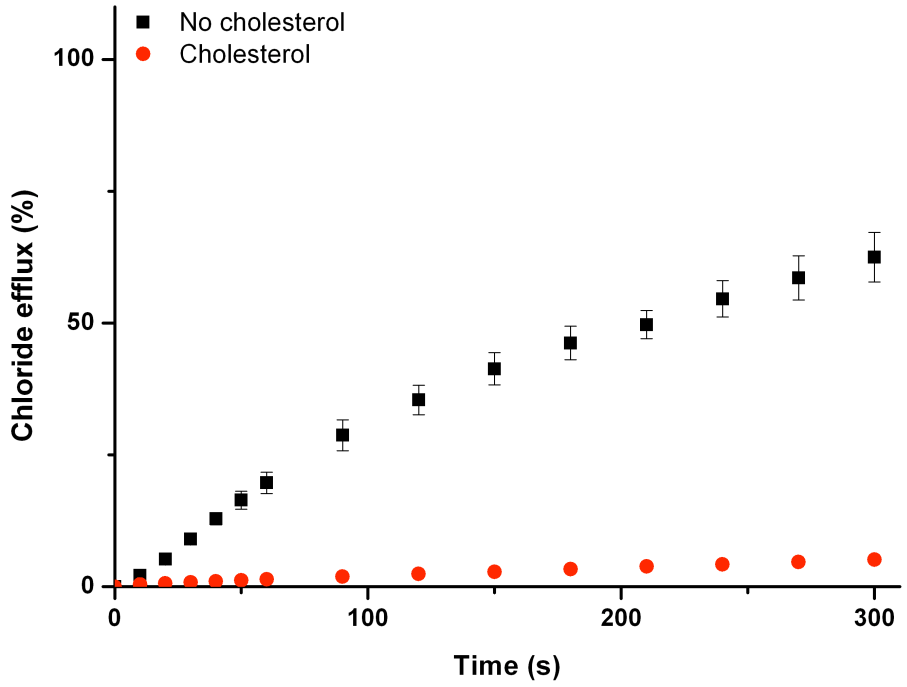

Figure 5.22: Chloride efflux mediated by receptor **289** (0.25 mol % with respect to lipid) from unilamellar POPC vesicles or unilamellar POPC/cholesterol (7:3) containing 451 mM CsCl buffered to pH 7.2 with 20 mM sodium phosphate salts. The vesicles were suspended in 150 mM Na_2SO_4 buffered to pH 7.2 with 20 mM sodium phosphate salts. At the end of the experiment, the vesicles were lysed to calibrate 100 % chloride efflux. Each point represents the average of three trials.

5.4.2 Dual Host Transport

In **Section 5.2** it was demonstrated that K^+/Cl^- co-transport can be facilitated by a dual host system comprising of a strapped calixpyrroles **267** and **268** (anionophore) and valinomycin **281** (cationophore).[535] This process can be visualised as two discrete coupled uniport pathways. A marker of suitability for use in a dual host system is the ability to facilitate an antiport process (essentially two coupled uniport steps). Compound **289** facilitates Cl^-/NO_3^- antiport and is thus a potential candidate for use as the chloride transporter in a K^+/Cl^- symport dual host system.[535]

K^+/Cl^- dual host transport activity was tested using an K^+/Cl^- symport ISE assay. Unilamellar POPC vesicles were prepared containing 451 mM KCl buffered to pH 7.2 with 20 mM sodium phosphate salts. The vesicles were suspended in 150 mM Na_2SO_4

buffered to pH 7.2 with 20 mM sodium phosphate salts. To initiate the experiment the test compound was added as a solution in DMSO to the vesicle suspension. At t = 10 s either a second compound was added as a solution in DMSO or 'blank' DMSO was added. The vesicles were lysed at t = 300 s to determine 100 % chloride efflux. Runs were performed with a DMSO control, valinomycin **281** (2 mol % with respect to lipid), compound **289** (2 mol % with respect to lipid) and both valinomycin **281** and compound **289** (2 mol % each with respect to lipid). A significant enhancement was observed when valinomycin **281** and compound **289** are added together, compared to the individual sum (**Figure 5.23**). This indicates that compound **289** can facilitate chloride uniport as part of a coupled transport process.

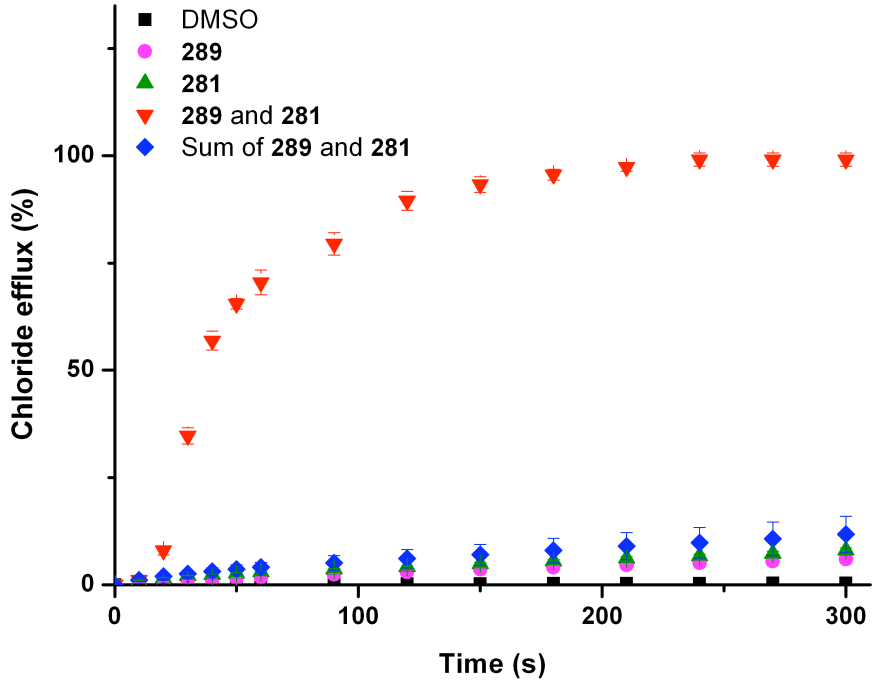

Figure 5.23: Chloride efflux from unilamellar POPC vesicles containing 451 mM KCl buffered to pH 7.2 with 20 mM sodium phosphate salts, suspended in 150 mM Na_2SO_4 buffered to pH 7.2 with 20 mM sodium phosphate salts upon addition of DMSO, **281** (2 mol % with respect to lipid), **289** (2 mol % with respect to lipid) and both **281** and **289** (2 mol % each with respect to lipid). At the end of the experiment, the vesicles were lysed to calibrate 100 % chloride efflux. Each point represents the average of three trials.

In **Section 5.3** it was demonstrated that compounds capable of facilitating chloride uniport in a K^+/Cl^- symport dual host system can also function as chloride

transporters in a dual host system for Cl^-/HCO_3^- antiport.[407] As transport processes in cells are coupled together, it is possible that any biological activity observed with compound **289** may stem from the compound's abilitiy to facilitate chloride uniport.

5.5 Conclusions

In **Section 5.2** it was demonstrated that a M^+/Cl^- coupled transport process can be considered as two discrete uniport pathways. By selecting a carrier capable of facilitating each uniport step it is possible to achieve a synergistic enhancement in the ion transport rates when using the two carriers in unison. In **Section 5.3** the same principle was applied to Cl^-/HCO_3^- antiport, which again can be considered to be two discrete uniport pathways. This is a unique example of an anion antiport pathway facilitated by a dual host mechanism. In **Section 5.4** the biological activity of strapped calixpyrrole **289** was examined. This compound was shown to be able to facilitate the chloride uniport pathway in a K^+/Cl^- symport dual host system. The biological activity of this compound may thus stem from the coupling of chloride transport to other transport processes within biological systems. Further, such a system permits the development of transporters that have their selectivity tuned for the transport of one component in a dual host system.

Chapter 6
Conclusions and Future Work

Owing to the hydrophobic nature of anions, their transport through biological membranes is achieved by a range of membrane spanning transporter proteins (see **Sections 1.1** and **1.4**). Defective transmembrane transport of anions by these proteins can result in a myriad of disease states typified by cystic fibrosis (see **Section 1.5**). Synthetic molecules capable of facilitating the transmembrane transport of ionic species may offer a strategy for treating such channelopathies. A range of synthetic molecules are capable of facilitating ion transport in model systems, operating either through a mobile carrier mechanism or functioning as synthetic ion channels (see **Section 1.8**). The progress made in developing new molecules capable of binding and transporting anions was discussed in **Chapters 2-5**.

In **Chapter 2** diindolylureas containing pendant amide functionalities were examined as anion hosts. These compounds were demonstrated to possess good affinity for oxo-anions in polar 10 % H_2O/DMSO-d_6 mixtures (see **Section 2.2.2**). Interestingly, the extra amide NH groups did not interact with Y-shaped carboxylate anions but did interact with tetrahedral dihydrogen phosphate anions. Despite the promising anion complexation behaviour these compounds they facilitated only low levels of chloride transport in POPC vesicles (see **Section 2.2.4**). A range of tripodal urea and thiourea bearing receptors were then examined. The tripodal arrangement of hydrogen-bond donors led to these compounds functioning as effective hosts for chloride and sulphate. Solid state studies revealed that the presence of alkyl or aromatic substituents facilitate anion encapsulation by a lipophilic coat (see **Section 2.3.2**).

Inspired by the anion hosts developed in **Chapter 2**, molecules based on the indolylurea and indolylthiourea scaffolds were explored in **Chapter 3**. Simple alkyl urea substited indolylureas were found to be poor ion transporters (see **Section 3.2.2**) but the introduction of thiourea functionalities into the scaffold yielded compounds capable of facilitating both Cl^-/NO_3^- and Cl^-/HCO_3^- antiport (see **Section 3.3**). The poor activity of the urea analogues was rationalised as due to their lower lipophilicities and may also be linked to the propensity of the urea compounds to aggregate.[372, 373] In an attempt to

improve the 'drug-like' properties of indolylurea and indolylthiourea scaffolds trifluoromethyl groups were introduced into the host scaffold. The trifluoromethyl functionalised compounds were found to have higher chloride and bicarbonate affinities than their unfluorinated analogues owing to the electron withdrawing influence of the trifluoromethyl substituents (see **Section 3.4.2**). In addition the fluorinated compounds were found to be more lipophilic and thus more active anion transporters than their unfluorinated analogues (see **Section 3.4.4**). Owing to the potent Cl^-/HCO_3^- transport activity exhibited in vesicle assays, the transport properties of the series were studied *in vitro* (see **Section 3.4.5**) The fluorinated compounds were found to exhibit selective toxicity towards GLC4 and A375 cancer cell lines and apoptotic cell death induced by changes in intracellular pH was demonstrated for members of the series. These findings demonstrated that the transport activity observed in vesicle assays can be indicative of biological activity *in vitro*.

In **Chapter 4** the urea group was again utilised in the study of *ortho*-phenylenediamine based bisureas. In an attempt to construct active urea containing transporters electron withdrawing substituents were added to both the peripheral and core phenyl groups. The most active compound contained electron withdrawing *para*-nitrophenyl substituents and was found to facilitate chloride efflux at loadings of 0.1 mmol % - the lowest loading of a synthetic mobile carrier reported to facilitate transport (see **Section 4.2.4**). Significantly the most active transporters in the series were shown indirectly to facilitate Cl^-/carboxylate antiport, perhaps offering new potential biological applications for this type of ion transporter (see **Section 4.2.5**).

The work described in **Chapter 5** builds on the findings in **Chapters 3** and **4**, demonstrating that both symport and antiport ion transport processes can be considered to be two coupled uniport pathways. The Cl^-/HCO_3^- antiport dual host system described in **Section 5.3** is the first example of a dual host system being applied to an anion antiport pathway. By utilising transporters that were selective for each of the uniport steps it was possible to achieve a synergistic enhancement in transport activity by using combinations of ionophores. Importantly, individual transporters that were found to facilitate antiport processes were suitable for application in a dual host system whilst those that could only facilitate symport pathways through the transport of an ion pair were inactive. Crucially

the transport properties of a biologically active molecule were examined (see **Section 5.4**). It was demonstrated that the observed transport activity occurring *in vitro* may be the consequence of dual host chloride uniport.

The construction of ion transporters that complex anions through hydrogen bonding interactions has been demonstrated as an approach that can ultimately yield compounds that exhibit a biological function *in vitro*. A variety of new transporter scaffolds have been discovered that may lead to the development of therapeutic agents for the treatment of diseases caused by defective ion transport. It appears that a fine balance must be struck between receptor lipophilicity and anion affinity to afford compounds that function as mobile anion carriers. Additionally, since ion distribution in biological systems is not uniform, as illustrated by **Table 6.1**, it should be possible to target specific uniport steps that are likely to be coupled to ion gradients within the biological system being studied.[17]

Ion	Cell (mM)	Blood (mM)
K^+	139	4
Na^+	12	145
Cl^-	4	116
HCO_3^-	12	29

Figure 6.1: Typical ion gradients present between cells and the blood in mammalian systems.

The work discussed within this thesis has opportunities for further expansion. Firstly, the ability of the indole compounds discussed in **Chapter 3** to partition into phospholipid bilayers could be examined by fluorescence techniques, owing to the highly solvent sensitive nature of indole fluorescence.[537] Analagous studies have been performed with *para*-nitrophenyl functionalised thioureas; wherein the positioning of the chromophore within the bilayer can be measured by UV-vis spectroscopy. Since nitrophenyl functionalities are utilised in the bisurea receptors discussed in **Chapter 4**, it may be possible to use these techniques to visualise the transporters partitioning within the membrane or assess the ability of these compounds to self associate under assay

conditions.[358] The compounds discussed in **Chapter 4** show good activity as Cl^-/NO_3^- and Cl^-/HCO_3^- antiport agents, comparable with the fluorinated compounds discussed in **Chapter 3**. Consequently, the bisureas may exhibit transport activity *in vitro* in an analogous manner. It would also be useful to demonstrate the transport of carboxylic acids by utilising NMR techniques (see **Section 1.9.5**). This would permit observation of the transmembrane transport of ^{13}C labelled maleate or fumarate directly. In addition, the precipitates formed upon addition of TBA maleate or TBA fumarate to 0.5 % H_2O/DMSO-d_6 solutions of bisureas **263**, **264** and **265** require further investigation in order to determine their composition.

Finally, the dual host work discussed in **Chapter 5** could be adapted for a range of other transport systems. Perhaps most suitable for exploration would be a dual host system for H^+/Cl^- symport.[538] Protonophores have already been utilised in dual host systems for K^+/H^+ antiport and could likely be similarly applied to a H^+/Cl^- symport system (see **Section 5.1.1**), whilst chloride carriers were utilised in both the M^+/Cl^- symport and Cl^-/HCO_3^- antiport systems. Such Cl^-/HCO_3^- antiport and H^+/Cl^- symport dual host systems may have biological applications (see **Section 1.5.4**). Furthermore, it appears that carrier function *in vitro* may be linked to the participation of transporters in such dual host systems, with carrier mediated ion transport linked to cell protein transporter function.

Chapter 7
Experimental Details

7.1 General Information

^{1}H NMR (300 MHz), ^{19}F{^{1}H} (282 MHz) and ^{13}C{^{1}H} NMR (75 MHz) spectra were determined on a Bruker AV300 spectrometer whilst ^{1}H NMR (400 MHz) and ^{13}C{^{1}H} (100 MHz) were determined on a Bruker AV400 spectrometer. Chemical shifts reported in parts per million (ppm), calibrated to the appropriate solvent peak. The abbreviations used for spin multiplicity are; s = singlet, d = doublet, t = triplet, m = multiplet. Melting points were recorded using open capillary tubes in a Gallenkamp melting apparatus. Infrared (IR) spectra were recorded on a Matterson Satellite (ATR). Fourier transform infrared (FTIR) spectra are reported in wavenumbers (cm^{-1}). Low resolution mass spectra (LRMS) were recorded on a Walters ZMD single quadrupole spectrometer. High resolution mass spectra (HRMS) were recorded by the mass spectrometry service at the University of Southampton using a Bruker Apex III spectrometer. Both HRMS and LRMS are reported as *m/z*. All solvents and reagents were obtained from commercial sources (Sigma Aldrich, Tokyo Chemical Industry UK or Alfa Aesar) and used without further purification unless stated otherwise. Dry DCM and chloroform were obtained by distillation over CaH_2. 2-butyl-7-nitro-5-trifluoromethyl-1*H*-indole was synthesised according to literature procedures.[385, 386]

7.2 NMR Methods

7.2.1 ^{1}H NMR Titrations

A solution of host (0.01 M, 1.5 mL) in 0.5 % H_2O/DMSO-d_6 was prepared. 0.5 mL of this solution was placed inside an NMR tube. The appropriate tetrabutylammonium (TBA) or tetraethylammonium (TEA) salt, having been dried under high vacuum, was added to the remainder of the host solution such that the concentration of the anion salt was 0.15 M. Small quantities of the anion solution were added stepwise to the host solution, typically 10 μL (x2), 5 μL (x9), 10 μL (x4) and 50 μL (x5). This resulted in an increase in the concentration of the anion salt within the NMR tube, whilst

the concentration of host remained constant. A ^{1}H NMR spectrum was recorded after each addition of anion. The chemical shifts observed were calibrated to the DMSO-d_6 solvent peak. The relevant NMR data was then fitted to an appropriate binding model using WinEQNMR2 fitting software.[340]

7.2.2 Job Plots

A solution of host (0.01 M, 3 mL) and a solution of anion salt (0.01 M, 3 mL) in 0.5 % H_2O/DMSO-d_6 were prepared. Combinations of these solutions were added to separate NMR tubes, typically; 0.5 mL host, 0.45 mL host and 0.05 mL guest, 0.40 mL host and 0.10 mL guest, 0.35 mL host and 0.15 mL guest, 0.30 mL host and 0.20 mL guest, 0.25 mL host and 0.25 mL guest, 0.20 mL host and 0.30 mL guest, 0.15 mL host and 0.35 mL guest, 0.10 mL host and 0.40 mL guest, and 0.05 mL host and 0.45 mL guest. A ^{1}H NMR spectrum was recorded for each sample and was calibrated to the DMSO-d_6 solvent peak. The relevant chemical shift data was then used to construct a Job plot.[539]

7.3 Vesicle Studies

7.3.1 General Method

A chloroform solution of 1-palmitoyl-2-oleoyl-*sn*-glycero-3-phosphocholine (POPC) (22.32 mg mL^{-1}) (Genzyme) was evaporated under reduced pressure to give a thin film. The lipid film was dried under high vacuum for at least 2 hours and rehydrated with the **internal** solution by vortexing. The lipid suspension was then subjected to nine freeze–thaw cycles and twenty-nine extrusions through a 200 nm polycarbonate nucleopore membrane using a LiposoFast Basic extruder (Avestin, Inc.) to obtain unilamellar vesicles. The liposomes underwent dialysis in the **external** solution. The vesicles were diluted to 5 mL with the **external** solution to form a stock solution of lipid.

Samples for assay were prepared by diluting lipid stock solution to 5 mL (using the **external** solution) to give a solution of 1 mM lipid. Chloride efflux was monitored using a chloride selective electrode (Accumet or Cole-Parmer). To initiate the experiment compounds were added as solutions in DMSO, to give a 1:50 compound to lipid ratio (2 mol %). At the end of the experiment detergent (octaethylene glycol monododecyl ether)

was added to allow the determination of 100 % chloride efflux. Experiments were repeated in triplicate and all traces presented are the average of three trials. The chloride electrode was calibrated against sodium chloride solutions of known concentration.

7.3.2 Cl^-/NO_3^- Antiport Assay

Internal solution: 488 mM sodium chloride buffered to pH 7.2 with 5 mM sodium phosphate salts.

External solution: 488 mM sodium nitrate buffered to pH 7.2 with 5 mM sodium phosphate salts.

Compound was added at t = 0. Detergent was added at t = 5 mins.

7.3.3 Cl^-/NO_3^- Antiport Assay with Cholesterol

Internal solution: 488 mM sodium chloride buffered to pH 7.2 with 5 mM sodium phosphate salts.

External solution: 488 mM sodium nitrate buffered to pH 7.2 with 5 mM sodium phosphate salts.

To the freeze dried lipid film a chloroform solution of cholesterol was added to achieve a lipid to cholesterol molar ratio of 7:3. The chloroform was removed under reduced pressure to give a thin film. The film was dried under high vacuum for at least 2 hours and vesicles were prepared by the standard method. Compound was added at t = 0. Detergent was added at t = 5 mins.

7.3.4 Cl^-/HCO_3^- Antiport Assay

Internal solution: 451 mM sodium chloride buffered to pH 7.2 with 20 mM sodium phosphate salts.

External solution: 150 mM sodium sulphate buffered to pH 7.2 with 20 mM sodium phosphate salts.

Compound was added at t = 0. A ‘pulse’ of sodium bicarbonate in external solution was added at t = 2 mins, such that the external concentration of bicarbonate was 40 mM. Detergent was added at t = 7 mins.

7.3.5 Sulphate 'Blank' Assay

Internal solution: 451 mM sodium chloride buffered to pH 7.2 with 20 mM sodium phosphate salts.

External solution: 150 mM sodium sulphate buffered to pH 7.2 with 20 mM sodium phosphate salts.

Compound was added at t = 0. Detergent was added at t = 7 mins.

7.3.6 M^+/Cl^- Symport Assay (M = Li, Na, K, Rb or Cs)

Internal solution: 451 mM metal chloride buffered to pH 7.2 with 20 mM sodium phosphate salts.

External solution: 150 mM sodium sulphate buffered to pH 7.2 with 20 mM sodium salts (except M = Na, where potassium phosphate salts were used).

Compound was added at t = 0. Detergent was added at t = 5 mins.

7.3.7 Cs^+/Cl^- Symport Assay with Cholesterol

Internal solution: 451 mM caesium chloride buffered to pH 7.2 with 20 mM sodium phosphate salts.

External solution: 150 mM sodium sulphate buffered to pH 7.2 with 20 mM sodium phosphate salts.

To the freeze dried lipid film a chloroform solution of cholesterol was added to achieve a lipid to cholesterol molar ratio of 7:3. The chloroform was removed under reduced pressure to give a thin film. The film was dried under high vacuum for at least 2 hours and vesicles were prepared by the standard method. Compound was added at t = 0. Detergent was added at t = 5 mins.

7.3.8 HEPES Buffer Assay

Internal solution: 451 mM sodium chloride buffered to pH 7.2 with 20 mM HEPES buffer.

External solution: 150 mM sodium sulphate buffered to pH 7.2 with 20 mM HEPES buffer.

Compound was added at t = 0. Detergent was added at t = 5 mins.

7.3.9 Cl^-/Carboxylate Antiport Assay at pH 7.2

Internal solution: 451 mM sodium chloride buffered to pH 7.2 with 20 mM sodium phosphate salts.

External solution: 150 mM sodium sulphate buffered to pH 7.2 with 20 mM sodium phosphate salts.

Compound was added at t = 0. A 'pulse' of either sodium maleate or sodium fumarate in external solution was added at t = 2 mins, such that the external concentration of carboxylate was 40 mM. Detergent was added at t = 7 mins.

7.3.10 Cl^-/Carboxylate Antiport Assay at pH 4.0

Internal solution: 451 mM sodium chloride buffered to pH 7.2 with 20 mM sodium citrate salts.

External solution: 150 mM sodium sulphate buffered to pH 7.2 with 20 mM sodium citrate salts.

Compound was added at t = 0. A 'pulse' of either sodium maleate or sodium fumarate in external solution was added at t = 2 mins, such that the external concentration of carboxylate was 40 mM. Detergent was added at t = 7 mins.

7.3.11 pH Gradient Assay

Internal solution: 451 mM sodium chloride buffered to pH 4.0 with 20 mM sodium citrate salts.

External solution: 150 mM sodium sulphate buffered to pH 7.2 with 20 mM sodium phosphate salts.

Compound was added at t = 0. Detergent was added at t = 5 mins.

7.3.12 Lucigenin Fluorescence Assay for Sulphate Transport

Internal solution: 100 mM sodium chloride and 2 mM lucigenin dye buffered to pH 7.2 with 20 mM sodium phosphate salts.

External solution: 100 mM sodium chloride buffered to pH 7.2 with 20 mM sodium phosphate salts.

Vesicles were prepared as described previously (see **Section 7.3.1**). Instead of dialysis, vesicles were purified by size exclusion chromatography using sephadex gel (G-50). Samples for assay were prepared by diluting the lipid stock solution to 3 mL (using the **external** solution) to give a solution of 1 mM lipid. Fluorescence spectra were obtained using a Varian Cary Eclipse Fluorescence Spectrophotometer. Lucigenin fluorescence was monitored by excitation at 455 nm and emission at 506 nm. At t = 30 s a solution of sodium sulphate was added, such that the external concentration of sulphate was 40 mM. At t = 1 min compounds were added as solutions in methanol.

7.3.13 HPTS Fluorescence Assay

Internal solution: 451 mM sodium chloride and 1 mM HPTS buffered to pH 7.2 with 20 mM sodium phosphate salts.

External solution: 150 mM sodium sulphate buffered to pH 7.2 with 20 mM sodium phosphate salts.

Vesicles were prepared as described previously (see **Section 7.3.1**). Instead of dialysis, vesicles were purified by size exclusion chromatography using sephadex gel (G-50). Samples for assay were prepared by diluting the lipid stock solution to 3 mL (using the **external** solution). Fluorescence spectra were obtained using a Varian Cary Eclipse Fluorescence Spectrophotometer. HPTS fluorescence was monitored by excitation at 405 nm and 460 nm, and emission at 506 nm. At t = 0 compounds were added as solutions in methanol.

7.3.14 Lucigenin Fluorescence Assay for Dual Host Studies

Internal solution: 71 mM sodium sulphate and 1 mM lucigenin dye buffered to pH 7.2 with 5 mM sodium phosphate salts.

External solution: 71 mM sodium sulphate buffered to pH 7.2 with 5 mM sodium phosphate salts.

Vesicles were prepared as described previously (see **Section 7.3.1**). Instead of dialysis, vesicles were purified by size exclusion chromatography using sephadex gel (G-50). Samples for assay were prepared by diluting the lipid stock solution to 3 mL (using the **external** solution) to give a solution of 1 mM lipid. Fluorescence spectra were obtained

using a Varian Cary Eclipse Fluorescence Spectrophotometer. Lucigenin fluorescence was monitored by excitation at 455 nm and emission at 506 nm. At t = 10 s, 100 μL of MCl (M = Na, K or Rb) stock solution (in 71 mM sodium sulphate buffered to pH 7.2 with sodium phosphate salts) was added such that the concentration of MCl in the eternal solution was 100 mM. Compounds were added at t = 40 s as solutions in acetone. Lucigenin fluorescence was converted to chloride concentration using the Stern-Volmer constant obtained under assay conditions. Internal chloride concentrations were standardised against the internal chloride concentration at t = 40 s.

To measure the Stern-Volmer constant, liposomes were prepared using the aforementioned method. Melittin was added at t = 10 s as a solution in ethanol (0.2 mol% with respect to lipid). 5 μL of a stock solution of sodium chloride (in 71 mM sodium sulphate, buffered to pH 7.2 with sodium phosphate salts) was added at 20 s intervals, such that each addition increased the chloride concentration of the solution by 2 mM. A plot of the inverse of the relative fluorescence (F_0/F) against chloride concentration (mM) gave a straight line that could be fitted to the Stern-Volmer equation (see **Appendix A5.3**).

7.3.15 Cl^-/HCO_3^- Antiport Assay for Dual Host Studies

Internal solution: 451 mM sodium chloride buffered to pH 7.2 with 20 mM sodium phosphate salts.

External solution: 150 mM sodium sulphate buffered to pH 7.2 with 20 mM sodium phosphate salts.

Compounds were added at t = 0. A 'pulse' of sodium bicarbonate in external solution was added at t = 2 mins, such that the external concentration of bicarbonate is 40 mM. In all cases the total volume of solution added was 20 μL. At t = 60 s a bicarbonate 'pulse' was introduced to the system such that the concentration of sodium bicarbonate in the external solution was 40 mM. At t = 660 s of detergent was added. Control experiments were performed using the same procedure, but without the sodium bicarbonate pulse at t = 60 s.

7.4 U-tube Assays

Source phase: 488 mM sodium chloride solution buffered to pH 7.2 with 5 mM sodium phosphate salts.

Receiving phase: 488 mM sodium nitrate solution buffered to pH 7.2 with 5 mM sodium phosphate salts.

The source phase and the receiving phase (7.5 mL each) were placed in u-tube apparatus, separated by the organic phase (1 mM compound and 1 mM tetrabutylammonium hexafluorophosphate in nitrobenzene, 15 mL). The organic phase was stirred at room temperature and the chloride concentration in the receiving phase was determined using a chloride selective electrode (Accumet) after 24 hours, 60 hours and 96 hours.

7.5 *In vitro* Assays

The assays described in this section were performed by V. Soto-Cerrato at the University of Barcelona, but are included for the sake of completeness.

7.5.1 Cell lines and Culture Conditions

Human lung cancer cell line GLC4 was obtained from the laboratory of Dr. N.H. Mulder and was cultured in Roswell Park Memorial Institute media (Biological Industries). Human melanoma (A375), human colon adenocarcinoma (SW480), human oral adenosquamos carcinoma (CAL27) and mammary epithelial (MCF-10A) cell lines were purchased from the American Type Culture Collection. Cells were cultured in Dulbecco's Modified Eagle Medium (DMEM) (Biological Industries) supplemented with 10 % heat-inactivated foetal bovine serum (FBS) (Life Technologies), penicillin (100 μg mL^{-1}), streptomycin (100 μg mL^{-1}) and *L*-glutamine (2 mM) (Biological Industries). The MCF10A cell line was cultured in DMEM/Nutrient Mixture F12 (1:1) (Biological Industries) supplemented with 5 % horse serum (Life Technologies), Epidermal growth factor (20 ng mL^{-1}), Hydrocortisone (0.5 μg mL^{-1}), Cholera toxin (100 ng mL^{-1}), insulin (10 μg mL^{-1}) (Sigma-Aldrich) and penicillin (100 μg mL^{-1}), streptomycin (100 μg mL^{-1}) and *L*-glutamine (2 mM) (Biological Industries). Cells were grown at 37 ºC in a 5 % CO_2 atmosphere.

7.5.2 Cell Viability Assay

Adherent cells (1 x 10^5 cells mL^{-1}) or floating cells (GLC4, 2 x 10^5 cells mL^{-1}) were seeded in 96-well plates and allowed to grow for 24 hours. They were then treated with the test compound (10 μM) for 48 hours. Cell viability was determined by 3-(4, 5-dimethylthiazol-2-yl)-2,5-diphenyltetrazolium bromide (MTT) assay. Following treatment, MTT (10 μM) was added to each well for an additional 4 hours. DMSO was added as a control. The resulting blue MTT formazan precipitate was dissolved in 100 μl of isopropanol/ HCl (1 M) (24:1). The absorbance at 570 nm was measured on a multiwell plate reader. Cell viability was expressed as a percentage of the control, and the data displayed are the mean value of two independent experiments performed in triplicate.

7.5.3 Acridine Orange Staining

Cells (2 x 10^5 cells mL^{-1}) were seeded on glass slices and 24 hours later were treated with the test compound (10 μM) for 1 hour. Cells were then washed twice with phosphate buffered saline (PBS) solution and incubated in acridine orange solution (5 μg mL^{-1}) for 30 minutes at room temperature. The cells were then washed with FBS/PBS (1:9) and examined by fluorescence using a NIKON eclipse E800 microscope.

7.5.4 Hoechst Staining

Cells (1 x 10^5 cells mL^{-1}) were seeded in 24-well plates, allowed to grow for 24 hours and then treated with the test compound (10 μM) for 48 hours. They were washed in PBS, suspended in Hoechst 33342 (2 μg mL^{-1}) (Sigma-Aldrich) and incubated for 30 minutes at 37 ºC in the dark. Finally, cells were washed with PBS and examined by fluorescence using a NIKON eclipse E800 microscope.

7.6 Synthetic Procedures

7.6.1 Chapter 2

***N*-benzyl-7-nitro-1*H*-indole-2-carboxamide** *(Novel compound)*

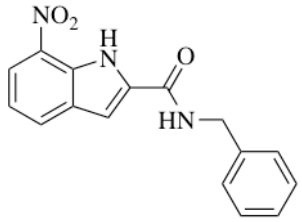

7-nitro-1*H*-indole-2-carboxylic acid (0.410 g, 1.99 mmol) and CDI (0.405 g, 2.50 mmol) were dissolved in chloroform (50 mL). The reaction mixture was heated at reflux for 3 hours under argon. Benzylamine (0.10 mL, 1.90 mmol) was dissolved in dry chloroform (20 mL) and then added dropwise to the stirring reaction mixture. The reaction mixture was heated at reflux for 72 hours under argon. The reaction mixture was diluted with DCM (30 mL), washed with water (2 x 15 mL) and then dried with magnesium sulphate. The reaction mixture was reduced *in vacuo* and then purified by column chromatography (5 % ethyl acetate/DCM) to yield a yellow solid (0.511 g). 90 % yield; $\mathbf{M_p}$ = 173 °C; **^{1}H NMR (300 MHz, DMSO-d_6), δ (ppm)** = 11.38 (s, 1 H, NH), 9.50 (t, J = 5.67 Hz, 1 H, NH), 8.22 (t, J = 8.40 Hz, 2 H, aromatic CH), 7.44 (s, 1 H, aromatic CH), 7.40-7.24 (m, 6 H, aromatic CH), 4.55 (d, J = 5.85 Hz, 2 H, CH_2); **^{13}C NMR (75 MHz, DMSO-d_6): δ (ppm)** = 159.5 (CO), 139.0 (q), 134.5 (q), 133.1 (q), 130.9 (q), 130.6 (aromatic CH), 128.8 (q), 128.4 (aromatic CH), 127.5 (aromatic CH), 127.0 (aromatic CH), 121.1 (aromatic CH), 119.9 (aromatic CH), 106.6 (aromatic CH), 42.5 (CH_2); **IR (film):** ν_{max} (cm^{-1}) = 3457 (NH), 3380 (NH), 3085 (CH), 2963 (CH), 1650 (CO); **LRMS (ES^-): m/z** = 294.2 $[M-H]^-$; **HRMS (ES^+): m/z** = 318.0855 $[M+Na]^+$ (found), 318.0849 $[M+Na]^+$ (calculated).

1,3-di(7-(*N*-benzyl-1*H*-indole-2-carboxamide))urea, 152 *(Novel compound)*

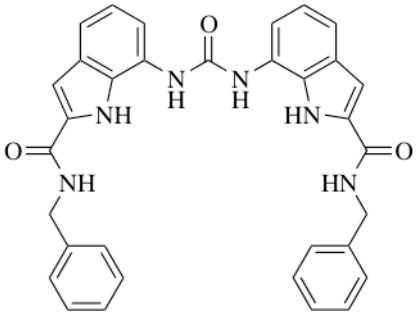

N-benzyl-7-nitro-1*H*-indole-2-carboxamide (0.243 g, 0.824 mmol) was dissolved in ethanol (20 mL). Palladium on carbon 10 % (0.025 g) was added. The reaction vessel was evacuated and placed under a hydrogen atmosphere and stirred at room temperature for 6 hours. The reaction mixture was then filtered through celite and reduced *in vacuo* to yield a white solid. Assumed yield 100 %. The white solid and triphosgene (0.051 g, 0.171 mmol) were dissolved in DCM (50 mL) with saturated sodium bicarbonate solution (50 mL) and stirred at room temperature for 2 hours. The two phase solution was then filtered. The resulting grey solid was sonicated in water (500 mL) for 1 hour. A solid was collected by filtration and washed with water (2 x 25 mL), DCM (10 mL) and diethyl ether (2 x 25 mL) to yield a white solid (0.129 g). 56 % yield; $\mathbf{M_p}$ = 162 °C; **^{1}H NMR (300 MHz, DMSO-d_6), δ (ppm)** = 11.46 (s, 2 H, NH), 9.13 (t, J = 5.85 Hz, 2 H, NH), 8.89 (s, 2 H, NH), 7.52 (d, J = 7.68 Hz, 2 H, aromatic CH), 7.20-7.38 (m, J = 7.68 Hz, 14 H, aromatic CH), 7.02 (t, J = 7.88 Hz, 2 H, aromatic CH), 4.53 (d, J = 5.85 Hz, 4 H, CH_2); **^{13}C NMR (75 MHz, DMSO-d_6), δ (ppm)** = 161.01 (CO), 153.21 (CO), 139.57 (q), 131.35 (q), 128.53 (q), 128.34 (aromatic CH), 128.05 (q), 127.29 (aromatic CH), 126.84 (q), 125.22 (aromatic CH), 120.30 (aromatic CH), 115.85 (aromatic CH), 113.33 (aromatic CH), 103.4 (aromatic CH), 42.2 (CH_2); **IR (film):** ν_{max} (cm^{-1}) = 3290 (NH), 1635 (CO), 1575 (CO); **LRMS (ES^-): m/z** = 555.3 $[M-H]^-$; **HRMS (ES^+): m/z** = 557.2294 $[M+H]^+$ (found), 557.2301 $[M+H]^+$ (calculated).

***N*-(pyridin-2-yl)-7-nitro-1*H*-indole-2-carboxamide** *(Novel compound)*

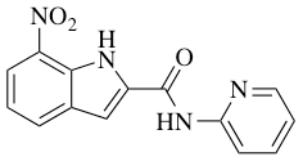

7-nitro-1*H*-indole-2-carboxylic acid (0.200 g, 0.970 mmol) and CDI (0.193 g, 1.19 mmol) were dissolved in dry chloroform. The reaction mixture was heated at reflux for 2 hours under argon. A solution of 2-aminopyridine (0.092 g, 0.967 mmol) in chloroform (5 mL) was added dropwise to the stirring reaction mixture. The reaction mixture was heated at reflux for 22 hours. The reaction mixture was washed with water (2 x 15 mL) and then dried with magnesium sulphate. The reaction mixture was then reduced *in vacuo* and purified by column chromatography (10 % ethyl acetate/DCM) to yield a yellow solid (0.220 g). 80 % yield; **M_p** = 194 °C; **^{1}H NMR (300 MHz, DMSO-d_6), δ (ppm)** = 11.97 (s, 1 H, NH), 11.57 (s, 1 H, NH), 8.43 (dd, J = 2.39, 1.11 Hz, 1 H, aromatic CH), 8.31-8.20 (m, 3 H, aromatic CH), 7.88 (dt, J = 7.32, 1.83 Hz, 1 H, aromatic CH), 7.71 (s, 1 H, aromatic CH), 7.35 (t, J = 8.04 Hz, 1 H, aromatic CH), 7.20 (ddd, J = 7.29, 4.74, 0.92 Hz, 1 H, aromatic CH); **^{13}C NMR (75 MHz, DMSO-d_6), δ (ppm)** = 158.4 (CO); 151.9 (q), 148.0 (aromatic CH), 138.3 (aromatic CH), 134.1 (q), 133.2 (q), 130.8 (q), 130.7 (aromatic CH), 129.3 (q), 121.7 (aromatic CH), 120.0 (aromatic CH), 120.0 (aromatic CH), 114.7 (aromatic CH), 109.2 (aromatic CH); **IR (film):** ν_{max} (cm^{-1}) = 3382 (NH), 3345 (NH), 1671 (CO); **LRMS (ES^-): m/z** = 281.2 $[M-H]^-$; **HRMS (ES^+): m/z** = 283.0831 $[M+H]^+$ (found), 283.0826 $[M+H]^+$ (calculated).

1,3-di(7-((2-pyridin-2-yl)-1H-indole-2-carboxamide))urea, 153 *(Novel compound)*

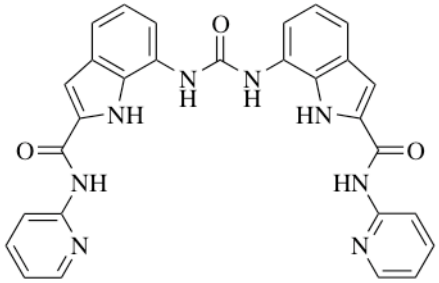

N-(pyridin-2-yl)-7-nitro-1*H*-indole-2-carboxamide (0.179 g, 0.635 mmol) was dissolved in ethanol (50 mL). Palladium on carbon 10 % (0.030 g) was added. The reaction vessel was evacuated and then supplied with hydrogen and stirred at room temperature for 6 hours. The reaction mixture was then filtered through celite and reduced *in vacuo* to yield a white solid. Assumed yield 100 %. The white solid and triphosgene (0.037 g, 0.125 mmol) were dissolved in DCM (50 mL) with saturated sodium bicarbonate solution (50 mL) and stirred at room temperature for 2 hours. The organic phase was separated and reduced *in vacuo*. The resulting brown solid was sonicated in water (500 mL) for 1 hour. The solid was filtered and washed with water (2 x 25 mL) and diethyl ether (2 x 25 mL) to yield a white solid (0.084 g). 55 % yield; $\mathbf{M_p}$ = 219 °C; **^{1}H NMR (300 MHz, DMSO-*d*$_6$), δ (ppm)** = 11.65 (s, 2 H, NH), 10.95 (s, 2 H, NH), 8.97 (s, 2 H, NH), 8.41 (d, J = 3.66 Hz, 2 H, aromatic CH), 8.25 (d, J = 8.40 Hz, 2 H, aromatic CH), 7.86 (m, 2 H, aromatic CH), 7.70 (s, 2 H, aromatic CH), 7.59 (d, J = 7.68 Hz, 2 H, aromatic CH), 7.38 (d, J = 8.04 Hz, 2 H, aromatic CH), 7.17 (dd, J = 6.57, 4.77 Hz, 2 H, aromatic CH), 7.06 (t, J = 7.68 Hz, 2 H, aromatic CH); **^{13}C NMR (75 MHz, DMSO-*d*$_6$), δ (ppm)** = 160.0 (CO), 153.1 (CO), 152.0 (q), 148.0 (aromatic CH), 138.2 (aromatic CH), 130.6 (q), 129.0 (q), 128.6 (q), 125.0 (q), 120.5 (aromatic CH), 119.7 (aromatic CH), 116.6 (aromatic CH), 114.6 (aromatic CH), 114.6 (aromatic CH), 105.8 (aromatic CH); **IR (film):** ν_{max} (cm^{-1}) = 3269 (NH), 1644 (CO), 1539 (CO); **LRMS (ES^-): m/z** = 529.2 $[M-H]^-$; **HRMS (ES^+): m/z** = 531.1879 $[M+H]^+$ (found), 531.1893 $[M+H]^+$ (calculated).

7.6.2 Chapter 3

1-butyl-3-(1*H*-indol-7-yl)urea, 202 *(Literature compound)*[370]

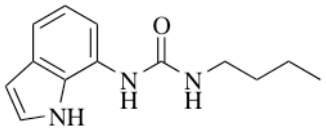

N-(1*H*-indol-7-yl)-1*H*-imidazole-1-carboxamide[371] (0.142 g, 0.628 mmol) was suspended in DCM (100 mL) with 1-butylamine (2.00 mL, 20.2 mmol) and the reaction mixture was heated at reflux for 18 hours. The reaction mixture was reduced *in vacuo* to yield an oil. The oil was triturated with hexane (50 mL) and ether (10 mL) to yield a white solid, which was removed by filtration. The solid was purified by column chromatography (10 % methanol/DCM) to yield a white solid (0.097 g). 67 % yield; **M_p** = 136 °C (literature value 137 °C)[370]; **^{1}H NMR (400 MHz, DMSO-*d*$_6$), δ (ppm)** = 10.69 (br. s, 1 H, NH), 8.35 (s, 1 H, NH), 7.30 (t, J = 2.78 Hz, 1 H, aromatic CH), 7.20 (d, J = 8.08 Hz, 1 H, aromatic CH), 7.07 (d, J = 7.58 Hz, 1 H, aromatic CH), 6.88 (t, J = 7.83 Hz, 1 H, aromatic CH), 6.39 (t, J = 2.27 Hz, 1 H, aromatic CH), 6.21 (t, J = 5.56 Hz, 1 H, NH), 3.14 (m, 2 H, CH_2), 1.51-1.41 (m, 2 H, CH_2), 1.34 (m, 2 H, CH_2), 0.91 (t, J = 7.33 Hz, 3 H, CH_3); **^{13}C NMR (100 MHz, DMSO-*d*$_6$), δ (ppm)** = 155.7 (CO), 129.1 (q), 127.8 (q), 125.0 (q), 124.8 (aromatic CH), 119.1 (aromatic CH), 114.5 (aromatic CH), 111.6 (aromatic CH), 101.5 (aromatic CH), 39.0 (CH_2), 31.9 (CH_2), 19.6 (CH_2), 13.7 (CH_3); **IR (film):** ν_{max} (cm^{-1}) = 3370 (NH), 3270 (NH), 2960 (CH), 2940 (CH), 2870 (CH), 1650 (CO); **LRMS (ES^+): m/z** = 232.3 $[M+H]^+$, 254.2 $[M+Na]^+$, 485.3 $[2M+Na]^+$; **HRMS (ES^+): m/z** = 254.1262 $[M+Na]^+$ (found), 254.1264 $[M+Na]^+$ (calculated).

1-pentyl-3-(1*H*-indol-7-yl)urea, 203 *(Novel compound)*

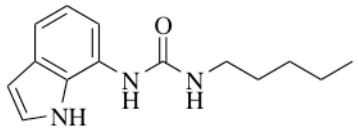

N-(1*H*-indol-7-yl)-1*H*-imidazole-1-carboxamide[371] (0.137 g, 0.606 mmol) was suspended in DCM (200 mL) with 1-pentylamine (0.65 mL, 5.63 mmol) and the reaction mixture was heated at reflux for 66 hours. The reaction mixture was reduced *in vacuo* and then purified by column chromatography (10 % ethyl acetate/DCM) to yield an off-white solid (0.060 g). 40 % yield; **M_p =** 137 °C; **^{1}H NMR (400 MHz, DMSO-*d_6*), δ (ppm)** = 10.66 (br. s., 1 H, NH), 8.27 (s, 1 H, NH), 7.30 (br. s, 1 H, aromatic CH), 7.20 (d, J = 8.08 Hz, 1 H, aromatic CH), 7.04 (d, J = 7.58 Hz, 1 H, aromatic CH), 6.88 (t, J = 7.83 Hz, 1 H, aromatic CH), 6.39 (br. s., 1 H, aromatic CH), 6.19 (t, J = 5.56 Hz, 1 H, NH), 3.17-3.09 (m, 2 H, CH_2), 1.51-1.44 (m, 2 H, CH_2), 1.36-1.25 (m, 4 H, 2 x CH_2), 0.89 (t, J = 6.57 Hz, 3 H, CH_3); **^{13}C NMR (100 MHz, DMSO-*d_6*), δ (ppm)** = 155.6 (CO), 129.2 (q), 127.9 (q), 125.0 (q), 124.8 (aromatic CH), 119.1 (aromatic CH), 114.6 (aromatic CH), 111.8 (aromatic CH), 101.5 (aromatic CH), 39.4 (CH_2), 29.5 (CH_2), 28.6 (CH_2), 21.9 (CH_2), 13.9 (CH_3); **IR (film):** ν_{max} (cm^{-1}) = 3390 (NH), 3310 (NH), 2950 (CH), 2930 (CH), 2870 (CH), 1630 (C=O); **LRMS (ES^+): m/z** = 246.2 $[M+H]^+$, 268.2 $[M+Na]^+$, 513.3 $[2M+Na]^+$; **HRMS (ES^+): m/z** = 268.1416 $[M+Na]^+$ (found), 268.1420 $[M+Na]^+$ (calculated).

1-hexyl-3-(1*H*-indol-7-yl)urea, 204 *(Novel compound)*

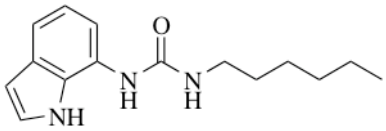

N-(1*H*-indol-7-yl)-1*H*-imidazole-1-carboxamide[371] (0.140 g, 0.619 mmol) was suspended in DCM (100 mL) with 1-hexylamine (2.50 mL, 18.9 mmol) and the reaction mixture was heated at reflux for 16 hours. The reaction mixture was washed with water (3 x 50 mL) and the organic fraction reduced *in vacuo* and then purified by column chromatography (10 % methanol/DCM) to yield a cream coloured solid (0.104 g). 65 % yield; **M_p =** 136 °C; **^{1}H NMR (400 MHz, DMSO-d_6), δ (ppm)** = 10.65 (br. s, 1 H, NH), 8.27 (s, 1 H, NH), 7.29 (t, J = 2.80 Hz, 1 H, aromatic CH), 7.20 (d, J = 8.08 Hz, 1 H, aromatic CH), 7.04 (d, J = 7.58 Hz, 1 H, aromatic CH), 6.92-6.82 (m, 1 H, aromatic CH), 6.39 (dd, J = 3.03, 2.02 Hz, 1 H, aromatic CH), 6.18 (t, J = 5.60 Hz, 1 H, NH), 3.18-3.06 (m, 2 H, CH_2) 1.54-1.40 (m, 2 H, CH_2) 1.37-1.23 (m, 6 H, 3 x CH_2), 0.87 (t, J = 7.60 Hz, 2 H, CH_3); **^{13}C NMR (100 MHz, DMSO-d_6), δ (ppm)** = 155.7 (CO), 129.2 (q), 127.9 (q), 125.0 (q), 124.8 (aromatic CH), 119.1 (aromatic CH), 114.6 (aromatic CH), 111.8 (aromatic CH), 101.5 (aromatic CH), 39.4 (CH_2), 31.0 (CH_2), 29.7 (CH_2), 26.1 (CH_2), 22.1 (CH_2), 13.9 (CH_3); **IR (film):** ν_{max} (cm^{-1}) = 3410 (NH), 3350 (NH), 3290 (NH), 2950 (CH), 2930 (CH), 2860 (CH), 1630 (CO); **LRMS (ES^+): m/z** = 260.2 $[M+H]^+$, 282.2 $[M+Na]^+$, 541.4 $[2M+Na]^+$; **HRMS (ES^+): m/z** = 282.1574 $[M+Na]^+$ (found), 282.1577 $[M+Na]^+$ (calculated).

1-heptyl-3-(1*H*-indol-7-yl)urea, 205 *(Novel compound)*

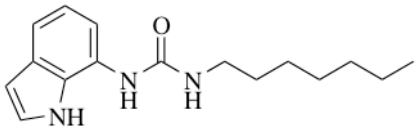

N-(1*H*-indol-7-yl)-1*H*-imidazole-1-carboxamide[371] (0.107 g, 0.473 mmol) was suspended in DCM (40 mL) with 1-heptylamine (0.50 mL, 3.38 mmol) and the reaction mixture was heated at reflux for 66 hours. The reaction mixture was reduced *in vacuo* and then purified by column chromatography (10 % methanol/DCM) to yield a white solid (0.670 g). 52 % yield; **M_p =** 128 °C; **^{1}H NMR (400 MHz, DMSO-*d_6*), δ (ppm)** = 10.70 (br. s, 1 H, NH), 8.33 (s, 1 H, NH), 7.29 (br. s, 1 H, aromatic CH), 7.19 (d, J = 7.58 Hz, 1 H, aromatic CH), 7.06 (d, J = 7.58 Hz, 1 H, aromatic CH), 6.88 (t, J = 7.58 Hz, 1 H, aromatic CH), 6.39 (br. s, 1 H, aromatic CH), 6.23 (t, J = 5.05 Hz, 1 H, NH), 3.13 (m, 2 H, CH_2), 1.47 (m, 2 H, CH_2), 1.35- 1.20 (m, 8 H, 4 x CH_2), 0.87 (t, J = 6.06 Hz, 3 H, CH_3); **^{13}C NMR (100 MHz, DMSO-*d_6*), δ (ppm)** = 155.7 (CO), 129.1 (q), 127.8 (q), 125.0 (q), 124.8 (aromatic CH), 119.1 (aromatic CH), 114.5 (aromatic CH), 111.7 (aromatic CH), 101.4 (aromatic CH), 39.4 (CH_2), 31.3 (CH_2), 29.8 (CH_2), 28.5 (CH_2), 26.4 (CH_2), 22.1 (CH_2), 13.9 (CH_3); **IR (film):** ν_{max} (cm^{-1}) = 3380 (NH), 3310 (NH), 2950 (CH), 2930 (CH), 2850 (CH), 1630 (CO); **LRMS (ES^+): m/z** = 274.2 $[M+H]^+$, 296.2 $[M+Na]^+$; **HRMS (ES^+): m/z** = 296.1736 $[M+Na]^+$ (found), 296.1733 $[M+Na]^+$ (calculated).

1-octyl-3-(1*H*-indol-7-yl)urea, 206 *(Literature compound)*[370]

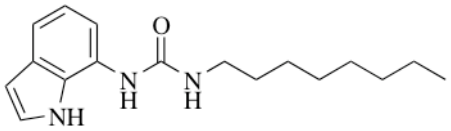

N-(1*H*-indol-7-yl)-1*H*-imidazole-1-carboxamide[374] (0.159 g, 0.703 mmol) was suspended in DCM (200 mL) with 1-octylamine (0.50 mL, 3.03 mmol) and the reaction mixture was heated at reflux for 17 hours. The reaction mixture was washed with water (150 mL) and then purified by column chromatography (10 % methanol/DCM) to yield a white solid (0.079 g). 39 % yield; **M_p =** 134 °C (literature value 137 °C)[370]; **^{1}H NMR (400 MHz, DMSO-*d*$_6$), δ (ppm)** = 10.65 (br. s, 1 H, NH), 8.27 (s, 1 H, NH), 7.29 (t, J = 2.53 Hz, 1 H, aromatic CH), 7.20 (d, J = 7.58 Hz, 1 H, aromatic CH), 7.03 (d, J = 7.58 Hz, 1 H, aromatic CH), 6.94-6.82 (m, 1 H, aromatic CH), 6.44-6.33 (m, 1 H, aromatic CH), 6.18 (t, J = 5.31 Hz, 1 H, NH), 3.13 (q, J = 6.23 Hz, 2 H, CH_2), 1.53-1.41 (m, 2 H, CH_2), 1.36-1.20 (m, 10 H, 5 x CH_2), 0.86 (t, J = 5.60 Hz, 3 H, CH_3); **^{13}C NMR (100 MHz, DMSO-*d*$_6$), δ (ppm)** = 155.6 (CO), 129.2 (q), 127.9 (q), 125.0 (q), 124.8 (aromatic CH), 119.1 (aromatic CH), 114.6 (aromatic CH), 111.8 (aromatic CH), 101.5 (aromatic CH), 39.4 (CH_2), 31.2 (CH_2), 29.8 (CH_2), 28.8 (CH_2), 28.7 (CH_2), 26.4 (CH_2), 22.1 (CH_2), 13.9 (CH_3); **IR (film):** ν_{max} (cm^{-1}) = 3390 (NH), 3310 (NH), 2950 (CH), 2920 (CH), 2850 (CH), 1630 (CO); **LRMS (ES^+): m/z** = 288.3 $[M+H]^+$, 310.3 $[M+Na]^+$, 597.5 $[2M+Na]^+$; **HRMS (ES^+): m/z** = 310.1892 $[M+Na]^+$ (found), 310.1890 $[M+Na]^+$ (calculated).

1-nonyl-3-(1*H*-indol-7-yl)urea, 207 *(Novel compound)*

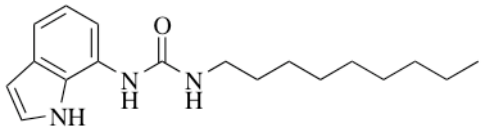

N-(1*H*-indol-7-yl)-1*H*-imidazole-1-carboxamide[371] (0.092 g, 0.407 mmol) was suspended in DCM (100 mL) with 1-nonylamine (0.50 mL, 2.73 mmol) and the reaction mixture was heated at reflux for 5 hours. The reaction mixture was reduced *in vacuo* and then purified by column chromatography (10 % ethyl acetate/DCM) to yield a white solid (0.081 g). 66 % yield; **M_p =** 130 °C; **^{1}H NMR (400 MHz, DMSO-*d_6*), δ (ppm)** = 10.66 (br. s, 1 H, NH), 8.27 (s, 1 H, NH), 7.29 (t, J = 2.53 Hz, 1 H, aromatic CH), 7.20 (d, J = 8.08 Hz, 1 H, aromatic CH), 7.04 (d, J = 7.58 Hz, 1 H, aromatic CH), 6.88 (t, J = 7.58 Hz, 1 H, aromatic CH), 6.39 (br. s., 1 H, aromatic CH), 6.19 (t, J = 5.56 Hz, 1 H, NH), 3.17-3.03 (m, 2 H, CH_2), 1.52-1.42 (m, 2 H, CH_2), 1.27 (s, 12 H, 6 x CH_2), 0.86 (t, J = 6.32 Hz, 3 H, CH_3); **^{13}C NMR (100 MHz, DMSO-*d_6*), δ (ppm)** = 155.6 (CO), 129.2 (q), 127.9 (q), 125.0 (q), 124.8 (aromatic CH), 119.1 (aromatic CH), 114.5 (aromatic CH), 111.7 (aromatic CH), 101.4 (aromatic CH), 39.4 (CH_2), 31.3 (CH_2), 29.8 (CH_2), 29.0 (CH_2), 28.8 (CH_2), 28.7 (CH_2), 26.4 (CH_2), 22.1 (CH_2), 13.9 (CH_3); **IR (film):** ν_{max} (cm^{-1}) = 3390 (NH), 3300 (NH), 2950 (CH), 2920 (CH), 2850 (CH), 1630 (CO); **LRMS (ES^+): m/z** = 302.3 $[M+H]^+$, 324.3 $[M+Na]^+$, 625.5 $[2M+Na]^+$; **HRMS (ES^+): m/z** = 324.2045 $[M+Na]^+$ (found), 324.2046 $[M+Na]^+$ (calculated).

1-decyl-3-(1*H*-indol-7-yl)urea, 208 *(Novel compound)*

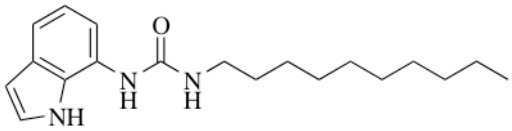

N-(1*H*-indol-7-yl)-1*H*-imidazole-1-carboxamide[371] (0.113 g, 0.499 mmol) was suspended in DCM (50 mL) with 1-decylamine (0.50 mL, 2.50 mmol) and the reaction mixture was heated at reflux for 18 hours. The reaction mixture was reduced *in vacuo* and sonicated in water for 30 minutes. The resulting solid was removed by filtration, sonicated in DCM for 15 minutes and then purified by column chromatography (10 % methanol/DCM) to yield a cream coloured solid (0.099 g). 79 % yield; **M_p =** 126 °C; **^{1}H NMR (400 MHz, DMSO-*d_6*), δ (ppm)** = 10.67 (br. s, 1 H, NH), 8.31 (s, 1 H, NH), 7.29 (t, J = 2.53 Hz, 1 H, aromatic CH), 7.19 (d, J = 7.58 Hz, 1 H, aromatic CH), 7.06 (s, 1 H, aromatic CH), 6.93-6.83 (m, 1 H, aromatic CH), 6.42-6.35 (m, 1 H, aromatic CH), 6.20 (t, J = 5.56 Hz, 1 H, NH), 3.18-3.07 (m, 2 H, CH_2), 1.52-1.40 (m, 2 H, CH_2), 1.34-1.17 (m, 14 H, 7 x CH_2), 0.86 (t, J = 6.82 Hz, 3 H, CH_3); **^{13}C NMR (100 MHz, DMSO-*d_6*), δ (ppm)** = 155.6 (CO), 129.1 (q), 127.8 (q), 125.0 (q), 124.8 (aromatic CH), 119.1 (aromatic CH), 114.5 (aromatic CH), 111.7 (aromatic CH), 101.4 (aromatic CH), 39.4 (CH_2), 31.3 (CH_2), 29.8 (CH_2), 29.1 (CH_2), 29.0 (CH_2), 28.8 (CH_2), 28.7 (CH_2), 26.4 (CH_2), 22.1 (CH_2), 13.9 (CH_3); **IR (film):** ν_{max} (cm^{-1}) = 3380 (NH), 3310 (NH), 2950 (CH), 2920 (CH), 2850 (CH), 1630 (CO); **LRMS (ES^+): m/z** = 316.3 $[M+H]^+$, 338.3 $[M+Na]^+$, 653.6 $[2M+Na]^+$; **HRMS (ES^+): m/z** = 338.2203 $[M+Na]^+$ (found), 338.2203 $[M+Na]^+$ (calculated).

1-(*iso*-pentyl)-3-(1*H*-indol-7-yl)urea, 215 *(Novel compound)*

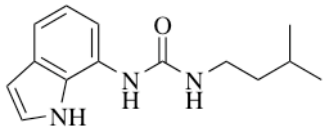

N-(1*H*-indol-7-yl)-1*H*-imidazole-1-carboxamide[371] (0.229 g, 1.01 mmol) was suspended in DCM (150 mL) under nitrogen. *Iso*-pentlyamine (2 mL, 17.23 mmol) was added to the reaction mixture, which was then heated at reflux for 18 hours. On cooling, the crude mixture was purified by column chromatography (15 % ethyl acetate/DCM) to yield compound a white solid (163 mg). 66 % yield; **M_p =** 159-160 °C; **^{1}H NMR (300 MHz, DMSO-*d_6*), δ (ppm)** = 10.66 (s, 1 H, NH), 8.27 (s, 1 H, NH), 7.30 (t, J = 2.94 Hz, 1 H, aromatic CH), 7.20 (d, J = 7.68 Hz, 1 H, aromatic CH), 7.04 (d, J = 6.96 Hz, 1 H, aromatic CH), 6.88 (t, J = 7.68 Hz, 1 H, aromatic CH), 6.40-6.38 (m, 1 H, aromatic CH), 6.16 (t, J = 5.49 Hz, 1 H, NH), 3.19-3.12 (m, 2 H, CH_2), 1.68-1.57 (m, 1 H, CH), 1.40-1.33 (m, 2 H, CH_2), 0.91 (d, J = 6.60 Hz, 6 H, CH_3); **^{13}C NMR (75 MHz, DMSO-*d_6*), δ (ppm)** = 155.7 (CO), 129.2 (q), 127.9 (q), 125.0 (q), 124.9 (aromatic CH), 119.1 (aromatic CH), 114.6 (aromatic CH), 111.8 (aromatic CH), 101.5 (aromatic CH), 38.8 (CH_2), 37.6 (CH_2), 25.2 (CH), 22.5 (CH_3); **IR (film):** ν_{max} (cm^{-1}) = 3390 (NH), 3280 (NH), 1650 (CO); **LRMS (ES^-): m/z** = 244.2 $[M-H]^-$; **HRMS (ES^+): m/z** = 268.1423 $[M+Na]^+$ (found), 268.1423 $[M+Na]^+$ (calculated).

1-hexyl-3-(1*H*-indol-7-yl)thiourea, 223 *(Novel compound)*

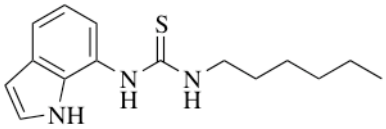

7-nitro-1*H*-indole (0.205 g, 1.26 mmol) was dissolved in methanol (30 mL) with palladium on carbon (~ 0.05 g) and the reaction vessel flooded with hydrogen. The mixture was stirred for three hours at room temperature. The palladium catalyst was removed by filtration and the filtrate reduced *in vacuo*. The crude product was dissolved in DCM (30 mL) with thiophosgene (0.1 mL, 1.30 mmol). Saturated aqueous sodium bicarbonate solution (30 mL) was added and the reaction mixture stirred for fifteen hours. The organic phase was separated and hexylamine (0.3 mL, 2.27 mmol) added. The reaction mixture was stirred at reflux for fifteen hours. The crude reaction mixture was washed with water (200 mL) and the organic phase reduced *in vacuo* to yield an orange oil. The crude mixture was purified by column chromatography (10 % methanol/DCM), the product fractions were combined and reduced *in vacuo* and the resulting oil triturated in hexane (50 mL). The precipitate was removed by filtration and dried under vacuum to yield a cream coloured solid (0.221 g). 64 % yield. **M_p** = 97-99 °C; **^{1}H NMR (300 MHz, DMSO-*d*$_6$), δ (ppm)** = 10.89 (s, 1 H, NH), 9.22 (s, 1 H, NH), 7.51-7.40 (m, 2 H, aromatic CH), 7.29 (t, J = 2.55 Hz, 1 H, aromatic CH), 7.02-6.93 (m, 2 H, aromatic CH, NH), 6.46 (dd, J = 1.83, 2.91 Hz, 1 H, aromatic CH), 3.55-3.40 (m, 2 H, CH_2), 1.52 (m, 2 H, CH_2), 1.26 (br. s, 6 H, CH_2), 0.87 (t, J = 6.60 Hz, 3 H, CH_3); **^{13}C NMR (100 MHz, DMSO-*d*$_6$), δ (ppm)** = 180.7 (CS), 131.2 (q), 129.5 (q), 125.6 (aromatic CH), 122.9 (q), 119.0 (aromatic CH), 118.0 (aromatic CH), 118.0 (aromatic CH), 101.6 (aromatic CH), 44.3 (CH_2), 31.0 (CH_2), 28.5 (CH_2), 26.0 (CH_2), 22.0 (CH_2), 13.9 (CH_3); **IR (film):** ν_{max} (cm^{-1}) = 3380 (NH), 3330 (NH), 3190 (NH), 3020 (CH), 2920 (CH), 2860 (CH); **LRMS (ES^-): m/z** = 274.2 $[M-H]^-$; **HRMS (ES^+): m/z** = 298.1356 $[M+Na]^+$ (found), 298.1354 $[M+Na]^+$ (calculated).

1-(2-butyl-5-(trifluoromethyl)-1*H*-indol-7-yl)-3-hexylurea, 224 *(Novel compound)*

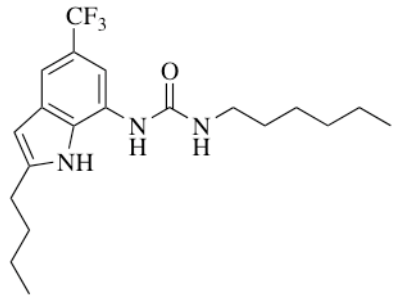

2-butyl-7-nitro-5(trifluoromethyl)-1*H*-indole[385, 386] (0.106 g, 0.37 mmol) was dissolved in ethanol (25 mL) with palladium on carbon (~ 0.05 g) and the reaction vessel flooded with hydrogen. The reaction mixture was heated at reflux for 5 hours. The palladium catalyst was removed by filtration and the filtrate reduced *in vacuo* to yield a white solid. The solid was dissolved in DCM (50 mL) with CDI (0.234 g, 1.44 mmol). The reaction mixture was stirred under nitrogen at room temperature for five hours. Hexylamine (2.0 mL, 15.14 mmol) was added and the reaction mixture was stirred at reflux for eighteen hours. The reaction mixture was reduced *in vacuo* to yield a brown oil which was purified by column chromatography (2 % methanol/hexane) to yield a white solid (0.085 g). 60 % yield. **M_p** = 102-104 °C; **^{1}H NMR (300 MHz, DMSO-*d*$_6$), δ (ppm)** = 10.89 (s, 1 H, NH), 8.38 (s, 1 H, NH), 7.53 (s, 1 H, aromatic CH), 7.43 (s, 1 H, aromatic CH), 6.28 (br. s, 2 H, aromatic CH, NH), 3.13 (dt, J = 7.08, 6.04 Hz, 2 H, CH_2), 2.76 (app. t, J = 7.56 Hz, 2 H, CH_2), 1.75-1.63 (m, 2 H, CH_2), 1.53-1.42 (m, 2 H, CH_2), 1.42-1.22 (m, 8 H, CH_2), 0.92 (t, J = 7.08 Hz, 3 H, CH_3), 0.88 (t, J = 7.04 Hz, 3 H, CH_3); **^{13}C NMR (100 MHz, DMSO-*d*$_6$), δ (ppm)** = 155.3 (CO), 141.8 (q), 128.9 (q), 128.6 (q), 125.6 (CF_3, [q, J = 269.8 Hz]), 125.1 (q), 119.9 (q, [q, J = 30.2Hz]), 110.6 (aromatic CH), 106.6 (aromatic CH), 100.0 (aromatic CH), 39.4 (CH_2), 31.1 (CH_2), 30.8 (CH_2), 29.7 (CH_2), 27.2 (CH_2), 26.1 (CH_2), 22.1 (CH_2), 21.8 (CH_2), 14.0 (CH_3), 13.7 (CH_3); **^{19}F NMR (282 MHz, DMSO-*d*$_6$), δ (ppm)** = -58.67 (CF_3); **IR (film):** ν_{max} (cm^{-1}) = 3390 (NH), 3350 (NH), 2960 (CH), 2930 (CH), 2870 (CH), 1630 (CO), 1110 (CF); **LRMS (ES^-): m/z** = 382.3 $[M-H]^-$; **HRMS (ES^+): m/z** = 406.2072 $[M+Na]^+$ (found), 406.2082 $[M+Na]^+$ (calculated).

1-(2-butyl-5-(trifluoromethyl)-1*H*-indol-7-yl)3-hexylthiourea, 225 *(Novel compound)*

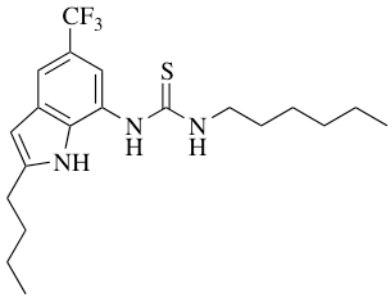

2-butyl-7-nitro-5-trifluoromethyl-1*H*-indole[385, 386] (0.100 g, 0.35 mmol) was dissolved in methanol (20 mL) with palladium on carbon (~ 0.05 g) and the reaction vessel flooded with hydrogen. The reaction mixture was heated at reflux for 3 hours. The palladium catalyst was removed by filtration and the filtrate reduced *in vacuo* to yield a white solid. The solid was dissolved in DCM (50 mL) with thiophosgene (0.3 mL, 3.91 mmol). Saturated aqueous sodium bicarbonate solution (100 mL) was added to the reaction mixture which was then stirred at room temperature for five hours. The organic portion was separated and reduced *in vacuo* to yield an orange oil. This oil was dissolved in DCM (50 mL) with hexylamine (2.0 mL, 15.14 mmol) and stirred at reflux for eighteen hours. The reaction mixture was reduced *in vacuo* to yield a yellow oil which was purified by column chromatography (DCM). The product fractions were combined and reduced *in vacuo* to yield a colourless oil. The oil was triturated in water (50 mL) to yield a cream solid (0.065 g). 47 % yield. **M_p** = 78-80 °C; **^{1}H NMR (300 MHz, DMSO-*d*$_6$), δ (ppm)** = 11.19 (s, 1 H, NH), 9.25 (s, 1 H, NH), 7.72 (br. s, 1 H, NH), 7.65 (s, 1 H, aromatic CH), 7.20 (s, 1 H, aromatic CH), 6.33 (s, 1 H, aromatic CH), 3.45 (br. m, 2 H, CH_2), 2.74 (t, J = 7.53 Hz, 2 H, CH_2), 1.67 (m, 2 H, CH_2), 1.53 (br. s, 2 H, CH_2), 1.40-1.20 (m, 8 H, CH_2), 0.91 (t, J = 7.14 Hz, 3 H, CH_3), 0.87 (t, J = 7.98 Hz, 3 H, CH_3); **^{13}C NMR (100 MHz, DMSO-*d*$_6$), δ (ppm)** = 180.8 (CS), 143.2 (q), 132.7 (q), 129.6 (q), 125.4 (CF_3, [q, J = 269.2 Hz]), 123.0 (q), 119.6 (q, [q, J = 30.8 Hz]), 114.1 (aromatic CH), 113.5 (aromatic CH), 99.9 (aromatic CH), 44.4 (CH_2), 31.1 (CH_2), 30.9 (CH_2), 28.4 (CH_2), 27.1 (CH_2), 26.1 (CH_2), 22.1 (CH_2), 21.8 (CH_2), 13.9 (CH_3), 13.7 (CH_3); **^{19}F NMR (282 MHz, DMSO-*d*$_6$), δ (ppm)** = -58.45 (CF_3); **IR (film):** ν_{max} (cm^{-1}) = 3390

(NH), 3290 (NH), 2850 (NH), 2950 (CH), 2930 (CH), 2850 (CH), 1100 (CF); **LRMS (ES^-): m/z** = 398.2 $[M-H]^-$; **HRMS (ES^+): m/z** = 400.2019 $[M+H]^+$ (found), 400.2034 $[M+H]^+$ (calculated).

1-(1*H*-indol-7-yl)-3-phenylurea, 226 *(Literature compound)*[305]

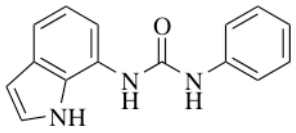

N-(1*H*-indol-7-yl)-1*H*-imidazole-1-carboxamide[371] (0.231 g, 1.02 mmol) was dissolved in 1:1 DCM/chloroform (100 mL). Aniline (1 mL, 10.97 mmol) was added and the reaction mixture was heated at reflux for 24 hours. The reaction mixture was reduced *in vacuo*, suspended in hexane (40 mL) and filtered to yield a white solid (0.085 g). 33 % yield. **M_p** = 218-220 °C; **^{1}H NMR (400 MHz, DMSO-*d*$_6$), δ (ppm)** = 10.67 (s, 1 H, NH), 8.75 (s, 1 H, NH), 8.47 (s, 1 H, NH), 7.50 (d, J = 7.56 Hz, 2 H, aromatic CH), 7.35-7.30 (m, 2 H, aromatic CH), 7.27 (d, J = 8.08 Hz, 2 H, aromatic CH), 7.09 (d, J = 7.60 Hz, 1 H, aromatic CH), 6.99-6.91 (m, 2 H, aromatic CH), 6.43 (dd, J = 2.88, 2.08 Hz, 1 H, aromatic CH); **^{13}C NMR (75 MHz, DMSO-*d*$_6$), δ (ppm)** = 153.1 (CO), 139.9 (q), 129.2 (q), 129.0 (q), 128.7 (aromatic CH), 125.2 (aromatic CH), 123.7 (q), 121.7 (aromatic CH), 119.0 (aromatic CH), 118.3 (aromatic CH), 115.8 (aromatic CH), 113.7 (aromatic CH), 101.5 (aromatic CH); **IR (film):** ν_{max} (cm^{-1}) = 3390 (NH), 3280 (NH), 1640 (CO); **LRMS (ES^-): m/z** = 250.1 $[M-H]^-$; **HRMS (ES^+): m/z** = 274.0950 $[M+Na]^+$ (found), 274.0956 $[M+Na]^+$ (calculated).

1-(1*H*-indol-7-yl)-3-phenylthiourea, 227 *(Novel compound)*

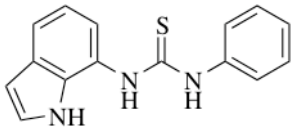

7-nitro-1*H*-indole (0.457 g, 2.82 mmol) was dissolved in methanol (25 mL) with palladium on carbon (~ 0.05 g) and the reaction vessel flooded with hydrogen. The mixture was stirred for 90 minutes at room temperature. The palladium catalyst was removed by filtration and the filtrate reduced *in vacuo* to yield a white solid (0.412 g). A portion of the solid (0.201 g, 1.52 mmol) was dissolved in pyridine (5 mL) with phenylisothiocyanate (0.4 mL, 3.34 mmol) and stirred under nitrogen for 18 hours at room temperature. Pyridine was removed *in vacuo* to yield a cream coloured solid. The crude product was purified by column chromatography (2 % methanol/DCM). Product fractions were combined and reduced *in vacuo* to yield a white solid (0.088 g). 20 % yield. **M_p** = 230-232 °C; **^{1}H NMR (400 MHz, DMSO-d_6), δ (ppm)** = 10.97 (s, 1 H, NH), 9.72 (s, 1 H, NH), 9.54 (s, 1 H, NH), 7.56 (d, J = 8.01 Hz, 2 H, aromatic CH), 7.44 (d, J = 7.32 Hz, 1 H, aromatic CH), 7.38-7.27 (m, 3 H, aromatic CH), 7.12 (t, J = 7.32 Hz, 1 H, aromatic CH), 7.08- 6.93 (m, 2 H, aromatic CH), 6.47 (s, 1 H, aromatic CH); **^{13}C NMR (75 MHz, DMSO-d_6), δ (ppm)** = 180.3 (CS), 139.7 (q), 131.6 (q), 129.4 (q), 128.3 (aromatic CH), 125.5 (aromatic CH), 124.3 (aromatic CH), 123.8 (aromatic CH), 123.6 (q), 118.9 (aromatic CH), 118.8 (aromatic CH), 118.2 (aromatic CH), 101.5 (aromatic CH); **IR (film):** ν_{max} (cm^{-1}) = 3320 (NH), 3120 (NH), 2970 (NH); **LRMS (ES^-): m/z** = 266.1 $[M-H]^-$; **HRMS (ES^+): m/z** = 290.0727 $[M+Na]^+$ (found), 290.0728 $[M+Na]^+$ (calculated).

1-(1*H*-indol-7-yl)-3-(4-(trifluoromethyl)phenyl)urea, 228 *(Novel compound)*

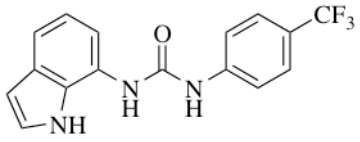

7-nitro-1*H*-indole (0.199 g, 1.23 mmol) was dissolved in methanol (20 mL) with palladium on carbon (~ 0.05 g) and the reaction vessel flooded with hydrogen. The mixture was stirred for two hours at room temperature. The palladium catalyst was removed by filtration and the filtrate reduced *in vacuo* to yield a white solid. The solid was dissolved in DCM (50 mL) with 4-(trifluoromethyl)phenyl isocyanate (0.3 mL, 2.10 mmol) and stirred under nitrogen for 90 minutes. The reaction mixture was filtered and the resulting solid washed with DCM (200 mL) to yield a grey solid (0.201 g,). 51 % yield. **M_p =** 225-226 °C; **^{1}H NMR (300 MHz, DMSO-*d*$_6$), δ (ppm)** = 10.73 (s, 1 H, NH), 9.23 (s, 1 H, NH), 8.59 (s, 1 H, NH), 7.71 (d, J = 8.67 Hz, 2 H, aromatic CH), 7.64 (d, J = 8.67 Hz, 2 H, aromatic CH), 7.36-7.31 (m, 2 H, aromatic CH), 7.10 (d, J = 7.17 Hz, 1 H, aromatic CH), 6.95 (t, J = 7.89 Hz, 1 H, aromatic CH), 6.45 (dd, J = 2.64, 1.89 Hz, 1 H, aromatic CH); **^{13}C NMR (75 MHz, DMSO-*d*$_6$), δ (ppm)** = 152.8 (CO), 143.6 (q), 129.3 (q), 129.2 (q), 126.0 (aromatic CH), 125.2 (aromatic CH), 124.6 (CF_3, [q, J = 269.1 Hz]), 123.2 (q), 121.6 (q, [q, J = 32.0 Hz]), 118.9 (aromatic CH), 117.9 (aromatic CH), 116.2 (aromatic CH), 114.4 (aromatic CH), 101.5 (aromatic CH); **^{19}F NMR (282 MHz, DMSO-*d*$_6$), δ (ppm)** = -60.08 (CF_3); **IR (film):** ν_{max} (cm^{-1}) = 3390 (NH), 3310 (NH), 3290 (NH), 1640 (CO), 1100 (CF); **LRMS (ES^-): m/z** = 318.1 $[M-H]^-$; **HRMS (ES^+): m/z** = 342.0823 $[M+Na]^+$ (found), 342.0830 $[M+Na]^+$ (calculated).

1-(1*H*-indol-7-yl)-3-(4-(trifluoromethyl)phenyl)thiourea, 229 *(Novel compound)*

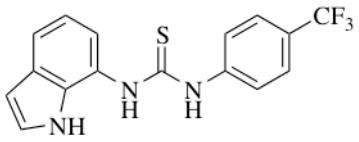

7-nitro-1*H*-indole (0.457 g, 2.82 mmol) was dissolved in methanol (25 mL) with palladium on carbon (~ 0.05 g) and the reaction vessel flooded with hydrogen. The mixture was stirred for 90 minutes at room temperature. The palladium catalyst was removed by filtration and the filtrate reduced *in vacuo* to yield a white solid (0.412 g). A portion of the solid (0.211 g, 1.60 mmol) was dissolved in pyridine (5 mL) with 4-(trifluoromethyl)phenylisothiocyanate (0.307 g, 1.51 mmol) and stirred under nitrogen for eighteen hours at room temperature. Pyridine was removed *in vacuo* to yield a cream coloured solid. The crude product was purified by column chromatography (2 % methanol/DCM). Product fractions were combined and reduced *in vacuo* to yield a white solid (0.109 g). 20 % yield. **M_p** = 158-160 °C; **^{1}H NMR (400 MHz, DMSO-*d_6*), δ (ppm)** = 10.99 (s, 1 H, NH), 10.05 (s, 1 H, NH), 9.80 (s, 1 H, NH), 7.84 (d, J = 8.60 Hz, 2 H, aromatic CH), 7.67 (d, J = 7.08 Hz, 2 H, aromatic CH), 7.46 (d, J = 7.60 Hz, 1 H, aromatic CH), 7.32 (s, 1 H, aromatic CH), 7.08-6.95 (m, 2 H, aromatic CH), 6.47 (br. s, 1 H, aromatic CH); **^{13}C NMR (100 MHz, DMSO-*d_6*), δ (ppm)** = 180.4 (CS), 143.7 (q), 131.6 (q) 129.4 (q), 125.5 (aromatic CH), 125.4 (aromatic CH), 125.4 (aromatic CH), 124.4 (CF_3, [q, J = 269.1 Hz]), 123.9 (q, [q, J = 32.0 Hz]), 123.4 (q), 123.1 (aromatic CH), 118.8 (aromatic CH), 118.5 (aromatic CH), 101.6 (aromatic CH); **^{19}F NMR (282 MHz, DMSO-*d_6*), δ (ppm)** = -60.42 (CF_3); **IR (film):** ν_{max} (cm^{-1}) = 3390 (NH), 3140 (NH), 2950 (NH), 1100 (CF); **LRMS (ES^-): m/z** = 334.1 $[M-H]^-$; **HRMS (ES^+): m/z** = 358.0591 $[M+Na]^+$ (found), 358.0602 $[M+Na]^+$ (calculated).

1-hexyl-3-(4-(trifluoromethyl)phenyl)urea, 232 *(Novel compound)*

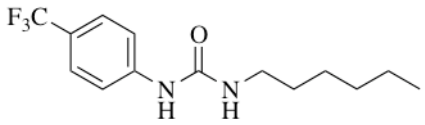

Hexylamine (0.47 mL, 3.56 mmol) was dissolved in dry DCM (10 mL) with 4-(trifluoromethyl)phenyl isocyanate (0.50 mL, 3.50 mmol) under nitrogen. The reaction mixture was allowed to stir for 1 hour whereupon a white precipitate formed. The precipitate was removed by filtration and washed with DCM (2 x 25 mL) to yield a white solid (0.693 g). 69 % yield. **M_p** = 103 °C; **^{1}H NMR (400 MHz, DMSO-*d*$_6$), δ (ppm)** = 8.81 (s, 1 H, NH), 7.58 (d, J = 9.12 Hz, 2 H, aromatic CH), 7.54 (d, J = 9.12 Hz, 2 H, aromatic CH), 6.25 (t, J = 5.56 Hz, 1 H, NH), 3.08 (dt, J = 7.04, 5.56 Hz, 2 H, CH_2), 1.50-1.35 (m, 2 H, CH_2), 1.35-1.20 (m, 6 H, CH_2), 0.87 (t, J = 7.08 Hz, 3 H, CH_3); **^{13}C NMR (100 MHz, DMSO-*d*$_6$), δ (ppm)** = 154.8 (CO), 144.3 (q), 125.9 (aromatic CH), 124.6 (CF_3, [q, J = 269.1 Hz]), 120.8 (q, [q, J = 31.8 Hz]), 117.1 (aromatic CH), 39.0 (CH_2), 31.0 (CH_2), 29.6 (CH_2), 26.0 (CH_2), 22.1 (CH_2), 13.9 (CH_3); **^{19}F NMR (282 MHz, DMSO-*d*$_6$), δ (ppm)** = -60.05 (CF_3); **IR (film):** ν_{max} (cm^{-1}) = 3340 (NH), 3330 (NH), 1640 (CO), 1110 (CF); **LRMS (ES^+): m/z** = 289.1 $[M+H]^+$, 311.1 $[M+Na]^+$, 327.1 $[M+K]^+$, 599.3 $[2M+Na]^+$; **HRMS (ES^+): m/z** = 289.1523 $[M+H]^+$ (found), 289.1528 $[M+H]^+$ (calculated).

1-hexyl-3-(4-(trifluoromethyl)phenyl)thiourea, 233 *(Novel compound)*

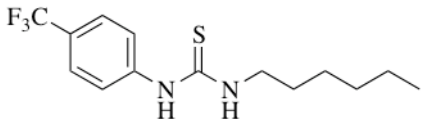

Hexylamine (0.33 mL, 2.50 mmol) was dissolved in dry DCM (10 mL) with 4-(trifluoromethyl)phenylisothiocyanate (0.509 g, 2.51 mmol) under nitrogen. The reaction mixture was allowed to stir for 18 hours. The reaction mixture was reduced *in vacuo* to yield an oily solid. The solid was washed with cold DCM (2 x 10 mL) to yield a white solid (0.355 g). 47 % yield. **M_p** = 94-95 °C; **^{1}H NMR (400 MHz, DMSO-*d_6*), δ (ppm)** = 9.77 (s, 1 H, NH), 8.03 (s, 1 H, NH), 7.73 (d, J = 8.60 Hz, 2 H, aromatic CH), 7.63 (d, J = 8.60 Hz, 2 H, aromatic CH), 3.55-3.40 (m, 2 H, CH_2), 1.65-1.50 (m, 2 H, CH_2), 1.40-1.25 (m, 6 H, CH_2), 0.87 (t, J = 6.56 Hz, 3 H, CH_3); **^{13}C NMR (100 MHz, DMSO-*d_6*), δ (ppm)** = 180.2 (CS), 143.5 (q), 125.5 (aromatic CH), 124.7 (CF_3, [q, J = 269.1 Hz]), 123.2 (q, [q, J = 29.1 Hz]), 121.6 (aromatic CH), 43.8 (CH_2), 31.0 (CH_2), 28.2 (CH_2), 26.1 (CH_2), 22.0 (CH_2), 13.8 (CH_3); **^{19}F NMR (282 MHz, DMSO-*d_6*), δ (ppm)** = -60.49 (CF_3); **IR (film):** ν_{max} (cm^{-1}) = 3220 (NH), 1560 (CO), 1110 (CF); **LRMS (ES^+): m/z** = 305.2 $[M+H]^+$, 327.1 $[M+Na]^+$, 343.2 $[M+K]^+$, 631.0 $[2M+Na]^+$; **HRMS (ES^+): m/z** = 305.1293 $[M+H]^+$ (found), 305.1299 $[M+H]^+$ (calculated).

7.6.3 Chapter 4

1,1'-(4,5-difluoro-1,2-phenylene)bis(3-phenylurea), 262 *(Novel compound)*

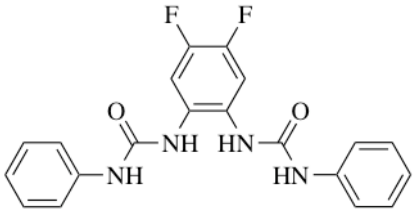

4,5-difluoro-2-nitroaniline (0.212 g, 1.22 mmol) was dissolved in methanol (20 mL) with palladium/carbon catalyst (~ 5 mg). The reaction mixture was stirred at room temperature for 4 hours under hydrogen. The catalyst was removed by filtration and the filtrate reduced *in vacuo* to yield a green oil. The oil was dissolved in DCM (20 mL) and pyridine (5 mL) with phenyl isocyanate (0.265 mL, 2.44 mmol). The reaction mixture was stirred at room temperature under nitrogen for 2 hours. The resulting precipitate was removed by filtration and sonicated in DCM (200 mL) for 1 hour. The suspension was filtered to yield a white solid (0.174 g). 37 % yield. **M_p =** 196 °C; **^{1}H NMR (400 MHz, DMSO-*d*$_6$), δ (ppm)** = 9.11 (s, 2 H, NH), 8.13 (s, 2 H, NH), 7.72 (t, J = 10.6 Hz, 2 H, aromatic CH), 7.48 (d, J = 8.60 Hz, 4 H, aromatic CH), 7.29 (t, J = 7.56 Hz, 4 H, aromatic CH), 6.98 (br. t, J = 7.60 Hz, 2 H, aromatic CH); **^{13}C NMR (100 MHz, DMSO-*d*$_6$), δ (ppm)** = 153.0 (CO), 145.3 (CF, [dd, J = 243.0, 16.0 Hz]) 139.5 (q), 128.8 (aromatic CH), 127.9 (q), 122.0 (aromatic CH), 118.3 (aromatic CH), 112.2 (aromatic CH, [dd, J = 11.6, 8.7Hz]); **^{19}F NMR (282 MHz, DMSO-*d*$_6$), δ (ppm)** = -143.16 (aromatic CF); **IR (film):** ν_{max} (cm^{-1}) = 3330 (NH), 3070 (NH), 1630 (CO), 1600 (CO); **LRMS (ES^+): m/z** = 405.1 $[M+Na]^+$, 787.4 $[2M+Na]^+$; **HRMS (ES^+): m/z** = 405.1131 $[M+Na]^+$ (found), 405.1134 $[M+Na]^+$ (calculated).

1,1'-(1,2-phenylene)bis(3-(4-cyanophenyl)urea), 263 *(Novel compound)*

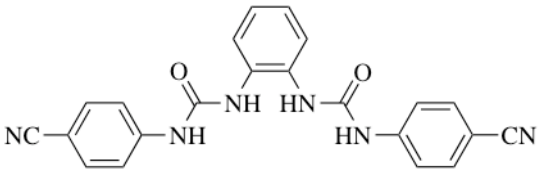

Ortho-phenylenediamine (0.204 g, 1.89 mmol) was dissolved in DCM (20 mL) and pyridine (5 mL) with 4-cyanophenyl isocyanate (0.541 g, 3.75 mmol). The reaction mixture was stirred at room temperature under nitrogen for 18 hours. The resulting precipitate was removed by filtration and sonicated in DCM (200 mL) for 15 minutes. The suspension was filtered to yield a white solid (0.290 g). 39 % yield. **M_p =** 217-218 °C; **^{1}H NMR (400 MHz, DMSO-*d*$_6$), δ (ppm)** = 9.59 (s, 2 H, NH), 8.23 (s, 2 H, NH), 7.73 (d, J = 8.60 Hz, 4 H, aromatic CH), 7.66 (d, J = 9.12 Hz, 4 H, aromatic CH), 7.62-7.58 (m, 2 H, aromatic CH), 7.16-7.12 (m, 2 H, aromatic CH); **^{13}C NMR (100 MHz, DMSO-*d*$_6$), δ (ppm)** = 152.8 (CO), 144.3 (q), 133.3 (aromatic CH), 131.0 (q), 124.6 (aromatic CH), 124.4 (aromatic CH), 119.3 (q), 118.0 (aromatic CH), 103.3 (CN); **IR (film):** ν_{max} (cm^{-1}) = 3370 (NH), 2220 (CN), 1670 (CO), 1590 (CO); **LRMS (ES^+): m/z** = 419.0 $[M+Na]^+$, 815.3 $[2M+Na]^+$; **HRMS (ES^+): m/z** = 419.1227 $[M+Na]^+$ (found), 419.1227 $[M+Na]^+$ (calculated).

1,1'-(1,2-phenylene)bis(3-(4-(trifluoromethyl)phenyl)urea), 264 *(Novel compound)*

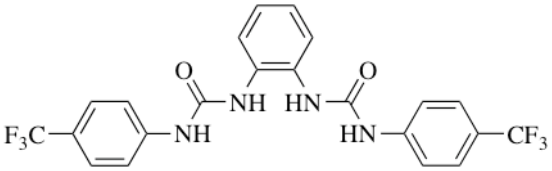

*Ortho-p*henylenediamine (0.244 g, 2.26 mmol) was dissolved in DCM (20 mL) with 4-(trifluoromethyl)phenyl isocyanate (0.650 mL, 4.55 mmol). The reaction mixture was stirred at room temperature under nitrogen for 48 hours. The resulting precipitate was removed by filtration and washed with DCM (2 x 25 mL) to yield a white solid (0.917g). 84 % yield. **M_p =** 210 °C; **^{1}H NMR (400 MHz, DMSO-*d*$_6$), δ (ppm)** = 9.50 (s, 2 H, NH), 8.20 (s, 2 H, NH), 7.71 (d, 4 H, J = 8.60 Hz, aromatic CH), 7.65-7.60 (m, 6 H, aromatic CH), 7.13 (dd, J = 6.04, 3.52 Hz, 2 H, aromatic CH); **^{13}C NMR (100 MHz, DMSO-*d*$_6$), δ (ppm)** = 153.0 (CO), 143.6 (q), 131.2 (q), 126.1 (aromatic CH), 124.6 (CF_3, [q, J = 269.1 Hz]), 124.4 (aromatic CH), 124.3 (aromatic CH), 121.8 (q, [q, J = 32.0 Hz]), 117.8 (aromatic CH); **^{19}F NMR (282 MHz, DMSO-*d*$_6$), δ (ppm)** = -60.26 (CF_3); **IR (film):** ν_{max} (cm^{-1}) = 3310 (NH), 1560 (CO), 1110 (CF), 1060 (CF); **LRMS (ES^+): m/z** = 505.1 $[M+Na]^+$; **HRMS (ES^+): m/z** = 505.1075 $[M+Na]^+$ (found), 505.1070 $[M+Na]^+$ (calculated).

1,1'-(1,2-phenylene)bis(3-(3-nitrophenyl)urea, 265 *(Novel compound)*

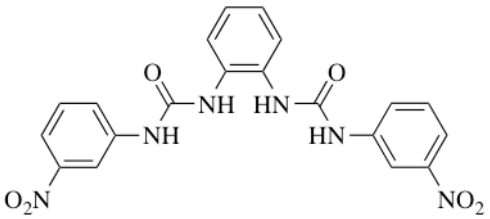

*Ortho-p*henylenediamine (0.212 g, 1.96 mmol) was dissolved in DCM (20 mL) and pyridine (5 mL) with 3-nitrophenyl isocyanate (0.644 g, 3.92 mmol). The reaction mixture was stirred at room temperature under nitrogen for 24 hours. The resulting precipitate was removed by filtration and sonicated in DCM (200 mL) for 15 minutes. The suspension was filtered to yield a yellow solid (0.705 g). 82 % yield. **M_p** = 206-207 °C; **^{1}H NMR (400 MHz, DMSO-*d*$_6$), δ (ppm)** = 9.64 (s, 2 H, NH), 8.57 (m, 2 H, aromatic CH), 8.22 (s, 2 H, NH), 8.81 (dd, J = 8.08, 2.04 Hz, 2 H, aromatic CH), 7.74 (dd, J = 8.56, 1.52 Hz, 2 H, aromatic CH), 7.63 (m, 2 H, aromatic CH), 7.56 (t, J = 8.08 Hz, 2 H, aromatic CH), 7.17-7.14 (m, 2 H, aromatic CH); **^{13}C NMR (100 MHz, DMSO-*d*$_6$), δ (ppm)** = 153.2 (CO), 148.2 (q), 141.2 (q), 131.2 (q), 130.0 (aromatic CH), 124.6 (aromatic CH), 124.5 (aromatic CH), 124.2 (aromatic CH), 116.2 (aromatic CH), 112.1 (aromatic CH); **IR (film):** ν_{max} (cm^{-1}) = 3340 (NH), 3270 (NH), 1650 (CO), 1520 (NO); **LRMS (ES^+): m/z** = 437.2 $[M+H]^+$, 459.1 $[M+Na]^+$; **HRMS (ES^+): m/z** = 459.1025 $[M+Na]^+$ (found), 459.1024 $[M+Na]^+$ (calculated).

References

1. A. M. King, L. Cromarty, C. Paterson and J. S. Boyd, *Vetinary Record*, 2007, **160**, 94-96
2. Lehn J. -M., *Supramolecular Chemistry - Scope and Perspectives; Molecules - Supermolecules - Molecular Devices*, Nobel Lecture, 1987
3. J. W. Steed and J. L. Atwood, *Supramolecular Chemistry*, 2002, Chichester, John Wiley and Sons, Inc.
4. J. T. Davis, O. Okunola and R. Quesada, *Chem. Soc. Rev.*, 2010, **39**, 3843-3862
5. P. A. Gale, *Acc. Chem. Res.*, 2011, **44**, 216-226
6. A. L. Sisson, M. R. Shah, S. Bhosale and S. Matile, *Chem. Soc. Rev.*, 2006, **35**, 1269-1286
7. A. P. Davis, D. N. Sheppard and B. D. Smith, *Chem. Soc. Rev.*, 2007, **36**, 348-357
8. B. A. McNally, W. M. Leevy and B. D. Smith, *Supramol. Chem.*, 2007, **19**, 29-37
9. G. W. Gokel and N. Barkey, *New J. Chem.*, 2009, **33**, 947-963
10. T. M. Fyles, *Chem. Soc. Rev.*, 2007, **36**, 335-347
11. E. D. Korn, *Science*, 1966, **153**, 1491-1498
12. J. M. Sanderson, *Org. Biomol. Chem.*, 2005, **3**, 201-212
13. S. J. Singer and G.L. Nicolson, *Science*, 1972, **175**, 720-731
14. S. J. Singer, *Annu. Rev. Cell Biol.*, 1990, **6**, 247-296
15. J. K. Blasie, L. Herbette and J. Pachence, *J. Membrane Biol.*, 1985, **86**, 1-7
16. K. B. Storey, Functional Metabolism: Regulation and Adaptation, 2004, Hoboken, John Wiley and Sons, Inc.
17. H. Lodish, A. Berk, C. A. Kaiser, M. Krieger, M. P. Scott, A. Bretscher, H. Ploegh and P. Matsudaira, *Molecular Cell Biology, 6th Ed.*, 2008, New York, W. H. Freeman and Company
18. S. Paula, A. G. Volkov and D. W. Deamer, *Biophys. J.*, 1998, **74**, 319-327
19. H. Hunter, M. C. Phillips and M. Stubbs, *Nature*, 1972, **239**, 342-344
20. Y. Zhang and P. S. Cremer, *Curr. Opin. Chem. Biol.*, 2006, **10**, 658-663
21. A. L. Sisson, J. P. Clare, L. H. Taylor, J. P. H. Charmant and A. P. Davis, *Chem. Commun.*, 2003, 2246-2247
22. Y. Marcus, *J. Chem. Soc. Faraday Trans.*, 1991, **81**, 2995-2999
23. P. J. Cragg, *Sci. Prog.*, 2002, **85**, 219-241
24. G. R. Dubyak, *Adv. Physiol. Educ.*, 2004, **28**, 143-154
25. R. MacKinnon, *FEBS Letters*, 2003, **555**, 62-65
26. F. M. Ashcroft, *Ion Channels and Disease*, 2000, Academic Press, San Diego
27. B. Nilius and G. Droogmans, *Acta. Physiol. Scand.*, 2003, **177**, 119-147
28. M. Maduke, C. Miller and J. A. Mindell, *Annu. Rev. Biophys. Biomol. Struct.*, 2000, **29**, 411-438
29. J. A. Mindell, M. Maduke, C. Miller and N. Grigorieff, *Nature*, 2001, **409**, 219-223
30. E. Gouaux and R. MacKinnon, *Science*, 2005, **310**, 1461-1465
31. R. Dutzler, E. B. Campbell, M. Cadene, B. T. Chait, and R. MacKinnon, *Nature*, 2002, **415**, 287-294
32. B. Corry and S-H. Chung, *Cell Mol. Life Sci.*, 2006, **63**, 301-315

33. L. Feng, E. B. Campbell, Y. Hsiung, and R. MacKinnon, *Science*, 2010, **330**, 635-641
34. J. A. Mindell, *Science*, 2010, **330**, 601-602
35. R. Dutzler, E. B. Campbell and R. MacKinnon, *Science*, 2003, **300**, 108-112
36. L. Puljak and G. Kilic, *Biochim. Biophys. Acta*, 2006, **1762**, 404-413
37. R. Planells-Cases and T. J. Jentsch, *Biochim. Biophys. Acta*, 2009, **1792**, 173-189
38. J. R. Casey, *Biochem. Cell Biol.*, 2006, **84**, 930-939
39. A. Lambert and A. G. Lowe, *J. Physiol.*, 1978, **275**, 51-63
40. J. O. Wieth, O. S. Andersen, J. Brahm, P. J. Bjerrum and C. L. Borders, Jr., *Phil. Trans. R. Soc. Lond. B*, 1982, **299**, 383-399
41. E. Cordat and J. R. Casey, *Biochem. J.*, 2009, **417**, 423-439
42. X. F. Wang, C. X. Zhou, Q. X. Shi, Y. Y. Yuan, M. K. Yu, L. C. Ajonuma, L. S. Ho, P. S. Lo, L. L. Tsang, Y. Liu, S. Y. Lam, L. N. Chan, W. C. Shao, Y. W. Chung and H. C. Chan, *Nat. Cell Biol.*, 2003, **5**, 902-906
43. W. M. Xu, Q. X. Shi, W. Y. Chen, C. X. Zhou, Y. Ni, D. K. Rowlands, G. Y. Liu, H. Zhu, Z. G. Ma. X. F. Wang, Z. H. Chen, S. C. Zhou, H. S. Dong, X. H. Zhang, Y. W. Chung, Y. Y. Yuan, W. X. Yang, and H. C. Chan, *Proc. Natl. Acad. Sci. U.S.A.*, 2007, **104**, 9816-9821
44. P. M. Quinton, *Acta Physiol. Sin.*, 2007, **59**, 397-415
45. J. -H. Chen, D. A. Stoltz, P. H. Karp, S. E. Ernst, A. A. Pezzulo, T. O. Moninger, M. V. Rector, L. R. Reznikov, J. L. Launspach, K. Chaloner, J. Zabner and M. J. Welsh, *Cell*, 2010, **143**, 911-923
46. J. Y. Choi, D. Muallem, K. Kiselyov, M. G. Lee, P. J. Thomas and S. Muallem, *Nature*, 2001, **410**, 94-97
47. M. A. S. Garcia, N. Yang, P. M. Quinton, *J. Clin. Invest.*, 2009, **119**, 2613-2622
48. P. M. Quinton, *Lancet*, 2008, **372**, 415-417
49. L. Tang, M. Fatehi and P. Linsdell, *J. Cyst. Fibros.*, 2009, **8**, 115-121
50. D. N. Sheppard, D. P. Rich, L. S. Ostedgaard, R. J. Gregory, A. E. Smith, and M. J. Welsh, *Nature*, 1993, **362**, 160-164
51. M. Pucéat, *Cell. Mol. Life Sci.*, 1999, **55**, 1216-1229
52. J. Fujinaga, F. B. Loiselle, and J. R. Casey, *Biochem. J.*, 2003, **371**, 687-696
53. D. Bok, G. Galbraith, I. Lopez, M. Woodruff, S. Nusinowitz, H. BeltrandelRio, W. Huang, S. Zhao, R. Geske, C. Montgomery, I. Van Sligtenhorst, C. Friddle, K. Platt, M. J. Sparks, A. Pushkin, N. Abuladze, A. Ishiyama, R. Dukkipati, W. Liu, and I. Kurtz, *Nat. Genet.*, 2003, **34**, 313-319
54. A. -V. Rousselle and D. Heymann, *Bone*, 2002, **30**, 533-540
55. O. A. Weisz, *Traffic*, 2003, **4**, 57-64
56. S. Matsuyama, J. Llopis, Q. L. Deveraux, R. Y. Tsien, and J. C. Reed, *Nat. Cell Biol.*, 2000, **2**, 318-325
57. T. J. Jentsch, T. Maritzen, and A. A. Zdebik, *J. Clin. Invest.*, 2005, **115**, 2039-2046
58. T. Sato, H. Konno, Y. Tanaka, T. Kataoka, K. Nagai, H. H. Wasserman, and S. Ohkuma, *J. Biol. Chem.*, 1998, **273**, 21455-21462
59. S. Ohkuma, T. Sato, M. Okamoto, H. Matsuya, T. Kataoka, K. Nagai, and H. H. Wasserman, *Biochem. J.*, 1998, **334**, 731-741

60. M. Grabe and G. Oster, *J. Gen. Physiol.*, 2001, **117**, 329-343
61. S. M. Simon, *Drug Discov. Ther.*, 1999, **4**, 32-38
62. N. Altan, Y. Chen, M. Schindler and S. M. Simon, *J. Exp. Med.*, 1998, **187**, 1583-1598
63. Y. Chen, M. Schindler and S. M. Simon, *J. Biol. Chem.*, 1999, **274**, 18364-18373
64. N. Raghunand and R. J. Gillies, *Drug Resist. Update.*, 2000, **3**, 39-47
65. Y. Okada, *J. Membrane Biol.*, 2006, **209**, 1-2
66. K. Kunzelmann, *J. Membrane Biol.*, 2005, **205**, 159-173
67. Y. Okada, T. Shimizu, E. Maeno, S. Tanabe, X. Wang and N. Takahashi, *J. Membrane Biol.*, 2006, **209**, 21-29
68. E. L. Lee, T. Shimizu, T. Ise, T. Numata, K. Kohno and Y. Okada, *J. Cell. Physiol.*, 2007, **211**, 513-521
69. T. R. Seth, R. M. Henderson, S. B. Hladky and A. W. Cuthbert, *Biochim. Biophys. Acta.*, 1992, **1107**, 179-185
70. E. J. Jeong, E. J. Kang, L. T. Sung, S. K. Hong and E. Lee, *J. Am. Chem. Soc.*, 2002, **124**, 14655-14662
71. A. Fürstner, *Angew. Chem. Int. Ed.*, 2003, **42**, 3582-3603
72. A. J. Castro, G. R. Gale, G. E. Means and G. Tertzakian, *J. Med. Chem.*, 1967, **10**, 29-32
73. A. J. Castro, *Nature*, 1967, **213**, 903-904
74. J. E. Lazaro, J. Nitcheu, R. Z. Predicala, G. C. Mangalindan, F. Nesslany, D. Marzin, G. P. Concepcion and B. Diquet, *J. Nat. Toxins*, 2002, **11**, 367-377
75. M. Isaka, A. Jaturapat, J. Kramyu, M. Tanticharoen and Y. Thebtaranonth, *Antimicrob. Agents Chemother.*, 2002, **46**, 1112-1113
76. D. Yamamoto, Y. Kiyozuka, Y. Uemura, C. Yamamoto, H. Takemoto, H. Hirata, K. Tanaka, K. Hioki and A. Tsubura, *J. Cancer Res. Clin. Oncol.*, 2000, **126**, 191-197
77. C. Diaz-Ruiz, B. Montaner and R. Pérez-Tomás, *Hisol. Histo-pathol.*, 2001, **16**, 415-421
78. B. Montaner and R. Pérez-Tomás, *Life Sci.*, 2001, **68**, 2025-2026
79. B. Montaner, S. Navarro, M. Piqué, M. Vilaseca, M. Martinell, E. Giralt, J. Gil and R. Pérez-Tomás, *Br. J. Pharmacol.*, 2000, **131**, 585-593
80. C. Campàs, M. Dalmau, B. Montaner, M. Barragán, B. Bellosillo, D. Colomer, G. Pons, R. Pérez-Tomás and J. Gil, *Leukemia*, 2003, **17**, 746-750
81. R. Pérez-Tomás, B. Montaner, E. Llagostera and V. Soto-Cerrato, *Biochem. Pharmacol.*, 2003, **66**, 1447-1452
82. M. Monge, M. Vilaseca, V. Soto-Cerrato, B. Montaner, E. Giralt and R. Pérez-Tomás, *Invest. New Drugs*, 2006, **25**, 21-29
83. R. D' Alessio, A. Bargiotti, O. Carlini, F. Colotta, M. Ferrari, P. Gnocchi, A. Isetta, N. Mongelli, P. Motta, A. Rossi, M. Rossi, M. Tibolla and E. Vanotti, *J. Med. Chem.*, 2000, **43**, 2557-2565
84. R. I. Sáez Diaz, J. Regourd, P. V. Santacroce, J. T. Davis, D. L. Jakeman and A. Thompson, *Chem. Commun.*, 2007, 2701-2703
85. M. S. Melvin, J. T. Tomlinson, G. R. Saluta, G. L. Kucera, N. Lindquist and R. A. Manderville, *J. Am. Chem. Soc.*, 2000, **122**, 6333-6334

86. H. Konno, H. Matsuya, M. Okamoto, T. Sato, Y. Tanaka, K. Yokoyama, T. Kataoka, K. Nagai, H. H. Wasserman and S. Ohkuma, *J. Biochem.*, 1998, **124**, 547-556
87. C. Yamamoto, H. Takemoto, K. Kuno, D. Yamamoto, A. Tsubura, K. Kamata, H. Hirata, A. Yamamoto, H. Kano, T. Seki and K. Inoue, *Hepatology*, 2003, **30**, 894-902
88. S. Jenkins, C. D. Incarvito, J. Parr and H. H. Wasserman, *CrystEngComm*, 2009, **11**, 242-245
89. J. L. Seganish and J. T. Davis, *Chem. Commun.*, 2005, 5781-5783
90. J. T. Davis, P. A. Gale, O. A. Okunola, P. Prados, J. C. Iglesias-Sánchez, T. Torroba and R. Quesada, *Nature Chem.*, 2009, **1**, 138-144
91. J. L. Sessler, L. R. Eller, W-S. Cho, S. Nicolaou, A. Aguilar, J. T. Lee, V. M. Lynch and D. J. Magda, *Angew. Chem. Int. Edit.*, 2005, **44**, 5989-5992
92. P. K. Paik, C. M. Rudin, M. C. Pietanza, A. Brown, N. A. Rizvi, N. Takebe, W. Travis, L. James, M. S. Ginsberg, R. Juergens, S. Markus, L. Tyson, S. Subzwari, M. G. Kris and L. M. Krug, *Lung Cancer*, 2011, **74**, 481-485
93. Y. Tang, H. A. Hamed, N. Cruickshanks, P. B. Fisher, S. Grant and P. Dent, *Mol. Pharmacol.*, 2012, **81**, 527-540
94. B. D. de Greñu, P. I. Hernández, M. Espona, D. Quiñonero, M. E. Light, T. Torroba, R. Pérez-Tomás and R. Quesada, *Chem. Eur. J.*, 2011, **17**, 14074-14083
95. B. Carté and D. J. Faulkner, *J. Org. Chem.*, 1983, **48**, 2314-2318
96. N. Lindquist and W. Fenical, *Experientia*, 1991, **47**, 504-506
97. A. J. Blackman and C. Li, *Aus. J. Chem.*, 1994, **47**, 1625-1629
98. K. Tanigaki, T. Suto, Y. Tanaka, T. Ochi, A. Nishikawa, K. Nagai, H. Kawashima and S. Ohkuma, *FEBS Lett.*, 2002, **524**, 37-42
99. B. C. Cavalcanti, H. V. N. Júnior, M. H. R. Seledhim, R. G. S. Berlinck, G. M. A. Cunha, M. O. Moraes and C. Pessoa, *Chem. –Biol. Interact.*, 2008, **174**, 155-162
100. K. Kojiri, S. Nakajima, H. Suzuki, A. Okura and H. Suda, *J. Antibiot.*, 1993, **46**, 1799-1803
101. P. I. Hernández, D. Moreno, A. A. Javier, T. Torroba, R. Pérez-Tomás and R. Quesada, *Chem. Commun.*, 2012, **48**, 1556-1558
102. W. Zheng, J. Kollmeyer, H. Symolon, A. Momin, E. Munter, E. Wang, S. Kelly, J. C. Allegood, Y. Liu, Q. Peng, H. Ramaraju, M. C. Sullards, M. Cabot and A. H. Merrill, Jr., *Biochim. Biophys. Acta*, 2006, **1758**, 1864-1884
103. L. M. Obeid, C. M. Linardic, L. A. Karolak and Y. A. Hannun, *Science*, 1993, **259**, 1769-1771
104. L. J. Siskind and M. Colombini, *J. Biol. Chem.*, 2000, **275**, 38640-38644
105. L. J. Siskind, R. N. Kolesnick, and M. Colombini, *Mitochondrion*, 2006, **6**, 118-125
106. M. N. Perera, V. Ganesan, L. J. Siskind, Z. M. Szulc, J. Bielawski, A. Bielawska, R. Bittman and M. Columbini, *Biochim. Biophys. Acta*, 2012, **1818**, 1291-1301
107. W. A. Harrell, Jr., M. L. Bergmeyer, P. Y. Zavalij and J. T. Davis, *Chem. Commun.*, 2010, **46**, 3950-3952
108. C. M. Armstrong and B. Hille, *Neuron*, 1998, **20**, 371-380
109. H. C. Rodgers and A. J. Knox, *Eur. Respir. J.*, 2001, **17**, 1314-1321

110. L. Gao, J. R. Broughman, T. Iwamoto, J. M. Tomich, C. J. Venglarik and H. J. Forman, *Am. J. Physiol Lung Cell Mol. Physiol.*, 2001, **281**, 24-30
111. G. Deng, T. Dewa and S. L. Regen, *J. Am. Chem. Soc.*, 1996, **118**, 8975-8976
112. C. Jiang, E. R. Lee, M. B. Lane, Y. -F. Xiao, D. J. Harris and S. H. Cheng, *Am. J. Physiol. Lung Cell Mol. Physiol.*, 2001, **281**, 1164-1172
113. F. P. Schmidtchen, *Chem. Soc. Rev.*, 2010, **39**, 3916-3935
114. Y. K. Kim, Y.-H. Lee, H. -Y. Lee, M. K. Kim, G. S. Cha and K. H. Ahn, *Org. Lett.*, 2003, **5**, 4003-4006
115. D. -S. Kim, Y. -M. Chung, M. Jin and K. H. Ahn, *J. Org. Chem.*, 2009, **74**, 4849-4854
116. S. Basurto, D. Miguel, D. Moreno, A. G. Neo, R. Quesada and T. Torroba, *Org. Biomol. Chem.*, 2010, **8**, 552-558
117. H. -J. Pyun, J. Chu, Y. M. Jun and D. J. Kim, *Bull. Korean Chem. Soc.*, 1999, **20**, 112-116
118. O. B. Berryman, V. S. Bryanstev, D. P. Stay, D. W. Johnson and B. P. Hay, *J. Am. Chem. Soc.*, 2007, **129**, 48-58
119. J. Mísek, A. V. Jentzsch, S. Sakurai, D. Emery, J. Mareda and S. Matile, *Angew. Chem. Int. Ed.*, 2010, **49**, 7680-7683
120. S. K. Kim and J. L. Sessler, *Chem. Soc. Rev.*, 2010, **39**, 3784-3809
121. H. Miyaji, D. -S. Kim, B. -Y. Chang, S. -M. Park and K. H. Ahn, *Bull. Korean Chem. Soc.*, 2008, **29**, 2355-2360
122. M. Wenzel, J. R. Hiscock and P. A. Gale, *Chem. Soc. Rev.*, 2012, **41**, 480-520
123. P. A. Gale, *Chem. Soc. Rev.*, 2010, **39**, 3746-3771
124. C. Caltagirone and P.A. Gale, *Chem. Soc. Rev.*, 2009, **38**, 520-563
125. X. Shang and S. Tian, *J. Recept. Sig. Transd.*, 2009, **29**, 274-279
126. Y. Hua and A. H. Flood, *Chem. Soc. Rev.*, 2010, **39**, 1262-1271
127. M. G. Chudzinski, C. A. McClary and M. S. Taylor, *J. Am. Chem. Soc.*, 2011, **133**, 10559-10567
128. A. P. Davis, *Coordin. Chem. Rev.*, 2006, **250**, 2939-2951
129. P. R. Brotherhood and A. P. Davis, *Chem. Soc. Rev.*, 2010, **39**, 3633-3647
130. A. P. Davis, J. J. Perry and R. S. Wareham, *Tetrahedron Lett.*, 1998, **39**, 4569-4572
131. A. J. Ayling, M. N. Pérez-Payán and A. P. Davis, *J. Am. Chem. Soc.*, 2001, **123**, 12716-12717
132. J. P. Clare, A. J. Ayling, J. -B. Joos, A. L. Sisson, G. Magro, M. N. Pérez-Payán, T. N. Lambert, R. Shukla, B. D. Smith and A. P. Davis, *J. Am. Chem. Soc.*, 2005, **127**, 10739-10746
133. E. P. Kyba, R. C. Helgeson, K. Madan, G. W. Gokel, T. L. Tarnowski, S. S. Moore and D. J. Cram, *J. Am. Chem. Soc.*, 1977, **98**, 2564-2571
134. A. J. Ayling, S. Broderick, J. P. Clare, A. P. Davis, M. N. Pérez-Payán, M. Lahtinen, M. J. Nissinen and K. Rissanen, *Chem. Eur. J.*, 2002, **8**, 2197-2203
135. B. Baragaña, A. G. Blackburn, P. Breccia, A. P. Davis, J. de Mendoza, J. M. Padrón-Carrillo, P. Prados, J. Riedner and J. G. de Vries, *Chem. Eur. J.*, 2002, **8**, 2931-2936

136. A. V. Koulov, T. N. Lambert, R. Shukla, M. Jain, J. M. Boon, B. D. Smith, H. Li, D. N. Sheppard, J. -B. Joos, J. P. Clare and A. P. Davis, *Angew. Chem. Int. Ed.*, 2003, **42**, 4931-4933
137. B. A. McNally, A. V. Koulov, B. D. Smith, J. -B. Joos and A. P. Davis, *Chem. Commun.*, 2005, 1087-1089
138. B. A. McNally, A. V. Koulov, T. N. Lambert, B. D. Smith, J.-B. Joos, A. L. Sisson, J. P. Clare, V. Sgarlata, L. W. Judd, G. Magro and A. P. Davis, *Chem. Eur. J.*, 2008, **14**, 9599-9606
139. T. N. Lambert, J. M. Boon, B. D. Smith, M. N. Pérez-Payán and A. P. Davis, *J. Am. Chem. Soc.*, 2002, **124**, 5276-5277
140. J. M. Boon, T. N. Lambert, A. L. Sisson, A. P. Davis and B. D. Smith, *J. Am. Chem. Soc.*, 2003, **125**, 8195-8201
141. L. W. Judd and A. P. Davis, *Chem. Commun.*, 2010, **46**, 2227-2229
142. N. Sakai and S. Matile, *Tetrahedron Lett.*, 1997, **38**, 2613-1616
143. M. Merritt, M. Lanier, G. Deng and S. L. Regen, *J. Am. Chem. Soc.*, 1998, **120**, 8494-8501
144. S. D. Whitmarsh, A. P. Redmond, V. Sgarlata and A. P. Davis, *Chem. Commun.*, 2008, 3669-3671
145. S. Hussain, P. R. Brotherhood, L. W. Judd and A. P. Davis, *J. Am. Chem. Soc.*, 2011, **133**, 1614-1617
146. P. V. Santacroce, J. T. Davis, M. E. Light, P. A. Gale, J. C. Iglesias-Sánchez, P. Prados and R. Quesada, *J. Am. Chem. Soc.*, 2007, **129**, 1886-1887
147. P. A. Gale, J. Garric, M. E. Light, B. A. McNally and B. D. Smith, *Chem. Commun.*, 2007, 1736-1738
148. C. R. Yamnitz, S. Negin, I. A. Carasel, R. K. Winter and G. W. Gokel, *Chem. Commun.*, 2010, **46**, 2838-2840
149. X. Li, B. Shen, X. -Q. Yao and D. Yang, *J. Am. Chem. Soc.*, 2007, **129**, 7264-7265
150. X. Li, B. Shen, X. -Q. Yao and D. Yang, *J. Am. Chem. Soc.*, 2009, **131**, 13676-13680
151. A. V. Koulov, J. M. Mahoney and B. D. Smith, *Org. Biomol. Chem.*, 2003, **1**, 27-29
152. P. A. Gale, M. E. Light, B. McNally, K. Navakhun, K. E. Sliwinski and B. D. Smith, *Chem. Commun.*, 2005, 3773-3775
153. H. -J. Lin, H. Szmacinski and J. R. Lakowicz, *Anal. Biochem.*, 1999, **269**, 162-167
154. K. J. Winstanley, A. M. Sayer and D. K. Smith, *Org. Biomol. Chem.*, 2006, **4**, 1760-1767
155. K. J. Winstanley and D. K. Smith, *J. Org. Chem.*, 2007, **72**, 2803-2815
156. S. K. Berezin and J. T. Davis, *J. Am. Chem. Soc.*, 2009, **131**, 2458-2459
157. T. Pomorski and A. K. Menon, *Cell. Mol. Life Sci.*, 2006, **63**, 2908-2921
158. A. J. Verkleij and J. A. Post, *J. Membrane Biol.*, 2000, **178**, 1-10
159. S. Manno, Y. Takakuwa and N. Mohandas, *Proc. Natl. Acad. Sci. U.S.A.*, 2002, **99**, 1943-1948
160. A. Zachowski, *Bochem. J.*, 1993, **294**, 1-14
161. J. M. Boon and B. D. Smith, *J. Am. Chem. Soc.*, 1999, **121**, 11924-11925

162. J. M. Boon and B. D. Smith, *J. Am. Chem. Soc.*, 2001, **123**, 6221-6226
163. J. M. Boon, R. Shukla, B. D. Smith, G. Licini and P. Scrimin, *Chem. Commun.*, 2002, 260-261
164. J. M. Boon, T. N. Lambert, B. D. Smith, A. M. Beatty, V. Ugrinova and S. N. Brown, *J. Org. Chem.*, 2002, **67**, 2168-2174
165. Y. Sasaki, R. Shukla and B. D. Smith, *Org. Biomol. Chem.*, 2004, **2**, 214-219
166. K. M. Divittorio, F. T. Hofmann, J. R. Johnson, L. Abu-Esba, and B. D. Smith, *Bioorgan. Med. Chem.*, 2009, **17**, 141-148
167. T. Sakamoto, A. Ojida and I. Hamachi, *Chem. Commun.*, 2009, 141-152
168. J. V. Carolan, S. J. Butler and K. A. Jolliffe, *J. Org. Chem.*, 2009, **74**, 2992-2996
169. S. J. Butler and K. A. Jolliffe, *Org. Biomol. Chem.*, 2011, **9**, 3471-3483
170. W. M. Leevy, S. T. Gammon, H. Jiang, J. R. Johnson, D. J. Maxwell, E. N. Jackson, M. Marquez, D. Piwnica-Worms and B. D. Smith, *J. Am. Chem. Soc.*, 2006, **128**, 16476-16477
171. W. M. Leevy, J. R. Johnson, C. Lakshmi, J. Morris, M. Marquez and B. D. Smith, *Chem. Commun.*, 2006, 1595-1597
172. B. A. Smith, W. J. Akers, W. M. Leevy, A. J. Lampkins, S. Xiao, W. Wolter, M. A. Suckow, S. Achilefu and B. D. Smith, *J. Am. Chem. Soc.*, 2010, **132**, 67-69
173. E. J. O'Neil and B. D. Smith, *Coordin. Chem. Rev.*, 2006, **250**, 3068-3080
174. K. M. DiVittorio, W. M. Leevy, E. J. O'Neil, J. R. Johnson, S. Vakulenko, J. D. Morris, K. D. Rosek, N. Serazin, S. Hilkert, S. Hurley, M. Marquez, and B. D. Smith, *ChemBioChem*, 2008, **9**, 286-293
175. T. Kohira, K. Honda, A. Ojida and I. Hamachi, *ChemBioChem*, 2008, **9**, 698-701
176. G. Fujii, J. -E. Chang, T. Coley and B. Steere, *Biochemistry*, 1997, **36**, 4959-4968
177. V. Khutorsky, *Biophys. J.*, 1996, **71**, 2984-2995
178. A. Asendei and T. Luchian, *Colloid. Surface. B.*, 2008, **67**, 99-106
179. N. Sakai, K. C. Brennan, L. A. Weiss and S. Matile, *J. Am. Chem. Soc.*, 1997, **119**, 8726-8727
180. L. A. Weiss, N. Sakai, B. Ghebremariam, C. Ni and S. Matile, *J. Am. Chem. Soc.*, 1997, **119**, 12142-12149
181. J. Mareda and S. Matile, *Chem. Eur. J.*, 2009, **15**, 28-37
182. V. Gorteau, G. Bollot, J. Mareda and S. Matile, *Org. Biomol. Chem.*, 2007, **5**, 3000-3012
183. V. Gorteau, G. Bollot, J. Mareda, A. Perez-Velasco and S. Matile, *J. Am. Chem. Soc.*, 2006, **128**, 14788-14789
184. N. Sakai, D. Gerard and S. Matile, *J. Am. Chem. Soc.*, 2001, **123**, 2517-2524
185. V. Gorteau, M. D. Julliard and S. Matile, *J. Membrane Sci.*, 2008, **321**, 37-42
186. F. Mora, D. -H. Tran, N. Oudry, G. Hopfgartner, D. Jeannerat, N. Sakai and S. Matile, *Chem. Eur. J.*, 2008, **14**, 1947-1953
187. A. Perez-Velasco, V. Gorteau and S. Matile, *Angew. Chem. Int. Ed.*, 2008, **47**, 921-923
188. C. -R. Elie, N. Noujeim, C. Pardin and A. R. Schmitzer, *Chem. Commun.*, 2011, **47**, 1788-1790
189. V. Sidorov, F. W. Kotch, J. L. Kuebler, Y. -F. Lam and J. T. Davis, *J. Am. Chem. Soc.*, 2003, **125**, 2840-2841

190. J. L. Seganish, J. C. Fettinger and J. T. Davis, *Supramol. Chem.*, 2006, **18**, 257-264
191. V. Sidorov, F. W. Kotch, G. Abdrakhmanova, R. Mizani, J. C. Fettinger and J. T. Davis, *J. Am. Chem. Soc.*, 2002, **124**, 2267-2278
192. J. L. Seganish, P. V. Santacroce, K. J. Salimian, J. C. Fettinger, P. Zavalij and J. T. Davis, *Angew. Chem. Int. Ed.*, 2006, **45**, 3334-3338
193. O. A. Okunola, J. L. Seganish, K. J. Salimian, P. Y. Zavalij and J. T. Davis, *Tetrahedron*, 2007, **63**, 10743-10750
194. M. Durmaz, S. Bozkurt, H. N. Naziroglu, M. Yilmaz and A. Sirit, *Tetrahedron-Asymmetr.*, 2011, **22**, 791-796
195. P. V. Santacroce, O. A. Okunola, P. Y. Zavalij and J. T. Davis, *Chem. Commun.*, 2006, 3246-3248
196. D. L. Granger, R. R. Taintor, K. S. Broockvar and J. B. Hibbs, *Method. Enzymol.*, **268**, 142-151
197. J. B. Fox, Jr., *Anal. Chem.*, 1979, **51**, 1493-1502
198. A. V. Jentzsch, D. Emery, J. Mareda, P. Metrangolo, G. Resnati and S. Matile, *Angew. Chem. Int. Ed.*, 2011, **50**, 11675-11678
199. N. Madhavan, E. C. Robert and M. S. Gin, *Angew. Chem. Int. Ed.*, 2005, **44**, 7584-7587
200. N. Madhavan and M. S. Gin, *ChemBioChem*, 2007, **8**, 1834-1840
201. P. V. Jog and M. S. Gin, *Org. Lett.*, 2008, **10**, 3693-3696
202. S. Licen, C. Coppola, J. D'Onofrio, D. Montesarchio and P. Tecilla, *Org. Biomol. Chem.*, 2009, **7**, 1060-1063
203. M. A. Ciardiello, D. Meleleo, G. Saviano, R. Crescenzo, V. Carratore, L. Camardella, E. Gallucci, S. Micelli, T. Tancredi, D. Picone and M. Tamburrini, *J. Pept. Sci.*, 2008, **14**, 742-754
204. T. R. Sheth, R. M. Henderson, S. B. Hladky and A. W. Cuthbert, *B. B. A. – Biomembranes*, 1992, **1107**, 179-185
205. H. Grasemann, F. Stehling, H. Brunar, R. Widmann, T. W. Laliberte, L. Molina, G. Döring and F. Ratjen, *Chest*, 2007, **131**, 1461-1466
206. G. L. Reddy, T. Iwamoto, J. M. Tomich and M. Montal, *J. Biol. Chem.*, 1993, **268**, 14608-14615
207. J. R. Broughman, L. P. Shank, O. Prakash, B. D. Schultz, T. Iwamoto, J. M. Tomich and K. Mitchell, *J. Membrane Biol.*, 2002, **190**, 93-103
208. J. M. Tomich, D. Wallace, K. Henderson, K. E. Mitchell, G. Radke, R. Brandt, C. A. Ambler, A. J. Scott, J. Grantham, L. Sullivan and T. Iwamoto, *Biophys. J.*, 1998, **74**, 256-267
209. G. A. Cook, O. Prakash, K. Zang, L. P. Shank, W. A. Takeguchi, A. S. Robbins, Y. -X. Gong, T. Iwamoto, B. D. Schultz and J. M. Tomich, *Biophys. J.*, 2004, **86**, 1424-1435
210. L. P. Shank, J. R. Broughman, W. A. Takeguchi, G. A. Cook, A. S. Robbins, L. Hahn, G. Radke, T. Iwamoto, B. D. Schultz and J. M. Tomich, *Biophys. J.*, 2006, **90**, 2138-2150
211. P. H. Schlesinger, R. Ferdani, J. Liu, J. Pajewski, M. Saito, H. Shabany and G. W. Gokel, *J. Am. Chem. Soc.*, 2002, **124**, 1848-1849

212. R. Pajewski, R. Ferdani, J. Pajewska, R. Li and G. W. Gokel, *J. Am. Chem. Soc.*, 2005, **127**, 18281-18295
213. G. A. Cook, R. Pajewski, M. Aburi, P. E. Smith, O. Prakash, J. M. Tomich and G. W. Gokel, *J. Am. Chem. Soc.*, 2006, **128**, 1633-1638
214. P. H. Schlesinger, N. K. Djedovic, R. Ferdani, J. Pajewska, R. Pajewski and G. W. Gokel, *Chem. Commun.*, 2003, 308-309
215. R. Ferdani, R. Li, R. Pajewski, J. Pajewska, R. K. Winter and G. W. Gokel, *Org. Biomol. Chem.*, 2007, **5**, 2423-2432
216. E. K. Elliott, M. M. Daschbach and G. W. Gokel, *Chem. Eur. J.*, 2008, **14**, 5871-5879
217. R. Pajewski, J. Pajewska, R. Li, M. M. Daschbach, E. A. Fowler and G. W. Gokel, *New J. Chem.*, 2007, **31**, 1960-1972
218. R. Ferdani, R. Pajewski, J. Pajewska, P. H. Schlesinger and G. W. Gokel, *Chem. Commun.*, 2006, 439-441
219. N. Djedovic, R. Ferdani, E. Harder, J. Pajewska, R. Pajewski, M. E. Weber, P. H. Schlesinger and G. W. Gokel, *New J. Chem.*, 2005, **29**, 291-305
220. P. H. Schlesinger, R. Ferdani, J. Pajewska, R. Pajewski and G. W. Gokel, *New J. Chem.*, 2003, **27**, 60-67
221. R. Ferdani, R. Pajewski, N. Djedovic, J. Pajewska, P. H. Schlesinger and G. W. Gokel, *New J. Chem.*, 2005, **29**, 673-680
222. G. A. Arteca and Z. Li, *Chem. Phys. Lett.*, 2004, **399**, 496-502
223. L. You, R. Ferdani, R. Li, J. P. Kramer, R. E. K. Winter and G. W. Gokel, *Chem. Eur. J.*, 2008, **14**, 382-396
224. L. You, R. Li and G. W. Gokel, *Org. Biomol. Chem.*, 2008, **6**, 2914-2923
225. E. K. Elliott, K. J. Stine and G. W. Gokel, *J. Membrane Sci.*, 2008, **321**, 43-50
226. R. Pajewski, R. Ferdani, J. Pajewska, N. Djedovic, P. H. Schlesinger and G. W. Gokel, *Org. Biomol. Chem.*, 2005, **3**, 619-625
227. L. You and G. W. Gokel, *Chem. Eur. J.*, 2008, **14**, 5861-5870
228. D. T. Bong, T. D. Clark, J. R. Granja and M. R. Ghadiri, *Angew. Chem. Int. Ed.*, 2001, **40**, 988-1011
229. A. Hennig, L. Fischer, G. Guichard and S. Matile, *J. Am. Chem. Soc.*, 2009, **131**, 16889-16895
230. L. Fischer, M. Decossas, J. -P. Briand, C. Didierjean and G. Guichard, *Angew. Chem. Int. Ed.*, 2009, **48**, 1625-1628
231. M. Kondo, M. Mehiri and S. L. Regen, *J. Am. Chem. Soc.*, 2008, **130**, 13771-13777
232. V. Janout, B. Jing, I. V. Staina and S. L. Regen, *J. Am. Chem. Soc.*, 2003, **125**, 4436-4437
233. S. Matile, A. V. Jentzsch, J. Montenegro and A. Fin, *Chem. Soc. Rev.*, 2011, **40**, 2453-2474
234. M. Mehiri, W. -H. Chen, V. Janout and S. L. Regen, *J. Am. Chem. Soc.*, 2009, **131**, 1338-1339
235. W. -H. Chen, V. Janout, M. Kondo, A. Mosoian, G. Mosoyan, R. R. Petrov, M. E. Klotman and S. L. Regen, *Bioconjugate Chem.*, 2009, **20**, 1711-1715
236. R. R. Petrov, W. -H. Chen and S. L. Regen, *Bioconjugate Chem.*, 2009, **20**, 1037-1043

237. L. L. Cline, V. Janout, M. Fisher, R. L. Juliano and S. L. Regen, *Bioconjugate Chem.*, 2011, **22**, 2210-2216
238. B. A. McNally, E. J. O'Neil, A. Nguyen and B. D. Smith, *J. Am. Chem. Soc.*, 2008, **130**, 17274-17275
239. R. C. Macdonald, R. I. Macdonald, B. P. M. Menco, K. Takeshita, N. K. Subbarao and L. R. Hu, *Biochim. Biophys. Acta*, 1991, **1061**, 297-303
240. B. D. Smith and T. N. Lambert, *Chem. Commun.*, 2003, 2261-2268
241. C. Taupin, M. Dvolaitzky and C. Sautery, *Biochemistry*, 1975, **14**, 4771-4775
242. G. B. Levy, *Clin. Chem.*, 1981, **27**, 1435-1438
243. M. E. Meyerhoff, E. Pretsch, D. H. Welti and W. Simon, *Anal. Chem.*, 1987, **59**, 144-150
244. M. Maj-Zurawska, D. Ziemianek, A. Mikolajczuk, J. Mieczkowski, A. Lewenstam, A. Hulanicki and T. Sokalski, *Anal. Bioanal. Chem.*, 2003, **376**, 524-526
245. J. Wissing and J. A. C. Smith, *J. Membrane Biol.*, 2000, **177**, 199-208
246. N. R. Clement and J. M. Gould, *Biochemistry*, 1981, **20**, 1534-1538
247. G. A. Woolley, M. K. Kapral and C. M. Deber, *FEBS Lett.*, 1987, **224**, 337-342
248. W. Wang, R. Li and G. W. Gokel, *Chem. Commun.*, 2009, 911-913
249. N. Busschaert, M. Wenzel, M. E. Light, P. Iglesias-Hernández, R. Pérez-Tomás and P. A. Gale, *J. Am. Chem. Soc.*, 2011, **133**, 14136-14148
250. P. Bandyopadhyay, V. Janout, L. Zhang and S. L. Regen, *J. Am. Chem. Soc.*, 2001, **123**, 7691-7696
251. F. G. Riddell, S. Arumugam and A. Patel, *J. Chem. Soc., Chem. Commun.*, 1990, 74-76
252. F. G. Riddell and Z. Zhou, *J. Inorg. Biochem.*, 1994, **55**, 279-293
253. C. Urban and C. Schmuck, *Chem. Eur. J.*, 2010, **16**, 9502-9510
254. J. L. Sessler, D. A. Ford, M. J. Cyr and H. Furuta, *J. Chem. Soc., Chem. Commun.*, 1991, 1733-1735
255. B. Dietrich, T. M. Fyles, M. W. Hosseini, J. -M. Lehn and K. C. Kaye, *J. Chem. Soc., Chem. Commun.*, 1988, 691-692
256. R. A. Shapiro, A. J. Brindley and R. W. Martin, *J. Am. Chem. Soc.*, 2010, **132**, 11406-11407
257. T. Starke-Peterkovic, N. Turner, M. F. Vitha, M. P. Waller, D. E. Hibbs and R. J. Clarke, *Biophys. J.*, 2006, **90**, 4060-4070
258. V. Buzon and J. Cladera, *Biochemistry*, 2006, **45**, 15768-15775
259. W. K. Subczynski, A. Wisniewska, J. J. Yin, J. S. Hyde and A. Kusumi, *Biochemistry*, 1994, **33**, 7670-7861
260. F. A. Nezil and M. Bloom, *Biophys. J.*, 1992, **61**, 1176-1183
261. M. E. Weber, P. H. Schlesinger and G. W. Gokel, *J. Am. Chem. Soc.*, 2005, **127**, 636-642
262. H. Ohvo-Rekilä, B. Ramstedt, P. Leppimäki and J. P. Slotte, *Prog. Lipid Res.*, 2002, **41**, 66-97
263. M. J. Pregel, L. Jullien, J. Canceill, L. Lacombe and J. -M. Lehn, *J. Chem. Soc. Perkin Trans. 2*, 1995, 417-426
264. S. Otto, M. Osifchin and S. L. Regen, *J. Am. Chem. Soc.*, 1999, **121**, 10440-10441
265. A. V. Hill, *J. Physiol.*, 1910, **40**, 4-7

266. S. Goutelle, M. Maurin, F. Rougier, X. Barbaut, L. Bourguignon, M. Ducher and P. Maire, *Fundam. Clin. Pharmacol.*, 2008, **22**, 633-648
267. M. Goto, S. Ishida, N. Tamai, H. Matsuki and S. Kaneshina, *Chem. Phys. Lipids*, 2009, **161**, 65-76
268. L. Beney, J. -M. Perrier-Cornet, M. Hayert and P. Gervais, *Biophys. J.*, 1997, **72**, 1258-1263
269. R. Benz, O. Frohlich and P. Lauger, *Biochim. Biophys. Acta*, 1977, **464**, 465-481
270. C. J. E. Haynes, S. J. Moore, J. R. Hiscock, I. Marques, P. J. Costa, V. Félix and P. A. Gale, *Chem. Sci.*, 2012, **3**, 1436-1444
271. T. M. Fyles, R. Knoy, K. Müllen and M. Sieffert, *Langmuir*, 2001, **17**, 6669-6674
272. O. P. Hamill, A. Marty, E. Neher, B. Sakmann and F. J. Sigworth, *Pflügers Arch.*, 1981, **391**, 85-100
273. G. Riquelme, E. Lopez, L. M. Garciasegura, J. A. Ferragut and J. M. Gonzalezros, *Biochemistry*, 1990, **29**, 11215-11222
274. D. N. Sheppard, M. A. Gray, X. Gong, Y. Sohma, I. Kogan, D. J. Benos, T. S. Scott-Ward, J. -H. Chen, H. Li, Z. Cai, J. Gupta, C. Li, M. Ramjeesingh, B. K. Berdiev, I. I. Ismailov, C. E. Bear, T. -C. Hwang, P. Linsdell and M. J. Hug, *J. Cyst. Fibros.*, 2004, **3**, 101-108
275. H. Li, D. N. Sheppard and M. J. Hug, *J. Cyst. Fibros.*, 2004, **3**, 123-126
276. F. Zoccarato, L. Cavallini and A. Alexandre, *J. Neurochem.*, 1999, **72**, 625-633
277. C. S. Wilcox, E. Kim, D. Romano, L. H. Kuo, A. L. Burt and D. P. Curran, *Tetrahedron*, 1995, **51**, 621-634
278. P. A. Gale, *Chem. Commun.*, 2008, 4525-4540
279. F. G. Bordwell, G. E. Drucker and H. E. Fried, *J. Org. Chem.*, 1981, **46**, 632-635
280. J. J. He and F. A. Quiocho, *Science*, 1991, **251**, 1479-1481
281. N. M. Koropatkin, H. B. Pakrasi and T. J. Smith, *Proc. Natl. Acad. Sci. U.S.A.*, 2006, **103**, 9820-9825
282. N. M. Koropatkin, D. W. Koppenaal, H. B. Pakrasi and T. J. Smith, *J. Biol. Chem.*, 2007, **282**, 2606-2614
283. K. H. G. Verschueren, F. Seljée, H. J. Rozeboom, K. H. Kalk and B. W. Dijkstra, *Nature*, 1993, **363**, 693-698
284. K. -J. Chang, M. K. Chae, C. Lee, J. -Y. Lee and K. -S. Jeong, *Tetrahedron Lett.*, 2006, **47**, 6385-6388
285. G. W. Lee, N. -K. Kim and K. -S. Jeong, *Org. Lett.*, 2010, **12**, 2634-2637
286. J. Kim, H. Juwarker, X. Liu, M. S. Lah and K. -S. Jeong, *Chem. Commun.*, 2010, **46**, 764-766
287. D. Curiel, A. Espinosa, M. Más-Montoya, G. Sánchez, A. Tárraga and P. Molina, *Chem. Commun.*, 2009, 7539-7541
288. T. Wang, H. -F. Wang and X. -P. Yan, *CrystEngComm*, 2010, **12**, 3177-3182
289. T. Wang and X. -P. Yan, *Chem. Eur. J.*, 2010, **16**, 4639-4649
290. J. L. Sessler, D. -G. Cho and V. Lynch, *J. Am. Chem. Soc.*, 2006, **126**, 16518-16519
291. C. Bejger, J. S. Park, E. S. Silver and J. L. Sessler, *Chem. Commun.*, 2010, **46**, 7745-7747
292. P. Dydio, T. Zielinski and J. Jurczak, *Chem. Commun.*, 2009, 4560-4562
293. P. Dydio, T. Zielinski and J. Jurczak, *Org. Lett.*, 2010, **12**, 1076-1078

294. C. Caltagirone, A. Mulas, F. Isaia, V. Lippolis, P. A. Gale and M. E. Light, *Chem. Commun.*, 2009, 6279-6281
295. K. Kavillieratos, S. R. de Gala, D. J. Austin and R. H. Crabtree, *J. Am. Chem. Soc.*, 1997, **119**, 2325-2326
296. C. A. Hunter and L. D. Sarson, *Angew. Chem. Int. Ed. Engl.*, 1994, **33**, 2313-2316
297. T. Zielinski, P. Dydio and J. Jurczak, *Tetrahedron*, 2008, **64**, 568-574
298. G. W. Bates, P. A. Gale and M. E. Light, *Chem. Commun.*, 2007, 2121-2123
299. C. Caltagirone, P. A. Gale, J. R. Hiscock, M. B. Hursthouse, M. E. Light and G. J. Tizzard, *Supramol. Chem.*, 2009, **21**, 125-130
300. C. Caltagirone, P. A. Gale, J. R. Hiscock, S. J. Brooks, M. B. Hursthouse and M. E. Light, *Chem. Commun.*, 2008, 3007-3009
301. C. Caltagirone, J. R. Hiscock, M. B. Hursthouse, M. E. Light and P. A. Gale, *Chem. Eur. J.*, 2008, **14**, 10236-10243
302. P. A. Gale, J. R. Hiscock, N. Lalaoui, M. E. Light, N. J. Wells and M. Wenzel, *Org. Biomol. Chem.*, 2012, Advance Article, DOI: 10.1039/C1OB06800H
303. J. R. Hiscock, C. Caltagirone, M. E. Light, M. B. Hursthouse and P. A. Gale, *Org. Biomol. Chem.*, 2009, **7**, 1781-1783
304. J. R. Hiscock, P. A. Gale, C. Caltagirone, M. B. Hursthouse and M. E. Light, *Supramol. Chem.*, 2010, **22**, 647-652
305. P. R. Edwards, J. R. Hiscock and P. A. Gale, *Tetrahedron Lett.*, 2009, **50**, 4922-4924
306. P. R. Edwards, J. R. Hiscock, P. A. Gale and M. E. Light, *Org. Biomol. Chem.*, 2010, **8**, 100-106
307. M. Arunachalam and P. Ghosh, *Chem. Commun.*, 2009, 5389-5391
308. M. Arunachalam and P. Ghosh, *Inorg. Chem.*, 2010, **49**, 943-951
309. P. Mateus, R. Delgado, P. Brandão, S. Carvalho and V. Félix, *Org. Biomol. Chem.*, 2009, **7**, 4661-4673
310. G. V. Zyryanov, M. A. Palacios and P. Anzenbacher, Jr., *Angew. Chem. Int. Ed.*, 2007, **46**, 7849-7852
311. C. M. G. dos Santos, E. M. Boyle, S. De Solis, P. E. Kruger and T. Gunnlaugsson, *Chem. Commun.*, 2011, **47**, 12176-12178
312. I. Ravikumar and P. Ghosh, *Chem. Commun.*, 2010, **46**, 6741-6743
313. P. G. Young and K. A. Jolliffe, *Org. Biomol. Chem.*, 2012, **10**, 2664-2672
314. M. de Loos, A. G. J. Ligtenbarg, J. van Esch, H. Kooijman, A. L. Spek, R. Hage, R. M. Kellogg and B. L. Feringa, *Eur. J. Org. Chem.*, 2000, 3675-3678
315. A. Danby, L. Seib, N. W. Alcock and K. Bowman-James, *Chem. Commun.*, 2000, 973-974
316. K. J. Winstanley, S. J. Allen and D. K. Smith, *Chem. Commun.*, 2009, 4299-4301
317. I. Ravikumar, P. S. Lakshminarayanan and P. Ghosh, *Inorg. Chim. Acta*, 2010, **363**, 2886-2895
318. C. Raposo, M. Almaraz, M. Martín, V. Weinrich, L. Mussóns, V. Alcázar, C. Caballero and J. R. Morán, *Chem. Lett.*, 1995, **9**, 759-760
319. F. Werner and H. -J. Schneider, *Helv. Chim. Acta*, 2000, **83**, 465-478
320. M. J. Berrocal, A. Cruz, I. H. A. Badr and L. G. Bachas, *Anal. Chem.*, 2000, **72**, 5295-5299

321. P. S. Lakshminarayanan, I. Ravikumar, E. Suresh, and P. Ghosh, *Inorg. Chem.*, 2007, **46**, 4769-4771
322. P. Bose, I. Ravikumar and P. Ghosh, *Inorg. Chem.*, 2011, **50**, 10693-10702
323. P. S. Lakshminarayanan, I. Ravikumar, E. Suresh and P. Ghosh, *Chem. Commun.*, 2007, 5214-5216
324. I. Ravikumar, P. S. Lakshminarayanan, M. Arunachalam, E. Suresh and P. Ghosh, *Dalton Trans.*, 2009, **21**, 4160-4168
325. I. Ravikumar and P. Ghosh, *Chem. Commun.*, 2010, **46**, 1082-1084
326. R. Custelcean, P. Remy, P. V. Bonnesen, D. Jiang and B. A. Moyer, *Angew. Chem. Int. Ed.*, 2008, **47**, 1866-1870
327. B. Wu, J. Liang, J. Yang, C. Jia, X. -J. Yang, H. Zhang, N. Tang and C. Janiak, *Chem. Commun.*, 2008, 1762-1764
328. F. Zhuge, B. Wu, J. Liang, J. Yang, Y. Liu, C. Jia, C. Janiak, N. Tang and X. -J. Yang, *Inorg. Chem.*, 2009, **48**, 10249-10256
329. R. Custelcean, A. Bock and B. A. Moyer, *J. Am. Chem. Soc.*, 2010, **132**, 7177-7185
330. R. Custelcean, B. A. Moyer and B. P. Hay, *Chem. Commun.*, 2005, 5971-5973
331. Y. Li, K. M. Mullen, T. D. W. Claridge, P. J. Costa, V. Felix and P. D. Beer, *Chem. Commun.*, 2009, 7134-7136
332. D. A. Jose, D. K. Kumar, B. Ganguly and A. Das, *Inorg. Chem.*, 2007, **46**, 5817-5819
333. S. K. Dey and G. Das, *Dalton Trans.*, 2011, **40**, 12048-12051
334. K. J. Bell, A. N. Westra, R. J. Warr, J. Chartres, R. Ellis, C. C. Tong, A. J. Blake, P. A. Tasker and M. Schröder, *Angew. Chem. Int. Ed.*, 2008, **47**, 1745-1748
335. R. J. Warr, A. N. Westra, K. J. Bell, J. Chartres, R. Ellis, C. C. Tong, T. G. Simmance, A. Gadzhieva, A. J. Blake, P. A. Tasker and M. Schröder, *Chem. Eur. J.*, 2009, **15**, 4836-4850
336. R. J. Fitzmaurice, F. Gaggini, N. Srinivasan and J. D. Kilburn, *Org. Biomol. Chem.*, 2007, **5**, 1706-1714
337. D. E. Gross, V. Mikkilneni, V. M. Lynch and J. L. Sessler, *Supramol. Chem.*, 2010, **22**, 135-141
338. F. Bigi, R. Maggi and G. Sartori, *Green Chem.*, 2000, **2**, 140-148
339. K. Hirose, *J. Incl. Phenom. Macro.*, 2001, **39**, 193-209
340. M. J. Hynes, *J. Chem. Soc., Dalton Trans.*, 1993, 311-312
341. D. Makuc, J. R. Hiscock, M. E. Light, P. A. Gale and J. Plavec, *Bellstein J. Org. Chem.*, 2011, **7**, 1205-1214
342. P. A. Gale, J. R. Hiscock, S. J. Moore, C. Caltagirone, M. B. Hursthouse and M. E. Light, *Chem. Asian J.*, 2010, **5**, 555-561
343. M. Wenzel, K. Gloe, K. Gloe, G. Bernhard, J. K. Clegg, X. -K. Ji and L. F. Lindoy, *New. J. Chem.*, 2008, **32**, 132-137
344. K. -S. Jeong, K. -M. Hahn and Y. L. Cho, *Tetrahedron Lett.*, 1998, **39**, 3779-3782
345. D. Zielinska, A. Gil, M. Pietraszkiewicz, O. Pietraszkiewicz, D. Van der Vijver and L. J. Nagens, *Anal. Chim. Acta*, 2004, **523**, 177-184
346. T. Tarantelli and B. Chiari, *J. Inorg. Nucl. Chem.*, 1975, **37**, 2291-2295

347. N. Busschaert, P. A. Gale, C. J. E. Haynes, M. E. Light, S. J. Moore, C. C. Tong, J. T. Davis and W. A. Harrell Jr., *Chem. Commun.*, 2010, **46**, 6252-6254
348. V. Amendola, L. Fabbrizzi and L. Mosca, *Chem. Soc. Rev.*, 2010, **39**, 3889-3915
349. A. -F. Li, J. -H. Wang, F. Wang and Y. -B. Jiang, *Chem. Soc. Rev.*, 2010, **39**, 3729-3745
350. F. M. Pfeffer, K. F. Lim and K. J. Sedgwick, *Org. Biomol. Chem.*, 2007, **5**, 1795-1799
351. G. W. Bates, Triyanti, M. E. Light, M. Albrecht and P. A. Gale, *J. Org. Chem.*, 2007, **72**, 8921-8927
352. D. Makuc, M. Lenarcic, G. W. Bates, P. A. Gale and J. Plavec, *Org. Biomol. Chem.*, 2009, **7**, 3505-3511
353. D. Makuc, M. Albrecht and J. Plavec, *Supramol. Chem.*, 2010, **22**, 603-611
354. M. Stocks, L. Alcaraz and E. Griffen, *On Chemistry - 4. On Medicinal Chemistry*, 2007, Sci-Ink Limited, Brackley
355. M. P. Gleeson, *J. Med. Chem.*, 2008, **51**, 817-834
356. C. A. Lipinski, F. Lombardo, B. W. Dominy and P. J. Feeney, *Adv. Drug Deliver. Rev.*, 1997, **23**, 3-25
357. D. F. Veber, S. R. Johnson, H. -Y. Cheng, B. R. Smith, K. W. Ward and K. D. Kopple, *J. Med. Chem.*, 2002, **45**, 2615-2623
358. T. Hayashita, T. Onodera, R. Kato, S. Nishizawa and N. Teramae, *Chem. Commun.*, 2000, 755-756
359. E. H. Kerns and L. Di, *Drug-like properties: concepts, structure design and methods*, 2008, Academic Press, Amsterdam
360. V. Saggiomo, S. Otto, I. Marques, V. Félix, T. Torroba and R. Quesada, *Chem. Commun.*, 2012, **48**, 5274-5276
361. M. Wenzel, M. E. Light, A. P. Davis and P. A. Gale, *Chem. Commun.*, 2011, **47**, 7641-7643
362. P. B. Smith and C. Crespi, *Biochem. Pharmacol.*, 2002, **63**, 1941-1948
363. R. C. A. Onderwater, J. N. M. Commandeur, E. J. Groot, A. Sitters, W. M. P. B. Menge and N. P. E. Vermeulen, *Toxicity*, 1998, **125**, 117-129
364. S. A. Svarovsky, R. H. Simoyi and S. V. Makarov, *J. Phys. Chem. B*, 2001, **105**, 12634-12643
365. P. A. Gale, C. C. Tong, C. J. E. Haynes, O. Adeosun, D. E. Gross, E. Karnas, E. M. Sedenberg, R. Quesada and J. L. Sessler, *J. Am. Chem. Soc.*, 2010, **132**, 3240-3241
366. P. Anzenbacher, Jr., A. C. Try, H. Miyaji, K. Jursíková, V. M. Lynch, M. Marquez and J. L. Sessler, *J. Am. Chem. Soc.*, 2000, **122**, 10268-10272
367. C. C. Tong, R. Quesada, J. L. Sessler, and P. A. Gale, *Chem. Commun.*, 2008, 6321-6323
368. A. V. Jentzsch, D. Emery, J. Mareda, S. K. Nayak, P. Metrangolo, G. Resnati, N. Sakai and S. Matile, *Nat. Commun.*, 2012, **3**,DOI:10.1038/ncomms1902
369. N. Busschaert, I. L. Kirby, S. Young, S. J. Coles, P. N. Horton, M. E. Light and P. A. Gale, *Angew. Chem.*, 2012, **124**, 4502-4506
370. D. Makuc, Triyanti, M. Albrecht, J. Pavec, K. Rissanen, A. Valkonen, and C. A. Schalley, *Eur. J. Org. Chem.*, 2009, 4854-4866

371. N.J. Andrews, C. J. E. Haynes, M. E. Light, S. J. Moore, C. C. Tong, J. T. Davis, W. A. Harrell Jr. and P. A. Gale, *Chem. Sci.*, 2011, **2**, 256-260
372. M. C. Stumpe and H. Grubmüller, *J. Phys. Chem. B*, 2007, **111**, 6220-6228
373. M. Obrzud, M. Rospenk and A. Koll, *J. Phys. Chem. B*, 2010, **14**, 15905-15912
374. J. W. Steed, *Chem. Soc. Rev.*, 2010, **39**, 3686-3699
375. S. A. Wildman and G. M. Crippen, *Chem. Inf. Comput. Sci.*, 1999, **39**, 868-873
376. P. Ertl, B. Rhode and P. Selzer, *J. Med. Chem.*, 2000, **43**, 3714-3737
377. Fieldview Version 2.0.2 for Macintosh, Cresset, 2011
378. S. Purser, P. R. Moore, S. Swallow and V. Gouverneur, *Chem. Soc. Rev.*, 2008, **37**, 320-330
379. B. E. Smart, *J. Fluorine Chem.*, 2001, **109**, 3-11
380. W. K. Hagmann, *J. Med. Chem.*, 2008, **51**, 4359-4369
381. H. -J. Böhm, D. Banner, S. Bendels, M. Kamsy, B. Kuhn, K. Müller, U. Obst-Sander and M. Stahl, *ChemBioChem*, 2004, **5**, 637-643
382. P. Shah and A. D. Westwell, *J. Enzym. Inhib. Med. Ch.*, 2007, **22**, 527-540
383. V. Amendola, M. Boiocchi, B. Colasson and L. Fabbrizzi, *Inorg. Chem.*, 2006, **45**, 6138-6147
384. A. K. Ghose, V.N. Viswanadhan and J.J. Wendoloski. *J. Combin. Chem.* 1999, **1**, 55-68
385. A. L. Rodriguez, C. Koradin, W. Dohle and P. Knochel, *Angew. Chem. Int. Ed.*, 2000, **39**, 2488-2490
386. C. Koradin, W. Dohle, A. L. Rodriquez, B. Schmid and P. Knochel, *Tetrahedron*, 2003, **59**, 1571-1587
387. F. Shi, Y. Deng, T. SiMa and H. Yang, *Tetrahedron Lett.*, 2001, **42**, 2161-2163
388. F. Shi, Q. Zhang, Y. Gu and Y. Deng, *Adv. Synth. Catal.*, 2005, **347**, 225-230
389. P. Adams, 1964, U.S. Patent No. 3,161,676
390. A. Barnard, S. J. Dickson, M. J. Paterson, A. M. Todd and J. W. Steed, *Org. Biomol. Chem.*, 2009, **7**, 1554-1561
391. P. Ballester and G. Gil-Ramírez, *Proc. Natl. Acad. Sci. U. S. A.*, 2009, **106**, 10455-10459
392. K. D. Shimizu and J. Rebek, Jr., *Proc. Natl. Acad. Sci. U. S. A.*, 1995, **92**, 12403-12407
393. M. Alajarín, A. Pastor, R.-Á. Orenes and J. W. Steed, *J. Org. Chem.*, 2002, **67**, 7091-7095
394. M. George, G. Tan, V. T. John and R. G. Weiss, *Chem. Eur. J.*, 2005, **11**, 3243-3254
395. L. Pauling, *J. Am. Chem. Soc.*, 1932, **54**, 3570-3582
396. F. G. Bordwell, *Acc. Chem. Res.*, 1988, **21**, 456-463
397. D. E. Gómez, L. Fabbrizzi, M. Licchelli and E. Monzani, *Org. Biomol. Chem.*, 2005, **3**, 1495-1500
398. V. S. Bryantsev, T. K. Firman and B. P. Hay, *J. Phys. Chem. A*, 2005, **109**, 832-842
399. V. S. Bryantsev and B. P. Hay, *J. Phys. Chem. A*, 2006, **110**, 4678-4688
400. W. W. Cleland, T. J. Andrews, S. Gutteridge, F. C. Hartman and G. H. Lorimer, *Chem. Rev.*, 1998, **98**, 549-561

401. R. D. Vaughan-Jones, K. W. Spitzer and P. Swietach, *J. Mol. Cell. Cardiol.*, 2009, **46**, 318-331
402. O. Murillo, I. Suzuki, E. Abel, C. L. Murray, E. S. Meadows, T. Jin and G. W. Gokel, *J. Am. Chem. Soc.*, 1997, **119**, 5540-5549
403. M. F. McCarty and J. Whitaker, *Altern. Med. Rev.*, 2010, **15**, 264-272
404. I. H. Madshus, *Biochem. J.*, 1988, **250**, 1-8
405. A. C. Allison and M. R. Young, *Lysosomes in Biology and Pathology, Vol. 2.*, 1969, North-Holland Publishing Co., Amsterdam
406. M. Yamagate and I. F. Tannock, *Br. J. Cancer*, 1996, **73**, 1328-1334
407. S. J. Moore, M. G. Fisher, M. Yano, C. C. Tong and P. A. Gale, *Dalton Trans.*, 2011, **40**, 12017-12020
408. J. F. Kerr, A. H. Wyllie and A. R. Currie, *Br. J. Cancer*, 1972, **26**, 239-257
409. A. De Milito, E. Lessi, M. Logozzi, F. Lozupone, M. Spada, M. L. Marino, C. Federici, M. Perdicchio, P. Matarrese, L. Lugini, A. Nilsson and S. Fais, *Cancer Res.*, 2007, **67**, 5408-5417
410. S. Bahmanjah, N. Zhang and J. T. Davis, *Chem. Commun.*, 2012, **48**, 4432-4434
411. G. Godeau, H. Arnion, C. Brun, C. Staedel and P. Barthélémy, *Med. Chem. Commun.*, 2010, **1**, 76-78
412. L. Dafik, V. Kalsani, A. K. L. Leung and K. Kumar, *J. Am. Chem. Soc.*, 2009, **131**, 12091-12093
413. M. -O. M. Piepenbrock, G. O. Lloyd, N. Clarke and J. W. Steed, *Chem. Commun.*, 2008, 2644-2646
414. G. O. Lloyd, M.-O. M. Piepenbrock, J. A. Foster, N. Clarke and J. W. Steed, *Soft Matter*, 2012, **8**, 204-216
415. E. J. Cho, J. W. Moon, S. W. Ko, J. Y. Lee, S. K. Kim, J. Yoon and K. C. Nam, *J. Am. Chem. Soc.*, 2003, **125**, 12376-12377
416. H. Yang, T. Yi, Z. Zhou, Y. Zhou, J. Wu, M. Xu, F. Li and C. Huang, *Langmuir*, 2007, **23**, 8224-8230
417. C. Wang, D. Zhang and D. Zhu, *Langmuir*, 2007, **23**, 1478-1482
418. M. Formica, V. Fusi. E. Macedi, P. Paoli, G. Piersanti, P. Rossi, G. Zappia and P. Orlando, *New J. Chem.*, 2008, **32**, 1204-1214
419. C. N. Carroll, O. B. Berryman, C. A. Johnson, L. N. Zakharov, M. M. Haley and D. W. Johnson, *Chem. Commun.*, 2009, 2520-2522
420. J. Shao, H. Lin, X. -F. Shang, H. -M. Chen and H. -K. Lin, *J. Incl. Phenom. Macrocycl. Chem.*, 2007, **59**, 371-375
421. T. D. Thangadurai, N. J. Singh, I. -C. Hwang, J. W. Lee, R. P. Chandran and K. S. Kim, *J. Org. Chem.*, 2007, **72**, 5461-5464
422. R. Breslow, *Artificial Enzymes*, 2005, Weinheim, Wiley-VCH
423. E. Fan, S. A. Van Arman, S. Kincaid and A. D. Hamilton, *J. Am. Chem. Soc.*, 1993, **115**, 369-370
424. S. Nishizawa, P. Bühlmann, M. Iwao and Y. Umezawa, *Tetrahedron Lett.*, 1995, **36**, 6483-6486
425. J. N. Babu, V. Bhalla, M. Kumar, R. K. Puri and R. K. Mahajan, *New. J. Chem.*, 2009, **33**, 675-681
426. A. N. Swinburne, M. J. Paterson, A. Beeby and J. W. Steed, *Chem. Eur. J.*, 2010, **16**, 2714-2718

427. C. Mendoza, J. Benet-Buchholz, M. A. Pericás and R. Vilar, *Dalton Trans.*, 2009, 2974-2985
428. S. J. Brooks, P. A. Gale and M. E. Light, *Chem. Commun.*, 2005, 4696-4698
429. S. J. Brooks, P. R. Edwards, P. A. Gale and M. E. Light, *New J. Chem.*, 2006, **30**, 65-70
430. S. J. Brooks, P. A. Gale and M. E. Light, *CrystEngComm*, 2005, **7**, 586-591
431. C. Bied, J. J. E. Moreau and M. W. C. Man, *Tetrahedron Asymmetr.*, 2001, **12**, 329-336
432. E. G. Klauber, C. K. De, T. K. Shah and D. Seidel, *J. Am. Chem. Soc.*, 2010, **132**, 13624-13626
433. J. van Esch, F. Schoonbeek, M. de Loos, H. Kooijman, A. L. Spek, R. M. Kellogg and B. L. Feringa, *Chem. Eur. J.*, 1999, **5**, 937-950
434. Y. –J. Kim, H. Kwak, S. J. Lee, J. S. Lee, H. J. Kwon, S. H. Nam, K. Lee and C. Kim, *Tetrahedron*, 2006, **62**, 9635-9640
435. D. A. Jose, D. K. Kumar, B. Ganguly and A. Das, *Tetrahedron Lett.*, 2005, **46**, 5343-5346
436. H. Yang, Z. -G. Zhou, J. Xu, F. -Y. Li, T. Yi and C. -H. Huang, *Tetrahedron*, 2007, **63**, 6732-6736
437. M. O. Odago, D. M. Colabello and A. J. Lees, *Tetrahedron*, 2010, **66**, 7465-7471
438. V. Amendola, M. Boiocchi, D. Esteban-Gómez, L. Fabbrizzi and E. Monzani, *Org. Biomol. Chem.*, 2005, **3**, 2632-2639
439. S. J. Brooks, P. A. Gale and M. E. Light, *Supramol. Chem.*, 2007, **19**, 9-15
440. C. Jia, B. Wu, S. Li, Z. Yang, Q. Zhao, J. Liang, Q. -S. Li and X. -J. Yang, *Chem. Commun.*, 2010, **46**, 5376-5378
441. C. Jia, B. Wu, S. Li, X. Huang and X. -J. Yang, *Org. Lett.*, 2010, **12**, 5612-5615
442. S. Li, M. Wei, X. Huang, X. -J. Yang and B. Wu, *Chem. Commun.*, 2012, **48**, 3097-3099
443. C. Jia, B. Wu, S. Li, X. Huang, Q. Zhao, Q. -S. Li and X. -J. Yang, *Angew. Chem. Int. Ed.*, 2011, **50**, 486-490
444. S. J. Brooks, S. E. García-Garrido, M. E. Light, P. A. Cole and P. A. Gale, *Chem. Eur. J.*, 2007, **13**, 3320-3329
445. S. J. Brooks, P. A. Gale and M. E. Light, *Chem. Commun.*, 2006, 4344-4346
446. H. Rahaman, A. Madarász, I. Pápai and P. M. Pihko, *Angew. Chem. Int. Ed.*, 2011, **50**, 6123-6127
447. S. N. Gavade, R. S. Balaskar, M. S. Mane, P. N. Pabrekar, M. S. Shingare and D. V. Mane, *Chinese Chem. Lett.*, 2011, **22**, 675-678
448. B. J. Kotecki, D. P. Fernando, A. R. Height and K. A. Lukin, *Org. Lett.*, 2009, **11**, 947-950
449. M. Miyahara, *Chem. Pharm. Bull.*, 1986, **34**, 1950-1960
450. G. A. Artamkina, A. G. Sergeev and I. P. Beletskaya, *Tetrahedron Lett.*, 2001, **42**, 4381-4384
451. G. A. Artamkina, A. G. Sergeev and I. P. Beletskaya, *Russ. J. Org. Chem.*, 2002, **38**, 538-545
452. Y. Ge, L. Miller, T. Ouimet and D. K. Smith, *J. Org. Chem.*, 2000, **65**, 8831-8838
453. J. Scheele, P. Timmerman and D. N. Reinhoudt, *Chem. Commun.*, 1998, 2613-2614

454. H. Iwamura, T. Fujita, S. Koyama, K. Koshimizu and Z. Kumazawa, *Phytochemistry*, 1980, **19**, 1309-1319
455. M. Bonizzoni, L. Fabbrizzi, A. Taglietti and F. Tiengo, *Eur. J. Org. Chem.*, 2006, 3567-3574
456. V. Amendola, D. Esteban-Gómez, L. Fabbrizzi and M. Licchelli, *Acc. Chem. Res.*, 2006, **39**, 343-353
457. S. E. García-Garrido, C. Caltagirone, M. E. Light and P. A. Gale, *Chem. Commun.*, 2007, 1450-1452
458. M. Boiocchi, L. Del Boca, D. Esteban-Gómez, L. Fabbrizzi, M. Licchelli and E. Monzani, *Chem. Eur. J.*, 2005, **11**, 3097-3104
459. D. Esteban-Gómez, L. Fabbrizzi and M. Licchelli, *J. Org. Chem.*, 2005, **70**, 5717-5720
460. Y. Shao, B. Linton, A. D. Hamilton and S. G. Weber, *J. Electroanal. Chem.*, 1998, **441**, 33-37
461. E. N. Kitova, A. El-Hawiet, P. D. Schnier and J. S. Klassen, *J. Am. Soc. Mass Spectrom.*, 2012, **23**, 431-441
462. L. Jaquillard, F. Saab, F. Schoentgen and M. Cadene, *J. Am. Soc. Mass. Spectrom.*, 2012, **23**, 908-922
463. M. G. Fisher, P. A. Gale, J. R. Hiscock, M. B. Hursthouse, M. E. Light, F. P. Schmidtchen and C. C. Tong, *Chem. Commun.*, 2009, 3017-3019
464. M. Yano, C. C. Tong, M. E. Light, F. P. Schmidtchen and P. A. Gale, *Org. Biomol. Chem.*, 2010, **8**, 4356-4363
465. C. Kirby, J. Clarke and G. Gregoriadis, *Biochem. J.*, 1980, **186**, 591-598
466. D. H. McDaniel and H. C. Brown, *J. Org. Chem.*, 1958, **23**, 420-427
467. R. J. Fitzmaurice, G. M. Kyne, D. Douheret and J. D. Kilburn, *J. Chem. Soc., Perkin Trans. 1*, 2002, 841-864
468. S. Piyaauksornsak, T. Tangthongkul, R. Wanbayor, B. Wanno and V. Ruangpornvisuti, *Struct. Chem.*, 2009, **20**, 767-780
469. K. -S. Jeong, J. W. Park and Y. L. Cho, *Tetrahedron Lett.*, 1996, **37**, 2795-2798
470. A. J. Lowe and F. M. Pfeffer, *Org. Biomol. Chem.*, 2009, **7**, 4233-4240
471. F. Sancenón, R. Martínez-Máñez, M. A. Miranda, M. –J. Seguí, and J. Soto, *Angew. Chem. Int. Ed.*, 2003, **42**, 647-650
472. S. L. Wiskur, P. N. Floriano, E. V. Anslyn and J. T. McDevitt, *Angew. Chem.*, 2003, **115**, 2116-2118
473. A. Bencini, A. Bianchi, M. I. Burguete, P. Dapporto, A. Doménech, E. Garcia-España, S. V. Luis, P. Paoli and J. A. Ramírez, *J. Chem. Soc. Perkin Trans. 2*, 1994, 569-577
474. J. -H. Yi and A. S. Hazell, *Neurochem. Int.*, 2006, **48**, 394-403
475. G. Tian, L. Lai, H. Guo, Y. Lin, M. E. R. Butchbach, Y. Chang and C. G. Lin, *J. Biol. Chem.*, 2007, **282**, 1727-1737
476. R. E. McCullumsmith and J. H. Meador-Woodruff, *Neuropsychopharmacol.*, 2002, **26**, 368-375
477. B. T. Hyman, G. W. Van Hoesen and A. R. Damasio, *Ann. Neurol.*, 1987, **22**, 37-40
478. E. Foran and D. Trotti, *Antioxid. Redox. Signal.*, 2009, **11**, 1587-1602
479. W. Masliah, L. Hansen, M. Alford, R. Deteresa and M. Mallory, *Ann. Neurol.*,

1996, **40**, 759-766
480. S. Li, M. Mallory, M. Alford, S. Tanaka and E. Masliah, J. Neuropath. *Exp. Neur.*, 1997, **56**, 901-911
481. P. F. Behrens, P. Franz, B. Woodman, K. S. Lindenberg and G. B. Landwehrmeyer, *Brain*, 2002, **125**, 1908-1922
482. A. Plaitakis, S. Berl and M. D. Yahr, *Ann. Neurol.*, 1984, **15**, 144-153
483. J. W. Olney, *Neurotoxicology*, 1994, **15**, 535-544
484. S. R. Marengo and A. M. P. Romani, *Nat. Clin. Pract. Nephrol.*,2008, **4**, 368-377
485. J. S. Clark, D. H. Vandrope, M. N. Chernova, J. F. Heneghan, A. K. Stewart and S. L. Alper, *J. Physiol.*, 2008, **586**, 1291-1306
486. S. -M. Kuo and P. S. Aronson, *J. Biol. Chem.*, 1988, **263**, 9710-9717
487. Y. -P. Tseng, G. -M. Tu, C. -H. Lin, C. -T. Chang, C. -Y. Lin and Y. -P. Yen, *Org. Biomol. Chem.*, 2007, **5**, 3592-3598
488. Y. -P. Yen and K. -W. Ho, *Tetrahedron Lett.*, 2006, **47**, 7357-7361
489. M. B. Jiménez, V. Alcázar, R. Peláez, F. Sanz, Á. L. Fuentes de Arriba and M. C. Caballero, *Org. Biomol. Chem.*, 2012, **10**, 1181-1185
490. S. Goswami, N. K. Das, D. Sen, G. Hazra, J. H. Goh, Y. C. Sing and H. -K. Fun, *New J. Chem*., 2011, **35**, 2811-2819
491. J. C. Kim, A. J. Lough, H. Park and Y. C. Kang, *Inorg. Chem. Commun.*, 2006, **9**, 514-517
492. A. M. Costero, M. Colera, P. Gaviña and S. Gil, *Chem. Commun.*, 2006, 761-763
493. H. A. Krebs, *The Citric Acid Cycle*, Nobel Lecture, 1953
494. S. Eiam-ong, M. Spohn, N. A. Kurtzman and S. Sabatini, *Kidney Int.*, 1995, **48**, 1542-1548
495. A. Gougoux, G. Lemieux and N. Lavoie, *Am. J. Physiol.*, 1976, **231**, 1010-1017
496. C. M. Michuda and M. Martinez-Carrion, *J. Biol. Chem.*, 1970, **245**, 262-269
497. D. R. Lide, *CRC Handbook of Chemistry and Physics 89th Edition*, 2008, CRC Press, Boca Raton
498. A. R. Cardoso, B. B. Queliconi, and A. J. Kowaltowski, *Biochim. Biophys. Acta*, 2010, **1797**, 832-838
499. M. M. G. Antonisse and D. N. Reinhoudt, *Chem. Commun.*, 1998, 443-448
500. G. J. Kirkovits, J. A. Shriver, P. A. Gal, and J. L. Sessler, *J. Incl. Phenom. Macro.*, 2001, **41**, 69-75
501. G. Cafeo, G. Gattuso, F. H. Kohnke, A. Notti, S. Occhipinti, S. Pappalardo and M. F. Parisi, *Angew. Chem. Int. Ed.*, 2002, **41**, 2122-2126
502. S. Roelens, A. Vacca, O. Franceson and C. Venturi, *Chem. Eur. J.*, 2009, **15**, 8296-8302
503. M. T. Reetz, J. Huff, J. Rudolph, K. Töllner, A. Deege and R. Goddard, *J. Am. Chem. Soc.*, 1994, **116**, 11588-11589
504. A. Aydogan, D. J. Coady, S. K. Kim, A. Akar, C. W. Beilawski, M. Marquez and J. L. Sessler, *Angew. Chem. Int. Ed.*, 2008, **47**, 9648-9652
505. L. A. J. Chrisstoffels, F. de Jong, D. N. Reinhoudt, S. Sivelli, L. Gazzola, A. Casnati and R. Ungaro, *J. Am. Chem. Soc.*, 1999, **121**, 10142-10151
506. H. C. Visser, D. M. Rudkevich, W. Verboom, F. de Jong and D. N. Reinhoudt, *J. Am. Chem. Soc.*, 1994, **116**, 11554-11555

507. D. G. Clark, T. F. McElligott and E. Weston Hurst, *Brit. J. Indust. Med.*, 1966, **23**, 126-132
508. G. Cafeo, C. Gargiulli, G. Gattuso, F. H. Kohnke, A. Notti, S. Occhipinti, S. Pappalardo and M. F. Parisi, *Tetrahedron Lett.*, 2002, **43**, 8103-8106
509. K. Kavallieratos, R. A. Sachleben, G. J. Van Berkel and B. A., Moyer, *Chem. Commun.*, 2000, 187-188
510. K. Kavallieratos, A. Danby, G. J. Van Berkel, M. A. Kelly, R. A. Sachleben, B. A. Moyer and K. Bowman-James, *Anal. Chem.*, 2000, **72**, 5258-5264
511. I. Ravikumar, S. Saha and P. Ghosh, *Chem. Commun.*, 2011, **47**, 4721-4723
512. B. M. Tulk, P. H. Schlesinger, S. A. Kapadia and J. C. Edwards, *J. Biol. Chem.*, 2000, **275**, 26986-26993
513. A. Yamaguchi and Y. Anraku, *Biochim. Biophys. Acta*, 1978, **501**, 136-149
514. V. N. Orlov, Y. N. Antonenko, A. A. Bulychev and L. S. Yaguzhinsky, *FEBS Lett.*, 1994, **345**, 104-106
515. B. S. Prabhananda and M. H. Kombrabail, *Biochim. Biophys. Acta*, 1996, **1282**, 193-199
516. J. Hudson, A. E. G. Cass and B. S. Prabhananda, *Phys. Chem. Chem. Phys.*, 2002, **4**, 2072-2707
517. A. Lerner, R. Shnaiderman and Y. Avi-Dor, *FEBS Lett.*, 1982, **146**, 9-12
518. G. Krishnamoorthy, *FEBS Lett.*, 1988, **232**, 199-203
519. T. J. Marrone and K. M. Merz, Jr., *J. Am. Chem. Soc.*, 1995, **117**, 779-791
520. M. Hillar, *Arch. Int. Phys. Bioch.*, 1978, **86**, 227-233
521. B. C. Pressman, E. J. Harris, W. S. Jagger and J. H. Johnson, *Proc. Nat. Acad. Sci. U. S. A.*, 1967, **58**, 1949-1956
522. L. Becucci, M. R. Moncelli, R. Naumann and R. Guidelli, *J. Am. Chem. Soc.*, 2005, **127**, 13316-13323
523. S. B. Hladky, J. C. H. Leung and W. J. Fitzgerald, *Biophys. J.*, 1995, **69**, 1758-1772
524. S. Krasne, G. Eisenman and G. Szabo, *Science*, 1971, **174**, 412-415
525. R. M. Izatt, J. S. Bradshaw, S. A. Nielsen, J. D. Lamb and J. J. Christensen, *Chem. Rev.*, 1985, **85**, 271-339
526. P. A. Gale, J. L. Sessler, V. Král, and V. Lynch, *J. Am. Chem. Soc.*, 1996, **118**, 5140-5141
527. P. A. Gale, J. L. Sessler, and V. Král, *Chem. Commun.*, 1998, 1-8
528. R. Custelcean, L. H. Delmau, B. A. Moyer, J. L. Sessler, W. -S. Cho, D. Gross, G. W. Bates, S. J. Brooks, M. E. Light, and P. A. Gale, *Angew. Chem. Int. Ed.*, 2005, **44**, 2537-2542
529. C. -H. Lee, H. Mijaji, D. -W. Yoon and J. L. Sessler, *Chem. Commun.*, 2008, 24-34
530. I. -W. Park, J. Yoo, B. Kim, S. Adhikari, S. K. Kim, Y. Yeon, C. J. E. Haynes, J. L. Sutton, C. C. Tong, V. M. Lynch, J. L. Sessler, P. A. Gale and C. –H. Lee, *Chem. Eur. J.*, 2012, **18**, 2514-2523
531. K. D. Legg and D. M. Hercues, *J. Phys. Chem.*, 1970, **74**, 2114-2118
532. M. Mally, J. Majhenc, S. Svetina and B. Zeks, *Biochim. Biophys. Acta*, 2007, **1768**, 1179-1189

533. R. Smith, F. Separovic, T. J. Milne, A. Whittaker, F. M. Bennett, B. A. Cornell and A. Makriyannis, *J. Mol. Biol.*, 1994, **241**, 456-466
534. M. C. McGahan, R. L. Hazard and P. J. Bentley, *Comp. Biochem. Physiol. C*, 1985, **82**, 291-296
535. S. J. Moore, M. G. Fisher, M. Yano, C. C. Tong and P. A. Gale, *Chem. Commun.*, 2011, **47**, 689-691
536. J. L. Sessler unpublished results
537. H. -T. Yu, W. J. Colucci, M. L. McLaughlin and M. D. Barkley, *J. Am. Chem. Soc.*, 1992, **114**, 8449-8454
538. S. Ozaki, K. Kano and O. Shirai, *Phys. Chem. Chem. Phys.*, 2008, **10**, 4449-4455
539. P. Job, *Annali di Chimica Applicata*, 1928, **9**, 113-203

Appendix 1

Amino Acid Codes

List of the 20 common amino acid groups found in proteins, shown in the ionised forms that exist at pH 7. The three letter abbreviations are listed alongside the relevant structure.[17]

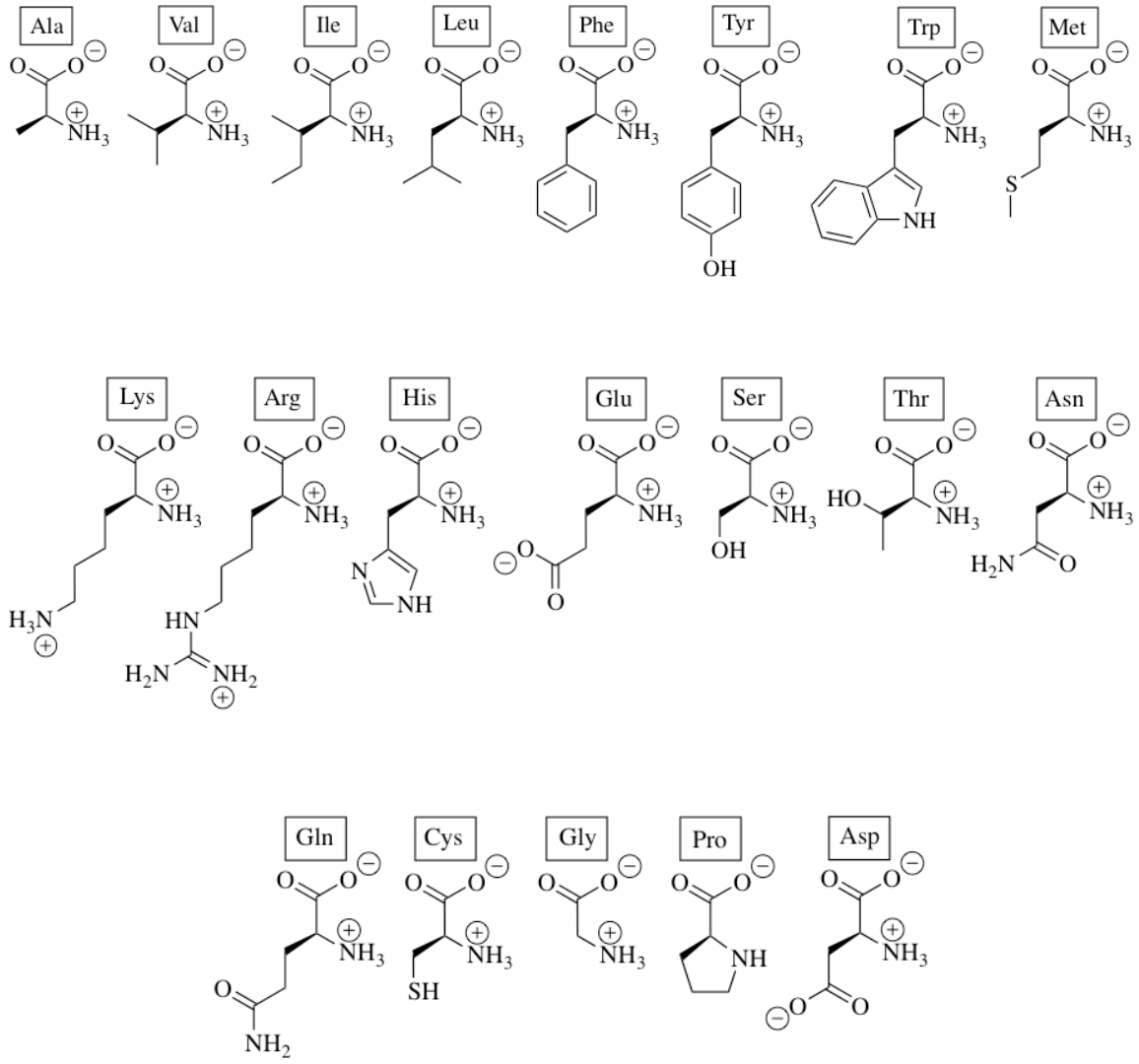
Ala
Val
Ile
Leu
Phe
Tyr
Trp
Met
Lys
Arg
His
Glu
Ser
Thr
Asn
Gln
Cys
Gly
Pro
Asp

Amino Acid	Three Letter Code	Single Letter Code
Alanine	Ala	A
Valine	Val	V
Isoleucine	Ile	I
Leucine	Leu	L
Phenylalanine	Phe	F
Tyrosine	Tyr	Y
Tryptophan	Trp	W
Methionine	Met	M
Lysine	Lys	K
Arginine	Arg	R
Histidine	His	H
Glutamic acid	Glu	E
Serine	Ser	S
Threonine	Thr	T
Asparagine	Asn	N
Glutamine	Gln	Q
Cysteine	Cys	C
Glycine	Gly	G
Proline	Pro	P
Aspartic acid	Asp	D

Appendix 2

^{1}H NMR Titration Data

The stability constants for receptor molecules with various anions were determined by ^{1}H NMR titration with the relevant anion (added as either the TBA or TEA salt) in either 0.5 % H_2O/DMSO-d_6 or 10 % H_2O/DMSO-d_6 at 298 K. The data was fitted to a suitable binding model using WinEQNMR2.[340] In addition, selected Job plot analyses, graphs depicting the change in chemical shift of selected ^{1}H signals and deprotonation experiments are included.

A2.1 NMR Data from Chapter 2

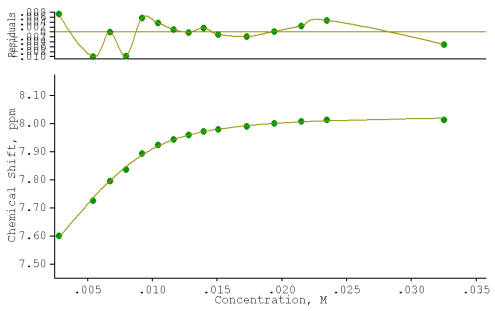

Figure A2.1.1: Binding curve from the ^{1}H NMR titration of receptor **152** with TBA benzoate in 0.5 % H_2O/DMSO-d_6 following the indolyl (6- position) CH group. This data was fitted to a 1:1 binding model using WinEQNMR 2. K_a = 1490 M^{-1} (9 % error).

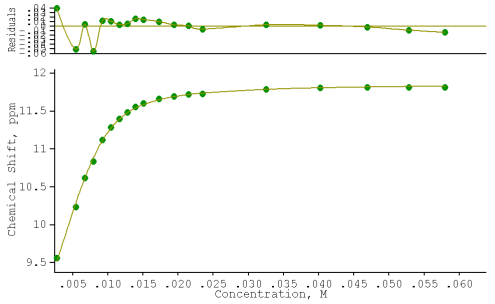

Figure A2.1.2: Binding curve from the ^{1}H NMR titration of receptor **152** with TBA benzoate in 0.5 % H_2O/DMSO-d_6 following the urea NH group. This data was fitted to a 1:1 binding model using WinEQNMR 2. K_a = 1580 M^{-1} (5 % error).

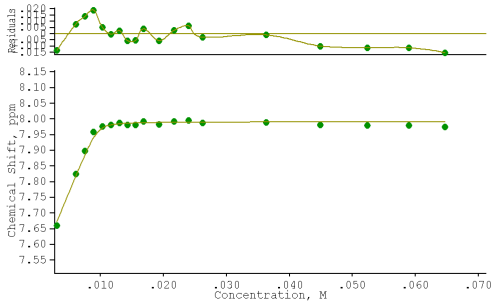

Figure A2.1.3: Binding curve from the ^{1}H NMR titration of receptor **152** with TBA acetate in 0.5 % H_2O/DMSO-d_6 following the indolyl (6- position) CH group. This data was fitted to a 1:1 binding model using WinEQNMR 2. $K_a > 10^4$ M^{-1}.

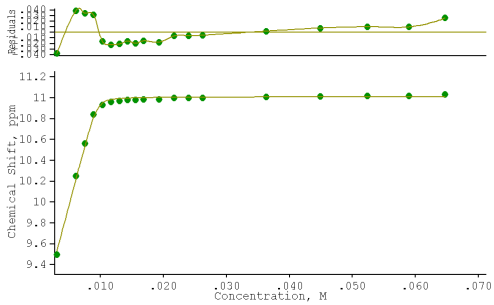

Figure A2.1.4: Binding curve from the ^{1}H NMR titration of receptor **152** with TBA acetate in 0.5 % H_2O/DMSO-d_6 following the urea NH group. This data was fitted to a 1:1 binding model using WinEQNMR 2. $K_a > 10^4\ M^{-1}$.

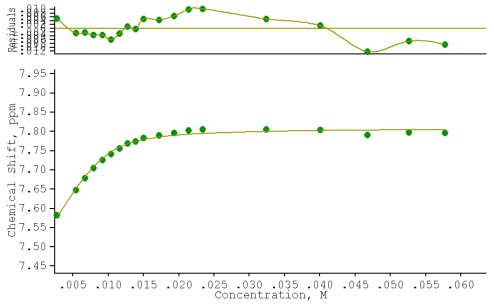

Figure A2.1.5: Binding curve from the ^{1}H NMR titration of receptor **152** with TEA bicarbonate in 0.5 % H_2O/DMSO-d_6 following the indolyl (6- position) CH group. This data was fitted to a 1:1 binding model using WinEQNMR 2. $K_a = 1420\ M^{-1}$ (4 % error).

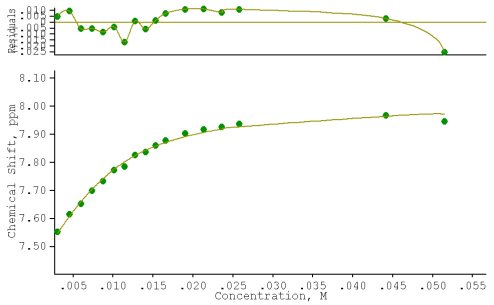

Figure A2.1.6: Binding curve from the ^{1}H NMR titration of receptor **152** with TBA benzoate in 10 % H_2O/DMSO-d_6 following the indolyl (6- position) CH group. This data was fitted to a 1:1 binding model using WinEQNMR 2. $K_a = 368\ M^{-1}$ (10 % error).

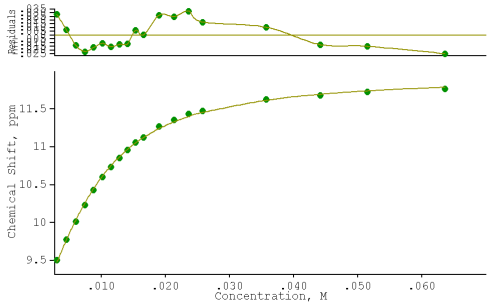

Figure A2.1.7: Binding curve from the ^{1}H NMR titration of receptor **152** with TBA benzoate in 10 % H_2O/DMSO-d_6 following the urea NH group. This data was fitted to a 1:1 binding model using WinEQNMR 2. K_a = 284 M^{-1} (4 % error).

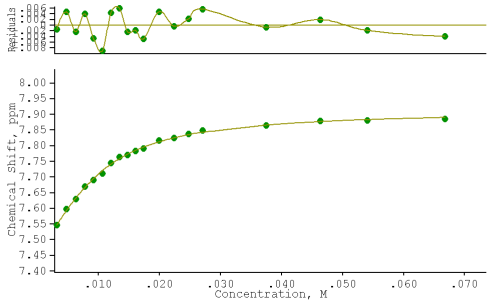

Figure A2.1.8: Binding curve from the ^{1}H NMR titration of receptor **152** with TBA acetate in 10 % H_2O/DMSO-d_6 following the indolyl (6- position) CH group. This data was fitted to a 1:1 binding model using WinEQNMR 2. K_a = 278 M^{-1} (5 % error).

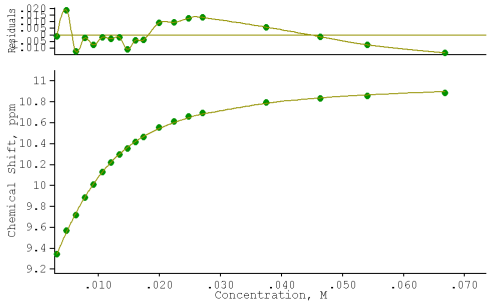

Figure A2.1.9: Binding curve from the ^{1}H NMR titration of receptor **152** with TBA acetate in 10 % H_2O/DMSO-d_6 following the urea NH group. This data was fitted to a 1:1 binding model using WinEQNMR 2. K_a = 293 M^{-1} (4 % error).

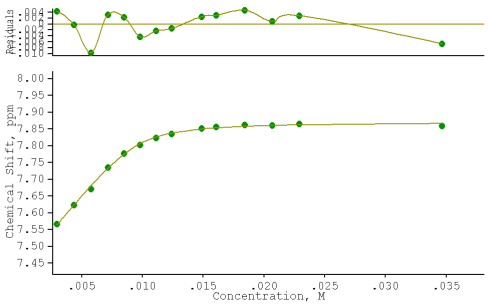

Figure A2.1.10: Binding curve from the ^{1}H NMR titration of receptor **152** with TBA dihydrogen phosphate in 10 % H_2O/DMSO-d_6 following the indolyl (6- position) CH group. This data was fitted to a 1:1 binding model using WinEQNMR 2. K_a = 2960 M^{-1} (13 % error).

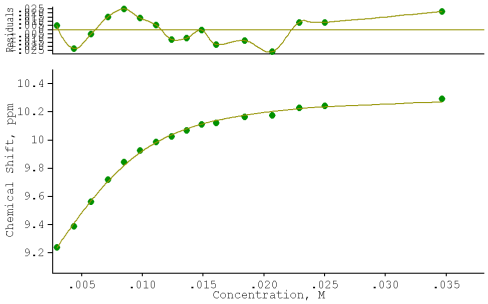

Figure A2.1.11: Binding curve from the ^{1}H NMR titration of receptor **152** with TBA dihydrogen phosphate in 10 % H_2O/DMSO-d_6 following the urea NH group. This data was fitted to a 1:1 binding model using WinEQNMR 2. K_a = 812 M^{-1} (10 % error).

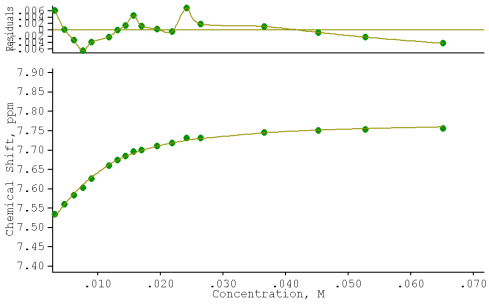

Figure A2.1.12: Binding curve from the ^{1}H NMR titration of receptor **152** with TEA bicarbonate in 10 % H_2O/DMSO-d_6 following the indolyl (6- position) CH group. This data was fitted to a 1:1 binding model using WinEQNMR 2. K_a = 319 M^{-1} (7 % error).

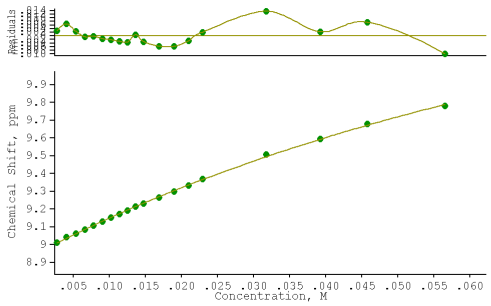

Figure A2.1.13: Binding curve from the ^{1}H NMR titration of receptor **153** with TBA chloride in 0.5 % H_2O/DMSO-d_6 following the urea NH group. This data was fitted to a 1:1 binding model using WinEQNMR 2. $K_a < 10\ M^{-1}$.

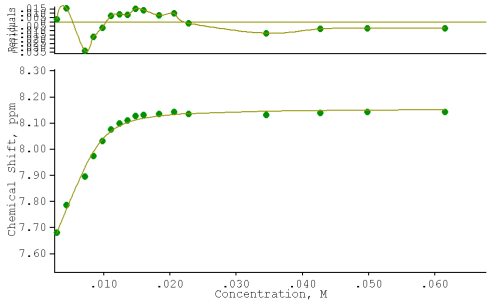

Figure A2.1.14: Binding curve from the ^{1}H NMR titration of receptor **153** with TBA benzoate in 0.5 % H_2O/DMSO-d_6 following the indolyl (6- position) CH group. This data was fitted to a 1:1 binding model using WinEQNMR 2. $K_a = 2430\ M^{-1}$ (19 % error).

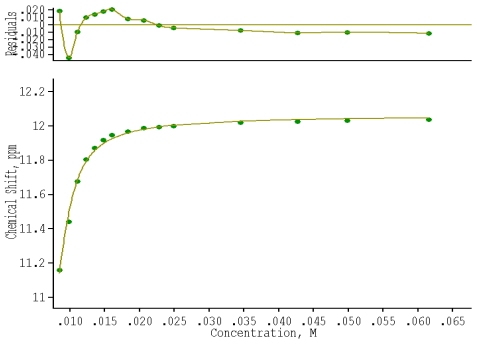

Figure A2.1.15: Binding curve from the ^{1}H NMR titration of receptor **153** with TBA benzoate in 0.5 % H_2O/DMSO-d_6 following the urea NH group. This data was fitted to a 1:1 binding model using WinEQNMR 2. $K_a = 4760\ M^{-1}$ (1 % error).

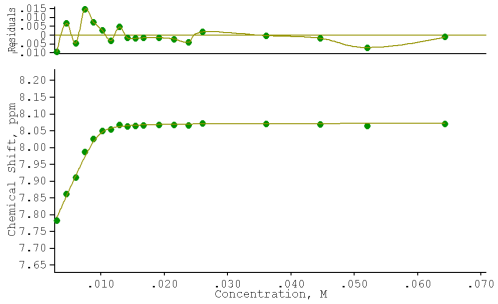

Figure A2.1.16: Binding curve from the ^{1}H NMR titration of receptor **153** with TBA acetate in 0.5 % H_2O/DMSO-d_6 following the indolyl (6- position) CH group. This data was fitted to a 1:1 binding model using WinEQNMR 2. $K_a > 10^4\ M^{-1}$.

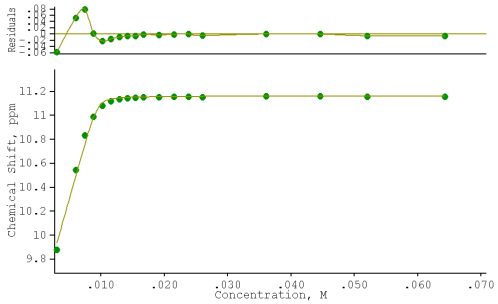

Figure A2.1.17: Binding curve from the ^{1}H NMR titration of receptor **153** with TBA acetate in 0.5 % H_2O/DMSO-d_6 following the urea NH group. This data was fitted to a 1:1 binding model using WinEQNMR 2. $K_a > 10^4\ M^{-1}$.

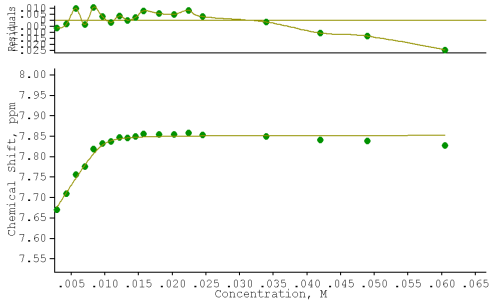

Figure A2.1.18: Binding curve from the ^{1}H NMR titration of receptor **153** with TEA bicarbonate in 0.5 % H_2O/DMSO-d_6 following the indolyl (6- position) CH group. This data was fitted to a 1:1 binding model using WinEQNMR 2. $K_a = 7660\ M^{-1}$ (13 % error).

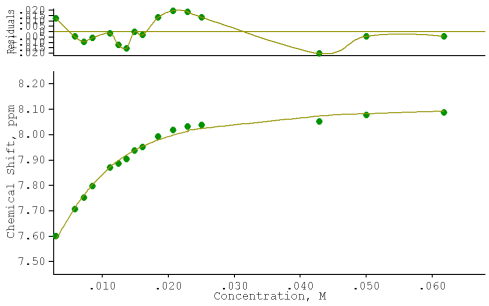

Figure A2.1.19: Binding curve from the ^{1}H NMR titration of receptor **153** with TBA benzoate in 10 % H_2O/DMSO-d_6 following the indolyl (6- position) CH group. This data was fitted to a 1:1 binding model using WinEQNMR 2. K_a = 298 M^{-1} (9 % error).

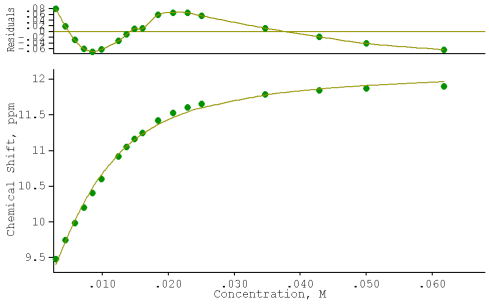

Figure A2.1.20: Binding curve from the ^{1}H NMR titration of receptor **153** with TBA benzoate in 10 % H_2O/DMSO-d_6 following the urea NH group. This data was fitted to a 1:1 binding model using WinEQNMR 2. K_a = 304 M^{-1} (10 % error).

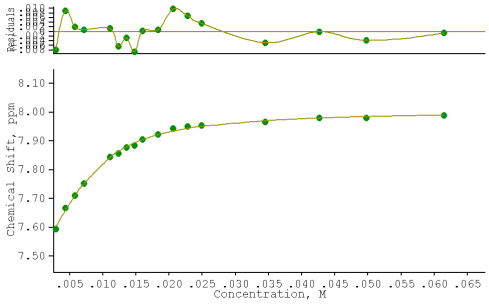

Figure A2.1.21: Binding curve from the ^{1}H NMR titration of receptor **153** with TBA acetate in 10 % H_2O/DMSO-d_6 following the indolyl (6- position) CH group. This data was fitted to a 1:1 binding model using WinEQNMR 2. K_a = 485 M^{-1} (7 % error).

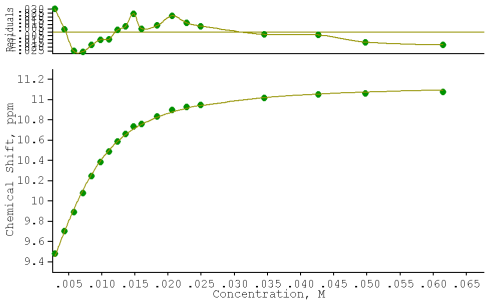

Figure A2.1.22: Binding curve from the ^{1}H NMR titration of receptor **153** with TBA acetate in 10 % H_2O/DMSO-d_6 following the urea NH group. This data was fitted to a 1:1 binding model using WinEQNMR 2. K_a = 544 M^{-1} (5 % error).

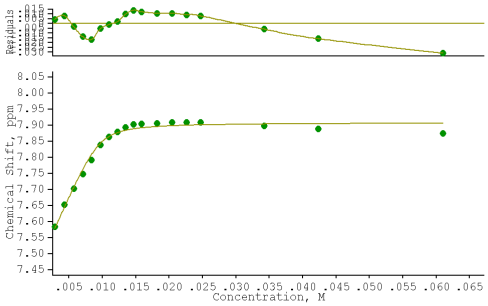

Figure A2.1.23: Binding curve from the ^{1}H NMR titration of receptor **153** with TBA dihydrogen phosphate in 10 % H_2O/DMSO-d_6 following the indolyl (6- position) CH group. This data was fitted to a 1:1 binding model using WinEQNMR 2. K_a = 2560 M^{-1} (1 % error).

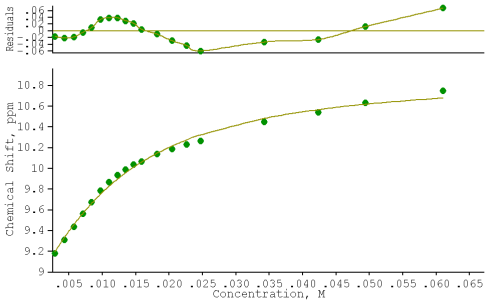

Figure A2.1.24: Binding curve from the ^{1}H NMR titration of receptor **153** with TBA dihydrogen phosphate in 10 % H_2O/DMSO-d_6 following the urea NH group. This data was fitted to a 1:1 binding model using WinEQNMR 2. K_a = 128 M^{-1} (10 % error).

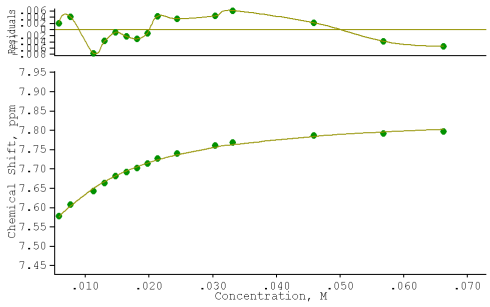

Figure A2.1.25: Binding curve from the ^{1}H NMR titration of receptor **153** with TEA bicarbonate in 10 % H_2O/DMSO-d_6 following the indolyl (6- position) CH group. This data was fitted to a 1:1 binding model using WinEQNMR 2. K_a = 149 M^{-1} (9 % error).

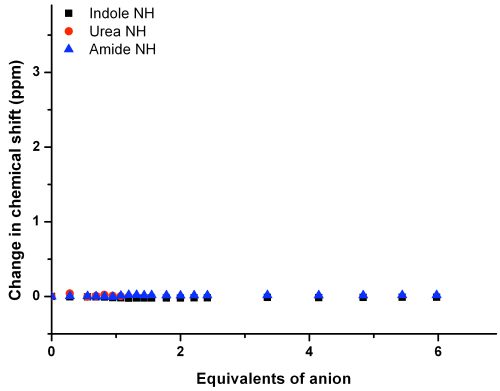

Figure A2.1.26: Change in ^{1}H NMR chemical shifts of indole, urea and amide NH groups during titration of receptor **152** with TBA chloride in 0.5 % H_2O/DMSO-d_6.

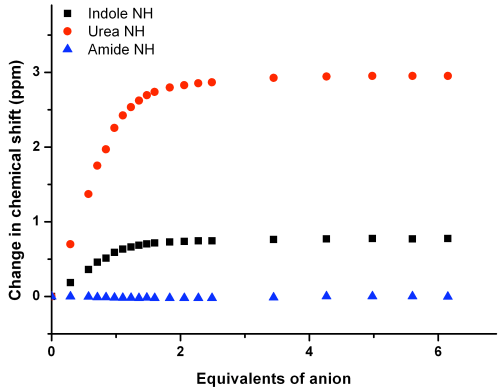

Figure A2.1.27: Change in ^{1}H NMR chemical shifts of indole, urea and amide NH groups during titration of receptor **152** with TBA benzoate in 0.5 % H_2O/DMSO-d_6.

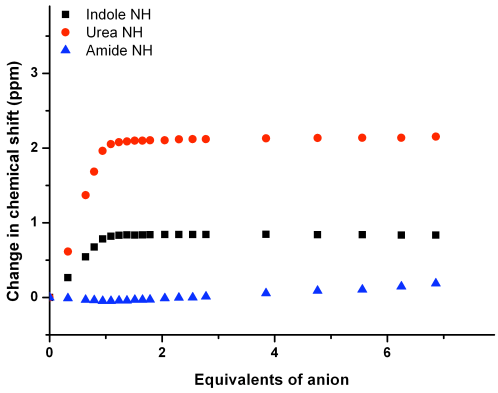

Figure A2.1.28: Change in ^{1}H NMR chemical shifts of indole, urea and amide NH groups during titration of receptor **152** with TBA acetate in 0.5 % H_2O/DMSO-d_6.

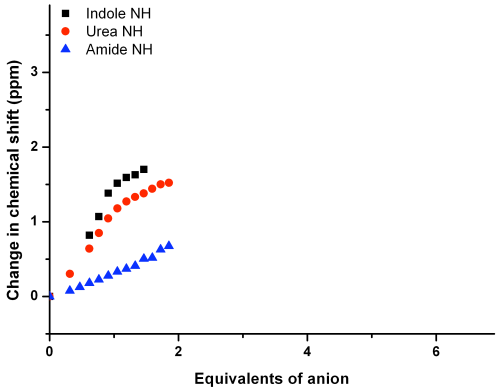

Figure A2.1.29: Change in ^{1}H NMR chemical shifts of indole, urea and amide NH groups during titration of receptor **152** with TBA dihydrogen phosphate in 0.5 % H_2O/DMSO-d_6.

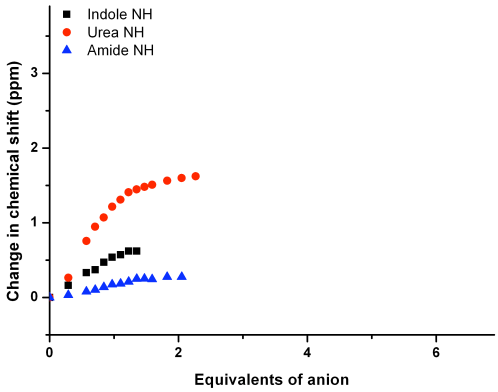

Figure A2.1.30: Change in ^{1}H NMR chemical shifts of indole, urea and amide NH groups during titration of receptor **152** with TEA bicarbonate in 0.5 % H_2O/DMSO-d_6.

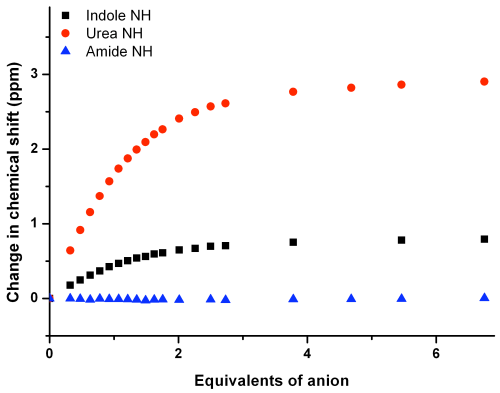

Figure A2.1.31: Change in ^{1}H NMR chemical shifts of indole, urea and amide NH groups during titration of receptor **152** with TBA benzoate in 10 % H_2O/DMSO-d_6.

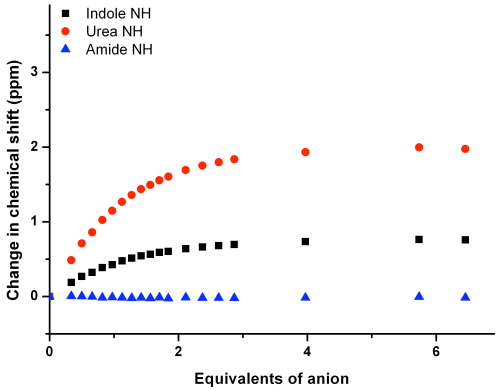

Figure A2.1.32: Change in ^{1}H NMR chemical shifts of indole, urea and amide NH groups during titration of receptor **152** with TBA acetate in 10 % H_2O/DMSO-d_6.

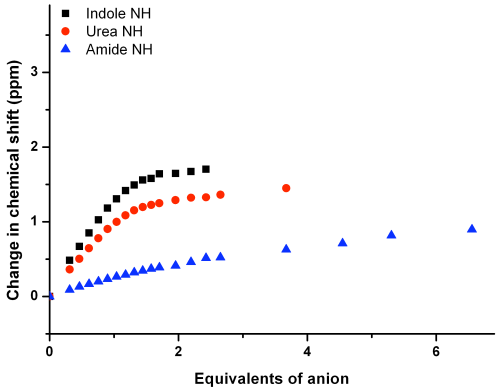

Figure A2.1.33: Change in ^{1}H NMR chemical shifts of indole, urea and amide NH groups during titration of receptor **152** with TBA dihydrogen phosphate in 10 % H_2O/DMSO-d_6.

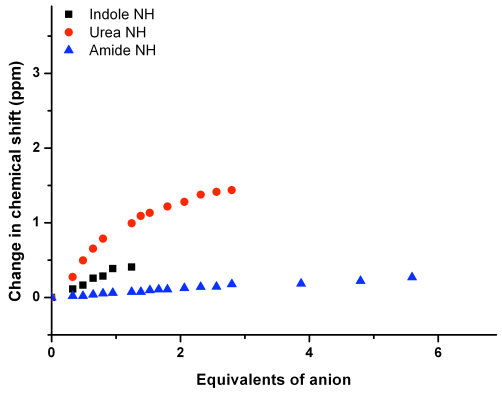

Figure A2.1.34: Change in ^{1}H NMR chemical shifts of indole, urea and amide NH groups during titration of receptor **152** with TEA bicarbonate in 10 % H_2O/DMSO-d_6.

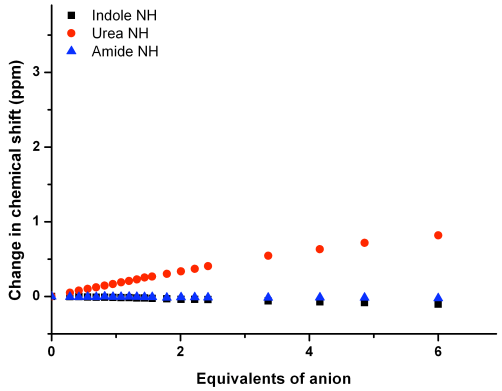

Figure A2.1.35: Change in ^{1}H NMR chemical shifts of indole, urea and amide NH groups during titration of receptor **153** with TBA chloride in 0.5 % H_2O/DMSO-d_6.

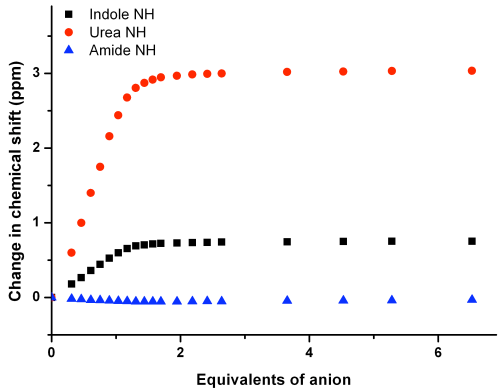

Figure A2.1.36: Change in ^{1}H NMR chemical shifts of indole, urea and amide NH groups during titration of receptor **153** with TBA benzoate in 0.5 % H_2O/DMSO-d_6.

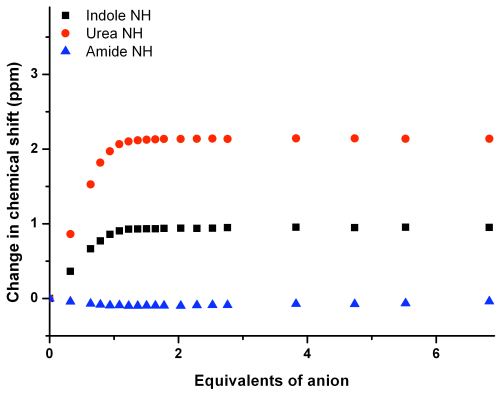

Figure A2.1.37: Change in ^{1}H NMR chemical shifts of indole, urea and amide NH groups during titration of receptor **153** with TBA acetate in 0.5 % H_2O/DMSO-d_6.

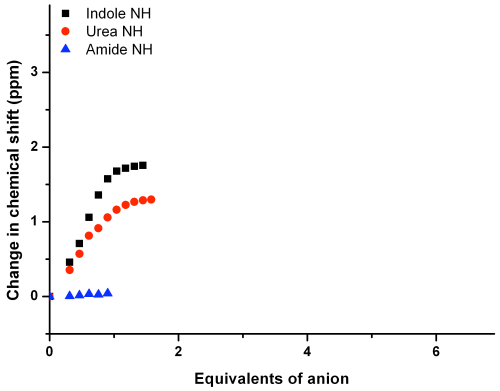

Figure A2.1.38: Change in ^{1}H NMR chemical shifts of indole, urea and amide NH groups during titration of receptor **153** with TBA dihydrogen phosphate in 0.5 % H_2O/DMSO-d_6.

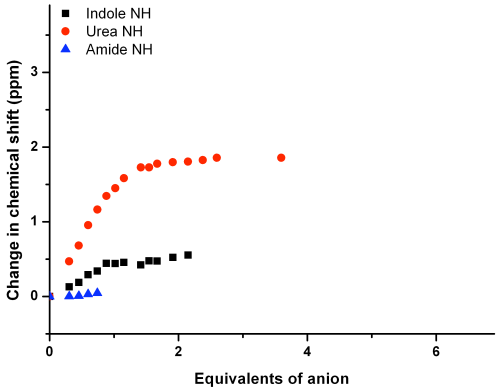

Figure A2.1.39: Change in ^{1}H NMR chemical shifts of indole, urea and amide NH groups during titration of receptor **153** with TEA bicarbonate in 0.5 % H_2O/DMSO-d_6.

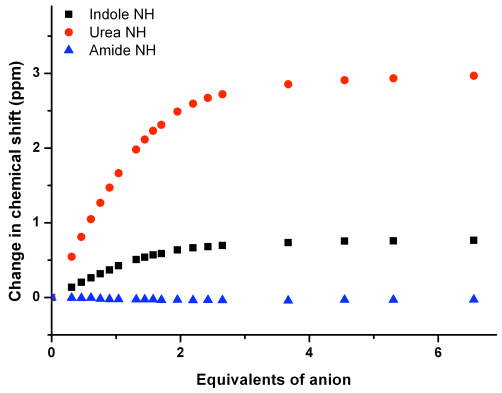

Figure A2.1.40: Change in ^{1}H NMR chemical shifts of indole, urea and amide NH groups during titration of receptor **153** with TBA benzoate in 10 % H_2O/DMSO-d_6.

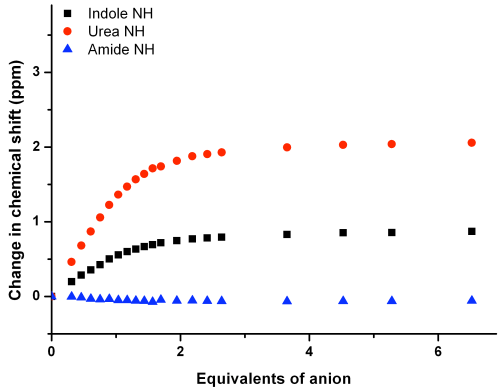

Figure A2.1.41: Change in ^{1}H NMR chemical shifts of indole, urea and amide NH groups during titration of receptor **153** with TBA acetate in 10 % H_2O/DMSO-d_6.

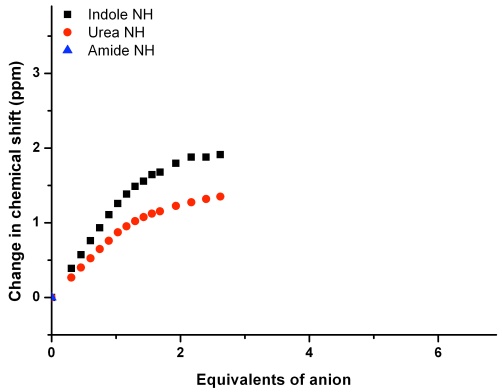

Figure A2.1.42: Change in ^{1}H NMR chemical shifts of indole, urea and amide NH groups during titration of receptor **153** with TBA dihydrogen phosphate in 10 % H_2O/DMSO-d_6.

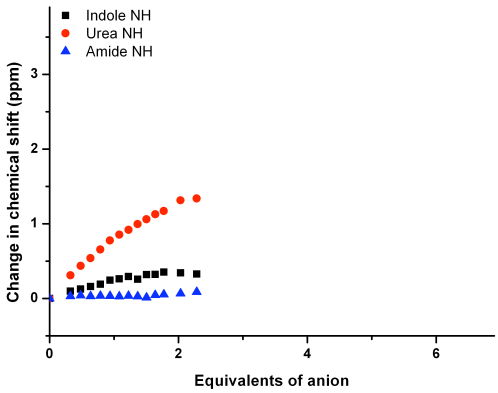

Figure A2.1.43: Change in ^{1}H NMR chemical shifts of indole, urea and amide NH groups during titration of receptor **153** with TEA bicarbonate in 10 % H_2O/DMSO-d_6.

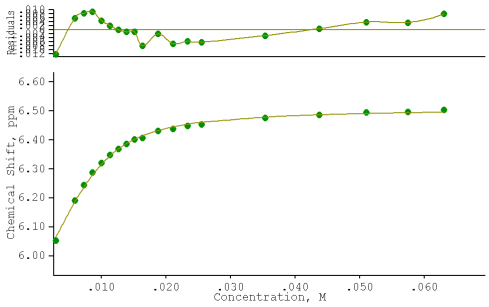

Figure A2.1.44: Binding curve from the ^{1}H NMR titration of receptor **155** with TBA chloride in 0.5 % H_2O/DMSO-d_6 following the most downfield urea NH group. This data was fitted to a 1:1 binding model using WinEQNMR 2. K_a = 655 M^{-1} (7 % error).

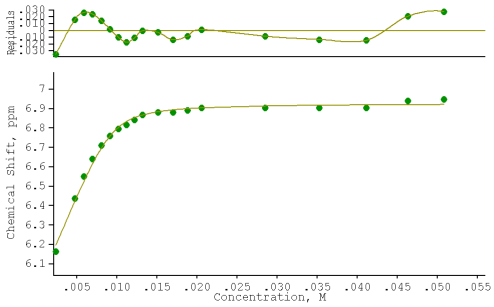

Figure A2.1.45: Binding curve from the ^{1}H NMR titration of receptor **155** with TBA dihydrogen phosphate in 0.5 % H_2O/DMSO-d_6 following the most downfield urea NH group. This data was fitted to a 1:1 binding model using WinEQNMR 2. K_a = 3450 M^{-1} (6 % error).

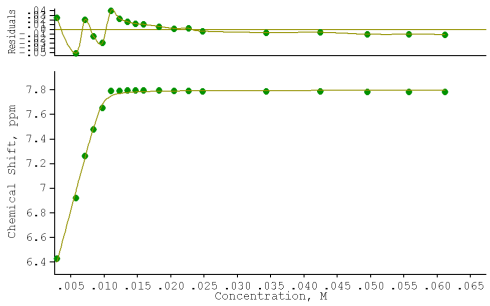

Figure A2.1.46: Binding curve from the ^{1}H NMR titration of receptor **155** with TBA sulphate in 0.5 % H_2O/DMSO-d_6 following the most downfield urea NH group. This data was fitted to a 1:1 binding model using WinEQNMR 2. $K_a > 10^4\ M^{-1}$.

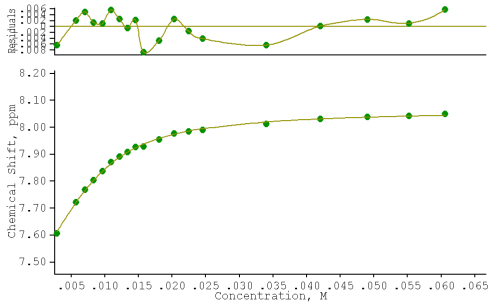

Figure A2.1.47: Binding curve from the ^{1}H NMR titration of receptor **156** with TBA chloride in 0.5 % H_2O/DMSO-d_6 following the most downfield urea NH group. This data was fitted to a 1:1 binding model using WinEQNMR 2. $K_a = 440\ M^{-1}$ (3 % error).

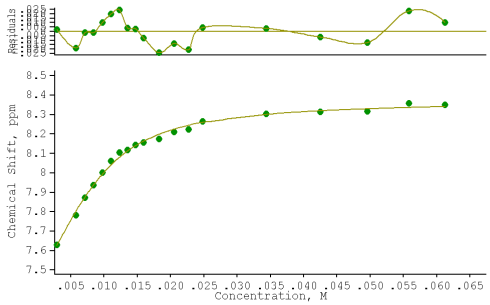

Figure A2.1.48: Binding curve from the ^{1}H NMR titration of receptor **156** with TEA bicarbonate in 0.5 % H_2O/DMSO-d_6 following the most downfield urea NH group. This data was fitted to a 1:1 binding model using WinEQNMR 2. $K_a = 451\ M^{-1}$ (8 % error).

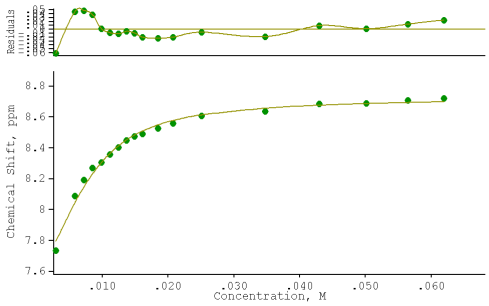

Figure A2.1.49: Binding curve from the ^{1}H NMR titration of receptor **156** with TBA dihydrogen phosphate in 0.5 % H_2O/DMSO-d_6 following the most downfield urea NH group. This data was fitted to a 1:1 binding model using WinEQNMR 2. K_a = 540 M^{-1} (14 % error).

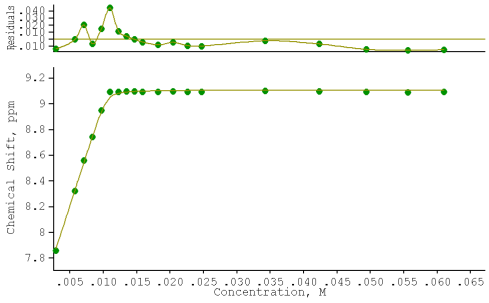

Figure A2.1.50: Binding curve from the ^{1}H NMR titration of receptor **156** with TBA sulphate in 0.5 % H_2O/DMSO-d_6 following the most downfield urea NH group. This data was fitted to a 1:1 binding model using WinEQNMR 2. $K_a > 10^4$ M^{-1}.

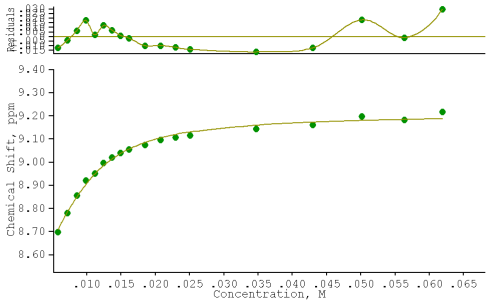

Figure A2.1.51: Binding curve from the ^{1}H NMR titration of receptor **143** with TBA chloride in 0.5 % H_2O/DMSO-d_6 following the most downfield urea NH group. This data was fitted to a 1:1 binding model using WinEQNMR 2. K_a = 777 M^{-1} (8 % error).

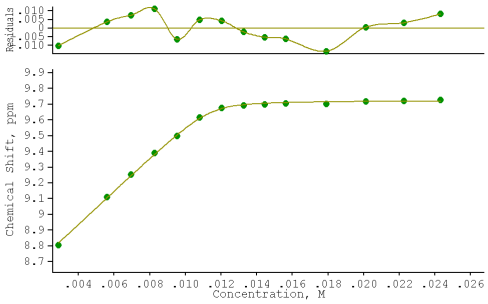

Figure A2.1.52: Binding curve from the ^{1}H NMR titration of receptor **143** with TBA dihydrogen phosphate in 0.5 % H_2O/DMSO-d_6 following the most downfield urea NH group. This data was fitted to a 1:1 binding model using WinEQNMR 2. $K_a > 10^4\ M^{-1}$.

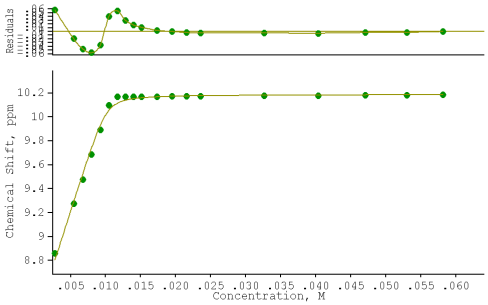

Figure A2.1.53: Binding curve from the ^{1}H NMR titration of receptor **143** with TBA sulphate in 0.5 % H_2O/DMSO-d_6 following the most downfield urea NH group. This data was fitted to a 1:1 binding model using WinEQNMR 2. $K_a > 10^4\ M^{-1}$.

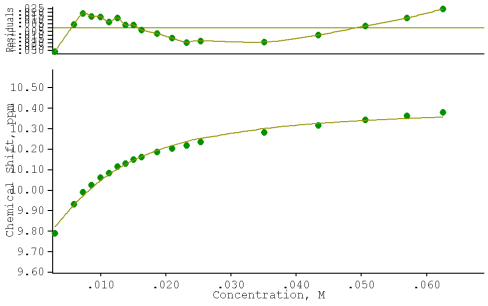

Figure A2.1.54: Binding curve from the ^{1}H NMR titration of receptor **144** with TBA chloride in 0.5 % H_2O/DMSO-d_6 following the most downfield urea NH group. This data was fitted to a 1:1 binding model using WinEQNMR 2. $K_a = 191\ M^{-1}$ (13 % error).

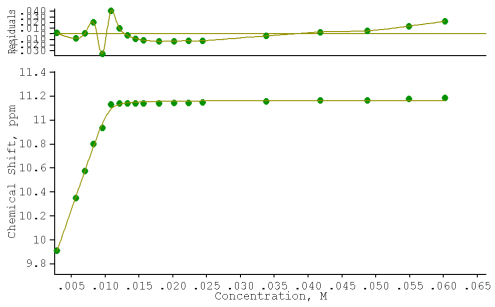

Figure A2.1.55: Binding curve from the ^{1}H NMR titration of receptor **144** with TBA sulphate in 0.5 % H_2O/DMSO-d_6 following the most downfield urea NH group. This data was fitted to a 1:1 binding model using WinEQNMR 2. $K_a > 10^4\ M^{-1}$.

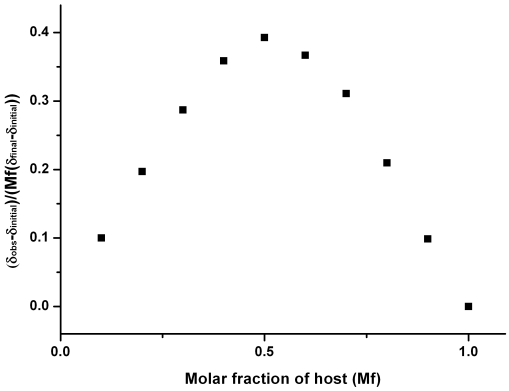

Figure A2.1.56: Job plot from the ^{1}H NMR titration of receptor **155** with TEA bicarbonate in 0.5 % H_2O/DMSO-d_6 following the most downfield urea NH group.

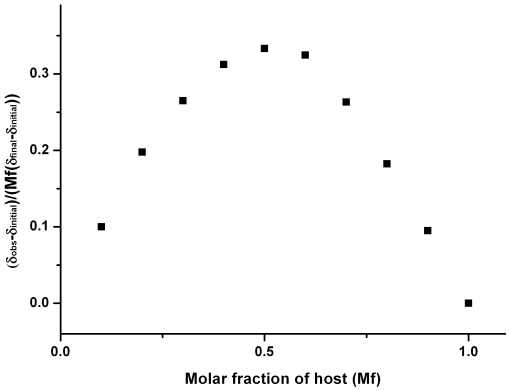

Figure A2.1.57: Job plot from the ^{1}H NMR titration of receptor **156** with TBA chloride in 0.5 % H_2O/DMSO-d_6 following the most downfield urea NH group.

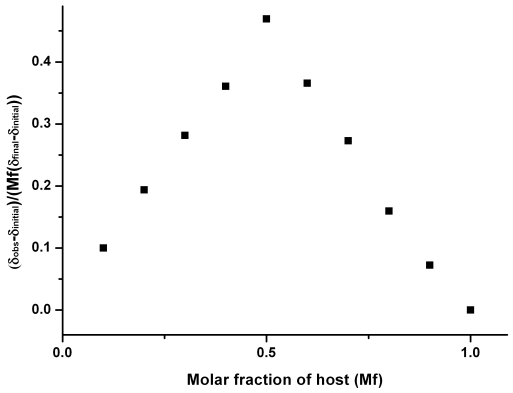

Figure A2.1.58: Job plot from the ^{1}H NMR titration of receptor **156** with TEA bicarbonate in 0.5 % H_2O/DMSO-d_6 following the most downfield urea NH group.

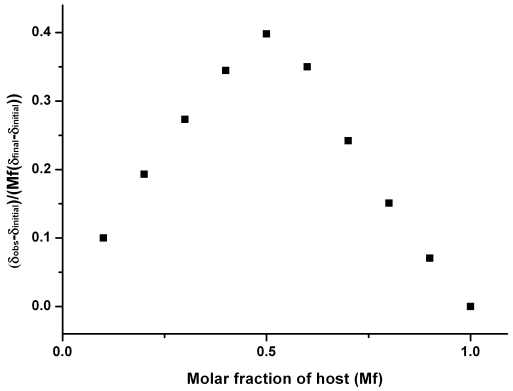

Figure A2.1.59: Job plot from the ^{1}H NMR titration of receptor **156** with TBA dihydrogen phosphate in 0.5 % H_2O/DMSO-d_6 following the most downfield urea NH group.

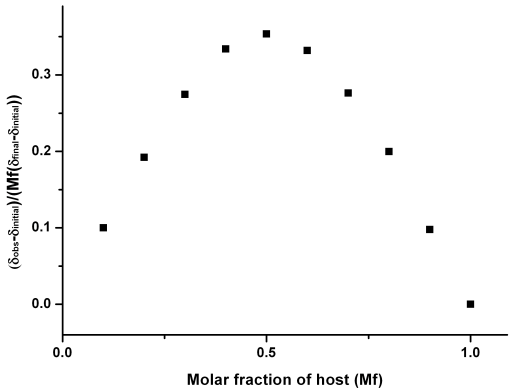

Figure A2.1.60: Job plot from the ^{1}H NMR titration of receptor **143** with TBA chloride in 0.5 % H_2O/DMSO-d_6 following the most downfield urea NH group.

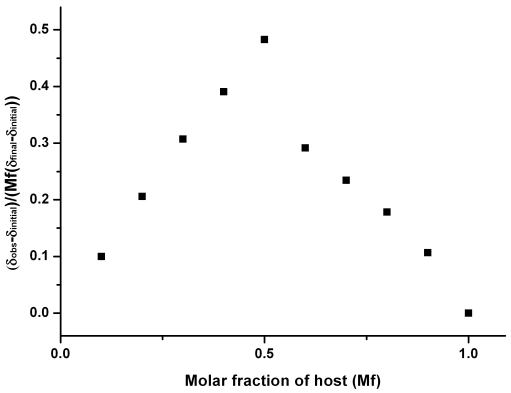

Figure A2.1.61: Job plot from the ^{1}H NMR titration of receptor **143** with TEA bicarbonate in 0.5 % H_2O/DMSO-d_6 following the most downfield urea NH group.

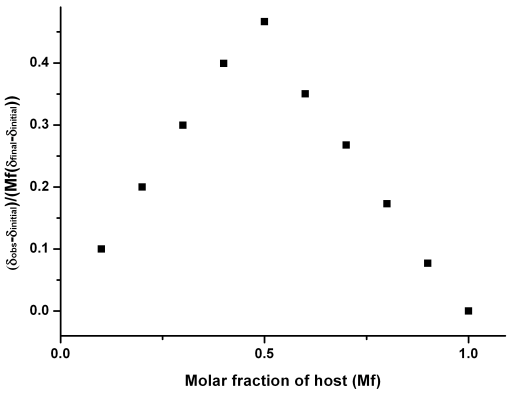

Figure A2.1.62: Job plot from the ^{1}H NMR titration of receptor **143** with TBA sulphate in 0.5 % H_2O/DMSO-d_6 following the most downfield urea NH group.

A2.2 NMR Data from Chapter 3

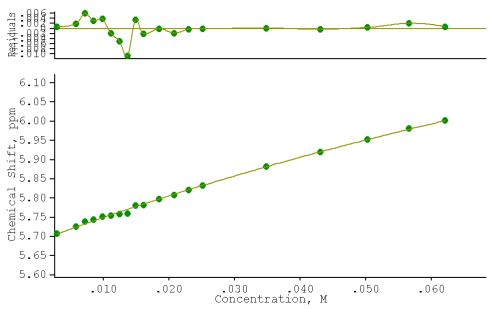

Figure A2.2.1: Binding curve from the ^{1}H NMR titration of receptor **211** with TBA chloride in 0.5 % H_2O/DMSO-d_6 following the *iso*-pentyl urea NH group. This data was fitted to a 1:1 binding model using WinEQNMR 2. $K_a < 10\ M^{-1}$.

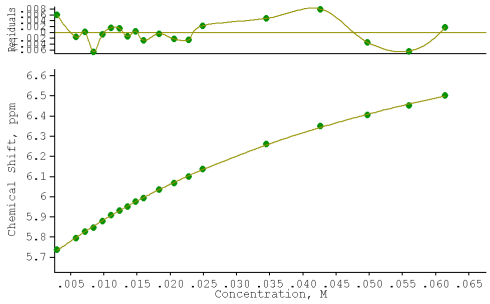

Figure A2.2.2: Binding curve from the ^{1}H NMR titration of receptor **211** with TEA bicarbonate in 0.5 % H_2O/DMSO-d_6 following the *iso*-pentyl urea NH group. This data was fitted to a 1:1 binding model using WinEQNMR 2. $K_a = 18\ M^{-1}$ (4 % error).

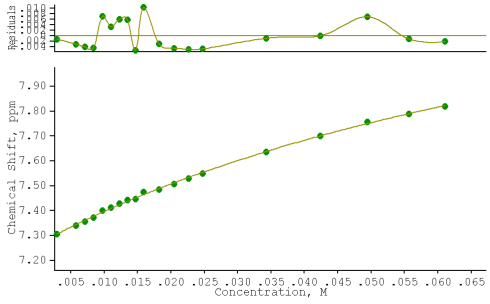

Figure A2.2.3: Binding curve from the ^{1}H NMR titration of receptor **212** with TBA chloride in 0.5 % H_2O/DMSO-d_6 following the *iso*-pentyl urea NH group. This data was fitted to a 1:1 binding model using WinEQNMR 2. $K_a = 10\ M^{-1}$ (9 % error).

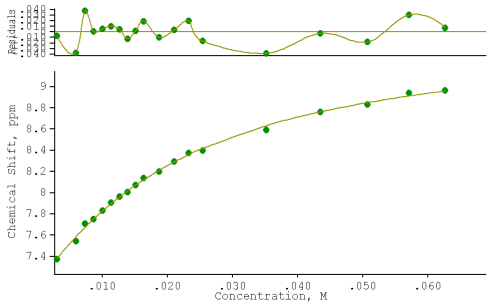

Figure A2.2.4: Binding curve from the ^{1}H NMR titration of receptor **212** with TEA bicarbonate in 0.5 % H_2O/DMSO-d_6 following the *iso*-pentyl urea NH group. This data was fitted to a 1:1 binding model using WinEQNMR 2. K_a = 58 M^{-1} (7 % error).

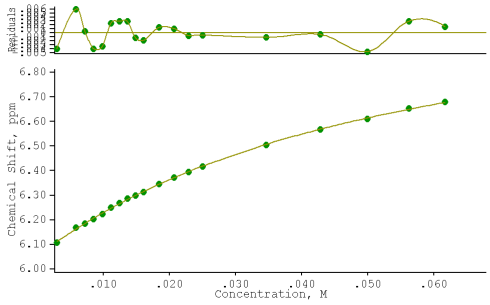

Figure A2.2.5: Binding curve from the ^{1}H NMR titration of receptor **213** with TBA chloride in 0.5 % H_2O/DMSO-d_6 following the *iso*-pentyl urea NH group. This data was fitted to a 1:1 binding model using WinEQNMR 2. K_a = 21 M^{-1} (4 % error).

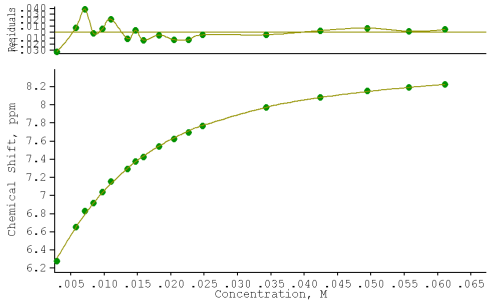

Figure A2.2.6: Binding curve from the ^{1}H NMR titration of receptor **213** with TEA bicarbonate in 0.5 % H_2O/DMSO-d_6 following the *iso*-pentyl urea NH group. This data was fitted to a 1:1 binding model using WinEQNMR 2. K_a = 135 M^{-1} (4 % error).

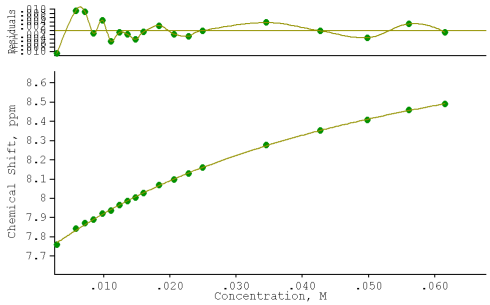

Figure A2.2.7: Binding curve from the ^{1}H NMR titration of receptor **214** with TBA chloride in 0.5 % H_2O/DMSO-d_6 following the *iso*-pentyl urea NH group. This data was fitted to a 1:1 binding model using WinEQNMR 2. K_a = 22 M^{-1} (5 % error).

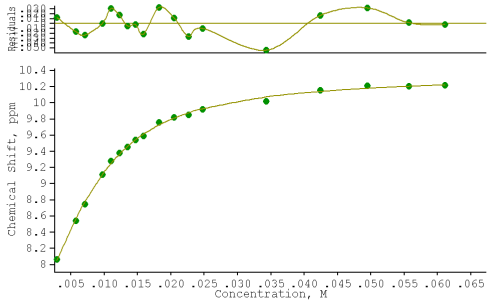

Figure A2.2.8: Binding curve from the ^{1}H NMR titration of receptor **214** with TEA bicarbonate in 0.5 % H_2O/DMSO-d_6 following the *iso*-pentyl urea NH group. This data was fitted to a 1:1 binding model using WinEQNMR 2. K_a = 343 M^{-1} (5 % error).

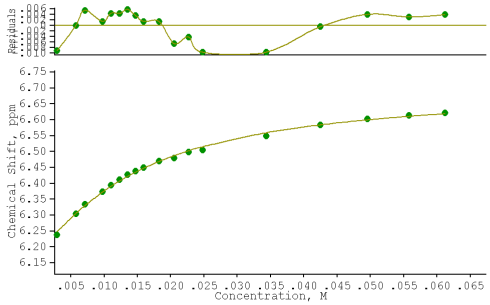

Figure A2.2.9: Binding curve from the ^{1}H NMR titration of receptor **215** with TBA chloride in 0.5 % H_2O/DMSO-d_6 following the *iso*-pentyl urea NH group. This data was fitted to a 1:1 binding model using WinEQNMR 2. K_a = 96 M^{-1} (6 % error).

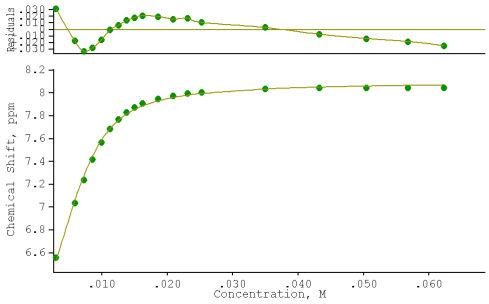

Figure A2.2.10: Binding curve from the ^{1}H NMR titration of receptor **215** with TEA bicarbonate in 0.5 % H_2O/DMSO-d_6 following the *iso*-pentyl urea NH group. This data was fitted to a 1:1 binding model using WinEQNMR 2. K_a = 1170 M^{-1} (7 % error).

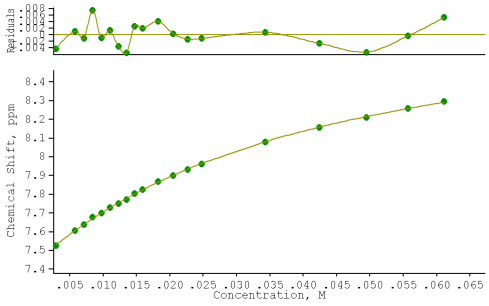

Figure A2.2.11: Binding curve from the ^{1}H NMR titration of receptor **216** with TBA chloride in 0.5 % H_2O/DMSO-d_6 following the *iso*-pentyl urea NH group. This data was fitted to a 1:1 binding model using WinEQNMR 2. K_a = 28 M^{-1} (3 % error).

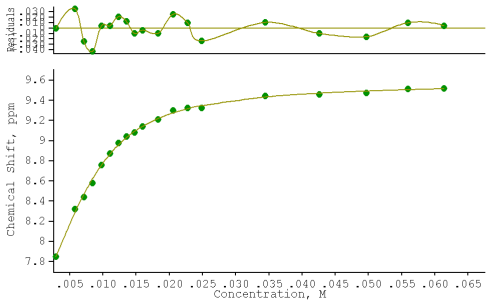

Figure A2.2.12: Binding curve from the ^{1}H NMR titration of receptor **216** with TEA bicarbonate in 0.5 % H_2O/DMSO-d_6 following the *iso*-pentyl urea NH group. This data was fitted to a 1:1 binding model using WinEQNMR 2. K_a = 516 M^{-1} (5 % error).

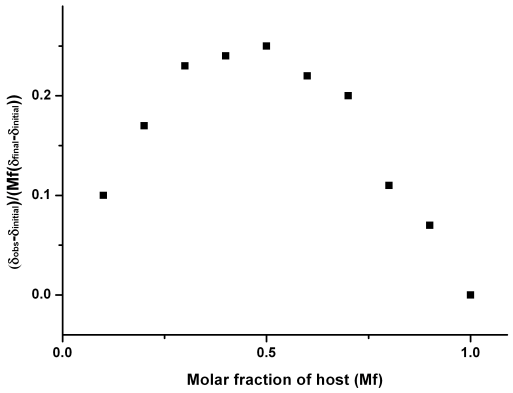

Figure A2.2.13: Job plot from the ^{1}H NMR titration of receptor **211** with TEA bicarbonate in 0.5 % H_2O/DMSO-d_6 following the most downfield urea NH group.

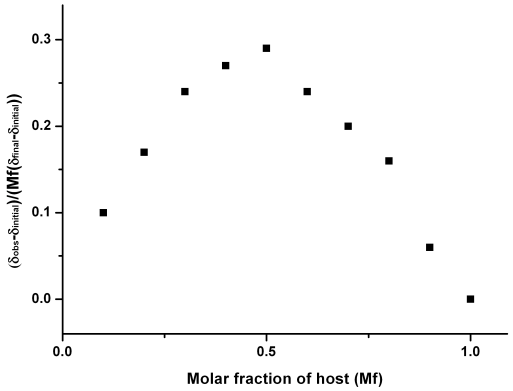

Figure A2.2.14: Job plot from the ^{1}H NMR titration of receptor **212** with TBA chloride in 0.5 % H_2O/DMSO-d_6 following the *iso*-pentyl urea NH group.

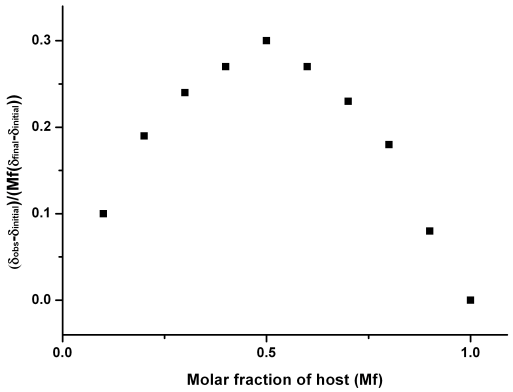

Figure A2.2.15: Job plot from the ^{1}H NMR titration of receptor **212** with TEA bicarbonate in 0.5 % H_2O/DMSO-d_6 following the *iso*-pentyl urea NH group.

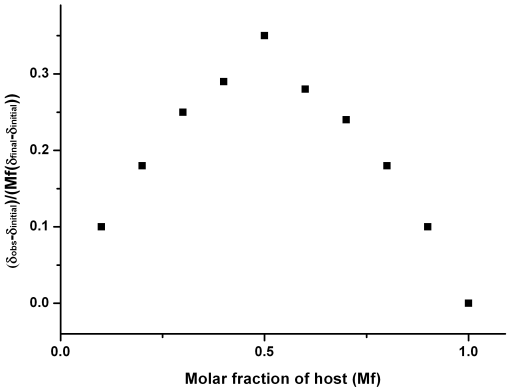

Figure A2.2.16: Job plot from the ^{1}H NMR titration of receptor **213** with TBA chloride in 0.5 % H_2O/DMSO-d_6 following the *iso*-pentyl urea NH group.

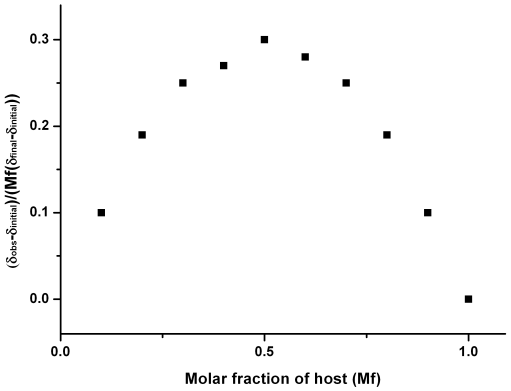

Figure A2.2.17: Job plot from the ^{1}H NMR titration of receptor **213** with TEA bicarbonate in 0.5 % H_2O/DMSO-d_6 following the *iso*-pentyl urea NH group.

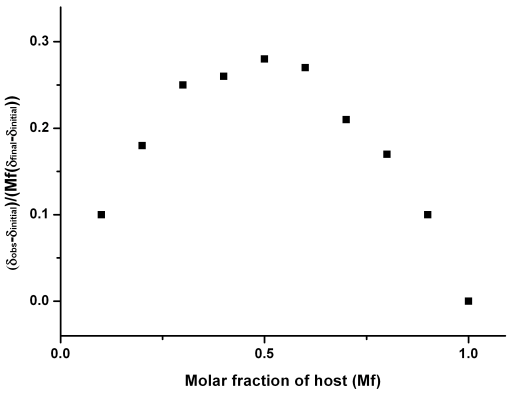

Figure A2.2.18: Job plot from the ^{1}H NMR titration of receptor **214** with TBA chloride in 0.5 % H_2O/DMSO-d_6 following the *iso*-pentyl urea NH group.

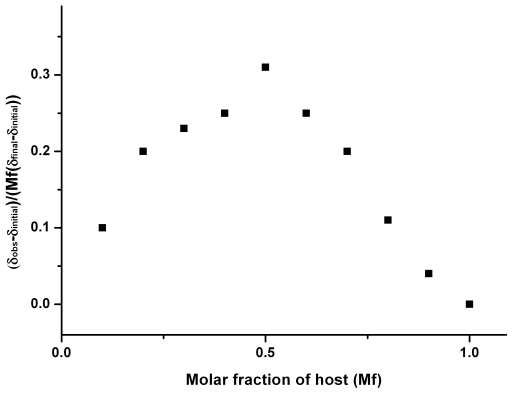

Figure A2.2.19: Job plot from the ^{1}H NMR titration of receptor **215** with TBA chloride in 0.5 % H_2O/DMSO-d_6 following the *iso*-pentyl urea NH group.

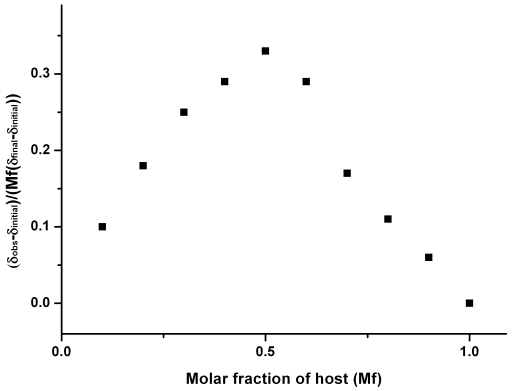

Figure A2.2.20: Job plot from the ^{1}H NMR titration of receptor **216** with TBA chloride in 0.5 % H_2O/DMSO-d_6 following the *iso*-pentyl urea NH group.

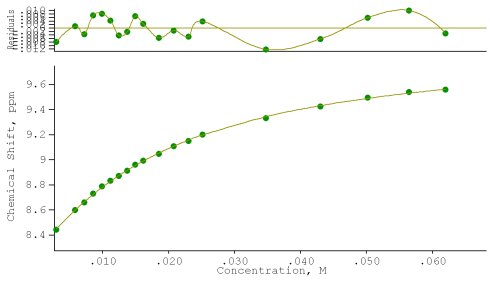

Figure A2.2.21: Binding curve from the ^{1}H NMR titration of receptor **204** with TBA chloride in 0.5 % H_2O/DMSO-d_6 following the most downfield urea NH group. This data was fitted to a 1:1 binding model using WinEQNMR 2. K_a = 64 M^{-1} (3 % error).

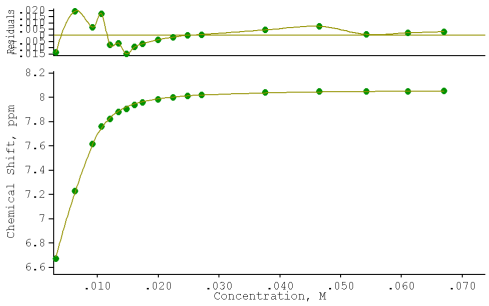

Figure A2.2.22: Binding curve from the ^{1}H NMR titration of receptor **204** with TEA bicarbonate in 0.5 % H_2O/DMSO-d_6 following the most upfield urea NH group. This data was fitted to a 1:1 binding model using WinEQNMR 2. K_a = 2330 M^{-1} (5 % error).

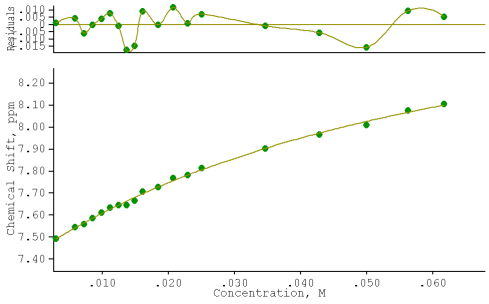

Figure A2.2.23: Binding curve from the ^{1}H NMR titration of receptor **223** with TBA chloride in 0.5 % H_2O/DMSO-d_6 following the most upfield urea NH group. This data was fitted to a 1:1 binding model using WinEQNMR 2. K_a = 17 M^{-1} (12 % error).

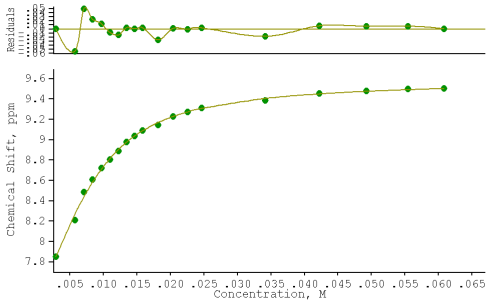

Figure A2.2.24: Binding curve from the ^{1}H NMR titration of receptor **223** with TEA bicarbonate in 0.5 % H_2O/DMSO-d_6 following the most upfield urea NH group. This data was fitted to a 1:1 binding model using WinEQNMR 2. K_a = 414 M^{-1} (6 % error).

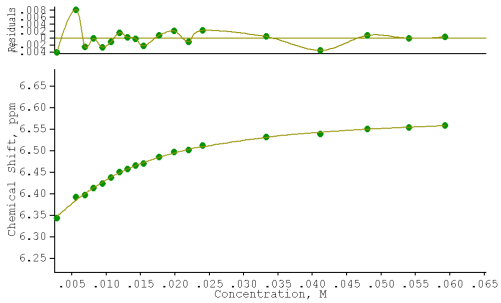

Figure A2.2.25: Binding curve from the ^{1}H NMR titration of receptor **224** with TBA chloride in 0.5 % H_2O/DMSO-d_6 following the most upfield urea NH group. This data was fitted to a 1:1 binding model using WinEQNMR 2. K_a = 154 M^{-1} (6 % error).

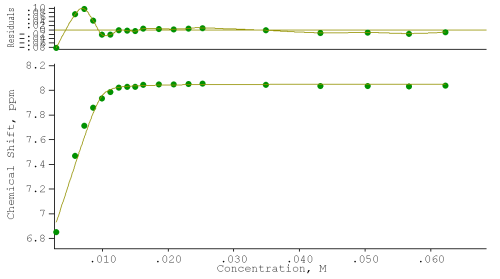

Figure A2.2.26: Binding curve from the ^{1}H NMR titration of receptor **224** with TEA bicarbonate in 0.5 % H_2O/DMSO-d_6 following the most upfield urea NH group. This data was fitted to a 1:1 binding model using WinEQNMR 2. $K_a > 10^4$ M^{-1} (5 % error).

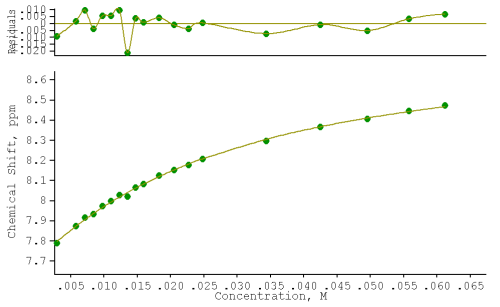

Figure A2.2.27: Binding curve from the ^{1}H NMR titration of receptor **225** with TBA chloride in 0.5 % H_2O/DMSO-d_6 following the most upfield urea NH group. This data was fitted to a 1:1 binding model using WinEQNMR 2. K_a = 40 M^{-1} (7 % error).

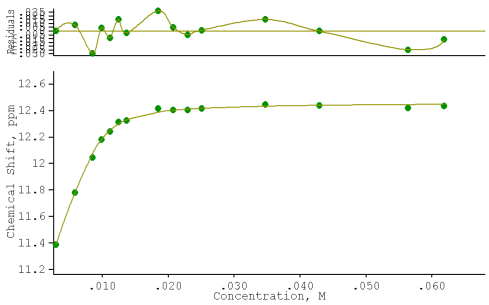

Figure A2.2.28: Binding curve from the ^{1}H NMR titration of receptor **225** with TEA bicarbonate in 0.5 % H_2O/DMSO-d_6 following the indole NH group. This data was fitted to a 1:1 binding model using WinEQNMR 2. K_a = 2150 M^{-1} (10 % error).

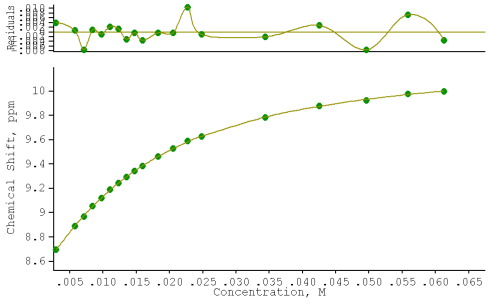

Figure A2.2.29: Binding curve from the ^{1}H NMR titration of receptor **226** with TBA chloride in 0.5 % H_2O/DMSO-d_6 following the most upfield urea NH group. This data was fitted to a 1:1 binding model using WinEQNMR 2. K_a = 95 M^{-1} (2 % error).

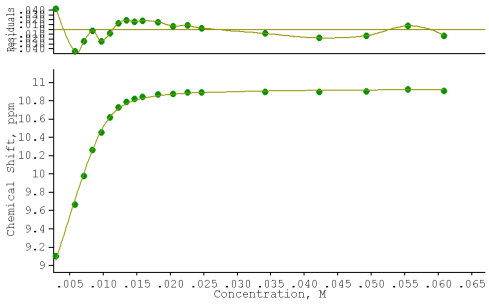

Figure A2.2.30: Binding curve from the ^{1}H NMR titration of receptor **226** with TEA bicarbonate in 0.5 % H_2O/DMSO-d_6 following the most upfield urea NH group. This data was fitted to a 1:1 binding model using WinEQNMR 2. K_a = 3860 M^{-1} (9 % error).

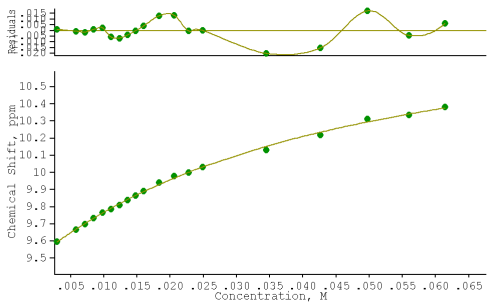

Figure A2.2.31: Binding curve from the ^{1}H NMR titration of receptor **227** with TBA chloride in 0.5 % H_2O/DMSO-d_6 following the most upfield urea NH group. This data was fitted to a 1:1 binding model using WinEQNMR 2. K_a = 25 M^{-1} (8 % error).

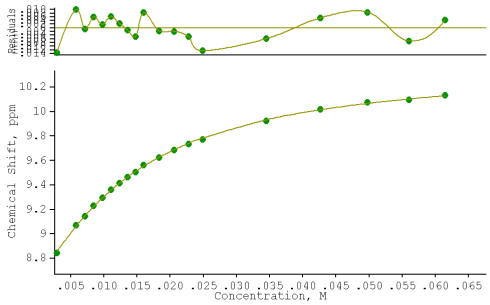

Figure A2.2.32: Binding curve from the ^{1}H NMR titration of receptor **228** with TBA chloride in 0.5 % H_2O/DMSO-d_6 following the most upfield urea NH group. This data was fitted to a 1:1 binding model using WinEQNMR 2. K_a = 101 M^{-1} (3 % error).

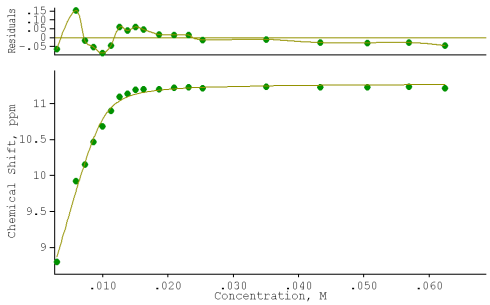

Figure A2.2.33: Binding curve from the ^{1}H NMR titration of receptor **228** with TEA bicarbonate in 0.5 % H_2O/DMSO-d_6 following the most upfield urea NH group. This data was fitted to a 1:1 binding model using WinEQNMR 2. K_a = 4050 M^{-1} (19 % error).

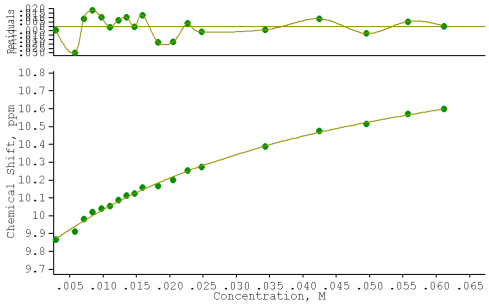

Figure A2.2.34: Binding curve from the ^{1}H NMR titration of receptor **229** with TBA chloride in 0.5 % H_2O/DMSO-d_6 following the most upfield urea NH group. This data was fitted to a 1:1 binding model using WinEQNMR 2. K_a = 26 M^{-1} (12 % error).

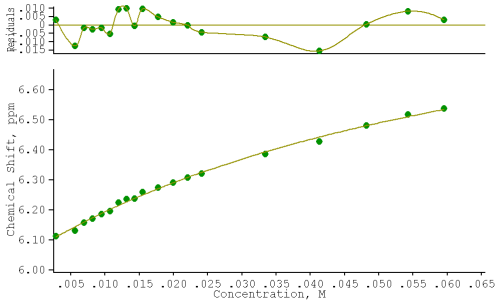

Figure A2.2.35: Binding curve from the ^{1}H NMR titration of receptor **230** with TBA chloride in 0.5 % H_2O/DMSO-d_6 following the most upfield urea NH group. This data was fitted to a 1:1 binding model using WinEQNMR 2. K_a = 16 M^{-1} (14 % error).

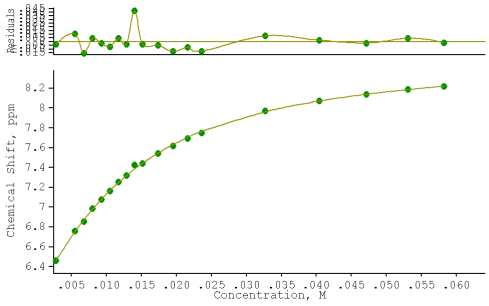

Figure A2.2.36: Binding curve from the ^{1}H NMR titration of receptor **230** with TEA bicarbonate in 0.5 % H_2O/DMSO-d_6 following the most upfield urea NH group. This data was fitted to a 1:1 binding model using WinEQNMR 2. K_a = 121 M^{-1} (3 % error).

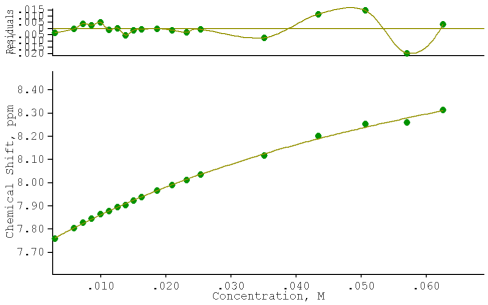

Figure A2.2.37: Binding curve from the ^{1}H NMR titration of receptor **231** with TBA chloride in 0.5 % H_2O/DMSO-d_6 following the most upfield urea NH group. This data was fitted to a 1:1 binding model using WinEQNMR 2. K_a = 14 M^{-1} (12 % error).

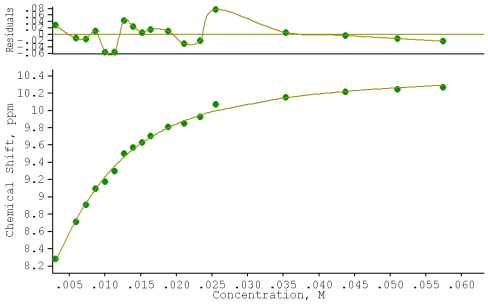

Figure A2.2.38: Binding curve from the ^{1}H NMR titration of receptor **231** with TEA bicarbonate in 0.5 % H_2O/DMSO-d_6 following the most upfield urea NH group. This data was fitted to a 1:1 binding model using WinEQNMR 2. K_a = 262 M^{-1} (8 % error).

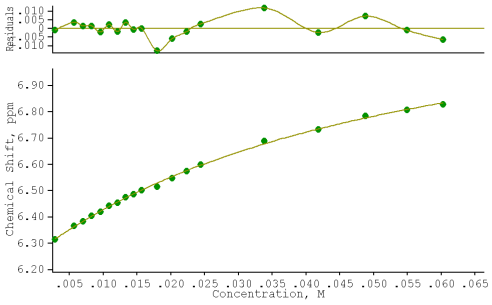

Figure A2.2.39: Binding curve from the ^{1}H NMR titration of receptor **232** with TBA chloride in 0.5 % H_2O/DMSO-d_6 following the most upfield urea NH group. This data was fitted to a 1:1 binding model using WinEQNMR 2. K_a = 23 M^{-1} (8 % error).

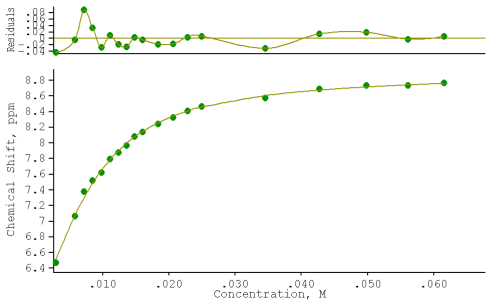

Figure A2.2.40: Binding curve from the ^{1}H NMR titration of receptor **232** with TEA bicarbonate in 0.5 % H_2O/DMSO-d_6 following the most upfield urea NH group. This data was fitted to a 1:1 binding model using WinEQNMR 2. K_a = 329 M^{-1} (6 % error).

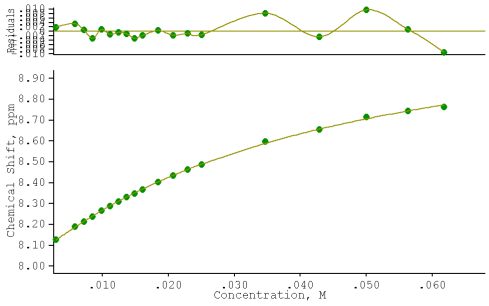

Figure A2.2.41: Binding curve from the ^{1}H NMR titration of receptor **233** with TBA chloride in 0.5 % H_2O/DMSO-d_6 following the most upfield urea NH group. This data was fitted to a 1:1 binding model using WinEQNMR 2. K_a = 26 M^{-1} (4 % error).

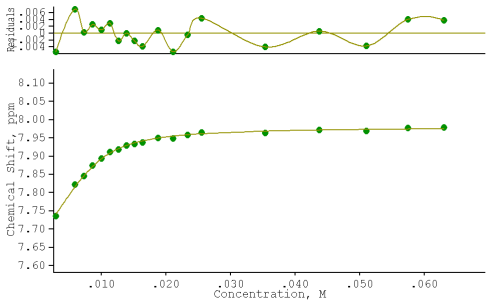

Figure A2.2.42: Binding curve from the ^{1}H NMR titration of receptor **233** with TEA bicarbonate in 0.5 % H_2O/DMSO-d_6 following an aromatic CH group. This data was fitted to a 1:1 binding model using WinEQNMR 2. K_a = 931 M^{-1} (8 % error).

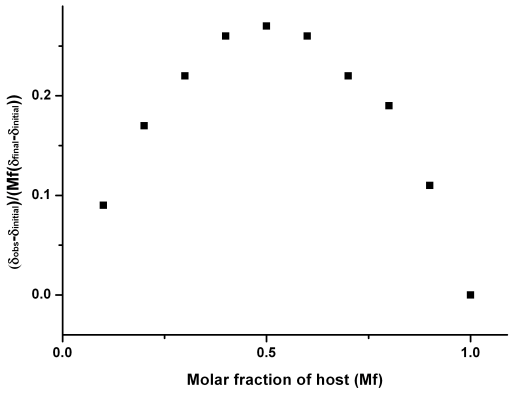

Figure A2.2.43: Job plot from the ^{1}H NMR titration of receptor **204** with TBA chloride in 0.5 % H_2O/DMSO-d_6 following the most downfield urea NH group.

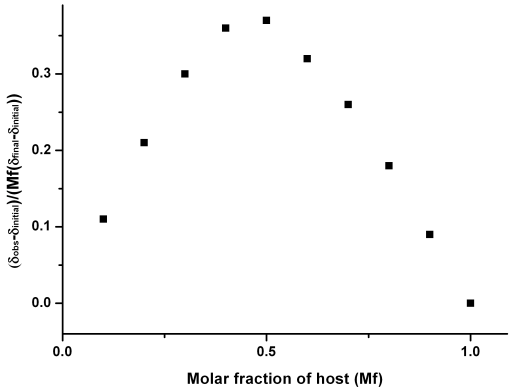

Figure A2.2.44: Job plot from the ^{1}H NMR titration of receptor **204** with TEA bicarbonate in 0.5 % H_2O/DMSO-d_6 following the most downfield urea NH group.

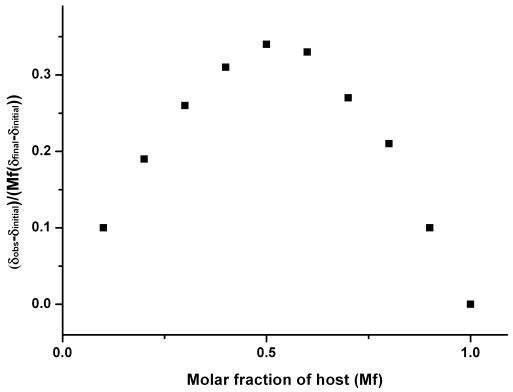

Figure A2.2.45: Job plot from the ^{1}H NMR titration of receptor **223** with TEA bicarbonate in 0.5 % H_2O/DMSO-d_6 following the most upfield urea NH group.

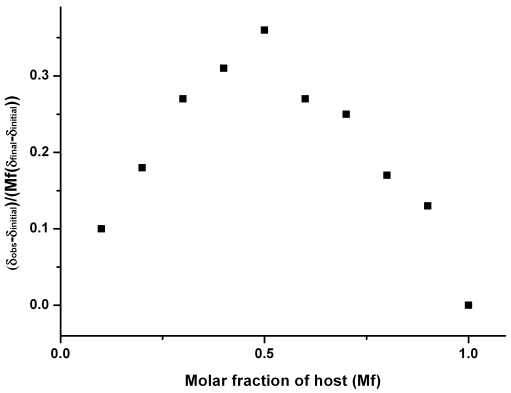

Figure A2.2.46: Job plot from the ^{1}H NMR titration of receptor **226** with TBA chloride in 0.5 % H_2O/DMSO-d_6 following the most upfield urea NH group.

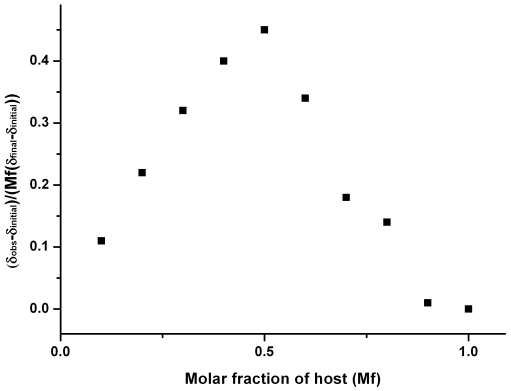

Figure A2.2.47: Job plot from the ^{1}H NMR titration of receptor **226** with TEA bicarbonate in 0.5 % H_2O/DMSO-d_6 following the most upfield urea NH group.

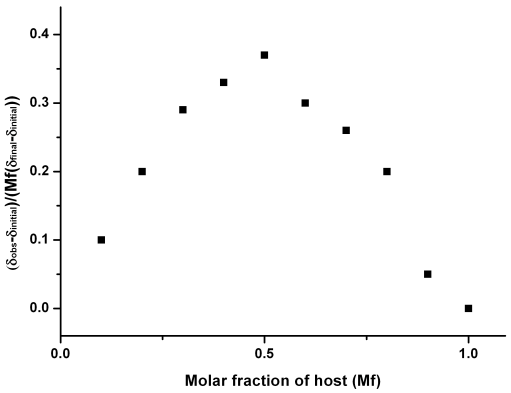

Figure A2.2.48: Job plot from the ^{1}H NMR titration of receptor **227** with TEA bicarbonate in 0.5 % H_2O/DMSO-d_6 following the most upfield urea NH group.

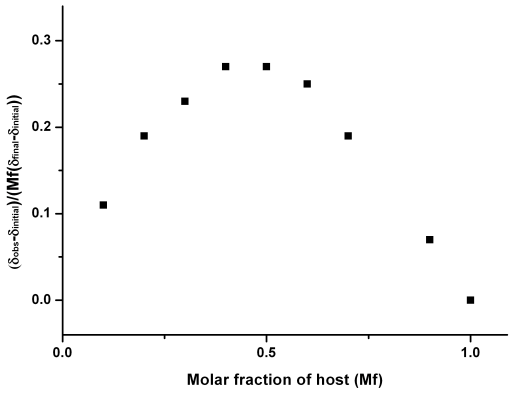

Figure A2.2.49: Job plot from the ^{1}H NMR titration of receptor **228** with TBA chloride in 0.5 % H_2O/DMSO-d_6 following the most upfield urea NH group.

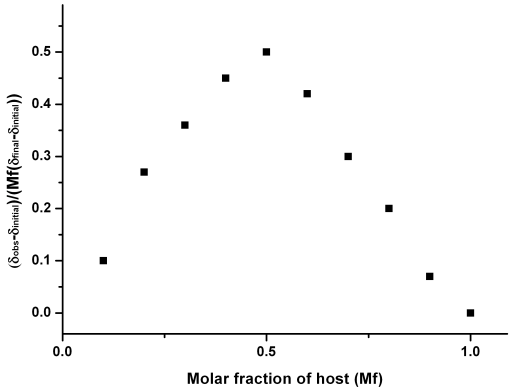

Figure A2.2.50: Job plot from the ^{1}H NMR titration of receptor **229** with TEA bicarbonate in 0.5 % H_2O/DMSO-d_6 following the most upfield urea NH group.

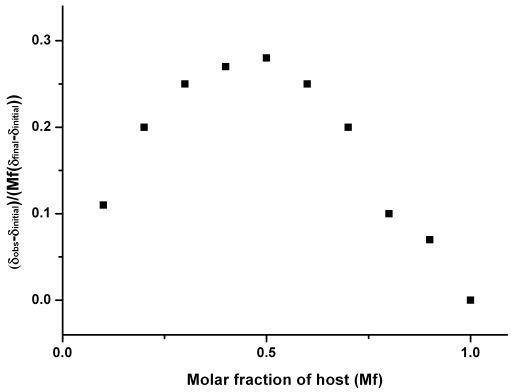

Figure A2.2.51: Job plot from the ^{1}H NMR titration of receptor **230** with TEA bicarbonate in 0.5 % H_2O/DMSO-d_6 following the most upfield urea NH group.

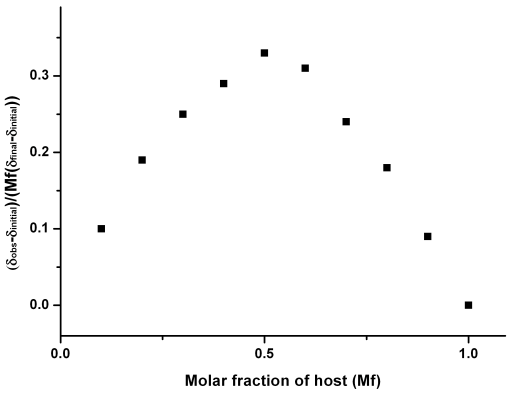

Figure A2.2.52: Job plot from the ^{1}H NMR titration of receptor **232** with TEA bicarbonate in 0.5 % H_2O/DMSO-d_6 following the most upfield urea NH group.

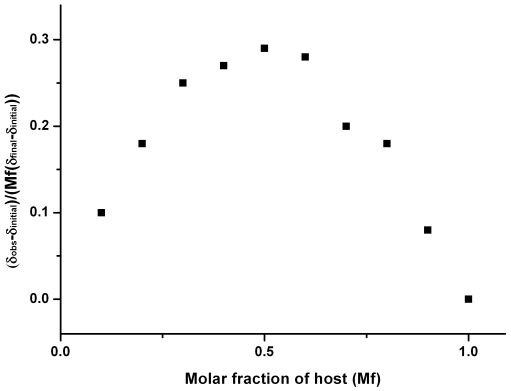

Figure A2.2.53: Job plot from the ^{1}H NMR titration of receptor **233** with TBA chloride in 0.5 % H_2O/DMSO-d_6 following the most upfield urea NH group.

A2.3 NMR Data from Chapter 4

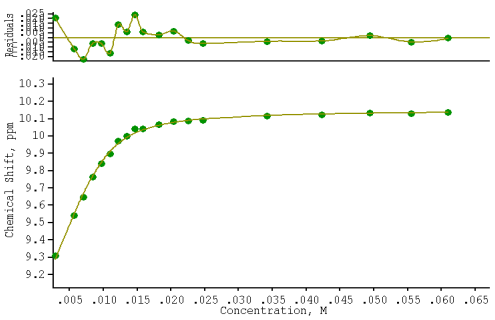

Figure A2.3.1: Binding curve from the ^{1}H NMR titration of receptor **244** with TEA bicarbonate in 0.5 % H_2O/DMSO-d_6 following the most downfield urea NH group. This data was fitted to a 1:1 binding model using WinEQNMR 2. K_a = 1370 M^{-1} (8 % error).

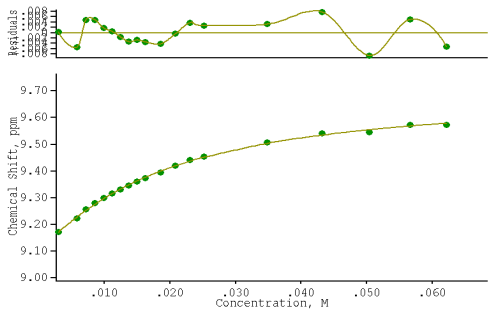

Figure A2.3.2: Binding curve from the ^{1}H NMR titration of receptor **262** with TBA chloride in 0.5 % H_2O/DMSO-d_6 following the most downfield urea NH group. This data was fitted to a 1:1 binding model using WinEQNMR 2. K_a = 73 M^{-1} (5 % error).

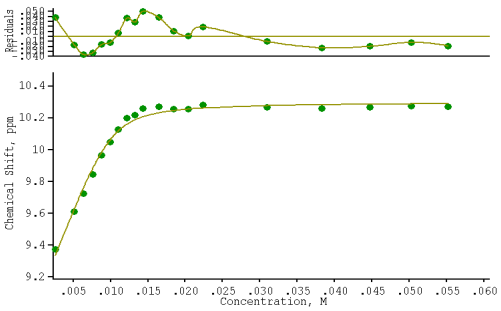

Figure A2.3.3: Binding curve from the ^{1}H NMR titration of receptor **245** with TEA bicarbonate in 0.5 % H_2O/DMSO-d_6 following the most downfield urea NH group. This data was fitted to a 1:1 binding model using WinEQNMR 2. K_a = 2570 M^{-1} (5 % error).

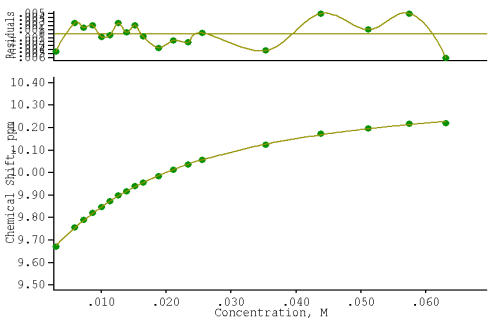

Figure A2.3.4: Binding curve from the ^{1}H NMR titration of receptor **263** with TBA chloride in 0.5 % H_2O/DMSO-d_6 following the most upfield urea NH group. This data was fitted to a 1:1 binding model using WinEQNMR 2. K_a = 74 M^{-1} (3 % error).

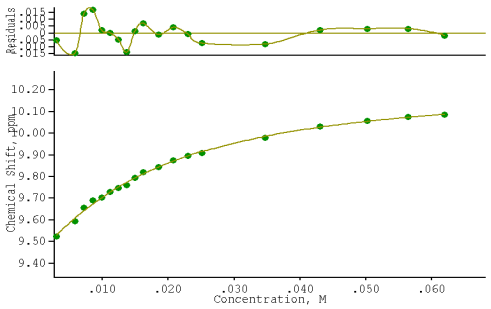

Figure A2.3.5: Binding curve from the ^{1}H NMR titration of receptor **264** with TBA chloride in 0.5 % H_2O/DMSO-d_6 following the most upfield urea NH group. This data was fitted to a 1:1 binding model using WinEQNMR 2. K_a = 78 M^{-1} (7 % error).

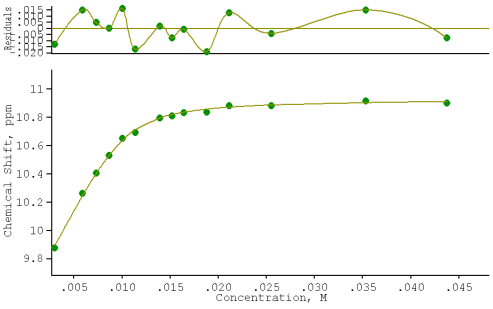

Figure A2.3.6: Binding curve from the ^{1}H NMR titration of receptor **264** with TEA bicarbonate in 0.5 % H_2O/DMSO-d_6 following the most upfield urea NH group. This data was fitted to a 1:1 binding model using WinEQNMR 2. K_a = 2090 M^{-1} (10 % error).

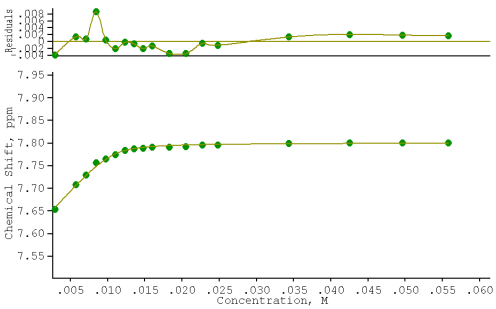

Figure A2.3.7: Binding curve from the ^{1}H NMR titration of receptor **247** with TEA bicarbonate in 0.5 % H_2O/DMSO-d_6 following the most upfield urea NH group. This data was fitted to a 1:1 binding model using WinEQNMR 2. K_a = 3770 M^{-1} (14 % error).

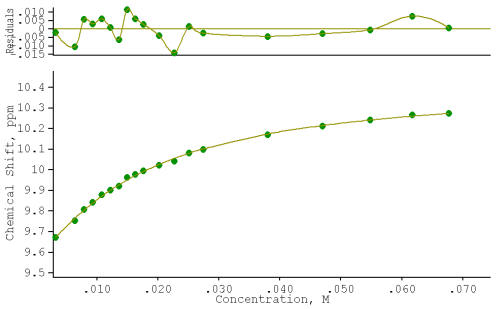

Figure A2.3.8: Binding curve from the ^{1}H NMR titration of receptor **265** with TBA chloride in 0.5 % H_2O/DMSO-d_6 following the most upfield urea NH group. This data was fitted to a 1:1 binding model using WinEQNMR 2. K_a = 81 M^{-1} (5 % error).

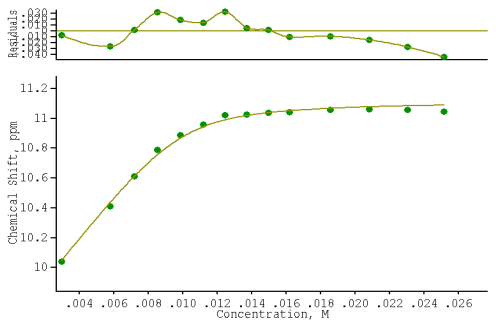

Figure A2.3.9: Binding curve from the ^{1}H NMR titration of receptor **265** with TEA bicarbonate in 0.5 % H_2O/DMSO-d_6 following the most upfield urea NH group. This data was fitted to a 1:1 binding model using WinEQNMR 2. K_a = 3140 M^{-1} (7 % error).

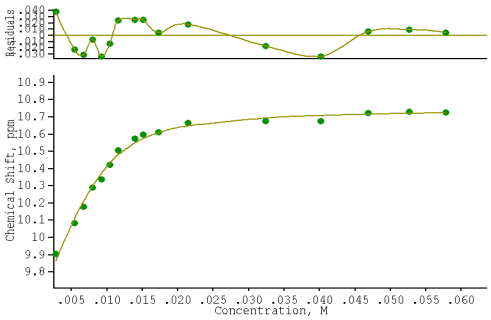

Figure A2.3.10: Binding curve from the ^{1}H NMR titration of receptor **248** with TEA bicarbonate in 0.5 % H_2O/DMSO-d_6 following the most upfield urea NH group. This data was fitted to a 1:1 binding model using WinEQNMR 2. K_a = 826 M^{-1} (14 % error).

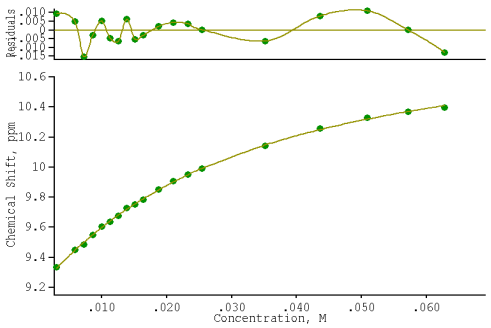

Figure A2.3.11: Binding curve from the ^{1}H NMR titration of receptor **266** with TBA chloride in 0.5 % H_2O/DMSO-d_6 following the most upfield urea NH group. This data was fitted to a 1:1 binding model using WinEQNMR 2. K_a = 41 M^{-1} (4 % error).

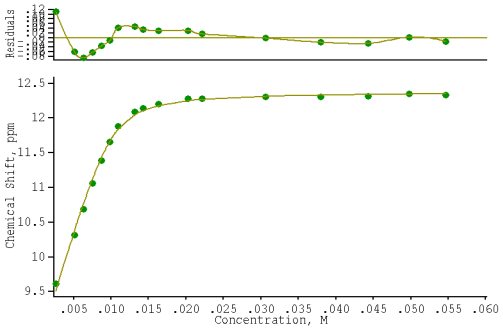

Figure A2.3.12: Binding curve from the ^{1}H NMR titration of receptor **266** with TEA bicarbonate in 0.5 % H_2O/DMSO-d_6 following the most upfield urea NH group. This data was fitted to a 1:1 binding model using WinEQNMR 2. K_a = 2580 M^{-1} (13 % error).

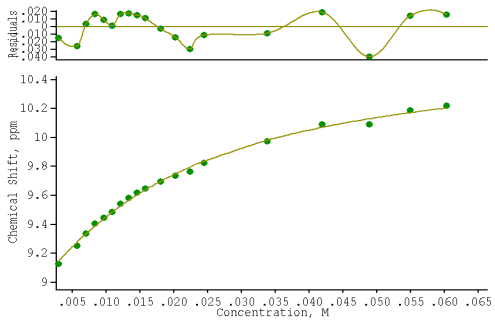

Figure A2.3.13: Binding curve from the ^{1}H NMR titration of receptor **267** with TBA chloride in 0.5 % H_2O/DMSO-d_6 following the most upfield urea NH group. This data was fitted to a 1:1 binding model using WinEQNMR 2. K_a = 61 M^{-1} (9 % error).

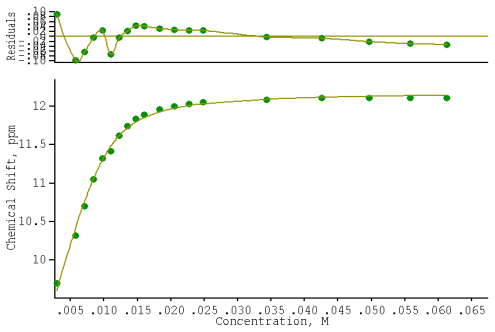

Figure A2.3.14: Binding curve from the ^{1}H NMR titration of receptor **267** with TEA bicarbonate in 0.5 % H_2O/DMSO-d_6 following the most upfield urea NH group. This data was fitted to a 1:1 binding model using WinEQNMR 2. K_a = 1380 M^{-1} (10 % error).

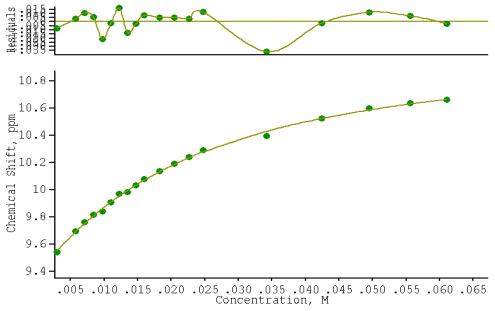

Figure A2.3.15: Binding curve from the ^{1}H NMR titration of receptor **268** with TBA chloride in 0.5 % H_2O/DMSO-d_6 following the most upfield urea NH group. This data was fitted to a 1:1 binding model using WinEQNMR 2. K_a = 57 M^{-1} (6 % error).

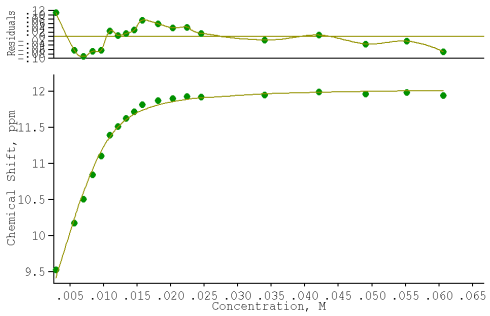

Figure A2.3.16: Binding curve from the ^{1}H NMR titration of receptor **268** with TEA bicarbonate in 0.5 % H_2O/DMSO-d_6 following the most upfield urea NH group. This data was fitted to a 1:1 binding model using WinEQNMR 2. K_a = 1630 M^{-1} (13 % error).

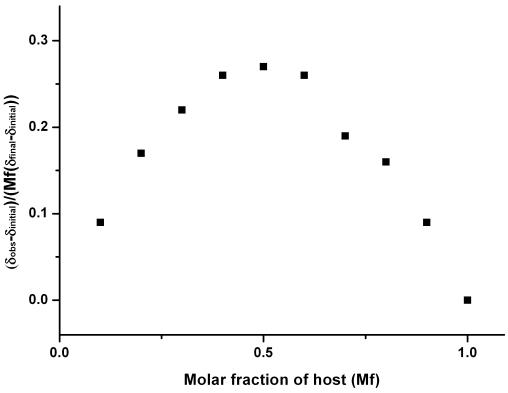

Figure A2.3.17: Job plot from the ^{1}H NMR titration of receptor **262** with TBA chloride in 0.5% H_2O/DMSO following the most upfield urea NH group.

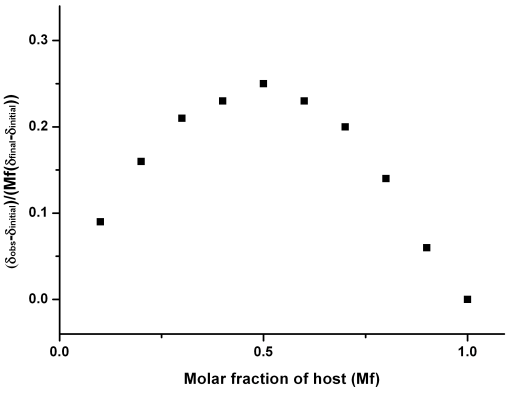

Figure A2.3.18: Job plot from the ^{1}H NMR titration of receptor **245** with TBA chloride in 0.5 % H_2O/DMSO-d_6 following the most upfield urea NH group.

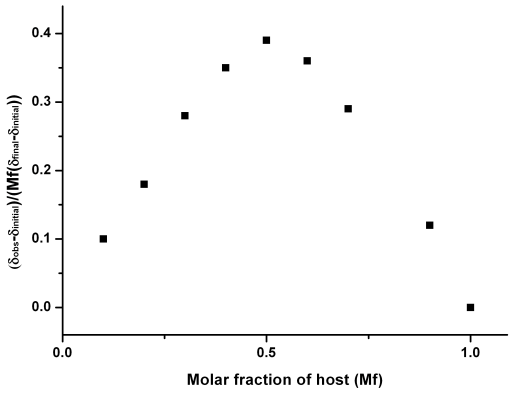

Figure A2.3.19: Job plot from the ^{1}H NMR titration of receptor **263** with TEA bicarbonate in 0.5 % H_2O/DMSO-d_6 following the most upfield urea NH group.

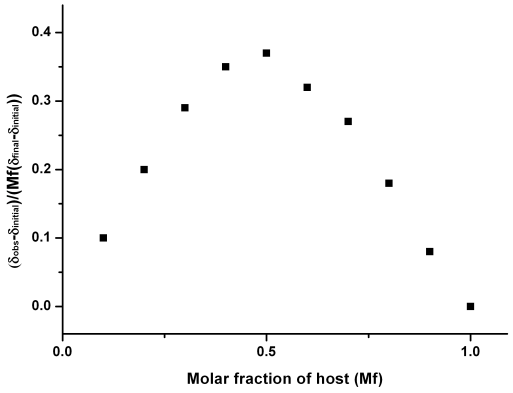

Figure A2.3.20: Job plot from the ^{1}H NMR titration of receptor **264** with TEA bicarbonate in 0.5 % H_2O/DMSO-d_6 following the most upfield urea NH group.

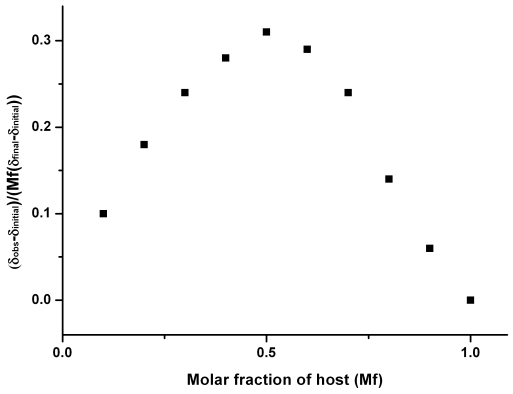

Figure A2.3.21: Job plot from the ^{1}H NMR titration of receptor **247** with TBA chloride in 0.5 % H_2O/DMSO-d_6 following the most upfield urea NH group.

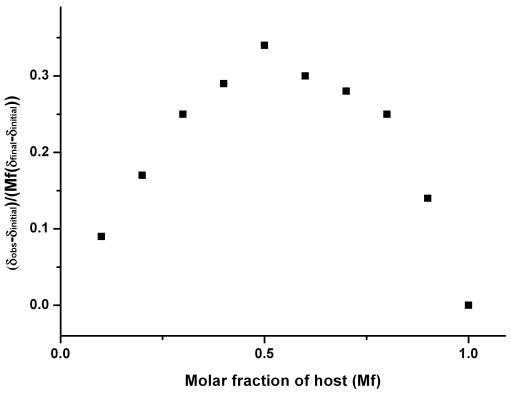

Figure A2.3.22: Job plot from the ^{1}H NMR titration of receptor **248** with TEA bicarbonate in 0.5 % H_2O/DMSO-d_6 following the most upfield urea NH group.

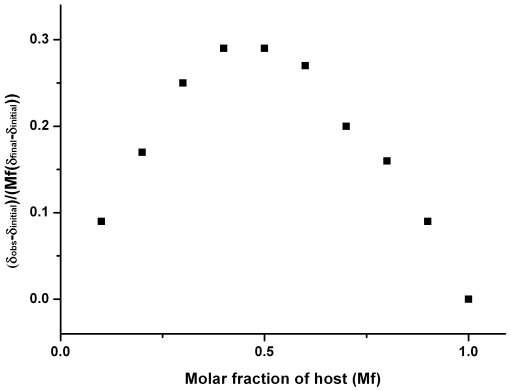

Figure A2.3.23: Job plot from the ^{1}H NMR titration of receptor **266** with TBA chloride in 0.5 % H_2O/DMSO-d_6 following the most upfield urea NH group.

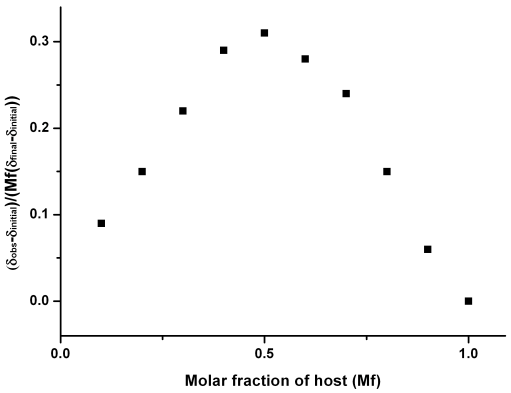

Figure A2.3.24: Job plot from the ^{1}H NMR titration of receptor **266** with TEA bicarbonate in 0.5 % H_2O/DMSO-d_6 following the most upfield urea NH group.

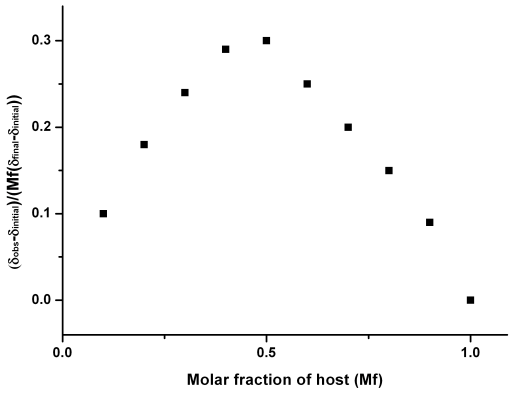

Figure A2.3.25: Job plot from the ^{1}H NMR titration of receptor **267** with TBA chloride in 0.5 % H_2O/DMSO-d_6 following the most upfield urea NH group.

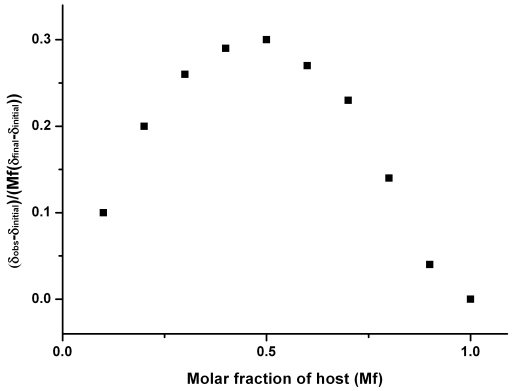

Figure A2.3.26: Job plot from the ^{1}H NMR titration of receptor **268** with TEA bicarbonate in 0.5 % H_2O/DMSO-d_6 following the most upfield urea NH group.

Appendix 3

X-ray Crystal Structure Data

The crystal structures presented in this thesis were solved by the EPSRC National Crystallography Service (M. E. Light). The refinement of these structures and the fractional coordinated are reported for the sake of completeness and so that the structures can be reproduced from the text if required.

A3.1 Structures from Chapter 2

A3.1.1 Receptor 152 (benzoate complex)

Table A3.1: Crystal data and structure refinement details.

Identification code	**2009sot1284**	
Empirical formula	$C_{79}H_{110}N_8O_7$	
Formula weight	1283.75	
Temperature	120(2) K	
Wavelength	0.71073 Å	
Crystal system	Triclinic	
Space group	P-1	
Unit cell dimensions	a = 18.6154(6) Å	α = 101.962(2)°
	b = 19.2475(4) Å	β = 96.8140(10)°
	c = 21.7372(7) Å	γ = 101.730(2)°
Volume	7354.3(4) Å^3	
Z	4	
Density (calculated)	1.159 Mg / m^3	
Absorption coefficient	0.074 mm^{-1}	
F(000)	2784	
Crystal	Fragment; Colourless	
Crystal size	0.20 × 0.10 × 0.03 mm^3	
θ range for data collection	2.92 – 25.03°	
Index ranges	$-22 \le h \le 22$, $-22 \le k \le 22$, $-25 \le l \le 25$	
Reflections collected	97583	
Independent reflections	25672 [R_{int} = 0.1589]	
Completeness to θ = 25.03°	98.9 %	
Absorption correction	Semi–empirical from equivalents	
Max. and min. transmission	0.9978 and 0.9853	
Refinement method	Full-matrix least-squares on F^2	
Data / restraints / parameters	25672 / 1154 / 1625	
Goodness-of-fit on F^2	1.035	
Final R indices [$F^2 > 2\sigma(F^2)$]	*R1* = 0.1786, *wR2* = 0.3531	
R indices (all data)	*R1* = 0.3147, *wR2* = 0.4354	
Largest diff. peak and hole	1.120 and –0.718 e Å^{-3}	

Diffractometer: *Nonius KappaCCD* area detector (ϕ scans and ω scans to fill *asymmetric unit*). **Cell determination:** DirAx (Duisenberg, A.J.M.(1992). J. Appl. Cryst. 25, 92-96.) **Data collection:** Collect (Collect: Data collection software, R. Hooft, Nonius B.V., 1998). **Data reduction and cell refinement**: *Denzo* (Z. Otwinowski & W. Minor, *Methods in Enzymology* (1997) Vol. **276**: *Macromolecular Crystallography*, part A, pp. 307–326; C. W. Carter, Jr. & R. M. Sweet, Eds., Academic Press). **Absorption correction**: Sheldrick, G. M. SADABS - Bruker Nonius area detector scaling and absorption correction - V2.10 **Structure solution**: *SHELXS97* (G. M. Sheldrick, Acta Cryst. (1990) A**46** 467–473). **Structure refinement**: *SHELXL97* (G. M. Sheldrick (1997), University of Göttingen, Germany). **Graphics:** Cameron - A Molecular Graphics Package. (D. M. Watkin, L. Pearce and C. K. Prout, Chemical Crystallography Laboratory, University of Oxford, 1993).
Special details: All hydrogen atoms were placed in idealised positions and refined using a riding model.

Table A3.2: Atomic coordinates [× 10^4], equivalent isotropic displacement parameters [Å^2 × 10^3] and site occupancy factors. U_{eq} is defined as one third of the trace of the orthogonalized U^{ij} tensor.

Atom	*x*	*y*	*z*	U_{eq}	*S.o.f.*
O1	−743(4)	−2953(3)	2719(3)	52(2)	1
O2	2214(3)	219(3)	4913(3)	45(2)	1
O3	−327(4)	1301(3)	2491(3)	51(2)	1
N1	−488(4)	−4043(4)	2792(4)	48(2)	1
N2	533(4)	−2199(4)	3606(3)	37(2)	1
N3	1479(4)	−696(4)	4111(3)	35(2)	1
N4	1611(4)	489(4)	4046(3)	35(2)	1
N5	906(4)	1431(3)	3387(3)	31(2)	1
N6	−103(5)	2532(4)	2599(4)	51(2)	1
C1	−1015(6)	−4128(5)	1145(5)	57(2)	1
C2	−685(7)	−4061(6)	615(5)	64(2)	1
C3	−23(7)	−4266(6)	551(5)	64(2)	1
C4	302(6)	−4548(6)	1008(5)	60(2)	1
C5	−30(6)	−4626(5)	1539(5)	54(2)	1
C6	−685(6)	−4403(5)	1615(5)	49(2)	1
C7	−1009(5)	−4449(5)	2206(5)	52(2)	1
C8	−358(5)	−3306(5)	2968(4)	39(2)	1
C9	271(5)	−2950(5)	3484(4)	40(2)	1
C10	724(5)	−3230(5)	3862(4)	43(2)	1
C11	1311(6)	−2632(5)	4235(4)	43(2)	1
C12	1938(6)	−2569(5)	4679(4)	49(2)	1
C13	2402(6)	−1908(6)	4915(5)	51(2)	1
C14	2266(5)	−1272(5)	4737(4)	45(2)	1
C15	1645(5)	−1302(5)	4314(4)	40(2)	1
C16	1175(5)	−1995(5)	4050(4)	37(2)	1
C17	1805(5)	21(5)	4402(4)	34(2)	1
C18	1864(5)	1251(5)	4203(4)	40(2)	1
C19	2454(6)	1645(5)	4686(4)	51(2)	1
C20	2677(6)	2395(5)	4829(5)	57(2)	1
C21	2306(6)	2797(5)	4496(5)	53(2)	1
C22	1719(5)	2436(5)	3997(4)	41(2)	1
C23	1226(5)	2652(5)	3576(4)	43(2)	1
C24	723(5)	2034(5)	3210(4)	39(2)	1
C25	1507(5)	1655(5)	3866(4)	36(2)	1
C26	56(5)	1926(5)	2730(4)	41(2)	1
C27	−784(6)	2504(6)	2191(5)	60(2)	1
C28	−666(6)	2615(6)	1549(5)	61(2)	1
C29	−355(7)	3279(6)	1447(6)	76(3)	1
C30	−258(8)	3378(7)	855(6)	81(3)	1

C31	−462(8)	2823(7)	337(6)	81(3)	1
C32	−800(8)	2147(7)	409(6)	90(3)	1
C33	−898(7)	2032(7)	1003(6)	78(3)	1
O4	5489(3)	3476(3)	2447(3)	46(2)	1
O5	2646(4)	4230(3)	35(3)	47(2)	1
O6	5313(4)	7527(4)	2245(5)	78(3)	1
N7	5441(4)	2277(4)	2356(4)	46(2)	1
N8	4282(4)	3184(3)	1488(3)	29(2)	1
N9	3359(4)	4003(4)	876(3)	36(2)	1
N10	3288(4)	5176(4)	885(3)	36(2)	1
N11	4022(4)	6725(4)	1466(3)	35(2)	1
N12	5034(5)	8603(4)	2184(5)	65(3)	1
C34	5931(8)	3072(8)	4011(7)	98(3)	1
C35	5657(9)	3067(9)	4583(7)	109(4)	1
C36	5176(9)	2459(8)	4647(7)	101(3)	1
C37	4961(8)	1839(8)	4174(6)	86(3)	1
C38	5244(7)	1833(7)	3612(6)	74(3)	1
C39	5740(7)	2433(7)	3523(6)	71(2)	1
C40	6016(6)	2403(7)	2900(5)	64(3)	1
C41	5207(5)	2839(5)	2170(4)	38(2)	1
C42	4600(5)	2631(4)	1627(4)	35(2)	1
C43	4239(5)	1995(4)	1222(4)	36(2)	1
C44	3660(5)	2133(4)	796(4)	36(2)	1
C45	3116(5)	1701(5)	293(4)	45(2)	1
C46	2620(6)	2029(5)	5(4)	45(2)	1
C47	2688(5)	2792(5)	188(4)	42(2)	1
C48	3232(5)	3239(4)	670(4)	36(2)	1
C49	3707(5)	2895(4)	995(4)	30(2)	1
C50	3064(5)	4448(5)	550(4)	40(2)	1
C51	3007(5)	5750(5)	729(4)	39(2)	1
C52	2339(5)	5652(5)	301(4)	43(2)	1
C53	2092(6)	6259(5)	169(4)	48(2)	1
C54	2472(6)	6965(5)	467(4)	45(2)	1
C55	3123(5)	7087(5)	903(4)	40(2)	1
C56	3637(5)	7703(5)	1285(5)	44(2)	1
C57	4178(5)	7485(5)	1616(5)	45(2)	1
C58	3380(5)	6471(4)	1028(4)	34(2)	1
C59	4875(6)	7868(5)	2047(5)	53(2)	1
C60	5764(6)	9045(6)	2500(8)	86(3)	1
C61	5833(7)	9290(6)	3199(9)	91(3)	1
C62	5731(7)	9970(7)	3479(9)	105(3)	1
C63	5797(8)	10203(8)	4145(9)	116(4)	1
C64	5985(8)	9757(8)	4541(9)	120(4)	1
C65	6092(7)	9092(8)	4233(9)	115(4)	1
C66	6000(7)	8841(7)	3597(9)	103(3)	1
O7	286(3)	−1021(3)	3102(3)	43(2)	1

O8	801(3)	−33(3)	2787(3)	40(2)	1
C67	−390(5)	−1746(5)	1853(5)	50(2)	1
C68	−708(6)	−2091(6)	1211(5)	61(2)	1
C69	−612(7)	−1712(7)	758(5)	72(3)	1
C70	−204(7)	−1007(7)	898(5)	76(3)	1
C71	100(6)	−674(6)	1531(5)	59(2)	1
C72	25(5)	−1039(5)	2006(4)	42(2)	1
C73	391(5)	−670(5)	2678(4)	39(2)	1
O9	4141(3)	4561(3)	2133(3)	39(2)	1
O10	4558(3)	5606(3)	1866(3)	42(2)	1
C74	4873(6)	5132(5)	3381(5)	51(2)	1
C75	5191(6)	5438(6)	4021(5)	66(3)	1
C76	5496(6)	6176(6)	4210(5)	68(3)	1
C77	5506(6)	6589(6)	3774(5)	58(2)	1
C78	5199(5)	6305(5)	3149(5)	47(2)	1
C79	4871(5)	5566(4)	2948(4)	36(2)	1
C80	4495(5)	5215(5)	2262(4)	33(2)	1
O11	691(5)	4018(4)	3142(4)	70(2)	1
O12	393(4)	5038(3)	3103(3)	56(2)	1
C81	−498(8)	4887(6)	4015(6)	149(2)	1
C82	−847(7)	4849(6)	4542(6)	149(2)	1
C83	−812(8)	4287(6)	4848(5)	149(2)	1
C84	−429(8)	3763(6)	4627(6)	149(2)	1
C85	−80(8)	3801(6)	4100(6)	149(2)	1
C86	−114(8)	4363(6)	3794(5)	149(2)	1
C87	323(9)	4468(8)	3284(7)	109(3)	1
O13	4264(4)	9609(3)	1823(3)	52(2)	1
O14	4750(4)	10792(3)	2053(3)	56(2)	1
C88	5691(9)	10605(7)	1145(8)	117(2)	1
C89	6065(9)	10496(7)	612(8)	117(2)	1
C90	5935(9)	9817(7)	211(8)	117(2)	1
C91	5497(9)	9265(7)	370(8)	117(2)	1
C92	5092(9)	9360(7)	851(8)	117(2)	1
C93	5180(10)	10044(7)	1245(8)	117(2)	1
C94	4698(8)	10151(6)	1745(6)	77(3)	1
N13	−1516(4)	−25(4)	3418(3)	46(2)	1
C95	−2035(6)	459(7)	3538(5)	64(3)	1
C96	−1771(6)	1234(7)	3465(6)	73(3)	1
C97	−2404(8)	1602(8)	3362(7)	93(3)	1
C98	−2054(9)	2479(9)	3449(8)	123(5)	1
C99	−736(4)	343(5)	3785(4)	37(2)	1
C100	−688(5)	527(5)	4512(4)	40(2)	1
C101	47(5)	1064(5)	4842(4)	46(2)	1
C102	97(6)	1849(5)	4779(4)	50(2)	1
C103	−1430(5)	−189(6)	2710(4)	49(2)	1

C104	−2147(6)	−520(7)	2247(5)	65(3)	1
C105	−1989(6)	−664(6)	1558(5)	66(3)	1
C106	−1744(8)	13(7)	1335(6)	92(4)	1
C107	−1841(6)	−739(6)	3601(5)	58(2)	1
C108	−1431(7)	−1339(6)	3461(5)	66(3)	1
C109	−1730(7)	−2003(7)	3748(6)	84(3)	1
C110	−2469(9)	−2394(8)	3453(8)	124(5)	1
N14	2688(4)	965(4)	2273(4)	45(2)	1
C111	1931(6)	1131(6)	2121(5)	58(2)	1
C112	1867(6)	1544(7)	1607(6)	74(2)	1
C13A	1095(7)	1643(7)	1432(6)	80(2)	0.473(15)
C14A	973(13)	1976(15)	903(11)	87(4)	0.473(15)
C13B	1095(7)	1643(7)	1432(6)	80(2)	0.527(15)
C14B	735(11)	972(12)	821(9)	87(4)	0.527(15)
C115	3302(6)	1656(5)	2471(5)	49(2)	1
C116	3235(6)	2192(5)	3056(5)	60(2)	1
C117	3833(7)	2894(5)	3180(5)	65(3)	1
C118	3834(9)	3446(7)	3758(6)	106(5)	1
C119	2866(6)	489(5)	1680(5)	56(3)	1
C120	2366(7)	−283(5)	1456(5)	65(3)	1
C121	2521(7)	−684(6)	826(6)	76(3)	1
C122	2188(9)	−430(7)	284(6)	101(4)	1
C123	2655(6)	565(5)	2804(5)	52(2)	1
C124	3345(6)	337(5)	3008(5)	54(2)	1
C125	3198(6)	−220(5)	3419(5)	57(2)	1
C126	2731(7)	−965(5)	3045(5)	70(3)	1
N15	6504(4)	4910(4)	1517(3)	39(2)	1
C127	6821(5)	5643(5)	1381(4)	43(2)	1
C128	6390(6)	6223(5)	1556(5)	52(2)	1
C129	6687(7)	6904(6)	1308(5)	65(3)	1
C130	7401(9)	7271(9)	1586(9)	136(6)	1
C131	6394(5)	4998(5)	2207(4)	43(2)	1
C132	7091(6)	5307(6)	2700(5)	55(2)	1
C133	6929(6)	5414(7)	3376(5)	66(3)	1
C134	7642(8)	5705(9)	3836(6)	109(5)	1
C135	5749(5)	4544(5)	1100(4)	39(2)	1
C136	5738(5)	4441(5)	392(4)	44(2)	1
C137	5035(5)	3868(5)	1(5)	50(2)	1
C138	5072(6)	3095(5)	2(5)	54(3)	1
C139	7059(5)	4441(5)	1369(5)	45(2)	1
C140	6829(5)	3662(5)	1436(5)	53(2)	1
C141	7461(6)	3282(5)	1418(5)	57(2)	1
C142	7225(7)	2494(6)	1423(7)	85(4)	1
N16	2454(4)	6043(4)	2863(4)	41(2)	1
C143	2463(6)	5399(5)	2316(5)	51(2)	1
C144	1752(6)	4798(6)	2117(5)	62(2)	1

C145	1868(7)	4109(7)	1720(6)	81(3)	1
C146	2290(8)	3697(7)	2105(8)	106(4)	1
C147	2306(6)	5790(6)	3461(5)	57(2)	1
C148	2864(7)	5398(7)	3725(6)	77(3)	1
C149	2655(9)	5220(9)	4345(7)	106(4)	1
C150	3205(12)	4933(11)	4670(9)	161(7)	1
C151	3217(5)	6569(5)	2979(5)	50(2)	1
C152	3319(6)	7236(5)	3525(5)	60(2)	1
C153	3995(6)	7830(6)	3502(6)	69(3)	1
C154	4119(7)	8481(6)	4091(6)	82(4)	1
C155	1835(5)	6401(5)	2687(4)	39(2)	1
C156	1895(5)	6787(5)	2138(4)	46(2)	1
C157	1298(6)	7222(5)	2104(5)	49(2)	1
C158	1339(6)	7626(6)	1573(5)	64(3)	1

Table A3.3: Hydrogen bonds [Å and °].

D–H···*A*	*d*(*D*–H)	*d*(H···*A*)	*d*(*D*···*A*)	∠(*D*H*A*)
N1–H1···O12^{i}	0.88	1.98	2.774(10)	149.0
N7–H7···O14^{i}	0.88	1.97	2.789(10)	154.1
N2–H2···O7	0.88	1.98	2.808(9)	156.5
N3–H3···O7	0.88	1.93	2.800(9)	171.4
N4–H4···O8	0.88	1.97	2.835(9)	165.7
N5–H5···O8	0.88	2.05	2.806(9)	144.1
N6–H6···O11	0.88	2.01	2.869(11)	165.0
N8–H8···O9	0.88	2.03	2.809(8)	147.3
N9–H9···O9	0.88	1.95	2.818(9)	168.0
N10–H10A···O10	0.88	1.98	2.846(9)	168.0
N11–H11···O10	0.88	1.96	2.799(9)	160.1
N12–H12A···O13	0.88	1.98	2.813(10)	156.6

Symmetry transformations used to generate equivalent atoms:
(i) x,y−1,z

A3.1.2 Receptor 155 (sulphate complex)

Table A3.4: Crystal data and structure refinement details.

Identification code	**2010sot0344**	
Empirical formula	$C_{74}H_{166}N_{16}O_{12}S$	
	$2(C_{21}H_{45}N_7O_3)$, $2(C_{16}H_{36}N)$, SO_4, $2(H_2O)$	
Formula weight	1504.29	
Temperature	120(2) K	
Wavelength	0.71073 Å	
Crystal system	Triclinic	
Space group	*P*–1	
Unit cell dimensions	a = 13.3171(4) Å	α = 90.1722(16)°
	b = 14.1510(6) Å	β = 103.847(3)°
	c = 24.6875(10) Å	γ = 90.899(2)°
Volume	4516.5(3) $Å^3$	
Z	2	
Density (calculated)	1.106 Mg / m^3	
Absorption coefficient	0.097 mm^{-1}	
F(000)	1668	
Crystal	Slab; Colourless	
Crystal size	0.35 × 0.24 × 0.08 mm^3	
θ range for data collection	2.92 – 26.47°	
Index ranges	$-16 \le h \le 15$, $-17 \le k \le 17$, $-30 \le l \le 30$	
Reflections collected	79090	
Independent reflections	18486 [R_{int} = 0.1410]	
Completeness to θ = 26.47°	99.0 %	
Absorption correction	Semi–empirical from equivalents	
Max. and min. transmission	0.9923 and 0.9668	
Refinement method	Full-matrix least-squares on F^2	
Data / restraints / parameters	18486 / 235 / 998	
Goodness-of-fit on F^2	1.006	
Final *R* indices [$F^2 > 2\sigma(F^2)$]	*R1* = 0.0757, *wR2* = 0.1687	
R indices (all data)	*R1* = 0.1687, *wR2* = 0.2075	
Extinction coefficient	0.0042(5)	
Largest diff. peak and hole	0.517 and –0.375 e $Å^{-3}$	

Diffractometer: *Nonius KappaCCD* area detector (ϕ scans and ω scans to fill *asymmetric unit*). **Cell determination:** DirAx (Duisenberg, A.J.M.(1992). J. Appl. Cryst. 25, 92-96.) **Data collection:** Collect (Collect: Data collection software, R. Hooft, Nonius B.V., 1998). **Data reduction and cell refinement**: *Denzo* (Z. Otwinowski & W. Minor, *Methods in Enzymology* (1997) Vol. **276**: *Macromolecular Crystallography*, part A, pp. 307–326; C. W. Carter, Jr. & R. M. Sweet, Eds., Academic Press). **Absorption correction**: Sheldrick, G. M. SADABS - Bruker Nonius area detector scaling and absorption correction - V2.10 **Structure solution**: *SHELXS97* (G. M. Sheldrick, Acta Cryst. (1990) A**46** 467–473). **Structure refinement**: *SHELXL97* (G. M. Sheldrick (1997), University of Göttingen, Germany). **Graphics:** Cameron - A Molecular Graphics Package. (D. M. Watkin, L. Pearce and C. K. Prout, Chemical Crystallography Laboratory, University of Oxford, 1993).

Special details: Hydrogen atoms were located in the difference map and then placed in idealised positions and refined using a riding model, those of the water were refined using distance restraints. Thermal and geometrical restraints were used to model the disorder of one arm of a TBA and 2 arms of the receptor.

Table A3.5: Atomic coordinates [× 10^4], equivalent isotropic displacement parameters [Å^2 × 10^3] and site occupancy factors. U_{eq} is defined as one third of the trace of the orthogonalized U^{ij} tensor.

Atom	*x*	*y*	*z*	U_{eq}	*S.o.f.*
O1	−799(2)	67(2)	1942(1)	34(1)	1
O2	2082(2)	1671(2)	4705(1)	47(1)	1
O3	−288(2)	5064(2)	2577(1)	40(1)	1
N1	−463(2)	2193(2)	3258(1)	26(1)	1
N2	450(2)	698(2)	2655(1)	31(1)	1
N3	662(2)	726(2)	1765(1)	37(1)	1
N4	1663(2)	2603(2)	3937(1)	31(1)	1
N6	77(2)	3530(2)	2425(1)	29(1)	1
N7	1374(2)	4648(2)	2626(1)	38(1)	1
C1	−938(2)	1272(2)	3069(1)	28(1)	1
C2	−125(2)	529(2)	3073(1)	30(1)	1
C3	47(2)	483(2)	2111(1)	30(1)	1
C4	328(3)	617(2)	1165(1)	40(1)	1
C5	−283(3)	1437(3)	893(2)	45(1)	1
C6	−576(3)	1367(3)	250(2)	49(1)	1
C7	313(3)	1588(3)	−2(2)	62(1)	1
C8	−183(2)	2264(2)	3868(1)	31(1)	1
C9	731(2)	2933(2)	4073(1)	33(1)	1
C10	2238(2)	1930(2)	4253(1)	31(1)	1
N5A	3008(2)	1582(2)	4044(1)	37(1)	0.566(4)
C11A	3834(8)	1007(6)	4365(6)	43(2)	0.566(4)
C12A	3621(6)	−43(5)	4321(3)	50(2)	0.566(4)
C13A	3486(6)	−444(5)	3738(3)	51(1)	0.566(4)
C14A	3478(12)	−1505(6)	3736(5)	78(3)	0.566(4)
N5B	3008(2)	1582(2)	4044(1)	37(1)	0.434(4)
C11B	3564(11)	763(7)	4300(8)	43(2)	0.434(4)
C12B	3190(8)	−118(6)	3958(4)	50(2)	0.434(4)
C13B	3757(7)	−986(6)	4260(4)	51(1)	0.434(4)
C14B	3389(16)	−1859(9)	3926(6)	78(3)	0.434(4)
C15	−1104(2)	2979(2)	2998(1)	29(1)	1
C16	−956(2)	3189(2)	2417(1)	31(1)	1
C17	349(2)	4451(2)	2547(1)	32(1)	1
C18	1817(3)	5583(2)	2777(2)	38(1)	1
C19	2587(3)	5606(3)	3345(2)	55(1)	1
C20	2145(4)	5327(3)	3826(2)	69(1)	1
C21	1286(4)	5950(4)	3912(2)	91(2)	1
O4	6341(2)	4624(2)	3035(1)	36(1)	1
O5	5600(2)	−308(2)	2218(1)	45(1)	1
O6	2911(2)	3333(2)	405(1)	44(1)	1
N8	5582(2)	2650(2)	1642(1)	28(1)	1

N9	4917(2)	4058(2)	2405(1)	31(1)	1
N11	5195(2)	1170(2)	2460(1)	33(1)	1
N12	3970(2)	−6(2)	2305(1)	48(1)	1
N13	3378(2)	2205(2)	1069(1)	32(1)	1
C22	6086(2)	3558(2)	1828(1)	29(1)	1
C23	5316(2)	4277(2)	1925(1)	30(1)	1
C24	5489(2)	4200(2)	2928(1)	30(1)	1
N10	5069(2)	3862(2)	3337(1)	38(1)	1
C25	5616(3)	3922(3)	3914(1)	40(1)	1
C26	4917(3)	3661(3)	4293(1)	44(1)	1
C27	5455(3)	3681(3)	4899(2)	54(1)	1
C28	4706(4)	3466(3)	5271(2)	67(1)	1
C29	6248(2)	1850(2)	1859(1)	30(1)	1
C30	6183(2)	1583(2)	2442(1)	32(1)	1
C31	4953(3)	260(2)	2322(2)	37(1)	1
C32	3554(3)	−947(2)	2149(2)	49(1)	1
C33	2760(3)	−989(3)	1592(2)	59(1)	1
C34	3145(4)	−664(3)	1096(2)	73(1)	1
C35	4013(4)	−1255(4)	981(2)	98(2)	1
C36	5181(2)	2606(2)	1044(1)	32(1)	1
C37	4263(2)	1929(2)	870(1)	32(1)	1
C38	2817(3)	2967(2)	845(1)	34(1)	1
N14A	2138(2)	3275(2)	1136(1)	39(1)	0.287(5)
C39A	1410(17)	4002(11)	916(15)	40(2)	0.287(5)
C40A	2008(14)	4920(10)	1085(7)	38(2)	0.287(5)
C41A	1279(10)	5738(8)	950(7)	44(1)	0.287(5)
C42A	1834(11)	6677(9)	1083(6)	54(2)	0.287(5)
N14B	2138(2)	3275(2)	1136(1)	39(1)	0.713(5)
C39B	1628(6)	4193(4)	1014(5)	40(2)	0.713(5)
C40B	2237(5)	5042(4)	1300(2)	38(2)	0.713(5)
C41B	1609(4)	5950(4)	1267(2)	44(1)	0.713(5)
C42B	1277(5)	6350(4)	679(2)	54(2)	0.713(5)
S1	2781(1)	2359(1)	2577(1)	25(1)	1
O7	1864(2)	2285(2)	2811(1)	30(1)	1
O8	3724(2)	2165(2)	3017(1)	34(1)	1
O9	2691(2)	1669(2)	2119(1)	33(1)	1
O10	2856(2)	3324(2)	2363(1)	32(1)	1
N15	2492(2)	2221(2)	6243(1)	27(1)	1
C43	3050(2)	1448(2)	6001(1)	28(1)	1
C44	3079(3)	485(2)	6254(2)	42(1)	1
C45	3548(3)	−200(2)	5922(2)	46(1)	1
C46	3543(3)	−1225(2)	6068(2)	48(1)	1
C47	3045(2)	2472(2)	6837(1)	30(1)	1
C48	4141(2)	2863(2)	6924(1)	34(1)	1
C49	4590(2)	3053(2)	7541(1)	32(1)	1
C50	5684(2)	3454(2)	7656(2)	41(1)	1

C51	2448(2)	3057(2)	5852(1)	29(1)	1
C52	1907(3)	3927(2)	5988(1)	34(1)	1
C53	1818(3)	4641(2)	5521(1)	36(1)	1
C54	1356(3)	5563(3)	5651(2)	49(1)	1
C55A	1406(2)	1892(2)	6257(1)	31(1)	0.458(14)
C56A	722(11)	1500(15)	5716(6)	36(3)	0.458(14)
C57A	−409(10)	1463(13)	5762(7)	46(3)	0.458(14)
C58A	−1124(15)	1230(15)	5195(9)	67(4)	0.458(14)
C55B	1406(2)	1892(2)	6257(1)	31(1)	0.542(14)
C56B	698(10)	1761(11)	5671(5)	36(3)	0.542(14)
C57B	−220(9)	1106(10)	5712(5)	46(3)	0.542(14)
C58B	−993(12)	869(13)	5176(7)	67(4)	0.542(14)
N16	7699(2)	7141(2)	1156(1)	27(1)	1
C59	8308(2)	7331(2)	1756(1)	28(1)	1
C60	9425(2)	7643(2)	1838(1)	31(1)	1
C61	9902(2)	7776(2)	2454(1)	34(1)	1
C62	11011(3)	8132(2)	2574(2)	40(1)	1
C63	7687(2)	8000(2)	789(1)	29(1)	1
C64	7186(3)	8875(2)	942(1)	35(1)	1
C65	7283(3)	9660(2)	532(2)	39(1)	1
C66	6825(3)	10579(3)	658(2)	56(1)	1
C67	6616(2)	6853(2)	1190(1)	29(1)	1
C68	5853(2)	6656(2)	641(1)	35(1)	1
C69	4924(3)	6090(3)	729(2)	45(1)	1
C70	4079(3)	5964(3)	196(2)	60(1)	1
C71	8194(2)	6367(2)	885(1)	28(1)	1
C72	8199(3)	5388(2)	1118(1)	37(1)	1
C73	8593(3)	4716(2)	735(1)	39(1)	1
C74	8582(3)	3694(3)	908(2)	55(1)	1
O11	7663(2)	5549(2)	2481(1)	38(1)	1
O12	7690(2)	9295(2)	2445(1)	35(1)	1

Table A3.6: Hydrogen bonds [Å and °].

D–H···*A*	*d*(*D*–H)	*d*(H···*A*)	*d*(*D*···*A*)	∠(*D*H*A*)
O12–H104···O1^{i}	0.855(17)	1.978(17)	2.814(3)	166(3)
O12–H103···O5^{ii}	0.834(17)	1.948(17)	2.772(3)	170(3)
O11–H102···O3^{iii}	0.840(17)	1.959(18)	2.779(3)	165(3)
O11–H101···O4	0.856(17)	1.952(19)	2.788(3)	165(4)
N2–H902···O7	0.88	2.14	2.872(3)	140.6
N3–H903···O9	0.88	2.06	2.932(3)	168.9
N4–H904···O7	0.88	2.21	2.891(3)	133.8
N6–H906···O7	0.88	2.24	2.955(3)	138.7
N7–H907···O10	0.88	2.06	2.924(3)	167.1
N5A–H5A1···O8	0.88	2.21	3.026(3)	154.7
N5A–H5A1···O7	0.88	2.49	3.229(3)	141.5
N9–H909···O10	0.88	2.02	2.898(3)	171.4
N11–H911···O8	0.88	2.16	3.013(3)	164.5
N12–H912···O9	0.88	2.15	2.914(3)	144.5
N13–H913···O9	0.88	2.22	3.044(3)	156.4
N10–H910···O8	0.88	2.25	2.962(3)	138.4
N14A–H14G···O10	0.88	2.23	2.952(4)	138.5
N14A–H14G···O9	0.88	2.52	3.291(4)	146.7
N14B–H14H···O10	0.88	2.44	2.952(4)	117.8
N14B–H14H···O9	0.88	2.53	3.291(4)	145.0

Symmetry transformations used to generate equivalent atoms:
(i) x+1,y+1,z (ii) x,y+1,z (iii) x+1,y,z

A.3.1.3 Receptor 156 (dihydrogen phosphate complex)

Table A3.7: Crystal data and structure refinement details.

Identification code	**2010sot0448**	
Empirical formula	$C_{39}H_{89}N_8O_5PS_4$	
	$C_{16}H_{36}N$, $C_{21}H_{45}N_7S_3$, C_2H_6O S, H_2PO_4	
Formula weight	909.39	
Temperature	120(2) K	
Wavelength	0.71073 Å	
Crystal system	Triclinic	
Space group	*P*–1	
Unit cell dimensions	a = 12.3418(3) Å	α = 94.0780(10)°
	b = 14.5410(2) Å	β = 90.6050(10)°
	c = 15.6431(3) Å	γ = 110.3830(10)°
Volume	2623.03(9) $Å^3$	
Z	2	
Density (calculated)	1.151 Mg / m^3	
Absorption coefficient	0.256 mm^{-1}	
F(000)	996	
Crystal	Fragment; Colourless	
Crystal size	0.20 × 0.10 × 0.03 mm^3	
θ range for data collection	3.00 – 25.03°	
Index ranges	$-14 \le h \le 14$, $-17 \le k \le 17$, $-18 \le l \le 18$	
Reflections collected	44018	
Independent reflections	9248 [R_{int} = 0.0472]	
Completeness to θ = 25.03°	99.7 %	
Absorption correction	Semi–empirical from equivalents	
Max. and min. transmission	0.9924 and 0.9505	
Refinement method	Full-matrix least-squares on F^2	
Data / restraints / parameters	9248 / 119 / 523	
Goodness-of-fit on F^2	1.017	
Final *R* indices [$F^2 > 2\sigma(F^2)$]	*R1* = 0.0880, *wR2* = 0.2231	
R indices (all data)	*R1* = 0.1077, *wR2* = 0.2417	
Largest diff. peak and hole	1.368 and –1.898 e $Å^{-3}$	

Diffractometer: *Nonius KappaCCD* area detector (ϕ scans and ω scans to fill *asymmetric unit*). **Cell determination:** DirAx (Duisenberg, A.J.M.(1992). J. Appl. Cryst. 25, 92-96.) **Data collection:** Collect (Collect: Data collection software, R. Hooft, Nonius B.V., 1998). **Data reduction and cell refinement**: *Denzo* (Z. Otwinowski & W. Minor, *Methods in Enzymology* (1997) Vol. **276**: *Macromolecular Crystallography*, part A, pp. 307–326; C. W. Carter, Jr. & R. M. Sweet, Eds., Academic Press). **Absorption correction**: Sheldrick, G. M. SADABS - Bruker Nonius area detector scaling and absorption correction - V2.10 **Structure solution**: *SHELXS97* (G. M. Sheldrick, Acta Cryst. (1990) A**46** 467–473). **Structure refinement**: *SHELXL97* (G. M. Sheldrick (1997), University of Göttingen, Germany). **Graphics:** Cameron - A Molecular Graphics Package. (D. M. Watkin, L. Pearce and C. K. Prout, Chemical Crystallography Laboratory, University of Oxford, 1993).

Special details: The DMSO is modelled as disordered over 2 slightly rotated orientations. The protons on the H2Po4 were clearly identified in the difference maps and subsequently refined using distance and thermal parameter restraints. Several of the TBA arms are disordered and the extent of this disorder has made the refinement slow to converge, and even after extensive modelling several large difference peaks remain in the vanity of the molecule.

Table A3.8: Atomic coordinates [$\times 10^4$], equivalent isotropic displacement parameters [$Å^2 \times 10^3$] and site occupancy factors. U_{eq} is defined as one third of the trace of the orthogonalized U^{ij} tensor.

Atom	*x*	*y*	*z*	U_{eq}	*S.o.f.*
S1	6970(1)	7139(1)	464(1)	33(1)	1
S2	12064(1)	7530(1)	1971(1)	45(1)	1
S3	8555(1)	5477(1)	5950(1)	35(1)	1
N1	7584(1)	8329(1)	1897(1)	32(1)	1
N2	7871(1)	6881(1)	1953(1)	28(1)	1
N3	10929(1)	8728(1)	2428(1)	42(1)	1
N4	10610(1)	7446(1)	3245(1)	30(1)	1
N5	9017(1)	7384(1)	5764(1)	35(1)	1
N6	7861(1)	6342(1)	4709(1)	28(1)	1
N7	8565(1)	5602(1)	3030(1)	25(1)	1
C1	4659(2)	9951(2)	1434(2)	53(1)	1
C2	5844(2)	9902(1)	1235(1)	39(1)	1
C3	6120(2)	9123(1)	1706(1)	35(1)	1
C4	7312(2)	9114(1)	1517(1)	34(1)	1
C5	7513(1)	7471(1)	1487(1)	27(1)	1
C6	8020(2)	5984(1)	1597(1)	32(1)	1
C7	7805(2)	5236(1)	2269(1)	31(1)	1
C8	10369(3)	11378(2)	867(2)	103(1)	1
C9	11117(3)	10697(2)	937(2)	74(1)	1
C10	10722(2)	10043(2)	1660(2)	73(1)	1
C11	11354(2)	9321(2)	1707(2)	51(1)	1
C12	11144(2)	7909(1)	2578(1)	35(1)	1
C13	10615(2)	6485(1)	3454(1)	30(1)	1
C14	9756(1)	5656(1)	2873(1)	29(1)	1
C15	13112(2)	8114(2)	6818(2)	63(1)	1
C16	11890(2)	7991(2)	7031(2)	53(1)	1
C17	11060(2)	7748(1)	6254(1)	42(1)	1
C18	9854(2)	7687(1)	6485(1)	41(1)	1
C19	8477(1)	6452(1)	5447(1)	29(1)	1
C20	7275(2)	5392(1)	4250(1)	32(1)	1
C21	8094(2)	5005(1)	3751(1)	30(1)	1
N8	6690(1)	4905(1)	−1679(1)	27(1)	1
C22	6258(1)	4146(1)	−2443(1)	29(1)	1
C23	4964(2)	3783(2)	−2634(1)	47(1)	1
C24	4621(2)	2969(2)	−3365(1)	52(1)	1
C25	5092(2)	3289(2)	−4223(1)	48(1)	1
C26A	6182(2)	4499(1)	−850(1)	33(1)	0.370(3)
C27A	6552(4)	3663(3)	−559(3)	33(1)	0.370(3)
C28A	6163(4)	3377(3)	336(3)	33(1)	0.370(3)
C29A	6501(4)	2594(3)	672(3)	33(1)	0.370(3)
C26B	6182(2)	4499(1)	−850(1)	33(1)	0.630(3)

C27B	6297(2)	3557(2)	−643(2)	33(1)	0.630(3)
C28B	5995(3)	3379(2)	299(2)	33(1)	0.630(3)
C29B	5846(2)	2359(2)	496(2)	33(1)	0.630(3)
C30	8005(1)	5180(1)	−1653(1)	30(1)	1
C31	8639(2)	5815(2)	−871(2)	58(1)	1
C32A	9946(2)	6110(2)	−961(2)	58(1)	0.80
C33A	10662(3)	6612(2)	−144(2)	58(1)	0.80
C32B	9946(2)	6110(2)	−961(2)	58(1)	0.10
C33B	11074(10)	6981(11)	−739(15)	58(1)	0.10
C32C	9946(2)	6110(2)	−961(2)	58(1)	0.10
C33C	11030(4)	6059(6)	−496(5)	58(1)	0.10
C34A	6341(2)	5798(2)	−1785(2)	69(1)	0.590(3)
C35A	6952(3)	6412(3)	−2515(3)	69(1)	0.590(3)
C36A	6391(4)	7189(2)	−2661(2)	69(1)	0.590(3)
C37A	6563(3)	7911(2)	−2044(2)	69(1)	0.590(3)
C34B	6341(2)	5798(2)	−1785(2)	69(1)	0.410(3)
C35B	6388(4)	6214(3)	−2663(3)	69(1)	0.410(3)
C36B	5581(4)	6854(3)	−2913(3)	69(1)	0.410(3)
C37B	5077(4)	7150(4)	−2209(3)	69(1)	0.410(3)
P1	8802(1)	9023(1)	4081(1)	25(1)	1
O1	7976(1)	9477(1)	3647(1)	43(1)	1
O2	8589(1)	8025(1)	3636(1)	28(1)	1
O3	8681(1)	9049(1)	5038(1)	27(1)	1
O4	10040(1)	9696(1)	3836(1)	38(1)	1
S4A	2831(1)	9269(1)	4604(1)	40(1)	0.3185(14)
O5A	3406(4)	9873(3)	5421(3)	43(1)	0.3185(14)
C38A	3501(5)	8366(4)	4445(5)	61(1)	0.3185(14)
C39A	3470(7)	10016(5)	3759(4)	61(1)	0.3185(14)
S4B	2857(1)	9536(1)	4539(1)	40(1)	0.6815(14)
O5B	3451(2)	10058(2)	5381(1)	43(1)	0.6815(14)
C38B	3627(3)	8736(3)	4197(2)	61(1)	0.6815(14)
C39B	3335(3)	10421(3)	3780(2)	61(1)	0.6815(14)

Table A3.9: Hydrogen bonds [Å and °].

D–H···*A*	*d*(*D*–H)	*d*(H···*A*)	*d*(*D*···*A*)	∠(*D*H*A*)
N1–H901···O2	0.88	2.29	3.100(2)	152.4
N1–H901···O1	0.88	2.30	3.045(2)	142.4
N2–H902···O2	0.88	2.14	2.9638(18)	156.5
N3–H903···O4	0.88	2.11	2.954(2)	160.2
N4–H904···O2	0.88	2.21	2.955(2)	141.5
N5–H905···O3	0.88	2.02	2.898(2)	172.0
N6–H6···O2	0.88	2.18	2.9496(19)	145.1
O4–H994···O3^{i}	0.823(11)	1.723(12)	2.5301(16)	166.2(19)
O1–H991···O5A^{ii}	0.835(12)	1.810(13)	2.629(5)	166.1(16)
O1–H991···O5B^{ii}	0.835(12)	1.743(12)	2.571(3)	171.1(13)

Symmetry transformations used to generate equivalent atoms:
(i) –x+2,–y+2,–z+1 (ii) –x+1,–y+2,–z+1

A3.1.4 Receptor 156 (chloride complex)

Table A3.10: Crystal data and structure refinement details.

Identification code	**2010sot0433**	
Empirical formula	$C_{37}H_{81}ClN_8S_3$ $C_{21}H_{45}N_7S_3$, $C_{16}H_{36}N$, Cl	
Formula weight	769.73	
Temperature	120(2) K	
Wavelength	0.71073 Å	
Crystal system	Triclinic	
Space group	*P*–1	
Unit cell dimensions	a = 13.6678(11) Å	α = 85.095(5)°
	b = 15.9682(16) Å	β = 74.096(6)°
	c = 22.901(2) Å	γ = 76.589(6)°
Volume	4674.5(7) Å^3	
Z	4 (Z' = 2)	
Density (calculated)	1.094 Mg / m^3	
Absorption coefficient	0.249 mm^{-1}	
F(000)	1696	
Crystal	Plate; Colourless	
Crystal size	0.30 × 0.18 × 0.03 mm^3	
θ range for data collection	2.92 – 25.03°	
Index ranges	$-16 \le h \le 16$, $-18 \le k \le 18$, $-27 \le l \le 27$	
Reflections collected	50328	
Independent reflections	15862 [R_{int} = 0.1351]	
Completeness to θ = 25.03°	96.0 %	
Absorption correction	Semi–empirical from equivalents	
Max. and min. transmission	0.9926 and 0.9291	
Refinement method	Full-matrix least-squares on F^2	
Data / restraints / parameters	15862 / 63 / 911	
Goodness-of-fit on F^2	1.065	
Final *R* indices [$F^2 > 2\sigma(F^2)$]	*R1* = 0.1510, *wR2* = 0.2726	
R indices (all data)	*R1* = 0.2553, *wR2* = 0.3310	
Largest diff. peak and hole	0.665 and –0.403 e Å^{-3}	

Diffractometer: *Nonius KappaCCD* area detector (ϕ scans and ω scans to fill *asymmetric unit*). **Cell determination:** DirAx (Duisenberg, A.J.M.(1992). J. Appl. Cryst. 25, 92-96.) **Data collection:** Collect (Collect: Data collection software, R. Hooft, Nonius B.V., 1998). **Data reduction and cell refinement**: *Denzo* (Z. Otwinowski & W. Minor, *Methods in Enzymology* (1997) Vol. **276**: *Macromolecular Crystallography*, part A, pp. 307–326; C. W. Carter, Jr. & R. M. Sweet, Eds., Academic Press). **Absorption correction**: Sheldrick, G. M. SADABS - Bruker Nonius area detector scaling and absorption correction - V2.10 **Structure solution**: *SHELXS97* (G. M. Sheldrick, Acta Cryst. (1990) A**46** 467–473). **Structure refinement**: *SHELXL97* (G. M. Sheldrick (1997), University of Göttingen, Germany). **Graphics:** Cameron - A Molecular Graphics Package. (D. M. Watkin, L. Pearce and C. K. Prout, Chemical Crystallography Laboratory, University of Oxford, 1993).

Special details: All hydrogen atoms were placed in idealised positions and refined using a riding model. One of the receptor molecule arms is modelled as disordered over 2 positions. Thermal parameter and geometric restraints were applied. This disorder is responsible for a close contact "H66C..H17C = 1.98 A" and a large Hirshfeld difference "C65--C66 = 0.26 A". It was evident that the data quality did not permit in finer detail disorder to be modelled.

Table A3.11: Atomic coordinates [$\times 10^4$], equivalent isotropic displacement parameters [$Å^2 \times 10^3$] and site occupancy factors. U_{eq} is defined as one third of the trace of the orthogonalized U^{ij} tensor.

Atom	*x*	*y*	*z*	U_{eq}	*S.o.f.*
S1	7358(2)	2278(2)	7479(1)	48(1)	1
S2	5100(2)	6877(2)	9655(1)	46(1)	1
S3	11378(2)	5244(2)	8943(1)	56(1)	1
N1	7563(6)	3895(5)	7223(4)	47(2)	1
N2	7709(6)	3426(5)	8149(3)	44(2)	1
N3	6624(6)	6788(5)	8637(4)	45(2)	1
N4	6726(6)	5602(5)	9232(3)	37(2)	1
N5	10205(6)	5806(6)	8180(4)	55(2)	1
N6	9670(5)	4781(5)	8856(3)	40(2)	1
N7	7988(5)	3877(5)	9321(3)	35(2)	1
C1	5572(10)	5341(9)	6631(6)	81(4)	1
C2	6668(10)	5491(9)	6586(6)	78(4)	1
C3	7536(10)	4729(9)	6285(5)	74(4)	1
C4	7477(10)	3870(7)	6597(5)	63(3)	1
C5	7548(6)	3245(7)	7622(5)	41(2)	1
C6	7869(7)	2797(7)	8622(4)	46(3)	1
C7	7479(7)	3186(6)	9253(4)	40(2)	1
C8	8577(9)	8750(8)	8236(6)	72(4)	1
C9	8001(8)	8041(7)	8247(5)	57(3)	1
C10	6835(8)	8295(6)	8538(5)	49(3)	1
C11	6247(7)	7648(7)	8435(5)	51(3)	1
C12	6207(7)	6390(7)	9146(4)	38(2)	1
C13	6403(7)	5023(6)	9721(4)	41(2)	1
C14	7344(7)	4384(6)	9850(4)	40(2)	1
C15A	11860(20)	5216(16)	6245(9)	106(8)	0.708(14)
C16A	11141(16)	5791(15)	6767(8)	72(6)	0.708(14)
C17A	11689(12)	5792(11)	7268(7)	69(5)	0.708(14)
C18A	10968(16)	6263(13)	7823(7)	60(5)	0.708(14)
C15B	11500(60)	5670(40)	6258(18)	106(8)	0.292(14)
C16B	11370(50)	5700(30)	6935(19)	72(6)	0.292(14)
C17B	10680(30)	6530(20)	7230(16)	69(5)	0.292(14)
C18B	10660(50)	6590(30)	7889(17)	60(5)	0.292(14)
C19	10367(8)	5290(7)	8636(5)	46(3)	1
C20	9661(7)	4206(7)	9374(4)	44(3)	1
C21	9032(7)	3530(6)	9390(4)	40(2)	1
S4	9338(2)	8758(2)	6373(1)	56(1)	1
S5	2989(2)	11035(2)	8080(1)	47(1)	1
S6	6698(2)	8216(2)	4472(1)	52(1)	1
N8	8001(6)	7726(5)	6583(4)	46(2)	1
N9	7300(6)	9073(5)	6928(4)	45(2)	1
N10	4058(6)	9422(5)	8136(4)	45(2)	1

N11	4242(6)	10017(5)	7192(4)	47(2)	1
N12	5780(7)	7688(6)	5570(4)	57(2)	1
N13	6317(6)	8928(6)	5551(4)	50(2)	1
N14	6130(6)	10400(5)	6267(3)	41(2)	1
C22	9232(11)	6248(8)	4599(6)	78(4)	1
C23	9402(10)	6281(8)	5225(6)	68(3)	1
C24	8629(8)	7004(7)	5598(5)	54(3)	1
C25	8745(8)	7025(6)	6232(5)	46(3)	1
C26	8145(8)	8500(7)	6640(4)	44(3)	1
C27	7236(8)	9980(7)	6970(4)	52(3)	1
C28	7096(8)	10477(7)	6402(4)	46(3)	1
C29	1618(10)	7906(10)	8929(7)	97(5)	1
C30	2691(11)	8183(9)	8795(6)	91(5)	1
C31	2600(10)	9058(8)	8953(6)	70(4)	1
C32	3631(7)	9361(7)	8797(4)	46(3)	1
C33	3800(7)	10123(7)	7796(5)	43(3)	1
C34	4233(8)	10694(7)	6732(5)	56(3)	1
C35	5230(8)	11030(7)	6584(5)	53(3)	1
C36	3091(13)	6603(14)	4922(8)	137(7)	1
C37	4144(11)	6371(10)	5111(6)	94(5)	1
C38	4504(10)	7159(9)	5202(6)	76(4)	1
C39	5550(9)	6948(8)	5345(5)	60(3)	1
C40	6255(7)	8288(8)	5237(5)	50(3)	1
C41	6828(7)	9623(7)	5299(4)	46(3)	1
C42	6220(8)	10456(7)	5613(5)	51(3)	1
N15	4100(5)	3061(5)	8617(3)	39(2)	1
C43	4738(7)	2149(6)	8567(4)	43(2)	1
C44	5250(7)	1826(7)	9080(5)	51(3)	1
C45	5882(8)	916(7)	8979(5)	55(3)	1
C46	6380(9)	550(8)	9492(5)	70(4)	1
C47	3288(7)	3212(7)	9236(4)	45(3)	1
C48	2545(7)	2610(7)	9409(4)	47(3)	1
C49	1866(8)	2822(9)	10047(5)	67(4)	1
C50	1076(9)	2257(9)	10267(5)	74(4)	1
C51	3512(7)	3214(7)	8126(4)	46(3)	1
C52	4199(8)	3267(7)	7486(4)	50(3)	1
C53	3556(9)	3308(8)	7028(5)	61(3)	1
C54	4135(9)	3506(8)	6390(5)	65(3)	1
C55	4791(7)	3703(6)	8535(5)	45(3)	1
C56	4287(7)	4630(7)	8496(4)	45(3)	1
C57	5069(8)	5195(8)	8316(5)	59(3)	1
C58	4554(8)	6130(7)	8227(5)	56(3)	1
N16	689(5)	10881(5)	6995(3)	38(2)	1
C59	–52(7)	10771(7)	7605(4)	45(3)	1
C60	287(8)	10870(7)	8161(4)	46(3)	1
C61	–422(7)	10577(7)	8732(4)	48(3)	1

C62	−229(9)	10815(8)	9311(5)	61(3)	1
C63	1688(7)	10188(6)	6895(5)	47(3)	1
C64	1570(8)	9258(7)	6949(6)	69(4)	1
C65	2653(9)	8661(7)	6772(7)	82(4)	1
C66	2639(12)	7750(11)	6875(9)	126(7)	1
C67	1040(6)	11731(6)	6949(4)	36(2)	1
C68	191(7)	12528(6)	6996(4)	43(2)	1
C69	600(8)	13321(7)	7050(5)	47(3)	1
C70	779(8)	13381(7)	7662(5)	57(3)	1
C71	94(7)	10836(7)	6526(4)	46(3)	1
C72	706(8)	10887(8)	5875(5)	53(3)	1
C73	11(9)	10929(8)	5455(5)	63(3)	1
C74	−828(10)	11745(9)	5487(5)	75(4)	1
Cl1	8309(2)	5317(2)	7796(1)	42(1)	1
Cl2	5413(2)	8029(2)	7000(1)	46(1)	1

Table A3.12: Hydrogen bonds [Å and °].

D–H···*A*	*d*(*D*–H)	*d*(H···*A*)	*d*(*D*···*A*)	∠(*D*H*A*)
N1–H1···Cl1	0.88	2.37	3.199(8)	157.8
N2–H2···Cl1	0.88	2.50	3.288(9)	148.7
N3–H3···Cl1	0.88	2.39	3.220(8)	157.9
N4–H4···Cl1	0.88	2.65	3.408(8)	145.3
N5–H5···Cl1	0.88	2.43	3.226(8)	151.5
N6–H6···Cl1	0.88	2.58	3.388(8)	153.3
N8–H8···Cl2	0.88	2.54	3.331(8)	149.6
N9–H9···Cl2	0.88	2.57	3.343(8)	147.1
N10–H10···Cl2	0.88	2.60	3.404(9)	151.5
N11–H11···Cl2	0.88	2.35	3.213(9)	165.8
N12–H12···Cl2	0.88	2.38	3.247(9)	167.3
N13–H13···Cl2	0.88	2.73	3.516(8)	149.2

A3.1.5 Receptor 144 (carbonate complex)

Table A3.13: Crystal data and structure refinement details.

Identification code	**2010sot0341**
Empirical formula	$C_{71}H_{106}N_{16}O_3S_6$ $2(C_{27}H_{33}N_7S_3)$, $2(C_8H_{20}N)$, CO_3
Formula weight	1424.08
Temperature	120(2) K
Wavelength	0.71069 Å
Crystal system	Monoclinic
Space group	*Cc*
Unit cell dimensions	a = 24.1742(5) Å b = 24.4456(7) Å β = 93.313(2)° c = 12.7595(4) Å
Volume	7527.7(4) Å^3
Z	4
Density (calculated)	1.257 Mg / m^3
Absorption coefficient	0.238 mm^{-1}
F(000)	3056
Crystal	Slab; Colourless
Crystal size	0.12 × 0.10 × 0.04 mm^3
θ range for data collection	2.91 – 27.48°
Index ranges	$-31 \le h \le 30$, $-31 \le k \le 31$, $-16 \le l \le 16$
Reflections collected	33393
Independent reflections	15112 [R_{int} = 0.0804]
Completeness to θ = 27.48°	99.4 %
Absorption correction	Semi–empirical from equivalents
Max. and min. transmission	0.9905 and 0.9720
Refinement method	Full-matrix least-squares on F^2
Data / restraints / parameters	15112 / 10 / 874
Goodness-of-fit on F^2	1.065
Final *R* indices [$F^2 > 2\sigma(F^2)$]	*R1* = 0.0856, *wR2* = 0.1532
R indices (all data)	*R1* = 0.1339, *wR2* = 0.1767
Absolute structure parameter	0.69(9) Refined as a racemic twin
Largest diff. peak and hole	0.460 and –0.408 e Å^{-3}

Diffractometer: *Nonius KappaCCD* area detector (ϕ scans and ω scans to fill *asymmetric unit*). **Cell determination:** DirAx (Duisenberg, A.J.M.(1992). J. Appl. Cryst. 25, 92-96.) **Data collection:** Collect (Collect: Data collection software, R. Hooft, Nonius B.V., 1998). **Data reduction and cell refinement**: *Denzo* (Z. Otwinowski & W. Minor, *Methods in Enzymology* (1997) Vol. **276**: *Macromolecular Crystallography*, part A, pp. 307–326; C. W. Carter, Jr. & R. M. Sweet, Eds., Academic Press). **Absorption correction**: Sheldrick, G. M. SADABS - Bruker Nonius area detector scaling and absorption correction - V2.10 **Structure solution**: *SHELXS97* (G. M. Sheldrick, Acta Cryst. (1990) A**46** 467–473). **Structure refinement**: *SHELXL97* (G. M. Sheldrick (1997), University of Göttingen, Germany). **Graphics:** Cameron - A Molecular Graphics Package. (D. M. Watkin, L. Pearce and C. K. Prout, Chemical Crystallography Laboratory, University of Oxford, 1993).
Special details: All hydrogen atoms were placed in idealised positions and refined using a riding model.

Table A3.14: Atomic coordinates [$\times 10^4$], equivalent isotropic displacement parameters [$Å^2 \times 10^3$] and site occupancy factors. U_{eq} is defined as one third of the trace of the orthogonalized U^{ij} tensor.

Atom	*x*	*y*	*z*	U_{eq}	*S.o.f.*
S1	−2823(1)	3065(1)	−115(1)	37(1)	1
S2	−1751(1)	302(1)	−512(1)	31(1)	1
S3	−1747(1)	3711(1)	−3916(1)	37(1)	1
N1	−1743(2)	2825(2)	223(4)	27(1)	1
N2	−2167(2)	2438(2)	−1214(4)	31(1)	1
N3	−1143(2)	1207(2)	6(4)	22(1)	1
N4	−1401(2)	1104(2)	−1705(4)	26(1)	1
N5	−1165(2)	3605(2)	−2068(4)	27(1)	1
N6	−1217(2)	2847(2)	−3081(4)	29(1)	1
N7	−1944(2)	1855(2)	−3105(4)	25(1)	1
C1	−1647(2)	3020(2)	1265(5)	21(1)	1
C2	−2017(3)	2965(2)	2035(5)	27(1)	1
C3	−1858(3)	3113(2)	3079(5)	30(2)	1
C4	−1335(3)	3323(2)	3322(5)	31(2)	1
C5	−963(3)	3384(2)	2546(5)	30(2)	1
C6	−1115(2)	3233(2)	1521(5)	28(1)	1
C7	−2222(2)	2762(2)	−378(5)	29(1)	1
C8	−2601(3)	2361(3)	−2045(5)	40(2)	1
C9	−2490(3)	1843(2)	−2672(5)	31(2)	1
C10	−1126(2)	1158(2)	1122(5)	25(1)	1
C11	−1075(2)	659(3)	1629(5)	30(2)	1
C12	−1092(3)	650(3)	2717(6)	39(2)	1
C13	−1156(3)	1128(4)	3287(6)	48(2)	1
C14	−1164(3)	1627(3)	2750(6)	41(2)	1
C15	−1152(3)	1639(3)	1685(5)	32(2)	1
C16	−1417(2)	898(2)	−737(5)	22(1)	1
C17	−1711(3)	890(2)	−2626(5)	29(1)	1
C18	−1767(3)	1314(2)	−3475(5)	27(1)	1
C19	−1211(3)	4155(2)	−1726(5)	29(2)	1
C20	−1323(3)	4250(3)	−687(5)	35(2)	1
C21	−1341(3)	4781(3)	−289(6)	42(2)	1
C22	−1251(3)	5219(3)	−956(6)	45(2)	1
C23	−1156(3)	5131(3)	−1990(7)	51(2)	1
C24	−1125(3)	4594(3)	−2375(6)	37(2)	1
C25	−1363(3)	3371(3)	−2982(5)	29(1)	1
C26	−1347(3)	2510(3)	−3994(5)	33(2)	1
C27	−1921(3)	2255(3)	−3971(5)	33(2)	1
S4	504(1)	223(1)	−960(1)	29(1)	1

S5	1874(1)	2684(1)	−1241(1)	35(1)	1
S6	782(1)	3592(1)	2636(1)	36(1)	1
N8	−20(2)	1181(2)	−1426(4)	23(1)	1
N9	200(2)	1030(2)	293(4)	25(1)	1
N10	759(2)	2670(2)	−1527(4)	34(1)	1
N11	1116(2)	2239(2)	−85(4)	32(1)	1
N12	260(2)	3534(2)	716(4)	28(1)	1
N13	223(2)	2768(2)	1711(4)	27(1)	1
N14	802(2)	1694(2)	1804(4)	24(1)	1
C28	−69(2)	1137(3)	−2521(5)	25(1)	1
C29	−209(2)	654(3)	−3060(5)	30(2)	1
C30	−252(3)	645(3)	−4145(5)	37(2)	1
C31	−173(3)	1119(4)	−4701(6)	46(2)	1
C32	−49(3)	1602(3)	−4187(6)	48(2)	1
C33	−5(3)	1615(3)	−3098(5)	37(2)	1
C34	222(2)	835(2)	−699(5)	20(1)	1
C35	467(3)	772(2)	1212(5)	26(1)	1
C36	542(3)	1178(2)	2110(5)	28(1)	1
C37	698(2)	2863(2)	−2577(5)	27(1)	1
C38	244(2)	3195(3)	−2833(5)	32(2)	1
C39	120(3)	3360(3)	−3861(5)	34(2)	1
C40	455(3)	3196(3)	−4631(6)	34(2)	1
C41	903(3)	2863(3)	−4399(5)	33(2)	1
C42	1028(2)	2691(2)	−3377(5)	24(1)	1
C43	1229(3)	2516(3)	−939(5)	29(1)	1
C44	1529(3)	2121(3)	773(6)	40(2)	1
C45	1352(3)	1628(3)	1401(5)	31(2)	1
C46	291(2)	4092(3)	450(5)	29(1)	1
C47	430(3)	4228(3)	−544(6)	38(2)	1
C48	409(3)	4776(3)	−885(7)	47(2)	1
C49	269(3)	5182(3)	−210(6)	41(2)	1
C50	135(3)	5041(3)	796(6)	38(2)	1
C51	144(3)	4505(3)	1134(6)	35(2)	1
C52	407(2)	3292(2)	1652(5)	27(1)	1
C53	286(3)	2425(3)	2650(5)	32(2)	1
C54	805(3)	2094(2)	2670(5)	29(1)	1
N15	−3012(2)	721(2)	1758(4)	27(1)	1
C55	−2817(3)	128(2)	1772(5)	30(1)	1
C56	−3267(3)	−290(3)	1932(6)	42(2)	1
C57	−3476(2)	806(3)	925(5)	30(2)	1
C58	−3339(3)	670(3)	−178(5)	41(2)	1
C59	−3240(3)	888(3)	2779(5)	31(1)	1
C60	−2835(3)	844(3)	3751(5)	39(2)	1
C61	−2508(2)	1060(2)	1508(5)	29(1)	1

C62	−2619(3)	1653(2)	1289(6)	36(2)	1
N16	−3098(2)	4631(2)	1906(5)	46(2)	1
C63	−3665(3)	4512(3)	1368(6)	43(2)	1
C64	−3701(3)	4050(3)	576(8)	61(2)	1
C65	−2879(4)	4150(4)	2479(8)	63(3)	1
C66	−3283(4)	3854(4)	3164(8)	70(3)	1
C67	−2675(3)	4775(3)	1119(7)	54(2)	1
C68	−2835(3)	5285(3)	455(6)	53(2)	1
C69	−3180(3)	5119(3)	2627(5)	38(2)	1
C70	−2662(3)	5415(3)	3066(6)	54(2)	1
C71	−515(2)	2443(2)	−668(5)	19(1)	1
O1	−945(2)	2212(2)	−1092(3)	25(1)	1
O2	−127(2)	2158(2)	−204(4)	30(1)	1
O3	−460(2)	2960(2)	−718(4)	34(1)	1

Table A3.15: Hydrogen bonds [Å and °].

D–H···*A*	*d*(*D*–H)	*d*(H···*A*)	*d*(*D*···*A*)	∠(*D*H*A*)
N1–H901···O1	0.88	2.21	3.027(6)	155.1
N1–H901···O3	0.88	2.61	3.407(7)	150.6
N2–H902···O1	0.88	2.20	3.001(6)	152.0
N3–H903···O1	0.88	2.10	2.882(6)	147.2
N3–H903···O2	0.88	2.59	3.403(6)	155.0
N4–H904···O1	0.88	2.26	3.012(6)	142.8
N5–H905···O3	0.88	1.96	2.832(6)	169.8
N6–H906···O1	0.88	2.20	3.016(7)	153.5
N8–H908···O2	0.88	2.07	2.873(6)	151.3
N8–H908···O1	0.88	2.60	3.413(6)	153.1
N9–H909···O2	0.88	2.17	2.927(6)	143.7
N10–H910···O2	0.88	2.28	3.070(7)	150.0
N10–H910···O3	0.88	2.44	3.257(8)	154.3
N11–H911···O2	0.88	2.18	3.006(6)	155.7
N12–H912···O3	0.88	2.00	2.824(6)	155.4
N13–H913···O2	0.88	2.09	2.945(7)	163.2

A3.2 Structures from Chapter 3

A3.2.1 Receptor 213

Table A3.16: Crystal data and structure refinement details.

Identification code	**2010sot0773**
Empirical formula	$C_{12}H_{18}N_2O$
Formula weight	206.28
Temperature	120(2) K
Wavelength	0.71073 Å
Crystal system	Orthorhombic
Space group	*Pccn*
Unit cell dimensions	a = 21.8777(7) Å b = 24.4332(8) Å c = 8.9667(2) Å
Volume	4793.1(2) Å^3
Z	16
Density (calculated)	1.143 Mg / m^3
Absorption coefficient	0.074 mm^{-1}
F(000)	1792
Crystal	Block; Colourless
Crystal size	0.20 × 0.10 × 0.04 mm^3
θ range for data collection	2.91 – 25.02°
Index ranges	$-26 \le h \le 26$, $-29 \le k \le 29$, $-10 \le l \le 9$
Reflections collected	55376
Independent reflections	4234 [R_{int} = 0.1849]
Completeness to θ = 25.02°	99.9 %
Absorption correction	Semi–empirical from equivalents
Max. and min. transmission	0.9971 and 0.9854
Refinement method	Full-matrix least-squares on F^2
Data / restraints / parameters	4234 / 189 / 287
Goodness-of-fit on F^2	1.153
Final R indices [$F^2 > 2\sigma(F^2)$]	*R1* = 0.1143, *wR2* = 0.1725
R indices (all data)	*R1* = 0.1841, *wR2* = 0.2013
Largest diff. peak and hole	0.247 and –0.261 e Å^{-3}

Diffractometer: *Nonius KappaCCD* area detector (ϕ scans and ω scans to fill *asymmetric unit*). **Cell determination:** DirAx (Duisenberg, A.J.M.(1992). J. Appl. Cryst. 25, 92-96.) **Data collection:** Collect (Collect: Data collection software, R. Hooft, Nonius B.V., 1998). **Data reduction and cell refinement**: *Denzo* (Z. Otwinowski & W. Minor, *Methods in Enzymology* (1997) Vol. **276**: *Macromolecular Crystallography*, part A, pp. 307–326; C. W. Carter, Jr. & R. M. Sweet, Eds., Academic Press). **Absorption correction**: Sheldrick, G. M. SADABS - Bruker Nonius area detector scaling and absorption correction - V2.10 **Structure solution**: *SHELXS97* (G. M. Sheldrick, Acta Cryst. (1990) A**46** 467–473). **Structure refinement**: *SHELXL97* (G. M. Sheldrick (1997), University of Göttingen, Germany). **Graphics:** Cameron - A Molecular Graphics Package. (D. M. Watkin, L. Pearce and C. K. Prout, Chemical Crystallography Laboratory, University of Oxford, 1993).
Special details: All hydrogen atoms were placed in idealised positions and refined using a riding model. The carbon chain is modelled as disordered over 2 positions.

Table A3.17: Atomic coordinates [$\times 10^4$], equivalent isotropic displacement parameters [$Å^2 \times 10^3$] and site occupancy factors. U_{eq} is defined as one third of the trace of the orthogonalized U^{ij} tensor.

Atom	*x*	*y*	*z*	U_{eq}	*S.o.f.*
C1	−808(2)	1310(2)	6504(5)	49(1)	1
C2	−1004(2)	770(2)	6400(6)	56(1)	1
C3	−801(2)	444(2)	5259(5)	52(1)	1
C4	−410(2)	661(2)	4214(4)	48(1)	1
C5	−211(2)	1194(2)	4307(4)	41(1)	1
C6	−406(2)	1526(2)	5473(4)	32(1)	1
C7	3(2)	2425(2)	4668(3)	29(1)	1
N2A	235(1)	2894(1)	5210(3)	37(1)	0.482(5)
C8A	302(4)	3365(2)	4189(7)	39(1)	0.482(5)
C9A	542(4)	3846(2)	5043(8)	38(1)	0.482(5)
C10A	894(5)	4336(4)	2655(7)	61(2)	0.482(5)
C11A	935(4)	4281(2)	4332(7)	45(1)	0.482(5)
C12A	910(6)	4822(3)	5154(10)	62(2)	0.482(5)
N2B	235(1)	2894(1)	5210(3)	37(1)	0.518(5)
C8B	575(3)	3303(2)	4360(7)	39(1)	0.518(5)
C9B	556(4)	3857(2)	5059(8)	38(1)	0.518(5)
C10B	1185(4)	4216(4)	2895(8)	61(2)	0.518(5)
C11B	681(3)	4343(2)	4030(7)	45(1)	0.518(5)
C12B	868(6)	4837(3)	4967(11)	62(2)	0.518(5)
N1	−194(1)	2063(1)	5704(3)	35(1)	1
O1	−34(1)	2332(1)	3311(3)	49(1)	1
C13	1643(2)	3819(2)	8744(5)	49(1)	1
C14	1392(2)	3304(2)	8988(5)	56(1)	1
C15	1512(2)	2878(2)	8030(6)	68(2)	1
C16	1883(2)	2967(2)	6808(7)	67(2)	1
C17	2140(2)	3473(2)	6567(5)	50(1)	1
C18	2023(2)	3909(2)	7526(4)	41(1)	1
C19	2356(2)	4858(2)	8099(4)	36(1)	1
N4	2570(2)	5311(1)	7440(3)	39(1)	1
C20	2728(2)	5795(1)	8311(4)	36(1)	1
C21	2966(2)	6250(1)	7343(4)	38(1)	1
C22	3644(2)	6661(2)	9339(5)	59(1)	1
C23	3138(2)	6766(1)	8210(4)	43(1)	1
C24	3321(2)	7220(2)	7130(5)	62(1)	1
N3	2274(2)	4422(1)	7175(3)	45(1)	1
O2	2245(1)	4844(1)	9462(3)	41(1)	1

Table A3.18: Hydrogen bonds [Å and °].

D–H···*A*	*d*(*D*–H)	*d*(H···*A*)	*d*(*D*···*A*)	∠(*D*H*A*)
N2A–H2A···O1^{i}	0.88	2.19	2.895(4)	136.4
N2B–H2B···O1^{i}	0.88	2.11	2.895(4)	149.0
N1–H1A···O1^{i}	0.88	1.95	2.788(4)	158.0
N4–H4A···O2^{ii}	0.88	2.16	2.933(4)	146.5
N3–H3A···O2^{ii}	0.88	2.01	2.844(4)	158.1

Symmetry transformations used to generate equivalent atoms:
(i) x,–y+1/2,z+1/2 (ii) –x+1/2,y,z–1/2

A3.2.2 Receptor 231

Table A3.19: Crystal data and structure refinement details.

Identification code	**2011sot0559**
Empirical formula	$C_{14}H_{19}F_3N_2O$
Formula weight	288.31
Temperature	100(2) K
Wavelength	0.71073 Å
Crystal system	Monoclinic
Space group	*P*21/*c*
Unit cell dimensions	a = 19.510(13) Å
	b = 4.657(3) Å β = 107.506(16)°
	c = 16.320(11) Å
Volume	1414.0(16) Å^3
Z	4
Density (calculated)	1.354 Mg / m^3
Absorption coefficient	0.113 mm^{-1}
F(000)	608
Crystal	Slab; Colourless
Crystal size	0.18 × 0.10 × 0.04 mm^3
θ range for data collection	3.13 – 25.03°
Index ranges	$-21 \le h \le 23$, $-5 \le k \le 4$, $-19 \le l \le 19$
Reflections collected	6403
Independent reflections	2496 [R_{int} = 0.0621]
Completeness to θ = 25.03°	99.6 %
Absorption correction	Semi–empirical from equivalents
Max. and min. transmission	0.9955 and 0.9800
Refinement method	Full-matrix least-squares on F^2
Data / restraints / parameters	2496 / 0 / 182
Goodness-of-fit on F^2	1.116
Final *R* indices [$F^2 > 2\sigma(F^2)$]	*R1* = 0.0702, *wR2* = 0.1316
R indices (all data)	*R1* = 0.1039, *wR2* = 0.1493
Largest diff. peak and hole	0.267 and –0.269 e Å

Diffractometer: *Rigaku AFC12 and Saturn724+ mounted at the window of RA-FRE+ HFM with Varimax optics.* **Cell determination, Data collection, Data reduction and cell refinement & Absorption correction**: CrystalClear-SM Expert 2.0 r7 (Rigaku, 2011) , **Structure solution**: *SHELXS97* (G. M. Sheldrick, Acta Cryst. (1990) A**46** 467–473). **Structure refinement**: *SHELXL97* (G. M. Sheldrick (1997), University of Göttingen, Germany). **Graphics:** CrystalMaker: a crystal and molecular structures program for Mac and Windows. CrystalMaker Software Ltd, Oxford, England (www.crystalmaker.com)
Special details: All hydrogen atoms were placed in idealised positions and refined using a riding model.

Table A3.20: Atomic coordinates [$\times 10^4$], equivalent isotropic displacement parameters [$Å^2 \times 10^3$] and site occupancy factors. U_{eq} is defined as one third of the trace of the orthogonalized U^{ij} tensor.

Atom	*x*	*y*	*z*	U_{eq}	*S.o.f.*
N1	590(1)	1221(5)	3895(2)	18(1)	1
F1	−2386(1)	−5220(4)	3348(1)	35(1)	1
O1	1205(1)	−3010(4)	4304(1)	22(1)	1
N2	1816(1)	1207(5)	4529(2)	20(1)	1
C2	−1513(2)	−2001(6)	3145(2)	19(1)	1
C5	−110(2)	66(6)	3642(2)	16(1)	1
C10	3128(2)	1903(6)	5148(2)	23(1)	1
C4	−618(2)	1158(6)	2913(2)	21(1)	1
C6	−318(2)	−2053(6)	4122(2)	20(1)	1
F3	−2752(1)	−1049(4)	2875(2)	47(1)	1
C7	−1015(2)	−3080(6)	3869(2)	21(1)	1
C9	2507(2)	−204(6)	4901(2)	21(1)	1
C8	1206(2)	−316(6)	4251(2)	18(1)	1
F2	−2461(1)	−4109(5)	2052(1)	44(1)	1
C3	−1312(2)	138(6)	2663(2)	21(1)	1
C1	−2266(2)	−3059(7)	2859(2)	26(1)	1
C12	4472(2)	2386(7)	5918(2)	27(1)	1
C11	3832(2)	394(6)	5585(2)	25(1)	1
C13	5171(2)	790(7)	6343(2)	34(1)	1
C14	5814(2)	2777(8)	6694(3)	45(1)	1

Table A3.21: Hydrogen bonds [Å and °].

D–H···*A*	*d*(*D*–H)	*d*(H···*A*)	*d*(*D*···*A*)	∠(*D*H*A*)
N1–H1···O1^{i}	0.88	2.16	2.936(3)	146.9
N2–H2···O1^{i}	0.88	2.13	2.923(3)	150.3

Symmetry transformations used to generate equivalent atoms:
(i) x,y+1,z

A3.2.3 Receptor 231

Table A3.22: Crystal data and structure refinement details.

Identification code	**2011sot0717**
Empirical formula	$C_{13}H_{20}N_2S$
Formula weight	236.37
Temperature	100(2) K
Wavelength	1.54187 Å
Crystal system	Orthorhombic
Space group	$P2_12_12_1$
Unit cell dimensions	a = 8.562(3) Å
	b = 10.271(4) Å
	c = 15.198(5) Å
Volume	1336.5(8) Å^3
Z	4
Density (calculated)	1.175 Mg / m^3
Absorption coefficient	1.945 mm^{-1}
F(000)	512
Crystal	Rod; Colourless
Crystal size	0.20 × 0.07 × 0.05 mm^3
θ range for data collection	6.73 – 66.56°
Index ranges	$-9 \le h \le 7$, $-11 \le k \le 12$, $-18 \le l \le 17$
Reflections collected	5374
Independent reflections	2245 [R_{int} = 0.0514]
Completeness to θ = 66.56°	97.2 %
Absorption correction	Semi–empirical from equivalents
Max. and min. transmission	0.9090 and 0.6971
Refinement method	Full-matrix least-squares on F^2
Data / restraints / parameters	2245 / 0 / 154
Goodness-of-fit on F^2	0.996
Final R indices [$F^2 > 2\sigma(F^2)$]	$R1$ = 0.0317, $wR2$ = 0.0712
R indices (all data)	$R1$ = 0.0330, $wR2$ = 0.0717
Absolute structure parameter	0.038(16)
Largest diff. peak and hole	0.225 and –0.276 e Å^{-3}

Diffractometer: *Rigaku AFC11 and Saturn944+ mounted at the window of RA-Micro7 HFM with Varimax optics.* **Cell determination, Data collection, Data reduction and cell refinement & Absorption correction**: CrystalClear-SM Expert 2.0 r7 (Rigaku, 2011) , **Structure solution**: *SHELXS97* (G. M. Sheldrick, Acta Cryst. (1990) A**46** 467–473). **Structure refinement**: *SHELXL97* (G. M. Sheldrick (1997), University of Göttingen, Germany). **Graphics:** CrystalMaker: a crystal and molecular structures program for Mac and Windows. CrystalMaker Software Ltd, Oxford, England (www.crystalmaker.com)
Special details: All hydrogen atoms were placed in idealised positions and refined using a riding model, except the NHs which were freely refined.

Table A3.23: Atomic coordinates [× 10^4], equivalent isotropic displacement parameters [$Å^2$ × 10^3] and site occupancy factors. U_{eq} is defined as one third of the trace of the orthogonalized U^{ij} tensor.

Atom	*x*	*y*	*z*	U_{eq}	*S.o.f.*
S1	7999(1)	9250(1)	5245(1)	17(1)	1
N1	10017(2)	7773(2)	4305(1)	17(1)	1
N2	10342(2)	7746(2)	5783(1)	19(1)	1
C1	8624(2)	9044(2)	3159(1)	18(1)	1
C2	8039(2)	9085(2)	2306(1)	19(1)	1
C3	8176(2)	8032(2)	1748(1)	20(1)	1
C4	8898(2)	6907(2)	2041(1)	21(1)	1
C5	9467(2)	6842(2)	2901(1)	20(1)	1
C6	9332(2)	7903(2)	3464(1)	14(1)	1
C7	9518(2)	8208(2)	5103(1)	15(1)	1
C8	10035(2)	7996(2)	6707(1)	18(1)	1
C9	8966(2)	6996(2)	7127(1)	21(1)	1
C10	8676(2)	7278(2)	8097(1)	21(1)	1
C11	7647(2)	6279(2)	8554(1)	20(1)	1
C12	7402(3)	6555(2)	9530(1)	25(1)	1
C13	6425(3)	5530(2)	9991(1)	33(1)	1

Table A3.24: Hydrogen bonds [Å and °].

D–H···*A*	*d*(*D*–H)	*d*(H···*A*)	*d*(*D*···*A*)	∠(*D*H*A*)
N1–H91···S1^{i}	0.90(3)	2.47(3)	3.363(2)	174(2)
N2–H92···S1^{i}	0.80(3)	2.68(3)	3.437(2)	158(2)

Symmetry transformations used to generate equivalent atoms:
(i) x+1/2,–y+3/2,–z+1

A3.2.4 Receptor 224 (chloride complex)

Table A3.25: Crystal data and structure refinement details.

Identification code	**2011sot0549**
Empirical formula	$C_{36}H_{64}ClF_3N_4O$ $C_{20}H_{28}F_3N_3O$, $C_{16}H_{36}N$, Cl
Formula weight	661.36
Temperature	120(2) K
Wavelength	0.71073 Å
Crystal system	Monoclinic
Space group	$P2_1/c$
Unit cell dimensions	a = 17.0415(6) Å b = 14.5286(8) Å β = 116.023(2)° c = 17.7209(10) Å
Volume	3942.7(3) Å^3
Z	4
Density (calculated)	1.114 Mg / m^3
Absorption coefficient	0.142 mm^{-1}
F(000)	1440
Crystal	Plate; Colourless
Crystal size	0.20 × 0.13 × 0.02 mm^3
θ range for data collection	2.92 – 25.03°
Index ranges	$-20 \le h \le 20$, $-17 \le k \le 17$, $-21 \le l \le 20$
Reflections collected	31420
Independent reflections	6931 [R_{int} = 0.1506]
Completeness to θ = 25.03°	99.6 %
Absorption correction	Semi–empirical from equivalents
Max. and min. transmission	0.9972 and 0.9722
Refinement method	Full-matrix least-squares on F^2
Data / restraints / parameters	6931 / 0 / 412
Goodness-of-fit on F^2	1.147
Final R indices [$F^2 > 2\sigma(F^2)$]	$R1$ = 0.1167, $wR2$ = 0.1858
R indices (all data)	$R1$ = 0.2056, $wR2$ = 0.2232
Largest diff. peak and hole	0.431 and –0.335 e Å^{-3}

Diffractometer: *Nonius KappaCCD* area detector (ϕ scans and ω scans to fill *asymmetric unit*). **Cell determination:** DirAx (Duisenberg, A.J.M.(1992). J. Appl. Cryst. 25, 92-96.) **Data collection:** Collect (Collect: Data collection software, R. Hooft, Nonius B.V., 1998). **Data reduction and cell refinement**: *Denzo* (Z. Otwinowski & W. Minor, *Methods in Enzymology* (1997) Vol. **276**: *Macromolecular Crystallography*, part A, pp. 307–326; C. W. Carter, Jr. & R. M. Sweet, Eds., Academic Press). **Absorption correction**: Sheldrick, G. M. SADABS - Bruker Nonius area detector scaling and absorption correction - V2.10 **Structure solution**: *SHELXS97* (G. M. Sheldrick, Acta Cryst. (1990) A**46** 467–473). **Structure refinement**: *SHELXL97* (G. M. Sheldrick (1997), University of Göttingen, Germany). **Graphics:** Cameron - A Molecular Graphics Package. (D. M. Watkin, L. Pearce and C. K. Prout, Chemical Crystallography Laboratory, University of Oxford, 1993).
Special details: All hydrogen atoms were placed in idealised positions and refined using a riding model.

Table A3.26: Atomic coordinates [$\times 10^4$], equivalent isotropic displacement parameters [$Å^2 \times 10^3$] and site occupancy factors. U_{eq} is defined as one third of the trace of the orthogonalized U^{ij} tensor.

Atom	*x*	*y*	*z*	U_{eq}	*S.o.f.*
Cl1	1681(1)	6926(1)	5716(1)	32(1)	1
F1	1815(2)	2627(3)	2825(2)	46(1)	1
F2	3119(3)	2208(3)	3576(3)	66(1)	1
F3	2851(3)	3219(3)	2633(3)	69(1)	1
O1	180(2)	4696(3)	3329(2)	29(1)	1
N1	3198(3)	5792(3)	5524(3)	30(1)	1
N2	1388(3)	5340(3)	4416(3)	28(1)	1
N3	6(3)	5763(3)	4177(3)	30(1)	1
C1	4373(7)	8914(7)	5652(7)	104(4)	1
C2	4512(5)	7845(6)	5761(5)	68(2)	1
C3	4307(5)	7445(6)	6429(5)	61(2)	1
C4	4586(4)	6463(5)	6628(4)	44(2)	1
C5	4100(4)	5797(4)	5928(4)	31(2)	1
C6	4409(4)	5113(4)	5597(3)	30(1)	1
C7	3673(3)	4662(4)	4962(3)	25(1)	1
C8	3570(4)	3935(4)	4407(4)	27(1)	1
C9	2733(3)	3689(4)	3849(3)	24(1)	1
C10	1984(3)	4131(4)	3817(3)	22(1)	1
C11	2073(3)	4851(4)	4368(3)	24(1)	1
C12	2929(3)	5109(4)	4929(3)	26(1)	1
C13	2633(4)	2950(4)	3237(4)	29(1)	1
C14	495(3)	5219(4)	3930(3)	24(1)	1
C15	−942(3)	5710(4)	3781(4)	27(1)	1
C16	−1325(3)	6428(4)	4142(4)	28(1)	1
C17	−2323(3)	6404(4)	3728(4)	26(1)	1
C18	−2723(4)	7148(4)	4054(4)	34(2)	1
C19	−3711(4)	7173(5)	3600(4)	47(2)	1
C20	−4113(5)	7922(6)	3925(5)	73(3)	1
N4	1312(3)	7710(3)	2905(3)	27(1)	1
C21	1757(4)	8590(4)	2808(3)	30(1)	1
C22	2538(4)	8923(4)	3593(4)	35(2)	1
C23	2980(4)	9734(5)	3376(4)	41(2)	1
C24	3476(4)	9464(6)	2896(5)	57(2)	1
C25	1939(4)	6911(4)	3161(4)	33(2)	1
C26	2382(4)	6701(5)	2605(4)	41(2)	1
C27	2933(5)	5844(5)	2884(5)	53(2)	1
C28	3365(5)	5583(6)	2333(5)	69(3)	1
C29	1003(4)	7829(4)	3582(3)	31(1)	1
C30	283(4)	8518(4)	3400(3)	26(1)	1
C31	139(4)	8698(4)	4180(4)	30(1)	1

C32	−643(4)	9325(5)	3996(4)	42(2)	1
C33	547(4)	7563(4)	2042(3)	28(1)	1
C34	−29(4)	6739(4)	1960(4)	30(1)	1
C35	−768(4)	6746(4)	1061(4)	35(2)	1
C36	−1421(4)	5965(5)	901(4)	44(2)	1

Table A3.27: Hydrogen bonds [Å and °].

D–H···*A*	*d*(*D*–H)	*d*(H···*A*)	*d*(*D*···*A*)	∠(*D*H*A*)
N1–H1···Cl1	0.88	2.34	3.208(5)	166.7
N2–H2···Cl1	0.88	2.27	3.140(5)	170.1
N3–H3···Cl1	0.88	2.61	3.406(5)	151.2

A3.2.5 Receptor 227 (chloride complex)

Table A3.28: Crystal data and structure refinement details.

Identification code	**2011sot0370**
Empirical formula	$C_{31}H_{49}ClN_4S$
Formula weight	545.25
Temperature	120(2) K
Wavelength	0.71073 Å
Crystal system	Monoclinic
Space group	*Pc*
Unit cell dimensions	a = 10.0881(4) Å b = 9.5939(2) Å β = 104.8840(10)° c = 17.0202(7) Å
Volume	1592.02(10) Å^3
Z	2
Density (calculated)	1.137 Mg / m^3
Absorption coefficient	0.210 mm^{-1}
F(000)	592
Crystal	Slab; Colourless
Crystal size	0.32 × 0.24 × 0.04 mm^3
θ range for data collection	3.26 – 25.03°
Index ranges	$-12 \le h \le 12$, $-11 \le k \le 11$, $-20 \le l \le 20$
Reflections collected	17355
Independent reflections	5499 [R_{int} = 0.0520]
Completeness to θ = 25.03°	99.6 %
Absorption correction	Semi–empirical from equivalents
Max. and min. transmission	0.9916 and 0.9357
Refinement method	Full-matrix least-squares on F^2
Data / restraints / parameters	5499 / 2 / 338
Goodness-of-fit on F^2	1.037
Final R indices [$F^2 > 2\sigma(F^2)$]	$R1$ = 0.0374, $wR2$ = 0.0823
R indices (all data)	$R1$ = 0.0443, $wR2$ = 0.0858
Absolute structure parameter	0.07(5)
Largest diff. peak and hole	0.165 and –0.174 e Å^{-3}

Diffractometer: *Nonius KappaCCD* area detector (ϕ scans and ω scans to fill *asymmetric unit*). **Cell determination:** DirAx (Duisenberg, A.J.M.(1992). J. Appl. Cryst. 25, 92-96.) **Data collection:** Collect (Collect: Data collection software, R. Hooft, Nonius B.V., 1998). **Data reduction and cell refinement**: *Denzo* (Z. Otwinowski & W. Minor, *Methods in Enzymology* (1997) Vol. **276**: *Macromolecular Crystallography*, part A, pp. 307–326; C. W. Carter, Jr. & R. M. Sweet, Eds., Academic Press). **Absorption correction**: Sheldrick, G. M. SADABS - Bruker Nonius area detector scaling and absorption correction - V2.10 **Structure solution**: *SHELXS97* (G. M. Sheldrick, Acta Cryst. (1990) A**46** 467–473). **Structure refinement**: *SHELXL97* (G. M. Sheldrick (1997), University of Göttingen, Germany). **Graphics:** Cameron - A Molecular Graphics Package. (D. M. Watkin, L. Pearce and C. K. Prout, Chemical Crystallography Laboratory, University of Oxford, 1993).
Special details: All hydrogen atoms were placed in idealised positions and refined using a riding model.

Table A3.29: Atomic coordinates [× 10^4], equivalent isotropic displacement parameters [Å^2 × 10^3] and site occupancy factors. U_{eq} is defined as one third of the trace of the orthogonalized U^{ij} tensor.

Atom	*x*	*y*	*z*	U_{eq}	*S.o.f.*
S1	3561(1)	8424(1)	2178(1)	32(1)	1
N1	−1577(2)	7865(2)	2335(1)	26(1)	1
N2	1440(2)	7917(2)	2838(1)	25(1)	1
N3	2857(2)	6110(2)	2858(1)	28(1)	1
C1	−2930(3)	8271(3)	2067(2)	33(1)	1
C2	−2995(3)	9674(3)	1924(2)	39(1)	1
C3	−1631(3)	10200(2)	2117(2)	29(1)	1
C4	−1021(3)	11522(3)	2120(2)	36(1)	1
C5	376(3)	11630(3)	2348(2)	36(1)	1
C6	1232(3)	10475(2)	2585(2)	30(1)	1
C7	672(2)	9152(2)	2596(1)	24(1)	1
C8	−757(2)	9037(2)	2375(1)	23(1)	1
C9	2596(2)	7460(2)	2642(2)	24(1)	1
C10	4005(2)	5296(3)	2802(2)	27(1)	1
C11	5342(2)	5769(3)	3106(2)	34(1)	1
C12	6423(3)	4897(3)	3078(2)	42(1)	1
C13	6188(3)	3560(4)	2774(2)	49(1)	1
C14	4856(3)	3084(3)	2491(2)	50(1)	1
C15	3769(3)	3955(3)	2502(2)	36(1)	1
N4	−13(2)	8668(2)	−60(1)	21(1)	1
C16	−1344(2)	9138(2)	−658(1)	24(1)	1
C17	−2414(2)	9746(2)	−272(2)	29(1)	1
C18	−3741(3)	10081(3)	−905(2)	37(1)	1
C19	−4801(3)	10742(3)	−521(2)	39(1)	1
C20	669(2)	9898(2)	460(2)	23(1)	1
C21	1141(2)	11078(2)	−3(2)	26(1)	1
C22	1877(3)	12181(3)	605(2)	35(1)	1
C23	2448(3)	13371(3)	191(2)	41(1)	1
C24	916(2)	8088(2)	−560(2)	26(1)	1
C25	2322(2)	7615(3)	−64(2)	31(1)	1
C26	3196(3)	7145(3)	−629(2)	36(1)	1
C27	4613(3)	6652(3)	−171(2)	42(1)	1
C28	−303(2)	7574(2)	520(1)	24(1)	1
C29	−1061(3)	6289(2)	104(2)	29(1)	1
C30	−1173(4)	5173(3)	702(2)	61(1)	1
C31	−1924(4)	3890(3)	275(2)	64(1)	1
Cl1	12(1)	5109(1)	3185(1)	29(1)	1

Table A3.30: Hydrogen bonds [Å and °].

D–H···*A*	*d*(*D*–H)	*d*(H···*A*)	*d*(*D*···*A*)	∠(*D*H*A*)
N1–H901···Cl1	0.88	2.39	3.235(2)	160.1
N2–H902···Cl1	0.88	2.44	3.1813(19)	141.6
N3–H903···Cl1	0.88	2.38	3.208(2)	156.9

A3.3 Structures from Chapter 4

A3.3.1 Receptor 265 (carbonate complex)

Table A3.31: Crystal data and structure refinement details.

Identification code	**2011sot0753**	
Empirical formula	$C_{57}H_{72}N_{14}O_{15}$ $2(C_{20}H_{16}N_6O_6)$, $2(C_8H_{20}N)$, CO_3	
Formula weight	1193.29	
Temperature	100(2) K	
Wavelength	0.71075 Å	
Crystal system	Triclinic	
Space group	*P*–1	
Unit cell dimensions	a = 14.1445(18) Å	α = 86.271(8)°
	b = 14.338(2) Å	β = 81.687(8)°
	c = 16.719(3) Å	γ = 61.358(5)°
Volume	2944.5(8) Å^3	
Z	2	
Density (calculated)	1.346 Mg / m^3	
Absorption coefficient	0.099 mm^{-1}	
F(000)	1264	
Crystal	Prism; Yellow	
Crystal size	0.12 × 0.10 × 0.08 mm^3	
θ range for data collection	2.91 – 27.48°	
Index ranges	$-16 \le h \le 18$, $-18 \le k \le 18$, $-19 \le l \le 21$	
Reflections collected	33949	
Independent reflections	13317 [R_{int} = 0.0279]	
Completeness to θ = 27.48°	98.5 %	
Absorption correction	Semi–empirical from equivalents	
Max. and min. transmission	0.9921 and 0.9882	
Refinement method	Full-matrix least-squares on F^2	
Data / restraints / parameters	13317 / 36 / 770	
Goodness-of-fit on F^2	1.078	
Final *R* indices [$F^2 > 2\sigma(F^2)$]	*R1* = 0.0618, *wR2* = 0.1432	
R indices (all data)	*R1* = 0.0780, *wR2* = 0.1535	
Largest diff. peak and hole	0.630 and –0.513 e Å^{-3}	

Diffractometer: *Rigaku AFC12* goniometer equipped with an enhanced sensitivity (HG) *Saturn724+* detector mounted at the window of an *FR-E+ SuperBright* molybdenum rotating anode generator with HF *Varimax* optics (100μm focus). **Cell determination, Data collection, Data reduction and cell refinement & Absorption correction**: CrystalClear-SM Expert 2.0 r7 (Rigaku, 2011) , **Structure solution**: SHELXS97 (G. M. Sheldrick, Acta Cryst. (1990) A**46** 467–473). S**tructure refinement**: SHELXL97 (G. M. Sheldrick (1997), University of Göttingen, Germany). **Graphics:** CrystalMaker: a crystal and molecular structures program for Mac and Windows. CrystalMaker Software Ltd, Oxford, England (www.crystalmaker.com)
Special details: The counter-ions balancing the 2 negative charges of the carbonate ion comprise 1 whole and 2 half TEA molecules. The 2 half molecules lie on inversion centres and were refined using thermal parameter and geometrical restraints.

Table A3.32: Atomic coordinates [$\times 10^4$], equivalent isotropic displacement parameters [$Å^2 \times 10^3$] and site occupancy factors. U_{eq} is defined as one third of the trace of the orthogonalized U^{ij} tensor.

Atom	*x*	*y*	*z*	U_{eq}	*S.o.f.*
N14	5000	0	0	41(1)	1
C50A	5788(4)	−1031(4)	7(3)	43(1)	0.50
C51A	6690(5)	−1295(5)	556(4)	43(1)	0.50
C52A	4655(4)	−852(4)	343(3)	43(1)	0.50
C53A	4126(5)	−621(4)	1225(3)	43(1)	0.50
C50B	5928(4)	−160(4)	487(3)	43(1)	0.50
C51B	6911(4)	−1187(4)	487(4)	43(1)	0.50
C52B	4390(4)	530(4)	848(3)	43(1)	0.50
C53B	3851(5)	−72(4)	1329(3)	43(1)	0.50
N15	0	0	0	40(1)	1
C54A	1049(4)	−32(4)	166(3)	40(1)	0.50
C55A	1517(5)	−381(5)	891(4)	40(1)	0.50
C56A	−773(4)	282(4)	820(3)	40(1)	0.50
C57A	−1112(4)	1415(4)	1081(3)	40(1)	0.50
C54B	375(4)	−494(4)	681(3)	40(1)	0.50
C55B	1397(5)	−573(5)	945(4)	40(1)	0.50
C56B	−334(4)	1284(4)	−1(3)	40(1)	0.50
C57B	−1094(4)	1836(4)	753(3)	40(1)	0.50
O1	723(2)	2380(2)	712(2)	65(1)	1
O2	1799(2)	2320(1)	1534(1)	55(1)	1
O3	−253(1)	7804(1)	1838(1)	35(1)	1
O4	4069(1)	8005(1)	2750(1)	37(1)	1
O5	7713(1)	2619(1)	2820(1)	48(1)	1
O6	9177(1)	2782(1)	2674(1)	56(1)	1
N1	1026(2)	2812(2)	1152(1)	46(1)	1
N2	762(1)	6030(1)	2122(1)	28(1)	1
N3	972(1)	7267(1)	2755(1)	28(1)	1
N4	2846(1)	7361(1)	2899(1)	24(1)	1
N5	4654(1)	6204(1)	2762(1)	25(1)	1
N6	8184(2)	3163(2)	2747(1)	37(1)	1
C1	851(2)	4469(2)	1621(1)	31(1)	1
C2	432(2)	3979(2)	1209(2)	36(1)	1
C3	−498(2)	4527(2)	841(2)	42(1)	1
C4	−1013(2)	5629(2)	894(2)	42(1)	1
C5	−621(2)	6159(2)	1300(1)	35(1)	1
C6	317(2)	5577(2)	1675(1)	29(1)	1
C7	431(2)	7099(2)	2211(1)	28(1)	1
C8	904(2)	8262(2)	2897(1)	28(1)	1
C9	−93(2)	9189(2)	2966(2)	37(1)	1

C10	−156(2)	10166(2)	3083(2)	43(1)	1
C11	776(2)	10223(2)	3151(2)	39(1)	1
C12	1779(2)	9310(2)	3101(1)	32(1)	1
C13	1856(2)	8318(2)	2966(1)	26(1)	1
C14	3864(2)	7264(2)	2792(1)	25(1)	1
C15	5772(2)	5830(2)	2741(1)	24(1)	1
C16	6266(2)	6482(2)	2701(1)	32(1)	1
C17	7380(2)	6029(2)	2698(2)	37(1)	1
C18	8028(2)	4943(2)	2719(1)	35(1)	1
C19	7523(2)	4321(2)	2742(1)	29(1)	1
C20	6413(2)	4732(2)	2759(1)	25(1)	1
O7	−2273(2)	6287(2)	4688(1)	64(1)	1
O8	−1096(2)	6438(2)	3776(1)	52(1)	1
O9	2893(1)	1112(1)	3682(1)	38(1)	1
O10	6538(1)	1634(1)	813(1)	27(1)	1
O11	5913(2)	6696(1)	794(1)	54(1)	1
O12	6813(2)	6597(1)	−384(1)	43(1)	1
N7	−1384(2)	5912(2)	4262(2)	47(1)	1
N8	2094(1)	2911(2)	3434(1)	29(1)	1
N9	3798(1)	1840(1)	2826(1)	28(1)	1
N10	5454(1)	2196(1)	2032(1)	24(1)	1
N11	5627(1)	3403(1)	1164(1)	26(1)	1
N12	6382(2)	6239(1)	145(1)	31(1)	1
C21	361(2)	4350(2)	3861(1)	33(1)	1
C22	−641(2)	4768(2)	4335(2)	38(1)	1
C23	−960(2)	4155(2)	4868(2)	46(1)	1
C24	−236(2)	3086(2)	4902(2)	45(1)	1
C25	770(2)	2633(2)	4430(1)	38(1)	1
C26	1082(2)	3269(2)	3911(1)	31(1)	1
C27	2919(2)	1885(2)	3344(1)	28(1)	1
C28	4860(2)	979(2)	2734(1)	25(1)	1
C29	5124(2)	−49(2)	3013(1)	31(1)	1
C30	6193(2)	−848(2)	2931(1)	35(1)	1
C31	7025(2)	−655(2)	2563(1)	33(1)	1
C32	6771(2)	354(2)	2267(1)	28(1)	1
C33	5701(2)	1171(2)	2341(1)	24(1)	1
C34	5924(2)	2350(2)	1295(1)	22(1)	1
C35	6065(2)	3811(2)	514(1)	23(1)	1
C36	6496(2)	3317(2)	−243(1)	28(1)	1
C37	6903(2)	3776(2)	−860(1)	31(1)	1
C38	6883(2)	4739(2)	−745(1)	28(1)	1
C39	6440(2)	5212(2)	9(1)	23(1)	1
C40	6033(2)	4777(2)	639(1)	24(1)	1
O13	2902(1)	4141(1)	2567(1)	34(1)	1
O14	2707(1)	5515(1)	3252(1)	33(1)	1

O15	4338(1)	4377(1)	2638(1)	28(1)	1
C49	3316(2)	4671(2)	2818(1)	23(1)	1
N13	5921(2)	2116(1)	4766(1)	30(1)	1
C41	5281(2)	3028(2)	4217(1)	33(1)	1
C42	4451(2)	4050(2)	4652(2)	40(1)	1
C43	5164(2)	1819(2)	5331(1)	34(1)	1
C44	4489(2)	1488(2)	4918(2)	39(1)	1
C45	6722(2)	1190(2)	4223(1)	38(1)	1
C46	7465(2)	201(2)	4653(2)	49(1)	1
C47	6495(2)	2444(2)	5300(1)	37(1)	1
C48	7294(2)	2782(3)	4863(2)	53(1)	1

Table A3.33: Hydrogen bonds [Å and °].

D–H···*A*	*d*(*D*–H)	*d*(H···*A*)	*d*(*D*···*A*)	∠(*D*H*A*)
N2–H902···O13	0.88	2.26	3.095(2)	158.7
N2–H902···O14	0.88	2.59	3.326(2)	142.2
N3–H903···O14	0.88	1.90	2.726(2)	155.7
N4–H904···O14	0.88	1.90	2.765(2)	166.9
N5–H905···O15	0.88	2.03	2.885(2)	165.1
N5–H905···O14	0.88	2.61	3.329(2)	139.0
N8–H908···O13	0.88	1.91	2.765(2)	163.1
N9–H909···O13	0.88	2.19	2.939(2)	142.8
N10–H910···O15	0.88	2.12	2.918(2)	150.2
N10–H910···O13	0.88	2.63	3.368(2)	142.5
N11–H911···O15	0.88	2.02	2.838(2)	154.5

Symmetry transformations used to generate equivalent atoms:
(i) –x+1,–y,–z (ii) –x,–y,–z

Appendix 4

Predicted logP and TPSA values

Predicted values for Wildman-Crippen logP (wclogP) and topological polar surface area (TPSA) were calculated for the compounds discussed in **Chapters 2-4** using Fieldview version 2.0.2 for Macintosh.[375-377]

A4.1 Compounds in Chapter 2

Compound	wclogP	TPSA (Å)
118	4.29	72.7
152	6.15	130.9
153	5.59	156.7
154	6.80	130.9
129	5.35	130.9
155	1.59	126.6
156	2.08	75.4
143	3.75	126.6
144	4.25	75.4

A4.2 Compounds in Chapter 3

Compound	wclogP	TPSA (Å)
202	3.09	56.9
203	3.48	56.9
204	3.87	56.9
205	4.26	56.9
206	4.65	56.9
207	5.04	56.9
208	5.43	56.9
209	5.82	56.9
210	6.21	56.9
211	2.13	41.1
212	2.30	24.1
213	2.85	41.1
214	3.02	24.1

215	3.34	56.9
216	3.50	39.8
217	2.34	29.1
218	3.14	12.0
219	3.06	29.1
220	3.86	12.0
221	3.54	44.9
222	4.34	27.8
223	4.03	39.8
224	6.23	56.9
225	6.40	39.8
226	3.81	56.9
227	3.98	39.8
228	4.83	56.9
229	5.00	39.8
230	3.39	41.1
231	3.55	24.1
232	4.41	41.1
233	4.57	24.1

A4.3 Compounds in Chapter 4

Compound	wclogP	TPSA (Å)
244	4.97	82.3
262	5.80	82.3
245	6.33	82.3
263	4.72	129.8
264	7.01	82.3
247	4.58	173.9
265	4.58	173.9

248	4.58	173.9
266	3.20	64.9
267	4.35	41.1
268	3.13	86.9

Appendix 5

Ion Transport Assays

Ion transport assays using POPC vesicles were performed using the assay conditions described in **Appendix 1**. Ion transport was measured using either a chloride ISE or fluorescence techniques.

A5.1 Ion Transport Assays from Chapter 3

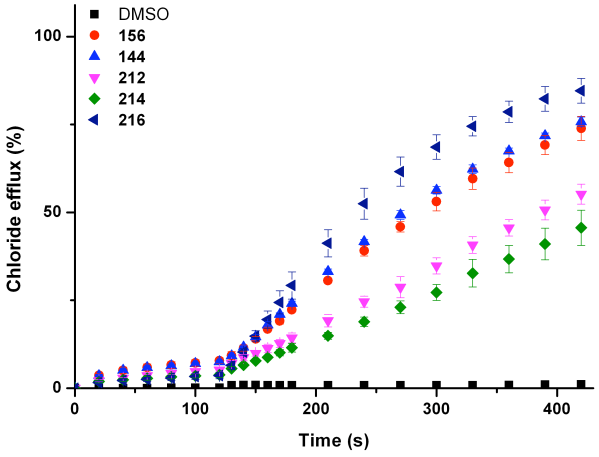

Figure 5.1.1: Chloride efflux promoted by addition of receptors **156**, **144**, **212**, **214** and **216** (2 mol % each with respect to lipid) to unilamellar POPC vesicles loaded with 451 mM NaCl buffered to pH 7.2 with 20 mM sodium phosphate salts upon addition of a $NaHCO_3$ 'pulse' to make the extravesicular bicarbonate concentration 40 mM. The vesicles were suspended in 150 mM Na_2SO_4 buffered to pH 7.2 with 20 mM sodium phosphate salts. At the end of the experiment, detergent was added to lyse the vesicles and calibrate the ISE to 100 % chloride efflux. Each point represents an average of three trials.

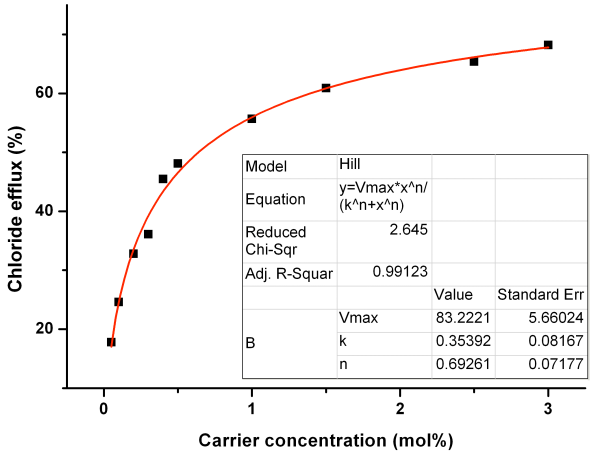

Figure 5.1.2: Hill plot for the Cl^-/HCO_3^- antiport promoted by receptor **212**.

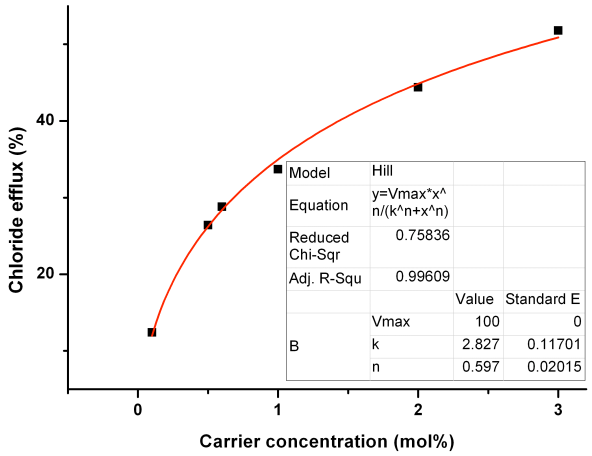

Figure 5.1.3: Hill plot for the Cl^-/HCO_3^- antiport promoted by receptor **214**.

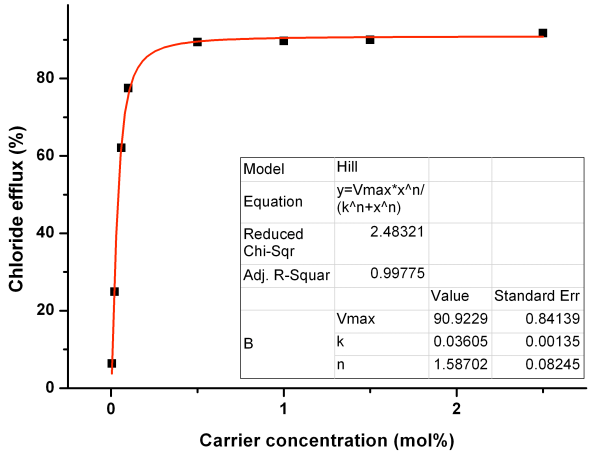

Figure 5.1.4: Hill plot for the Cl^-/HCO_3^- antiport promoted by receptor **216**.

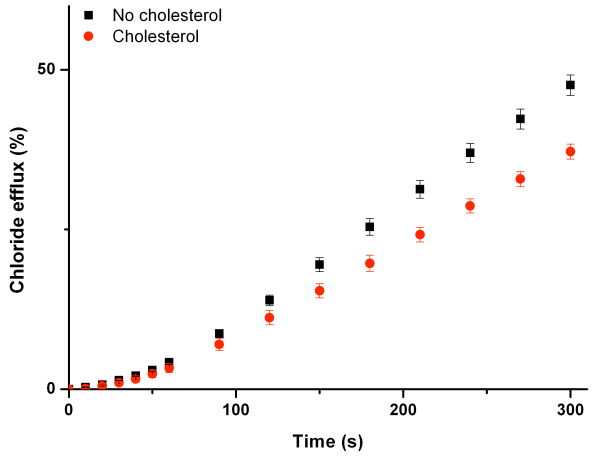

Figure 5.1.5: Chloride efflux promoted by addition of receptor **212** (0.2 mol % with respect to lipid) to unilamellar vesicles composed of either POPC or POPC/cholesterol (7:3 molar ratio) loaded with 488 mM NaCl buffered to pH 7.2 with 5 mM sodium phosphate salts. The vesicles were suspended in 488 mM $NaNO_3$ buffered to pH 7.2 with 5 mM sodium phosphate salts. At the end of the experiment, detergent was added to lyse the vesicles and calibrate the ISE to 100 % chloride efflux. Each point represents an average of three trials.

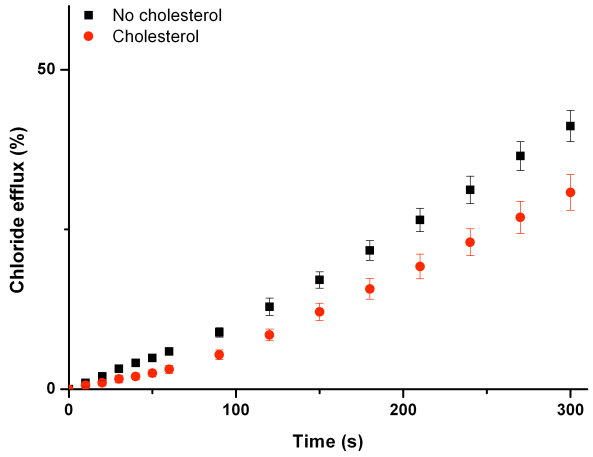

Figure 5.1.6: Chloride efflux promoted by addition of receptor **214** (3 mol % with respect to lipid) to unilamellar vesicles composed of either POPC or POPC/cholesterol (7:3 molar ratio) loaded with 488 mM NaCl buffered to pH 7.2 with 5 mM sodium phosphate salts. The vesicles were suspended in 488 mM $NaNO_3$ buffered to pH 7.2 with 5 mM sodium phosphate salts. At the end of the experiment, detergent was added to lyse the vesicles and calibrate the ISE to 100 % chloride efflux. Each point represents an average of three trials.

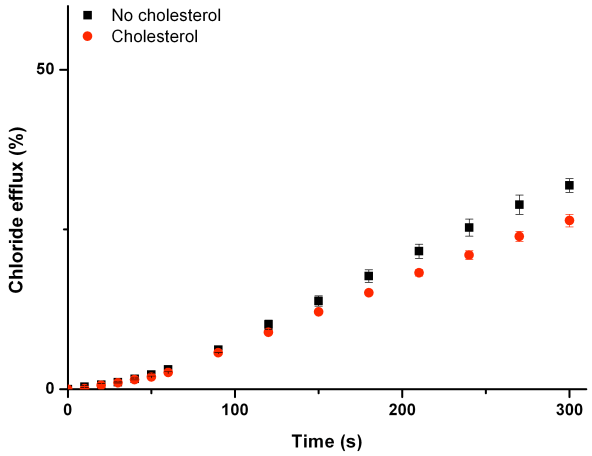

Figure 5.1.7: Chloride efflux promoted by addition of receptor **216** (0.03 mol % with respect to lipid) to unilamellar vesicles composed of either POPC or POPC/cholesterol (7:3 molar ratio) loaded with 488 mM NaCl buffered to pH 7.2 with 5 mM sodium phosphate salts. The vesicles were suspended in 488 mM $NaNO_3$ buffered to pH 7.2 with 5 mM sodium phosphate salts. At the end of the experiment, detergent was added to lyse the vesicles and calibrate the ISE to 100 % chloride efflux. Each point represents an average of three trials.

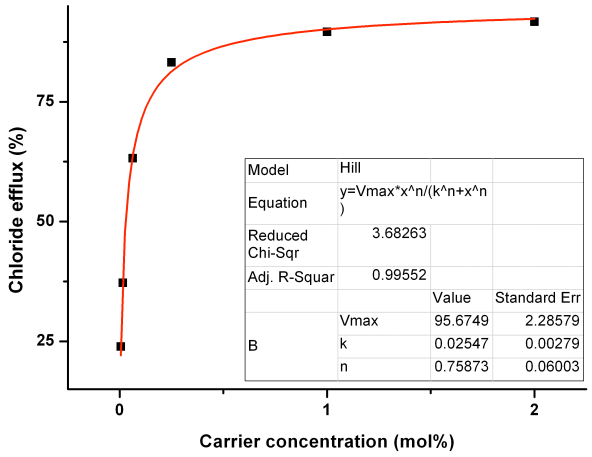

Figure 5.1.8: Hill plot for the Cl^-/NO_3^- antiport promoted by receptor **223**.

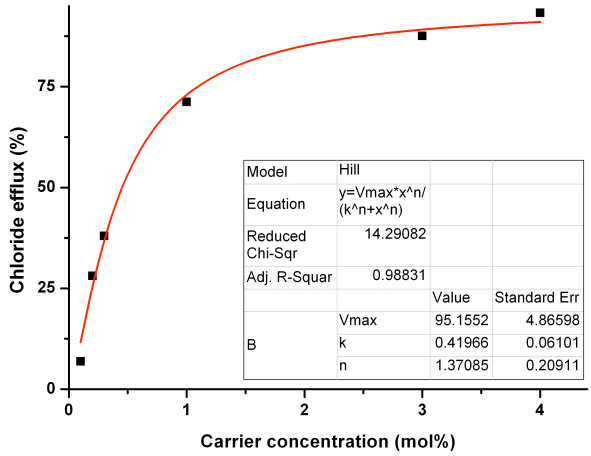

Figure 5.1.9: Hill plot for the Cl^-/NO_3^- antiport promoted by receptor **224**.

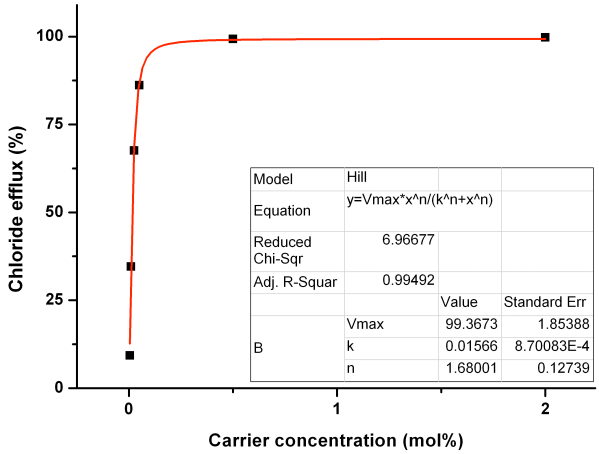

Figure 5.1.10: Hill plot for the Cl^-/NO_3^- antiport promoted by receptor **225**.

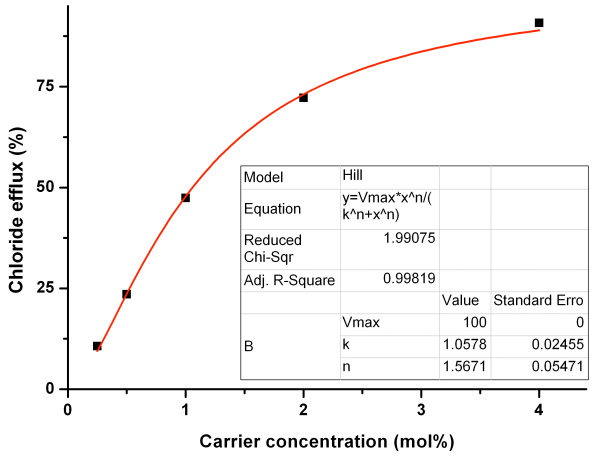

Figure 5.1.11: Hill plot for the Cl^-/NO_3^- antiport promoted by receptor **228**.

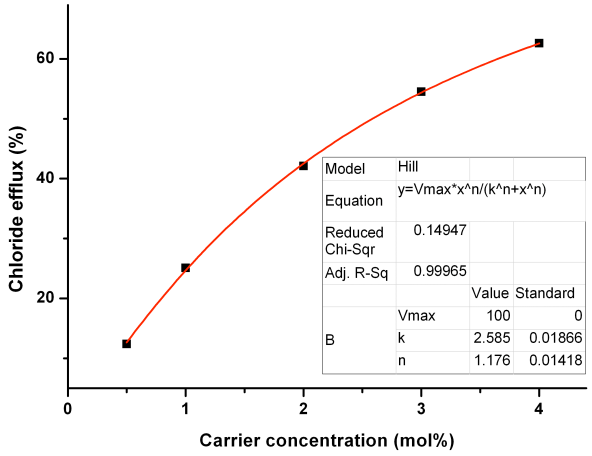

Figure 5.1.12: Hill plot for the Cl^-/NO_3^- antiport promoted by receptor **229**.

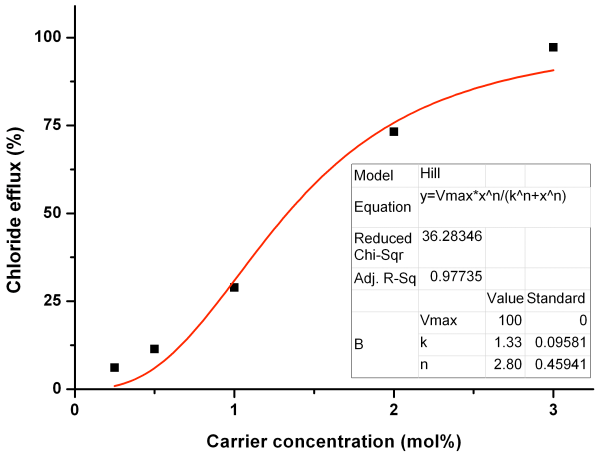

Figure 5.1.13: Hill plot for the Cl^-/NO_3^- antiport promoted by receptor **232**.

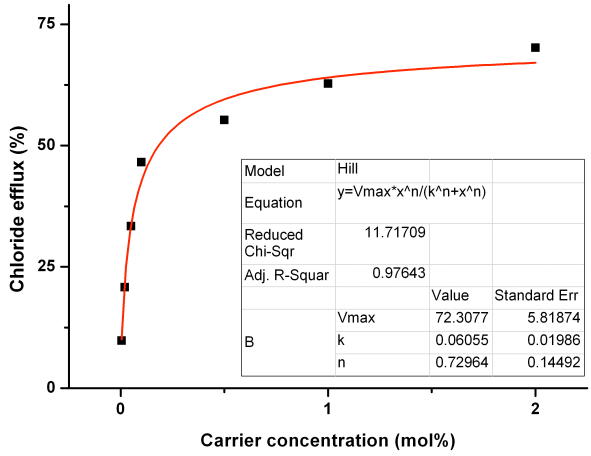

Figure 5.1.14: Hill plot for the Cl^-/HCO_3^- antiport promoted by receptor **223**.

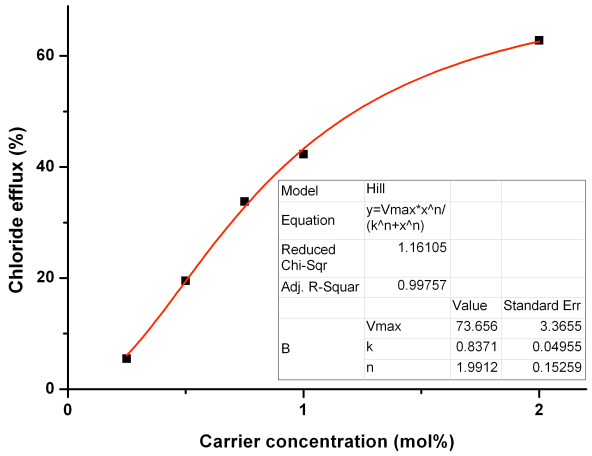

Figure 5.1.15: Hill plot for the Cl^-/HCO_3^- antiport promoted by receptor **224**.

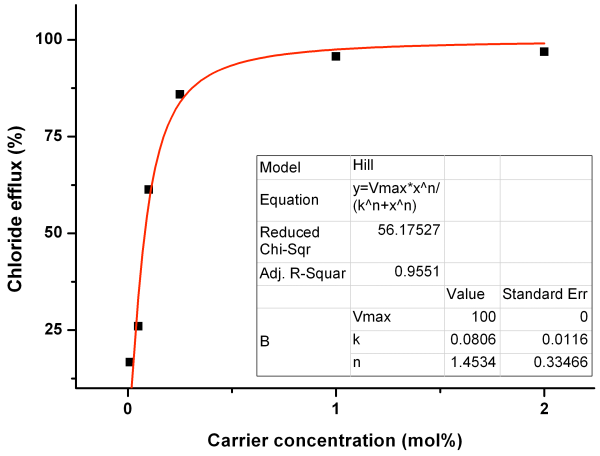

Figure 5.1.16: Hill plot for the Cl^-/HCO_3^- antiport promoted by receptor **225**.

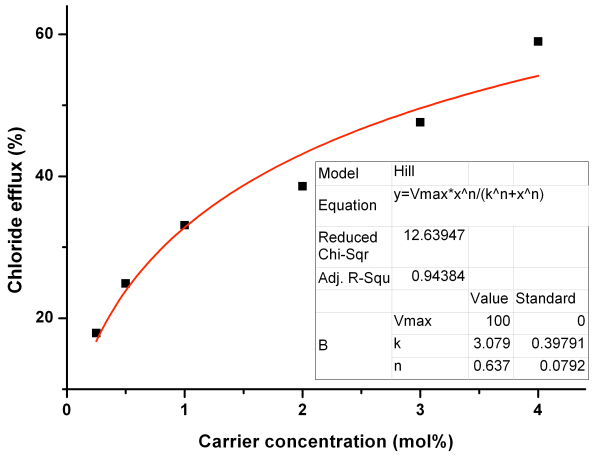

Figure 5.1.17: Hill plot for the Cl^-/HCO_3^- antiport promoted by receptor **231**.

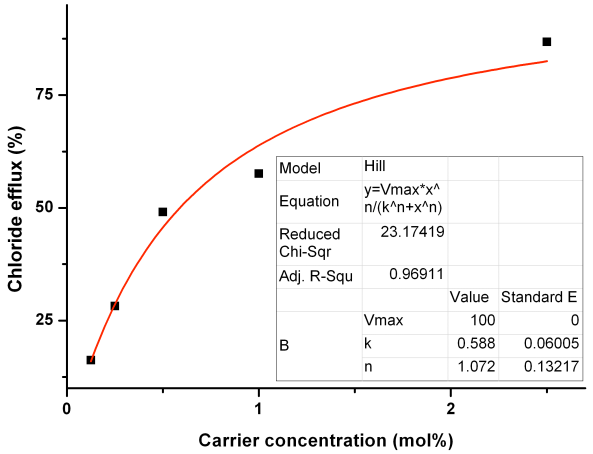

Figure 5.1.18: Hill plot for the Cl^-/HCO_3^- antiport promoted by receptor **233**.

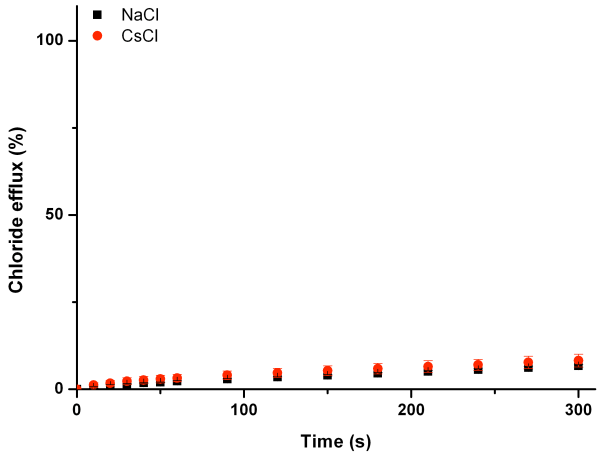

Figure 5.1.19: Chloride efflux promoted by addition of receptor **204** (2 mol % with respect to lipid) to unilamellar POPC vesicles loaded with either 451 mM NaCl or 451 mM CsCl, buffered to pH 7.2 with 20 mM sodium phosphate salts. The vesicles were suspended in 150 mM Na_2SO_4 buffered to pH 7.2 with 20 mM sodium phosphate salts. At the end of the experiment, detergent was added to lyse the vesicles and calibrate the ISE to 100 % chloride efflux. Each point represents an average of three trials.

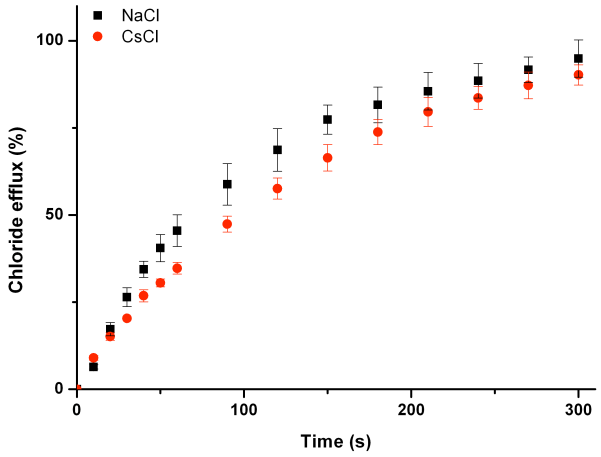

Figure 5.1.20: Chloride efflux promoted by addition of receptor **223** (2 mol % with respect to lipid) to unilamellar POPC vesicles loaded with either 451 mM NaCl or 451 mM CsCl, buffered to pH 7.2 with 20 mM sodium phosphate salts. The vesicles were suspended in 150 mM Na_2SO_4 buffered to pH 7.2 with 20 mM sodium phosphate salts. At the end of the experiment, detergent was added to lyse the vesicles and calibrate the ISE to 100 % chloride efflux. Each point represents an average of three trials.

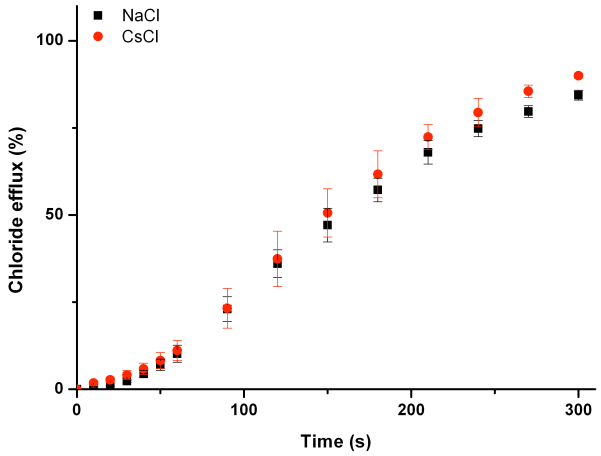

Figure 5.1.21: Chloride efflux promoted by addition of receptor **224** (2 mol % with respect to lipid) to unilamellar POPC vesicles loaded with either 451 mM NaCl or 451 mM CsCl, buffered to pH 7.2 with 20 mM sodium phosphate salts. The vesicles were suspended in 150 mM Na_2SO_4 buffered to pH 7.2 with 20 mM sodium phosphate salts. At the end of the experiment, detergent was added to lyse the vesicles and calibrate the ISE to 100 % chloride efflux. Each point represents an average of three trials.

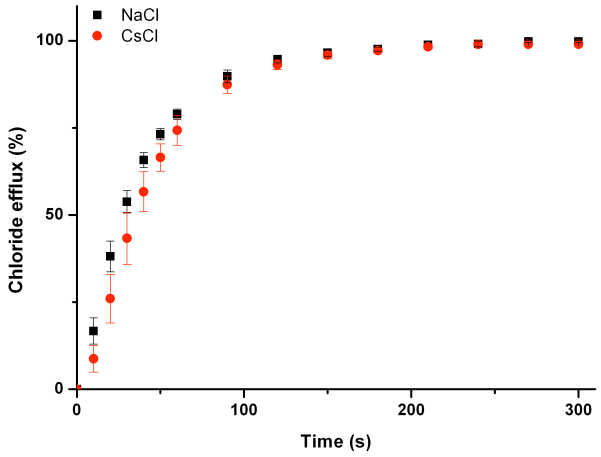

Figure 5.1.22: Chloride efflux promoted by addition of receptor **225** (2 mol % with respect to lipid) to unilamellar POPC vesicles loaded with either 451 mM NaCl or 451 mM CsCl, buffered to pH 7.2 with 20 mM sodium phosphate salts. The vesicles were suspended in 150 mM Na_2SO_4 buffered to pH 7.2 with 20 mM sodium phosphate salts. At the end of the experiment, detergent was added to lyse the vesicles and calibrate the ISE to 100 % chloride efflux. Each point represents an average of three trials.

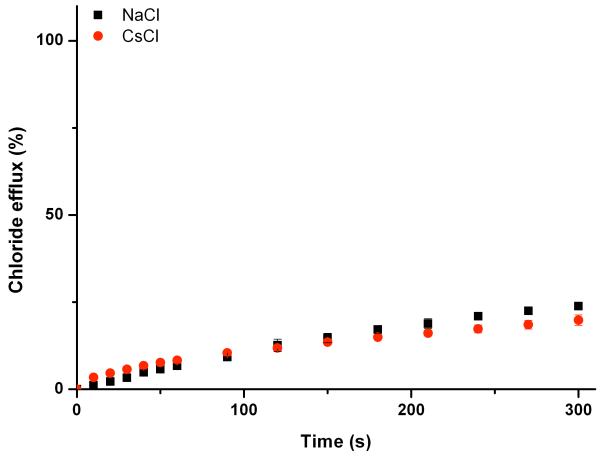

Figure 5.1.23: Chloride efflux promoted by addition of receptor **226** (2 mol % with respect to lipid) to unilamellar POPC vesicles loaded with either 451 mM NaCl or 451 mM CsCl, buffered to pH 7.2 with 20 mM sodium phosphate salts. The vesicles were suspended in 150 mM Na_2SO_4 buffered to pH 7.2 with 20 mM sodium phosphate salts. At the end of the experiment, detergent was added to lyse the vesicles and calibrate the ISE to 100 % chloride efflux. Each point represents an average of three trials.

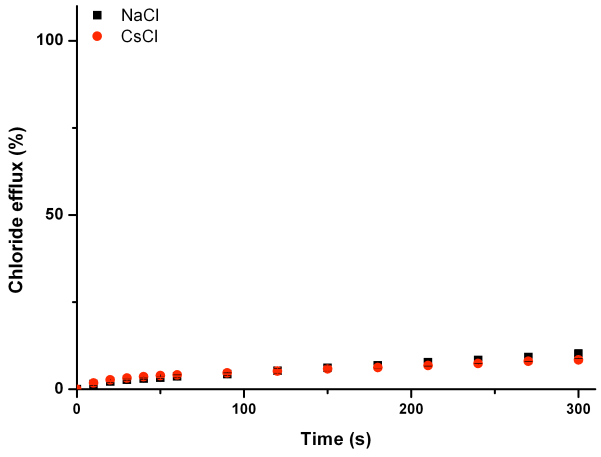

Figure 5.1.24: Chloride efflux promoted by addition of receptor **227** (2 mol % with respect to lipid) to unilamellar POPC vesicles loaded with either 451 mM NaCl or 451 mM CsCl, buffered to pH 7.2 with 20 mM sodium phosphate salts. The vesicles were suspended in 150 mM Na_2SO_4 buffered to pH 7.2 with 20 mM sodium phosphate salts. At the end of the experiment, detergent was added to lyse the vesicles and calibrate the ISE to 100 % chloride efflux. Each point represents an average of three trials.

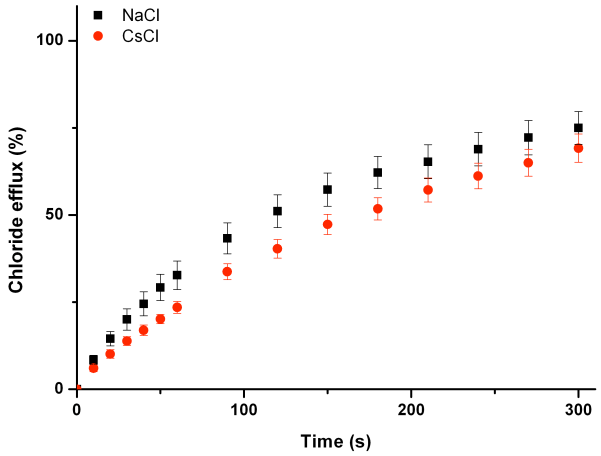

Figure 5.1.25: Chloride efflux promoted by addition of receptor **228** (2 mol % with respect to lipid) to unilamellar POPC vesicles loaded with either 451 mM NaCl or 451 mM CsCl, buffered to pH 7.2 with 20 mM sodium phosphate salts. The vesicles were suspended in 150 mM Na_2SO_4 buffered to pH 7.2 with 20 mM sodium phosphate salts. At the end of the experiment, detergent was added to lyse the vesicles and calibrate the ISE to 100 % chloride efflux. Each point represents an average of three trials.

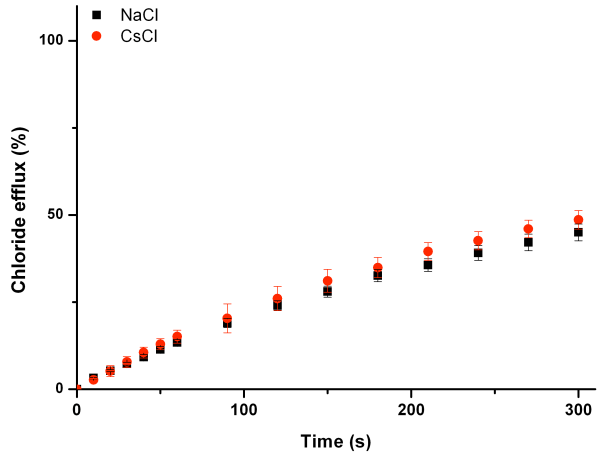

Figure 5.1.26: Chloride efflux promoted by addition of receptor **229** (2 mol % with respect to lipid) to unilamellar POPC vesicles loaded with either 451 mM NaCl or 451 mM CsCl, buffered to pH 7.2 with 20 mM sodium phosphate salts. The vesicles were suspended in 150 mM Na_2SO_4 buffered to pH 7.2 with 20 mM sodium phosphate salts. At the end of the experiment, detergent was added to lyse the vesicles and calibrate the ISE to 100 % chloride efflux. Each point represents an average of three trials.

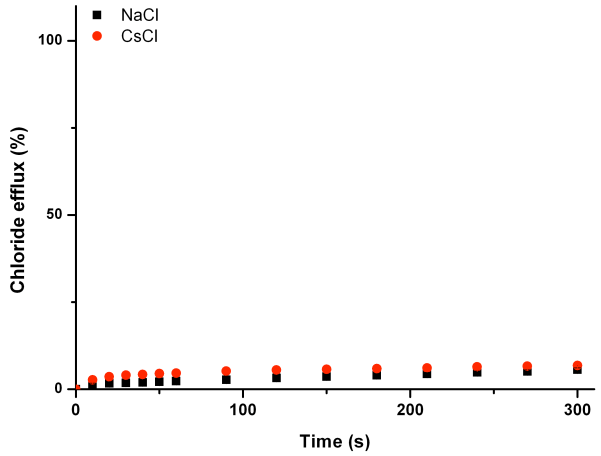

Figure 5.1.27: Chloride efflux promoted by addition of receptor **230** (2 mol % with respect to lipid) to unilamellar POPC vesicles loaded with either 451 mM NaCl or 451 mM CsCl, buffered to pH 7.2 with 20 mM sodium phosphate salts. The vesicles were suspended in 150 mM Na_2SO_4 buffered to pH 7.2 with 20 mM sodium phosphate salts. At the end of the experiment, detergent was added to lyse the vesicles and calibrate the ISE to 100 % chloride efflux. Each point represents an average of three trials.

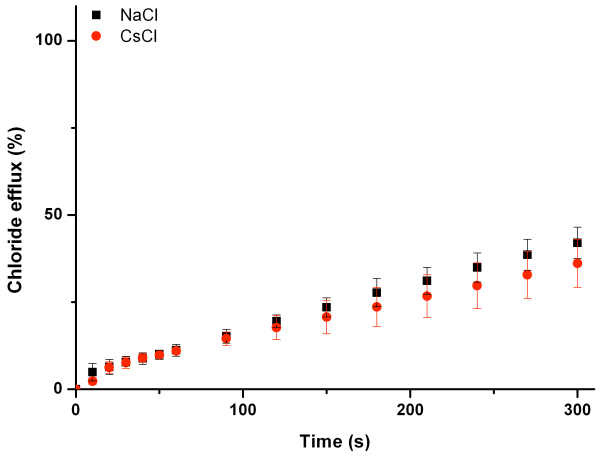

Figure 5.1.28: Chloride efflux promoted by addition of receptor **231** (2 mol % with respect to lipid) to unilamellar POPC vesicles loaded with either 451 mM NaCl or 451 mM CsCl, buffered to pH 7.2 with 20 mM sodium phosphate salts. The vesicles were suspended in 150 mM Na_2SO_4 buffered to pH 7.2 with 20 mM sodium phosphate salts. At the end of the experiment, detergent was added to lyse the vesicles and calibrate the ISE to 100 % chloride efflux. Each point represents an average of three trials.

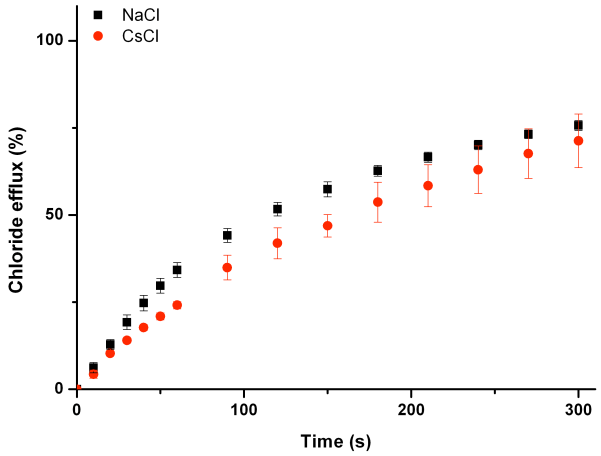

Figure 5.1.29: Chloride efflux promoted by addition of receptor **232** (2 mol % with respect to lipid) to unilamellar POPC vesicles loaded with either 451 mM NaCl or 451 mM CsCl, buffered to pH 7.2 with 20 mM sodium phosphate salts. The vesicles were suspended in 150 mM Na_2SO_4 buffered to pH 7.2 with 20 mM sodium phosphate salts. At the end of the experiment, detergent was added to lyse the vesicles and calibrate the ISE to 100 % chloride efflux. Each point represents an average of three trials.

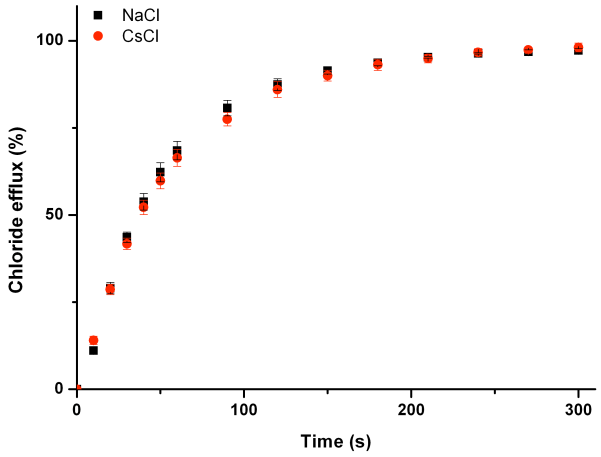

Figure 5.1.30: Chloride efflux promoted by addition of receptor **233** (2 mol % with respect to lipid) to unilamellar POPC vesicles loaded with either 451 mM NaCl or 451 mM CsCl, buffered to pH 7.2 with 20 mM sodium phosphate salts. The vesicles were suspended in 150 mM Na_2SO_4 buffered to pH 7.2 with 20 mM sodium phosphate salts. At the end of the experiment, detergent was added to lyse the vesicles and calibrate the ISE to 100 % chloride efflux. Each point represents an average of three trials.

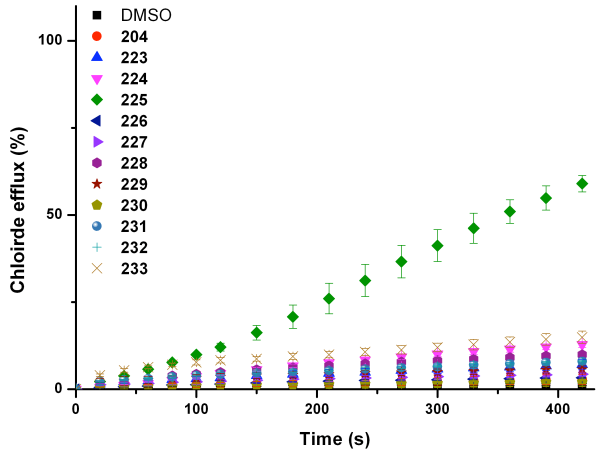

Figure 5.1.31: Chloride efflux promoted by addition of receptors **204** and **223-233** (2 mol % each with respect to lipid) to unilamellar POPC vesicles loaded with 451 mM NaCl buffered to pH 7.2 with 20 mM sodium phosphate salts. The vesicles were suspended in 150 mM Na_2SO_4 buffered to pH 7.2 with 20 mM sodium phosphate salts. At the end of the experiment, detergent was added to lyse the vesicles and calibrate the ISE to 100 % chloride efflux. Each point represents an average of three trials.

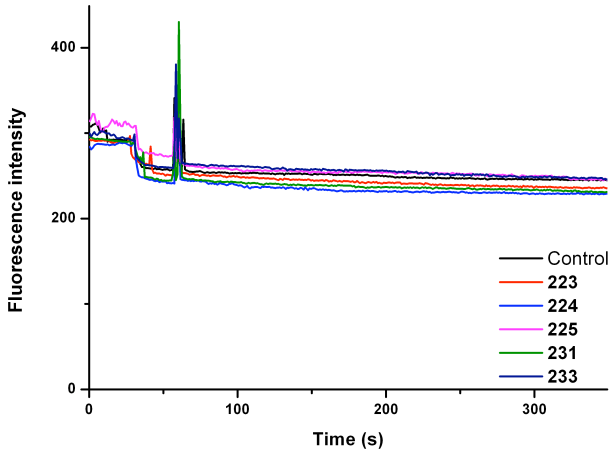

Figure 5.1.32: Change in lucigenin fluorescence intensity (excitation at 455 nm, emission at 506 nm) upon addition of receptors **223-225**, **231** and **233** (2 mol % each with respect to lipid) to unilamellar POPC vesicles loaded with 100 mM NaCl and 2 mM lucigenin buffered to pH 7.2 with 20 mM sodium phosphate salts following the addition of a Na_2SO_4 'pulse' to make the extravesicular sulphate concentration 40 mM. The vesicles were suspended in 100 mM NaCl buffered to pH 7.2 with 20 mM sodium phosphate salts. Each trace represents an average of three trials.

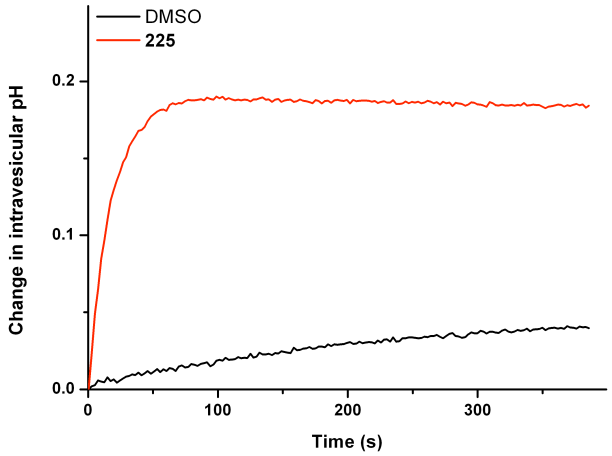

Figure 5.1.33: Change in intravesicular pH upon addition upon addition of receptors **225** (2 mol % with respect to lipid) to unilamellar POPC vesicles loaded with 451 mM NaCl and 1mM HPTS buffered to pH 7.2 with 20 mM sodium phosphate salts. The vesicles were suspended in 150 mM Na_2SO_4 buffered to pH 7.2 with 20 mM sodium phosphate salts. Each trace represents an average of three trials.

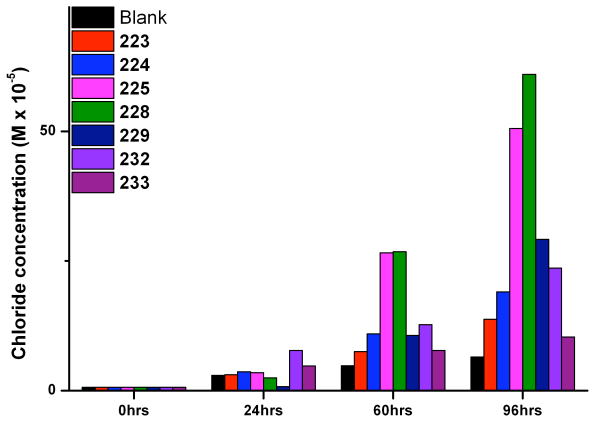

Figure 5.1.34: Change in chloride concentration of the receiving phase in a U-tube assay facilitated by compounds **223-225**, **228**, **229**, **232** and **233** (1 mM each) dissolved in a nitrobenzene organic phase (15 mL) in the presence of TBA hexafluorophosphate (1 mM). The source phase (7.5 mL) contained 488 mM NaCl buffered to pH 7.2 with 5 mM sodium phosphate salts and the receiving phase (7.5 mL) contained 488 mM $NaNO_3$ buffered to pH 7.2 with 5 mM sodium phosphate salts.

A5.2 Ion Transport Assays from Chapter 4

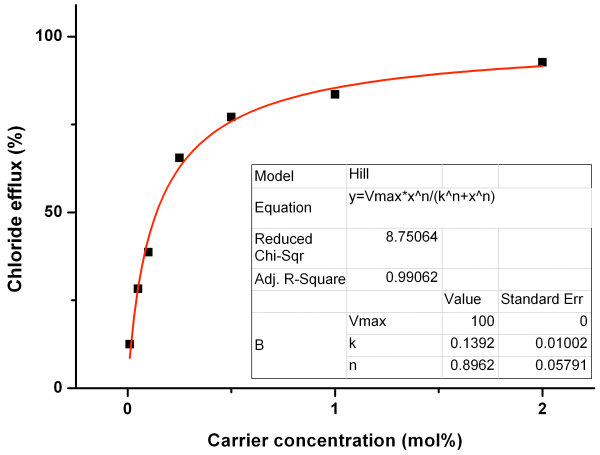

Figure 5.2.1: Hill plot for the Cl^-/NO_3^- antiport promoted by receptor **262**.

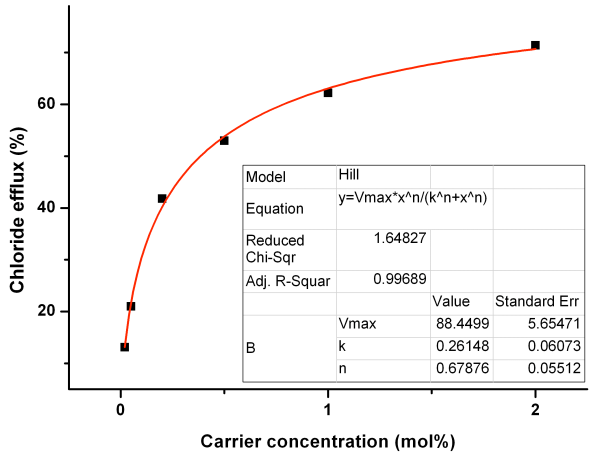

Figure 5.2.2: Hill plot for the Cl^-/NO_3^- antiport promoted by receptor **245**.

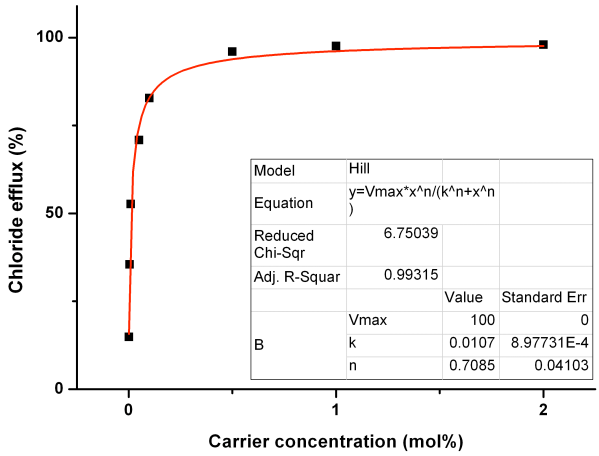

Figure 5.2.3: Hill plot for the Cl^-/NO_3^- antiport promoted by receptor **263**.

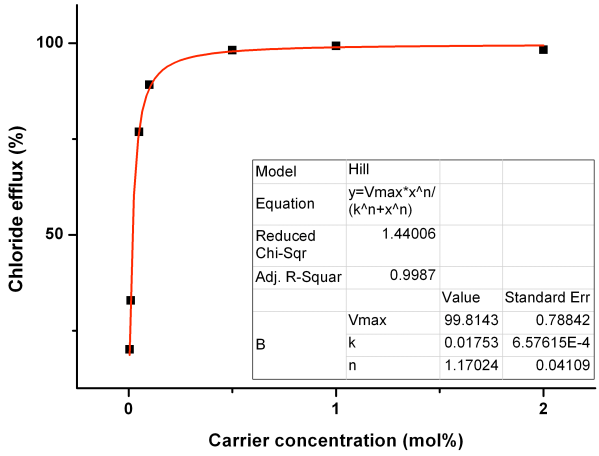

Figure 5.2.4: Hill plot for the Cl^-/NO_3^- antiport promoted by receptor **264**.

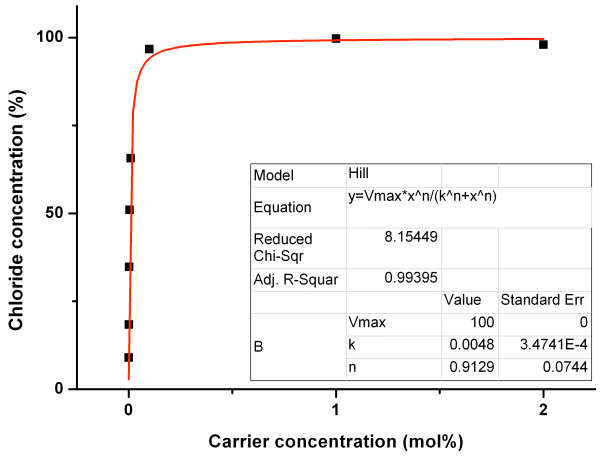

Figure 5.2.5: Hill plot for the Cl^-/NO_3^- antiport promoted by receptor **247**.

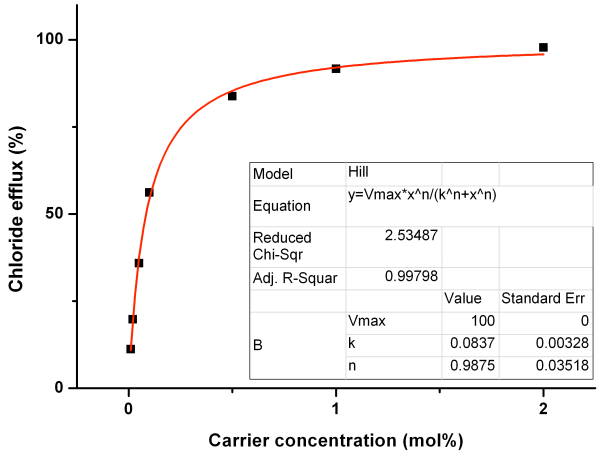

Figure 5.2.6: Hill plot for the Cl^-/NO_3^- antiport promoted by receptor **265**.

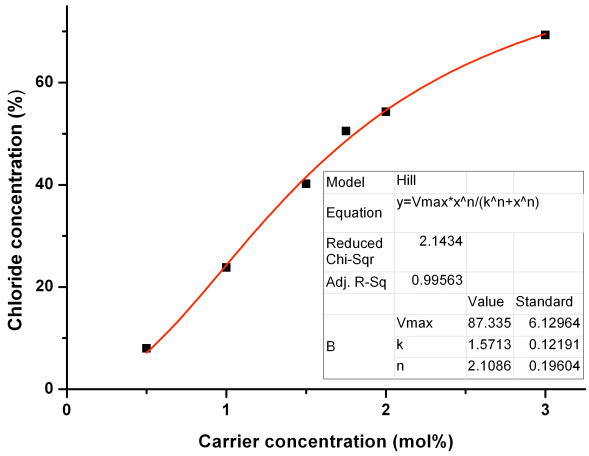

Figure 5.2.7: Hill plot for the Cl^-/NO_3^- antiport promoted by receptor **267**.

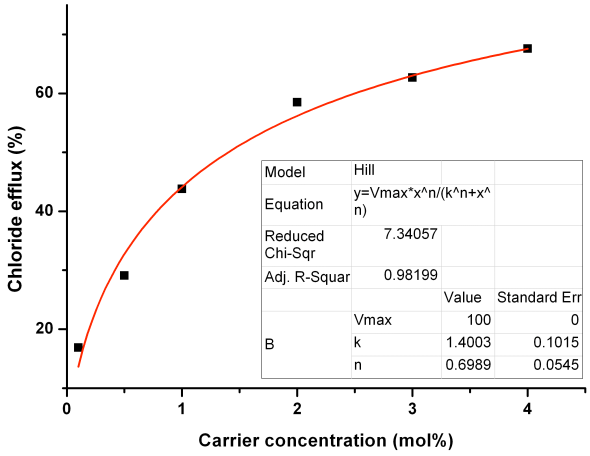

Figure 5.2.8: Hill plot for the Cl^-/HCO_3^- antiport promoted by receptor **262**.

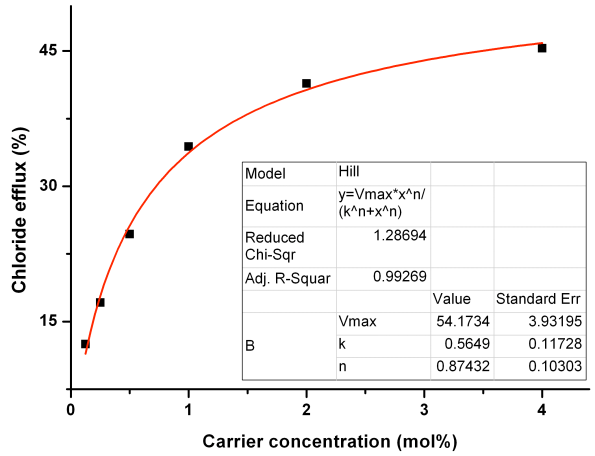

Figure 5.2.9: Hill plot for the Cl^-/HCO_3^- antiport promoted by receptor **245**.

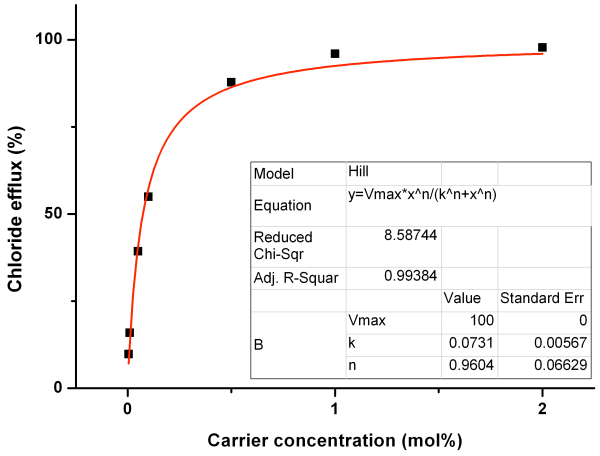

Figure 5.2.10: Hill plot for the Cl^-/HCO_3^- antiport promoted by receptor **263**.

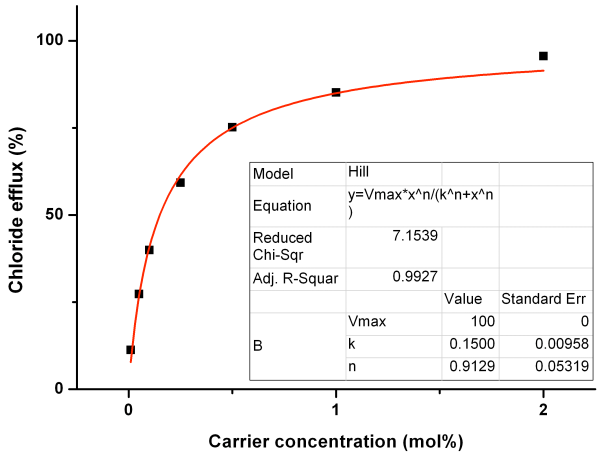

Figure 5.2.11: Hill plot for the Cl^-/HCO_3^- antiport promoted by receptor **264**.

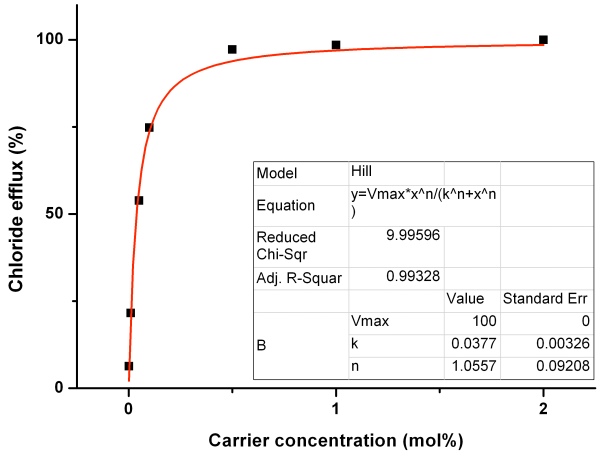

Figure 5.2.12: Hill plot for the Cl^-/HCO_3^- antiport promoted by receptor **247**.

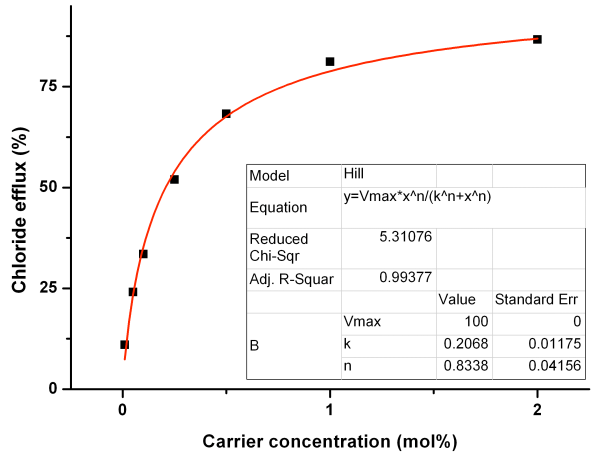

Figure 5.2.13: Hill plot for the Cl^-/HCO_3^- antiport promoted by receptor **265**.

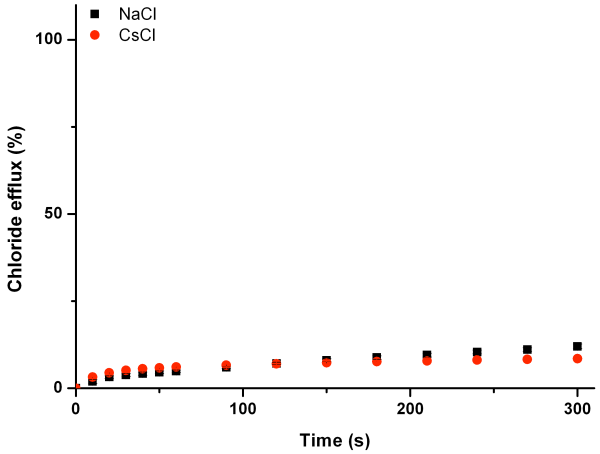

Figure 5.2.14: Chloride efflux promoted by addition of receptor **244** (2 mol % with respect to lipid) to unilamellar POPC vesicles loaded with either 451 mM NaCl or 451 mM CsCl, buffered to pH 7.2 with 20 mM sodium phosphate salts. The vesicles were suspended in 150 mM Na_2SO_4 buffered to pH 7.2 with 20 mM sodium phosphate salts. At the end of the experiment, detergent was added to lyse the vesicles and calibrate the ISE to 100 % chloride efflux. Each point represents an average of three trials.

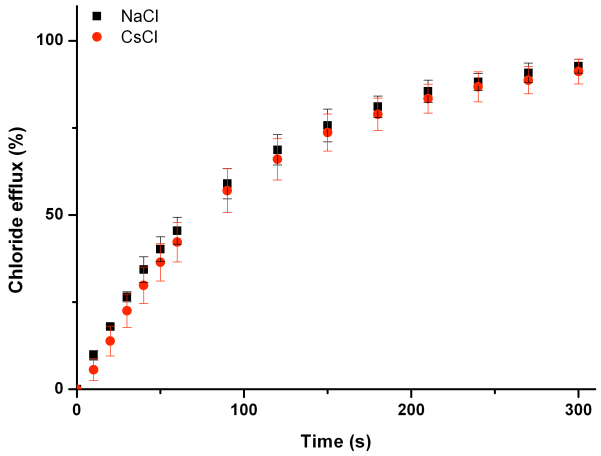

Figure 5.2.15: Chloride efflux promoted by addition of receptor **262** (2 mol % with respect to lipid) to unilamellar POPC vesicles loaded with either 451 mM NaCl or 451 mM CsCl, buffered to pH 7.2 with 20 mM sodium phosphate salts. The vesicles were suspended in 150 mM Na_2SO_4 buffered to pH 7.2 with 20 mM sodium phosphate salts. At the end of the experiment, detergent was added to lyse the vesicles and calibrate the ISE to 100 % chloride efflux. Each point represents an average of three trials.

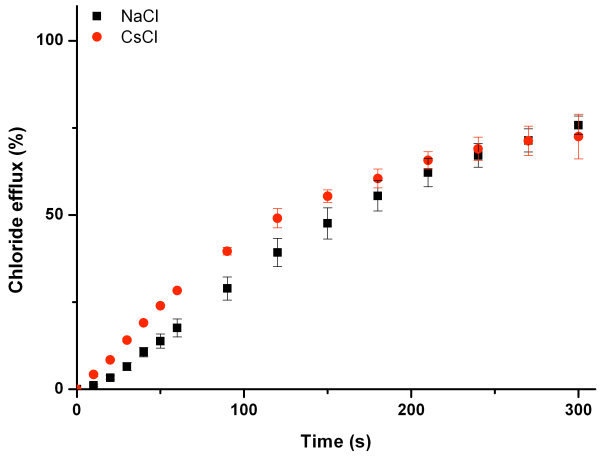

Figure 5.2.16: Chloride efflux promoted by addition of receptor **245** (2 mol % with respect to lipid) to unilamellar POPC vesicles loaded with either 451 mM NaCl or 451 mM CsCl, buffered to pH 7.2 with 20 mM sodium phosphate salts. The vesicles were suspended in 150 mM Na_2SO_4 buffered to pH 7.2 with 20 mM sodium phosphate salts. At the end of the experiment, detergent was added to lyse the vesicles and calibrate the ISE to 100 % chloride efflux. Each point represents an average of three trials.

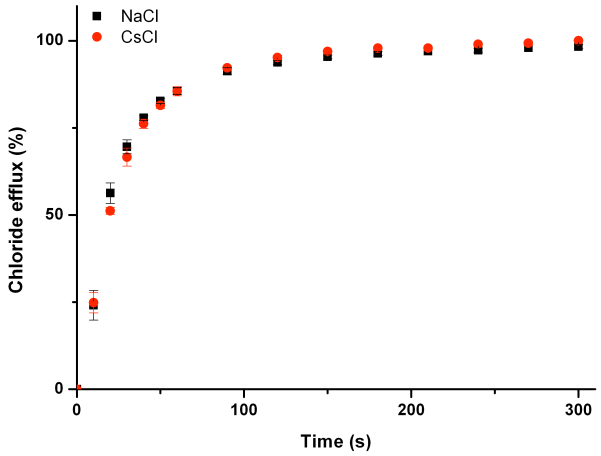

Figure 5.2.17: Chloride efflux promoted by addition of receptor **263** (2 mol % with respect to lipid) to unilamellar POPC vesicles loaded with either 451 mM NaCl or 451 mM CsCl, buffered to pH 7.2 with 20 mM sodium phosphate salts. The vesicles were suspended in 150 mM Na_2SO_4 buffered to pH 7.2 with 20 mM sodium phosphate salts. At the end of the experiment, detergent was added to lyse the vesicles and calibrate the ISE to 100 % chloride efflux. Each point represents an average of three trials.

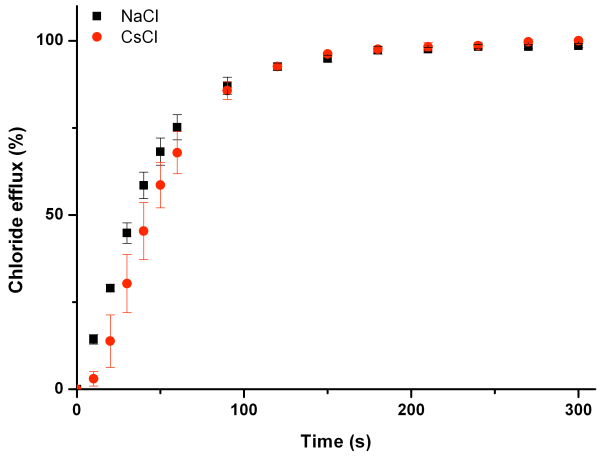

Figure 5.2.18: Chloride efflux promoted by addition of receptor **264** (2 mol % with respect to lipid) to unilamellar POPC vesicles loaded with either 451 mM NaCl or 451 mM CsCl, buffered to pH 7.2 with 20 mM sodium phosphate salts. The vesicles were suspended in 150 mM Na_2SO_4 buffered to pH 7.2 with 20 mM sodium phosphate salts. At the end of the experiment, detergent was added to lyse the vesicles and calibrate the ISE to 100 % chloride efflux. Each point represents an average of three trials.

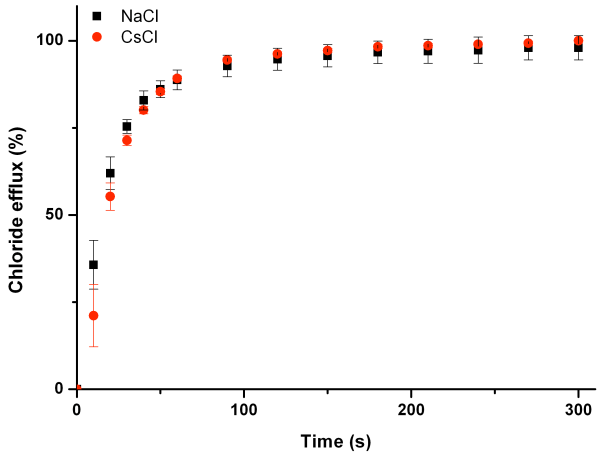

Figure 5.2.19: Chloride efflux promoted by addition of receptor **247** (2 mol % with respect to lipid) to unilamellar POPC vesicles loaded with either 451 mM NaCl or 451 mM CsCl, buffered to pH 7.2 with 20 mM sodium phosphate salts. The vesicles were suspended in 150 mM Na_2SO_4 buffered to pH 7.2 with 20 mM sodium phosphate salts. At the end of the experiment, detergent was added to lyse the vesicles and calibrate the ISE to 100 % chloride efflux. Each point represents an average of three trials.

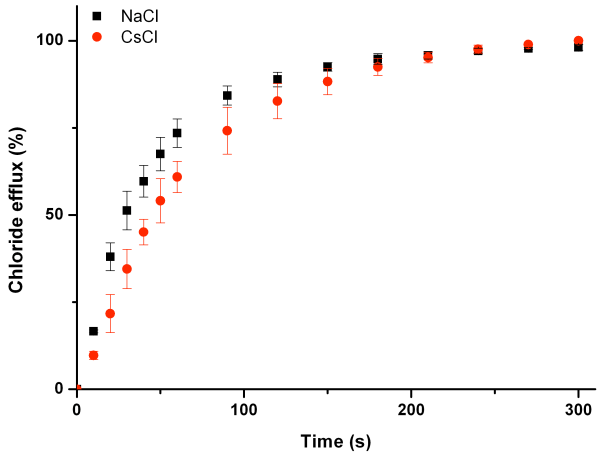

Figure 5.2.20: Chloride efflux promoted by addition of receptor **265** (2 mol % with respect to lipid) to unilamellar POPC vesicles loaded with either 451 mM NaCl or 451 mM CsCl, buffered to pH 7.2 with 20 mM sodium phosphate salts. The vesicles were suspended in 150 mM Na_2SO_4 buffered to pH 7.2 with 20 mM sodium phosphate salts. At the end of the experiment, detergent was added to lyse the vesicles and calibrate the ISE to 100 % chloride efflux. Each point represents an average of three trials.

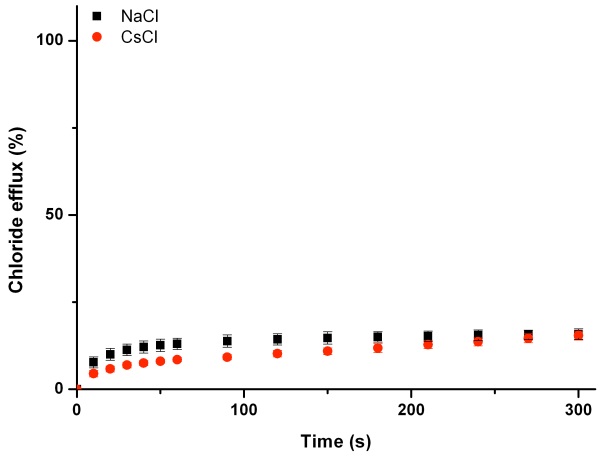

Figure 5.2.21: Chloride efflux promoted by addition of receptor **248** (2 mol % with respect to lipid) to unilamellar POPC vesicles loaded with either 451 mM NaCl or 451 mM CsCl, buffered to pH 7.2 with 20 mM sodium phosphate salts. The vesicles were suspended in 150 mM Na_2SO_4 buffered to pH 7.2 with 20 mM sodium phosphate salts. At the end of the experiment, detergent was added to lyse the vesicles and calibrate the ISE to 100 % chloride efflux. Each point represents an average of three trials.

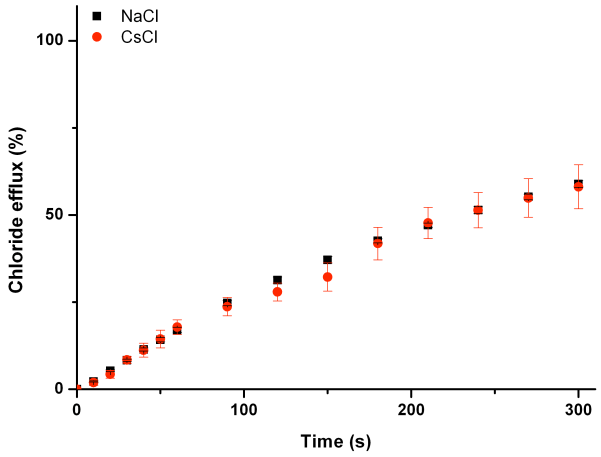

Figure 5.2.22: Chloride efflux promoted by addition of receptor **266** (2 mol % with respect to lipid) to unilamellar POPC vesicles loaded with either 451 mM NaCl or 451 mM CsCl, buffered to pH 7.2 with 20 mM sodium phosphate salts. The vesicles were suspended in 150 mM Na_2SO_4 buffered to pH 7.2 with 20 mM sodium phosphate salts. At the end of the experiment, detergent was added to lyse the vesicles and calibrate the ISE to 100 % chloride efflux. Each point represents an average of three trials.

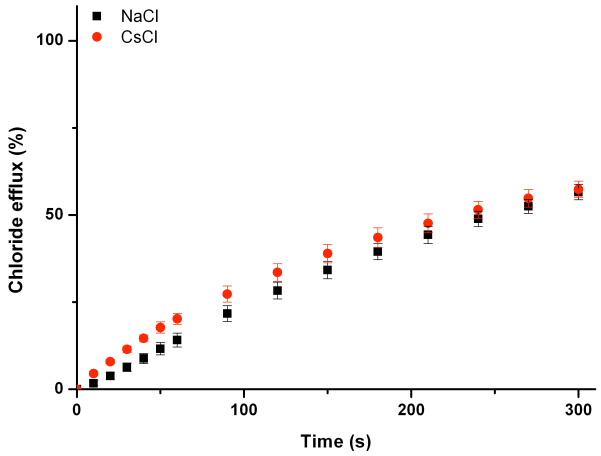

Figure 5.2.23: Chloride efflux promoted by addition of receptor **267** (2 mol % with respect to lipid) to unilamellar POPC vesicles loaded with either 451 mM NaCl or 451 mM CsCl, buffered to pH 7.2 with 20 mM sodium phosphate salts. The vesicles were suspended in 150 mM Na_2SO_4 buffered to pH 7.2 with 20 mM sodium phosphate salts. At the end of the experiment, detergent was added to lyse the vesicles and calibrate the ISE to 100 % chloride efflux. Each point represents an average of three trials.

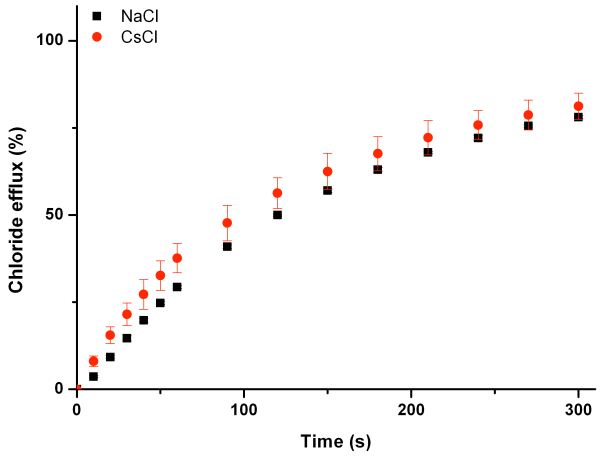

Figure 5.2.24: Chloride efflux promoted by addition of receptor **268** (2 mol % with respect to lipid) to unilamellar POPC vesicles loaded with either 451 mM NaCl or 451 mM CsCl, buffered to pH 7.2 with 20 mM sodium phosphate salts. The vesicles were suspended in 150 mM Na_2SO_4 buffered to pH 7.2 with 20 mM sodium phosphate salts. At the end of the experiment, detergent was added to lyse the vesicles and calibrate the ISE to 100 % chloride efflux. Each point represents an average of three trials.

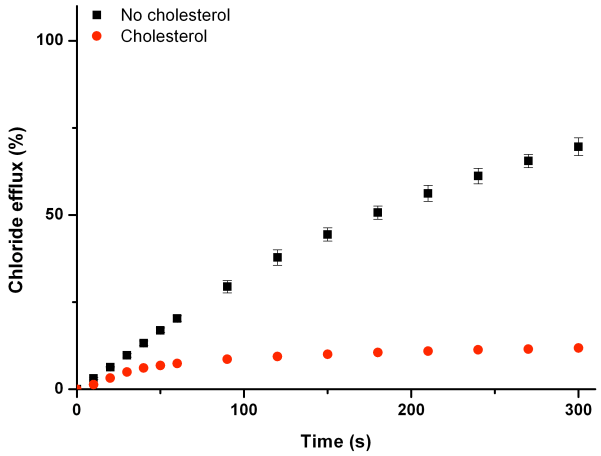

Figure 5.2.25: Chloride efflux promoted by addition of receptor **262** (0.25 mol % with respect to lipid) to unilamellar vesicles composed of either POPC or POPC/cholesterol (7:3 molar ratio) loaded with 488 mM NaCl buffered to pH 7.2 with 5 mM sodium phosphate salts. The vesicles were suspended in 488 mM $NaNO_3$ buffered to pH 7.2 with 5 mM sodium phosphate salts. At the end of the experiment, detergent was added to lyse the vesicles and calibrate the ISE to 100 % chloride efflux. Each point represents an average of three trials.

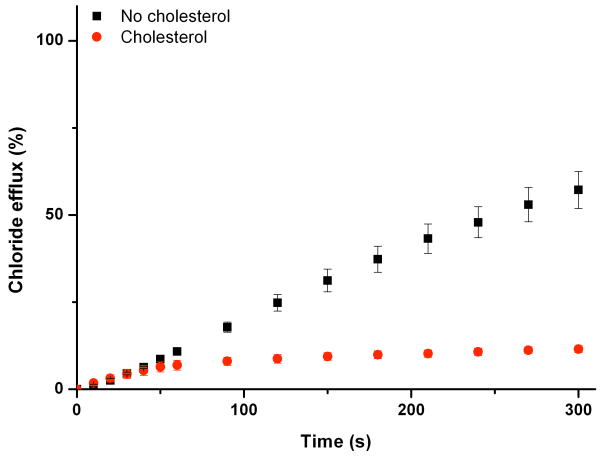

Figure 5.2.26: Chloride efflux promoted by addition of receptor **245** (0.5 mol % with respect to lipid) to unilamellar vesicles composed of either POPC or POPC/cholesterol (7:3 molar ratio) loaded with 488 mM NaCl buffered to pH 7.2 with 5 mM sodium phosphate salts. The vesicles were suspended in 488 mM $NaNO_3$ buffered to pH 7.2 with 5 mM sodium phosphate salts. At the end of the experiment, detergent was added to lyse the vesicles and calibrate the ISE to 100 % chloride efflux. Each point represents an average of three trials.

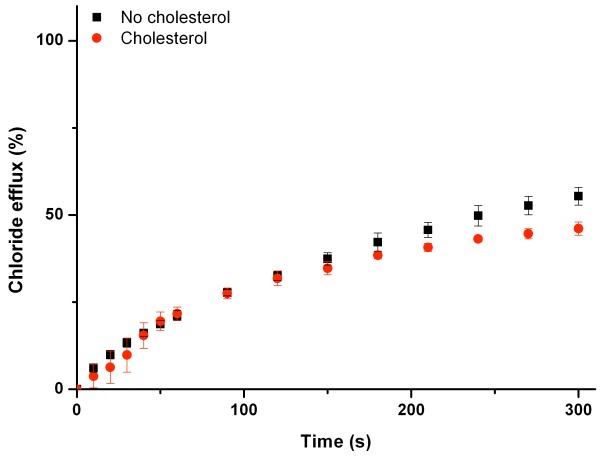

Figure 5.2.27: Chloride efflux promoted by addition of receptor **263** (0.01 mol % with respect to lipid) to unilamellar vesicles composed of either POPC or POPC/cholesterol (7:3 molar ratio) loaded with 488 mM NaCl buffered to pH 7.2 with 5 mM sodium phosphate salts. The vesicles were suspended in 488 mM $NaNO_3$ buffered to pH 7.2 with 5 mM sodium phosphate salts. At the end of the experiment, detergent was added to lyse the vesicles and calibrate the ISE to 100 % chloride efflux. Each point represents an average of three trials.

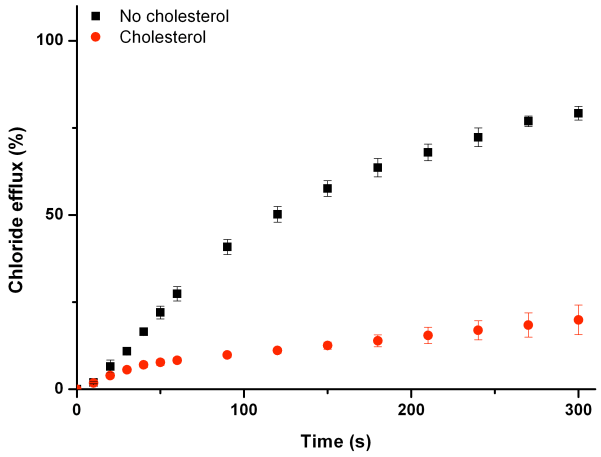

Figure 5.2.28: Chloride efflux promoted by addition of receptor **264** (0.05 mol % with respect to lipid) to unilamellar vesicles composed of either POPC or POPC/cholesterol (7:3 molar ratio) loaded with 488 mM NaCl buffered to pH 7.2 with 5 mM sodium phosphate salts. The vesicles were suspended in 488 mM $NaNO_3$ buffered to pH 7.2 with 5 mM sodium phosphate salts. At the end of the experiment, detergent was added to lyse the vesicles and calibrate the ISE to 100 % chloride efflux. Each point represents an average of three trials.

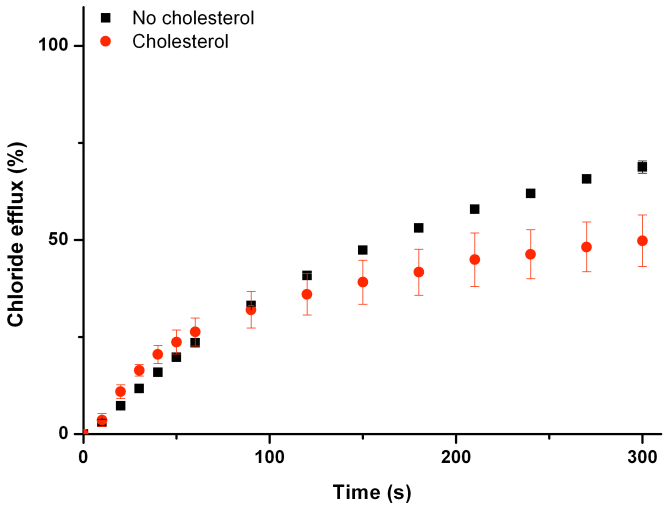

Figure 5.2.29: Chloride efflux promoted by addition of receptor **247** (0.01 mol % with respect to lipid) to unilamellar vesicles composed of either POPC or POPC/cholesterol (7:3 molar ratio) loaded with 488 mM NaCl buffered to pH 7.2 with 5 mM sodium phosphate salts. The vesicles were suspended in 488 mM $NaNO_3$ buffered to pH 7.2 with 5 mM sodium phosphate salts. At the end of the experiment, detergent was added to lyse the vesicles and calibrate the ISE to 100 % chloride efflux. Each point represents an average of three trials.

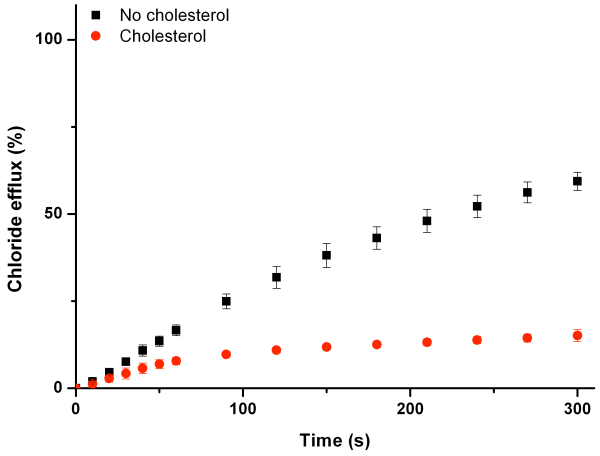

Figure 5.2.30: Chloride efflux promoted by addition of receptor **265** (0.1 mol % with respect to lipid) to unilamellar vesicles composed of either POPC or POPC/cholesterol (7:3 molar ratio) loaded with 488 mM NaCl buffered to pH 7.2 with 5 mM sodium phosphate salts. The vesicles were suspended in 488 mM $NaNO_3$ buffered to pH 7.2 with 5 mM sodium phosphate salts. At the end of the experiment, detergent was added to lyse the vesicles and calibrate the ISE to 100 % chloride efflux. Each point represents an average of three trials.

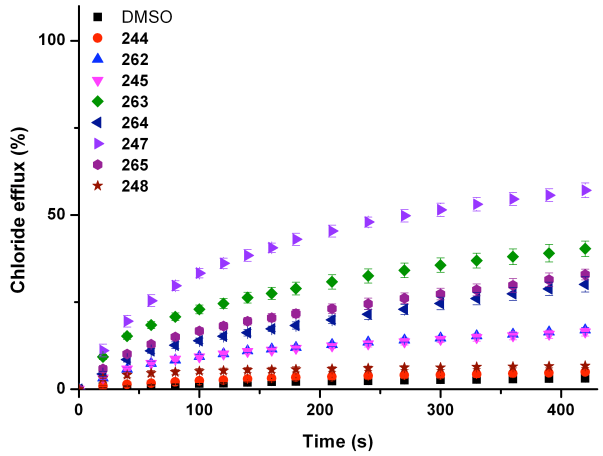

Figure 5.2.31: Chloride efflux promoted by addition of receptors **244**, **245**, **247**, **248** and **262-265** (2 mol % each with respect to lipid) to unilamellar POPC vesicles loaded with 451 mM NaCl buffered to pH 7.2 with 20 mM sodium phosphate salts. The vesicles were suspended in 150 mM Na_2SO_4 buffered to pH 7.2 with 20 mM sodium phosphate salts. At the end of the experiment, detergent was added to lyse the vesicles and calibrate the ISE to 100 % chloride efflux. Each point represents an average of three trials.

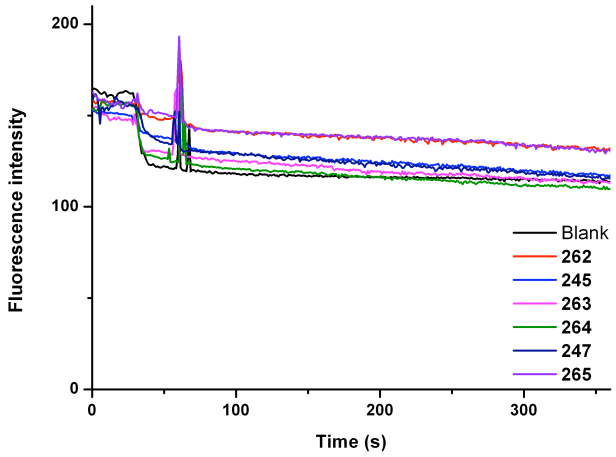

Figure 5.2.32: Change in lucigenin fluorescence intensity (excitation at 455 nm, emission at 506 nm) upon addition of receptors **245**, **247** and **262-265** (2 mol % each with respect to lipid) to unilamellar POPC vesicles loaded with 100 mM NaCl and 2mM lucigenin buffered to pH 7.2 with 20 mM sodium phosphate salts following the addition of a Na_2SO_4 'pulse' to make the extravesicular sulphate concentration 40 mM. The vesicles were suspended in 100 mM NaCl buffered to pH 7.2 with 20 mM sodium phosphate salts. Each trace represents an average of three trials.

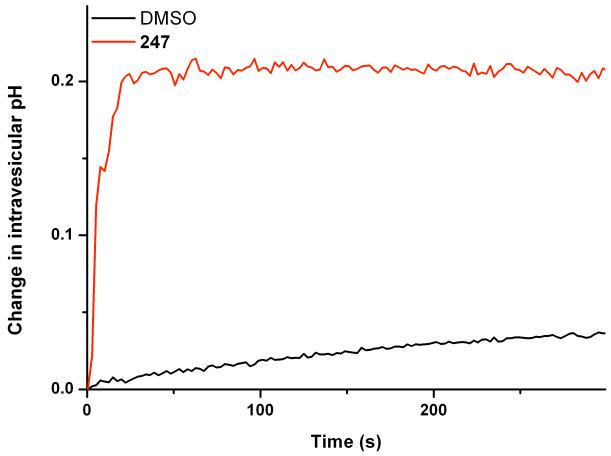

Figure 5.2.33: Change in intravesicular pH upon addition upon addition of receptors **247** (2 mol % with respect to lipid) to unilamellar POPC vesicles loaded with 451 mM NaCl and 1mM HPTS buffered to pH 7.2 with 20 mM sodium phosphate salts. The vesicles were suspended in 150 mM Na_2SO_4 buffered to pH 7.2 with 20 mM sodium phosphate salts. Each trace represents an average of three trials.

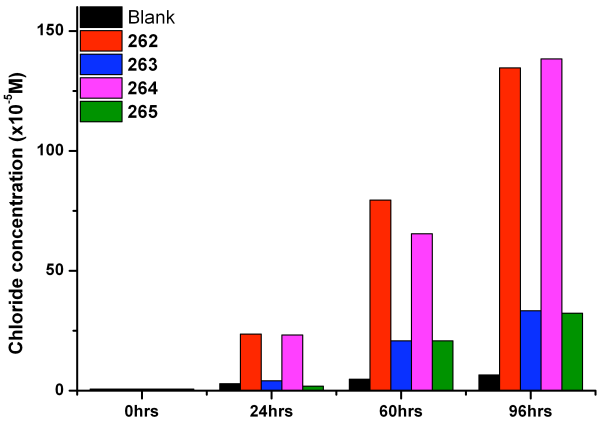

Figure 5.2.34: Change in chloride concentration of the receiving phase in a U-tube assay facilitated by compounds **262-265** (1 mM each) dissolved in a nitrobenzene organic phase (15 mL) in the presence of TBA hexafluorophosphate (1 mM). The source phase (7.5 mL) contained 488 mM NaCl buffered to pH 7.2 with 5 mM sodium phosphate salts and the receiving phase (7.5 mL) contained 488 mM $NaNO_3$ buffered to pH 7.2 with 5mM sodium phosphate salts.

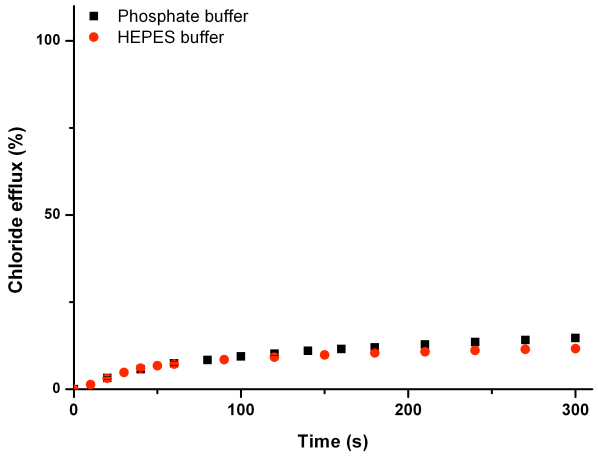

Figure 5.2.35: Chloride efflux promoted by addition of receptors **262** (2 mol % with respect to lipid) to unilamellar POPC vesicles loaded with 451 mM NaCl buffered to pH 7.2 with either 20 mM sodium phosphate salts or 20 mM HEPES buffer. The vesicles were suspended in 150 mM Na_2SO_4 buffered to pH 7.2 with either 20 mM sodium phosphate salts or 20 mM HEPES buffer. At the end of the experiment, detergent was added to lyse the vesicles and calibrate the ISE to 100% chloride efflux. Each point represents an average of three trials.

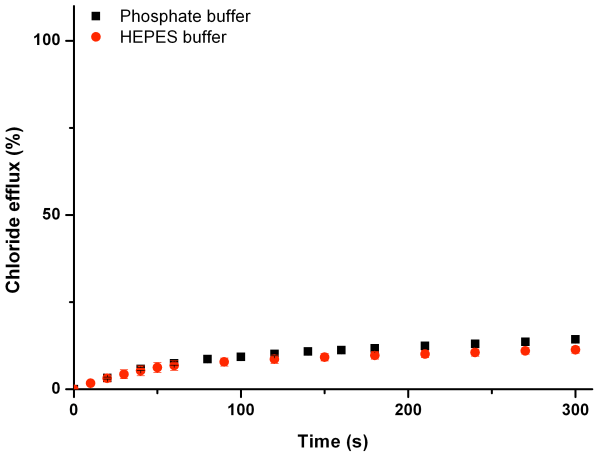

Figure 5.2.36: Chloride efflux promoted by addition of receptors **245** (2 mol % with respect to lipid) to unilamellar POPC vesicles loaded with 451 mM NaCl buffered to pH 7.2 with either 20 mM sodium phosphate salts or 20 mM HEPES buffer. The vesicles were suspended in 150 mM Na_2SO_4 buffered to pH 7.2 with either 20 mM sodium phosphate salts or 20 mM HEPES buffer. At the end of the experiment, detergent was added to lyse the vesicles and calibrate the ISE to 100 % chloride efflux. Each point represents an average of three trials.

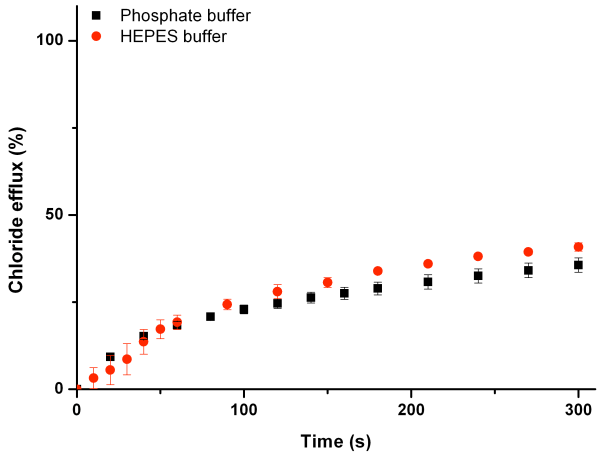

Figure 5.2.37: Chloride efflux promoted by addition of receptors **263** (2 mol % with respect to lipid) to unilamellar POPC vesicles loaded with 451 mM NaCl buffered to pH 7.2 with either 20 mM sodium phosphate salts or 20 mM HEPES buffer. The vesicles were suspended in 150 mM Na_2SO_4 buffered to pH 7.2 with either 20 mM sodium phosphate salts or 20 mM HEPES buffer. At the end of the experiment, detergent was added to lyse the vesicles and calibrate the ISE to 100 % chloride efflux. Each point represents an average of three trials.

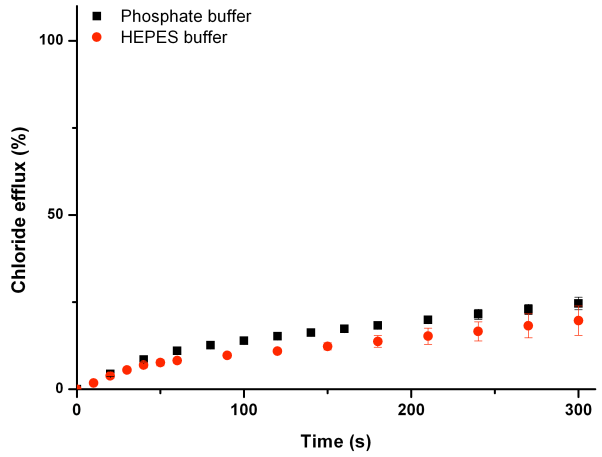

Figure 5.2.38: Chloride efflux promoted by addition of receptors **264** (2 mol % with respect to lipid) to unilamellar POPC vesicles loaded with 451 mM NaCl buffered to pH 7.2 with either 20 mM sodium phosphate salts or 20 mM HEPES buffer. The vesicles were suspended in 150 mM Na_2SO_4 buffered to pH 7.2 with either 20 mM sodium phosphate salts or 20 mM HEPES buffer. At the end of the experiment, detergent was added to lyse the vesicles and calibrate the ISE to 100 % chloride efflux. Each point represents an average of three trials.

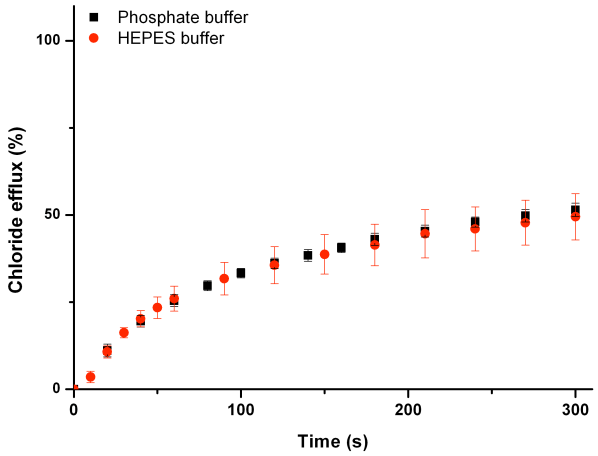

Figure 5.2.39: Chloride efflux promoted by addition of receptors **247** (2 mol % with respect to lipid) to unilamellar POPC vesicles loaded with 451 mM NaCl buffered to pH 7.2 with either 20 mM sodium phosphate salts or 20 mM HEPES buffer. The vesicles were suspended in 150 mM Na_2SO_4 buffered to pH 7.2 with either 20 mM sodium phosphate salts or 20 mM HEPES buffer. At the end of the experiment, detergent was added to lyse the vesicles and calibrate the ISE to 100 % chloride efflux. Each point represents an average of three trials.

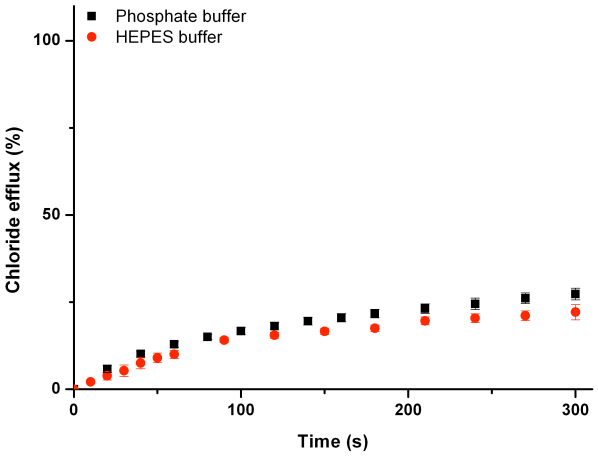

Figure 5.2.40: Chloride efflux promoted by addition of receptors **265** (2 mol % with respect to lipid) to unilamellar POPC vesicles loaded with 451 mM NaCl buffered to pH 7.2 with either 20 mM sodium phosphate salts or 20 mM HEPES buffer. The vesicles were suspended in 150 mM Na_2SO_4 buffered to pH 7.2 with either 20 mM sodium phosphate salts or 20 mM HEPES buffer. At the end of the experiment, detergent was added to lyse the vesicles and calibrate the ISE to 100 % chloride efflux. Each point represents an average of three trials.

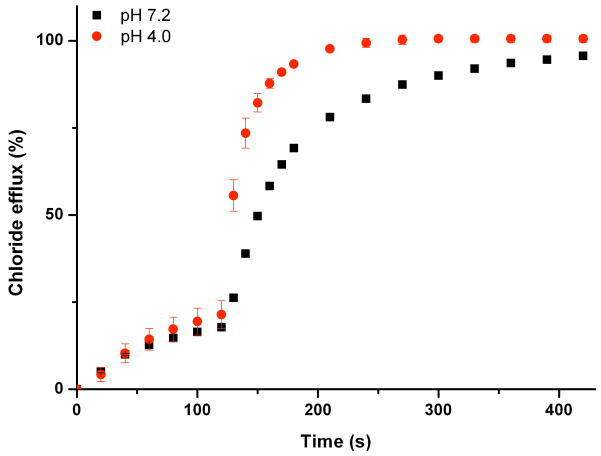

Figure 5.2.41: Chloride efflux promoted by a DMSO solution of compound **263** (2 mol % carrier to lipid) from unilamellar POPC vesicles loaded with either; i) 451 mM NaCl buffered to pH 7.2 with 20 mM sodium phosphate salts and dispersed in 150 mM Na_2SO_4 buffered to pH 7.2 with 20 mM sodium phosphate salts, or ii) 451 mM NaCl buffered to pH 4.0 with 20 mM sodium citrate salts and dispersed in 150 mM Na_2SO_4 buffered to pH 4.0 with 20 mM sodium citrate salts. At t = 120 s a solution of sodium maleate was added such that the external concentration of carboxylate was 40 mM. At the end of the experiment, detergent was added to lyse the vesicles and calibrate the ISE to 100 % chloride efflux. Each point represents an average of three trials.

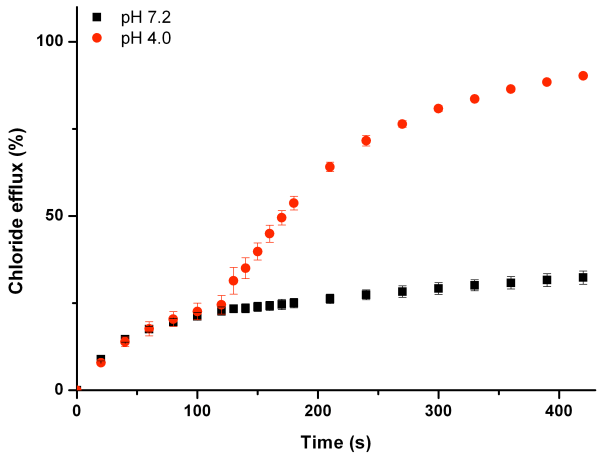

Figure 5.2.42: Chloride efflux promoted by a DMSO solution of compound **263** (2 mol % carrier to lipid) from unilamellar POPC vesicles loaded with either; i) 451 mM NaCl buffered to pH 7.2 with 20 mM sodium phosphate salts and dispersed in 150 mM Na_2SO_4 buffered to pH 7.2 with 20 mM sodium phosphate salts, or ii) 451 mM NaCl buffered to pH 4.0 with 20 mM sodium citrate salts and dispersed in 150 mM Na_2SO_4 buffered to pH 4.0 with 20 mM sodium citrate salts. At t = 120 s a solution of sodium fumarate was added such that the external concentration of carboxylate was 40 mM. At the end of the experiment, detergent was added to lyse the vesicles and calibrate the ISE to 100 % chloride efflux. Each point represents an average of three trials.

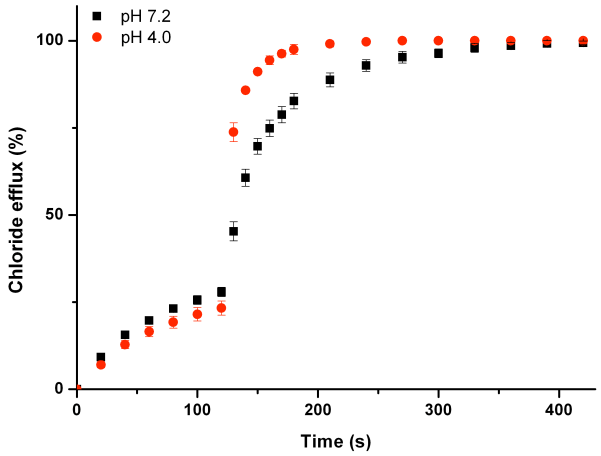

Figure 5.2.43: Chloride efflux promoted by a DMSO solution of compound **247** (2 mol % carrier to lipid) from unilamellar POPC vesicles loaded with either; i) 451mM NaCl buffered to pH 7.2 with 20mM sodium phosphate salts and dispersed in 150 mM Na_2SO_4 buffered to pH 7.2 with 20mM sodium phosphate salts, or ii) 451 mM NaCl buffered to pH 4.0 with 20 mM sodium citrate salts and dispersed in 150 mM Na_2SO_4 buffered to pH 4.0 with 20 mM sodium citrate salts. At t = 120 s a solution of sodium maleate was added such that the external concentration of carboxylate was 40 mM. At the end of the experiment, detergent was added to lyse the vesicles and calibrate the ISE to 100 % chloride efflux. Each point represents an average of three trials.

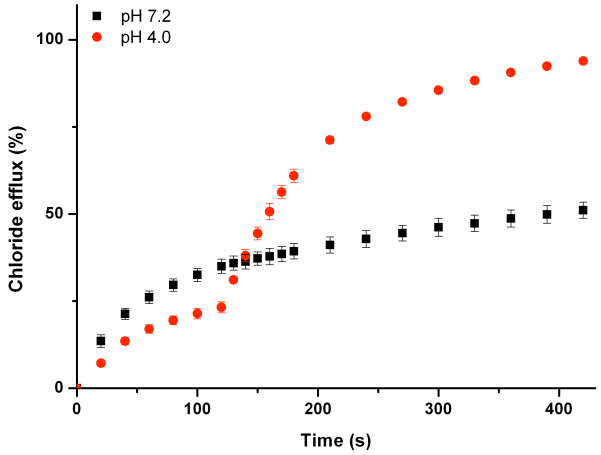

Figure 5.2.44: Chloride efflux promoted by a DMSO solution of compound **247** (2 mol % carrier to lipid) from unilamellar POPC vesicles loaded with either; i) 451 mM NaCl buffered to pH 7.2 with 20 mM sodium phosphate salts and dispersed in 150 mM Na_2SO_4 buffered to pH 7.2 with 20 mM sodium phosphate salts, or ii) 451 mM NaCl buffered to pH 4.0 with 20 mM sodium citrate salts and dispersed in 150 mM Na_2SO_4 buffered to pH 4.0 with 20 mM sodium citrate salts. At t = 120 s a solution of sodium fumarate was added such that the external concentration of carboxylate was 40 mM. At the end of the experiment, detergent was added to lyse the vesicles and calibrate the ISE to 100 % chloride efflux. Each point represents an average of three trials.

A5.3 Ion Transport Assays from Chapter 5

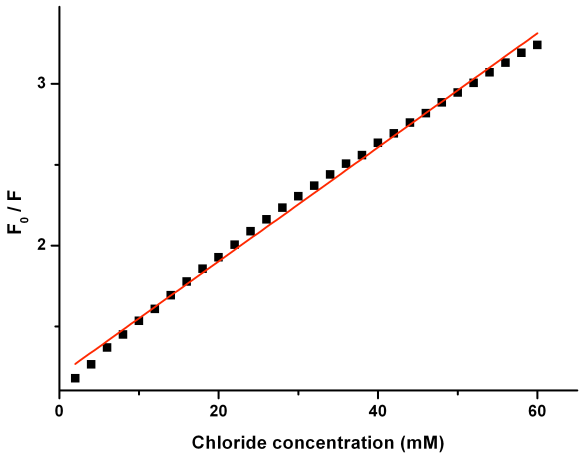

Figure 5.3.1: Stern-Volmer plot obtained by adding melattin (0.2 mol % with respect to lipid) to unilamellar POPC vesicles loaded with 1 mM lucigenin and 71 mM sodium sulphate, buffered to pH 7.2 with 5 mM sodium phosphate salts. The vesicles were suspended in a solution of 71 mM sodium sulphate, buffered to pH 7.2 with 5 mM sodium phosphate salts. Sodium chloride was added stepwise such that each addition increased the total chloride concentration by 2 mM. $K_{sv} = 42.55 \pm 0.44\ M^{-1}$.

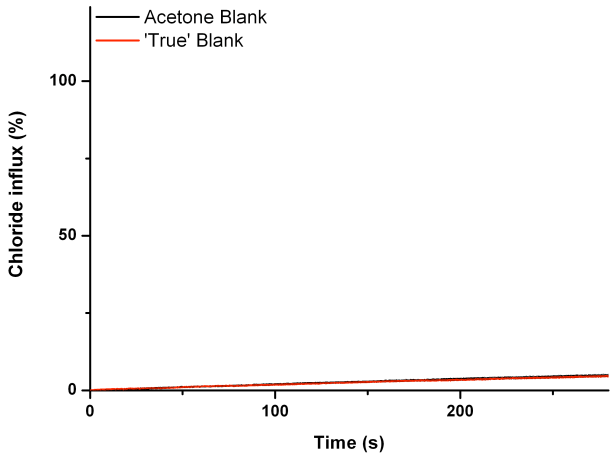

Figure 5.3.2: Standardised change in internal chloride concentration of unilamellar POPC vesicles containing 1 mM lucigenin and 71 mM sodium sulphate, buffered to pH 7.2 with 5 mM sodium phosphate salts and suspended in 71 mM sodium sulphate, buffered to pH 7.2 with 5 mM sodium phosphate salts, upon addition of acetone (6 µL, Acetone blank) and without addition ('True' blank) following a 'pulse' of NaCl such that the external concentration of NaCl was 100 mM.

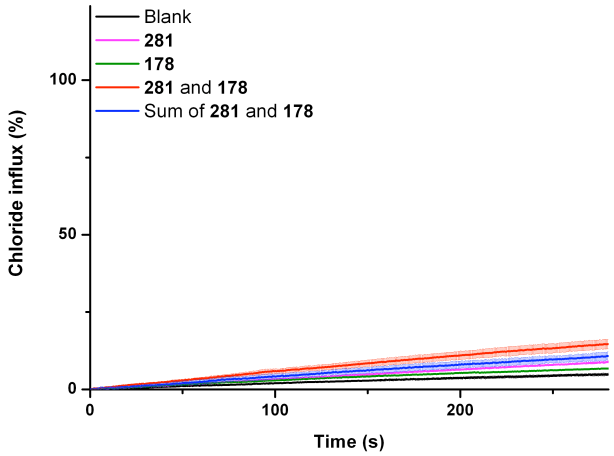

Figure 5.3.3: Chloride influx promoted by addition of acetone solutions of receptors **281** (2 mol % with respect to lipid), **178** (2 mol % with respect to lipid), and both **281** and **178** (2 mol % each with respect to lipid) to unilamellar POPC vesicles loaded with 1 mM lucigenin and 71 mM Na_2SO_4, buffered to pH 7.2 with 5 mM sodium phosphate salts, upon addition of a NaCl 'pulse' such that the extravesicular concentration of NaCl was 100 mM. The vesicles were suspended in 71 mM sodium sulphate, buffered to pH 7.2 with 5 mM sodium phosphate salts. Each plot represents an average of three trials. The corrected sum of compounds **281** and **178** added individually is shown for comparison.

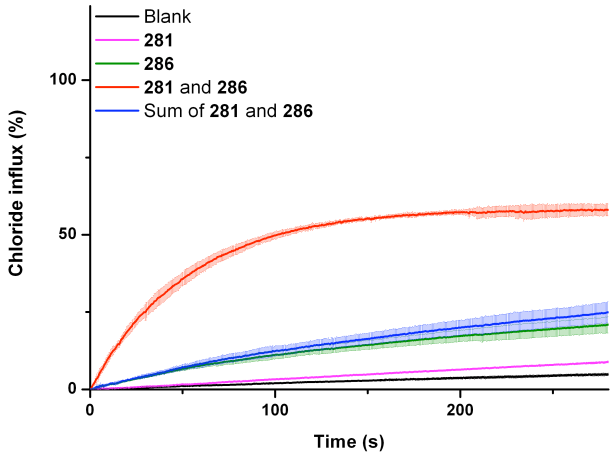

Figure 5.3.4: Chloride influx promoted by addition of acetone solutions of receptors **281** (2 mol % with respect to lipid), **286** (2 mol % with respect to lipid), and both **281** and **286** (2 mol % each with respect to lipid) to unilamellar POPC vesicles loaded with 1 mM lucigenin and 71 mM Na_2SO_4, buffered to pH 7.2 with 5 mM sodium phosphate salts, upon addition of a NaCl 'pulse' such that the extravesicular concentration of NaCl was 100 mM. The vesicles were suspended in 71 mM sodium sulphate, buffered to pH 7.2 with 5 mM sodium phosphate salts. Each plot represents an average of three trials. The corrected sum of compounds **281** and **286** added individually is shown for comparison.

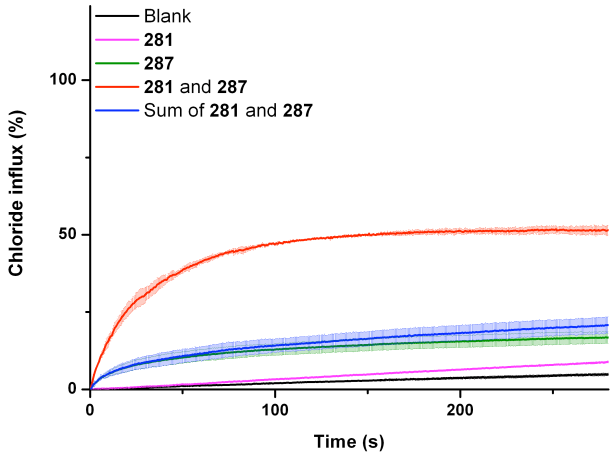

Figure 5.3.5: Chloride influx promoted by addition of acetone solutions of receptors **281** (2 mol % with respect to lipid), **287** (2 mol % with respect to lipid), and both **281** and **287** (2 mol % each with respect to lipid) to unilamellar POPC vesicles loaded with 1 mM lucigenin and 71 mM Na_2SO_4, buffered to pH 7.2 with 5 mM sodium phosphate salts, upon addition of a NaCl 'pulse' such that the extravesicular concentration of NaCl was 100 mM. The vesicles were suspended in 71 mM sodium sulphate, buffered to pH 7.2 with 5 mM sodium phosphate salts. Each plot represents an average of three trials. The corrected sum of compounds **281** and **287** added individually is shown for comparison.

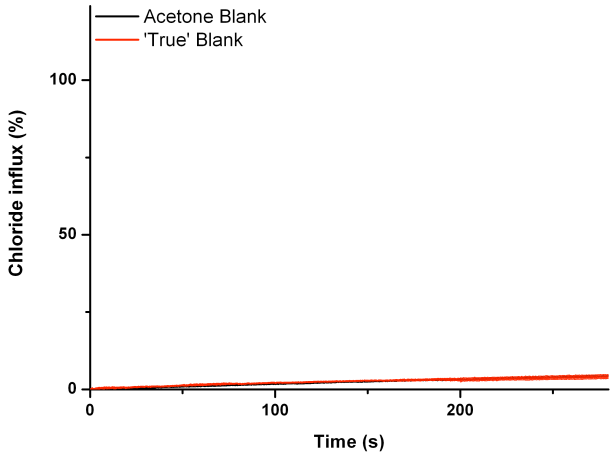

Figure 5.3.6: Standardised change in internal chloride concentration of unilamellar POPC vesicles containing 1 mM lucigenin and 71 mM sodium sulphate, buffered to pH 7.2 with 5 mM sodium phosphate salts and suspended in 71 mM sodium sulphate, buffered to pH 7.2 with 5 mM sodium phosphate salts, upon addition of acetone (6 µL, Acetone blank) and without addition ('True' blank) following a 'pulse' of KCl such that the external concentration of KCl was 100 mM.

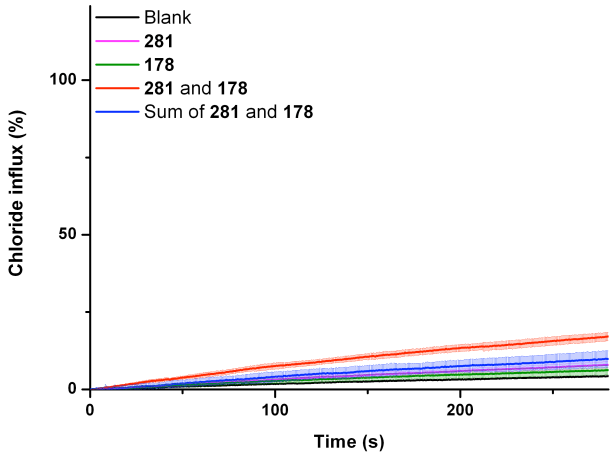

Figure 5.3.7: Chloride influx promoted by addition of acetone solutions of receptors **281** (2 mol % with respect to lipid), **178** (2 mo l% with respect to lipid), and both **281** and **178** (2 mol % each with respect to lipid) to unilamellar POPC vesicles loaded with 1 mM lucigenin and 71 mM Na_2SO_4, buffered to pH 7.2 with 5 mM sodium phosphate salts, upon addition of a KCl 'pulse' such that the extravesicular concentration of KCl was 100 mM. The vesicles were suspended in 71 mM sodium sulphate, buffered to pH 7.2 with 5 mM sodium phosphate salts. Each plot represents an average of three trials. The corrected sum of compounds **281** and **178** added individually is shown for comparison.

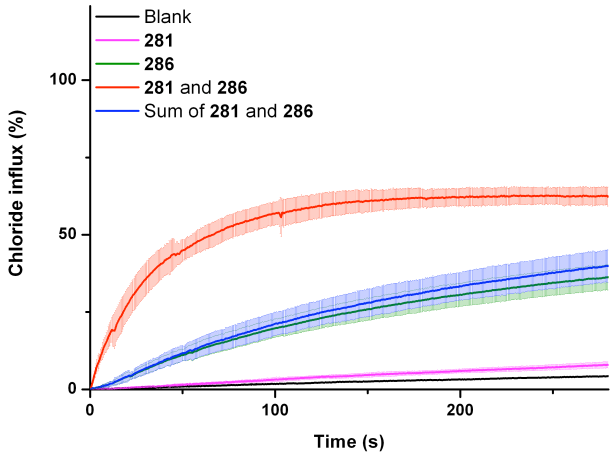

Figure 5.3.8: Chloride influx promoted by addition of acetone solutions of receptors **281** (2 mol % with respect to lipid), **286** (2 mol % with respect to lipid), and both **281** and **286** (2 mol % each with respect to lipid) to unilamellar POPC vesicles loaded with 1 mM lucigenin and 71 mM Na_2SO_4, buffered to pH 7.2 with 5 mM sodium phosphate salts, upon addition of a KCl 'pulse' such that the extravesicular concentration of KCl was 100 mM. The vesicles were suspended in 71 mM sodium sulphate, buffered to pH 7.2 with 5 mM sodium phosphate salts. Each plot represents an average of three trials. The corrected sum of compounds **281** and **286** added individually is shown for comparison.

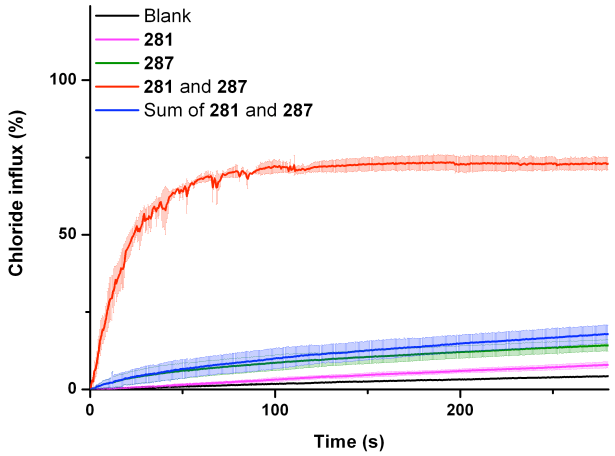

Figure 5.3.9: Chloride influx promoted by addition of acetone solutions of receptors **281** (2 mol % with respect to lipid), **287** (2 mol % with respect to lipid), and both **281** and **287** (2 mol % each with respect to lipid) to unilamellar POPC vesicles loaded with 1 mM lucigenin and 71 mM Na_2SO_4, buffered to pH 7.2 with 5 mM sodium phosphate salts, upon addition of a KCl 'pulse' such that the extravesicular concentration of KCl was 100 mM. The vesicles were suspended in 71 mM sodium sulphate, buffered to pH 7.2 with 5 mM sodium phosphate salts. Each plot represents an average of three trials. The corrected sum of compounds **281** and **287** added individually is shown for comparison.

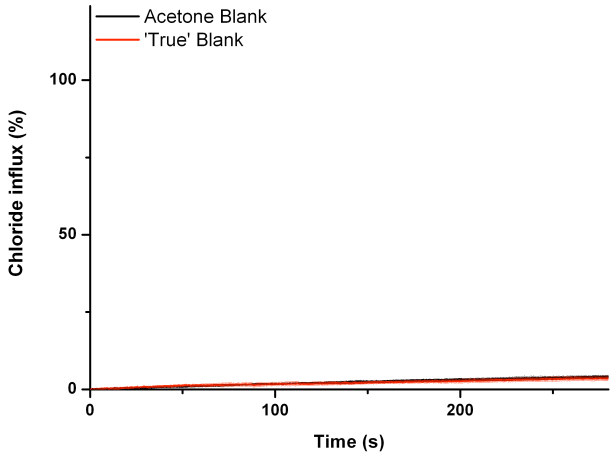

Figure 5.3.10: Standardised change in internal chloride concentration of unilamellar POPC vesicles containing 1 mM lucigenin and 71 mM sodium sulphate, buffered to pH 7.2 with 5 mM sodium phosphate salts and suspended in 71 mM sodium sulphate, buffered to pH 7.2 with 5 mM sodium phosphate salts, upon addition of acetone (6 μL, Acetone blank) and without addition ('True' blank) following a 'pulse' of RbCl such that the external concentration of RbCl was 100 mM.

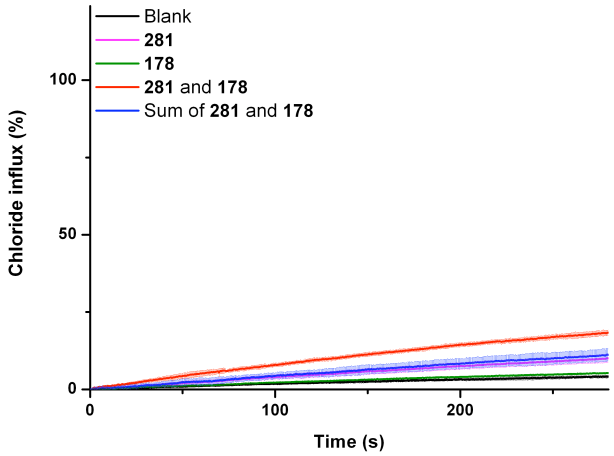

Figure 5.3.11: Chloride influx promoted by addition of acetone solutions of receptors **281** (2 mol % with respect to lipid), **178** (2 mol % with respect to lipid), and both **281** and **178** (2 mol % each with respect to lipid) to unilamellar POPC vesicles loaded with 1 mM lucigenin and 71 mM Na_2SO_4, buffered to pH 7.2 with 5 mM sodium phosphate salts, upon addition of a RbCl 'pulse' such that the extravesicular concentration of RbCl was 100 mM. The vesicles were suspended in 71 mM sodium sulphate, buffered to pH 7.2 with 5 mM sodium phosphate salts. Each plot represents an average of three trials. The corrected sum of compounds **281** and **178** added individually is shown for comparison.

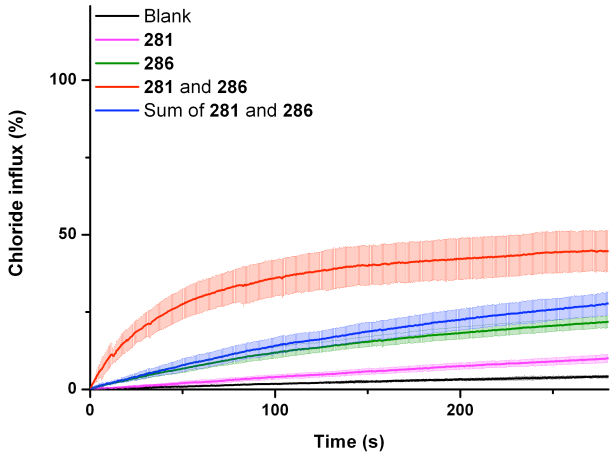

Figure 5.3.12: Chloride influx promoted by addition of acetone solutions of receptors **281** (2 mol % with respect to lipid), **286** (2 mol % with respect to lipid), and both **281** and **286** (2 mol % each with respect to lipid) to unilamellar POPC vesicles loaded with 1 mM lucigenin and 71 mM Na_2SO_4, buffered to pH 7.2 with 5mM sodium phosphate salts, upon addition of a RbCl 'pulse' such that the extravesicular concentration of RbCl was 100 mM. The vesicles were suspended in 71 mM sodium sulphate, buffered to pH 7.2 with 5 mM sodium phosphate salts. Each plot represents an average of three trials. The corrected sum of compounds **281** and **286** added individually is shown for comparison.

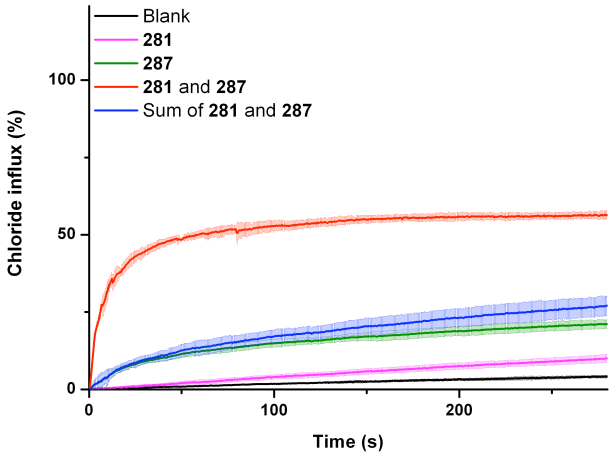

Figure 5.3.13: Chloride influx promoted by addition of acetone solutions of receptors **281** (2 mol % with respect to lipid), **287** (2 mol % with respect to lipid), and both **281** and **287** (2 mol % each with respect to lipid) to unilamellar POPC vesicles loaded with 1 mM lucigenin and 71 mM Na_2SO_4, buffered to pH 7.2 with 5 mM sodium phosphate salts, upon addition of a RbCl 'pulse' such that the extravesicular concentration of RbCl was 100 mM. The vesicles were suspended in 71 mM sodium sulphate, buffered to pH 7.2 with 5 mM sodium phosphate salts. Each plot represents an average of three trials. The corrected sum of compounds **281** and **287** added individually is shown for comparison.

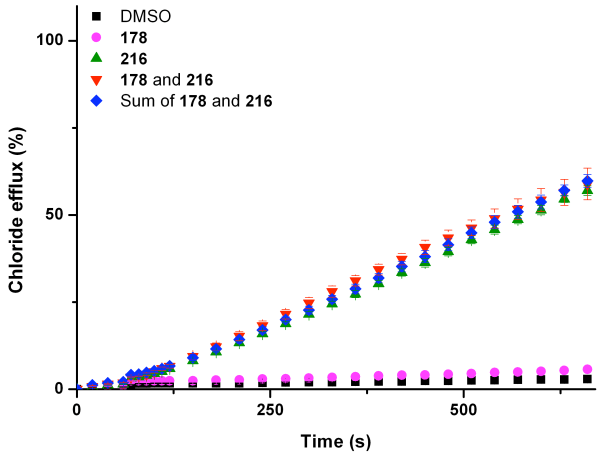

Figure 5.3.14: Chloride efflux promoted by addition of DMSO solutions of receptors **178** (2 mol % with respect to lipid), **216** (0.03 mol % with respect to lipid), and both **178** and **216** (2 mol % and 0.03 mol % respectively, with respect to lipid) to unilamellar POPC vesicles loaded with 451 mM NaCl buffered to pH 7.2 with 20 mM sodium phosphate salts upon addition of a $NaHCO_3$ 'pulse' at t = 60 s, such that the extravesicular concentration of bicarbonate was 40 mM. The vesicles were suspended in 150 mM Na_2SO_4 buffered to pH 7.2 with 20 mM sodium phosphate salts. At the end of the experiment, detergent was added to lyse the vesicles and calibrate the ISE to 100 % chloride efflux. Each point represents an average of three trials. The corrected sum of compounds **178** and **216** added individually is shown for comparison.

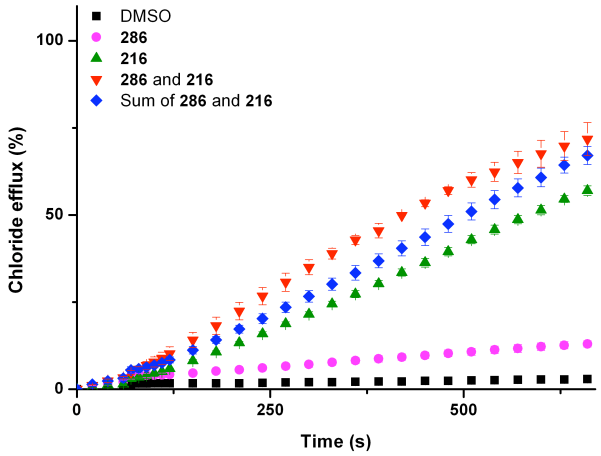

Figure 5.3.15: Chloride efflux promoted by addition of DMSO solutions of receptors **286** (2 mol % with respect to lipid), **216** (0.03 mol % with respect to lipid), and both **286** and **216** (2 mol % and 0.03 mol % respectively, with respect to lipid) to unilamellar POPC vesicles loaded with 451 mM NaCl buffered to pH 7.2 with 20 mM sodium phosphate salts upon addition of a $NaHCO_3$ 'pulse' at t = 60 s, such that the extravesicular concentration of bicarbonate was 40 mM. The vesicles were suspended in 150 mM Na_2SO_4 buffered to pH 7.2 with 20 mM sodium phosphate salts. At the end of the experiment, detergent was added to lyse the vesicles and calibrate the ISE to 100 % chloride efflux. Each point represents an average of three trials. The corrected sum of compounds **286** and **216** added individually is shown for comparison.

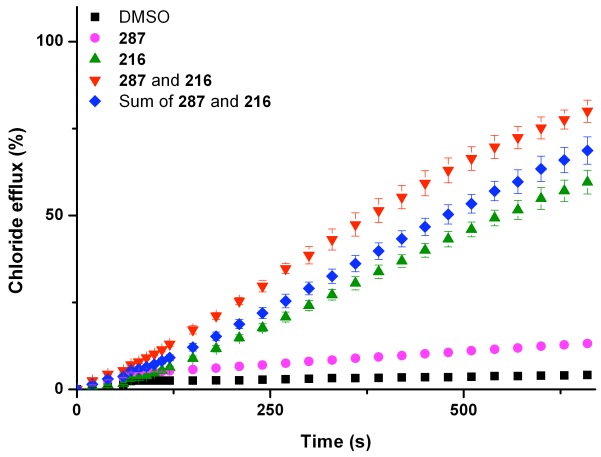

Figure 5.3.16: Chloride efflux promoted by addition of DMSO solutions of receptors **287** (2 mol % with respect to lipid), **216** (0.03 mol % with respect to lipid), and both **287** and **216** (2 mol % and 0.03 mol % respectively, with respect to lipid) to unilamellar POPC vesicles loaded with 451 mM NaCl buffered to pH 7.2 with 20 mM sodium phosphate salts upon addition of a $NaHCO_3$ 'pulse' at t = 60 s, such that the extravesicular concentration of bicarbonate was 40 mM. The vesicles were suspended in 150 mM Na_2SO_4 buffered to pH 7.2 with 20 mM sodium phosphate salts. At the end of the experiment, detergent was added to lyse the vesicles and calibrate the ISE to 100% chloride efflux. Each point represents an average of three trials. The corrected sum of compounds **287** and **216** added individually is shown for comparison.

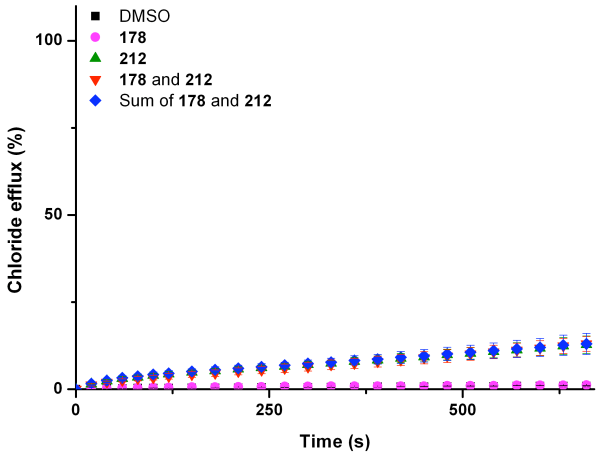

Figure 5.3.17: Chloride efflux promoted by addition of DMSO solutions of receptors **178** (2 mol % with respect to lipid), **212** (2 mol % with respect to lipid), and both **178** and **212** (2 mol % each with respect to lipid) to unilamellar POPC vesicles loaded with 451 mM NaCl buffered to pH 7.2 with 20 mM sodium phosphate salts. The vesicles were suspended in 150 mM Na_2SO_4 buffered to pH 7.2 with 20 mM sodium phosphate salts. At the end of the experiment, detergent was added to lyse the vesicles and calibrate the ISE to 100 % chloride efflux. Each point represents an average of three trials. The corrected sum of compounds **178** and **212** added individually is shown for comparison.

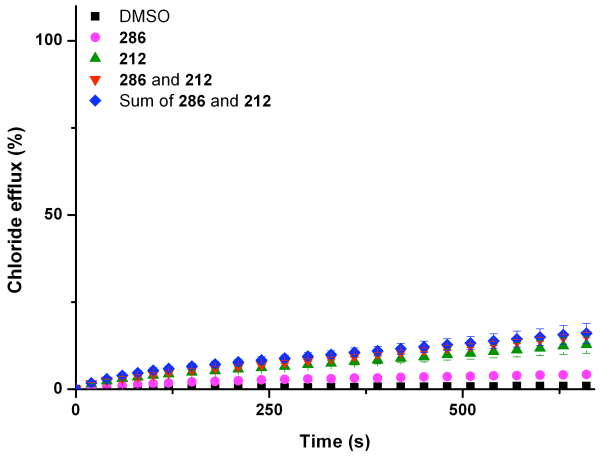

Figure 5.3.18: Chloride efflux promoted by addition of DMSO solutions of receptors **286** (2 mol % with respect to lipid), **212** (2 mol % with respect to lipid), and both **286** and **212** (2 mol % each with respect to lipid) to unilamellar POPC vesicles loaded with 451 mM NaCl buffered to pH 7.2 with 20 mM sodium phosphate salts. The vesicles were suspended in 150 mM Na_2SO_4 buffered to pH 7.2 with 20 mM sodium phosphate salts. At the end of the experiment, detergent was added to lyse the vesicles and calibrate the ISE to 100 % chloride efflux. Each point represents an average of three trials. The corrected sum of compounds **286** and **212** added individually is shown for comparison.

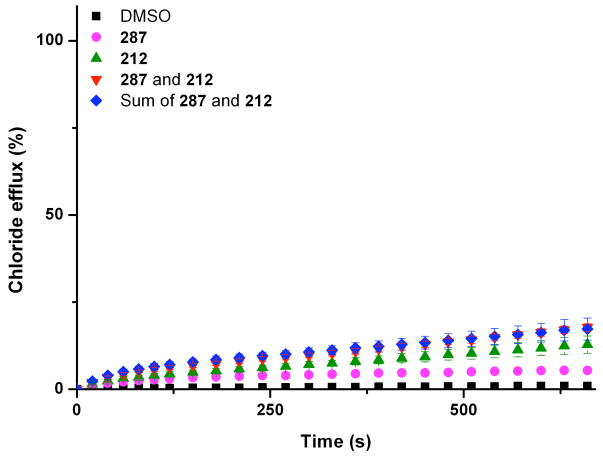

Figure 5.3.19: Chloride efflux promoted by addition of DMSO solutions of receptors **287** (2 mol % with respect to lipid), **212** (2 mol % with respect to lipid), and both **287** and **212** (2 mol % each with respect to lipid) to unilamellar POPC vesicles loaded with 451 mM NaCl buffered to pH 7.2 with 20 mM sodium phosphate salts. The vesicles were suspended in 150 mM Na_2SO_4 buffered to pH 7.2 with 20 mM sodium phosphate salts. At the end of the experiment, detergent was added to lyse the vesicles and calibrate the ISE to 100 % chloride efflux. Each point represents an average of three trials. The corrected sum of compounds **287** and **212** added individually is shown for comparison.

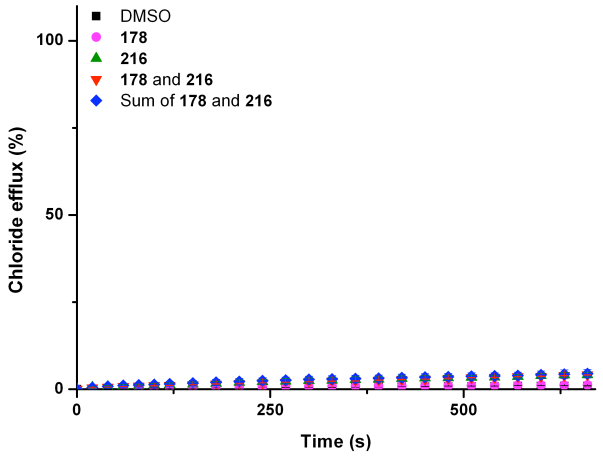

Figure 5.3.20: Chloride efflux promoted by addition of DMSO solutions of receptors **178** (2 mol % with respect to lipid), **216** (0.03 mol % with respect to lipid), and both **178** and **216** (2 mol % and 0.03 mol % respectively, with respect to lipid) to unilamellar POPC vesicles loaded with 451 mM NaCl buffered to pH 7.2 with 20 mM sodium phosphate salts. The vesicles were suspended in 150 mM Na_2SO_4 buffered to pH 7.2 with 20 mM sodium phosphate salts. At the end of the experiment, detergent was added to lyse the vesicles and calibrate the ISE to 100 % chloride efflux. Each point represents an average of three trials. The corrected sum of compounds **178** and **216** added individually is shown for comparison.

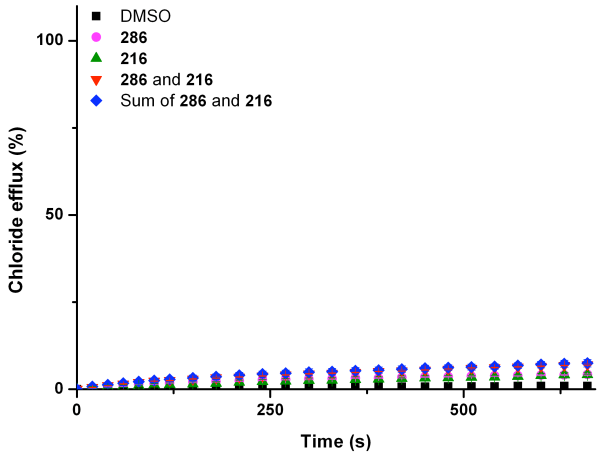

Figure 5.3.21: Chloride efflux promoted by addition of DMSO solutions of receptors **286** (2 mol % with respect to lipid), **216** (0.03 mol % with respect to lipid), and both **286** and **216** (2 mol % and 0.03 mol % respectively, with respect to lipid) to unilamellar POPC vesicles loaded with 451 mM NaCl buffered to pH 7.2 with 20 mM sodium phosphate salts. The vesicles were suspended in 150 mM Na_2SO_4 buffered to pH 7.2 with 20 mM sodium phosphate salts. At the end of the experiment, detergent was added to lyse the vesicles and calibrate the ISE to 100 % chloride efflux. Each point represents an average of three trials. The corrected sum of compounds **286** and **216** added individually is shown for comparison.

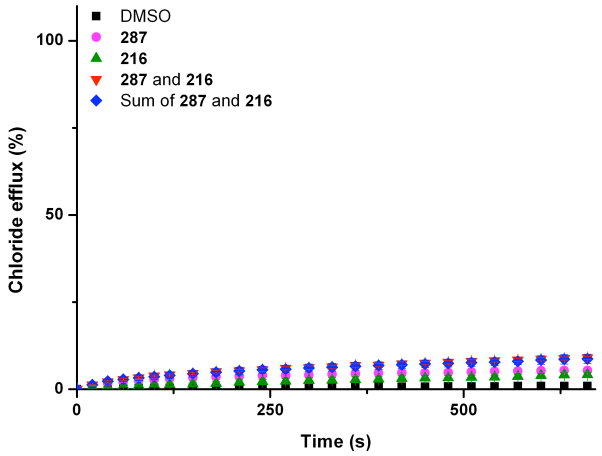

Figure 5.3.22: Chloride efflux promoted by addition of DMSO solutions of receptors **287** (2 mol % with respect to lipid), **216** (0.03 mol % with respect to lipid), and both **287** and **216** (2 mol % and 0.03 mol % respectively, with respect to lipid) to unilamellar POPC vesicles loaded with 451 mM NaCl buffered to pH 7.2 with 20 mM sodium phosphate salts. The vesicles were suspended in 150 mM Na_2SO_4 buffered to pH 7.2 with 20 mM sodium phosphate salts. At the end of the experiment, detergent was added to lyse the vesicles and calibrate the ISE to 100 % chloride efflux. Each point represents an average of three trials. The corrected sum of compounds **287** and **216** added individually is shown for comparison.

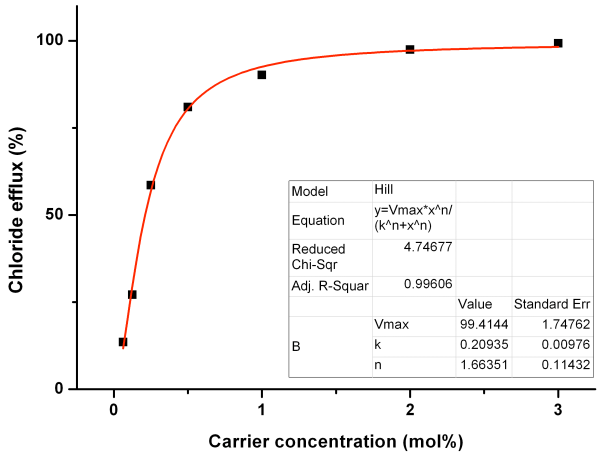

Figure 5.3.23: Hill plot for the Cs^{+}/Cl^{-} symport promoted by receptor **289**.

Appendix 6

Mass Spectrometry

The mass spectrometry experiments described in this section were performed by G. J. Langley and J. Herniman. Stock solutions of ligand and carboxylic acids (1 mg mL^{-1}) were prepared in methanol (analytical grade). Ligand stock solution (10 μL) was added to each experimental sample with the appropriate volume of carboxylic acid stock solution to achieve host:guest ratios of 1:0.4, 1:1, 1:2, 1:4, 1:6, 1:8 and 1:10, and the total volume of the solution made up to 1 mL. ESI-MS were run in the negative ionisation mode using a Bruker Apex III spectrometer, with the relative intensity of both the $[host]^-$ ($[H]^-$) and $[host + guest]^-$ ($[HG]^-$) species recorded. The ratio (R) of total abundances of the host and host + guest species ($[HG]^-/[H]^-$) at equilibrium serves as a relative measure of K_a.[461, 462]

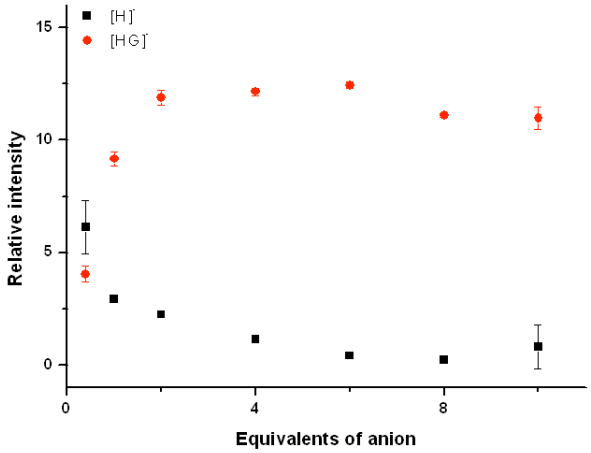

A6.1: Relative intensities of $[H]^-$ and $[HG]^-$ species detected by negative mode ESI-MS from mixtures of bis(urea) **264** and maleic acid in methanol. R = 5.3.

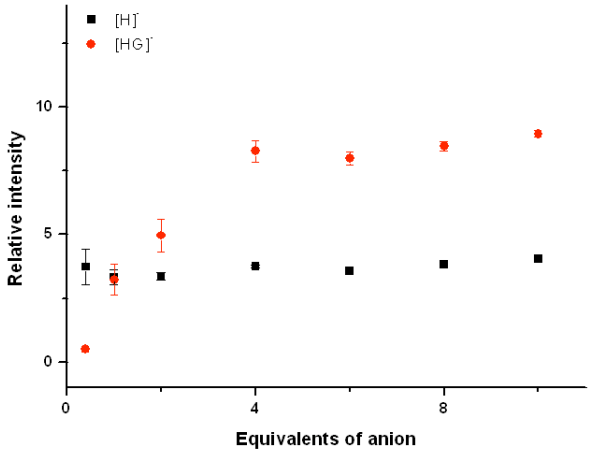

A6.2: Relative intensities of $[H]^-$ and $[HG]^-$ species detected by negative mode ESI-MS from mixtures of bis(urea) **264** and fumaric acid in methanol. R = 2.3.